MSC-DERIVED EXTRACELLULAR VESICLES AND SECRETED FACTORS AS 'CELL-FREE' THERAPEUTIC ALTERNATIVES IN REGENERATIVE MEDICINE

EDITED BY: Enrico Ragni, Antonietta Rosa Silini and Ornella Parolini
PUBLISHED IN: Frontiers in Bioengineering and Biotechnology

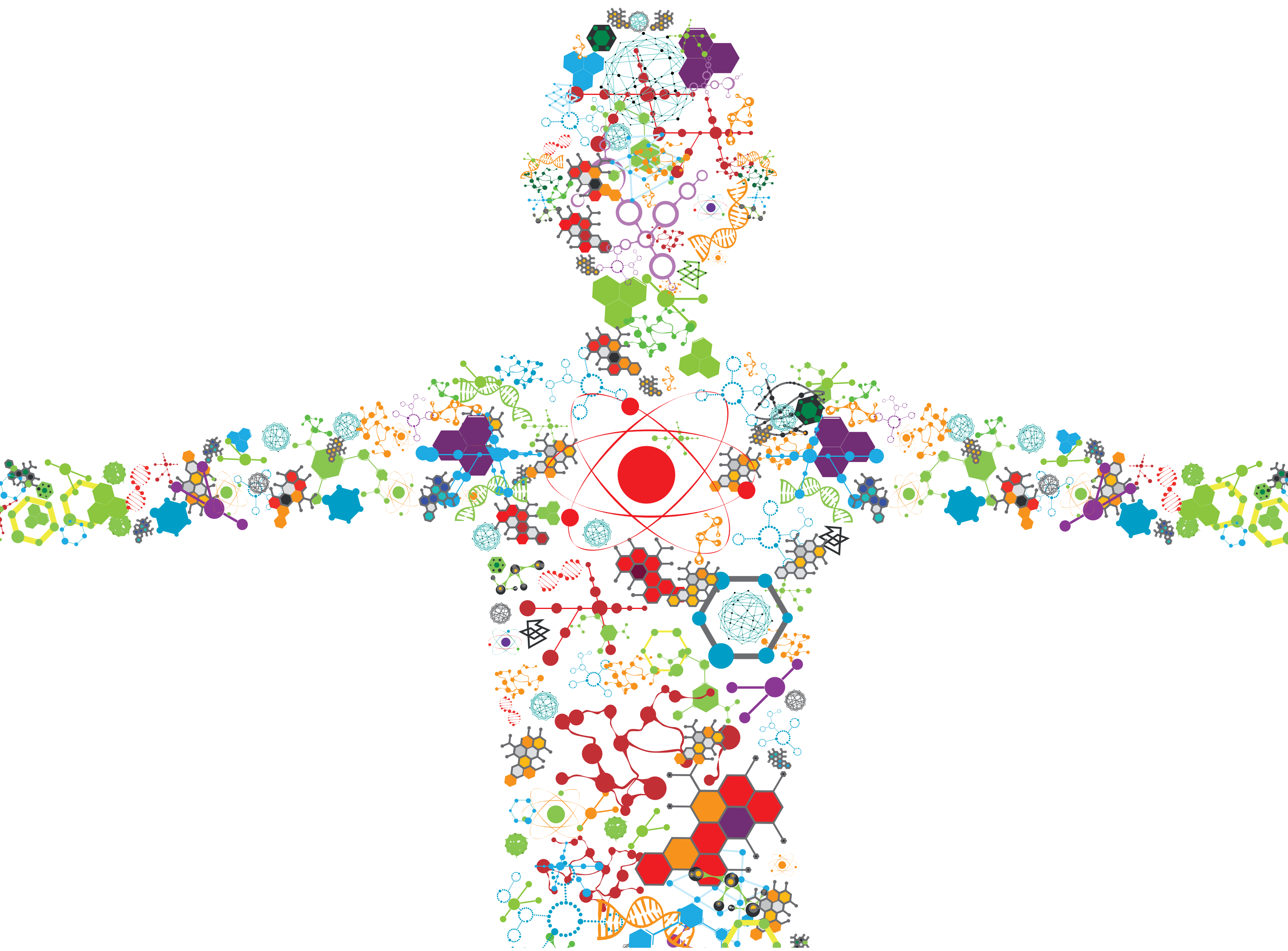

frontiers Research Topics

Frontiers eBook Copyright Statement

The copyright in the text of individual articles in this eBook is the property of their respective authors or their respective institutions or funders. The copyright in graphics and images within each article may be subject to copyright of other parties. In both cases this is subject to a license granted to Frontiers.

The compilation of articles constituting this eBook is the property of Frontiers.

Each article within this eBook, and the eBook itself, are published under the most recent version of the Creative Commons CC-BY licence. The version current at the date of publication of this eBook is CC-BY 4.0. If the CC-BY licence is updated, the licence granted by Frontiers is automatically updated to the new version.

When exercising any right under the CC-BY licence, Frontiers must be attributed as the original publisher of the article or eBook, as applicable.

Authors have the responsibility of ensuring that any graphics or other materials which are the property of others may be included in the CC-BY licence, but this should be checked before relying on the CC-BY licence to reproduce those materials. Any copyright notices relating to those materials must be complied with.

Copyright and source acknowledgement notices may not be removed and must be displayed in any copy, derivative work or partial copy which includes the elements in question.

All copyright, and all rights therein, are protected by national and international copyright laws. The above represents a summary only. For further information please read Frontiers' Conditions for Website Use and Copyright Statement, and the applicable CC-BY licence.

ISSN 1664-8714
ISBN 978-2-88974-508-1
DOI 10.3389/978-2-88974-508-1

About Frontiers

Frontiers is more than just an open-access publisher of scholarly articles: it is a pioneering approach to the world of academia, radically improving the way scholarly research is managed. The grand vision of Frontiers is a world where all people have an equal opportunity to seek, share and generate knowledge. Frontiers provides immediate and permanent online open access to all its publications, but this alone is not enough to realize our grand goals.

Frontiers Journal Series

The Frontiers Journal Series is a multi-tier and interdisciplinary set of open-access, online journals, promising a paradigm shift from the current review, selection and dissemination processes in academic publishing. All Frontiers journals are driven by researchers for researchers; therefore, they constitute a service to the scholarly community. At the same time, the Frontiers Journal Series operates on a revolutionary invention, the tiered publishing system, initially addressing specific communities of scholars, and gradually climbing up to broader public understanding, thus serving the interests of the lay society, too.

Dedication to Quality

Each Frontiers article is a landmark of the highest quality, thanks to genuinely collaborative interactions between authors and review editors, who include some of the world's best academicians. Research must be certified by peers before entering a stream of knowledge that may eventually reach the public - and shape society; therefore, Frontiers only applies the most rigorous and unbiased reviews.
Frontiers revolutionizes research publishing by freely delivering the most outstanding research, evaluated with no bias from both the academic and social point of view.
By applying the most advanced information technologies, Frontiers is catapulting scholarly publishing into a new generation.

What are Frontiers Research Topics?

Frontiers Research Topics are very popular trademarks of the Frontiers Journals Series: they are collections of at least ten articles, all centered on a particular subject. With their unique mix of varied contributions from Original Research to Review Articles, Frontiers Research Topics unify the most influential researchers, the latest key findings and historical advances in a hot research area! Find out more on how to host your own Frontiers Research Topic or contribute to one as an author by contacting the Frontiers Editorial Office: frontiersin.org/about/contact

MSC-DERIVED EXTRACELLULAR VESICLES AND SECRETED FACTORS AS 'CELL-FREE' THERAPEUTIC ALTERNATIVES IN REGENERATIVE MEDICINE

Topic Editors:
Enrico Ragni, Galeazzi Orthopedic Institute (IRCCS), Italy
Antonietta Rosa Silini, Fondazione Poliambulanza Istituto Ospedaliero, Italy
Ornella Parolini, Catholic University of the Sacred Heart, Italy

Citation: Ragni, E., Silini, A. R., Parolini, O., eds. (2022). MSC-derived Extracellular Vesicles and Secreted Factors as 'Cell-Free' Therapeutic Alternatives in Regenerative Medicine. Lausanne: Frontiers Media SA.
doi: 10.3389/978-2-88974-508-1

Table of Contents

frontiers in Bioengineering and Biotechnology

EDITORIAL
published: 26 January 2022
doi: 10.3389/fbioe.2022.842128

Editorial: MSC-Derived Extracellular Vesicles and Secreted Factors as "Cell-Free" Therapeutic Alternatives in Regenerative Medicine

Enrico Ragni[1], Ornella Parolini[2,3] and Antonietta Rosa Silini[4]*

[1]*IRCCS Istituto Ortopedico Galeazzi, Laboratorio di Biotecnologie Applicate All'Ortopedia, Milano, Italy,* [2]*Department of Life Science and Public Health, Università Cattolica Del Sacro Cuore, Rome, Italy,* [3]*Fondazione Policlinico Universitario "Agostino Gemelli" IRCCS, Rome, Italy,* [4]*Centro di Ricerca E. Menni, Fondazione Poliambulanza- Istituto Ospedaliero, Brescia, Italy*

Keywords: mesenchymal stromal (or stem) cells, extracellular vesicle (EV), secretome, biomaterials, therapeutics

Editorial on the Research Topic

MSC-Derived Extracellular Vesicles and Secreted Factors as "Cell-Free" Therapeutic Alternatives in Regenerative Medicine

OPEN ACCESS

Edited and reviewed by:
Andrea Banfi,
University of Basel, Switzerland

****Correspondence:***
Ornella Parolini
ornella.parolini@unicatt.it

Specialty section:
This article was submitted to Preclinical Cell and Gene Therapy, a section of the journal Frontiers in Bioengineering and Biotechnology

Received: *23 December 2021*
Accepted: *11 January 2022*
Published: *26 January 2022*

Citation:
Ragni E, Parolini O and Silini AR (2022) Editorial: MSC-Derived Extracellular Vesicles and Secreted Factors as "Cell-Free" Therapeutic Alternatives in Regenerative Medicine. Front. Bioeng. Biotechnol. 10:842128. doi: 10.3389/fbioe.2022.842128

In recent years, the concept of "regenerative medicine" has gained interest in the clinical scenario. Within this broad field, mesenchymal stromal cells (MSCs) have paved the way for their potential to stimulate reparative and anti-inflammatory mechanisms to restore healthy functions in damaged organs and tissues (Gomez-Salazar et al., 2020). All these features are ascribed to MSCs capacity to interact with the diseased environment and release soluble mediators, both free and conveyed within extracellular vesicles (EVs) (Phinney and Pittenger, 2017), collectively termed the "secretome". For these reasons, one of MSCs "fathers", Prof. Arnold Caplan, in 2011 defined MSCs as an "injury drugstore" (Caplan and Correa, 2011) and recently proposed a nomenclature change in "medicinal signaling cells" (Caplan, 2017). Accordingly, MSC secretomes have repeatedly shown both *in vitro* and *in vivo* to maintain several features of the cells from which they derive, and are increasingly been used for both regenerative and immune modulatory applications (Harman et al., 2021).

Due to these reasons, the secretome itself or its constituents (cytokines/chemokines, EVs and embedded molecules) were assumed to serve as a cell-free option in the field of regenerative medicine (Pokrovskaya et al., 2020), avoiding controversial issues related to conventional cell-based therapies (Lukomska et al., 2019). In this frame, several protocols have been developed for MSC-EVs production under good manufacturing practice (Wei et al., 2021), and many clinical trials are currently completed or recruiting (Maumus et al., 2020). Nevertheless, several critical issues have been put aside in the excitement to pursue clinical trials. In particular, a thorough dissection of EVs potential, starting from their rigorous characterization to *in vitro/in vivo* evidence, is sometimes missing or underestimated. These deficiencies and pitfalls greatly limit MSC-EVs translation into clinical practice, ultimately dampening their therapeutic potential and opening the door to unsatisfactory effects.

This Research Topic presents cutting edge and innovative data on MSC secretome-based research, encompassing both innovative and, when possible, clinical production scalable characterization methods and new results in different disease settings, to select the most characterized and data-driven MSC-based cell free product.

The first step to frame the MSC secretome, and in particular EVs, is a thorough and reliable definition of techniques and parameters with the choice of the most appropriate isolation procedure being a crucial issue. To this end, Phan et al. proposed several methods to effectively and uniformly isolate MSC-EVs from complex biological milieu. By using multiple techniques including optical, non-optical and high-resolution single vesicle characterization methods, the authors clearly showed that isolation techniques greatly influence EVs composition and biological properties. In particular, not a single but multiple and complimentary techniques are crucial to reliably evaluate EVs potential on a more complex level. In this frame, the need of reliable albeit easy to manage protocols is mandatory. Ragni et al. showed how the molecular characterization of EVs, especially for miRNAs, is largely dependent on the selection of the most appropriate reference genes (RGs) since, to date, a universal RG miRNA for MSC-EVs is missing. The authors presented several RG miRNAs for adipose (adipose derived-MSC, ASC)- and bone marrow (bone marrow derived-MSC, BMSC)-derived EVs and, most importantly, showed how an integrated analysis encompassing different EV types is a mandatory step. Finally, Carlomagno et al. exhibited an innovative approach to characterize both EVs and whole secretome based on Raman spectroscopy, which is a non-destructive vibrational investigation method. Their results clearly emphasize how this technique can confirm EVs and secretome isolation reproducibility, a major issue for clinical translation when batch to batch differences depend not only on the source but also on the technical pipeline. These new methodologies will help in accelerating translation to the clinic and regulatory approval reducing concerns related to technical workflow.

The second step for the dissection of the biological role of secretome and EVs requires data on *in vitro* and preclinical efficacy, allowing *in vitro–in vivo* correlation of therapeutic potency. When data are largely missing, *in vitro* analyses are crucial. Ghebes et al. showed how BMSCs ability to support hematopoietic stem cells (HSPCs) expansion relies on EV-shuttled molecules, both proteins and miRNAs, and how the divergent molecular fingerprints in EVs from foetal or adult BMSCs may differentially support *ex vivo* HSPCs expansion. The issue of molecular signature and composition was also addressed by Zhong et al. in the frame of cardiovascular diseases and heart failure. In an *in vitro* model of doxorubicin-induced heart failure, miR-100-5p embedded in umbilical cord MSC-EVs inhibited oxidative stress, ROS and apoptosis increase through the direct downregulation of NOX4 expression. A similar role for embedded molecules was shown by Pan et al., who demonstrated the role of lncRNA malat-1 in MSCs-EVs to promote chondrocyte proliferation and repair as well as alleviate cartilage inflammation and degeneration *in vitro* and *in vivo* in osteoarthritis models. Consistently, in Qi et al., the use of an animal model allowed to sharply define the modulation of secretome given by the pre-activation of MSCs with serum from colitis rats, which promoted the production of paracrine factors improving the therapeutic effects on the disease. Of note, when data cover a number of different pathologies and indications, a more defined picture may be framed as reported from Cargnoni et al. and Sandonà et al., In the first manuscript related to inflammatory pathologies, perinatal derived EVs were described to directly modulate the immune response by targeting the inflammatory microenvironment. In the second work related to musculoskeletal diseases, MSCs and their secretome were reported to enhance both myofiber regeneration and myogenesis, with EVs postulated as candidates for cell free-based muscle regeneration. In this frame, EVs targeted delivery to the injured site or diseased tissue is another crucial need. To improve the process, Driscoll et al. fabricated an engineered biomaterial composed of EVs cross-linked with graphene oxide and exhibiting cell-type dependent cytotoxicity on liver cancer cells with minimal impact on healthy hepatocytes. Thus, next step in EVs production will be their manipulation under tissue engineering approaches for regenerative medicine.

Altogether, this Research Topic highlights the need for proper EVs characterization and functional studies, both mandatory prerequisites for a faster and bioengineering-driven EVs translation from bench to bedside.

AUTHOR CONTRIBUTIONS

All authors listed have made a substantial, direct, and intellectual contribution to the work and approved it for publication.

FUNDING

This work was supported by Ministero della Salute Italiano, “Ricerca Corrente”, by the Italian Ministry of Research and University (MIUR, 5 × 1,000 years 2020), and PRIN 2017 program of Italian Ministry of Research and University (MIUR, Grant No. 2017RSAFK7).

REFERENCES

Caplan, A. I., and Correa, D. (2011). The MSC: An Injury Drugstore. *Cell Stem Cell* 9 (1), 11–15. doi:10.1016/j.stem.2011.06.008

Caplan, A. I. (2017). Mesenchymal Stem Cells: Time to Change the Name!. *Stem Cell Transl Med* 6 (6), 1445–1451. doi:10.1002/sctm.17-0051

Gomez-Salazar, M., Gonzalez-Galofre, Z. N., Casamitjana, J., Crisan, M., James, A. W., and Péault, B. (2020). Five Decades Later, Are Mesenchymal Stem Cells Still Relevant? *Front. Bioeng. Biotechnol.* 8, 148. doi:10.3389/fbioe.2020.00148

Harman, R. M., Marx, C., and Van de Walle, G. R. (2021). Translational Animal Models Provide Insight into Mesenchymal Stromal Cell (MSC) Secretome Therapy. *Front. Cel Dev. Biol.* 9, 654885. doi:10.3389/fcell.2021.654885

Lukomska, B., Stanaszek, L., Zuba-Surma, E., Legosz, P., Sarzynska, S., and Drela, K. (2019). Challenges and Controversies in Human Mesenchymal Stem Cell Therapy. *Stem Cell Int.* 2019, 9628536. doi:10.1155/2019/9628536

Maumus, M., Rozier, P., Boulestreau, J., Jorgensen, C., and Noël, D. (2020). Mesenchymal Stem Cell-Derived Extracellular Vesicles: Opportunities and Challenges for Clinical Translation. *Front. Bioeng. Biotechnol.* 8, 997. doi:10.3389/fbioe.2020.00997

Phinney, D. G., and Pittenger, M. F. (2017). Concise Review: MSC-Derived Exosomes for Cell-Free Therapy. *Stem Cells* 35 (4), 851–858. doi:10.1002/stem.2575

Pokrovskaya, L. A., Zubareva, E. V., Nadezhdin, S. V., Lysenko, A. S., and Litovkina, T. L. (2020). Biological Activity of Mesenchymal Stem Cells Secretome as a Basis for Cell-free Therapeutic Approach. *Res. Results Pharmacol.* 6 (1), 57–68. doi:10.3897/rrpharmacology.6.49413

Wei, W., Ao, Q., Wang, X., Cao, Y., Liu, Y., Zheng, S. G., et al. (2021). Mesenchymal Stem Cell-Derived Exosomes: A Promising Biological Tool in Nanomedicine. *Front. Pharmacol.* 11, 590470. doi:10.3389/fphar.2020.590470

Conflict of Interest: The authors declare that the research was conducted in the absence of any commercial or financial relationships that could be construed as a potential conflict of interest.

Publisher's Note: All claims expressed in this article are solely those of the authors and do not necessarily represent those of their affiliated organizations, or those of the publisher, the editors and the reviewers. Any product that may be evaluated in this article, or claim that may be made by its manufacturer, is not guaranteed or endorsed by the publisher.

Copyright © 2022 Ragni, Parolini and Silini. This is an open-access article distributed under the terms of the Creative Commons Attribution License (CC BY). The use, distribution or reproduction in other forums is permitted, provided the original author(s) and the copyright owner(s) are credited and that the original publication in this journal is cited, in accordance with accepted academic practice. No use, distribution or reproduction is permitted which does not comply with these terms.

frontiers in Bioengineering and Biotechnology

REVIEW
published: 05 February 2021
doi: 10.3389/fbioe.2021.637737

Extracellular Vesicles From Perinatal Cells for Anti-inflammatory Therapy

Anna Cargnoni[1†], Andrea Papait[1,2†], Alice Masserdotti[2], Anna Pasotti[1], Francesca Romana Stefani[1], Antonietta Rosa Silini[1] and Ornella Parolini[2,3]*

[1] Centro di Ricerca E. Menni, Fondazione Poliambulanza Istituto Ospedaliero, Brescia, Italy, [2] Department of Life Science and Public Health, Università Cattolica del Sacro Cuore, Rome, Italy, [3] Fondazione Policlinico Universitario "Agostino Gemelli" IRCCS, Rome, Italy

OPEN ACCESS

Edited by:
Georg A. Feichtinger, University of Leeds, United Kingdom

Reviewed by:
Muhammad Nawaz, University of Gothenburg, Sweden
Gaia Spinetti, MultiMedica (IRCCS), Italy

***Correspondence:**
Antonietta Rosa Silini
antonietta.silini@poliambulanza.it

† These authors have contributed equally to this work

Specialty section:
This article was submitted to Preclinical Cell and Gene Therapy, a section of the journal Frontiers in Bioengineering and Biotechnology

Received: *04 December 2020*
Accepted: *19 January 2021*
Published: *05 February 2021*

Citation:
Cargnoni A, Papait A, Masserdotti A, Pasotti A, Stefani FR, Silini AR and Parolini O (2021) Extracellular Vesicles From Perinatal Cells for Anti-inflammatory Therapy. Front. Bioeng. Biotechnol. 9:637737. doi: 10.3389/fbioe.2021.637737

Perinatal cells, including cells from placenta, fetal annexes (amniotic and chorionic membranes), umbilical cord, and amniotic fluid display intrinsic immunological properties which very likely contribute to the development and growth of a semiallogeneic fetus during pregnancy. Many studies have shown that perinatal cells can inhibit the activation and modulate the functions of various inflammatory cells of the innate and adaptive immune systems, including macrophages, neutrophils, natural killer cells, dendritic cells, and T and B lymphocytes. These immunological properties, along with their easy availability and lack of ethical concerns, make perinatal cells very useful/promising in regenerative medicine. In recent years, extracellular vesicles (EVs) have gained great interest as a new therapeutic tool in regenerative medicine being a cell-free product potentially capable, thanks to the growth factors, miRNA and other bioactive molecules they convey, of modulating the inflammatory microenvironment thus favoring tissue regeneration. The immunomodulatory actions of perinatal cells have been suggested to be mediated by still not fully identified factors (secretoma) secreted either as soluble proteins/cytokines or entrapped in EVs. In this review, we will discuss how perinatal derived EVs may contribute toward the modulation of the immune response in various inflammatory pathologies (acute and chronic) by directly targeting different elements of the inflammatory microenvironment, ultimately leading to the repair and regeneration of damaged tissues.

Keywords: perinatal derivatives, secretome, extracellular vesicles, immunomodulation, tissue regeneration

EXTRACELLULAR VESICLES

Extracellular vesicles (EVs) are membrane-bound vesicles secreted into the extracellular environment by healthy (Raposo and Stoorvogel, 2013) and apoptotic cells (Hristov et al., 2004). Exosomes (exo), microvesicles (MVs) and apoptotic bodies are the three main subtypes of EVs which are distinguished based upon their biogenesis, release pathways, size, content, and function (Zaborowski et al., 2015) (**Figure 1**). Among the subtypes, the most numerous are exosomes (Rani et al., 2015), whose diameters ranges from 40 to 120 nm. Exosomes form by fusion between multivesicular endosomes and plasma membrane. MVs are between 100 and 1,000 nm in size and bud directly from the plasma membrane. Apoptotic blebs' size ranges from 50 to 2,000 nm and the bodies are released by dying cells (Zaborowski et al., 2015).

Originally, EVs were thought to serve as a disposal mechanism by which cells eliminate unwanted proteins and other molecules. However, today EVs represent a well-known mechanism of cell-to-cell communication that goes beyond the classical signaling through cell-cell contact and secreted bioactive factors (*i.e.,* cytokines, inflammatory mediators, metabolites, and hormones) (Pitt et al., 2016). Therefore, EVs exert their biological effect through activation of cell signaling by physical ligand/receptor interactions or by fusing with their recipient cells, transferring their contents (miRNAs, mRNAs, proteins, phospholipids, or generally, a morphogen) into the cytosol, and modifying the physiological state of the recipient cells (**Figure 1**). EVs may also be endocytosed by the target cells or release their bioactive molecules, receptors and genetic information into the extracellular space (**Figure 1**) (Turturici et al., 2014).

Extracellular vesicles content and mechanism of release differs according to cell origin and it changes in response to fluctuations of physiological states or pathological conditions. During physiological processes EVs can regulate angiogenesis, immune responses, apoptosis, coagulation, cellular homeostasis, and intercellular signaling (Gurunathan et al., 2019). Furthermore, they play a role in the development and progression of diseases (*e.g.,* cancer, neurodegeneration, infections, and cardiovascular disease) (Zaborowski et al., 2015; Kao and Papoutsakis, 2019). EVs can be isolated from a variety of body fluids (*e.g.*, blood, semen, saliva, plasma, urine, cerebrospinal fluid, synovial fluid, malignant and pleural effusions of ascites, bronchoalveolar lavage (BAL) fluid, breast milk, and amniotic fluid) (Rani et al., 2015), and from solid tissues like lung tumors, brain (Hurwitz et al., 2019), and perinatal derivatives, such as placenta (Fitzgerald et al., 2018).

Extracellular vesicles are gaining increasing interest for a broad range of applications, such as potential tools for cancer diagnosis (Rahbarghazi et al., 2019) and therapeutic approaches in regenerative medicine. More specifically, given their role in modulating immune responses, EV-based therapeutics are being developed for the treatment of inflammatory diseases, autoimmune disorders and cancer (Robbins and Morelli, 2014). In order to pursue such applications involving EVs, a better understanding of the immunomodulatory mechanisms through which EVs act, such as deciphering their bioactive cargo and target cells, is needed. The aim of this review is to discuss the current status and advances of EVs from perinatal, or birth-associated, cells isolated from placenta, umbilical cord, and fetal membranes. Perinatal cells and their secretome have demonstrated robust immunomodulatory properties (Mattar and Bieback, 2015; Magatti et al., 2016, 2018, 2019; Abumaree et al., 2017; Lim, 2017; Silini et al., 2017), that have been correlated to their ability to contribute to tissue regeneration (Silini et al., 2017). Hence herein we will discuss the contribution of perinatal-derived EVs to the immune response, with a focus on their ability to promote reparation and regeneration of damaged tissues in the context of acute and chronic inflammation.

PERINATAL TISSUES AS SOURCES OF EXTRACELLULAR VESICLES

As mentioned previously, perinatal or birth-associated tissues, refer to tissues that are obtained from term placentas and fetal annexes and more specifically refers to the amniotic membrane, chorionic membrane, chorionic villi, umbilical cord (including Wharton's jelly), the placental basal plate (including maternal and fetal cells), and the amniotic fluid (Silini et al., 2020).

The fetal membranes enclose the fetus and its surrounding amniotic fluid, forming a highly specialized interface between the mother and the fetus that performs vital functions. The fetal membranes consist of two components: the amnion and the chorion. The amnion, the inner of the two fetal membranes, is a thin, avascular membrane, composed of an epithelial and a mesenchymal layer. The amniotic epithelium is in direct contact with the amniotic fluid and is composed of columnar and cuboidal epithelial cells; the amniotic mesoderm is composed of fibronectin and collagen (type I and III) and hosts rare macrophages and dispersed mesenchymal stromal cells (Silini et al., 2020). Weakly linked but not fused to the amnion, the chorionic membrane consists of a mesodermal region, containing chorionic mesenchymal stromal cells, and a trophoblastic area, rich in proliferating trophoblasts and fibrinoid deposits. In order to maximize exchange surface between mother and fetus tissues, finger-like structures, known as chorionic villi, develop from the outer region of the chorion. The chorionic villi anchor the placenta to maternal endometrium and are involved in fetal-maternal exchange (Silini et al., 2020).

The umbilical cord is an extraembryonic tissue connecting the placenta to the fetus, externally covered by a single epithelial layer of cells, supposed to derive from amniotic epithelium. The structure of umbilical cord is made up of a mucous connective tissue called Wharton's jelly, enriched in fibroblast-like cells. Within this glycosaminoglycan and collagen-rich matrix are immersed a vein and two umbilical arteries, essential for nutrient, metabolic and gas exchange (Anzalone et al., 2010).

The decidua is the maternal component of placenta and its formation is due to the growth and the proliferation of the functional layer cells of endometrium after implantation. The part of decidua that lies at the site of implantation and interacts with the trophoblasts is defined as decidua basalis, while decidua capsularis refers to the portion of decidua covering the conceptus on the luminal site. The remaining section of endometrium, blending by the fourth month of gestation with the decidua capsularis, is the decidua parietalis that lines the rest of uterus cavity (Abumaree et al., 2016; Turco and Moffett, 2019).

Several cell types can be obtained and expanded from the different regions of the human placenta and the fetal annexes,

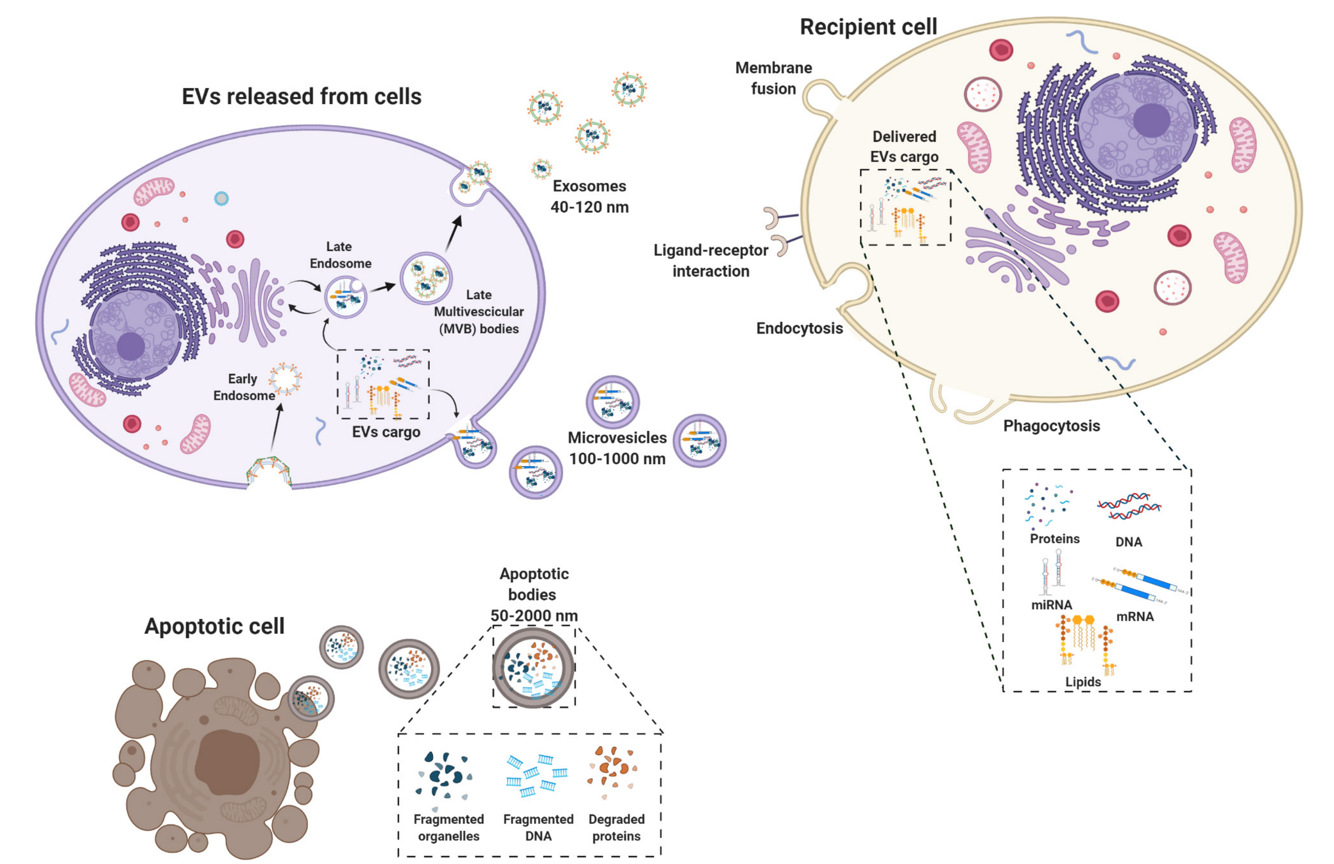

FIGURE 1 | Biogenesis of extracellular vesicles (EVs). EVs are a heterogeneous family of membrane-bound vesicles produced by a donor cell that target a recipient cell. EVs are distinguished into three main subtypes according to their size: microvesicles (100–1,000 nm), exosomes (40–120 nm), and apoptotic bodies (50–2,000 nm). Exosome biogenesis starts from the endosomal system, with the early endosome that transforms into a late endosome, deriving from the inward budding of intraluminal vesicles. EVs can carry many biologically active molecules such as proteins and genetic material (mRNA, miRNA, and DNA), with important immunomodulatory functions. The exosomes produced then can be released by the exocytotic pathway with the fusion between the multivescicular late endosome and the plasma membrane. Microvesicles present a less defined mechanism of biogenesis and release compared to exosomes with different mechanisms that have been identified for the shedding of the MVs depending also on the biological content. Apoptotic bodies are released by dying cells following the blebbing process. EVs are taken up by the recipient cell via different mechanisms including membrane fusion endocytosis, phagocytosis or ligand–receptor interactions. Created with Biorender.com.

the most prominent being epithelial cells, mesenchymal stromal cells (MSC), endothelial, and hematopoietic cells, and all of these produce and release EVs.

IMMUNOMODULATORY PROPERTIES OF PERINATAL CELLS AND THEIR EVs

The essential role of the placenta in maintaining a state of fetal-maternal tolerance during pregnancy initially suggested that cells derived from gestational tissues may possess intriguing immunomodulatory properties, exploitable for several regenerative medicine applications. Nowadays, the immunomodulatory properties of perinatal cells, especially MSC, have widely been demonstrated (Magatti et al., 2016). Indeed, different *in vitro* studies have demonstrated that perinatal cells target components of the innate and adaptive immune systems, including T and B lymphocytes, macrophages, dendritic cells, neutrophils and natural killer cells.

Specifically, they can suppress the proliferation of T lymphocytes (Magatti et al., 2008; Kronsteiner et al., 2011), and can inhibit the differentiation into Th1 and Th17, causing concurrently the formation of Th2 cells, with an immune regulatory cytokine profile, and the enhancement of regulatory T cells (Pianta et al., 2016; Khoury et al., 2020). In addition, perinatal cells directly interact with B cells, reducing proliferation and plasma cells formation as well as promoting regulatory B cells induction (Che et al., 2012; Magatti et al., 2020). Perinatal cells can also inhibit the migration and maturation of dendritic cells and promote the polarization of monocytes/macrophages toward an anti-inflammatory phenotype (Magatti et al., 2009, 2015; Banas et al., 2013; Croxatto et al., 2014; Abomaray et al., 2015; Abumaree et al., 2019).

In line with this, preclinical studies have shown that administration of perinatal cells or their secretome induces therapeutic effects in many models of inflammatory diseases such as liver (Lee et al., 2010; Manuelpillai et al., 2010, 2012; Jung et al., 2013; Cargnoni et al., 2018), and lung fibrosis

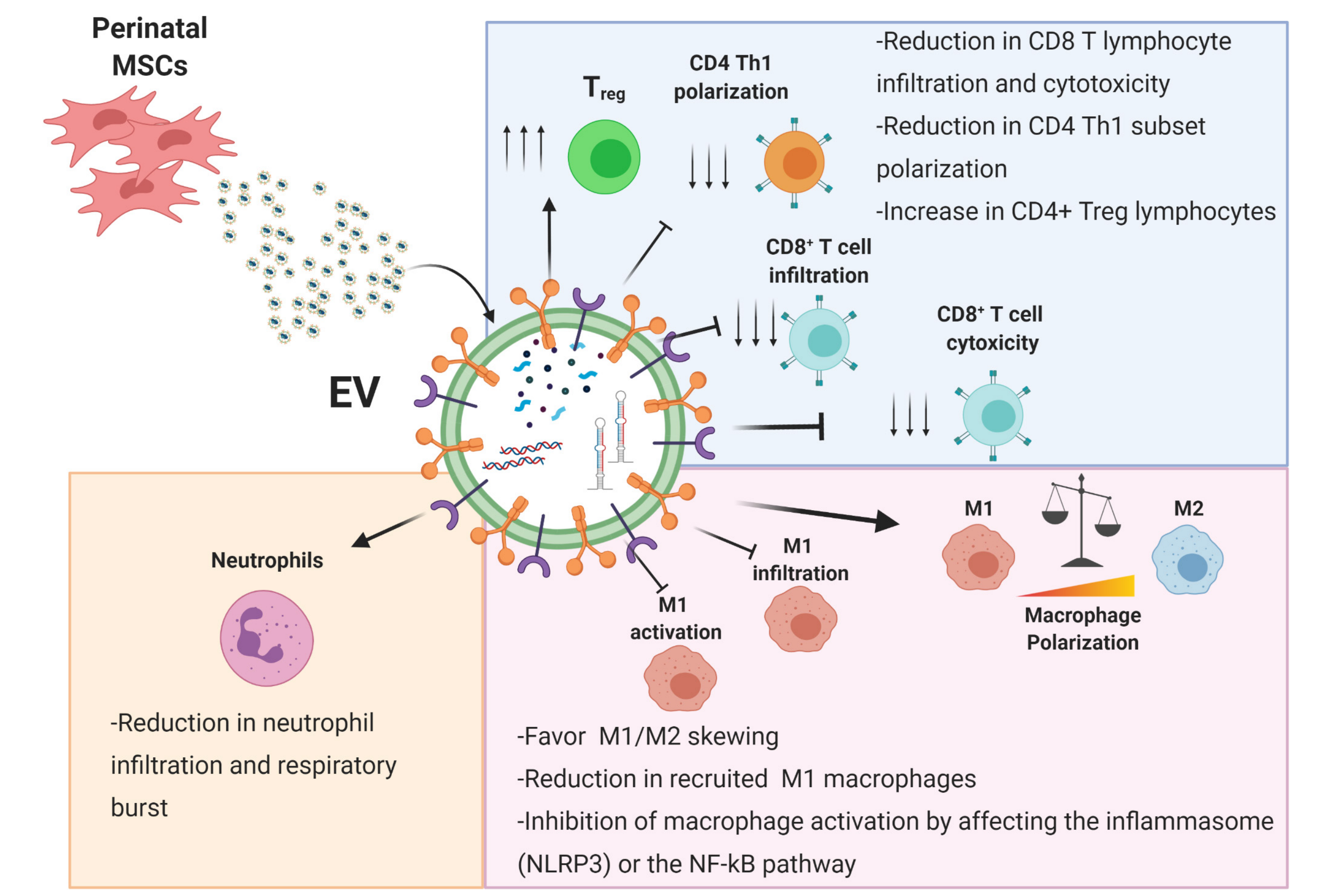

FIGURE 2 | Immunomodulatory effects of perinatal-MSC extracellular vesicles (EVs). The molecular content of perinatal MSC-EVs represented by proteins, lipids, and nucleic acids can strongly affect both the innate (neutrophils and macrophages) and adaptive immune response (T lymphocytes). Treg, T regulatory cell; Th1, T helper 1 cell; M1, macrophage type 1; M2, macrophage type 2; NLRP3, NLR family pyrin domain containing 3; NF-κB, nuclear factor kappa B. Created with Biorender.com.

(Cargnoni et al., 2009, 2020; Vosdoganes et al., 2011; Murphy et al., 2012; Moodley et al., 2013; Tan et al., 2014, 2017), collagen-induced arthritis (Parolini et al., 2014), experimental autoimmune encephalomyelitis (Parolini et al., 2014; Donders et al., 2015), cerebral ischemia (Lin et al., 2011), and diabetes (Wang et al., 2014; Tsai et al., 2015).

A large body of evidence has demonstrated that these effects are mediated by active molecules secreted by perinatal cells able to affect cell survival, function and repair in host damaged tissues (Gunawardena et al., 2019; Silini et al., 2019). As a matter of the fact, the delivery of conditioned medium (CM), generated from *in vitro* culture of perinatal cells, representing perinatal cell secretome, produced benefits similar to that obtained with parental cells (Cargnoni et al., 2012, 2014; Danieli et al., 2015; Pischiutta et al., 2016; Giampa et al., 2019).

In the last decade, several studies have reported that EVs from perinatal tissues are comparable to the parental cells when transplanted in several preclinical models of inflammatory mediated diseases such as wound healing (Li et al., 2016; Zhao et al., 2017), pulmonary fibrosis (Tan et al., 2018), hepatic fibrosis (Alhomrani et al., 2017); bronchopulmonary dysplasia (BPD) (Chaubey et al., 2018; Willis et al., 2018), liver failure (Jiang et al., 2019; Yao et al., 2019), vascular repair (Spinosa et al., 2018; Wei et al., 2019), renal injury (Zou et al., 2014, 2016), neurodegenerative diseases (Ding et al., 2018; Ma et al., 2019; Romanelli et al., 2019; Thomi et al., 2019), autoimmune diseases (Bai et al., 2017; Mao et al., 2017), and Duchenne muscular dystrophy (Bier et al., 2018). Furthermore, EVs have the advantage of being a cell-free therapy and therefore with reduced risks associated with the transplantation of live cells.

In relation to the therapeutic utility of perinatal EVs assessed in the above cited preclinical studies, there are five clinical trials applying EVs from perinatal cells reported in the ClinicalTrials.gov database and one reported in Chinese Clinical Trial Registry. They are phase I studies with the primary endpoint to establish the safety of the treatment. One of these (NCT03437759), will apply exosomes from human UC-MSCs to large and refractory macular holes (MHs). Another study (NCT04213248), explores whether the local delivery of exosomes from UC-MSCs is able to reduce dry-eye symptoms in patients with chronic Graft Versus Host Diseases (cGVHD). Exosomes from UC-MSCs will also be used to treat multiple organ dysfunction syndrome after surgical ascending aortic replacement (NCT04356300). Exosomes from another source, amniotic fluid, are under evaluation to treat, in combination with ultrasound therapy, depression, anxiety, and neurodegenerative dementia in patients resistant to any pharmacological treatment (NCT04202770).

Finally, two more trials, one using EVs derived from human amniotic fluid (NCT04384445) and the other using exosomes from umbilical cord MSCs (ChiCTR2000030484 study, from Chinese Clinical Trial Registry), will assess the ability of these treatments to suppress cytokine activation and any incidence of associated adverse events, in subjects suffering from COVID-19 infection with severe acute respiratory syndrome.

Impact of Perinatal EVs on Cells of the Myeloid Lineage

It is now widely recognized that the therapeutic effect of perinatal cells is largely mediated via secretion of bioactive factors rather than cell–cell interactions (Silini et al., 2019). Many studies have suggested the MSC EVs modulate inflammation and contribute to tissue regeneration (Fatima et al., 2017), however, the exact mechanism by which perinatal derived/secreted factors regulate the immune response is still unknown. Importantly, several recent papers focused their attention on EVs from perinatal MSC, highlighting their potential for a cell-free therapy (Robbins and Morelli, 2014; Phinney and Pittenger, 2017).

Innate immune cells, including neutrophils, NK cells, and phagocytic cells such as macrophages and dendritic cells, are the first cells to initiate an immune response against a potential pathogen, clear from residual apoptotic or necrotic cells, and remodel the extracellular matrix to prepare the "scenario" pivotal to the subsequent healing steps (White and Mantovani, 2013; MacLeod and Mansbridge, 2016). Perinatal EVs have been shown to interact with various innate immune cells (**Figure 2**). In the following sections we describe the interactions between perinatal EVs and immune cells (summarized in **Figure 2**) and identify several key molecules involved in these interactions (summarized in **Table 1**).

MSC-EVs Interfere With Infiltration and Accumulation of Neutrophils

Several studies have shown the ability of perinatal EVs to act on neutrophils. For example, in a rat model of hepatic ischemia-reperfusion injury, IV injection of EVs from human umbilical cord MSC (hUC-MSC) reduced serum biomarkers of liver injury (ALT, AST, and ALP), hepatic necrosis and hepatocyte apoptosis (Yao et al., 2019). These effects were mediated by EVs ability in reducing neutrophil hepatic infiltration, suppressing neutrophil respiratory burst (*in vitro* evidence) and in decreasing the expression and the levels of inflammatory cytokines (IL-1β, IL-6, and TNF-α) in hepatic tissues and serum, respectively. The authors suggested that the hepatic protective effects of hUC-MSC EVs may be mediated through the vesicular secretion of a crucial enzyme with anti-oxidant action (MnSOD) (Yao et al., 2019). However, no mechanism has been explored to explain EVs action on neutrophil recruitment.

Exosomes derived from Wharton's jelly MSC (hWJ-MSC) of premature neonates, injected intraperitoneally in a mouse model of hyperoxia-induced BPD, decreased lung inflammation, alveolar structural alterations, endothelial cell damage and demyelination in the brains (Chaubey et al., 2018). Interestingly, exosome treatment specifically suppressed the hyperoxia-induced neutrophil accumulation in BAL while it did not affect BAL macrophage levels. In the same study, a group of BPD animals received either the CM (hWJ-MSC-CM) or the exosome-depleted fraction of CM, and while both hWJ-MSC-CM and hWJ-MSC-exosome treatments improved BPD pathology, the exo-free fraction did not, suggesting that the exosome fraction is responsible for the beneficial effects observed. Interestingly, the authors detected the presence of tumor necrosis factor alpha-stimulated gene-6 (TSG-6) in exosomes and in CM and observed that the use of a TSG-6 neutralizing antibody or of exosomes obtained from TSG-6 siRNA knockdown hWJ-MSC abolished the therapeutic effects.

MSC-EVs Affect Macrophage Activation and Polarization

Human umbilical cord MSC EVs have been reported to differently affect the activity of inflammatory macrophages, by modulating their activation (Li et al., 2016), favoring a skewing toward anti-inflammatory M2 macrophages, or modulating their recruitment to the injured site of inflammation (Yu et al., 2016; Willis et al., 2018; Wei et al., 2019). Jiang et al. (2019) reported the capacity of UC-MSC-derived exosomes to directly inhibit M1 macrophage activation in a mouse model of acute liver failure by inhibiting the expression of the NLRP3 inflammasome complex and the production of inflammatory cytokines. These findings were also confirmed in a cell line of LPS-stimulated RAW 264.7 macrophages, where the administration of UC-MSC exosomes was able to reduce the expression of NLRP3, caspase 1 as well as of the inflammatory cytokines IL-1β and IL-6 (Jiang et al., 2019). In another mouse model of acute burn, administration of the UC-MSC-derived exosomes strongly reduced the activation of M1 macrophages by impairing the NF-κB/p65 pathway, consequently reducing the expression of TNFα, IL-1β and increasing the amount of IL-10 produced and released (Li et al., 2016). As a matter of fact, *in vitro* studies performed in a cell line of mouse macrophages identified a specific miRNA, miR-181c, as the one responsible for the effect observed. Indeed, this miRNA directly affects the expression of toll-like receptor 4 (TLR4), whose downregulation directly impacts NF-κB/p65 pathway activation (Li et al., 2016).

Importantly, EVs can regulate the phenotype polarization of M1 toward M2 macrophages thus reducing the release of inflammatory cytokines. Using the human monocytic cell line THP1, Ti et al. (2015) reported that exosomes from LPS-primed UC-MSC were able to affect the M1/M2 skewing and enhance the expression of miR-Let7b. The overexpression of this miRNA can directly impact M1 polarization favoring instead a skewing toward the M2 subset by downregulating the TLR4/NF-κB/STAT3/AKT signaling pathway which is essential for the regulation of macrophage plasticity (Ti et al., 2015). Comparable effects were observed when UC-MSC were primed with the inflammatory cytokine IL-1β. Indeed, researchers observed that the priming was able to trigger an increase in the total amount of miRNA-146a molecules contained in the UC-MSC EVs resulting in a strong polarization of bone marrow-derived macrophages

TABLE 1 | Summary of perinatal EVs mechanisms of action and biological effects.

Cell type	Model	Target cells	Key molecules/Molecular mechanism	Biological effect	References
hUC-MSC	Rat hepatic ischemia-reperfusion injury	Hepatocytes, Neutrophils	Mitochondrial manganese superoxide dismutase Mn(SOD), anti-oxidant activity	Decreased expression of inflammatory cytokines in hepatic tissue and serum, decreased hepatocyte necrosis	Yao et al. (2019)
hUC-MSC	Mouse model of acute liver failure; RAW 264.7 macrophages *in vitro* activated with LPS	Macrophages	Inhibition of NLRP3 inflammasome complex expression	Reduced caspase 1 and inflammatory cytokines (IL-1β and IL-6)	Jiang et al. (2019)
hUC-MSC	Mouse model of acute burn	Macrophages	miR-181c downregulation of TLR-4 receptor expression with consequent downregulation of NF-κB/p65 pathway	Reduction of M1 macrophage activation	Li et al. (2016)
hUC-MSC	Mouse model of aortic aneurysm	T lymphocytes	miR-147	Decreased expression of inflammatory cytokines, reduction of lymphocytes infiltration, improved aortic diameter, and elasticity	Spinosa et al. (2018)
hUC-MSC (LPS primed)	Wound healing model in diabetic rat	Macrophages	miR-let-7b down regulation of TLR4/NF-κB/STAT3/AKT signaling pathway	Promotion of M2 macrophage activation, enhanced diabetic cutaneous wound healing	Ti et al. (2015)
hUC-MSC (IL-1β primed)	Mouse model of sepsis	Macrophages	miR-146a	Increased polarization of macrophages toward the M2 anti-inflammatory subset	Song et al. (2017)
hUC-MSC	Mouse and rat spinal cord injury model	Macrophages	-	Reduction of inflammatory cytokines and M2 polarization	Romanelli et al. (2019); Sun et al. (2018)
hUC-MSC	Mouse model of inflammatory bowel disease	Macrophages	-	Reduced macrophage recruitment and reduced inflammation	Mao et al. (2017)
hUC-MSC	Mouse model of retinal laser injury	Macrophages	-	Downregulation of MCP1 and macrophage infiltration	Yu et al. (2016)
hUC-MSC	Rat model of experimental autoimmune uveoretinitis	CD4 T lymphocytes, NK cells, neutrophils and macrophages	-	Reduced infiltration of inflammatory immune cells	Bai et al. (2017)
hUC-MSC	Synthetic vascular grafts in rat model of hyperlipidemia	Macrophages	-	Reduced macrophage infiltration and enhanced M2 macrophage polarization, associated with reduced thrombosis and vascular intimal hyperplasia	Wei et al. (2019)
hUC-MSC	Alzheimer mouse model	Microglia	-	Reduced number of M1 microglial cells, promotion of M2 microglial polarization associated with reduced neuroinflammation and B amyloid deposition	Ding et al. (2018)
hUC-MSC	Human *in vitro* purified T lymphocytes	T lymphocytes	Adenosine signaling through CD73 expression	Reduced T lymphocyte activation	Kerkelä et al. (2016)
hUC-MSC	Mouse model of contact hypersensitivity	T lymphocytes	STAT1 signaling pathway inhibition	Reduced cytotoxic and Th1 lymphocyte infiltration and induced Treg with reduced tissue swelling	Guo et al. (2019)
hUC-MSC	Human *in vitro* purified T lymphocytes	T lymphocytes	-	Reduced T lymphocyte proliferation and inflammatory cytokine production	Monguió-Tortajada et al. (2017)
hUC-MSC	GVHD mouse model	T lymphocytes	-	Reduced CD8 cytotoxic T lymphocyte and reduced inflammatory cytokines in serum, alleviated GVHD manifestations and reduced mortality of the recipient mice	Wang et al. (2016)
hUC-MSC (β2 microglobulin deficient)	Rat model of myocardial infarction	CD8 T lymphocytes	miR-24	Reduced CD8 T lymphocyte cytotoxicity with improved preservation of cardiac function after myocardial infarction	Shao et al. (2020)

(Continued)

TABLE 1 | Continued

Cell type	Model	Target cells	Key molecules/Molecular mechanism	Biological effect	References
hUC-MSC (primed with TGFβ and IFNγ)	*In vitro* study on human PBMC	Treg	IDO1	Increased Treg polarization	Zhang et al. (2018)
hUC-MSC	*In vitro* study on hUC-MSC and hCB-MSC	miRNA profiling	miR-a25b, miR26a, miR145, miR181c-5p, miR-Let7e, miR-Let7c, miR-Let7f, and miR.106a	miRNAs with immunoregulatory functions	Meng et al. (2017)
hUC-MSC	Rat model of renal ischemic reperfusion injury	NK cells	CXC3L1, TLR-2	Reduced CXC3L1 and TLR-2 expression with consequent reduced NK cell recruitment	Zou et al. (2016)
hWJ-MSC	Mouse model of acute kidney injury	Macrophages	-	Decreased CXCL3 ligand 1, reduced macrophage and T lymphocyte infiltration, and reduced renal injury	Zou et al. (2014)
hWJ-MSC	Perinatal brain injury rat model	Microglia	TLR4/CD14 signaling pathway inhibition	Reduced expression of inflammatory cytokines by microglial cells	Thomi et al. (2019)
hWJ-MSC	Mouse model of hyperoxia-induced bronchopulmonary dysplasia (BPD)	Neutrophils	Tumor necrosis factor alpha-stimulated gene-6 (TSG-6)	Suppression of hyperoxia-induced neutrophil accumulation in bronchoalveolar lavage (BAL) with improvement of BPD pathology	Chaubey et al. (2018)
canine WJ-MSC	*In vitro* study with canine PBMC	CD4 T lymphocytes	TGF-β1/Adenosine signaling	Reduced CD4 T lymphocyte proliferation	Crain et al. (2019)
hWJ-MSC	Hyperoxia-induced bronchopulmonary dysplasia	Macrophages	-	Reduced M1 macrophage lung infiltration, enhanced M2 polarization	Willis et al. (2018)
hAF-MSC (primed with IFNγ)	*In vitro* co-culture with PBMC; mouse model of allogeneic skin graft transplantation	Treg	IDO1	Increased number of Treg cells promoting *in vivo* allograft survival	Romani et al. (2015)
hAF-MSC	*In vitro* THP1 macrophage cell line; mouse model of monoiodoacetate induced osteoarthritis	Macrophages	-	Promoted skewing of THP1 committed M1 macrophages toward M2 subset. *In vivo* increased pain tolerance and improved histopathological score	Zavatti et al. (2020)
hAF-SC	*In vitro* and *in vivo* models of skeletal muscle atrophy (HSA-Cre, SmnF7/F7 mice)	B lymphocytes	-	Reduced B lymphocyte maturation and decreased skeletal muscle inflammation associated with enhanced muscle strength and survival	Balbi et al. (2017)
hAEC	Mouse model of CCl4 induced liver fibrosis	Macrophages	-	Reduced liver fibrosis through promotion of M2 macrophage polarization	Alhomrani et al. (2017)
hAEC	Bleomycin-induced pulmonary fibrosis	Macrophages/T lymphocytes	-	Reduced lung fibrosis through promotion of M2 macrophage polarization and reduction of T cell infiltration	Tan et al. (2018)

hUC-MSC, human umbilical cord mesenchymal stromal cells; hAF-SC, human amniotic fluid stem cells; hAF-MSC, human amniotic fluid mesenchymal stromal cells; hWJ-MSC, human Wharton's jelly mesenchymal stromal cells; IDO1, indoleamine-2,3-dioxygenase-1; LPS, lipopolysaccharide; TLR-2/4, Toll like receptor 2 or 4; CXC3L1, chemokine (C-X3-C motif) ligand 1; GVHD, acute graft-vs-host disease; NK, natural killer cells; MCP-1, monocyte chemotactic protein-1, PBMC; human peripheral blood mononuclear cells.

toward M2 macrophages both *in vitro* and in an animal model of sepsis (Song et al., 2017). Similarly, IV injection of EVs and exosomes from hUC-MSCs was able to reduce inflammatory cytokines and induce M2 macrophage polarization with a concomitant improvement of motor function in models of spinal cord injury induced in mice (Sun et al., 2018) and in rats (Romanelli et al., 2019), respectively.

Analogous findings were observed by Zavatti et al. (2020) in a murine model of monoiodoacetate-induced osteoarthritis. The authors report the capability of amniotic fluid-derived MSC (hAF-MSC) to directly affect the differentiation of the THP1 cell line toward the M1 subset (Zavatti et al., 2020). Indeed, exposure of THP1 committed M1 macrophages to hAF-MSC EVs, strongly reduced the expression of canonical M1 markers like iNOS, the expression of the co-stimulatory molecules CD86 and IL1R favoring instead the acquisition of feature typical of M2 macrophages like the expression of arginase, CD163 and TGFβ (Zavatti et al., 2020). Moreover, the authors reported the ability of hAF-MSC-EVs to increase pain tolerance and improve histopathological scores (Zavatti et al., 2020).

MSC-EVs Prevent Inflammatory Immune Cell Recruitment

Furthermore, UC-MSC EVs can also affect the inflammatory microenvironment by preventing the migration of pro-inflammatory M1 macrophages (Zou et al., 2014; Yu et al., 2016; Bai et al., 2017). Injection of WJ-MSC EVs in an animal model of acute kidney injury was able to reduce the renal cell apoptosis by reducing the infiltration of inflammatory macrophages thus improving the survival and proliferation of the renal cells. This effect was due to the down-modulation of CXCL3 ligand 1, a chemotactic factor essential for monocyte and T lymphocyte recruitment in the injured area (Zou et al., 2014). Moreover, WJ-MSC EVs were able to strongly impact the total number of $CD68^{+}$ immune cells recruited, correlating the potential therapeutic effect of the treatment to the reduced amount of infiltrating inflammatory cells (Zou et al., 2014). hUC-MSC exosomes were also able to reduce acute inflammatory macrophage hepatic infiltration and related liver injury induced by intraperitoneal injection of LPS toxin (Jiang et al., 2019). hUC-MSC exosomes also reduced macrophage infiltration in colon tissues after injection in mice with dextran-induced inflammatory bowel disease (Mao et al., 2017).

In another study, Yu et al. (2016) reported the capacity of UC-MSC EVs to reduce the migration and infiltration of inflammatory cells in a mouse model of retinal laser injury. This effect was due to the reduction of MCP1, TNF-α, and ICAM1. Importantly, these findings were confirmed also in *in vitro* experiments where the treatment with UC-MSC EVs was able to reduce the expression of MCP1 thus positively impacting the amount of heat-induced apoptosis or death of retinal cells (Yu et al., 2016). These findings suggested that UC-MSC EVs exert their protective effect, at least partially, through regulation of MCP-1 and macrophage infiltration. Exosomes from hUC-MSC were also able to inhibit the autoimmune response in a rat model of experimental autoimmune uveoretinitis (EAU) (Bai et al., 2017). hUC-MSC exosomes reduced the amount of $CD4^{+}$ T cells, neutrophils, NK cells and macrophages infiltrating the retina.

Recently, Wei et al. (2019) used EVs from hUC-MSC to functionalize synthetic vascular grafts in order to reduce inflammatory-induced thrombosis and vascular intimal hyperplasia occurring in hyperlipidemic rats. hUC-MSC-derived EVs enhance the patency of vascular grafts by reducing macrophage infiltration and inducing M2 polarization. In another study performed in a mouse model of aortic aneurysm formation, mice treated with UC-MSC EVs displayed decreased expression of inflammatory cytokines and in parallel reduced lymphocyte infiltration thus improving aortic diameter and elasticity through the activity played by miR-147 (Spinosa et al., 2018).

Furthermore, EVs from human amniotic membrane epithelial cells (hAEC) were able to reduce macrophage infiltration in the liver and lung parenchyma in a model of CCl4-induced liver fibrosis (Alhomrani et al., 2017) and in a model of bleomycin-induced pulmonary fibrosis (Tan et al., 2018). hAEC-EVs were also able to promote M2 macrophage polarization (Alhomrani et al., 2017; Tan et al., 2018), while reducing pulmonary T cell infiltration (Tan et al., 2018). Interestingly, exosomes from WJ-MSC were also able to reduce macrophage lung infiltration when IV injected in a model of hyperoxia-induced BPD (Willis et al., 2018).

MSC-EVs Modulate the Microglial Inflammatory Response

Tissue resident macrophages of the central nervous system, microglia, play a pivotal role in modulating the inflammatory response (Lenz and Nelson, 2018). Thomi et al. (2019) reported that the administration of WJ-MSC-EVs was able to modulate the microglia response by interfering with the TLR4/CD14 signaling pathway thus dampening the expression of inflammatory cytokines such as TNF-α and IL-6 but without affecting the inflammasome pathway. Furthermore, in a transgenic mouse model of Alzheimer's disease exosomes derived from hUC-MSC ameliorated spatial learning and memory function and, in parallel, reduced the number of inflammatory M1 microglial cells and increased levels of M2 immunomodulatory microglia (Ding et al., 2018). In addition, reduced levels of inflammatory cytokines (IL-1β and TNF-α) and increased of anti-inflammatory ones (IL-10 and TGF-β) were found in peripheral blood and in brains of mice treated with hUC-MSC exosomes.

Impact of Perinatal EVs on Cells of the Lymphoid Lineage

Perinatal MSC-EVs Influence T Lymphocyte Activation and Polarization

In addition to the effect observed on innate immune cells, several groups have also shown that perinatal EVs modulate the adaptive immune response, as well as the infiltration of T lymphocytes in the inflamed tissues. Crain et al. (2019) reported that WJ-MSC EVs were able to inhibit CD4 T lymphocyte proliferation in a dose-dependent manner. The observed effect was possibly due to the high amount of TGFβ1 delivered by the EVs. Indeed, the administration of TGFβ1 neutralizing antibodies and TGFβ1R antagonist reverted the efficacy of the WJ-MSC EVs. Similar findings were also obtained when adenosine signaling was blocked, thus suggesting that the mechanism of action of WJ-MSC-EVs was based on the activation of these two axes (Crain et al., 2019). As a matter of fact, similar findings were observed also by Kerkelä et al. (2016), who reported the capacity of UC-MSC EVs to affect the extracellular microenvironment through the production of adenosine by the CD73 ectonucleotidase expressed on the surface of the EVs. The authors reported how CD39 expressed by the T lymphocyte synergizes with CD73 expressed on the surface of the exosomes to convert the extracellular ATP in ADP, AMP, and finally in adenosine, thus inhibiting the immune response (Kerkelä et al., 2016).

hUC-MSC EVs have been also used to treat immune-dysregulated diseases such as allergic dermatitis characterized by an excessive antigen-specific T cell reaction (Guo et al., 2019).

Application of hUC-MSC EVs in a mouse model of contact hypersensitivity (CHS) reduced ear swelling and ear leukocyte infiltration, reduced the percentages of IFN-γ producing $CD8^+$ and $CD4^+$ T cells, increased the levels of T regulatory (Treg) cells in the cervical lymph nodes, and finally, decreased serum levels of IFN-γ and TNF-α while increasing those of IL-10 (Guo et al., 2019). The authors suggested that the immunomodulatory action of hUC-MSC EVs may be mediated by their ability to suppress STAT1 activation (Guo et al., 2019).

The ability of UC-MSC EVs to affect T lymphocyte activation and proliferation was also observed in a comparison article aimed to determine whether the different fractions of the secretome display distinct immunomodulatory properties. Indeed, one study that compared the results obtained from the complete CM, the ultracentrifuged pellet, the non-EV fraction, and the EV fraction isolated by size-exclusion chromatography (SEC) (Monguió-Tortajada et al., 2017). Importantly, the authors reported that EVs do not induce monocyte polarization or cytokine secretion, but the non-EV fraction is able to trigger the expression of two M2 markers namely CD163 and CD206, while at the same time enhance the production of the inflammatory cytokine TNF-α (Monguió-Tortajada et al., 2017). Moreover, the SEC-purified EV fraction was the only fraction able to inhibit T lymphocyte proliferation and inflammatory cytokine production *in vitro*, resembling the effect of parental UC-MSC. Furthermore, the other fractions triggered the polarization of polyclonally stimulated T cells toward the inflammatory Th17 subset (Monguió-Tortajada et al., 2017). Additionally, the ability of UC-MSC EVs to affect Th subset polarization was also reported by Wang et al. (2016). Indeed, the authors highlighted how UC-MSC-EVs can trigger the conversion of inflammatory Th1 subset toward the Th2 subset by the downregulation of the pro-inflammatory cytokines TNFα and IFNγ, and instead trigger the expression of IL-10 and IL-4. Furthermore, when inoculated in a mouse model of graft versus host disease, UC-MSC EVs were able to reduce the serum level of inflammatory cytokines IL-2, TNFα, and IFNγ, increase the amount of IL-10, and reduce the absolute number of cytotoxic CD8 T lymphocytes (Wang et al., 2016).

In line with this, another study reported that EVs isolated from the B2 microglobulin negative fraction of UC-MSC lack of the capacity to trigger the activation of cytotoxic CD8 T lymphocytes. Moreover, authors observed an enrichment of miR-24 promoting survival of cardiomyocytes by targeting Bim. As a matter of fact, the authors highlighted the capacity of UC-MSC EVs to counteract fibrosis induced by the TGFβ pathway in an *in vivo* model of myocardial infarction in rats (Shao et al., 2020). These findings were also confirmed by Guo et al. (2019), who reported that, both *in vitro* and in an *in vivo* model of allergic contact dermatitis (ACD), UC-MSC-EVs were able to reduce the total amount of cytotoxic CD8 IFNγ + T lymphocytes, and inhibit the polarization of the inflammatory CD4 Th1 subset and instead foster the Treg polarization. In a different study, internalization of the EVs was able to reduce the STAT1 protein level thus affecting the transcriptional polarization toward the inflammatory and cytotoxic T lymphocyte subsets (Guo et al., 2019).

Perinatal EVs Impact Treg Polarization and T Lymphocyte Recruitment

Perinatal EVs can also affect Treg polarization. In this context, Zhang et al. (2018) reported how UC-MSC primed with TGFβ and IFNγ for 72 h were able to enhance Treg polarization, putatively through upregulation of IDO molecules.

Similarly, EVs isolated from primed amniotic fluid MSC were able to induce the polarization and expansion of CD4 Treg cells. Romani et al. (2015) reported that pre-treatment with IFNγ was able to strongly increase the amount of IDO1 conveyed by the EVs. These *in vitro* findings were confirmed in a mouse model of allogeneic skin graft transplantation, where the treatment with hAF-MSC EVs induced an increase in the number of Treg cells in the draining lymph nodes of recipient mice (Romani et al., 2015). Conversely, Balbi et al. (2017) highlighted how EVs isolated from hAF-SC were not able to affect the proliferation of human PBMC activated with different stimuli. Furthermore, they did not observe any significant effect in the polarization of CD4 Treg cells, while a significant reduction on B cell maturation was detected (Balbi et al., 2017). Finally, several studies also reported the ability of EVs isolated from UC-MSC and hAEC to inhibit the recruitment of inflamed T lymphocytes. Indeed, in a mouse model of uveoretinitis Bai et al. (2017) reported a reduction of IFN-γ- and IL-17-producing $CD4^+$ T cells in the damaged area. However, these findings were associated neither with a diminished T cell proliferation nor with increased cell apoptosis, but rather with the ability of hUC-MSC exosomes to inhibit T cell migration (Bai et al., 2017). Similar results were reported also by Tan et al. (2018), highlighting the potential immunomodulatory effect of hAEC EVs, able not only to induce polarization of monocytes toward anti-inflammatory M2 macrophages, but also to reduce the infiltration of T lymphocytes in a mouse model of bleomycin induced pulmonary fibrosis. Besides T-cells, *in vitro* and *in vivo* studies have reported the capacity of the exosomes isolated from UC-MSC to affect other lymphoid cells, such as the migration of NK cells by down modulating the expression of the C-X3-C motif chemokine ligand-1 (CX3CL1) and toll-like receptor-2 (TLR-2), thus affecting NK cell recruitment (Zou et al., 2016).

miRNAs REGULATE THE IMMUNE MODULATORY PROPERTIES OF PERINATAL EVs

Many of the observed effects can be in part attributable to the presence of bioactive molecules like the miRNAs. As a matter of fact, among the bioactive factors contained in EVs, miRNAs have emerged as one of the main effectors in regulating several biochemical and transcriptional pathways such as proliferation, differentiation, inflammation, metabolism, and apoptosis (He and Hannon, 2004). Indeed, several miRNAs have been associated with the modulation of T lymphocytes being able to boost or dampen their activation and polarization in order to maintain homeostasis (Rodríguez-Galán et al., 2018). At present, only a few studies have attempted to characterize the miRNA profile of the EVs isolated from perinatal MSC

(Fang et al., 2016; Balbi et al., 2017; Meng et al., 2017; Zou et al., 2018). Importantly, these studies reported the presence of a few specific and highly expressed miRNAs, previously described for their immunomodulatory potential, such as miR-16, miR-Let7-c, miR-181a, miR-125b, miR-26a, miR-145, miR-181c-5p, miR-Let-7e, miR-Let7-c, miR-Let-7f, and miR-106a (Meng et al., 2017). Moreover, UC-MSC EVs express high levels of miR16 and miR-Let-c (Zou et al., 2018). These two miRNA have been reported as directly targeting the 3′UTR of mTOR and RICTOR consequently reducing mTOR signaling and triggering Treg cell induction (Marcais et al., 2014). Since all these miRNAs impact the function of T lymphocytes, they represent possible mechanisms of action for the effects of EVs described so far.

The effects of perinatal EVs/exosomes may be mediated by a variety of miRNA that alter the activity of macrophages. For example, Ti et al. (2015) suggested that exosomes from LPS-primed hUC-MSC can affect macrophage plasticity through TLR4/NF-κB/STAT3/AKT regulatory signaling pathway via let-7b miRNA (Ding et al., 2018). The authors suggested that let-7b may activate AKT pathway which, in turn, suppresses macrophage TLR4/NF-κB activation and the resulting inflammatory response. TLR4/CD14 signaling pathway was affected also through exosomal delivery of miR-181c (Yao et al., 2019) and by the treatment with hWJ-MSC-exosomes which possibly act via the exosomal shuttle of miR-146a/b (Ma et al., 2019).

CONCLUSION, CHALLENGES AND FUTURE DIRECTIONS

The studies performed until now have on one hand demonstrated the attractive therapeutic potential of EVs derived from perinatal cells, but, on the other hand, they uncover the limitations of our knowledge and the need to solve many critical aspects before the translation of these products as therapeutic tools in clinic.

A common observation that should be outlined is the great heterogeneity in methods/techniques applied to obtain EVs/exosomes. Lack of standardized procedures does not assure the reproducibility, purity and maintenance of EV functional properties (Théry et al., 2018). The most applied EV-isolation methods in these papers are ultracentrifugation and precipitation kits each of which differ for recovery and specificity (Théry et al., 2018). Different methods of EV quantification have been applied, the most used is the total protein amount, some report the particle numbers (Alhomrani et al., 2017; Bier et al., 2018; Li et al., 2020), one the RNA concentration (Li et al., 2016) and others the injection volume (Alhomrani et al., 2017; Willis et al., 2018).

Another parameter that makes comparison difficult is referred to the conditioned media from which EVs/exosomes are isolated. The detailed preparation protocol for CM is often omitted in the publications, even if it is well known that culture conditions (cell passage, cell density, culture volume, culture medium, culture duration, etc.) affect cell functions as well as cell EV/exosome production. It is important to consider that supplements, such as serum, used in cell culture media, may contain EVs therefore ultimately affecting readouts. Although the use of serum-free medium or EV-depleted medium is strongly advisable, some studies use medium with serum (Li et al., 2016). Moreover, in order to exclude any possible contribution of the medium itself to EV composition, negative controls are needed. In this case, negative control means the "material" obtained from culture medium not conditioned by cells but processed in the same way as CM (Théry et al., 2018). Very few studies include this negative control in the planned treatment groups (Ding et al., 2018), while often this control is incorrectly replaced with a group treated with PBS, representing the vehicle in which EVs/exosomes are usually dissolved.

An important aim of some of the above reported studies is to compare the therapeutic efficacy of EVs/exosomes with respect to that of parental cells (Bier et al., 2018; Romanelli et al., 2019; Yao et al., 2019; Zavatti et al., 2020). However, this outcome is compromised by the lack of equivalent doses (Bier et al., 2018; Yao et al., 2019), differences in frequency and timing of delivery (Zavatti et al., 2020), and very few studies testing more than one dose (Sun et al., 2018).

Another important point, but that only a few studies have addressed (Alhomrani et al., 2017; Chaubey et al., 2018), is to establish whether treatment with EVs/exosomes is advantageous (for example, in terms of efficacy, effect duration, and tissue distribution) with respect to the treatment with CM in toto or with EV-depleted CM, to rationalize the time and money consuming procedure to isolate EVs from CM.

Some studies tried to approach another important point: the possible functional differences among EVs/exosomes derived from MSC from different sources and contrasting results have been reported. Willis et al. (2018) observed that, when IV injected in a murine model of hyperoxia-induced BPD, exosomes from bone marrow-derived MSC (BM-MSC) exerted therapeutic effects comparable to exosomes from WJ-MSC, while no benefits were observed after treatment with exosomes from human dermal fibroblasts. Instead, other authors found that in a model of bleomycin-induced pulmonary fibrosis exosomes from human lung fibroblasts show some of the anti-inflammatory effects observed when hAEC exosomes are used (Tan et al., 2018). In contrast with Willis et al. (2018); Bier et al. (2018) found that, in a model of Duchenne muscular dystrophy, BM-MSC-derived exosomes, unlike placenta-derived, did not ameliorate the pathology.

Another major point scarcely studied is the ability of EVs/exosomes to home to injury sites. Ma et al. (2019) injected fluorescent-labeled hUC-MSC EVs in rat tail vein and 24 h after injection EVs were found in the muscle lesioned by sciatic nerve transection, suggesting that EVs may maintain the tropism of parental cells.

Currently, there are a few ongoing clinical trials using MSC-derived EVs/exosomes. An updated search (December 2020) in the database of NIH https://clinicaltrials.gov/using the key words "MSC exosomes OR MSC extracellular vesicles" resulted in 13 clinical trials, most of these using exosomes derived from BM-MSC or from adipose MSC, and only 6, as mentioned previously, regarded the application of perinatal EVs.

Even considering the ongoing clinical trials, a concerted effort is still required to standardize perinatal EVs. Consortiums such as the COST SPRINT Action (CA17116), which aims to approach consensus for different aspects of perinatal derivatives (PnD) research, such as providing inputs for future standards for the processing, *in vitro* characterization and clinical application of perinatal cells and their secretome, will be fundamental to address this challenge.

Albeit cell heterogeneity doesn't seem to be a *sine qua non-condition* for EV efficacy as demonstrated by many preclinical studies and initial clinical trials. Rather, standardizing EVs and understanding heterogeneity is crucial to fine-tune EV preparations for specific therapeutic applications and to select EVs that will provide an optimal response to the disease.

AUTHOR CONTRIBUTIONS

AC, APap, AM, APas, and ARS: writing – original draft preparation. FRS, ARS, and OP: writing – review and editing. OP: supervision and final approval of the manuscript. All authors contributed to the article and approved the submitted version.

FUNDING

This work was supported by the Italian Ministry of Research and University (MIUR, 5 × 1,000 years 2017, 2018), intramural funds from the Università Cattolica del Sacro Cuore (*Linea D1-2018* and *Linea D1-2019*); PRIN 2017 program of Italian Ministry of Research and University (MIUR, grant no. 2017RSAFK7), and Fondazione Poliambulanza.

ACKNOWLEDGMENTS

This work contributes to the COST Action CA17116 International Network for Translating Research on Perinatal Derivatives into Therapeutic Approaches (SPRINT), supported by COST (European Cooperation in Science and Technology). We would like to acknowledge the Regenerative Medicine Research Center (CROME) of Università Cattolica del Sacro Cuore.

REFERENCES

Abomaray, F. M., Al Jumah, M. A., Kalionis, B., AlAskar, A. S., Al Harthy, S., Jawdat, D., et al. (2015). Human Chorionic Villous Mesenchymal Stem Cells Modify the Functions of Human Dendritic Cells, and Induce an Anti-Inflammatory Phenotype in CD1+ Dendritic Cells. *Stem Cell Rev. Rep.* 11, 423–441. doi: 10.1007/s12015-014-9562-8

Abumaree, M. H., Abomaray, F. M., Alshabibi, M. A., AlAskar, A. S., and Kalionis, B. (2017). Immunomodulatory properties of human placental mesenchymal stem/stromal cells. *Placenta* 59, 87–95. doi: 10.1016/j.placenta.2017.04.003

Abumaree, M. H., Abomaray, F. M., Alshehri, N. A., Almutairi, A., AlAskar, A. S., Kalionis, B., et al. (2016). Phenotypic and Functional Characterization of Mesenchymal Stem/Multipotent Stromal Cells From Decidua Parietalis of Human Term Placenta. *Reprod. Sci.* 23, 1193–1207. doi: 10.1177/1933719116632924

Abumaree, M. H., Harthy, S. Al, Subayyil, A.M. Al, Alshabibi, M. A., Abomaray, F. M., Khatlani, T., et al. (2019). Decidua Basalis Mesenchymal Stem Cells Favor Inflammatory M1 Macrophage Differentiation In Vitro. *Cells* 8:8020173. doi: 10.3390/cells8020173

Alhomrani, M., Correia, J., Zavou, M., Leaw, B., Kuk, N., Xu, R., et al. (2017). The Human Amnion Epithelial Cell Secretome Decreases Hepatic Fibrosis in Mice with Chronic Liver Fibrosis. *Front. Pharmacol.* 8:748. doi: 10.3389/fphar.2017.00748

Anzalone, R., Lo Iacono, M., Corrao, S., Magno, F., Loria, T., Cappello, F., et al. (2010). New emerging potentials for human Wharton's jelly mesenchymal stem cells: immunological features and hepatocyte-like differentiative capacity. *Stem Cells Dev.* 19, 423–438. doi: 10.1089/scd.2009.0299

Bai, L., Shao, H., Wang, H., Zhang, Z., Su, C., Dong, L., et al. (2017). Effects of Mesenchymal Stem Cell-Derived Exosomes on Experimental Autoimmune Uveitis. *Sci. Rep.* 7:4323.

Balbi, C., Piccoli, M., Barile, L., Papait, A., Armirotti, A., Principi, E., et al. (2017). First Characterization of Human Amniotic Fluid Stem Cell Extracellular Vesicles as a Powerful Paracrine Tool Endowed with Regenerative Potential. *Stem Cells Transl. Med.* 6, 1340–1355. doi: 10.1002/sctm.16-0297

Banas, R., Miller, C., Guzik, L., and Zeevi, A. (2013). Amnion-derived Multipotent Progenitor Cells Inhibit Blood Monocyte Differentiation into Mature Dendritic Cells. *Cell Transpl.* 23, 1111–1125. doi: 10.3727/096368913x670165

Bier, A., Berenstein, P., Kronfeld, N., Morgoulis, D., Ziv-Av, A., Goldstein, H., et al. (2018). Placenta-derived mesenchymal stromal cells and their exosomes exert therapeutic effects in Duchenne muscular dystrophy. *Biomaterials* 174, 67–78. doi: 10.1016/j.biomaterials.2018.04.055

Cargnoni, A., Farigu, S., Piccinelli, E. C., Signoroni, P. B., Romele, P., Vanosi, G., et al. (2018). Effect of human amniotic epithelial cells on pro-fibrogenic resident hepatic cells in a rat model of liver fibrosis. *J. Cell Mol. Med.* 22, 1202–1213.

Cargnoni, A., Gibelli, L., Tosini, A., Signoroni, P. B., Nassuato, C., Arienti, D., et al. (2009). Transplantation of allogeneic and xenogeneic placenta-derived cells reduces bleomycin-induced lung fibrosis. *Cell Transpl.* 18, 405–422. doi: 10.3727/096368909788809857

Cargnoni, A., Piccinelli, E. C., Ressel, L., Rossi, D., Magatti, M., Toschi, I., et al. (2014). Conditioned medium from amniotic membrane-derived cells prevents lung fibrosis and preserves blood gas exchanges in bleomycin-injured mice-specificity of the effects and insights into possible mechanisms. *Cytotherapy* 16, 17–32. doi: 10.1016/j.jcyt.2013.07.002

Cargnoni, A., Ressel, L., Rossi, D., Poli, A., Arienti, D., Lombardi, G., et al. (2012). Conditioned medium from amniotic mesenchymal tissue cells reduces progression of bleomycin-induced lung fibrosis. *Cytotherapy* 14, 153–161. doi: 10.3109/14653249.2011.613930

Cargnoni, A., Romele, P., Signoroni, P. B., Farigu, S., Magatti, M., Vertua, E., et al. (2020). Amniotic MSCs reduce pulmonary fibrosis by hampering lung B-cell recruitment, retention, and maturation. *Stem Cells Transl. Med.* 9, 1023–1035. doi: 10.1002/sctm.20-0068

Chaubey, S., Thueson, S., Ponnalagu, D., Alam, M. A., Gheorghe, C. P., Aghai, Z., et al. (2018). Early gestational mesenchymal stem cell secretome attenuates experimental bronchopulmonary dysplasia in part via exosome-associated factor TSG-6. *Stem Cell Res. Therapy* 9:173.

Che, N., Li, X., Zhou, S., Liu, R., Shi, D., Lu, L., et al. (2012). Umbilical cord mesenchymal stem cells suppress B-cell proliferation and differentiation. *Cell. Immunol.* 274, 46–53. doi: 10.1016/j.cellimm.2012.02.004

Crain, S. K., Robinson, S. R., Thane, K. E., Davis, A. M., Meola, D. M., Barton, B. A., et al. (2019). Extracellular Vesicles from Wharton's Jelly Mesenchymal Stem Cells Suppress CD4 Expressing T Cells Through Transforming Growth Factor Beta and Adenosine Signaling in a Canine Model. *Stem Cells Dev.* 28, 212–226. doi: 10.1089/scd.2018.0097

Croxatto, D., Vacca, P., Canegallo, F., Conte, R., Venturini, P. L., Moretta, L., et al. (2014). Stromal Cells from Human Decidua Exert a Strong Inhibitory Effect on NK Cell Function and Dendritic Cell Differentiation. *PLoS One* 9:e89006. doi: 10.1371/journal.pone.0089006

Danieli, P., Malpasso, G., Ciuffreda, M. C., Cervio, E., Calvillo, L., Copes, F., et al. (2015). Conditioned medium from human amniotic mesenchymal stromal cells limits infarct size and enhances angiogenesis. *Stem Cells Transl. Med.* 4, 448–458. doi: 10.5966/sctm.2014-0253

Ding, M., Shen, Y., Wang, P., Xie, Z., Xu, S., Zhu, Z., et al. (2018). Exosomes Isolated From Human Umbilical Cord Mesenchymal Stem Cells Alleviate

Neuroinflammation and Reduce Amyloid-Beta Deposition by Modulating Microglial Activation in Alzheimer's Disease. *Neurochem. Res.* 43, 2165–2177. doi: 10.1007/s11064-018-2641-5

Donders, R., Vanheusden, M., Bogie, J. F., Ravanidis, S., Thewissen, K., Stinissen, P., et al. (2015). Human Wharton's Jelly-Derived Stem Cells Display Immunomodulatory Properties and Transiently Improve Rat Experimental Autoimmune Encephalomyelitis. *Cell Transpl.* 24, 2077–2098. doi: 10.3727/096368914x685104

Fang, S., Xu, C., Zhang, Y., Xue, C., Yang, C., Bi, H., et al. (2016). Umbilical Cord-Derived Mesenchymal Stem Cell-Derived Exosomal MicroRNAs Suppress Myofibroblast Differentiation by Inhibiting the Transforming Growth Factor-β/SMAD2 Pathway During Wound Healing. *Stem Cells Translat. Med.* 5, 1425–1439. doi: 10.5966/sctm.2015-0367

Fatima, F., Ekstrom, K., Nazarenko, I., Maugeri, M., Valadi, H., Hill, A. F., et al. (2017). Non-coding RNAs in Mesenchymal Stem Cell-Derived Extracellular Vesicles: Deciphering Regulatory Roles in Stem Cell Potency, Inflammatory Resolve, and Tissue Regeneration. *Front. Genet.* 8:161. doi: 10.3389/fgene.2017.00161

Fitzgerald, W., Gomez-Lopez, N., Erez, O., Romero, R., and Margolis, L. (2018). Extracellular vesicles generated by placental tissues ex vivo: A transport system for immune mediators and growth factors. *Am. J. Reproduct. Immunol.* 80:e12860. doi: 10.1111/aji.12860

Giampa, C., Alvino, A., Magatti, M., Silini, A. R., Cardinale, A., Paldino, E., et al. (2019). Conditioned medium from amniotic cells protects striatal degeneration and ameliorates motor deficits in the R6/2 mouse model of Huntington's disease. *J. Cell Mol. Med.* 23, 1581–1592. doi: 10.1111/jcmm.14113

Gunawardena, T. N. A., Mohammad, T. R., Abdullah, B. J. J., and Kasim, N. H. A. (2019). Conditioned media serived from mesenchymal stem cell cultures: The next generation for regenerative medicine. *J. Tissue Eng. Regen. Med.* 13, 569–586. doi: 10.1002/term.2806

Guo, L., Lai, P., Wang, Y., Huang, T., Chen, X., Luo, C., et al. (2019). Extracellular vesicles from mesenchymal stem cells prevent contact hypersensitivity through the suppression of Tc1 and Th1 cells and expansion of regulatory T cells. *Int. Immunopharmacol.* 74:105663. doi: 10.1016/j.intimp.2019.05.048

Gurunathan, S., Kang, M.-H., Jeyaraj, M., Qasim, M., and Kim, J.-H. (2019). Review of the Isolation, Characterization, Biological Function, and Multifarious Therapeutic Approaches of Exosomes. *Cells* 8:307. doi: 10.3390/cells8040307

He, L., and Hannon, G. J. (2004). Correction: MicroRNAs: small RNAs with a big role in gene regulation. *Nat. Rev. Genet.* 5, 631–631. doi: 10.1038/nrg1415

Hristov, M., Erl, W., Linder, S., and Weber, P. C. (2004). Apoptotic bodies from endothelial cells enhance the number and initiate the differentiation of human endothelial progenitor cells in vitro. *Blood* 104, 2761–2766. doi: 10.1182/blood-2003-10-3614

Hurwitz, S. N., Olcese, J. M., and Meckes, D. G. Jr. (2019). Extraction of Extracellular Vesicles from Whole Tissue. *J. Visualized Exp.* 2019:59143.

Jiang, L., Zhang, S., Hu, H., Yang, J., Wang, X., Ma, Y., et al. (2019). Exosomes derived from human umbilical cord mesenchymal stem cells alleviate acute liver failure by reducing the activity of the NLRP3 inflammasome in macrophages. *Biochem. Biophys. Res. Commun.* 508, 735–741. doi: 10.1016/j.bbrc.2018.11.189

Jung, J., Choi, J. H., Lee, Y., Park, J. W., Oh, I. H., Hwang, S. G., et al. (2013). Human placenta-derived mesenchymal stem cells promote hepatic regeneration in CCl4 -injured rat liver model via increased autophagic mechanism. *Stem Cells* 31, 1584–1596. doi: 10.1002/stem.1396

Kao, C.-Y., and Papoutsakis, E. T. (2019). Extracellular vesicles: exosomes, microparticles, their parts, and their targets to enable their biomanufacturing and clinical applications. *Curr. Opin. Biotechnol.* 60, 89–98. doi: 10.1016/j.copbio.2019.01.005

Kerkelä, E., Laitinen, A., Räbinä., J., Valkonen, S., Takatalo, M., Larjo, A., et al. (2016). Adenosinergic Immunosuppression by Human Mesenchymal Stromal Cells Requires Co-Operation with T cells. *Stem Cells* 34, 781–790. doi: 10.1002/stem.2280

Khoury, O., Atala, A., and Murphy, S. V. (2020). Stromal cells from perinatal and adult sources modulate the inflammatory immune response in vitro by decreasing Th1 cell proliferation and cytokine secretion. *Stem Cells Translat. Med.* 9, 61–73. doi: 10.1002/sctm.19-0123

Kronsteiner, B., Wolbank, S., Peterbauer, A., Hackl, C., Redl, H., van Griensven, M., et al. (2011). Human mesenchymal stem cells from adipose tissue and amnion influence T-cells depending on stimulation method and presence of other immune cells. *Stem Cells Dev.* 20, 2115–2126. doi: 10.1089/scd.2011.0031

Lee, M.-J., Jung, J., Na, K.-H., Moon, J. S., Lee, H.-J., Kim, J.-H., et al. (2010). Anti-fibrotic effect of chorionic plate-derived mesenchymal stem cells isolated from human placenta in a rat model of CCl4-injured liver: Potential application to the treatment of hepatic diseases. *J. Cell Biochem.* 111, 1453–1463. doi: 10.1002/jcb.22873

Lenz, K. M., and Nelson, L. H. (2018). Microglia and Beyond: Innate Immune Cells As Regulators of Brain Development and Behavioral Function. *Front. Immunol.* 9:698. doi: 10.3389/fimmu.2018.00698

Li, B., Lee, C., O'Connell, J. S., Antounians, L., Ganji, N., Alganabi, M., et al. (2020). Activation of Wnt signaling by amniotic fluid stem cell-derived extracellular vesicles attenuates intestinal injury in experimental necrotizing enterocolitis. *Cell Death Dis.* 11:750.

Li, X., Liu, L., Yang, J., Yu, Y., Chai, J., Wang, L., et al. (2016). Exosome Derived From Human Umbilical Cord Mesenchymal Stem Cell Mediates MiR-181c Attenuating Burn-induced Excessive Inflammation. *EBioMedicine* 8, 72–82. doi: 10.1016/j.ebiom.2016.04.030

Lim, R. (2017). Concise Review: Fetal Membranes in Regenerative Medicine: New Tricks from an Old Dog? *Stem Cells Transl. Med.* 6, 1767–1776. doi: 10.1002/sctm.16-0447

Lin, Y. C., Ko, T. L., Shih, Y. H., Lin, M. Y., Fu, T. W., Hsiao, H. S., et al. (2011). Human umbilical mesenchymal stem cells promote recovery after ischemic stroke. *Stroke* 42, 2045–2053. doi: 10.1161/strokeaha.110.603621

Ma, Y., Dong, L., Zhou, D., Li, L., Zhang, W., Zhen, Y., et al. (2019). Extracellular vesicles from human umbilical cord mesenchymal stem cells improve nerve regeneration after sciatic nerve transection in rats. *J. Cell. Mol. Med.* 23, 2822–2835. doi: 10.1111/jcmm.14190

MacLeod, A. S., and Mansbridge, J. N. (2016). The Innate Immune System in Acute and Chronic Wounds. *Adv. Wound Care* 5, 65–78. doi: 10.1089/wound.2014.0608

Magatti, M., Abumaree, M. H., Silini, A. R., Anzalone, R., Saieva, S., Russo, E., et al. (2016). "The Immunomodulatory Features of Mesenchymal Stromal Cells Derived from Wharton's Jelly, Amniotic Membrane and Chorionic Villi," in *Vitro and In Vivo Data, in Placenta: The Tree of Life*, ed. O. Parolini (Boca Raton: CRC Press), 91–128. doi: 10.1201/b19620-6

Magatti, M., Caruso, M., Munari, S. D., Vertua, E., De, D., Manuelpillai, U., et al. (2015). Human Amniotic Membrane-Derived Mesenchymal and Epithelial Cells Exert Different Effects on Monocyte-Derived Dendritic Cell Differentiation and Function. *Cell Transpl.* 24, 1733–1752. doi: 10.3727/096368914x684033

Magatti, M., De Munari, S., Vertua, E., Gibelli, L., Wengler, G. S., and Parolini, O. (2008). Human amnion mesenchyme harbors cells with allogeneic T-cell suppression and stimulation capabilities. *Stem Cells* 26, 182–192. doi: 10.1634/stemcells.2007-0491

Magatti, M., De Munari, S., Vertua, E., Nassauto, C., Albertini, A., Wengler, G. S., et al. (2009). Amniotic mesenchymal tissue cells inhibit dendritic cell differentiation of peripheral blood and amnion resident monocytes. *Cell Transpl.* 18, 899–914. doi: 10.3727/096368909x471314

Magatti, M., Masserdotti, A., Signoroni, P. B., Vertua, E., Stefani, F. R., Silini, A. R., et al. (2020). B Lymphocytes as Targets of the Immunomodulatory Properties of Human Amniotic Mesenchymal Stromal Cells. *Front. Immunol.* 11:1156. doi: 10.3389/fimmu.2020.01156

Magatti, M., Stefani, F. R., Papait, A., Cargnoni, A., Masserdotti, A., Silini, A. R., et al. (2019). Perinatal Mesenchymal Stromal Cells and Their Possible Contribution to Fetal-Maternal Tolerance. *Cells* 8:1401. doi: 10.3390/cells8111401

Magatti, M., Vertua, E., Cargnoni, A., Silini, A., and Parolini, O. (2018). The Immunomodulatory Properties of Amniotic Cells: The Two Sides of the Coin. *Cell Transpl.* 27, 31–44. doi: 10.1177/0963689717742819

Manuelpillai, U., Lourensz, D., Vaghjiani, V., Tchongue, J., Lacey, D., Tee, J. Y., et al. (2012). Human amniotic epithelial cell transplantation induces markers of alternative macrophage activation and reduces established hepatic fibrosis. *PLoS One* 7:e38631. doi: 10.1371/journal.pone.0038631

Manuelpillai, U., Tchongue, J., Lourensz, D., Vaghjiani, V., Samuel, C. S., Liu, A., et al. (2010). Transplantation of human amnion epithelial cells reduces hepatic fibrosis in immunocompetent CCl(4)-treated mice. *Cell Transpl.* 19, 1157–1168. doi: 10.3727/096368910x504496

Mao, F., Wu, Y., Tang, X., Kang, J., Zhang, B., Yan, Y., et al. (2017). Exosomes Derived from Human Umbilical Cord Mesenchymal Stem Cells Relieve Inflammatory Bowel Disease in Mice. *BioMed. Res. Int.* 2017:5356760.

Marcais, A., Blevins, R., Graumann, J., Feytout, A., Dharmalingam, G., Carroll, T., et al. (2014). microRNA-mediated regulation of mTOR complex components facilitates discrimination between activation and anergy in CD4 T cells. *J. Exp. Med.* 211, 2281–2295. doi: 10.1084/jem.20132059

Mattar, P., and Bieback, K. (2015). Comparing the Immunomodulatory Properties of Bone Marrow, Adipose Tissue, and Birth-Associated Tissue Mesenchymal Stromal Cells. *Front. Immunol.* 6:560. doi: 10.3389/fimmu.2015.00560

Meng, X., Xue, M., Xu, P., Hu, F., Sun, B., and Xiao, Z. (2017). MicroRNA profiling analysis revealed different cellular senescence mechanisms in human mesenchymal stem cells derived from different origin. *Genomics* 109, 147–157. doi: 10.1016/j.ygeno.2017.02.003

Monguió-Tortajada, M., Roura, S., Gálvez-Montón, C., Pujal, J. M., Aran, G., Sanjurjo, L., et al. (2017). Nanosized UCMSC-derived extracellular vesicles but not conditioned medium exclusively inhibit the inflammatory response of stimulated T cells: implications for nanomedicine. *Theranostics* 7, 270–284. doi: 10.7150/thno.16154

Moodley, Y., Vaghjiani, V., Chan, J., Baltic, S., Ryan, M., Tchongue, J., et al. (2013). Anti-inflammatory effects of adult stem cells in sustained lung injury: a comparative study. *PLoS One* 8:e69299. doi: 10.1371/journal.pone.0069299

Murphy, S. V., Shiyun, S. C., Tan, J. L., Chan, S., Jenkin, G., Wallace, E. M., et al. (2012). Human amnion epithelial cells do not abrogate pulmonary fibrosis in mice with impaired macrophage function. *Cell Transpl.* 21, 1477–1492. doi: 10.3727/096368911x601028

Parolini, O., Souza-Moreira, L., O'Valle, F., Magatti, M., Hernandez-Cortes, P., Gonzalez-Rey, E., et al. (2014). Therapeutic effect of human amniotic membrane-derived cells on experimental arthritis and other inflammatory disorders. *Arthritis Rheumatol.* 66, 327–339. doi: 10.1002/art.38206

Phinney, D. G., and Pittenger, M. F. (2017). Concise Review: MSC-Derived Exosomes for Cell-Free Therapy. *Stem Cells* 35, 851–858. doi: 10.1002/stem.2575

Pianta, S., Magatti, M., Vertua, E., Signoroni, P. B., Muradore, I., Nuzzo, A. M., et al. (2016). Amniotic mesenchymal cells from pre-eclamptic placentae maintain immunomodulatory features as healthy controls. *J. Cell Mol. Med.* 20, 157–169. doi: 10.1111/jcmm.12715

Pischiutta, F., Brunelli, L., Romele, P., Silini, A., Sammali, E., Paracchini, L., et al. (2016). Protection of Brain Injury by Amniotic Mesenchymal Stromal Cell-Secreted Metabolites. *Crit. Care Med.* 44, 1118–1131e.

Pitt, J. M., Kroemer, G., and Zitvogel, L. (2016). Extracellular vesicles: masters of intercellular communication and potential clinical interventions. *J. Clin. Investig.* 126, 1139–1143. doi: 10.1172/jci87316

Rahbarghazi, R., Jabbari, N., Sani, N. A., Asghari, R., Salimi, L., Kalashani, S. A., et al. (2019). Tumor-derived extracellular vesicles: reliable tools for Cancer diagnosis and clinical applications. *Cell Communicat. Signal.* 17:73.

Rani, S., Ryan, A. E., Griffin, M. D., and Ritter, T. (2015). Mesenchymal Stem Cell-derived Extracellular Vesicles: Toward Cell-free Therapeutic Applications. *Mol. Ther.* 23, 812–823. doi: 10.1038/mt.2015.44

Raposo, G., and Stoorvogel, W. (2013). Extracellular vesicles: exosomes, microvesicles, and friends. *J. Cell Biol.* 200, 373–383. doi: 10.1083/jcb.201211138

Robbins, P. D., and Morelli, A. E. (2014). Regulation of Immune Responses by Extracellular Vesicles. *Nat. Rev. Immunol.* 14, 195–208. doi: 10.1038/nri3622

Rodríguez-Galán, A., Fernández-Messina, L., and Sánchez-Madrid, F. (2018). Control of Immunoregulatory Molecules by miRNAs in T Cell Activation. *Front. Immunol.* 9:2148. doi: 10.3389/fimmu.2018.02148

Romanelli, P., Bieler, L., Scharler, C., Pachler, K., Kreutzer, C., Zaunmair, P., et al. (2019). Extracellular Vesicles Can Deliver Anti-inflammatory and Anti-scarring Activities of Mesenchymal Stromal Cells After Spinal Cord Injury. *Front. Neurol.* 10:1225. doi: 10.3389/fneur.2019.01225

Romani, R., Pirisinu, I., Calvitti, M., Pallotta, M. T., Gargaro, M., Bistoni, G., et al. (2015). Stem cells from human amniotic fluid exert immunoregulatory function via secreted indoleamine 2,3-dioxygenase1. *J. Cell Mol. Med.* 19, 1593–1605. doi: 10.1111/jcmm.12534

Shao, L., Zhang, Y., Pan, X., Liu, B., Liang, C., Zhang, Y., et al. (2020). Knockout of beta-2 microglobulin enhances cardiac repair by modulating exosome imprinting and inhibiting stem cell-induced immune rejection. *Cell. Mol. Life Sci.* 77, 937–952. doi: 10.1007/s00018-019-03220-3

Silini, A. R., Di Pietro, R., Lang-Olip, I., Alviano, F., Banerjee, A., Basile, M., et al. (2020). Perinatal derivatives: where do we stand? A roadmap of the human placenta and consensus for tissue and cell nomenclature. *Front. Bioengine. Biotechnol.* 8:610544. doi: 10.3389/fbioe.2020.610544

Silini, A. R., Magatti, M., Cargnoni, A., and Parolini, O. (2017). Is Immune Modulation the Mechanism Underlying the Beneficial Effects of Amniotic Cells and Their Derivatives in Regenerative Medicine? *Cell Transpl.* 26, 531–539. doi: 10.3727/096368916x693699

Silini, A. R., Masserdotti, A., Papait, A., and Parolini, O. (2019). Shaping the Future of Perinatal Cells: Lessons From the Past and Interpretations of the Present. *Front. Bioengin. Biotechnol.* 7, 75–75. doi: 10.3389/fbioe.2019.00075

Song, Y., Dou, H., Li, X., Zhao, X., Li, Y., Liu, D., et al. (2017). Exosomal miR-146a Contributes to the Enhanced Therapeutic Efficacy of Interleukin-1β-Primed Mesenchymal Stem Cells Against Sepsis. *Stem Cells* 35, 1208–1221. doi: 10.1002/stem.2564

Spinosa, M., Lu, G., Su, G., Bontha, S. V., Gehrau, R., Salmon, M. D., et al. (2018). Human mesenchymal stromal cell-derived extracellular vesicles attenuate aortic aneurysm formation and macrophage activation via microRNA-147. *FASEB J.* 32, 6038–6050. doi: 10.1096/fj.201701138rr

Sun, G., Li, G., Li, D., Huang, W., Zhang, R., Zhang, H., et al. (2018). hucMSC derived exosomes promote functional recovery in spinal cord injury mice via attenuating inflammation. *Materials Sci. Engine. C* 89, 194–204. doi: 10.1016/j.msec.2018.04.006

Tan, J. L., Chan, S. T., Wallace, E. M., and Lim, R. (2014). Human amnion epithelial cells mediate lung repair by directly modulating macrophage recruitment and polarization. *Cell Transpl.* 23, 319–328. doi: 10.3727/096368912x661409

Tan, J. L., Lau, S. N., Leaw, B., Nguyen, H. P. T., Salamonsen, L. A., Saad, M. I., et al. (2018). Amnion Epithelial Cell-Derived Exosomes Restrict Lung Injury and Enhance Endogenous Lung Repair. *Stem Cells Transl. Med.* 7, 180–196. doi: 10.1002/sctm.17-0185

Tan, J. L., Tan, Y. Z., Muljadi, R., Chan, S. T., Lau, S. N., Mockler, J. C., et al. (2017). Amnion Epithelial Cells Promote Lung Repair via Lipoxin A(4). *Stem Cells Transl. Med.* 6, 1085–1095. doi: 10.5966/sctm.2016-0077

Théry, C., Witwer, K. W., Aikawa, E., Alcaraz, M. J., Anderson, J. D., Andriantsitohaina, R., et al. (2018). Minimal information for studies of extracellular vesicles 2018 (MISEV2018): a position statement of the International Society for Extracellular Vesicles and update of the MISEV2014 guidelines. *J. Extracell. Vesicles* 7:1535750.

Thomi, G., Surbek, D., Haesler, V., Joerger-Messerli, M., and Schoeberlein, A. (2019). Exosomes derived from umbilical cord mesenchymal stem cells reduce microglia-mediated neuroinflammation in perinatal brain injury. *Stem Cell Res. Therapy* 10:105.

Ti, D., Hao, H., Tong, C., Liu, J., Dong, L., Zheng, J., et al. (2015). LPS-preconditioned mesenchymal stromal cells modify macrophage polarization for resolution of chronic inflammation via exosome-shuttled let-7b. *J. Transl. Med.* 13:308.

Tsai, P.-J., Wang, H.-S., Lin, G.-J., Chou, S.-C., Chu, T.-H., Chuan, W.-T., et al. (2015). Undifferentiated Wharton's Jelly Mesenchymal Stem Cell Transplantation Induces Insulin-Producing Cell Differentiation and Suppression of T-Cell-Mediated Autoimmunity in Nonobese Diabetic Mice. *Cell Transplant.* 24, 1555–1570. doi: 10.3727/096368914x683016

Turco, M. Y., and Moffett, A. (2019). Development of the human placenta. *Development* 146:163428.

Turturici, G., Tinnirello, R., Sconzo, G., and Geraci, F. (2014). Extracellular membrane vesicles as a mechanism of cell-to-cell communication: advantages and disadvantages. *Am. J. Physiolo. Cell Physiol.* 306, C621–C633.

Vosdoganes, P., Hodges, R. J., Lim, R., Westover, A. J., Acharya, R. Y., Wallace, E. M., et al. (2011). Human amnion epithelial cells as a treatment for inflammation-induced fetal lung injury in sheep. *Am. J. Obstet. Gynecol.* 205, 156.e26–33. doi: 10.1016/j.ajog.2011.03.054

Wang, H., Qiu, X., Ni, P., Qiu, X., Lin, X., Wu, W., et al. (2014). Immunological characteristics of human umbilical cord mesenchymal stem cells and the therapeutic effects of their transplantion on hyperglycemia in diabetic rats. *Int. J. Mol. Med.* 33, 263–270. doi: 10.3892/ijmm.2013.1572

Wang, L., Gu, Z., Zhao, X., Yang, N., Wang, F., Deng, A., et al. (2016). Extracellular Vesicles Released from Human Umbilical Cord-Derived Mesenchymal Stromal Cells Prevent Life-Threatening Acute Graft-Versus-Host Disease in a Mouse

Model of Allogeneic Hematopoietic Stem Cell Transplantation. *Stem Cells Dev.* 25, 1874–1883. doi: 10.1089/scd.2016.0107

Wei, Y., Wu, Y., Zhao, R., Zhang, K., Midgley, A. C., Kong, D., et al. (2019). MSC-derived sEVs enhance patency and inhibit calcification of synthetic vascular grafts by immunomodulation in a rat model of hyperlipidemia. *Biomaterials* 204, 13–24. doi: 10.1016/j.biomaterials.2019.01.049

White, E. S., and Mantovani, A. R. (2013). Inflammation, wound repair, and fibrosis: reassessing the spectrum of tissue injury and resolution. *J. Pathol.* 229, 141–144. doi: 10.1002/path.4126

Willis, G. R., Fernandez-Gonzalez, A., Anastas, J., Vitali, S. H., Liu, X., Ericsson, M., et al. (2018). Mesenchymal Stromal Cell Exosomes Ameliorate Experimental Bronchopulmonary Dysplasia and Restore Lung Function through Macrophage Immunomodulation. *Am. J. Respir. Crit. Care Med.* 197, 104–116. doi: 10.1164/rccm.201705-0925oc

Yao, J., Zheng, J., Cai, J., Zeng, K., Zhou, C., Zhang, J., et al. (2019). Extracellular vesicles derived from human umbilical cord mesenchymal stem cells alleviate rat hepatic ischemia-reperfusion injury by suppressing oxidative stress and neutrophil inflammatory response. *FASEB J.* 33, 1695–1710. doi: 10.1096/fj.201800131rr

Yu, B., Shao, H., Su, C., Jiang, Y., Chen, X., Bai, L., et al. (2016). Exosomes derived from MSCs ameliorate retinal laser injury partially by inhibition of MCP-1. *Sci. Rep.* 6:34562.

Zaborowski, M. P., Balaj, L., Breakefield, X. O., and Lai, C. P. (2015). Extracellular Vesicles: Composition, Biological Relevance, and Methods of Study. *BioScience* 65, 783–797. doi: 10.1093/biosci/biv084

Zavatti, M., Beretti, F., Casciaro, F., Bertucci, E., and Maraldi, T. (2020). Comparison of the therapeutic effect of amniotic fluid stem cells and their exosomes on monoiodoacetate-induced animal model of osteoarthritis. *BioFactors* 46, 106–117. doi: 10.1002/biof.1576

Zhang, Q., Fu, L., Liang, Y., Guo, Z., Wang, L., Ma, C., et al. (2018). Exosomes originating from MSCs stimulated with TGF-β and IFN-γ promote Treg differentiation. *J. Cell. Physiol.* 233, 6832–6840. doi: 10.1002/jcp.26436

Zhao, B., Zhang, Y., Han, S., Zhang, W., Zhou, Q., Guan, H., et al. (2017). Exosomes derived from human amniotic epithelial cells accelerate wound healing and inhibit scar formation. *J. Mol. Histol.* 48, 121–132. doi: 10.1007/s10735-017-9711-x

Zou, X., Gu, D., Zhang, G., Zhong, L., Cheng, Z., Liu, G., et al. (2016). NK Cell Regulatory Property is Involved in the Protective Role of MSC-Derived Extracellular Vesicles in Renal Ischemic Reperfusion Injury. *Hum. Gene Therapy* 27, 926–935. doi: 10.1089/hum.2016.057

Zou, X., Yu, Y., Lin, S., Zhong, L., Sun, J., Zhang, G., et al. (2018). Comprehensive miRNA Analysis of Human Umbilical Cord-Derived Mesenchymal Stromal Cells and Extracellular Vesicles. *Kidney Blood Pressure Res.* 43, 152–161. doi: 10.1159/000487369

Zou, X., Zhang, G., Cheng, Z., Yin, D., Du, T., Ju, G., et al. (2014). Microvesicles derived from human Wharton's Jelly mesenchymal stromal cells ameliorate renal ischemia-reperfusion injury in rats by suppressing CX3CL1. *Stem Cell Res. Therapy* 5:40. doi: 10.1186/scrt428

Conflict of Interest: The authors declare that the research was conducted in the absence of any commercial or financial relationships that could be construed as a potential conflict of interest.

Copyright © 2021 Cargnoni, Papait, Masserdotti, Pasotti, Stefani, Silini and Parolini. This is an open-access article distributed under the terms of the Creative Commons Attribution License (CC BY). The use, distribution or reproduction in other forums is permitted, provided the original author(s) and the copyright owner(s) are credited and that the original publication in this journal is cited, in accordance with accepted academic practice. No use, distribution or reproduction is permitted which does not comply with these terms.

frontiers in Bioengineering and Biotechnology

ORIGINAL RESEARCH
published: 15 February 2021
doi: 10.3389/fbioe.2021.632440

Check for updates

miR-103a-3p and miR-22-5p Are Reliable Reference Genes in Extracellular Vesicles From Cartilage, Adipose Tissue, and Bone Marrow Cells

Enrico Ragni[1†], Alessandra Colombini[1†], Paola De Luca[1], Francesca Libonati[1], Marco Viganò[1], Carlotta Perucca Orfei[1], Luigi Zagra[2] and Laura de Girolamo[1]*

[1] IRCCS Istituto Ortopedico Galeazzi, Laboratorio di Biotecnologie Applicate all'Ortopedia, Milan, Italy, [2] IRCCS Istituto Ortopedico Galeazzi, Hip Department, Milan, Italy

OPEN ACCESS

Edited by:
Roberta Tasso, University of Genoa, Italy

Reviewed by:
Lagneaux Laurence, Université libre de Bruxelles, Belgium
Ryan Michael Porter, University of Arkansas for Medical Sciences, United States

***Correspondence:**
Enrico Ragni
enrico.ragni@grupposandonato.it

† These authors have contributed equally to this work

Specialty section:
This article was submitted to Preclinical Cell and Gene Therapy, a section of the journal Frontiers in Bioengineering and Biotechnology

Received: *23 November 2020*
Accepted: *18 January 2021*
Published: *15 February 2021*

Citation:
Ragni E, Colombini A, De Luca P, Libonati F, Viganò M, Perucca Orfei C, Zagra L and de Girolamo L (2021) miR-103a-3p and miR-22-5p Are Reliable Reference Genes in Extracellular Vesicles From Cartilage, Adipose Tissue, and Bone Marrow Cells. Front. Bioeng. Biotechnol. 9:632440. doi: 10.3389/fbioe.2021.632440

Cartilage cells (CCs), adipose tissue (ASC)- and bone marrow (BMSC)-derived mesenchymal stromal cells (MSCs) have been shown as promising candidates for the treatment of osteoarthritis (OA). Despite their adaptive ability, exposure to chronic catabolic and inflammatory processes can limit their survival and healing potential. An attractive cell-free alternative or complementary strategy is represented by their secreted extracellular vesicles (EVs), having homeostatic properties on OA chondrocytes and synovial cells. In view of clinical translation, a thorough characterization of the shuttled therapeutic molecules, like miRNAs, is greatly needed to fingerprint and develop the most effective EV formulation for OA treatment. To date, a crucial pitfall is given by the lack of EV-miRNA-associated reference genes (RGs) for the reliable quantification and comparison among different therapeutic EV-based therapeutic products. In this study, the stability of 12 putative miRNA RGs (let-7a-5p, miR-16-5p, miR-22-5p, miR-23a-3p, miR-26a-5p, miR-29a-5p, miR-101-3p, miR-103a-3p, miR-221-3p, miR-423-5p, miR-425-5p and miR-660-5p), already proposed by literature in EV products from alternative sources, was assessed in EVs isolated from three donor-matched ASCs, BMSCs, and CCs through geNorm, NormFinder, BestKeeper, and ΔCt algorithms and the geometric mean of rankings. ASC-EVs and BMSC-EVs shared more similar molecular signatures than cartilage-derived EVs, although overall miR-103a-3p consistently ranked as the first and miR-22-5p as the second most stable EV-miRNA RG, whereas miR-221-3p behaved poorly. Further, to emphasize the impact of incorrect RG choice, the abundance of four OA-therapeutic miRNAs (miR-93-5p, miR-125b-5p, miR-455-3p, and miR-27b-3p) was compared. The use of miR-221-3p led to less accurate EV fingerprinting and, when applied to sift therapeutic potency prediction, to misleading indication of the most appropriate clinical product. In conclusion, miR-103a-3p and miR-22-5p will represent reliable RGs for the quantification of miRNAs embedded in MSC- and CC-EVs, a mandatory step for the molecular definition and comparison of the clinical potency of these innovative cell-free-based therapeutic products for OA in particular, as well as for a wider array of regenerative-medicine-based approaches.

Keywords: cartilage cells, adipose tissue mesenchymal stromal cells, bone marrow mesenchymal stromal cells, miRNAs, reference genes, extracellular vesicles

INTRODUCTION

Articular cartilage cells (CCs) (Brittberg et al., 1994; Schuette et al., 2017; Kreuz and Kalkreuth, 2019), bone marrow- (BMSCs) and adipose tissue-derived stromal cells (ASCs) (Moroni and Fornasari, 2013) are considered the most clinically relevant cell types in the setting of cell-based therapy for the treatment of osteoarthritis (OA). The adaptive trophic and immunomodulatory potential of CCs, ASCs, and BMSCs along with the crosstalk with the resident and inflammatory infiltrated cells account for their capacity to actively modulate the local pathological environment (Colombini et al., 2019).

This was confirmed by the satisfactory outcomes in terms of pain relief and joint homeostasis restoration in osteoarthritic patients (Niemeyer et al., 2016; Colombini et al., 2019; Kim et al., 2019). However, the typical chronic catabolic and inflammatory processes of an OA joint represents, together with the activation trigger, a big hurdle to cell survival and healing performances (Colombini et al., 2019). Moreover, the achievement of a sufficient number of cells for autologous use is associated with expensive and time-consuming procedures, together with patients' discomfort (Lopa et al., 2019).

The switch toward allogeneic donors could be a cheaper and logistically more convenient solution for the MSC-based treatment of musculoskeletal conditions (Vega et al., 2015; Gupta et al., 2016). More importantly, the collection and characterization of several cell batches from healthy donors would allow us to select only those with the best potency. Likewise, allogeneic CCs have been demonstrated to possess potent immunomodulatory properties (Lohan et al., 2016) and similar efficacy in a rabbit model of cartilage defect when compared to autologous CCs (Boopalan et al., 2019). Nevertheless, the potential tumorigenicity (Barkholt et al., 2013) and pro-fibrogenic potential (Russo et al., 2006) of autologous or allogeneic MSCs and the production of allo-antibodies (Cho et al., 2008) or the host immune response mediated by allogeneic cells (Moskalewski et al., 2002) still remain a concern.

Waiting for the development and validation of safe and clinically effective allogeneic cell therapies for OA treatment, an attractive alternative, or a strategy to combine with autologous cells is represented by the use of non-immunogenic cell products such as a conditioned medium and/or extracellular vesicles (EVs) (Colombini et al., 2019; Yin et al., 2019; Wu et al., 2020). In particular, the conditioned medium from BMSCs (van Buul et al., 2012) or ASCs (Manferdini et al., 2013; Platas et al., 2013, 2016) had anti-inflammatory and homeostatic properties in inflamed or OA chondrocytes and synovial cells, mostly mediated by their EVs. When co-cultured with osteoarthritic CCs, human BMSC-EVs were able to stimulate the production of proteoglycans and type II collagen from CCs and to inhibit the catabolic effects induced by pro-inflammatory mediators (Vonk et al., 2018). In addition, EVs derived from BMSCs promoted cartilage tissue formation by enhancing proliferation and attenuating apoptosis of CCs (Cosenza et al., 2017; Toh et al., 2017; Zhang et al., 2018). EVs mediated also the ASC anti-inflammatory and chondro-protective action in osteoarthritic CCs stimulated with IL-1β (Tofiño-Vian et al., 2018). CCs treated with ASC-EVs showed a downregulation of COX-2, PGES-1, and iNOS expression, with a consequent reduction of the release of TNF-α, IL-6, PGE2, and NO and a reduced MMP activity and MMP13 expression. Moreover, the enhancement of the IL-10 release and the type II collagen expression suggested a trophic activity of ASC-EVs. Similar results were reported also for synovial fibroblasts isolated from osteoarthritic joints (Ragni et al., 2019c). Regarding CCs, recent findings showed that also their EVs stimulated chondrogenesis and were chondro-protective, by decreasing catabolic events in IL−1β−treated CCs (Liu et al., 2020). Moreover, *in vitro*, CC-EVs were able to stimulate proliferation, migration, and expression of chondrogenesis markers in constructs containing cartilage progenitor cells, while inhibiting angiogenesis (Chen et al., 2018). *In vivo*, CC-EVs stabilized these constructs, which efficiently and reproducibly developed into cartilage with increased collagen deposition, minimal hypertrophy, and vessel ingrowth. On the contrary, cartilage formed with BMSC-EVs was characterized by hypertrophic differentiation accompanied by vascular ingrowth (Chen et al., 2018). Therefore, CCs could also be exploited to produce EVs, possibly even more committed to cartilage healing and homeostasis. This rationale relies on the nature of the EV cargo that is cell type specific and resembles the properties of the secreting cells. Consistently, when compared with ASCs or BMSCs, CCs derived from OA donors showed higher chondrogenic ability, superior basal secretion of growth factors and cytokines, and noteworthy immunomodulatory behavior (De Luca et al., 2019).

In this scenario, the use of EVs has the considerable advantage of being potentially well characterized in terms of their contents at the molecular level, including lipids, proteins, or miRNAs. In the last years, miRNA fingerprint in EVs from several cell types, including MSCs (Ferguson et al., 2018; Qiu et al., 2018), has started to be deciphered, shedding light on shuttled biological functions and providing a platform for dissecting the overall EV potential. Therefore, a deep characterization and comparison of EVs from different cell types in terms of miRNA content would allow the selection of the most effective drug-like formulation to be used as a therapeutic tool in each specific pathology, including

OA. In this perspective, specific EV-miRNA engineering (Tao et al., 2017) or modifications of their natural amounts due to variable secreting cells or stage of differentiation (Wang et al., 2018) were postulated as a next-generation approach. Nevertheless, to achieve a complete miRNA characterization, high-throughput quantitative miRNA expression analysis should be performed. Global mean normalization (Mestdagh et al., 2009) is the more reliable strategy to compare outcomes, although it implies the need of a large amount of collected EVs due to the very low nucleic acid amount per particle. While this is possible for basic research, in the therapeutic pipeline, this would be time-consuming and non-cost-effective. Therefore, reliable reference genes (RGs) would be needed to both validate high-throughput data and establish focused assays to characterize different batches. Nevertheless, to date, a universal miRNA RG has not been defined yet, and each EV type or experimental setting must be investigated (D'Haene et al., 2012). The purpose of the present study was to characterize the stability of putative EV-miRNA RGs in donor-matched ASCs, BMSCs, and CCs via bioinformatic tools. The selection of the most stable RGs will allow a reliable comparison of the content of the EVs obtained from three different tissue sources, as well as from different donors.

MATERIALS AND METHODS

Ethics Approval Statement

Institutional review board approval (San Raffaele Hospital Ethics Committee approval on 8 March 2018, registered under number 6/int/2018) was obtained and sampling performed after the procurement of patient informed consent and following the 1964 Helsinki declaration and its later amendments.

CCs, BMSCs, and ASCs Isolation and Expansion

Articular cartilage, bone marrow, and subcutaneous adipose tissue were collected from the same three osteoartritic patients (two females aged 53 and 56 years and one male aged 41 years, Kellgren–Lawrence III–IV) who underwent total hip arthroplasty. Cartilage was detached with a scalpel from non-weight-bearing superficial areas of femoral head/neck (removed to allow implant positioning) and enzymatically digested (37°C, 22 h) with 0.15% w/v type II collagenase (Worthington Biochemical, Lakewood, NJ, United States) (Lopa et al., 2013). Bone marrow coming out from the femoral canal was collected, washed in phosphate-buffered saline (PBS), and centrifuged, and BMSCs were isolated for plastic adherence (Lopa et al., 2011). A small waste amount of subcutaneous adipose from local hip fat deposit tissue was collected, and ASCs were isolated by enzymatic digestion (37°C, 30 min) with 0.075% w/v type I collagenase (Worthington Biochemical, Lakewood, NJ, United States) (Lopa et al., 2014).

The obtained CCs were cultured in high-glucose (4.5 mg/ml) Dulbecco's Modified Eagle Medium (DMEM), and ASCs and BMSCs were cultured in minimum essential medium (αMEM). All cells were supplemented with 10% fetal bovine serum (FBS, Lonza), 0.29 mg/ml L-glutamine, 100 U/ml penicillin, 100 μg/ml streptomycin, 10 mM 4-(2-hydroxyethyl)piperazine-1-ethanesulfonic acid (HEPES), and 1 mM sodium pyruvate (all reagents from Thermo Fisher Scientific, Waltham, MA, United States).

To preserve MSC chondrogenic potential, 5 ng/ml of fibroblast growth factor 2 (FGF-2) (PeproTech, Rocky Hill, NJ, United States) was added to BMSCs and ASCs (Solchaga et al., 2005; Liu and Wagner, 2012). All the cell types were cultured at 37°C, 5% CO_2, and 95% humidity.

Experiments with EVs were performed on cells at passage 3, and flow cytometry was performed at passage 4.

Cell Characterization

Flow cytometry analysis was performed on 2.5×10^5 cells incubated with anti-human primary monoclonal antibodies: CD14-FITC, CD34-biotinylated, CD44-FITC, CD45-FITC, and CD105-biotinylated (Ancell Corporation, Bayport, MN, United States) and CD90-FITC and CD73-PE (Miltenyi Biotec, Bergisch Gladbach, Germany). Streptavidin–phycoerythrin (PE) (Ancell Corporation, Bayport, MN, United States) was added to biotinylated stained cells. Data were acquired using a FACSCalibur flow cytometer collecting a minimum of 10,000 events and analyzed using CellQuest software (BD Biosciences, San Jose, CA, United States).

EV Isolation and Nanoparticle Tracking Analysis (NTA)

To obtain the cell supernatants, the cells at 90% confluency were washed three times with PBS, and a medium without FBS was added. After 48 h and cell viability check with a NucleoCounter NC-3000 (ChemoMetec, Allerød, Denmark), 30 ml of culture supernatants was collected and differentially centrifuged at 4°C to remove debris and floating cells at 376 × *g* for 15 min, 1,000 × *g* for 15 min, 2,000 × *g* for 15 min, and twice at 4,000 × *g* for 15 min each (cleared supernatant). Dilutions of 1:3 were performed in PBS, and 1 ml dilution was analyzed with the NanoSight LM10-HS system (NanoSight Ltd., Amesbury, United Kingdom) (Ragni et al., 2017). Five recordings of 60 s were conducted for each EV sample, and an NTA-dedicated software was used to provide both concentration measurements and high-resolution particle size distribution profiles.

EV Characterization

The cleared supernatants, as previously reported, were ultracentrifuged at 100,000 × *g* for 3 h at 4°C in a 70 Ti rotor (Beckman Coulter). The pellets were suspended in 100 μl of PBS and processed as follows:

(a) Transmission electron microscopy (TEM): 5 μl of EVs in PBS was absorbed on formvar carbon-coated grids for 10 min, and particles were negatively stained with 2% uranyl acetate aqueous suspension for 10 min. Samples were analyzed with a TALOS L120C TEM (Thermo Fisher Scientific, Waltham, MA, United States) at 120 kV.
(b) Flow cytometry: EVs were diluted at 1:150 in PBS, and 0.05 μM carboxyfluorescein succinimidyl ester (CFSE) staining was performed for 30 min at 37°C in the dark.

TABLE 1 | Candidate RGs and cartilage-related miRNAs and target sequences.

Accession number	Gene name	Target sequence (5'–3')	References
MIMAT0000062	let-7a-5p	UGAGGUAGUAGGUUGUAUAGUU	Cazzoli et al., 2013; Li et al., 2015a,b
MIMAT0000069	miR-16-5p	UAGCAGCACGUAAAUAUUGGCG	Ge et al., 2014; Lange et al., 2017
MIMAT0004495	miR-22-5p	AGUUCUUCAGUGGCAAGCUUUA	Lange et al., 2017
MIMAT0000078	miR-23a-3p	AUCACAUUGCCAGGGAUUUCC	Gouin et al., 2017
MIMAT0000082	miR-26a-5p	UUCAAGUAAUCCAGGAUAGGCU	Li et al., 2015a; Gouin et al., 2017
MIMAT0004503	miR-29a-5p	ACUGAUUUCUUUUGGUGUUCAG	Ragni et al., 2019d
MIMAT0000099	miR-101-3p	UACAGUACUGUGAUAACUGAA	Gouin et al., 2017
MIMAT0000101	miR-103a-3p	AGCAGCAUUGUACAGGGCUAUGA	Li et al., 2015b
MIMAT0000278	miR-221-3p	AGCUACAUUGUCUGCUGGGUUUC	Li et al., 2015a,b
MIMAT0004748	miR-423-5p	UGAGGGGCAGAGAGCGAGACUUU	Santovito et al., 2014
MIMAT0003393	miR-425-5p	AAUGACACGAUCACUCCCGUUGA	Santovito et al., 2014
MIMAT0003338	miR-660-5p	UACCCAUUGCAUAUCGGAGUUG	Ragni et al., 2019d
miRNA targets			
MIMAT0000093	miR-93-5p	CAAAGUGCUGUUCGUGCAGGUAG	Ding et al., 2019; Xue et al., 2019; Wu et al., 2020
MIMAT0000419	miR-27b-3p	UUCACAGUGGCUAAGUUCUGC	Akhtar et al., 2010; Wu et al., 2014, 2020
MIMAT0000423	miR-125b-5p	UCCCUGAGACCCUAACUUGUGA	Matsukawa et al., 2013; Wu et al., 2014, 2020
MIMAT0004784	miR-455-3p	GCAGUCCAUGGGCAUAUACAC	Swingler et al., 2012; Wu et al., 2014, 2020

EVs without CFSE were used as a mock sample. Then, 1 µl of antibodies (BioLegend, San Diego, CA, United States) anti-CD9-APC (HI9A), CD63-APC (H5C6), and CD81-APC (5A6) (for EV markers) or CD44-APC, CD73-APC, and CD90-APC (for stomal markers) was added separately to 20 µl of CFSE-EVs, and incubation was performed for 30 min at 4°C in the dark. After a further 1:7 dilution with PBS, samples were analyzed with a CytoFLEX flow cytometer with a 10 µl/min flow rate. At least 30,000 events were acquired. Events were compared with those obtained when running FITC fluorescent beads of 160, 200, 240, and 500 nm (Biocytex, Marseille, France), and PBS or unstained EVs were used to gate FITC-positive events. PBS samples supplemented with CFSE and/or antibodies were used as negative controls for background in FITC and APC channels (Ragni et al., 2020b).

Candidate miRNA RG Selection

According to the literature, 12 miRNAs were selected for stability analysis (**Table 1**; Cazzoli et al., 2013; Ge et al., 2014; Santovito et al., 2014; Li et al., 2015a,b; Gouin et al., 2017; Lange et al., 2017; Ragni et al., 2019d).

TABLE 2 | Immunophenotype of CCs, BMSCs, and ASCs as a percentage of marker positivity.

	ASCs	BMSCs	CCs
CD14	1.5 ± 0.6	2.6 ± 1.3	6.0 ± 0.3
CD34	0.8 ± 0.4	0.4 ± 0.4	2.2 ± 0.6
CD45	0.5 ± 0.6	0.2 ± 0.2	2.1 ± 1.1
CD44	99.5 ± 0.3	99.7 ± 0.1	96.3 ± 5.7
CD73	99.8 ± 0.2	99.8 ± 0.1	99.8 ± 0.0
CD90	75.2 ± 17.4	48.1 ± 19.8	98.4 ± 0.6
CD105	93.0 ± 1.9	97.3 ± 0.6	92.4 ± 6.0

RNA Isolation and miRNA Profiling

Five milliliters of cleared culture supernatants containing similar number of EVs (10.6×10^9 EVs ± 1.3) was 1:1 diluted in PBS and ultracentrifuged at 100,000 × *g* for 9 h at 4°C, and the pellet was frozen at -80°C until RNA extraction and miRNA profiling as previously reported (Ragni et al., 2019c). Briefly, before RNA extraction, *Arabidopsis thaliana* ath-miR-159a (30 pg) synthetic miRNA (Life Technologies, Foster City, CA, United States) was spiked in each sample to monitor the efficiency of RNA recovery by miRNeasy and RNeasy cleanup kits (Qiagen, Hilden, Germany), and cDNA synthesis was performed with standard reverse transcription and pre-amplification steps (Cavalleri et al., 2017). miRNA expression analysis with the OpenArray system (Life Technologies) was performed in 384-well OpenArray plates, and miRNAs with C_{RT} values >27 and Amp Score <1.24 were considered as not present, following manufacturer's instruction[1]. The mean of each sample was used to equalize subtle differences in the amount of starting RNA. The amplification values of the following assays (Life Technologies) were analyzed for stability: hsa-miR-22-5p 002301; hsa-miR-23a-3p 000399; hsa-miR-29a-5p 002447; hsa-miR-221-3p 000524; hsa-miR-423-5p 002340; hsa-miR-16-5p 000391; hsa-miR-26a-5p 000405; hsa-miR-103a-3p 000439; hsa-miR-101-3p 002253; hsa-let-7d-5p 002283; hsa-miR-425-5p 001516; and hsa-miR-660-5p 001515. The following assays for cartilage-related miRNA analysis (**Table 1**): hsa-miR-93-5p 001090; hsa-miR-125b-5p 000449; hsa-miR-455-3p 002244; and hsa-miR-27b-3p 000409 (Akhtar et al., 2010; Swingler et al., 2012; Matsukawa et al., 2013; Wu et al., 2014, 2020; Ding et al., 2019; Xue et al., 2019).

[1] https://www.thermofisher.com/document-connect/document-connect.html?url=https%3A%2F%2Fassets.thermofisher.com%2FTFS-Assets%2FLSG%2Fbrochures%2FCO28730-Crt-Tech-note_FLR.pdf&title=Q3J0LCBhIHJlbGF0aXZlIHRocmVzaG9sZCBtZXRob2QgZm9yIHFQQ1IgZGF0YSBhbmFseXNpcyBvbiB0aGUgUXVhbnRTdHVkaW8mdHJhZGU7IDEySyBGbGV4IHN5c3RlbSB3aXRoIE9wZW5BcnJheSZyZWc7IHRlY2hub2xvZ3k=

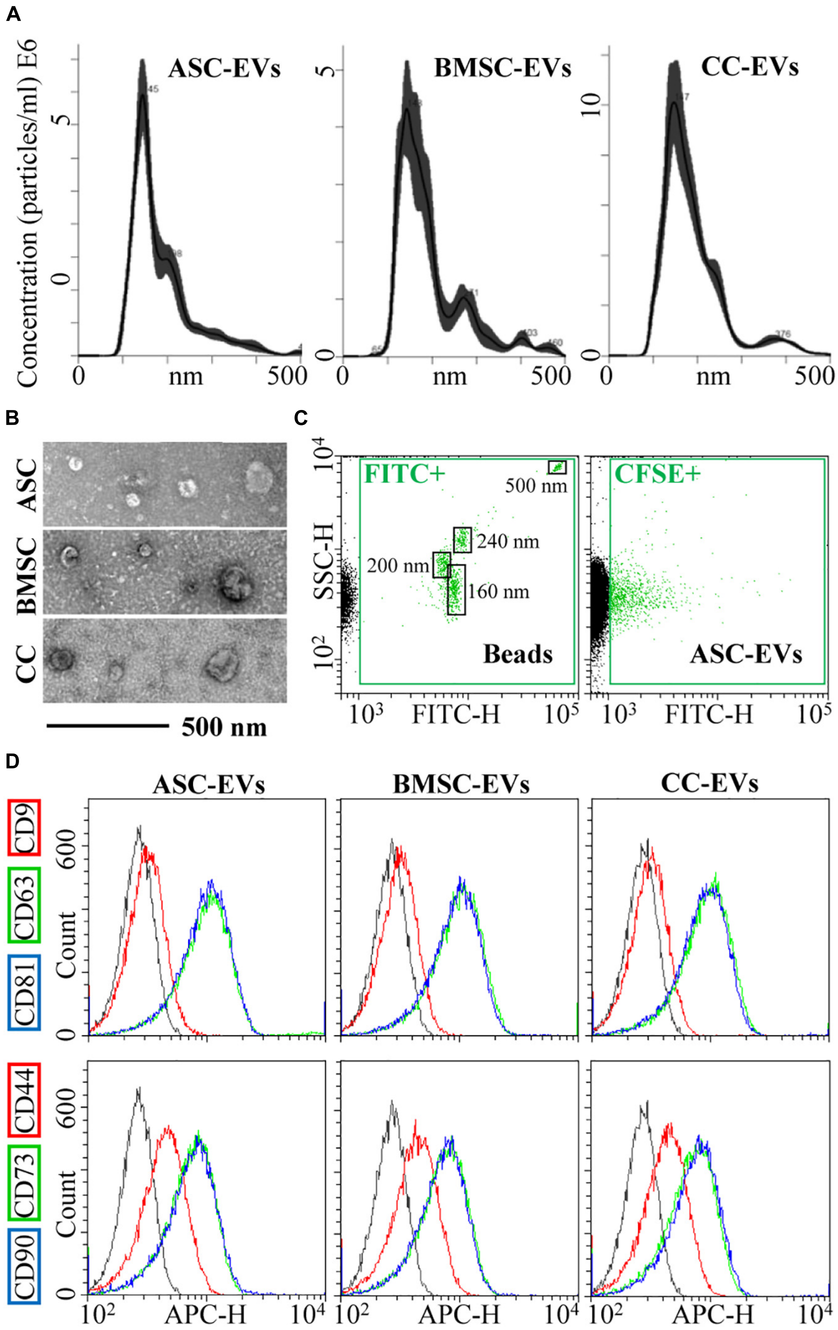

FIGURE 1 | CC-, BMSC-, and ASC-EV phenotype characterization. **(A)** Size distribution of nanoparticles by NanoSight particle tracking analysis. Representative plots are shown. **(B)** TEMs of EVs showing particles with characteristic cup-shaped morphology and size consistent with the NanoSight profile. **(C)** The resolution of the reference bead mix indicates the flow cytometer performance in light scattering at default settings. The first cytogram depicts the SSC-H vs. 535/35 (green fluorescence triggering) channel. Four fluorescent populations (160, 200, 240, and 500 nm) were resolved (FITC+ gate) from the instrument noise (in black). The second plot shows EVs stained with CFSE to allow their identification and gating in the FITC channel (CFSE+ gate) vs. background noise, debris, and unstained particles. **(D)** After CFSE+ gating, with respect to antibody-unstained samples (in gray), antibody-treated EVs showed the presence of EV-defining molecules CD63 and CD81, while CD9 staining gave a weak signal. EVs were also strongly positive for stromal markers CD73 and CD90, with CD44 labeling allowing a complete shift of the population although without a sharp separation with respect to antibody-unstained (gray curve) samples. Representative cytograms are presented.

Data Analysis

C_{RT} values of ath-miR-159 Ct spike-in were used for the equalization of technical differences during the whole process (Ragni et al., 2019c). geNorm, NormFinder, BestKeeper, and ΔCt method applets (Vandesompele et al., 2002; Andersen et al., 2004; Pfaffl et al., 2004; Silver et al., 2006) were used to assess miRNA RG stability. The geometric mean, hereafter indicated as geomean, of applet rankings was calculated, leading to an eventual consensus stability score.

Principal component analysis (PCA) plot and heat map were generated with the online package ClustVis[2] (Metsalu and Vilo, 2015). Raw C_{RT} values of miRNA RGs for heat map and cartilage-related miRNA C_{RT} values normalized with both stable miR-103a-3p/miR-22-5p and unstable miR-221-3p for PCA were analyzed. The following settings were used: for PCA, unit variance scaling was applied to rows; SVD with imputation was used to calculate principal components; and X and Y axes showed principal components 1 and 2; for heat map, rows were centered; unit variance scaling was applied to rows; and both rows and columns were clustered using correlation distance and average linkage.

Statistical Analysis

GraphPad Prism software version 5 (GraphPad, San Diego, CA, United States) was used to perform statistical analyses. Grubb's test was used to identify and exclude possible outliers. One-sample Student t-test with a significance level set at $p < 0.05$ was used when comparing BMSC-EVs and ASC-EVs with the amount of cartilage-related miRNAs with CC-EVs set as 1.

RESULTS

CCs, BMSCs, ASCs, and Derived EV Phenotypic Characterization

Flow cytometry analysis was used to confirm the immunophenotype of CCs, BMSCs, and ASCs. Characteristic MSC cell-surface antigens, including CD44, CD73, CD90, and CD105, were expressed, whereas hematoendothelial markers, such as CD14, CD34, and CD45, were not present (**Table 2**).

Cell viability after starvation always resulted to > 95%. EVs released by CCs, BMSCs, and ASCs were directly analyzed in the culture supernatant by NTA. All EVs were within the expected EV size range (mean of 181 nm ± 7 for CCs, 199 nm ± 9 for BMSCs, and 187 nm ± 5 for ASCs) (**Figure 1A**). D50, the size point below which 50% of the EVs are contained, resulted in 162 nm ± 7 for CCs, 175 nm ± 8 for BMSCs, and 161 nm ± 1 for ASCs, indicating enrichment in small vesicles. After ultracentrifugation, scanning electron microscopy showed the presence of particles within the expected size range, mainly between 50 and 250 nm, with the characteristic cup-shaped morphology (**Figure 1B**). The dimensional size range was confirmed by flow cytometry by direct comparison with FITC-labeled microbeads of defined size (160–200–240–500 nm) (**Figure 1C**), and particle integrity was assessed by positive CFSE staining (**Figure 1C**). Further, all particles strongly expressed both CD63 and CD81, consistent with previously reported characteristics of EVs (**Figure 1D**). CD9, another EV marker, staining gave a weak signal (**Figure 1D**). Eventually, stromal markers CD73 and CD90 showed a strong signal in fully and similarly labeled EVs collected from three cell types, while CD44

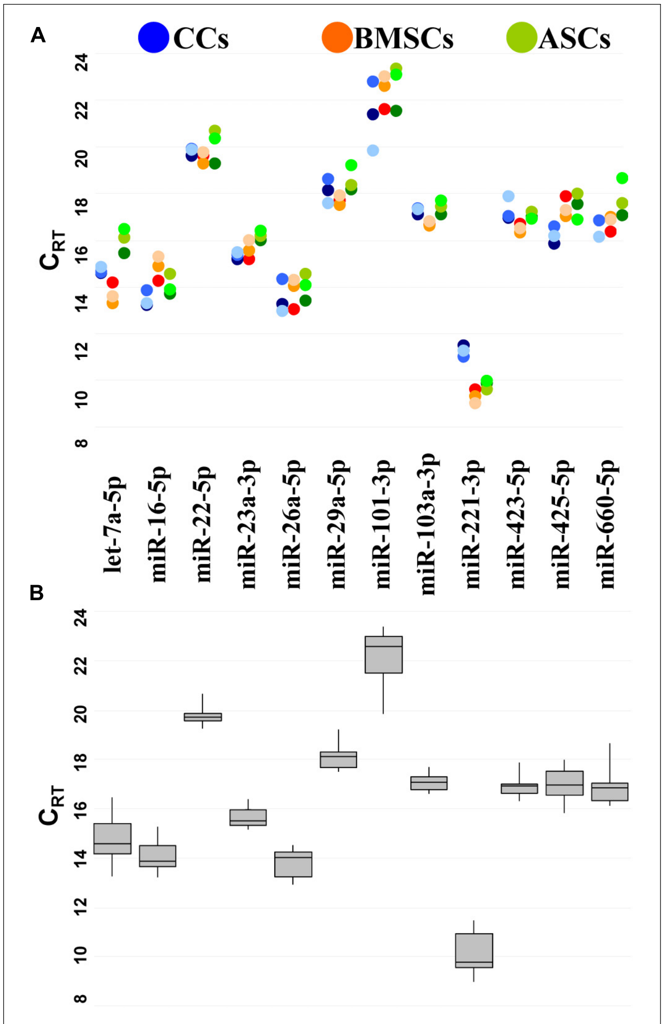

FIGURE 2 | Expression of candidate RG miRNAs in CC-, BMSC-, and ASC-EVs. **(A)** C_{RT} values for miRNA RGs in different donors. Color from dark to light stands for donors 1–3, respectively. **(B)** The box plot graphs of the C_{RT} values for each RG, regardless of the donor difference, illustrate the interquartile range (box) and median. The whisker plot depicts the range of the values.

resulted in a weaker signal, although the complete peak shift suggests a homogeneous staining of the particles rather than two distinct populations (**Figure 1D**).

Expression of Candidate RGs

To reduce likelihood of including co-regulated miRNAs in the stability analysis, miRNA genomic proximity was assessed. None of the 12 candidates resides in the same gene cluster, which makes their levels mutually independent. Then, the presence and amount of each RG were monitored by qRT-PCR. RGs were detected in all the samples at different levels of expression (**Figure 2A**).

miR-221-3p always had the lowest C_{RT} (high amount), whereas miR-101-3p the highest (**Figure 2B**). The difference between the most abundant miRNA, miR-221-3p in BMSC3 (C_{RT} 8.99), and the less expressed miRNA, miR-101-3p in ASC2

[2]https://biit.cs.ut.ee/clustvis/

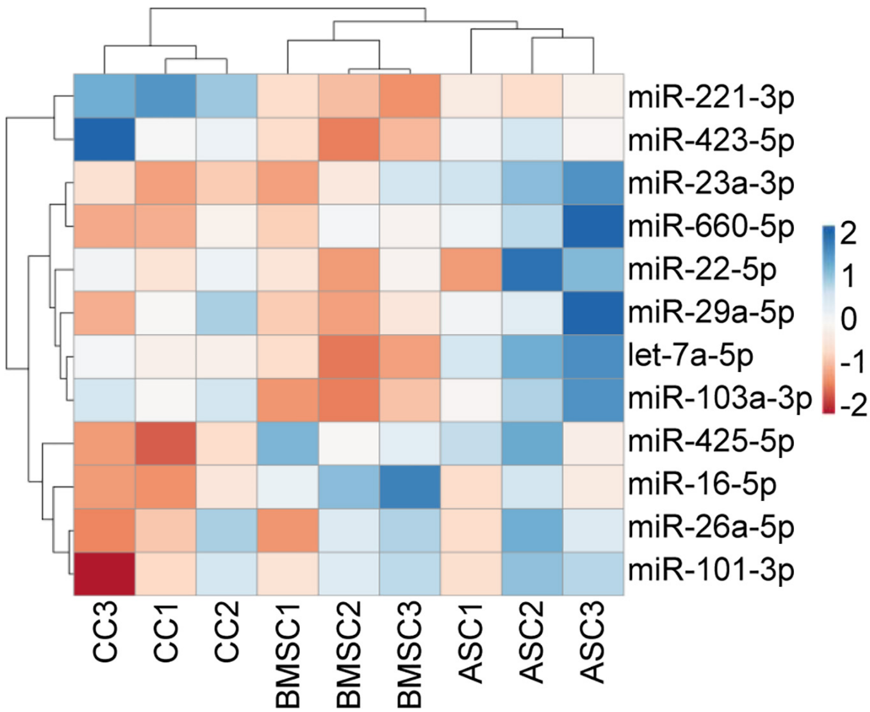

FIGURE 3 | Unsupervised hierarchical clustering for the miRNA RG C_{RT} values. In the dendrogram, each row represents a miRNA, and each column represents a sample. The sample clustering tree is shown at the top. The color scale shown in the map illustrates the relative expression levels of miRNAs across all samples: red shades represent high expression levels (low C_{RT}), and blue shades represent low expression levels (high C_{RT}).

(C_{RT} 23.35), indicates a range of expression along a 21,000-fold difference for the candidates under analysis. The majority of miRNAs were detected between 14 and 20 C_{RT} values.

RG Stability Analysis

Before performing the stability analysis of the 12 miRNA RGs under study, unsupervised hierarchical clustering was conducted on the qRT-PCR values. The heat map clearly showed that cell tissue source, and not the donor, tipped the scale toward the identification of similar molecular signatures, with MSCs (BMSCs and ASCs) clustering tighter and under the same node (**Figure 3**). In particular, with the donors taken into account, MSCs from donors 2 and 3 clustered together, whereas CCs from donor 2 was more similar to those of donor 1.

Following cluster analysis that shed light on the cell source similarity rather than the donor identity, four algorithms (geNorm, NormFinder, BestKeeper, and the comparative ΔCt method) were run, and geometric mean was used to rank the stability of the 12 RGs (**Table 3**). For all the cell types, miR-103a-3p was the most stable miRNA, whereas miR-101-3p was always ranked last. When MSCs (BMSC-EVs and ASC-EVs) were scored together, again miR-103a-3p was first in the ranking, with let-7a-5p emerging as less reliable and miR-101-3p once more being at the bottom of the list. Then, differences among donors were taken into account (**Table 4**). As appeared in the hierarchical clustering of the C_{RT} values, donors 1 and 2 were more similar, with miR-26-5p, being the most stable RG, and miR-221-3p in last and penultimate positions, respectively. For donor 3, miR-22-5p was the best RG, and miR-221-3p/miR-101-3p was at the bottom of the ranking. miR-103a-3p always laid in the first half of the list for the three donors, between the fourth and sixth positions.

Eventually, to obtain a definitive hierarchy, RG stability was calculated regardless of tissue source or donor, analyzing all the samples together (**Table 5**). miR-103a-3p was ranked first and miR-22-5p second, being in the top 3 positions in all algorithms used. On the contrary, miR-221-3p was at the end of the ranking, being in the last position in three algorithms out of four, making it an unfavorable choice.

Impact of RG Choice on the Quantification of Target Genes

Four miRNAs (miR-93-5p, miR-125b-5p, miR-455-3p, and miR-27b-3p), involved in cartilage homeostasis and OA pathology, were studied to evaluate the impact of the RG choice on the accurate expression of these selected miRNAs and on the most reliable establishment of similarities and differences between the three different EV types. Both stable (miR-103a-3p and miR-22-5p) and unreliable (miR-221-3p) RGs were used, with EVs from chondrocytes (CCs) as a touchstone.

Unsupervised clustering analysis of the three EV types was performed, and PCA, with principal components 1 and 2 explaining 99% of the variance, clearly showed that unreliable miR-221-3p led to a sharper separation of BMSC- and

ASC-EV samples with respect to CC-EVs (**Figure 4A**) that, as reported in **Figure 3**, appeared distinct from MSCs. Further, when using stable miR-103a-3p and miR-22-5p, BMSCs and ASCs grouped close and far from the samples normalized with miR-221-3p, indicating a similar outcome for the two most stable RGs.

TABLE 3 | Stability of candidate RGs in EVs from different cell types.

Source	Ranking	Geomean		Delta Ct		BestKeeper		NormFinder		geNorm	
CCs	1	miR-103a-3p	1.78	miR-22-5p	0.42	miR-23a-3p	0.10	miR-660-5p	0.02	miR-22-5p | miR-103a-3p	0.04
	2	miR-22-5p	2.00	miR-103a-3p	0.42	miR-103a-3p	0.10	miR-16-5p	0.04		
	3	miR-23a-3p	3.46	miR-16-5p	0.43	let-7a-5p	0.11	miR-425-5p	0.11	miR-23a-3p	0.06
	4	miR-16-5p	3.98	miR-23a-3p	0.45	miR-22-5p	0.12	miR-22-5p	0.18	let-7a-5p	0.09
	5	miR-660-5p	4.28	miR-425-5p	0.45	miR-221-3p	0.17	miR-103a-3p	0.19	miR-425-5p	0.18
	6	miR-425-5p	4.61	miR-660-5p	0.46	miR-425-5p	0.25	miR-23a-3p	0.27	miR-16-5p	0.21
	7	let-7a-5p	5.09	let-7a-5p	0.49	miR-16-5p	0.26	miR-29a-5p	0.30	miR-660-5p	0.24
	8	miR-221-3p	7.75	miR-29a-5p	0.57	miR-660-5p	0.32	let-7a-5p	0.36	miR-221-3p	0.30
	9	miR-29a-5p	8.21	miR-221-3p	0.64	miR-29a-5p	0.35	miR-26a-5p	0.47	miR-29a-5p	0.34
	10	miR-26a-5p	9.97	miR-26a-5p	0.66	miR-423-5p	0.40	miR-221-3p	0.51	miR-26a-5p	0.39
	11	miR-423-5p	10.74	miR-423-5p	0.78	miR-26a-5p	0.54	miR-423-5p	0.74	miR-423-5p	0.44
	12	miR-101-3p	12.00	miR-101-3p	1.38	miR-101-3p	1.00	miR-101-3p	1.37	miR-101-3p	0.60
BMSCs	1	miR-103a-3p	1.57	miR-103a-3p	0.38	miR-103a-3p	0.07	miR-29a-5p	0.03	miR-22-5p | miR-29a-5p	0.07
	2	miR-29a-5p	1.57	miR-29a-5p	0.39	miR-423-5p	0.12	miR-103a-3p	0.05		
	3	miR-22-5p	2.45	miR-22-5p	0.41	miR-29a-5p	0.14	miR-22-5p	0.17	miR-103a-3p	0.12
	4	miR-423-5p	3.36	miR-423-5p	0.42	miR-22-5p	0.18	miR-423-5p	0.24	miR-423-5p	0.15
	5	miR-23a-3p	6.12	miR-23a-3p	0.45	miR-221-3p	0.20	miR-23a-3p	0.24	miR-425-5p	0.25
	6	miR-660-5p	6.64	miR-660-5p	0.49	miR-660-5p	0.25	miR-660-5p	0.29	let-7a-5p	0.27
	7	miR-221-3p	6.88	miR-16-5p	0.51	miR-23a-3p	0.28	miR-16-5p	0.40	miR-221-3p	0.30
	8	miR-425-5p	7.54	miR-221-3p	0.58	miR-425-5p	0.33	miR-221-3p	0.48	miR-23a-3p	0.36
	9	miR-16-5p	8.37	miR-425-5p	0.60	let-7a-5p	0.34	miR-425-5p	0.56	miR-660-5p	0.40
	10	let-7a-5p	8.57	let-7a-5p	0.61	miR-16-5p	0.36	let-7a-5p	0.57	miR-16-5p	0.43
	11	miR-26a-5p	11.00	miR-26a-5p	0.64	miR-26a-5p	0.51	miR-26a-5p	0.60	miR-26a-5p	0.48
	12	miR-101-3p	12.00	miR-101-3p	0.67	miR-101-3p	0.53	miR-101-3p	0.65	miR-101-3p	0.51
ASCs	1	miR-103a-3p	1.41	miR-103a-3p	0.43	miR-423-5p	0.11	miR-103a-3p	0.09	miR-23a-3p | miR-103a-3p	0.10
	2	miR-23a-3p	1.68	miR-23a-3p	0.45	miR-23a-3p	0.14	miR-23a-3p	0.19		
	3	miR-423-5p	3.46	let-7a-5p	0.47	miR-221-3p	0.14	let-7a-5p	0.19	miR-221-3p	0.21
	4	let-7a-5p	4.05	miR-26a-5p	0.51	miR-103a-3p	0.21	miR-26a-5p	0.28	miR-423-5p	0.27
	5	miR-221-3p	5.20	miR-16-5p	0.53	miR-16-5p	0.33	miR-16-5p	0.33	let-7a-5p	0.33
	6	miR-16-5p	5.23	miR-423-5p	0.54	let-7a-5p	0.38	miR-423-5p	0.36	miR-16-5p	0.37
	7	miR-26a-5p	5.29	miR-22-5p	0.57	miR-26a-5p	0.39	miR-22-5p	0.41	miR-26a-5p	0.40
	8	miR-22-5p	8.15	miR-29a-5p	0.59	miR-425-5p	0.40	miR-29a-5p	0.46	miR-29a-5p	0.43
	9	miR-29a-5p	8.24	miR-221-3p	0.59	miR-29a-5p	0.42	miR-221-3p	0.46	miR-22-5p	0.45
	10	miR-660-5p	10.24	miR-660-5p	0.72	miR-22-5p	0.55	miR-660-5p	0.64	miR-660-5p	0.49
	11	miR-425-5p	10.84	miR-101-3p	0.76	miR-660-5p	0.59	miR-101-3p	0.67	miR-101-3p	0.53
	12	miR-101-3p	11.24	miR-425-5p	0.82	miR-101-3p	0.75	miR-425-5p	0.76	miR-425-5p	0.58
MSCs*	1	miR-103a-3p	1.41	miR-103a-3p	0.51	miR-423-5p	0.26	miR-103a-3p	0.11	miR-29a-5p | miR-103a-3p	0.23
	2	miR-23a-3p	2.45	miR-23a-3p	0.54	miR-221-3p	0.27	miR-23a-3p	0.15		
	3	miR-423-5p	2.45	miR-423-5p	0.57	miR-23a-3p	0.34	miR-423-5p	0.25	miR-23a-3p	0.26
	4	miR-29a-5p	3.50	miR-22-5p	0.59	miR-103a-3p	0.36	miR-22-5p	0.25	miR-423-5p	0.32
	5	miR-221-3p	4.36	miR-29a-5p	0.59	miR-425-5p	0.38	miR-29a-5p	0.31	miR-221-3p	0.34
	6	miR-22-5p	5.26	miR-221-3p	0.64	miR-29a-5p	0.43	miR-221-3p	0.40	miR-22-5p	0.39
	7	miR-26a-5p	7.24	miR-26a-5p	0.67	miR-26a-5p	0.45	miR-26a-5p	0.46	miR-660-5p	0.43
	8	miR-660-5p	8.18	miR-660-5p	0.71	miR-22-5p	0.46	miR-660-5p	0.50	miR-26a-5p	0.47
	9	miR-425-5p	8.41	miR-101-3p	0.77	miR-16-5p	0.47	miR-101-3p	0.61	miR-101-3p	0.52
	10	miR-101-3p	9.46	miR-425-5p	0.81	miR-660-5p	0.57	miR-425-5p	0.66	miR-425-5p	0.57
	11	miR-16-5p	10.46	miR-16-5p	0.95	miR-101-3p	0.64	miR-16-5p	0.86	miR-16-5p	0.62
	12	let-7a-5p	12.00	let-7a-5p	1.17	let-7a-5p	1.16	let-7a-5p	1.11	let-7a-5p	0.71

*Data from three different donors for each cell type were analyzed together to generate a miRNA stability ranking. *RG of BMSCs and ASCs scored together.*

Eventually, the differential amount of each candidate miRNAs was analyzed and compared to the value in CC-EVs that resulted in the less clustered sample in the PCA. Notably, the RG choice strongly altered the ratios between samples, exhorting a misleading conclusion (**Figure 4B**). With reliable RGs, miR-455-3p was downregulated (ratio 0.49, *p*-value 0.0032) in ASC-EVs using miR-103a-3p as RG, with a similar trend for miR-22-5p (ratio 0.57, *p*-value 0.0836). Also, miR-27b-3p got reduced in BMSC-EVs with both RGs. Conversely, when unreliable miR-221-3p was chosen for normalization, all four miRNAs appeared significantly downregulated with respect to CC-EVs. In fact, the mean modulation of the four miRNAs resulted to be 0.64 ± 0.28 and 0.80 ± 0.47 for BMSC- and ASC-EVs using miR-103a-3p, 0.81 ± 0.36 and 0.96 ± 0.55 with miR-22-5p, and 0.26 ± 0.10 and 0.27 ± 0.16 for miR-221-3p. Therefore, the best RG performers obtained through a computational approach allowed us to get closer to the true compositional variation by the reliable evaluation of subtle (around 2-fold) differences between donors.

DISCUSSION

In this study, among 12 putative stable EV-RGs, miR-103a-3p and miR-22-5p were found to be the most consistent for the reliable quantification of EV-embedded miRNAs released from donor-matched ASCs, BMSCs, and CCs.

EVs are biological delivery platforms used in cell-to-cell communication to shuttle a wide array of molecules, including proteins, lipids, and nucleic acids as miRNAs (Lotvall and Valadi, 2007). Due to their role in regulating physiological and

TABLE 4 | Stability of candidate RGs in EVs from single donors.

Source	Ranking	Geomean		ΔCt		BestKeeper		NormFinder		geNorm	
Donor1	1	miR-26a-5p	1.86	miR-26a-5p	0.44	miR-101-3p	0.09	miR-26a-5p	0.03	miR-29a-5p | miR-103a-3p	0.04
	2	miR-423-5p	2.21	miR-423-5p	0.45	miR-423-5p	0.13	miR-423-5p	0.03		
	3	miR-29a-5p	2.91	miR-29a-5p	0.47	miR-26a-5p	0.14	miR-101-3p	0.08	miR-423-5p	0.07
	4	miR-101-3p	2.94	miR-103a-3p	0.48	miR-22-5p	0.15	miR-29a-5p	0.15	miR-26a-5p	0.08
	5	miR-103a-3p	3.16	miR-101-3p	0.50	miR-29a-5p	0.20	miR-103a-3p	0.18	miR-101-3p	0.17
	6	miR-23a-3p	6.24	miR-23a-3p	0.54	miR-103a-3p	0.20	miR-23a-3p	0.29	miR-23a-3p	0.24
	7	miR-22-5p	6.73	miR-660-5p	0.57	miR-16-5p	0.35	miR-660-5p	0.33	miR-660-5p	0.29
	8	miR-660-5p	7.45	miR-22-5p	0.60	miR-23a-3p	0.35	miR-22-5p	0.34	miR-22-5p	0.32
	9	let-7a-5p	9.24	let-7a-5p	0.67	miR-660-5p	0.36	let-7a-5p	0.50	let-7a-5p	0.36
	10	miR-16-5p	9.46	miR-16-5p	0.75	let-7a-5p	0.46	miR-16-5p	0.58	miR-16-5p	0.43
	11	miR-425-5p	11.24	miR-425-5p	1.17	miR-221-3p	0.78	miR-425-5p	1.13	miR-425-5p	0.54
	12	miR-221-3p	11.74	miR-221-3p	1.21	miR-425-5p	0.83	miR-221-3p	1.18	miR-221-3p	0.66
Donor2	1	miR-26a-5p	2.21	miR-101-3p	0.46	miR-26a-5p	0.17	miR-423-5p	0.04	miR-23a-3p | miR-660-5p	0.05
	2	miR-101-3p	2.28	miR-423-5p	0.49	miR-101-3p	0.29	miR-26a-5p	0.08		
	3	miR-660-5p	2.66	miR-26a-5p	0.49	miR-660-5p	0.29	miR-101-3p	0.09	miR-101-3p	0.14
	4	miR-423-5p	2.78	miR-103a-3p	0.50	miR-23a-3p	0.32	miR-103a-3p	0.13	miR-26a-5p	0.20
	5	miR-23a-3p	3.60	miR-660-5p	0.51	miR-103a-3p	0.35	miR-660-5p	0.25	miR-423-5p	0.26
	6	miR-103a-3p	4.68	miR-23a-3p	0.53	miR-423-5p	0.35	miR-22-5p	0.25	miR-103a-3p	0.27
	7	miR-22-5p	7.17	miR-22-5p	0.57	miR-16-5p	0.38	miR-23a-3p	0.28	miR-22-5p	0.31
	8	miR-29a-5p	8.00	miR-29a-5p	0.63	miR-29a-5p	0.43	miR-29a-5p	0.42	miR-29a-5p	0.35
	9	miR-16-5p	9.15	miR-425-5p	0.70	miR-22-5p	0.48	miR-425-5p	0.55	miR-425-5p	0.40
	10	miR-425-5p	9.24	miR-16-5p	0.90	miR-425-5p	0.53	miR-16-5p	0.82	miR-16-5p	0.47
	11	miR-221-3p	11.00	miR-221-3p	1.08	miR-221-3p	0.69	miR-221-3p	1.02	miR-221-3p	0.57
	12	let-7a-5p	12.00	let-7a-5p	1.14	let-7a-5p	0.96	let-7a-5p	1.07	let-7a-5p	0.67
Donor3	1	miR-22-5p	1.68	miR-23a-3p	0.84	miR-22-5p	0.24	miR-22-5p	0.11	miR-26a-5p | miR-425-5p	0.20
	2	miR-23a-3p	2.06	miR-22-5p	0.87	miR-103a-3p	0.31	miR-23a-3p	0.16		
	3	miR-425-5p	3.16	miR-103a-3p	0.93	miR-23a-3p	0.32	miR-29a-5p	0.33	miR-23a-3p	0.35
	4	miR-103a-3p	3.31	miR-29a-5p	0.94	miR-425-5p	0.40	miR-103a-3p	0.36	miR-22-5p	0.46
	5	miR-26a-5p	3.83	miR-425-5p	0.97	miR-423-5p	0.53	miR-425-5p	0.50	miR-103a-3p	0.53
	6	miR-29a-5p	4.74	miR-26a-5p	0.98	miR-26a-5p	0.54	miR-26a-5p	0.53	miR-29a-5p	0.57
	7	miR-423-5p	7.33	miR-660-5p	1.21	miR-29a-5p	0.65	miR-660-5p	0.87	miR-660-5p	0.68
	8	miR-660-5p	7.65	miR-423-5p	1.32	miR-16-5p	0.76	miR-423-5p	1.10	miR-16-5p	0.78
	9	miR-16-5p	8.49	miR-16-5p	1.37	miR-221-3p	0.79	miR-16-5p	1.15	miR-423-5p	0.89
	10	let-7a-5p	10.24	let-7a-5p	1.47	miR-660-5p	0.96	let-7a-5p	1.24	let-7a-5p	0.99
	11	miR-221-3p	10.46	miR-221-3p	1.61	let-7a-5p	1.00	miR-221-3p	1.49	miR-221-3p	1.08
	12	miR-101-3p	12.00	miR-101-3p	1.76	miR-101-3p	1.42	miR-101-3p	1.64	miR-101-3p	1.19

Data from three different cell types for each donor were analyzed together to generate a miRNA stability ranking.

pathological molecular processes (O'Brien et al., 2018), miRNAs have been envisioned as therapeutic molecules (Chakraborty et al., 2017). This paradigm was recently applied to OA (Oliviero et al., 2019), also given the emerging roles of miRNA lack/gain in disease development (Wu et al., 2014, 2020). Therefore, due to their function as a shuttle, EVs were assumed to be a privileged means of miRNA vehicles and therapeutic biological particles for targeted therapies (Raimondo et al., 2019). In this perspective, a reliable normalization approach to compare the presence of potential therapeutic miRNAs between EV batches from different patients or tissue sources is imperative. This issue was recently debated for EVs from umbilical cord-derived MSCs for clinical approaches (Rohde et al., 2019), in order to facilitate translational research during the development and validation of these complex biological therapeutics. Nevertheless, for miRNAs, even when cellular, no univocal RGs have been released, and very often, each sample and each donor have to be tested for the most stable normalizers. To date, only few methods have been proposed. The most sensitive quantification approach is the miRNA global mean expression (Mestdagh et al., 2009). This strategy consists of the obtainment of the entire or at least a large portfolio of miRNome in all samples to be compared and the calculation of the mean expression value for each sample to be used as a normalizer. The major problem is the amount of required RNA that must be abundant enough to obtain the miRNome, especially when qRT-PCR technology is used. Due to the reduced RNA content per EV, approximately 70–25,000 small RNA molecules (Li et al., 2014) with miRNAs accounting only for around 30% of the total, this would imply that a large portion of each EV isolate would be needed for RG identification any time two different batches are compared. Although reasonable for research and preclinical studies aimed at identifying miRNA markers for a specific EV type or disease target, this would make the process economically unsustainable if used for clinical purposes. Thus, in view of translating basic research into potency assays to release disease-targeted EV batches, the availability of few donor/tissue/batch-independent and endogenous RGs is the most straightforward option (Pfaffl, 2001; Meyer et al., 2010; Schwarzenbach et al., 2015). As in cells, also in pure EVs or vesicle-enriched body fluids, U6 snRNA was suggested (Gray et al., 2015; Hayashi et al., 2017). Nevertheless, in recent reports scoring RG stability for EV-miRNAs, U6 snRNA was shown to be an unreliable candidate. In fact, similar to EVs released by cardiosphere-derived-cells (Gouin et al., 2017) and of particular importance for the cell types discussed in this manuscript, U6 snRNA performed poorly also in EVs released by MSCs isolated from adipose tissue (Ragni et al., 2019a,b,d) and amniotic membrane (Ragni et al., 2020a). This may be due to the mechanistical biogenesis of U6 snRNA that is processed by the Drosha complex in spite of the spliceosome (Lee et al., 2003).

Thus, for miRNAs and other small RNAs, it was postulated that miRNA RGs would be more appropriate. In this frame, in the last years, a bunch of reports identified few putative candidates in EVs from an array of different secreting cells (**Table 1**). Although of pioneering importance, as previously mentioned, a universal miRNA was not defined yet, possibly due to the still reduced number of datasets. In the present study, miR-103a-3p and miR-22-5p were found to be the best overall performers in the comparison of EVs released by CCs, BMSCs, and ASCs. The reported results highlight four crucial findings potentially useful for future comparative studies in the field of EVs:

(i) miR-22-5p was previously identified by our group as reliable EV-miRNA RG for ASCs (Ragni et al., 2019d), naïve or primed with IFNγ, as well as human placenta-derived MSCs (hAMSCs) (Ragni et al., 2020a). Similarly, in ASC-EVs, miR-103a-3p did not change its levels after IFNγ priming (Ragni et al., 2020b), although its absence in hAMSC-EVs (Ragni et al., 2020a) may raise the question of its reliability as a general MSC EV-miRNA RG. Also, both miRNAs were reported as being not influenced in BMSC-EVs by different conditions such as hypoxia or donor age (Zhu et al., 2018; Zhang et al., 2019; Boulestreau et al., 2020). Therefore, the presence of miR-22-5p as a stable miRNA in EVs from different MSC types under several conditions, as well as from CCs, opens the interesting possibility of its use as a reliable EV-miRNA RG to compare several MSCs and most likely any cells of stromal origin. To confirm this hypothesis, future comparative studies focused on miR-22-5p will be needed.

(ii) The tissue source rather than the donor tipped the scale in favor of fingerprint homogeneity (**Figure 3**). This is

TABLE 5 | Stability of candidate RGs through all samples.

Source	Ranking	Geomean		ΔCt		BestKeeper		NormFinder		GeNorm	
All	1	miR-103a-3p	1.32	miR-103a-3p	0.66	miR-103a-3p	0.29	miR-23a-3p	0.20	miR-22-5p | miR-103a-3p	0.31
	2	miR-22-5p	2.06	miR-23a-3p	0.67	miR-423-5p	0.30	miR-22-5p	0.21		
	3	miR-23a-3p	2.38	miR-22-5p	0.67	miR-22-5p	0.34	miR-103a-3p	0.23	miR-29a-5p	0.37
	4	miR-29a-5p	3.94	miR-29a-5p	0.70	miR-23a-3p	0.39	miR-29a-5p	0.28	miR-23a-3p	0.41
	5	miR-423-5p	5.12	miR-26a-5p	0.75	miR-29a-5p	0.40	miR-26a-5p	0.42	miR-26a-5p	0.48
	6	miR-26a-5p	5.23	miR-660-5p	0.80	miR-26a-5p	0.54	miR-660-5p	0.51	miR-660-5p	0.51
	7	miR-660-5p	6.24	miR-423-5p	0.83	miR-660-5p	0.55	miR-423-5p	0.58	miR-423-5p	0.56
	8	miR-425-5p	8.24	miR-425-5p	0.95	miR-16-5p	0.57	miR-425-5p	0.74	miR-425-5p	0.63
	9	miR-16-5p	8.74	miR-16-5p	0.96	miR-425-5p	0.58	miR-16-5p	0.77	miR-16-5p	0.68
	10	let-7a-5p	10.24	let-7a-5p	1.05	miR-221-3p	0.75	let-7a-5p	0.88	let-7a-5p	0.74
	11	miR-101-3p	11.24	miR-101-3p	1.11	let-7a-5p	0.82	miR-101-3p	0.97	miR-101-3p	0.79
	12	miR-221-3p	11.47	miR-221-3p	1.23	miR-101-3p	0.93	miR-221-3p	1.13	miR-221-3p	0.87

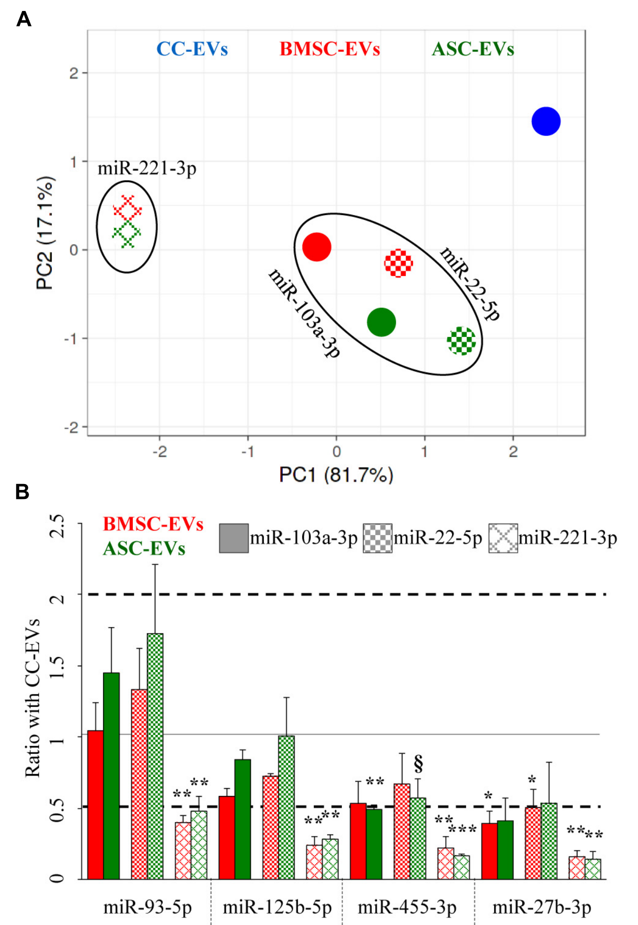

FIGURE 4 | Influence of RG selection on cartilage and OA-related EV-miRNA profile. **(A)** PCA for the BMSC- and ASC-EV molecular signature, based on the amount ratios with CC-EVs set as 1, of cartilage-related miRNAs after stable miR-103a-3p and miR-22-5p or unreliable miR-221-3p RG normalization. **(B)** Effects of RG normalization on the differential expression of single-cartilage-related miRNAs in BMSC- and ASC-EVs with respect to CC-EVs set as 1, $N = 3$, § $p < 0.1$, $^{*}p < 0.05$, $^{**}p < 0.01$, and $^{***}p < 0.001$.

of paramount importance, especially in view of clinical translation. In fact, it is reasonable to envision, for allogeneic use, biobanks formed of several EV batches grouped by the original tissue sources rather than by the different donors. Thus, when comparing two or more products with miRNA-based potency assays, e.g., CC-EV batches for cartilage regeneration, the use of cell-type-specific RGs would be of great help.

(iii) The ranking of the tissue sources and the donors differs, with miR-26a-5p being the best in two out of three donors but poor in stability in CCs, BMSCs, ASCs, and MSCs in general (**Tables 3, 4**). This suggests that in the unlikely, but possible, use of EVs for autologous applications, such as for cutting-edge approaches, where the most effective EV type has to be deciphered from those obtained by two or three tissue sources of the same patient, a different miRNA RG should be selected. miR-26a-5p can be a good starting point for CCs, BMSCs, and ASCs, but its variability between rankings suggests a specific and donor-guided validation.

(iv) Most importantly, even for allogeneic use, it is possible that a combination of tissue sources and donors will have to be screened and compared for the presence of miRNAs targeting a specific disease, if the most effective tissue source has not been defined yet. Only an integrated analysis will give solid outcomes, allowing potency assays to be reliably performed. In this perspective, for CC-, BMSC- and ASC-EVs, miR-103a-3p and miR-22-5p will be a milestone for therapeutic EV-miRNA fingerprint, while when assessing only BMSC- and ASC-EVs miR-103a-3p might be preferred, with miR-22-5p still being among the most stable ones and therefore again suggesting its overall reliability for EVs of mesenchymal origin.

Recently, on a global level, OA cartilage miRNA and mRNA sequencing data allowed the identification of an OA miRNA interactome (Coutinho de Almeida et al., 2019). Several miRNAs were found to regulate crucial pathways; therefore, both their upregulation and downregulation resulted in a key turning point in pathology. This led to the conclusion that EV batches, natural or bio-engineered with protective miRNAs and depleted of the destructive ones, might be more therapeutically relevant, and their comparison, at least for few disease-related candidates, might allow a proper selection. Although covering all the miRNAs related to OA is outside of this study's scope, we demonstrated the dramatic effect of suboptimal miRNA RG choice on four molecules affecting OA cartilage at different levels, allowing for a sharper definition of their abundance, as close as possible to real levels that, *a priori*, are impossible to know. miR-93-5p is significantly downregulated in the articular cartilages of OA mice, and its overexpression enhances viability, improves apoptosis, and attenuates the inflammatory response in chondrocytes (Ding et al., 2019). Also, miR-125b-5p is downregulated in OA chondrocytes, and its artificial augmentation suppressed the IL-1β-induced upregulation of its target aggrecanase-1 (Matsukawa et al., 2013). On the contrary, miR-455-3p was reported to be highly expressed in human OA cartilage (Swingler et al., 2012). Nevertheless, its upregulation was protective since miR-455-3p promotes TGF-β/Smad signaling inhibiting cartilage degeneration (Hu et al., 2019) and increasing the expression of cartilage-specific genes, and its deletion in mice leads to accelerated cartilage degeneration (Sun et al., 2018). Eventually, already 10 years ago, IL-1β was shown to downregulate miR-27b-3p in human chondrocytes, ending in the increased levels of its target and destructive proteinase MMP-13 (Akhtar et al., 2010). These results thus indicate that the four miRNAs are potential therapeutic agents for the treatment of OA, and their presence/enrichment in therapeutic EVs is a powerful tool. In this frame, the suboptimal choice of RGs, like miR-221-3p, led to an apparent reduction for all analyzed miRNAs in MSCs vs. CCs, erroneously suggesting a reduced therapeutic potential for EVs from BMSCs and ASCs. Future studies on other cartilage- and OA-related miRNAs, and more generally on those miRNAs involved in pathologies that are target of regenerative medicine approaches for a wider clinical translation, will be needed. This will give a more complete picture to compare the presence and/or absence of potentially therapeutic/destructive miRNAs in CC-, BMSC-, and ASC-derived EVs and to develop potency assays for off-the-shelf clinical products.

CONCLUSION

EVs from MSCs and CCs have already shown promising results *in vitro* and *in vivo* for the treatment of cartilage-related pathologies like OA. A deep characterization of their content at the molecular level remains a challenge due to the complexity of both cargo and target gene networks. In view of clinical translation, only the definition of reliable RGs will allow a correct quantification of therapeutically relevant embedded molecules, like miRNAs, to develop disease-focused potency assays and compare either cell/tissue sources or donors to make CC-, BMSC-, and ASC-EVs safe and efficacious cell-based miRNA delivery platforms for regenerative medicine-based approaches.

DATA AVAILABILITY STATEMENT

The datasets presented in this study can be found in online repositories. The names of the repository/repositories and accession number(s) can be found below: https://osf.io/yz6fq/?view_only=e65affa38ae546899bb4112bf4c728f2.

ETHICS STATEMENT

The studies involving human participants were reviewed and approved by the San Raffaele Hospital Ethics Committee approval on date 8 March 2018, registered under number 6/int/2018. The patients/participants provided their written informed consent to participate in this study.

AUTHOR CONTRIBUTIONS

AC and ER: conception and design, collection and assembly of the data, data analysis and interpretation, manuscript writing, and final approval of the manuscript. LdG: financial and administrative support and final approval of the manuscript. PDL and FL: collection and assembly of the data and final approval of the manuscript. MV: statistical analysis and final approval of the manuscript. CPO and LZ: data analysis and interpretation and final approval of the manuscript. All authors contributed to the article and approved the submitted version.

FUNDING

This research was financially supported by the Italian Ministry of Health "Ricerca Corrente."

ACKNOWLEDGMENTS

We want to thank all healthcare workers of IRCCS Istituto Ortopedico Galeazzi for their exceptional work during the COVID-19 pandemic, which allowed the proceedings of the research activity and the preparation of this manuscript.

REFERENCES

Akhtar, N., Rasheed, Z., Ramamurthy, S., Anbazhagan, A. N., Voss, F. R., and Haqqi, T. M. (2010). MicroRNA-27b regulates the expression of matrix metalloproteinase 13 in human osteoarthritis chondrocytes. *Arthritis Rheum.* 62, 1361–1371. doi: 10.1002/art.27329

Andersen, C. L., Jensen, J. L., and Ørntoft, T. F. (2004). Normalization of real-time quantitative reverse transcription-PCR data: a model-based variance estimation approach to identify genes suited for normalization, applied to bladder and colon cancer data sets. *Cancer Res.* 64, 5245–5250. doi: 10.1158/0008-5472.can-04-0496

Barkholt, L., Flory, E., Jekerle, V., Lucas-Samuel, S., Ahnert, P., Bisset, L., et al. (2013). Risk of tumorigenicity in mesenchymal stromal cell-based therapies–bridging scientific observations and regulatory viewpoints. *Cytotherapy* 15, 753–759. doi: 10.1016/j.jcyt.2013.03.005

Boopalan, P., Varghese, V. D., Sathishkumar, S., Arumugam, S., and Amarnath, V. (2019). Similar regeneration of articular cartilage defects with autologous & allogenic chondrocytes in a rabbit model. *Indian J. Med. Res.* 149, 650–655. doi: 10.4103/ijmr.IJMR_1233_17

Boulestreau, J., Maumus, M., Rozier, P., Jorgensen, C., and Noël, D. (2020). Mesenchymal stem cell derived extracellular vesicles in aging. *Front. Cell Dev. Biol.* 8:107. doi: 10.3389/fcell.2020.00107

Brittberg, M., Lindahl, A., Nilsson, A., Ohlsson, C., Isaksson, O., and Peterson, L. (1994). Treatment of deep cartilage defects in the knee with autologous chondrocyte transplantation. *N. Engl. J. Med.* 331, 889–895. doi: 10.1056/NEJM199410063311401

Cavalleri, T., Angelici, L., Favero, C., Dioni, L., Mensi, C., Bareggi, C., et al. (2017). Plasmatic extracellular vesicle microRNAs in malignant pleural mesothelioma and asbestos-exposed subjects suggest a 2-miRNA signature as potential biomarker of disease. *PLoS One* 12:e0176680. doi: 10.1371/journal.pone.0176680

Cazzoli, R., Buttitta, F., Di Nicola, M., Malatesta, S., Marchetti, A., Rom, W. N., et al. (2013). microRNAs derived from circulating exosomes as noninvasive biomarkers for screening and diagnosing lung cancer. *J. Thorac. Oncol.* 8, 1156–1162. doi: 10.1097/JTO.0b013e318299ac32

Chakraborty, C., Sharma, A. R., Sharma, G., Doss, C. G. P., and Lee, S. S. (2017). Therapeutic miRNA and siRNA: moving from bench to clinic as next generation medicine. *Mol. Ther. Nucleic Acids* 8, 132–143. doi: 10.1016/j.omtn.2017.06.005

Chen, Y., Xue, K., Zhang, X., Zheng, Z., and Liu, K. (2018). Exosomes derived from mature chondrocytes facilitate subcutaneous stable ectopic chondrogenesis of cartilage progenitor cells. *Stem Cell Res. Ther.* 9:318. doi: 10.1186/s13287-018-1047-2

Cho, P. S., Messina, D. J., Hirsh, E. L., Chi, N., Goldman, S. N., Lo, D. P., et al. (2008). Immunogenicity of umbilical cord tissue derived cells. *Blood* 111, 430–438. doi: 10.1182/blood-2007-03-078774

Colombini, A., Perucca Orfei, C., Kouroupis, D., Ragni, E., De Luca, P., ViganÒ, M., et al. (2019). Mesenchymal stem cells in the treatment of articular cartilage degeneration: New biological insights for an old-timer cell. *Cytotherapy* 21, 1179–1197. doi: 10.1016/j.jcyt.2019.10.004

Cosenza, S., Ruiz, M., Toupet, K., Jorgensen, C., and Noël, D. (2017). Mesenchymal stem cells derived exosomes and microparticles protect cartilage and bone from degradation in osteoarthritis. *Sci. Rep.* 7:16214. doi: 10.1038/s41598-017-15376-8

Coutinho de Almeida, R., Ramos, Y. F. M., Mahfouz, A., den Hollander, W., Lakenberg, N., Houtman, E., et al. (2019). RNA sequencing data integration reveals an miRNA interactome of osteoarthritis cartilage. *Ann. Rheum. Dis.* 78, 270–277. doi: 10.1136/annrheumdis-2018-213882

De Luca, P., Kouroupis, D., and Viganò, M. (2019). Human diseased articular cartilage contains a mesenchymal stem cell-like population of chondroprogenitors with strong immunomodulatory responses. *J. Clin. Med.* 8:423. doi: 10.3390/jcm8040423

D'Haene, B., Mestdagh, P., Hellemans, J., and Vandesompele, J. (2012). miRNA expression profiling: from reference genes to global mean normalization. *Methods Mol. Biol.* 822, 261–272. doi: 10.1007/978-1-61779-427-8_18

Ding, Y., Wang, L., Zhao, Q., Wu, Z., and Kong, L. (2019). MicroRNA-93 inhibits chondrocyte apoptosis and inflammation in osteoarthritis by targeting the TLR4/NF-κB signaling pathway. *Int. J. Mol. Med.* 43, 779–790. doi: 10.3892/ijmm.2018.4033

Ferguson, S. W., Wang, J., Lee, C. J., Liu, M., Neelamegham, S., Canty, J. M., et al. (2018). The microRNA regulatory landscape of MSC-derived exosomes: a systems view. *Sci. Rep.* 8:1419. doi: 10.1038/s41598-018-19581-x

Ge, Q., Zhou, Y., Lu, J., Bai, Y., Xie, X., and Lu, Z. (2014). miRNA in plasma exosome is stable under different storage conditions. *Molecules* 19, 1568–1575. doi: 10.3390/molecules19021568

Gouin, K., Peck, K., Antes, T., Johnson, J. L., Li, C., and Vaturi, S. D. (2017). A comprehensive method for identification of suitable reference genes in extracellular vesicles. *J. Extracell. Vesicles* 6:1347019. doi: 10.1080/20013078.2017.1347019

Gray, W. D., French, K. M., Ghosh-Choudhary, S., Maxwell, J. T., Brown, M. E., Platt, M. O., et al. (2015). Identification of therapeutic covariant microRNA clusters in hypoxia-treated cardiac progenitor cell exosomes using systems biology. *Circ. Res.* 116, 255–263. doi: 10.1161/circresaha.116.304360

Gupta, P. K., Chullikana, A., Rengasamy, M., Shetty, N., Pandey, V., Agarwal, V., et al. (2016). Efficacy and safety of adult human bone marrow-derived, cultured, pooled, allogeneic mesenchymal stromal cells (Stempeucel§): preclinical and clinical trial in osteoarthritis of the knee joint. *Arthritis Res. Ther.* 18:301. doi: 10.1186/s13075-016-1195-7

Hayashi, T., Lombaert, I. M., Hauser, B. R., Patel, V. N., and Hoffman, M. P. (2017). Exosomal microRNA transport from salivary mesenchyme regulates epithelial progenitor expansion during organogenesis. *Dev. Cell* 40, 95–103. doi: 10.1016/j.devcel.2016.12.001

Hu, S., Zhao, X., Mao, G., Zhang, Z., Wen, X., Zhang, C., et al. (2019). MicroRNA-455-3p promotes TGF-β signaling and inhibits osteoarthritis development by directly targeting PAK2. *Exp. Mol. Med.* 51, 1–13. doi: 10.1038/s12276-019-0322-3

Kim, S. H., Ha, C. W., and Park, Y. B. (2019). Intra-articular injection of mesenchymal stem cells for clinical outcomes and cartilage repair in osteoarthritis of the knee: a meta-analysis of randomized controlled trials. *Arch. Orthop. Trauma Surg.* 139, 971–980. doi: 10.1007/s00402-019-03140-8

Kreuz, P. C., and Kalkreuth, R. H. (2019). Long-term clinical and MRI results of matrix-assisted autologous chondrocyte implantation for articular cartilage defects of the knee. *Cartilage* 10, 305–313. doi: 10.1177/1947603518756463

Lange, T., Stracke, S., Rettig, R., Lendeckel, U., Kuhn, J., Schlüter, R., et al. (2017). Identification of miR-16 as an endogenous reference gene for the normalization of urinary exosomal miRNA expression data from CKD patients. *PLoS One* 12:e0183435. doi: 10.1371/journal.pone.0183435

Lee, Y., Ahn, C., Han, J., Choi, H., Kim, J., Yim, J., et al. (2003). The nuclear RNase III Drosha initiates microRNA processing. *Nature* 425, 415–419. doi: 10.1038/nature01957

Li, M., Zeringer, E., Barta, T., Schageman, J., Cheng, A., and Vlassov, A. V. (2014). Analysis of the RNA content of the exosomes derived from blood serum and urine and its potential as biomarkers. *Philos. Trans. R. Soc. Lond. B Biol. Sci.* 369:20130502. doi: 10.1098/rstb.2013.0502

Li, Y., Xiang, G. M., Liu, L. L., Liu, C., Liu, F., Jiang, D. N., et al. (2015a). Assessment of endogenous reference gene suitability for serum exosomal microRNA expression analysis in liver carcinoma resection studies. *Mol. Med. Rep.* 12, 4683–4691. doi: 10.3892/mmr.2015.3919

Li, Y., Zhang, L., Liu, F., Xiang, G., Jiang, D., and Pu, X. (2015b). Identification of endogenous controls for analyzing serum exosomal miRNA in patients with hepatitis B or hepatocellular carcinoma. *Dis. Markers* 2015:893594. doi: 10.1155/2015/893594

Liu, X., Shortt, C., Zhang, F., Bater, M. Q., Cowman, M. K., and Kirsch, T. (2020). Extracellular vesicles released from articular chondrocytes play a major role in cell-cell communication. *J. Orthop. Res.* 38, 731–739. doi: 10.1002/jor.24525

Liu, Y., and Wagner, D. R. (2012). Effect of expansion media containing fibroblast growth factor-2 and dexamethasone on the chondrogenic potential of human adipose-derived stromal cells. *Cell Biol. Int.* 36, 611–615. doi: 10.1042/cbi20110503

Lohan, P., Treacy, O., Lynch, K., Barry, F., Murphy, M., Griffin, M. D., et al. (2016). Culture expanded primary chondrocytes have potent immunomodulatory properties and do not induce an allogeneic immune response. *Osteoarthritis Cartilage* 24, 521–533. doi: 10.1016/j.joca.2015.10.005

Lopa, S., Colombini, A., de Girolamo, L., Sansone, V., and Moretti, M. (2011). New strategies in cartilage tissue engineering for osteoarthritic patients: infrapatellar fat pad as an alternative source of progenitor cells. *J. Biomater. Tissue Eng.* 1, 40–48. doi: 10.1166/jbt.2011.1010

Lopa, S., Colombini, A., Moretti, M., and de Girolamo, L. (2019). Injective mesenchymal stem cell-based treatments for knee osteoarthritis: from mechanisms of action to current clinical evidences. *Knee Surg. Sports Traumatol. Arthrosc.* 27, 2003–2020. doi: 10.1007/s00167-018-5118-9

Lopa, S., Colombini, A., Sansone, V., Preis, F. W., and Moretti, M. (2013). Influence on chondrogenesis of human osteoarthritic chondrocytes in co-culture with donor-matched mesenchymal stem cells from infrapatellar fat pad and subcutaneous adipose tissue. *Int. J. Immunopathol. Pharmacol.* 26(Suppl. 1), 23–31. doi: 10.1177/03946320130260s104

Lopa, S., Colombini, A., Stanco, D., de Girolamo, L., Sansone, V., and Moretti, M. (2014). Donor-matched mesenchymal stem cells from knee infrapatellar and subcutaneous adipose tissue of osteoarthritic donors display differential chondrogenic and osteogenic commitment. *Eur. Cell Mater.* 27, 298–311. doi: 10.22203/ecm.v027a21

Lotvall, J., and Valadi, H. (2007). Cell to cell signalling via exosomes through esRNA. *Cell Adh. Migr.* 1, 156–158. doi: 10.4161/cam.1.3.5114

Manferdini, C., Maumus, M., Gabusi, E., Piacentini, A., Filardo, G., Peyrafitte, J. A., et al. (2013). Adipose-derived mesenchymal stem cells exert antiinflammatory effects on chondrocytes and synoviocytes from osteoarthritis patients through prostaglandin E2. *Arthritis Rheum.* 65, 1271–1281. doi: 10.1002/art.37908

Matsukawa, T., Sakai, T., Yonezawa, T., Hiraiwa, H., Hamada, T., Nakashima, M., et al. (2013). MicroRNA-125b regulates the expression of aggrecanase-1 (ADAMTS-4) in human osteoarthritic chondrocytes. *Arthritis Res. Ther.* 15:R28. doi: 10.1186/ar4164

Mestdagh, P., Van Vlierberghe, P., De Weer, A., Muth, D., Westermann, F., Speleman, F., et al. (2009). A novel and universal method for microRNA RT-qPCR data normalization. *Genome Biol.* 10:R64. doi: 10.1186/gb-2009-10-6-r64

Metsalu, T., and Vilo, J. (2015). ClustVis: a web tool for visualizing clustering of multivariate data using Principal Component Analysis and heatmap. *Nucleic Acids Res.* 43, W566–W570. doi: 10.1093/nar/gkv468

Meyer, S. U., Pfaffl, M. W., and Ulbrich, S. E. (2010). Normalization strategies for microRNA profiling experiments: a 'normal' way to a hidden layer of complexity? *Biotechnol. Lett.* 32, 1777–1788. doi: 10.1007/s10529-010-0380-z

Moroni, L., and Fornasari, P. M. (2013). Human mesenchymal stem cells: a bank perspective on the isolation, characterization and potential of alternative sources for the regeneration of musculoskeletal tissues. *J. Cell Physiol.* 228, 680–687. doi: 10.1002/jcp.24223

Moskalewski, S., Hyc, A., and Osiecka-Iwan, A. (2002). Immune response by host after allogeneic chondrocyte transplant to the cartilage. *Microsc. Res. Tech.* 58, 3–13. doi: 10.1002/jemt.10110

Niemeyer, P., Albrecht, D., Andereya, S., Angele, P., Ateschrang, A., Aurich, M., et al. (2016). Autologous chondrocyte implantation (ACI) for cartilage defects of the knee: a guideline by the working group "Clinical Tissue Regeneration" of the German Society of Orthopaedics and Trauma (DGOU). *Knee* 23, 426–435. doi: 10.1016/j.knee.2016.02.001

O'Brien, J., Hayder, H., Zayed, Y., and Peng, C. (2018). Overview of MicroRNA biogenesis, mechanisms of actions, and circulation. *Front. Endocrinol. (Lausanne)* 9:402. doi: 10.3389/fendo.2018.00402

Oliviero, A., Della Porta, G., Peretti, G. M., and Maffulli, N. (2019). MicroRNA in osteoarthritis: physiopathology, diagnosis and therapeutic challenge. *Br. Med. Bull.* 130, 137–147. doi: 10.1093/bmb/ldz015

Pfaffl, M. W. (2001). A new mathematical model for relative quantification in real-time RT-PCR. *Nucleic Acids Res.* 29:e45. doi: 10.1093/nar/29.9.e45

Pfaffl, M. W., Tichopad, A., Prgomet, C., and Neuvians, T. P. (2004). Determination of stable housekeeping genes, differentially regulated target genes and sample integrity: BestKeeper–Excel-based tool using pair-wise correlations. *Biotechnol. Lett.* 26, 509–515. doi: 10.1023/b:bile.0000019559.84305.47

Platas, J., Guillén, M. I., del Caz, M. D., Gomar, F., Mirabet, V., and Alcaraz, M. J. (2013). Conditioned media from adipose-tissue-derived mesenchymal stem cells downregulate degradative mediators induced by interleukin-1β in osteoarthritic chondrocytes. *Mediat. Inflamm.* 2013:357014. doi: 10.1155/2013/357014

Platas, J., Guillén, M. I., Pérez Del Caz, M. D., Gomar, F., Castejón, M. A., Mirabet, V., et al. (2016). Paracrine effects of human adipose-derived mesenchymal stem cells in inflammatory stress-induced senescence features of osteoarthritic chondrocytes. *Aging (Albany NY)* 8, 1703–1717. doi: 10.18632/aging.101007

Qiu, G., Zheng, G., Ge, M., Wang, J., Huang, R., Shu, Q., et al. (2018). Mesenchymal stem cell-derived extracellular vesicles affect disease outcomes via transfer of microRNAs. *Stem Cell Res. Ther.* 9:320. doi: 10.1186/s13287-018-1069-9

Ragni, E., Banfi, F., Barilani, M., Cherubini, A., Parazzi, V., Larghi, P., et al. (2017). Extracellular vesicle-shuttled mRNA in mesenchymal stem cell communication. *Stem Cells* 35, 1093–1105. doi: 10.1002/stem.2557

Ragni, E., De Luca, P., Perucca Orfei, C., Colombini, A., Viganò, M., Lugano, G., et al. (2019a). Insights into inflammatory priming of adipose-derived mesenchymal stem cells: validation of extracellular vesicles-embedded miRNA reference genes as a crucial step for donor selection. *Cells* 8:369. doi: 10.3390/cells8040369

Ragni, E., Perucca Orfei, C., De Luca, P., and Colombini, A. (2019b). Identification of miRNA reference genes in extracellular vesicles from adipose derived mesenchymal stem cells for studying osteoarthritis. *Int. J. Mol. Sci.* 20:1108. doi: 10.3390/ijms20051108

Ragni, E., Perucca Orfei, C., De Luca, P., Lugano, G., Vigano, M., Colombini, A., et al. (2019c). Interaction with hyaluronan matrix and miRNA cargo as contributors for in vitro potential of mesenchymal stem cell-derived extracellular vesicles in a model of human osteoarthritic synoviocytes. *Stem Cell Res. Ther.* 10:109. doi: 10.1186/s13287-019-1215-z

Ragni, E., Perucca Orfei, C., De Luca, P., Mondadori, C., Viganò, M., Colombini, A., et al. (2020b). Inflammatory priming enhances mesenchymal stromal cell secretome potential as a clinical product for regenerative medicine approaches through secreted factors and EV-miRNAs: the example of joint disease. *Stem Cell Res. Ther.* 11:165. doi: 10.1186/s13287-020-01677-9

Ragni, E., Perucca Orfei, C., De Luca, P., Viganò, M., Colombini, A., Lugano, G., et al. (2019d). miR-22-5p and miR-29a-5p are reliable reference genes for analyzing extracellular vesicle-associated miRNAs in adipose-derived mesenchymal stem cells and are stable under inflammatory priming mimicking osteoarthritis condition. *Stem Cell Rev. Rep.* 15, 743–754. doi: 10.1007/s12015-019-09899-y

Ragni, E., Perucca Orfei, C., Silini, A. R., Colombini, A., Viganò, M., Parolini, O., et al. (2020a). miRNA reference genes in extracellular vesicles released from amniotic membrane-derived mesenchymal stromal cells. *Pharmaceutics* 12:347. doi: 10.3390/pharmaceutics12040347

Raimondo, S., Giavaresi, G., Lorico, A., and Alessandro, R. (2019). Extracellular vesicles as biological shuttles for targeted therapies. *Int. J. Mol. Sci.* 20:1848. doi: 10.3390/ijms20081848

Rohde, E., Pachler, K., and Gimona, M. (2019). Manufacturing and characterization of extracellular vesicles from umbilical cord-derived mesenchymal stromal cells for clinical testing. *Cytotherapy* 21, 581–592. doi: 10.1016/j.jcyt.2018.12.006

Russo, F. P., Alison, M. R., Bigger, B. W., Amofah, E., Florou, A., Amin, F., et al. (2006). The bone marrow functionally contributes to liver fibrosis. *Gastroenterology* 130, 1807–1821. doi: 10.1053/j.gastro.2006.01.036

Santovito, D., De Nardis, V., Marcantonio, P., Mandolini, C., Paganelli, C., Vitale, E., et al. (2014). Plasma exosome microRNA profiling unravels a new potential modulator of adiponectin pathway in diabetes: effect of glycemic control. *J. Clin. Endocrinol. Metab.* 99, E1681–E1685. doi: 10.1210/jc.2013-3843

Schuette, H. B., Kraeutler, M. J., and McCarty, E. C. (2017). Matrix-assisted autologous chondrocyte transplantation in the knee: a systematic review of mid- to long-term clinical outcomes. *Orthop. J. Sports Med.* 5:2325967117709250. doi: 10.1177/2325967117709250

Schwarzenbach, H., da Silva, A. M., Calin, G., and Pantel, K. (2015). Data normalization strategies for microRNA quantification. *Clin. Chem.* 61, 1333–1342. doi: 10.1373/clinchem.2015.239459

Silver, N., Best, S., Jiang, J., and Thein, S. L. (2006). Selection of housekeeping genes for gene expression studies in human reticulocytes using real-time PCR. *BMC Mol. Biol.* 7:33. doi: 10.1186/1471-2199-7-33

Solchaga, L. A., Penick, K., Porter, J. D., Goldberg, V. M., Caplan, A. I., and Welter, J. F. (2005). FGF-2 enhances the mitotic and chondrogenic potentials of human adult bone marrow-derived mesenchymal stem cells. *J. Cell Physiol.* 203, 398–409. doi: 10.1002/jcp.20238

Sun, H., Zhao, X., Zhang, C., Zhang, Z., Lun, J., Liao, W., et al. (2018). MiR-455-3p inhibits the degenerate process of chondrogenic differentiation through modification of DNA methylation. *Cell Death Dis.* 9:537. doi: 10.1038/s41419-018-0565-2

Swingler, T. E., Wheeler, G., Carmont, V., Elliott, H. R., Barter, M. J., Abu-Elmagd, M., et al. (2012). The expression and function of microRNAs in chondrogenesis and osteoarthritis. *Arthritis Rheum.* 64, 1909–1919. doi: 10.1002/art.34314

Tao, S. C., Yuan, T., Zhang, Y. L., Yin, W. J., Guo, S. C., and Zhang, C. Q. (2017). Exosomes derived from miR-140-5p-overexpressing human synovial mesenchymal stem cells enhance cartilage tissue regeneration and prevent osteoarthritis of the knee in a rat model. *Theranostics* 7, 180–195. doi: 10.7150/thno.17133

Tofiño-Vian, M., Guillén, M. I., Pérez Del Caz, M. D., Silvestre, A., and Alcaraz, M. J. (2018). Microvesicles from human adipose tissue-derived mesenchymal stem cells as a new protective strategy in osteoarthritic chondrocytes. *Cell Physiol. Biochem.* 47, 11–25. doi: 10.1159/000489739

Toh, W. S., Lai, R. C., Hui, J. H. P., and Lim, S. K. (2017). MSC exosome as a cell-free MSC therapy for cartilage regeneration: Implications for osteoarthritis treatment. *Semin. Cell Dev. Biol.* 67, 56–64. doi: 10.1016/j.semcdb.2016.11.008

van Buul, G. M., Villafuertes, E., Bos, P. K., Waarsing, J. H., Kops, N., Narcisi, R., et al. (2012). Mesenchymal stem cells secrete factors that inhibit inflammatory processes in short-term osteoarthritic synovium and cartilage explant culture. *Osteoarthritis Cartil.* 20, 1186–1196. doi: 10.1016/j.joca.2012.06.003

Vandesompele, J., De Preter, K., Pattyn, F., Poppe, B., Van Roy, N., De Paepe, A., et al. (2002). Accurate normalization of real-time quantitative RT-PCR data by geometric averaging of multiple internal control genes. *Genome Biol.* 3:Research0034. doi: 10.1186/gb-2002-3-7-research0034

Vega, A., Martín-Ferrero, M. A., Del Canto, F., Alberca, M., García, V., Munar, A., et al. (2015). Treatment of knee osteoarthritis with allogeneic bone marrow mesenchymal stem cells: a randomized controlled trial. *Transplantation* 99, 1681–1690. doi: 10.1097/tp.0000000000000678

Vonk, L. A., van Dooremalen, S. F. J., Liv, N., Klumperman, J., Coffer, P. J., Saris, D. B. F., et al. (2018). Mesenchymal stromal/stem cell-derived extracellular vesicles promote human cartilage regeneration in vitro. *Theranostics* 8, 906–920. doi: 10.7150/thno.20746

Wang, X., Omar, O., Vazirisani, F., Thomsen, P., and Ekström, K. (2018). Mesenchymal stem cell-derived exosomes have altered microRNA profiles and induce osteogenic differentiation depending on the stage of differentiation. *PLoS One* 13:e0193059. doi: 10.1371/journal.pone.0193059

Wu, C., Tian, B., Qu, X., Liu, F., Tang, T., Qin, A., et al. (2014). MicroRNAs play a role in chondrogenesis and osteoarthritis (review). *Int. J. Mol. Med.* 34, 13–23. doi: 10.3892/ijmm.2014.1743

Wu, X., Wang, Y., Xiao, Y., Crawford, R., Mao, X., and Prasadam, I. (2020). Extracellular vesicles: potential role in osteoarthritis regenerative medicine. *J. Orthop. Transl.* 21, 73–80. doi: 10.1016/j.jot.2019.10.012

Xue, H., Tu, Y., Ma, T., Wen, T., Yang, T., Xue, L., et al. (2019). miR-93-5p attenuates IL-1β-induced chondrocyte apoptosis and cartilage degradation in osteoarthritis partially by targeting TCF4. *Bone* 123, 129–136. doi: 10.1016/j.bone.2019.03.035

Yin, K., Wang, S., and Zhao, R. C. (2019). Exosomes from mesenchymal stem/stromal cells: a new therapeutic paradigm. *Biomark Res.* 7:8. doi: 10.1186/s40364-019-0159-x

Zhang, S., Chuah, S. J., Lai, R. C., Hui, J. H. P., Lim, S. K., and Toh, W. S. (2018). MSC exosomes mediate cartilage repair by enhancing proliferation, attenuating apoptosis and modulating immune reactivity. *Biomaterials* 156, 16–27. doi: 10.1016/j.biomaterials.2017.11.028

Zhang, X., Sai, B., Wang, F., Wang, L., Wang, Y., Zheng, L., et al. (2019). Hypoxic BMSC-derived exosomal miRNAs promote metastasis of lung cancer cells via STAT3-induced EMT. *Mol. Cancer* 18, 40. doi: 10.1186/s12943-019-0959-5

Zhu, L.-P., Tian, T., Wang, J.-Y., He, J.-N., Chen, T., Pan, M., et al. (2018). Hypoxia-elicited mesenchymal stem cell-derived exosomes facilitates cardiac repair through miR-125b-mediated prevention of cell death in myocardial infarction. *Theranostics* 8, 6163–6177. doi: 10.7150/thno.28021

Conflict of Interest: The authors declare that the research was conducted in the absence of any commercial or financial relationships that could be construed as a potential conflict of interest.

Copyright © 2021 Ragni, Colombini, De Luca, Libonati, Viganò, Perucca Orfei, Zagra and de Girolamo. This is an open-access article distributed under the terms of the Creative Commons Attribution License (CC BY). The use, distribution or reproduction in other forums is permitted, provided the original author(s) and the copyright owner(s) are credited and that the original publication in this journal is cited, in accordance with accepted academic practice. No use, distribution or reproduction is permitted which does not comply with these terms.

frontiers in Bioengineering and Biotechnology

ORIGINAL RESEARCH
published: 25 February 2021
doi: 10.3389/fbioe.2021.640419

Extracellular Vesicles Derived From Adult and Fetal Bone Marrow Mesenchymal Stromal Cells Differentially Promote *ex vivo* Expansion of Hematopoietic Stem and Progenitor Cells

Corina A. Ghebes[1], Jess Morhayim[2], Marion Kleijer[1], Merve Koroglu[1], Stefan J. Erkeland[3], Remco Hoogenboezem[2], Eric Bindels[2], Floris P. J. van Alphen[4], Maartje van den Biggelaar[4], Martijn A. Nolte[1,4], Bram C. J. van der Eerden[5], Eric Braakman[2], Carlijn Voermans[1]*† and Jeroen van de Peppel[5]*†

[1] Department of Hematopoiesis, Sanquin Research, Amsterdam, Netherlands, [2] Department of Hematology, Erasmus MC, University Medical Center, Rotterdam, Netherlands, [3] Department of Immunology, Erasmus MC, University Medical Center, Rotterdam, Netherlands, [4] Department of Molecular Hematology, Sanquin Research, Amsterdam, Netherlands, [5] Department of Internal Medicine, Erasmus MC, University Medical Center, Rotterdam, Netherlands

OPEN ACCESS

Edited by:
Ornella Parolini, Catholic University of the Sacred Heart, Italy

Reviewed by:
Pavel Makarevich, Lomonosov Moscow State University, Russia
Elisabeth Ferreira, University of Arkansas for Medical Sciences, United States

****Correspondence:***
Carlijn Voermans
c.voermans@sanquin.nl
Jeroen van de Peppel
h.vandepeppel@erasmusmc.nl

† These authors have contributed equally to this work

Specialty section:
This article was submitted to Preclinical Cell and Gene Therapy, a section of the journal Frontiers in Bioengineering and Biotechnology

Received: *11 December 2020*
Accepted: *02 February 2021*
Published: *25 February 2021*

Citation:
Ghebes CA, Morhayim J, Kleijer M, Koroglu M, Erkeland SJ, Hoogenboezem R, Bindels E, van Alphen FPJ, van den Biggelaar M, Nolte MA, van der Eerden BCJ, Braakman E, Voermans C and van de Peppel J (2021) Extracellular Vesicles Derived From Adult and Fetal Bone Marrow Mesenchymal Stromal Cells Differentially Promote ex vivo Expansion of Hematopoietic Stem and Progenitor Cells. Front. Bioeng. Biotechnol. 9:640419. doi: 10.3389/fbioe.2021.640419

Recently, we and others have illustrated that extracellular vesicles (EVs) have the potential to support hematopoietic stem and progenitor cell (HSPC) expansion; however, the mechanism and processes responsible for the intercellular communication by EVs are still unknown. In the current study, we investigate whether primary human bone marrow derived mesenchymal stromal cells (BMSC) EVs isolated from two different origins, fetal (fEV) and adult (aEV) tissue, can increase the relative low number of HSPCs found in umbilical cord blood (UCB) and which EV-derived components are responsible for *ex vivo* HSPC expansion. Interestingly, aEVs and to a lesser extent fEVs, showed supportive *ex vivo* expansion capacity of UCB-HSPCs. Taking advantage of the two BMSC sources with different supportive effects, we analyzed the EV cargo and investigated how gene expression is modulated in HSPCs after incubation with aEVs and fEVs. Proteomics analyses of the protein cargo composition of the supportive aEV vs. the less-supportive fEV identified 90% of the Top100 exosome proteins present in the ExoCarta database. Gene Ontology (GO) analyses illustrated that the proteins overrepresented in aEVs were annotated to oxidation-reduction process, mitochondrial ATP synthesis coupled proton transport, or protein folding. In contrast, the proteins overrepresented in fEVs were annotated to extracellular matrix organization positive regulation of cell migration or transforming growth factor beta receptor (TGFBR) signaling pathway. Small RNA sequencing identified different molecular signatures between aEVs and fEVs. Interestingly, the microRNA cluster miR-99b/let-7e/miR-125a, previously identified to increase the number of HSPCs by targeting multiple pro-apoptotic genes, was highly and significantly enriched in aEVs. Although we identified significant differences in the supportive effects of aEVs and fEVs, RNAseq analyses of the 24 h treated HSPCs indicated that a limited set of genes was differentially regulated when compared to cells that were treated with cytokines only. Together, our study provides novel insights into the complex biological role of EVs and illustrates that aEVs and fEVs differentially support *ex vivo* expansion capacity of UCB-HSPCs. Together opening new means for the application of EVs in the discovery of therapeutics for more efficient *ex vivo* HSPC expansion.

Keywords: extracellular vesicles, BMSCs, HSPC expansion, transplantation, hematopoietic niche, intercellular communication, EV cargo

INTRODUCTION

Allogeneic hematopoietic stem cell transplantation (HSCT) has become a common practice for the treatment of (malignant-) hematopoietic diseases (Copelan, 2006; Juric et al., 2016). However, most patients in need for HSCT do not have a suitable human leukocyte antigen (HLA)-matched related donor, and of these, less than half can find an HLA-matched unrelated donor (Gragert et al., 2014). For these patients, umbilical cord blood (UCB) has become an important hematopoietic stem and progenitor cell (HSPC) source for allogeneic HSCT. In contrast to peripheral blood stem cell transplantation (PBSCT), UCB has fewer mature T lymphocytes, thus allowing UCB transplantation with a greater degree of HLA mismatch (Stanevsky et al., 2009), and the large number of banked UCB units can easily facilitate the finding of an HLA-matched graft (Mayani et al., 2020). However, the relatively low number of HSPCs present in one UCB unit is a major limitation for UCB transplantation (de Lima et al., 2012; Kindwall-Keller and Ballen, 2020). This is associated with delayed engraftment and higher risk of graft failure, and leads to restriction in their widespread application (Mattsson et al., 2008). To overcome these limitations, the development of efficient culture conditions and the discovery of new compounds that boost *ex vivo* HSPC expansion will therefore help toward the treatment of malignant hematopoietic diseases.

In the bone marrow microenvironment, HSPCs are supported by a large heterogeneous population of stromal cells in the perivascular niche, such as endothelial and mesenchymal cells that generate signals regulating hematopoietic stem cells (HSC) self-renewal, quiescence and differentiation (Boulais and Frenette, 2015; Crane et al., 2017). We and others have shown that *ex vivo* co-culture of UCB-CD34^{+} cells with bone marrow-derived mesenchymal stromal cells (BMSCs) increases the number of HSPCs regardless of the presence of growth factors, such as SCF, Flt3L, TPO, IL6, and G-CSF, making BMSCs an exceptional tool to identify novel HSPC regulators (de Lima et al., 2012; Paciejewska et al., 2016; Cooney, 2018). Recent findings suggest that BMSC-derived extracellular vesicles (EVs) may play an important role in the biological functions of their parental cells (Vonk et al., 2018; Harrell et al., 2019). We therefore postulate that EVs derived from BMSCs may recapitulate the hematopoietic supportive effects of their parental cells and can help us to identify new molecules capable of *ex vivo* expansion of relevant UCB-HSPC numbers for the treatment of patients in need for stem cell transplantation.

The HSPCs in the fetal and adult bone marrow niche actively expand, however, the cellular and extracellular compartment within the fetal- and adult bone marrow differ a lot (Gao et al., 2018). Here we aim to assess whether the EVs released by primary human BMSCs of different origins, e.g., fetal and adult BMSCs, have similar differential supportive effects as their parental cells (Paciejewska et al., 2016) and identify the EVs cargo molecules that mediate the HSPC-supporting capacity of stromal cells. To achieve this, we identified the EV cargo molecules by performing proteomics and small non-coding RNA analyses, and studied their effects on the gene expression of UCB-CD34^{+} cells by next generation sequencing. This study identified new regulatory proteins for the application of EVs in the discovery of therapeutics for more efficient *ex vivo* HSPC expansion.

MATERIALS AND METHODS

Isolation and Culture of Human Bone Marrow Derived MSCs

Adult human bone marrow aspirates (40–70 years old) were obtained from the sternum of patients undergoing cardiac surgery after given informed consent and approval of the medical ethics review board of the AMC (MEC:04/042#04.17.370). Collection of fetal tissues for research purposes was approved by the medical ethical review board of the Academic Medical Centre (AMC) (MEC: 03/038). The fetal human bone marrow samples were obtained from the HIS facility of the AMC, Amsterdam. All material has been collected from donors from whom a written informed consent for the use of the material for research purposes had been obtained by the Bloemenhove clinic (Heemstede, The Netherlands). These informed consents are kept together with the medical record of the donor by the clinic. Low-density mononuclear cells (MNC) were separated by Ficoll gradient centrifugation and cultured in Dulbecco's modified Eagle's medium, GlutaMAX^{TM} and low glucose (Thermo Fisher Scientific, United States) supplemented with 10% fetal bovine serum (FBS, Bodinco, The Netherlands) and 1% penicillin-streptomycin (Sigma Aldrich, Germany), referred in this article as BMSC medium. Non-adherent cells were removed by replacing the medium after 48 h of incubation. Cells were either frozen or expanded up to passage 5, in order to harvest sufficient amounts of EVs.

Isolation and Culture of Human UCB-CD34$^+$ Cells

UCB was collected after informed consent, according to the guidelines of NetCord FACT (by the Sanquin Cord Blood bank, The Netherlands). CD34$^+$ cells were isolated by magnetic cell sorting (MACS, Miltenyi Biotec, Germany), using the human CD34$^+$ Microbead kit (Miltenyi; 130-046-703, Germany) according to manufacturer instructions and within 48 h after initial sample collection. This resulted in a purity of more than 90% CD34$^+$ cells, as determined by flow cytometry and were immediately frozen. After thawing of frozen cells, 10,000 viable UCB-CD34$^+$ CD45$^+$ cells, referred here as UCB-CD34$^+$, were cultured in 48 well plates in growth factor driven serum-free expansion media, Cellgenix GMP SCGM (Cellgenix, Germany) supplemented with stem cell factor (recombinant human SCF, 50 ng/mL, Biolegend, United States) and FMS-like tyrosine kinase 3 ligand (Flt3L, 50 ng/mL, Prepotech, United Kingdom), with or without EVs. Cells were refreshed every 2–3 days. After 10 days the total number of cells (TNCs), CD34$^+$ cells and primitive HSC was counted. TNC number was obtained using fluorescence counting beads in combination with DAPI (diamidino-2-phenylindole, Sigma Aldrich, Germany) for live/dead staining. For the TGFB1 receptor inhibitor experiment, cells were incubated in the absence or presence of fEVs, 1 μM TGFB1 receptor inhibitor (LY 2157299 from Axon Medchem, Netherlands) and DMSO (control TGFB1R inhibitor).

Colony Forming Unit (CFU) Assay

UCB-CD34$^+$ cells, non-cultured and cultured for 10 days, were plated in a 24-well plate at 150 cell/well in cytokine-supplemented methylcellulose medium (MethoCult H4435, StemCell Technologies, Canada) and further cultured for 14 days at 37°C and 5% CO_2. Colony forming unit colonies were counted using an inverted bright field microscope (Leica, Germany).

Isolation and Characterization of Human MSC Derived EVs

Adult and Fetal BMSC-derived EVs were isolated from BMSCs supernatant, after confluent layers of cells cultured in T175 flasks were exposed for 24 h to serum-free BMSC medium. The conditioned BMSC supernatant was exposed to low speed centrifugation (300 g for 5 min, 2,000 g for 10 min) followed by ultracentrifugation (20,000 g for 30 min and 100,000 g for 1 h) using the Ti50.2 rotor (Beckman Coulter, United States). The EV pellets, further referred in this article as EVs, were collected from the last ultracentrifugation step after the supernatant containing no EV was removed, in expansion media or PBS dependent on the assay to follow.

Concentration and Size Distribution

Concentration and size distribution of BMSC-derived EVs were determined using NanoSight NS300 (Nanosight Ltd., United Kingdom) equipped with a 405 nm laser. The particles in each sample were recorded for 5 times 60 s. The data was processed by NTA 2.3 software.

Flow Cytometry

UCB-CD34$^+$ cells, before and after 10 days' culture, were examined for surface markers and viability. Absolute numbers were determined using fluorescence reference counting beads (Thermo Fisher Scientific, United States), anti-APC-CD34$^+$ (Biolegend, United Kingdom) or anti-PeCy7-CD34$^+$ (BD Bioscience, United States), anti-FITC-CD45 (BD Bioscience, United States), anti-APC-CD38 (eBioscience, Thermo Fisher Scientific, United States), anti-PE-CD45RA (Diaclone, France), and DAPI (Sigma Aldrich, Germany). All samples were analyzed using LRS II (BD Biosciences, United States) and data was analyzed using FlowJo software (Tree Star, Inc., United States).

Transmission Electron Microscopy (TEM)

TEM images were taken by negative staining of the EVs, as previously described (Morhayim et al., 2020). Freshly carbon sputtered and formvar coated copper grids were incubated on EV preparations, washed rapidly in water and contrasted with 3.5% uranyl acetate. Grids were blotted and dried before the analysis using a Tecnai T12 G2 Biotwin at 120 kV.

Western Blot Analyses

We compared BMSC supernatant with BMSC-derived EVs and supernatant depleted EVs. For this experiment we have collected the supernatants and EVs from confluent cell layers of five T175 flasks, adult and fetal MSCs each, exposed for 24 h in serum free BMSC medium. For supernatant before centrifugation and supernatant depleted EVs we collected 4 ml and concentrated to a volume of approx. 150 μl using a 3 k molecular weight cut-off amicon ultra centrifugation filter (Merck Millipore, Germany). While the aEVs and fEVs were collected from 30 ml of supernatant following the ultracentrifugation steps and resuspended in $\sim$150 μl of serum free BMSC medium. Protein samples were prepared by immediately mixing with 4X reducing sample buffer containing β-mercaptoethanol (Sigma Aldrich, Germany). EVs proteins were separated by SDS-PAGE at 100 V and transferred onto a nitrocellulose membrane (Whatman Gmbh, Germany). After incubation with 5% BSA for 1 h, the membrane was incubated with primary antibodies against Annexin A2 (ANXA2; rabbit polyclonal. 1:1,000, Abcam, Cambridge, United Kingdom). Membranes were probed with secondary antibody goat anti-rabbit-HRP (Dako, United States) and films were processed with a Konica Minolta, SRX-101A.

RNA Isolation, Next-Generation Sequencing and Bioinformatic Analysis of EV Derived Small RNA

EV pellets were collected for each sample from confluent cell layers of 10×T175 flasks, as previously described (Morhayim et al., 2020). Total EV-RNA was isolated using the TRIzol LS reagent (Thermo Fisher Scientific, United States) according to the manufacturer's instructions. RNA concentration and size distribution profile were analyzed on an Agilent Bioanalyzer RNA 6000 Pico chip (Thermo Fisher Scientific, United States). Small RNA libraries were prepared with the NEBNext Small RNA library preparation kit (New England Biolabs, United States) according to the manufacturer's instructions. Finished small RNA libraries were quantified on a Bioanalyzer High Sensitivity

DNA chip (Agilent, United States) and subsequently normalized and pooled. Single end 50-bp sequencing was performed on a Miseq (Illumin). Subsequently demultiplexing was done using Illumina's bcl2fastq program allowing for one mismatch in the barcode. Quality metrics on the resulting FASTQ files were generated using fastqc in combination with multiqc. The illumina universal adapters were removed using trim galore. Subsequently alignment was performed using bowtie1 using very sensitive settings (-l15 –tryhard –all –best –strata) Finally quantification of abundance per feature was performed using in house developed software. During quantification fragments were assigned only once to the best matching feature. The feature set used originate from the DASHR (v2) small RNA database. Total number of reads per small RNA ID were counted. Differential gene expression analysis was done with DESeq2 (Love et al., 2014). All small RNAs with a sum count of 2 and higher in all samples were included in the analysis. The sequencing data are available in the Gene Expression Omnibus (GEO) database repository (GSE165323)[1]. miRPathDB v2.0 was used to categorize the miRNA into GO annotations (Kehl et al., 2020).

RNA Isolation and RNA Profiling of UCB-CD34$^+$ Cells Transcriptome

Freshly isolated UCB-CD34$^+$ cells were immediately frozen or cultured for 24 h in the absence or presence of aEVs or fEVs. Total RNA was isolated using NucleoSpin RNA XS kit (Macherey-Nagel, Germany) according to the manufacturer's instructions. RNA concentration and size distribution profile were analyzed on an Agilent Bioanalyzer RNA 6000 Pico chip (Thermo Fisher Scientific, United States). The SMARTer version v4 Ultra Low Input RNA kit for sequencing (Clontech) was used to generate cDNA. Subsequent bulk RNAseq libraries were generated with the Truseq nano DNA sample prep kit (illumina) according to manufacturer's instructions. The resulting libraries were quality checked and sequenced paired-end 100 cycles on a Novaseq6000 instrument (Illumina). The resulting base-calls from sequencing were converted to FASTQ files using Illumina's bcl2fastq software allowing for one mismatch in the barcode. Quality metrics of the resulting FASTQ files were summarized using fastqc in combination with multiqc. SMARTer adapters and poly-T tails were removed using fqtrim. Pseudo counts per transcript were measured using salmon. The per transcript pseudo counts were summarized to per gene pseudo counts using the R package tximport. After mapping the reads, differential gene expression analysis was done with DESeq2 (Love et al., 2014) using p.adj $<$ 0.05 as a cutoff for differential gene expression. The sequencing data are available in the Gene Expression Omnibus (GEO) database repository with accession number: GSE165921 (see text footnote 1).

Mass Spectrometry and Bioinformatics Analysis of Proteins

Tryptic peptides were prepared according to the method described by Kulak et al. (2014) with some adjustments. Briefly, 4–8 $\times$ 10^9 fEVs and 2–6 $\times$ 10^9 aEVs were isolated, and lysed in 2% Sodium deoxycholate lysis buffer (Sigma Aldrich, Germany), 20 mM TCEP (Tris(2-CarboxyEthyl)Phosphine, Thermo Fisher Scientific, United States), 80 mM ChloroAcetamide (Sigma Aldrich, Germany) and 200 mM TRIS-HCl pH 8.0 (Life Technologies, United Kingdom), boiled at 95°C for 5 min and sonicated for 10 cycles of 30 s on/off in a Bioruptor (Diagenode, Belgium). After an overnight digestion with 100 ng Trypsin-LysC (Promega, United States) at room temperature, samples were acidified with 10% trifluoroacetic acid (Thermo Fisher Scientific, United States) and loaded on in-house prepared SDB-RPS STAGEtips (Empore, United States). The tips were washed with ethyl acetate (Sigma Aldrich, Germany) and 0.2% trifluoroacetic acid (Thermo Fisher Scientific, United States) and the peptides were eluted in three fractions by increasing concentrations (100 mM and 150 mM) of ammonium formate (VWR Chemicals, Belgium) or 5% (v/v) ammonium hydroxide (Merck Millipore, Germany) and acetonitrile (40, 60, and 80% v/v) (BioSolve, France). Sample volume was reduced by SpeedVac and supplemented with 2% acetonitrile, 0.1% TFA to a final volume of 10 μl. Three microliter of each sample was injected for MS analysis. Tryptic peptides were separated by nanoscale C18 reverse phase chromatography coupled on line to an Orbitrap Fusion Lumos Tribrid mass spectrometer (Thermo Fisher Scientific, United States) via a nanoelectrospray ion source (Nanospray Flex Ion Source, Thermo Fisher Scientific, United States). All data was acquired with Xcalibur 4.1 software. The raw mass spectrometry files were processed with the MaxQuant computational platform, 1.6.2.10. Proteins and peptides were identified using the Andromeda search engine by querying the human Uniprot database (downloaded Feb 2019). Standard settings with the additional options match between runs, Label Free Quantification (LFQ), and only unique peptides for quantification were selected. The data was filtered for potential contaminants, reverse hits and "only identified by site" using Perseus 1.6.5.0 (Tyanova et al., 2016). The proteins were filtered for 100% valid values in at least one of the experimental groups. Missing values were imputed by normal distribution (width = 0.3, shift = 1.8), assuming these proteins were close to the detection limit. Double-sided t-test (FDR 0.05 and S0 of 4) was used to determine significant differences between aEV and fEV. David Bioinformatics Resources 6.8 was used for gene ontology (GO) analysis, using all the proteins identified by the whole EV lysate proteomics experiment as background. ExoCarta top 100 exosome proteins were downloaded to map the percentage of proteins found back in our proteomics experiment (Keerthikumar et al., 2016). The mass spectrometry proteomics data have been deposited to the ProteomeXchange Consortium[2] via the PRIDE partner repository with the dataset identifier: PXD022851 (Perez-Riverol et al., 2019).

Statistics

Statistical analyses were performed with Graphpad Prism 8, unless otherwise stated. Significance was calculated using Student's t-test and two-way ANOVA test. Mean values plus or

[1]https://www.ncbi.nlm.nih.gov/geo/

[2]http://proteomecentral.proteomexchange.org

minus standard deviation of the mean are shown. $^{*}P < 0.05$; $^{**}P < 0.01$; $^{***}P < 0.001$.

RESULTS

BMSC-Derived EVs Contain Supportive Factors for *ex vivo* Expansion of Human UCB-CD34^{+} Cells

To analyze whether BMSC-derived EVs are able to support UCB-derived CD34^{+} cells *ex vivo,* we expanded BMSCs from adult and fetal bone marrow and harvested EVs from the conditioned medium by a series of ultracentrifugation steps. We quantified the number of EVs that were produced by the BMSCs and added different numbers of EVs (25,000, 50,000, or 100,000) per human UCB-CD34^{+} cell. *Ex vivo* expansion experiments illustrated that 100,000 EVs were able to support the UCB-CD34^{+} cells, whereas adding a lower number of EVs did not significantly increase the total number of viable nucleated cells as compared to control culture (SCF and Flt3L only) after expansion (**Supplementary Figure 1A**). Next, we investigated if the isolated BMSC-derived EVs were responsible for *ex vivo* expansion of UCB-CD34^{+} cells or whether other secreted factors were present in the EV-depleted supernatant or serum-free MSC medium. **Supplementary Figure 1B** illustrates that only the isolated EV-fraction consistently contributed to the increase in the number of viable nucleated cells. These results suggest the presence of supporting factors in the BMSC-derived EVs for the *ex vivo* expansion of UCB-CD34^{+} cells.

UCB-CD34^{+} Cell Support by BMSC-Derived EVs Is Dependent on the Origin of the BMSCs

Next, we compared the supportive effects of BMSC-derived EVs isolated from different origins. UCB-CD34^{+} cells from a single donor were exposed to EVs isolated from adult (aEVs) or fetal (fEVs) BMSCs in growth factor- (SCF and Flt3L) driven serum-free expansion media (**Figure 1A**). aEVs caused a significant increase in the total number of viable nucleated cells (1.6 fold, $p < 0.05$) and CD34^{+} cell subset (1.8-fold, $p < 0.01$), while fEVs caused a non-significant increase of 1.2 and 1.4 fold, respectively (**Figures 1B,C**). The expanded UCB-CD34^{+} cells were further examined for their *in vitro* colony forming capacity by performing Colony Forming Unit Granulocyte-Macrophage (CFU-GM) assay. Corrected for input cell numbers, we observed that UCB-CD34^{+} cells treated with either aEVs or fEVs retained their colony forming potential (**Figure 1D**). This indicates that progenitors did not differentiate, but maintained their stemness. This notion was further supported by analyzing the presence of a more immature CD34^{+} subset (CD34^{+} CD38-CD45RA−, addressed here as primitive HSCs) and observed that the number of primitive HSCs was also maintained by both aEVs and fEVs treatment, comparable to the control culture condition (**Figure 1E**). Together, these findings demonstrate that aEVs support the *ex vivo* expansion of UCB-CD34^{+} cells while maintaining primitive HSCs in culture.

Both Adult and Fetal BMSCs Release EVs With Similar Morphological Characteristics

Next, we used various methods to characterize the EVs obtained from the different sets of BMSCs. Nanoparticle tracking analysis (NTA) of the isolated EVs indicated that the majority of detected particles were in the same size range of 100–200 nm, with no difference in mean size observed between aEVs (162 ± 9 nm) and fEVs (164 ± 6 nm) (**Figure 2A**). Transmission electron microscopy (TEM) analysis confirmed the presence of a heterogeneous EV population, with particles size comparable to the NTA-derived data. The isolated EVs displayed a cup shaped morphology that is characteristic for EVs analyzed by TEM (van Niel et al., 2018) and we observed no differences in morphology between aEVs and fEVs (**Figure 2B**). Western blot analysis using an EVs specific marker, Annexin A2, confirmed the enrichment of EVs in the 100,000 g EV pellet compared to supernatant before centrifugation, and the absence of Annexin A2 in the supernatant after centrifugation (**Figure 2C**). These findings, in line with the aforementioned functional assays, strengthen our hypothesis that BMSC secrete EVs with supportive factors for *ex vivo* expansion of the UCB-CD34^{+} cells.

Protein Profiling of Adult and Fetal BMSC-Derived EVs Identifies TGFB1 as a Key Suppressor in the Expansion of UCB-CD34^{+} Cells by Fetal MSC Derived EVs

To assess whether the differences between aEVs and fEVs in supportive expansion of UCB-CD34^{+} cells can be attributed to their protein cargo, we performed label-free mass spectrometry-based proteomics analysis. We identified a total of 2,283 proteins that were detected in all biological replicates in at least one group (aEV or fEV) with 139 and 27 proteins quantified exclusively in fEV or aEVs, respectively. The proteins that were quantified in both subsets included 90 of the Top 100 most frequently identified exosomal proteins, as defined by the ExoCarta database (Keerthikumar et al., 2016; **Supplementary Table 1**). Principal component analysis with the identified proteins illustrated that the first two components account for 80.2% of the total variance and were able to separate the aEVs and fEVs on the first principal component (**Figure 3A**). Differential enrichment analysis indicated that 156 proteins were significantly enriched in aEVs (orange) and 255 proteins in fEVs (green) (**Figure 3B**). The top highly abundant proteins detected in both aEVs and fEVs are the well-defined EV marker proteins ANXA1, ANXA2, ANXA5, and GAPDH (blue) (**Figure 3B**). To further investigate the function of our differentially expressed proteins, we conducted Gene Ontology (GO) enrichment analysis using DAVID (Huang et al., 2009), and identified that the processes, such as oxidation-reduction process (GO:0055114; HADHA, HADHB), mitochondrial ATP synthesis coupled proton transport (GO:0042776; ATP5A1, ATP5B, and ATP5O)

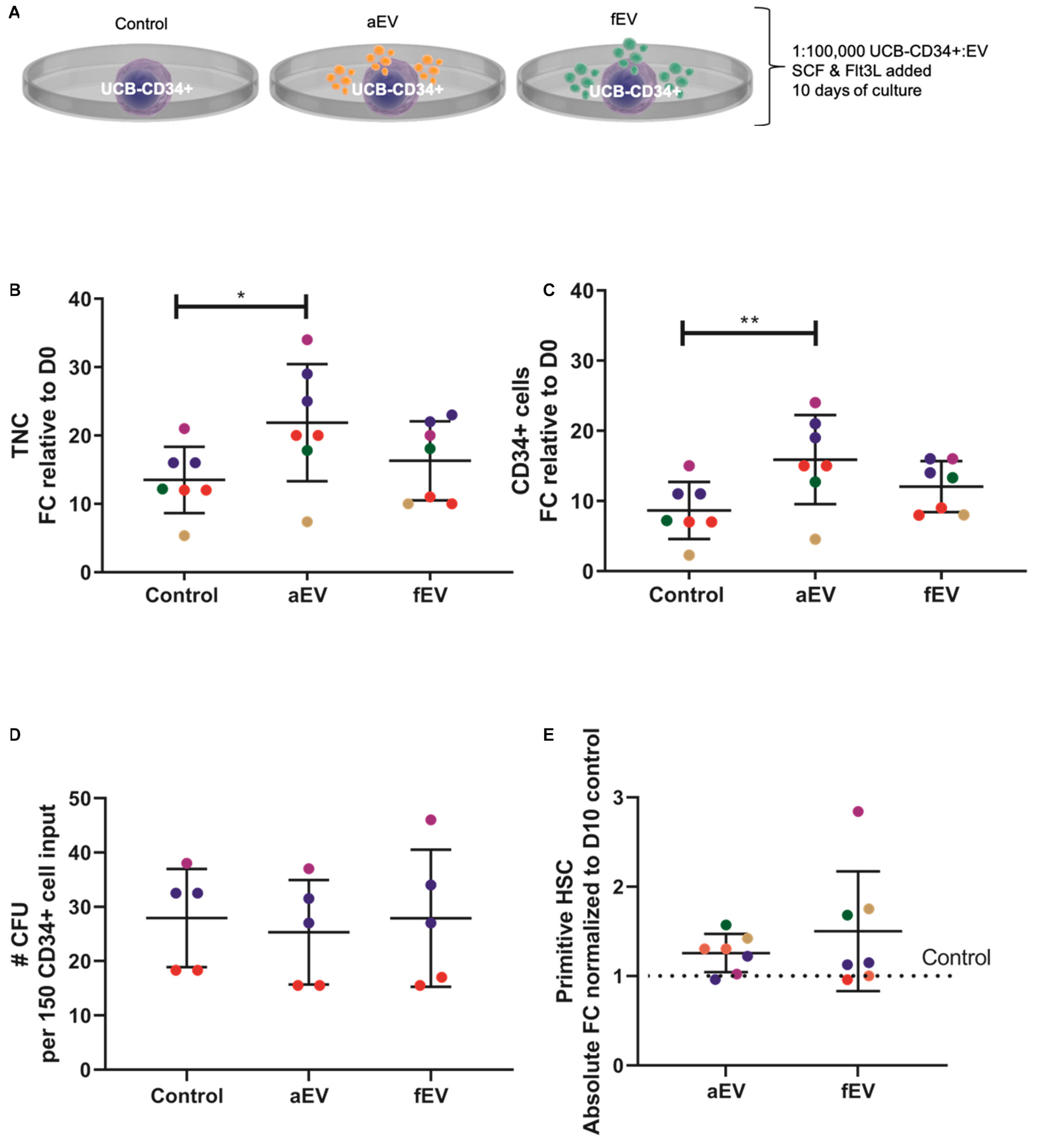

FIGURE 1 | Role of MSC derived EVs in *ex vivo* expansion of UCB-CD34$^+$ cells. **(A)** UCB-CD34$^+$ cells were cultured for 10 days in growth factor (SCF and Flt3L) driven serum-free expansion media and in the presence of aEVs and fEVs. We compared the effect of single aEVs (n = 7) and fEVs (n = 7) donors on the expansion of UCB-CD34$^+$ cells of the same donor. Each datapoint color represents a different UCB CD34$^+$ cell donor, n = 5. UCB CD34$^+$ cell donors in red and blue were exposed to two different aEV and fEV donors, each. Statistics was performed for all n = 7 different aEV and fEV donors. **(B)** Proliferation of viable total nucleated cells, TNC and **(C)** CD34$^+$ cells shown as fold change increase relative to Day 0 (D0) input. **(D)** Total number of colony forming cells after being cultured for 10 days in growth factor-driven serum-free expansion media and in the presence of aEVs and fEVs. **(E)** Maintenance of primitive HSC (CD34$^+$ CD38-CD45RA-) subset, shown as absolute fold change normalized to D10 cell culture control. $^*P < 0.05$, $^{**}P < 0.01$.

and protein folding (GO:0006457; FKBP11, FKBP10, FKBP2, MESDC2) were overrepresented in aEVs (**Figure 3C**). In contrast, the majority of the proteins overrepresented in fEVs were annotated to extracellular matrix organization (GO:0030198; FN1, COL12A1, COL1A1, COL6A1, CCDC80, and others), positive regulation of cell migration (GO:0030335;

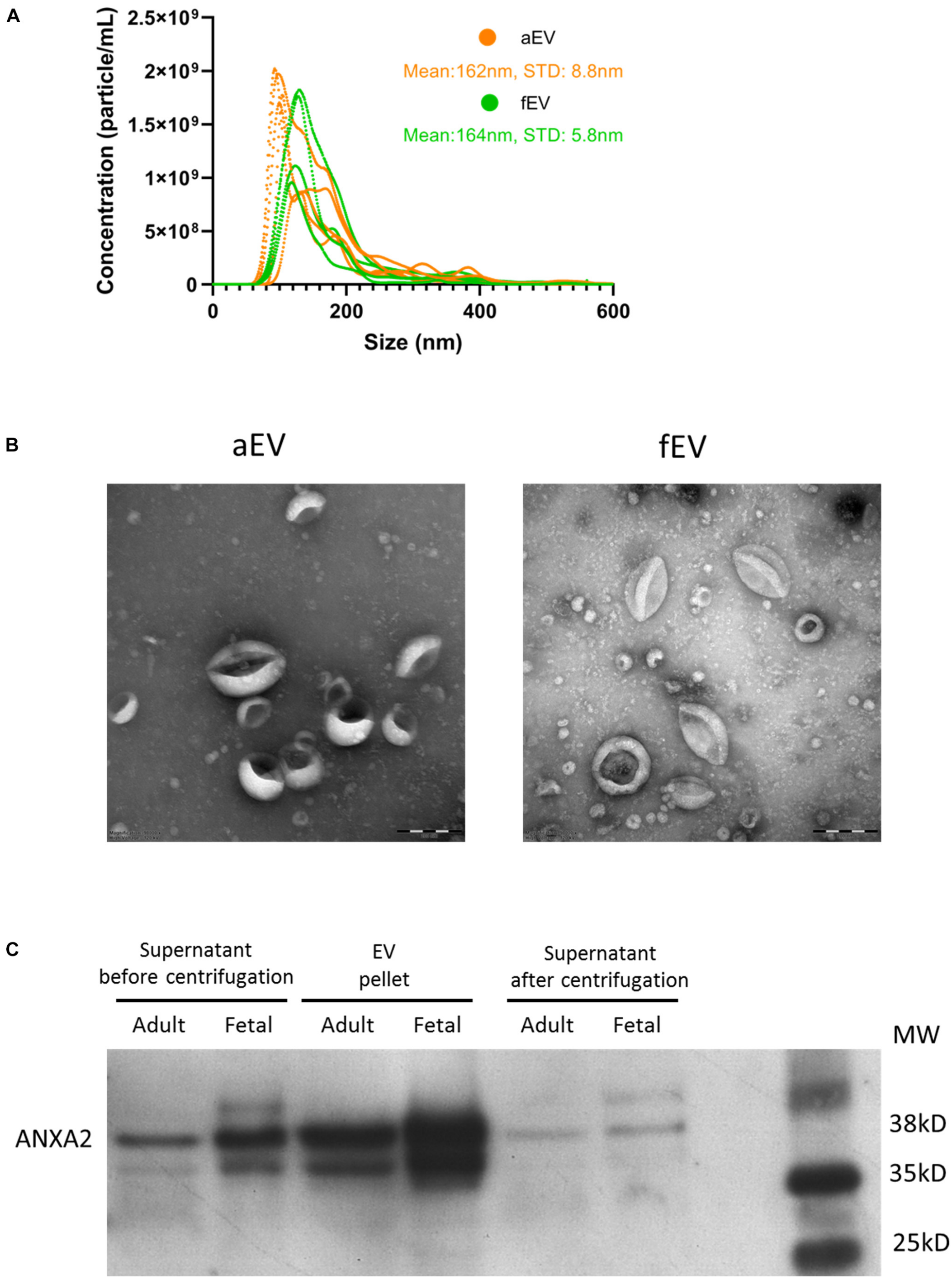

FIGURE 2 | MSC derived EVs characterization. **(A)** EV size and concentration (particle/mL) were analyzed using nanoparticle tracking analysis. We used $n = 5$ aEV ($n = 3$ single and $n = 2$ pooled donors) and $n = 4$ fEV (single donors). The highest concentration of particles detected in aEVs and fEVs have the size of 100–200 nm, with a mean particle size of 162 and 164 nm, respectively. **(B)** Transmission electron microscopy images confirm the presence of different sized EVs, characterized by the cup-shaped morphology. Scale bar = 200 nm. **(C)** Western blot analysis of the MSC supernatant before centrifugation, EV pellet and supernatant after centrifugation (containing no EVs), and using Annexin A2 as a positive marker for EVs, confirms the enrichment of EVs in the EV pellet.

ITGA4, ITGA6, GDF15, SEMA3, APDSD6, MMP14, ICAM1, FGFR1, PDGFRA, ADAMTS1), and proteins involved the transforming growth factor beta receptor signaling pathway (GO:0007179; TGFBR1, TGFB1, LTBP1, TGFBR2, LTBP2, BMPR1A, GDF5, GDF15, PARP1, RPS27A, COL3A1, TGFB2; **Figures 3C,D**).

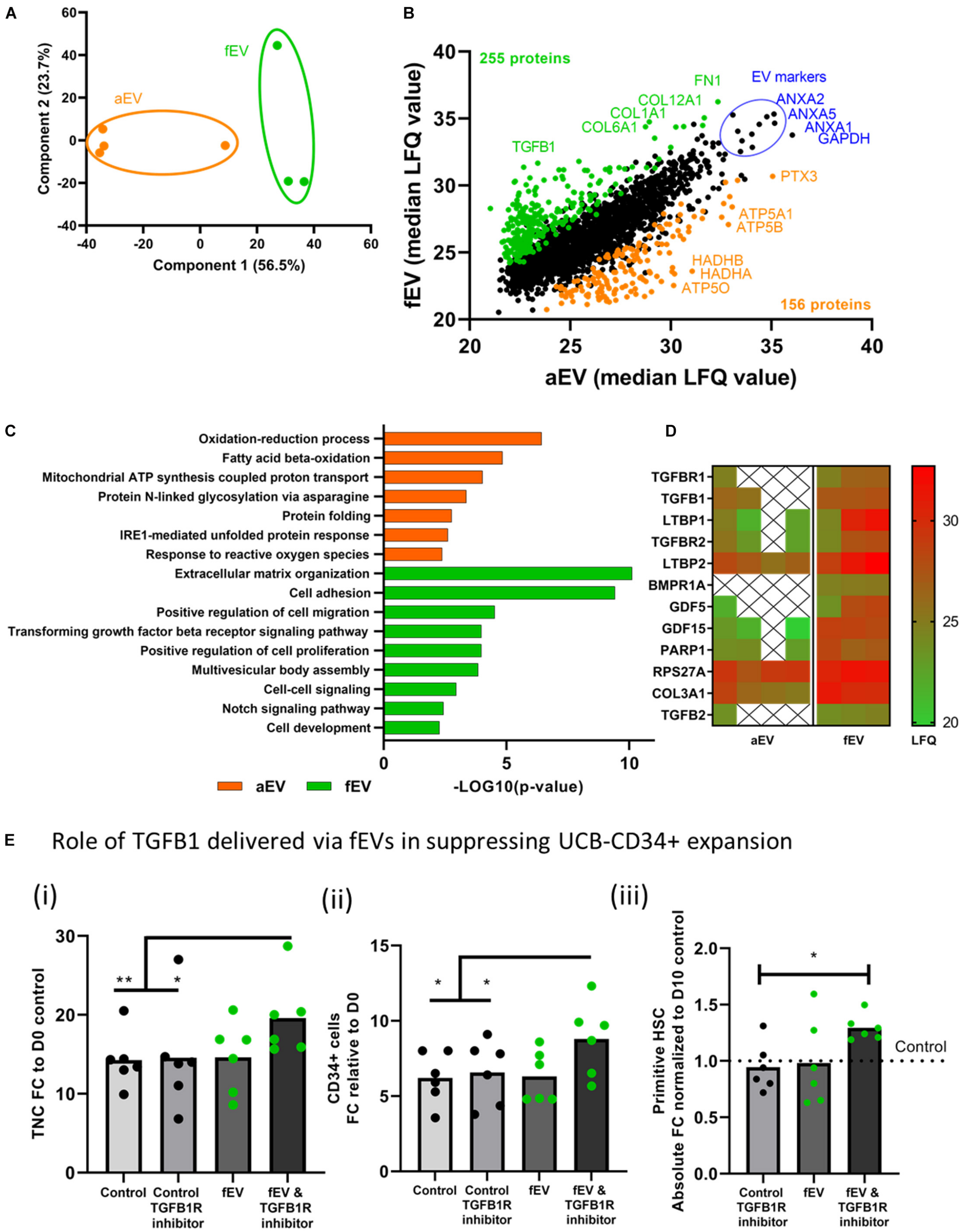

FIGURE 3 | Proteomic profiling of adult- and fetal MSC derived EVs. **(A)** Principal Component Analyses, PCA, based on the LFQ intensity values of proteins that were quantified in all samples, showing a separation between aEVs and fEVs. Each datapoint represents one independent sample ($n = 2$ single and $n = 2$ pooled adult MSC EV donors and $n = 3$, single fetal MSC EV donors). **(B)** Scatterplot results of all quantified proteins, represented as median LFQ values after imputation, showing 156 differentially expressed proteins identified in aEVs (orange) vs. 255 differentially expressed proteins in fEVs (green). The top highly expressed proteins are representative EV protein markers (blue). **(C)** Gene Ontology enrichment analysis of the differentially expressed proteins based on the "Biological process." **(D)** Heatmap showing significantly enriched fEV proteins involved in transforming growth factor receptor signaling pathway and potentially responsible for limiting the effect of fEVs to support the *ex vivo* expansion of UCB CD34$^+$ cells. Each column represents one independent sample (X = not quantified). **(E)** Inhibition of TGFB1 signaling pathway in UCB-CD34$^+$ cells. UCB-CD34$^+$ cells ($n = 6$ donors) were cultured for 10 days in growth factor-driven serum-free expansion media in the presence or absence of fEVs ($n = 6$, single donors) and TGFB1R inhibitor; (i) proliferation of viable total nucleated cells, TNC and (ii) CD34$^+$ cells shown as fold change increase compared to D0 input.; (iii) proliferation of primitive HSC (CD34$^+$ CD38-CD45RA-) subset, shown as absolute fold change normalized to D10 control. Blocking TGFBR1 shows a non-significant trend in increased expansion of total nucleated cells ($P = 0.14$), the CD34$^+$ cell subset ($P = 0.11$) and the primitive HSCs ($P = 0.09$) when compared to fEVs. $^*P < 0.05$, $^{**}P < 0.01$.

For the latter one, we used a heat map to visualize the detection intensities of the proteins involved in the transforming growth factor beta receptor signaling pathway and noticed that some of these proteins were limited or not quantified in the aEVs, whereas they were quite abundant in the fEVs (**Figure 3D**). Since TGFB1 was previously described in literature to negatively regulate the number and function of hematopoietic stem cells (Wang et al., 2018), we investigated whether TGFB1 transported by the fEVs is responsible for the suppression of the potentially supportive factors within the EV cargo. Therefore, we exposed UCB-CD34$^+$ cells to fEVs in the absence or presence of transforming growth factor beta receptor 1 inhibitor (TGFBR1 inhibitor). We found that blocking TGFBR1 significantly increased the expansion of total nucleated cells, the CD34$^+$ cell subset and the primitive HSCs when compared to control culture conditions (**Figures 3Ei–iii**). These results are compatible with the hypothesis that TGFB1 present in fEVs impairs their supportive effects on the HSC expansion, but it also indicates that both aEVs and fEVs contain supportive factors for *ex vivo* expansion of UCB-CD34$^+$ cells. Therefore, we investigated the top 30 highly expressed proteins between aEVs and fEVs to identify candidates that may induce UCB-CD34$^+$ cell expansion (**Supplementary Figure 2**). Among them, we identified well defined EV markers (blue), proteins involved in extracellular matrix organization (GO:0030198; green) and proteins involved in cell activation (GO: 0001775).

Together, we found various proteins (e.g., TGFB) that were differentially quantified between adult and fetal EV cargo, and suggests that aEVs contain a more favorable ratio of HPSC supportive protein cargo.

Identification of Small RNA Expression Signature in EVs Derived From Adult and Fetal BMSCs

Besides the identified proteins transfered via the BMSC-derived EVs, the presence of a selective repertoire of small RNAs can additionally contribute to the *ex vivo* expansion of UCB-CD34$^+$ cells. Small non-coding RNAs represent an interesting group of bioactive molecules that may be involved in reprogramming UCB-CD34$^+$ cell fate (De Luca et al., 2016). To assess which small RNAs are selectively packed in the BMSC derived EVs and may be transferred to UCB-CD34$^+$ cells, we performed next generation sequencing of aEVs and fEVs.

Analysis of the total RNA from both adult and fetal MSC-derived EVs revealed a typical RNA size distribution profile of vesicles, which were enriched for small RNAs and highly reduced in the 18S and 28S rRNA peaks, when compared to their parental cells (**Figure 4A**). Principal component analysis of small RNA sequencing depicted a separation between the vesicular and cellular small RNAs, and between the adult and fetal origin (**Figure 4B**). To identify the small RNA distribution biotypes, we mapped all detected RNA reads to known small RNA sequences and determined that 19% of the miRNA, 1% of the piRNA, 100% of the yRNA, and rRNA, 70% of the snoRNA, 92% of the snRNA, and 16% of the tRNA, were present in our EV samples (**Figure 4C**). Next, we determined whether there are differences between aEVs and fEVs in the number of reads identified per RNA species (**Figures 4D,E**). We found that EV samples were more abundant in rRNA (49.9% $\pm$ 7.5), miRNA (25.2 $\pm$ 8.5%) and yRNA (16.9 $\pm$ 7.5%), while snoRNA was mainly only identified in fEVs (4.2 $\pm$ 2%) and limited in aEVs (0.7 $\pm$ 0.4%). While little is known about the contribution of this different small RNA species to the hematopoietic processes, miRNAs have been lately described to play a key role in the hematopoietic system, being involved in the maintenance of self-renewal of hematopoietic stem cells and differentiation into mature blood cells. Moreover, miRNA are highly abundant in aEVs and fEVs and encouraged us to search for candidate miRNAs that may drive UCB-CD34$^+$ cell expansion. Hence, we outlined all miRNAs that have a Log2 (mean normalized reads) count, over all adult, and fetal samples, higher than nine (**Figure 4F**) and used miRPathDB to determine the top GO biological processes associated with the listed miRNAs (Kehl et al., 2020). Target genes of the miRNAs were mostly annotated to regulation of metabolic process (miR-21-5p, miR-26a-5p, miR-23a-3p, miR-125b-5p, miR-127-3p, miR-99b-5p, miR-27a-3p, miR-199a-5p) and cell morphogenesis or development (miR-125b-5p, miR-10a-5p, miR-152-3p, miR-22-3p, miR-125a-5p, miR-148b-3p). Among these miRNAs, we identified interesting miRNA clusters, such as miR-99b, let-7e, and miR-125a or miR-99a/100, let-7, and miR-125b, which were previously found to increase the number of HSCs *in vivo* (Guo et al., 2010; Emmrich et al., 2014), making them potential candidates for the induction of *ex vivo* UCB-CD34$^+$ cell expansion.

EVs Derived From Adult and Fetal BMSCs Result in a Unique Transcriptional Response in UCB-CD34$^+$ Cells

The proteomics and small RNA sequencing analyses of the EV cargo resulted in many targets that may be responsible or partly responsible for the supportive effects of the aEVs. To analyze what functional changes occur upon addition of aEV and fEVs, we determined the gene expression changes after 24 h vesicle incubation with UCB-CD34$^+$ cells and compared this with the cells treated with cytokine only.

Our results indicated that the variation between the UCB-CD34$^+$ cells from the different donors was larger than the differences of the treatment (**Figure 5A**). However, gene expression analyses indicated 93 genes that were differentially expressed between the various conditions and only 10 genes that were differentially expressed when cells were treated with fEVs compared to aEVs. Of these, we identified 5 genes, (e.g., MTF1, PER1, HOMER1, HSPA6, ENSG00000260534) that were significantly upregulated in response to aEV compared to fEV treatment of UCB-CD34$^+$ cells (**Figure 5B** and **Supplementary Table 2**). Moreover we identified that 31 and 75 genes were differentially expressed ($p < 0.05$) upon aEV and fEV treatment, respectively, when compared to the UCB-CD34$^+$ cells that were treated with cytokines only (**Figures 5B–D**).

Functional analysis of the 31 differentially expressed genes upon treatment with aEVs indicated that gene ontology terms

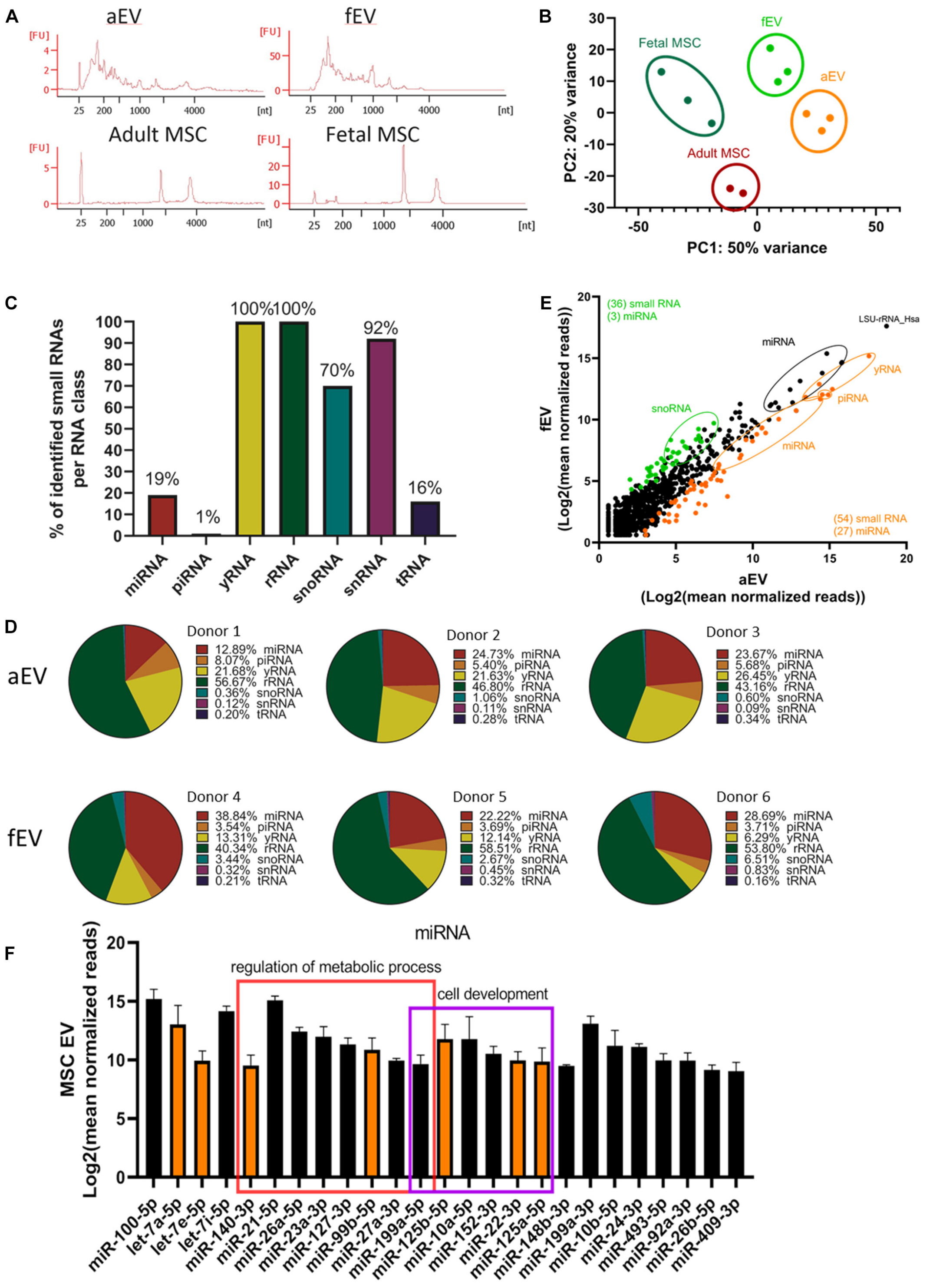

FIGURE 4 | Small RNA profiling of adult and fetal MSC derived EVs. **(A)** Representative RNA profiles of aEVs (*n* = 1 single and *n* = 2 pooled donors) and fEVs (*n* = 3, single donors) compared to their parental cells. (FU, Fluorescent Units) **(B)** Principal component analyses of normalized small RNA sequencing data showing a nice separation between the different biological replicates. **(C)** Percentages of identified small RNAs per RNA class. **(D)** Pie charts mapping the composition in percentage of the diverse small RNA species, per each biological replicate. For each EV sample we individually summed the number of reads per RNA species, and presented the results in percentages in form of pie-charts **(E)** Scatterplot mapping Log2 (mean normalized reads) of aEVs (differentially expressed in orange) and fEVs (differentially expressed in green). **(F)** Common most abundant miRNAs identified in aEVs and fEVs with Log2 (mean normalized reads) higher than nine. Some of the miRNAs were significantly expressed in aEVs (orange); some miRNAs were annotated to regulation of metabolic process (red square) and cell morphogenesis or development (purple square). Error bars represent the standard deviation of the normalized reads from all EVs (3× fEVs and 3× aEVs) combined.

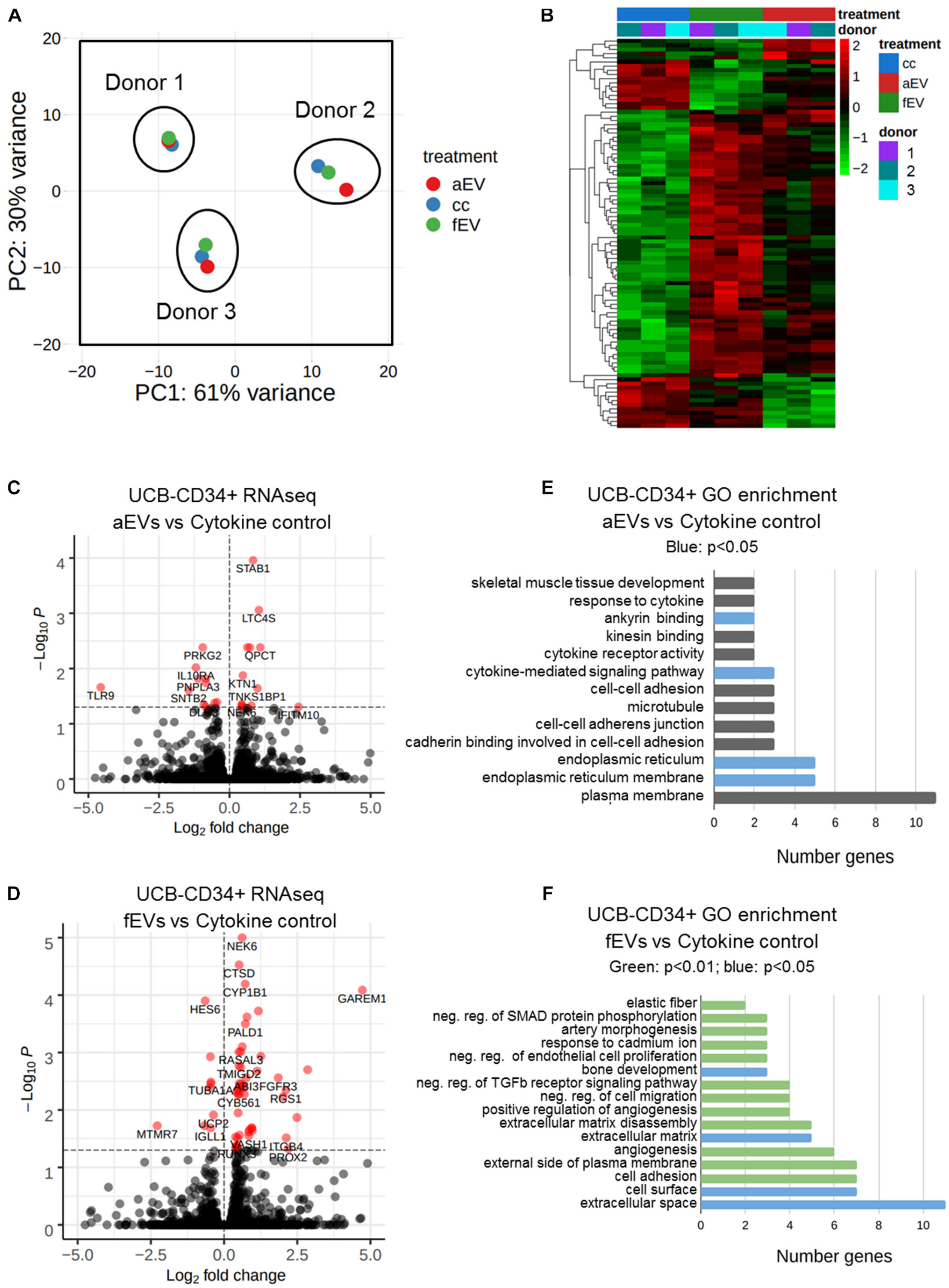

FIGURE 5 | Differential gene expression analyses of UBC-CD34+ cells upon exposure to adult and fetal MSC EVs. **(A)** Principal component analysis of RNA sequencing data of UCB-CD34+ ($n = 3$) upon exposure for 24 h to cytokine cocktail with or without aEVs ($n = 3$, pooled donors) or fEVs ($n = 3$, single donors). **(B)** Heatmap of all differential expressed genes (p.adj < 0.05) in all comparisons aEV vs. cytokine control (cc), fEV vs. cc and aEV vs. fEV. **(C)** Volcano plot of UCB-CD34+ cells treated with aEVs vs. cc. **(D)** Volcano plot of UCB-CD34+ cells treated with fEVs vs. cc. **(E)** GO enrichment analyses using DAVID of all genes differentially regulated of UCB-CD34+ cells treated with aEVs vs. cc. Blue bars represent significant ($p < 0.05$) GO-term enrichment **(F)** GO enrichment analyses using DAVID of all genes differentially regulated of UCB-CD34+ treated with fEVs vs. cc. Blue and Green ($p < 0.01$) represent significant ($p < 0.05$ and $p < 0.01$, respectively) GO-term enrichment.

such as endoplasmatic reticulum (GO:0005783), cytokine-mediated signaling pathway (GO:0019221) or involvement in ankyrin binding (GO:0030506) were enriched (**Figure 5E**). Interestingly, among the 75 genes differentially expressed upon addition of fEVs we identified GO categories, such as cell adhesion (GO:0007155), extracellular matrix (GO:0031012) and negative regulation of transforming growth factor beta receptor signaling pathway (GO:0030512) (**Figure 5F**).

In summary, our results on protein and miRNA cargo analyses of the EVs together with the gene analysis of the $CD34^+$ cells suggests that especially the TGFB pathway hampers the effect of the fEVs and that the aEVs contain specific miRNA clusters that favor HSPC expansion.

DISCUSSION

In the current study, we illustrate that primary human BMSC-derived EVs isolated from fetal and adult bone marrow sources have a different supportive role on UCB-$CD34^+$ cell expansion. We systematically investigated the bioactive cargo released by aEVs and fEVs, i.e., proteins and small RNA, and identified potential regulators that may have a positive supportive role on the *ex vivo* expansion of UBC-$CD34^+$ cells while retaining CFU-GM capacity.

Among the bioactive molecules that we identified, small non-coding RNAs may represent as key regulators of UCB-$CD34^+$ cell fate. Previous work of us and others have already illustrated that small non-coding RNAs are present in EVs that were isolated from osteoprogenitors and osteoblasts (De Luca et al., 2016; Morhayim et al., 2016, 2020; Xie et al., 2016). Here, we show that aEVs and fEVs contain many small RNAs with different abundances. While aEVs are abundant for small non-coding RNAs of the categories: yRNA and piRNA; snoRNAs were more present in fEVs. This illustrates the large differences found in small RNAs identified in body fluids (Godoy et al., 2018). Especially of interest is the microRNA cluster containing miR-99b, let-7e, and miR-125a that was higher enriched in the aEVs and within the Top50 most abundant miRNAs. miR-125a controls the size of the stem cell population by regulating hematopoietic stem/progenitor cell apoptosis (Guo et al., 2010; Wojtowicz et al., 2019). Although downregulation of proapoptotic genes were not identified in the RNAseq analyses of UCB-$CD34^+$ cells in response to aEVs and fEVs, inhibition of apoptosis could take place at later stage or only present in subset of expanding UCB-$CD34^+$ cells. In more recent work by Wojtowicz et al. (2019), miR-125a was identified to expand murine long-term repopulating hematopoietic stem cells and increase the number of hematopoietic stem cells *in vivo*. In addition, similar to the study of Xie et al., we identified miR-21 that has been reported to be involved in hematopoiesis (Bhagat et al., 2013; Xie et al., 2016). Altogether, we demonstrate that EVs contain molecules that may be directly involved in the supportive action and recent data suggests that miR-125a is sufficient to increase *ex vivo* of HSPCs.

Another interesting finding is the identification of proteins associated with TGF-β signaling and the regulation of negative regulators of TGF-β in UCB-$CD34^+$ in response to fEVs. The low abundance of proteins involved in TGF-β signaling in aEVs let us further investigate whether the presence of TGFβ signaling is inhibitory in the fEVs assisted expansion conditions. Previously we showed that Transforming Growth Factor Beta Induced (*TGFBI*) expression in the bone marrow niche is essential for a balanced HSPC proliferation and differentiation, and only in the presence of BMSCs, TGFBI levels were reduced in HSPCs enhanced HSC maintenance (Klamer et al., 2018). This correlates very well with the reduced abundance of *TGF*-β in aEVs and their increased supportive effects. Nevertheless, several reports illustrated that TGF-β1 results in a biphasic dose-dependent response in HSC (Vaidya and Kale, 2015). Low concentrations of TGF-β1 are able to induce p44/42 MAPK-STAT pathway whereas high concentrations result in induced SMAD3 pathway activation and proliferation. In addition, TGF-β1 regulates distinct HSC subtypes. Early HSPC seem to be more sensitive to the inhibition by TGF-β1 while more differentiated progenitors get stimulated. Moreover, we also observed that genes involved in the negative regulation of TGFβ signaling were affected upon fEVs addition. Although we only identify 4 genes (*SKIL*, *SMAD7*, *LDLRAD4*, *ENG*), it is interesting to speculate that fEVs induce a TGF-β response with reduced *ex vivo* HSPC support. Inhibition of TGFBR by a neutralizing antibody prior to fEV addition indicated that an increased *ex vivo* expansion of UCB-$CD34^+$ is obtained and suggests additional mode of action.

The question remains whether our findings could eventually lead to an innovative EV component-based GMP-compliant approach to *ex vivo* expand UCB-derived HSCs for therapeutic purposes. In previous years various clinical studies were initiated in which UCB derived $CD34^+$ cells were expanded *ex vivo* using several factors, like StemRegenin 1, UM 171, TEPA, immobilized notch ligand Delta1 and nicotinamide (Lima et al., 2008; Delaney et al., 2010; Fares et al., 2014, 2017; Horwitz et al., 2014; Wagner et al., 2016; Stiff et al., 2018; Cohen et al., 2020). All components have shown to enhance HSC self-renewal and/or inhibit differentiation, and were suggested to improve *ex vivo* expansion of (primitive) HSCs. In all previous studies the HSPC support was established by the use of the specific component, as aEVs exerted their effect in this study, in combination with a cocktail of cytokines. However, the cytokine combinations used in the above-mentioned clinical studies were in general more extensive than our cocktail consisting of only two cytokines, SCF and Flt3L. Therefore it is difficult to compare the *in vitro* enhancing effects of the various compounds with our approach. In general, these clinical studies revealed that a higher total cell number (TNC) was closely associated with faster neutrophil engraftment in transplanted patients compared to historical controls, while in some cases platelet recovery was also statistically improved. Furthermore, only the studies using nicotinamide, UM171 and StemRegenin 1 reported long-term chimerism after transplantation of the expanded UCB-unit. These studies suggest that there is still much room for improvement for patient outcome and that the *in vivo* function of EVs and their role in hematopoietic support has to be further studied.

In conclusion, our study gives novel insights into the complex biological role of EVs in the bone marrow microenvironment.

Systematic analyses of supportive and less supportive primary BMSC derived extracellular vesicles indicated known molecules, e.g., microRNA cluster miR-99b/let-7e/miR-125a, and the presence of TGFb pathway components that are important regulators in the cell-cell communication via EVs and open new means for the application of EVs in the discovery of therapeutics for more efficient *ex vivo* HSPC expansion.

DATA AVAILABILITY STATEMENT

The datasets presented in this study can be found in online repositories. The names of the repository/repositories and accession number(s) can be found in the article/**Supplementary Material**.

AUTHOR CONTRIBUTIONS

CG, JM, EBr, BE, CV, and JP contributed to the conception and design of the experiments. CG, MKl, and MKo isolated EVs, perform *ex vivo* expansion experiment, flow cytometry experiments, and data analyses. CG, FA, and MB performed mass spectrometry analyses. EBi and RH performed smallRNA and RNAseq experiments. JP analyzed smallRNA and CD34 RNAseq data. CG performed statistical data analyses, generated the figures, and wrote the first versions of the manuscript, supervised by CV and JP. CG, JM, MKl, MKo, SE, RH, EBi, FA, MB, MN, BE, EBr, CV, and JP contributed to manuscript revisions, read, and approved the submitted version. All authors contributed to the article and approved the submitted version.

FUNDING

This work was supported by the grants from Erasmus MC (Mrace grant 2015) and Sanquin (PPOC-16-05).

ACKNOWLEDGMENTS

We thank N. van der Wel and A. E. Grootemaat at AMC-UvA for assisting with electron microscopy. M. ter Borg for contribution in scientific discussion. C. Kuijk for helping with the collection of biological samples.

SUPPLEMENTARY MATERIAL

The Supplementary Material for this article can be found online at: https://www.frontiersin.org/articles/10.3389/fbioe.2021.640419/full#supplementary-material

Supplementary Figure 1 | (A) Concentration dependent effect of fEVs on TNC proliferation of UCB CD34$^+$ cells. Different UCB-CD34$^+$ cell donors (n = 3) co-cultures with EVs derived from different single donors (n = 3), **(B)** aEVs (single donors, n = 2), but not serum free MSC medium or supernatant after EVs isolation, show a trend in positive contribution to the proliferation of UCB CD34$^+$ cells over a period of 10 days.

Supplementary Figure 2 | Top 30 most abundant proteins among both aEVs and fEVs displayed according to their expression level (mean ± SD), colors are in accordance with previous description.

Supplementary Table 1 | Proteomics data. Proteomics identification of all proteins present in aEVs and fEVs (n = 3 each). Proteins identified in both (1) aEVs and fEVS (2283 proteins), proteins that were identified only in aEVs (2) or fEVs (3), proteins that were overrepresented in aEVs (4), or in fEVs (5), comparison of the top100 Exocarta (6) proteins identified in fEVs and aEVs.

Supplementary Table 2 | small RNAseq data. Result output of the differential gene expression analyses of small RNA sequencing content of adult cells (AMSC, n = 2), adult EVs (AMSC.EV, n = 3), fetal Cells (FMSC, n = 3 donors), fetal EVs (FMSC.EV, n = 3 donors). Result output after differential gene expression analyses with DESeq2 (Love et al., 2014).

Supplementary Table 3 | Differential gene expression analyses of human UCB-CD34$^+$ 24 h incubated with aEVs, fEVs, and cytokine control. Result output of the differential gene expression analyses in UCB-CD34$^+$ incubated for 24 h with aEVs, fEVs or cytokine control (CC) (n = 3 per treatment). Result output after differential gene expression analyses with DESeq2 (Love et al., 2014).

REFERENCES

Bhagat, T. D., Zhou, L., Sokol, L., Kessel, R., Caceres, G., Gundabolu, K., et al. (2013). miR-21 mediates hematopoietic suppression in MDS by activating TGF-β signaling. *Blood* 121, 2875–2881. doi: 10.1182/blood-2011-12-397067

Boulais, P. E., and Frenette, P. S. (2015). Making sense of hematopoietic stem cell niches. *Blood* 125, 2621–2629. doi: 10.1182/blood-2014-09-570192

Cohen, S., Roy, J., Lachance, S., Delisle, J.-S., Marinier, A., Busque, L., et al. (2020). Hematopoietic stem cell transplantation using single UM171-expanded cord blood: a single-arm, phase 1-2 safety and feasibility study. *Lancet Haematol* 7, e134–e145. doi: 10.1016/S2352-3026(19)30202-9

Cooney, J. (2018). Expansion of cord blood stem cells and enhancing their mobilization and homing potential using mesenchymal stromal cells. *Blood* 132, 3344–3344.

Copelan, E. A. (2006). Hematopoietic stem-cell transplantation. *N. Engl. J. Med.* 354, 1813–1826. doi: 10.1056/NEJMra052638

Crane, G. M., Jeffery, E., and Morrison, S. J. (2017). Adult haematopoietic stem cell niches. *Nat. Rev. Immunol.* 17, 573–590. doi: 10.1038/nri.2017.53

Delaney, C., Heimfeld, S., Brashem-Stein, C., Voorhies, H., Manger, R. L., and Bernstein, I. D. (2010). Notch-mediated expansion of human cord blood progenitor cells capable of rapid myeloid reconstitution. *Nat. Med.* 16, 232–236. doi: 10.1038/nm.2080

de Lima, M., McNiece, I., Robinson, S. N., Munsell, M., Eapen, M., Horowitz, M., et al. (2012). Cord-blood engraftment with ex vivo mesenchymal-cell coculture. *N. Engl. J. Med.* 367, 2305–2315. doi: 10.1056/NEJMoa1207285

De Luca, L., Trino, S., Laurenzana, I., Simeon, V., Calice, G., Raimondo, S., et al. (2016). MiRNAs and piRNAs from bone marrow mesenchymal stem cell extracellular vesicles induce cell survival and inhibit cell differentiation of cord blood hematopoietic stem cells: a new insight in transplantation. *Oncotarget* 7, 6676–6692. doi: 10.18632/oncotarget.6791

Emmrich, S., Rasche, M., and Schöning, J. (2014). miR-99a/100∼ 125b tricistrons regulate hematopoietic stem and progenitor cell homeostasis by shifting the balance between TGFβ and Wnt signaling. *Genes* 2014, 858–874.

Fares, I., Chagraoui, J., Gareau, Y., Gingras, S., Ruel, R., Mayotte, N., et al. (2014). Pyrimidoindole derivatives are agonists of human hematopoietic stem cell self-renewal. *Science* 345, 1509–1512. doi: 10.1126/science.1256337

Fares, I., Chagraoui, J., Lehnertz, B., MacRae, T., Mayotte, N., Tomellini, E., et al. (2017). EPCR expression marks UM171-expanded CD34 cord blood stem cells. *Blood* 129, 3344–3351. doi: 10.1182/blood-2016-11-750729

Gao, X., Xu, C., Asada, N., and Frenette, P. S. (2018). The hematopoietic stem cell niche: from embryo to adult. *Development* 145:139691. doi: 10.1242/dev.139691

Godoy, P. M., Bhakta, N. R., Barczak, A. J., Cakmak, H., Fisher, S., MacKenzie, T. C., et al. (2018). Large Differences in Small RNA Composition Between Human Biofluids. *Cell Rep.* 25, 1346–1358. doi: 10.1016/j.celrep.2018.10.014

Gragert, L., Eapen, M., Williams, E., Freeman, J., Spellman, S., Baitty, R., et al. (2014). HLA match likelihoods for hematopoietic stem-cell grafts in the U.S. registry. *N. Engl. J. Med.* 371, 339–348. doi: 10.1056/NEJMsa1311707

Guo, S., Lu, J., Schlanger, R., Zhang, H., Wang, J. Y., Fox, M. C., et al. (2010). MicroRNA miR-125a controls hematopoietic stem cell number. *Proc. Natl Acad. Sci.* 107, 14229–14234. doi: 10.1073/pnas.0913574107

Harrell, C. R., Jovicic, N., Djonov, V., Arsenijevic, N., and Volarevic, V. (2019). Mesenchymal Stem Cell-Derived Exosomes and Other Extracellular Vesicles as New Remedies in the Therapy of Inflammatory Diseases. *Cells* 8:8121605. doi: 10.3390/cells8121605

Horwitz, M. E., Chao, N. J., Rizzieri, D. A., Long, G. D., Sullivan, K. M., Gasparetto, C., et al. (2014). Umbilical cord blood expansion with nicotinamide provides long-term multilineage engraftment. *J. Clin. Invest.* 124, 3121–3128. doi: 10.1172/JCI74556

Huang, D. W., Sherman, B. T., and Lempicki, R. A. (2009). Systematic and integrative analysis of large gene lists using DAVID bioinformatics resources. *Nat. Protoc.* 4, 44–57. doi: 10.1038/nprot.2008.211

Juric, M. K., Ghimire, S., Ogonek, J., Weissinger, E. M., Holler, E., van Rood, J. J., et al. (2016). Milestones of Hematopoietic Stem Cell Transplantation - From First Human Studies to Current Developments. *Front. Immunol.* 7:470. doi: 10.3389/fimmu.2016.00470

Keerthikumar, S., Chisanga, D., Ariyaratne, D., Al Saffar, H., Anand, S., Zhao, K., et al. (2016). ExoCarta: A Web-Based Compendium of Exosomal Cargo. *J. Mol. Biol.* 428, 688–692. doi: 10.1016/j.jmb.2015.09.019

Kehl, T., Kern, F., Backes, C., Fehlmann, T., Stöckel, D., Meese, E., et al. (2020). miRPathDB 2.0: a novel release of the miRNA Pathway Dictionary Database. *Nucleic Acids Res.* 48, D142–D147. doi: 10.1093/nar/gkz1022

Kindwall-Keller, T. L., and Ballen, K. K. (2020). Umbilical cord blood: The promise and the uncertainty. *Stem Cells Transl. Med.* 2020, 0288. doi: 10.1002/sctm.19-0288

Klamer, S. E., Dorland, Y. L., Kleijer, M., Geerts, D., Lento, W. E., van der Schoot, C. E., et al. (2018). TGFBI Expressed by Bone Marrow Niche Cells and Hematopoietic Stem and Progenitor Cells Regulates Hematopoiesis. *Stem Cells Dev.* 27, 1494–1506. doi: 10.1089/scd.2018.0124

Kulak, N. A., Pichler, G., Paron, I., Nagaraj, N., and Mann, M. (2014). Minimal, encapsulated proteomic-sample processing applied to copy-number estimation in eukaryotic cells. *Nat. Methods* 11, 319–324. doi: 10.1038/nmeth.2834

Lima, M., de, de Lima, M., McMannis, J., Gee, A., Komanduri, K., et al. (2008). Transplantation of ex vivo expanded cord blood cells using the copper chelator tetraethylenepentamine: a phase I/II clinical trial. *Bone Marrow Transplant.* 41, 771–778. doi: 10.1038/sj.bmt.1705979

Love, M. I., Huber, W., and Anders, S. (2014). Moderated estimation of fold change and dispersion for RNA-seq data with DESeq2. *Genome Biol.* 15:550. doi: 10.1186/s13059-014-0550-8

Mattsson, J., Ringdén, O., and Storb, R. (2008). Graft failure after allogeneic hematopoietic cell transplantation. *Biol. Blood Marrow Transplant.* 14, 165–170. doi: 10.1016/j.bbmt.2007.10.025

Mayani, H., Wagner, J. E., and Broxmeyer, H. E. (2020). Cord blood research, banking, and transplantation: achievements, challenges, and perspectives. *Bone Marrow Transplant.* 55, 48–61. doi: 10.1038/s41409-019-0546-9

Morhayim, J., Ghebes, C. A., Erkeland, S. J., Ter Borg, M. N. D., Hoogenboezem, R. M., Bindels, E. M. J., et al. (2020). Identification of osteolineage cell-derived extracellular vesicle cargo implicated in hematopoietic support. *FASEB J.* 34, 5435–5452. doi: 10.1096/fj.201902610R

Morhayim, J., van de Peppel, J., Braakman, E., Rombouts, E. W. J. C., Ter Borg, M. N. D., Dudakovic, A., et al. (2016). Osteoblasts secrete miRNA-containing extracellular vesicles that enhance expansion of human umbilical cord blood cells. *Sci. Rep.* 6:32034. doi: 10.1038/srep32034

Paciejewska, M. M., Maijenburg, M. W., Gilissen, C., Kleijer, M., Vermeul, K., Weijer, K., et al. (2016). Different Balance of Wnt Signaling in Adult and Fetal Bone Marrow-Derived Mesenchymal Stromal Cells. *Stem Cells Dev.* 25, 934–947. doi: 10.1089/scd.2015.0263

Perez-Riverol, Y., Csordas, A., Bai, J., Bernal-Llinares, M., Hewapathirana, S., Kundu, D. J., et al. (2019). The PRIDE database and related tools and resources in 2019: improving support for quantification data. *Nucleic Acids Res.* 47, D442–D450. doi: 10.1093/nar/gky1106

Stanevsky, A., Goldstein, G., and Nagler, A. (2009). Umbilical cord blood transplantation: pros, cons and beyond. *Blood Rev.* 23, 199–204. doi: 10.1016/j.blre.2009.02.001

Stiff, P. J., Montesinos, P., Peled, T., Landau, E., Goudsmid, N. R., Mandel, J., et al. (2018). Cohort-Controlled Comparison of Umbilical Cord Blood Transplantation Using Carlecortemcel-L, a Single Progenitor–Enriched Cord Blood, to Double Cord Blood Unit Transplantation. *Biol. Blood Marrow Transplant.* 24, 1463–1470. doi: 10.1016/j.bbmt.2018.02.012

Tyanova, S., Temu, T., Sinitcyn, P., Carlson, A., Hein, M. Y., Geiger, T., et al. (2016). The Perseus computational platform for comprehensive analysis of (prote)omics data. *Nat. Methods* 13, 731–740.

Vaidya, A., and Kale, V. P. (2015). TGF-β signaling and its role in the regulation of hematopoietic stem cells. *Syst. Synth. Biol.* 9, 1–10. doi: 10.1007/s11693-015-9161-2

van Niel, G., D'Angelo, G., and Raposo, G. (2018). Shedding light on the cell biology of extracellular vesicles. *Nat. Rev. Mol. Cell Biol.* 19, 213–228. doi: 10.1038/nrm.2017.125

Vonk, L. A., van Dooremalen, S. F. J., Liv, N., Klumperman, J., Coffer, P. J., Saris, D. B. F., et al. (2018). Mesenchymal Stromal/stem Cell-derived Extracellular Vesicles Promote Human Cartilage Regeneration In Vitro. *Theranostics* 8, 906–920. doi: 10.7150/thno.20746

Wagner, J. E. Jr., Brunstein, C. G., Boitano, A. E., DeFor, T. E., McKenna, D., Sumstad, D., et al. (2016). Phase I/II Trial of StemRegenin-1 Expanded Umbilical Cord Blood Hematopoietic Stem Cells Supports Testing as a Stand-Alone Graft. *Cell Stem Cell* 18, 144–155. doi: 10.1016/j.stem.2015.10.004

Wang, X., Dong, F., Zhang, S., Yang, W., Yu, W., Wang, Z., et al. (2018). TGF-β1 Negatively Regulates the Number and Function of Hematopoietic Stem Cells. *Stem Cell Reports* 11, 274–287. doi: 10.1016/j.stemcr.2018.05.017

Wojtowicz, E. E., Broekhuis, M. J. C., Weersing, E., Dinitzen, A., Verovskaya, E., Ausema, A., et al. (2019). MiR-125a enhances self-renewal, lifespan, and migration of murine hematopoietic stem and progenitor cell clones. *Sci. Rep.* 9:4785. doi: 10.1038/s41598-019-38503-z

Xie, H., Sun, L., Zhang, L., Liu, T., Chen, L., Zhao, A., et al. (2016). Mesenchymal Stem Cell-Derived Microvesicles Support Ex Vivo Expansion of Cord Blood-Derived CD34(+) Cells. *Stem Cells Int.* 2016:6493241. doi: 10.1155/2016/6493241

Conflict of Interest: The authors declare that the research was conducted in the absence of any commercial or financial relationships that could be construed as a potential conflict of interest.

Copyright © 2021 Ghebes, Morhayim, Kleijer, Koroglu, Erkeland, Hoogenboezem, Bindels, van Alphen, van den Biggelaar, Nolte, van der Eerden, Braakman, Voermans and van de Peppel. This is an open-access article distributed under the terms of the Creative Commons Attribution License (CC BY). The use, distribution or reproduction in other forums is permitted, provided the original author(s) and the copyright owner(s) are credited and that the original publication in this journal is cited, in accordance with accepted academic practice. No use, distribution or reproduction is permitted which does not comply with these terms.

frontiers in Bioengineering and Biotechnology

BRIEF RESEARCH REPORT
published: 13 April 2021
doi: 10.3389/fbioe.2021.640617

Raman Fingerprint of Extracellular Vesicles and Conditioned Media for the Reproducibility Assessment of Cell-Free Therapeutics

Cristiano Carlomagno[1†‡], Chiara Giannasi[2,3†‡], Stefania Niada[3‡], Marzia Bedoni[1‡], Alice Gualerzi[1‡$] and Anna Teresa Brini[2,3*‡$]

[1] IRCCS Fondazione Don Carlo Gnocchi ONLUS, Milan, Italy, [2] Department of Biomedical Surgical and Dental Sciences, University of Milan, Milan, Italy, [3] IRCCS Istituto Ortopedico Galeazzi, Milan, Italy

Extracellular Vesicles (EVs) and Conditioned Medium (CM) are promising cell-free approaches to repair damaged and diseased tissues for regenerative rehabilitation purposes. They both entail several advantages, mostly in terms of safety and handling, compared to the cell-based treatment. Despite the growing interest in both EVs and CM preparations, in the light of a clinical translation, a number of aspects still need to be addressed mainly because of limits in the reproducibility and reliability of the proposed protocols. Raman spectroscopy (RS) is a non-destructive vibrational investigation method that provides detailed information about the biochemical composition of a sample, with reported ability in bulk characterization of clusters of EVs from different cell types. In the present brief report, we acquired and compared the Raman spectra of the two most promising cell-free therapeutics, i.e., EVs and CM, derived from two cytotypes with a history in the field of regenerative medicine, adipose-derived mesenchymal stem/stromal cells (ASCs) and dermal fibroblasts (DFs). Our results show how RS can verify the reproducibility not only of EV isolation, but also of the whole CM, thus accounting for both the soluble and the vesicular components of cell secretion. RS can provide hints for the identification of the soluble factors that synergistically cooperate with EVs in the regenerative effect of CM. Still, we believe that the application of RS in the pipeline of cell-free products preparation for therapeutic purposes could help in accelerating translation to clinics and regulatory approval.

Keywords: mesenchymal stem/stromal cells, Raman spectroscopy, extracellular vesicles, conditioned medium, secretome, orthobiologics

OPEN ACCESS

Edited by:
Elizabeth R. Balmayor,
Maastricht University, Netherlands

Reviewed by:
Cecile Martinat,
Institut National de la Santé et de la Recherche Médicale (INSERM), France
Alice C. Rodrigues,
University of São Paulo, Brazil

****Correspondence:***
Anna Teresa Brini
anna.brini@unimi.it

†These authors have contributed equally to this work and share first authorship

‡ORCID:
Cristiano Carlomagno
orcid.org/0000-0002-5543-0505
Chiara Giannasi
orcid.org/0000-0002-7186-7432
Stefania Niada
orcid.org/0000-0003-3655-9968
Marzia Bedoni
orcid.org/0000-0003-2618-3661
Alice Gualerzi
orcid.org/0000-0003-2996-5714
Anna Teresa Brini
orcid.org/0000-0002-7848-8099

$These authors have contributed equally to this work and share last authorship

Specialty section:
This article was submitted to Preclinical Cell and Gene Therapy, a section of the journal Frontiers in Bioengineering and Biotechnology

Received: *11 December 2020*
Accepted: *10 March 2021*
Published: *13 April 2021*

Citation:
Carlomagno C, Giannasi C, Niada S, Bedoni M, Gualerzi A and Brini AT (2021) Raman Fingerprint of Extracellular Vesicles and Conditioned Media for the Reproducibility Assessment of Cell-Free Therapeutics. Front. Bioeng. Biotechnol. 9:640617. doi: 10.3389/fbioe.2021.640617

INTRODUCTION

Over the years, mesenchymal stem/stromal cells (MSCs) have gained popularity as therapeutics in a variety of clinical scenarios thanks to their ability to promote tissue regeneration and reduce inflammation. Among the most common MSC harvesting sources, the stromal vascular fraction of adipose tissue stands out as one of the most convenient in terms of both harvesting procedure and cell yield (Chu et al., 2019). To date, the clinical studies relying on the use of Adipose-derived MSCs (ASCs) comprise different applications, ranging from musculoskeletal diseases such as osteoarthritis to diabetes mellitus, colitis, and autoimmune disorders (Chu et al., 2019). Of note, in recent months ASC administration has also been evaluated as a therapeutic strategy for the treatment of Acute Respiratory Distress Syndrome in COVID-19 patients (Rogers et al., 2020).

Also recently, the therapeutic potential of dermal fibroblasts (DFs) has attracted scientific interest, mainly in the field of wound healing and skin grafts (Ichim et al., 2018). While the most common therapeutic applications include the treatment of acute and chronic wounds, burns, epidermolysis bullosa, and ulcers, we recently gave evidence also of a pro-osteogenic potential of DF secretome (Niada et al., 2018).

ASCs and DFs share common characteristics (such as immunophenotypic profile and differentiative potential) and, when implanted at the damaged site, both of them are able to exert immunomodulatory and regenerative actions (Nilforoushzadeh et al., 2017; Ichim et al., 2018).

Despite the overall success obtained in clinical trials, cell therapy presents several challenges, such as safety/regulatory concerns and technical aspects (harvesting procedure, cell expansion, and storage of the final product). In the past decade, increasing evidence has led to a paradigm shift in the mechanism of action of cell-based therapies, from the initial belief in a direct replacement of the damaged tissue to the evidence of paracrine signaling orchestrating the regenerative process. In comparison with cell-based strategies, cell-free approaches entail several advantages, mostly in terms of safety and handling. Nevertheless, in the light of a clinical translation a number of aspects still need to be addressed.

Extracellular vesicle-related (EV) research and application have attracted considerable commercial interest and investment thanks to their potential in diagnosis and therapy. In the field of regenerative medicine and regenerative rehabilitation (Willett et al., 2020), EVs released by MSCs have demonstrated their ability to foster recovery and repair of damaged and aged tissues. Despite the proven advantages, application methods and efficacy are debated mainly because of limits in the reproducibility and reliability of the proposed protocols. Indeed, the technical challenge is still open as no appropriate and quantifiable performance metrics have been developed yet to objectively assess the repeatability and efficiency of the multitude of suggested methods for separation and isolation of EVs from an MSC-derived culture medium. Therefore, data interpretation and assessment of EV treatment efficacy in regeneration studies are difficult to achieve.

Since their discovery as therapeutic agents, the EV efficacy as cell-free therapy has been compared to that of a conditioned medium (CM), which represents a mixture of different factors secreted by the cells, including growth factors and cytokines, enzymes, nucleic acids, bioactive lipids, and of course, EVs. From this perspective, the potential of MSC-derived EVs and CM as innovative biological approaches for the treatment of osteoarthritis is currently a hot topic in the orthopedic field (D'Arrigo et al., 2019). Although the production of CM preparations is simple in principle, their characterization and standardization are a major issue that needs to be overcome to deliver clinically acceptable products. Up to now, CM preparations are mainly analyzed for the presence of pro-inflammatory factors (Sriramulu et al., 2018), while EV preparations are commonly characterized by the size and number of particles, presence of EV-specific surface markers, and total protein concentration (Thery et al., 2018). Conversely, the correlation between the folds of concentration (routine CM concentrates) or protein concentration/number of particles (EV preparations) and product safety and potency is extremely limited or not even addressed (Bogatcheva and Coleman, 2019).

EVs are a subproduct of CM preparations. For this reason, it is important to consider that isolated EV populations can vary significantly depending on the isolation method considered and/or concentration procedure. Distinct isolation methods can lead to EV products with different purity levels, EV dimensions, intracellular origin, and thus with heterogeneous biochemical composition, and possibly regenerative effects. Differences in isolation procedures have brought confusing results and misleading opinions about EV application in regenerative medicine.

Raman spectroscopy (RS) is a non-destructive vibrational investigation method that can provide detailed information about the biochemical composition of a sample by taking advantage of the vibration modes of the chemical bonds present within molecules irradiated by laser. The collected spectrum is a combination of signals provided by lipids, proteins, nucleic acids, and metabolites in relation with their presence, concentration, coordination, modifications, interactions, and environment. The Raman bulk characterization of clusters of MSC-derived EVs can help assessing their purity and effective isolation (Gualerzi et al., 2019). Moreover, RS distinguishes with high accuracy EVs derived from different cell types (Gualerzi et al., 2017). For the present brief report, we acquired and compared the Raman spectra of two promising cell-free therapeutics, i.e., EVs and CM, derived from two cytotypes with a history in the field of regenerative medicine, ASCs and DFs. Our results show how RS can verify the reproducibility not only of EV isolation from ASCs and DFs, but also of an even more complex type of sample, the whole CM, accounting for both the soluble and the vesicular components of cell secretion. Moreover, RS can provide hints for the identification of the soluble factors that synergistically cooperate with EVs in the regenerative effect of CM.

MATERIALS AND METHODS

Cell Isolation and Maintenance

ASCs and DFs were isolated from the waste tissues collected at IRCCS Istituto Ortopedico Galeazzi under the Institutional Review Board approval. ASCs were derived from two male and four female donors (mean age 44 ± 16 y/o) undergoing aesthetic (n = 4) or prosthetic (n = 2) surgery, following well-established protocols (de Girolamo et al., 2009). Briefly, the subcutaneous adipose tissue was fragmented with a scalpel and digested with 0.75 mg/ml type I Collagenase (Worthington Biochemical Corporation, Lakewood, NJ, United States) for 30 min at 37°C. DFs were derived from three female donors (mean age 39 ± 12 y/o) undergoing aesthetic surgery, following standard protocols

(Niada et al., 2018). Briefly, the abdominal dermis was first subjected to a mechanical fragmentation and then enzymatically digested with 0.1% type I collagenase for 30 min at 37°C. Isolated ASCs and DFs were then plated at the density of 10^5 cells/cm^2 in high glucose DMEM plus 10% FBS (EuroClone, Pero, Italy), 2 mM l-glutammine (Sigma-Aldrich, St. Louis, MO, United States), 50 U/ml penicillin and 50 μg/ml streptomycin (Sigma-Aldrich, St. Louis, MO, United States) and expanded for IV-VI passages for EV and CM production.

EV Isolation and CM Production

Conditioned media were collected from 80 to 90% confluent ASCs and DFs cultured for 3 days in starving conditions (absence of FBS). Supernatants were first centrifuged at 2,500 g for 15 min at 4°C to remove dead cells, large apoptotic bodies, and debris, and then they followed different routes in order to isolate EVs rather than obtain CM. EV isolation was performed through differential centrifugation at 100,000 g in a SW 41 Ti swinging-bucket rotor (Beckman Coulter, Brea, CA, United States) (Gualerzi et al., 2017) while CM concentration was achieved by spinning the samples for 90 min at 4,000 g through Amicon Ultra-15 Centrifugal Filter Devices with 3 kDa cut-off (Merck Millipore, Burlington, MA, United States) (Niada et al., 2018).

Nanoparticle Tracking Analysis

For each cell type, coupled EV and CM samples were diluted in 0.22 μm triple-filtered PBS and the nanoparticle tracking analysis (NTA) was performed by NanoSight NS300 (Malvern PANalytical, Salisbury, United Kingdom). Each measurement consisted in three videos lasting 1 min. All captures complied with the quality criteria of 20–120 particles/frame, concentration ranging from 10^6 to 4×10^9 particles/ml and valid tracks > 20%. Data analysis was performed with the in-build NanoSight Software NTA.

Western Blot

Prior to Western Blot analysis, an aliquot of each CM sample was quantified through the Bio-Rad Protein Assay (Bio-Rad, Milan, Italy), while EV pellets were directly lysed in the appropriate buffer without protein quantification (Niada et al., 2020). The amount of 10 μg of CM, corresponding to ∼25 μl, and EVs derived from 1.5×10^6 ASCs or DFs were lysed in 5% 2-Mercaptoethanol and 2X Laemmli Buffer (Bio-Rad, Milan, Italy), separated in a 4–15% polyacrylamide gel (Bio-Rad, Milan, Italy) and transferred to a nitrocellulose membrane (GE Healthcare, Chicago, IL, United States) (Niada et al., 2020). After being blocked with 5% non-fat dried milk (AppliChem, Darmstadt, Germany) and 0.1% Tween (Promega, Madison, WI, United States) in PBS, samples were probed overnight at 4°C for the expression of Alix (NBP1-90201, 1:1,000 diluted, Novus Biologicals, Centennial, CO, United States), FLOT-1 (1:500 diluted, BD Transduction Laboratories, San Jose, CA, United States), TSG101 (T5701, 1:1,000 diluted, Millipore, Burlington, MA, United States), and CD9 (1:1,000 diluted, System Biosciences, Palo Alto, CA, United States). All washing steps were performed with 0.1% Tween in PBS, and after incubation with appropriate peroxidase-conjugated secondary antibodies (sc-2004, 1:5,000 diluted, Santa Cruz Biotechnology, Dallas, TX, United States and 62-6520, 1:20,000 diluted, Thermo Fisher Scientific, Waltham, MA, United States and System Biosciences, Palo Alto, CA, United States), bands were revealed using ECL (Cyanagen, Bologna, Italy). Images were acquired with the ChemiDoc imaging system (Bio-Rad, Milan, Italy).

Raman Spectroscopy

Samples were analyzed by RS following a previously reported protocol for the bulk characterization of EVs (Gualerzi et al., 2017, 2019). Briefly, 5–10 μl of EV suspension or CM were deposited on a calcium fluoride slide and air-dried. Measurements were performed with Raman microspectroscopy (LabRAM Aramis, Horiba Jobin Yvon S.A.S., Lille, France) equipped with a 532 nm laser and with a 50× objective (N.A. 0.75), 1,800 grooves/mm diffraction grating, 400 μm entrance slit, and confocal mode (300 μm pinhole) in the spectral ranges 600–1,800 and 2,600–3,200 cm^{-1}. Calibration was performed using silicon reference peak (520.7 cm^{-1}). Taking advantage of the integrated software Labspec 6 (Horiba Jobin Yvon S.A.S., Lille, France), we performed a baseline correction (fourth-degree polynomial curve), unit vector normalization, and post-acquisition calibration before the statistical analysis of spectra.

Statistical Analysis

Descriptive and multivariate statistical analysis of Raman spectra were performed by Origin 2018 (OriginLab, Northampton, MA, United States) as previously described (Gualerzi et al., 2017, 2019). Principal component analysis (PCA) of the normalized and aligned spectra was performed and followed by linear discriminant analysis (LDA). The classification model created, based on leave-one-out cross-validation, allowed us to evaluate the discrimination power between cell sources of EVs and CM. The non-parametric Kruskal-Wallis test was then performed on canonical variable scores to verify that the means of each group were significantly different, despite within-group variance. The Kruskal-Wallis test was performed also to evaluate the inter-donor variability of canonical variable 1 and 2 scores, with a p-value of 0.05.

RESULTS

EV and CM preparations were obtained in conformity with previously reported protocols with tested efficacy in regeneration studies. To compare the two cell-free preparations, size distribution and concentration of particles were assessed.

NTA revealed a similar size distribution between all samples (**Figures 1A–E**), with 50% of the events falling inside the dimensional range of 150 nm. No significant difference was observed in size distribution between EV and CM samples (non-parametric Mann-Whitney test; $p > 0.05$). Given the same number of donor cells, the vesicular yield is comparable between the ASCs and DFs. As expected, EV preparations showed a lower number of particles/10^6 cells in comparison with coupled CM samples. Indeed, the post-ultracentrifugation

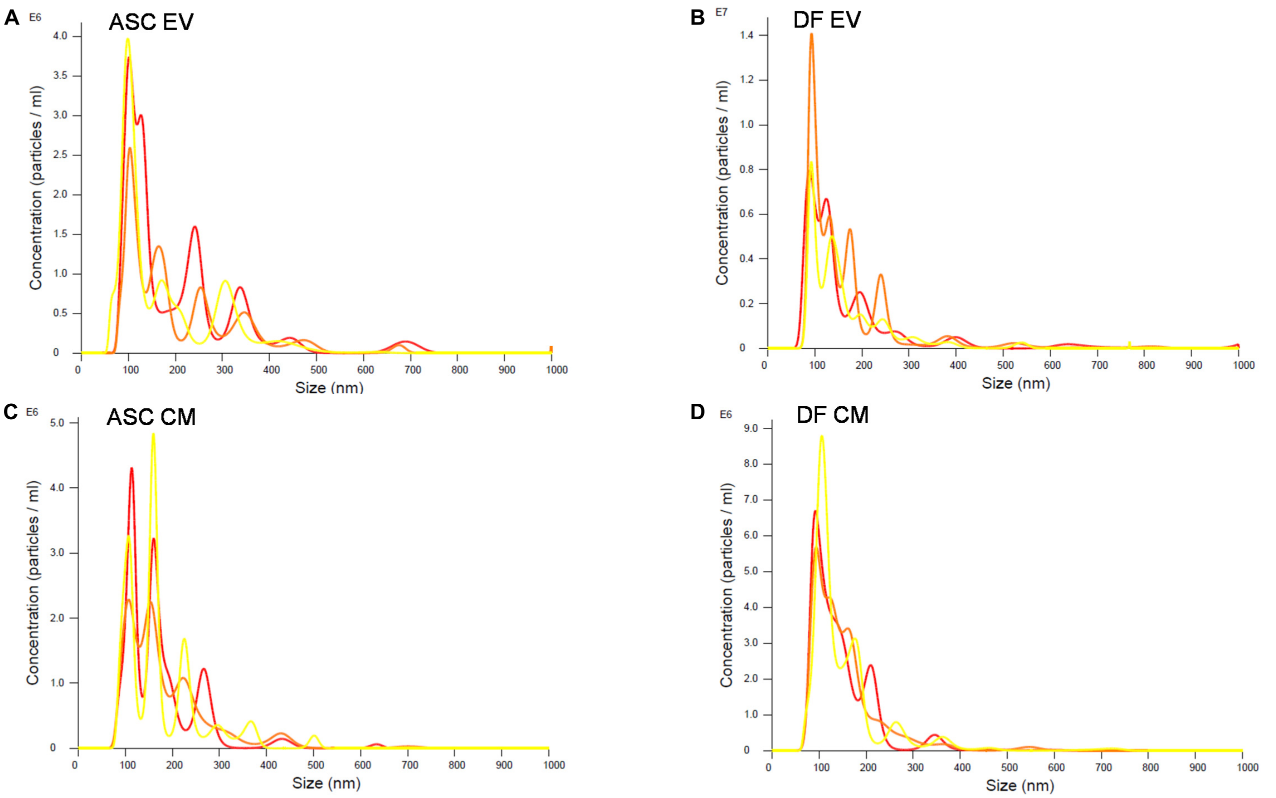

E

	Particle size (nm)				
	Mean	Mode	D10	D50	D90
ASC EV	182.7±26.7	100.4±9.0	90.0±8.1	137.6±22.4	324.9±41.7
DF EV	183.6±17.2	117.1±31.1	98.7±14.3	150.7±24.2	287.6±25.3
ASC CM	169.9±18.7	118.3±29.1	95.0±11.8	150.1±17.0	275.5±28.2
DF CM	175.4±25.1	116.5±24.7	101.9±13.7	153.2±28.5	280.3±37.6

F

	Yield (particles/10^6 cells)
ASC EV	$2.6 \pm 0.8 \times 10^8$
DF EV	$3.7 \pm 0.6 \times 10^8$
ASC CM	$8.5 \pm 3.9 \times 10^8$
DF CM	$8.4 \pm 2.8 \times 10^8$

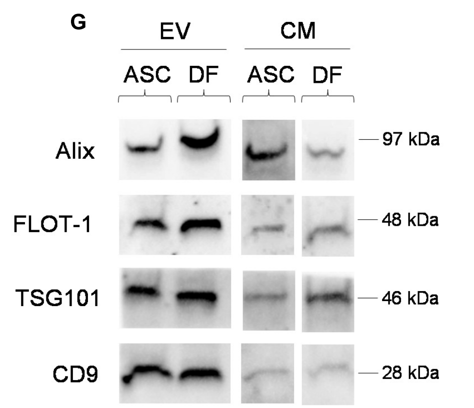

FIGURE 1 | (A–D) Representative NTA of EV and CM samples derived from ASCs and DFs. Each graph shows the size distribution of 3 consecutive 1 min runs for each sample. **(E–F)** Size distribution and vesicular yield deriving from 6 NTA measurements/group shown as mean ± SD. **(G)** Western Blot of CM and EV samples from ASCs and DFs, showing the expression of the vesicular markers Alix, FLOT-1, TSG101 and CD9. In each lane, 10μg of CM or EV deriving from 1.5×10^6 cells were loaded.

recovery was about 30% of the input for ASCs and 44% for DFs, as shown in **Figure 1F**. Besides, we obtained the purity score by calculating the ratio between the number of particles and the total protein content on the same sample (Gualerzi et al., 2019). The data demonstrated that EV preparations from both ASCs and DFs have higher purity scores compared to CM samples, as expected (data not shown). The expression of the canonical markers Alix, FLOT-1, TSG101, and CD9 was confirmed in all samples by Western Blot, as shown in **Figure 1G**.

Raman spectroscopy analysis of EV suspensions and CM preparations were performed on dried drops layed on Raman-transparent calcium fluoride slides. Data were obtained in the spectral range 600–1,800 and 2,600–3,200 cm^{-1} with a good signal-to-noise ratio and a good reproducibility of the spectra in the acquisition conditions considered, as attested by the values of standard deviation (**Figures 2A–D**). Raman data were acquired for all of the EV and CM samples from both ASCs and DFs, obtained from the cells of six and three different donors, respectively.

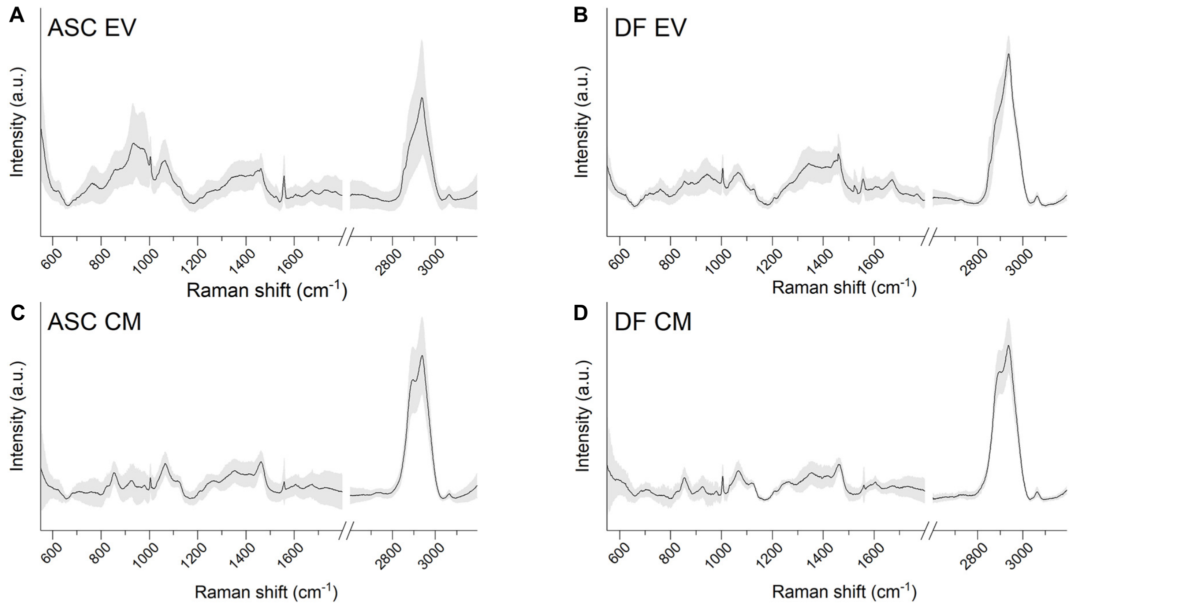

FIGURE 2 | (A–D) Average Raman spectra obtained with 532 nm laser line on air-dried drops of EV or CM samples lied on calcium fluoride slides. Both ASC-derived and DF-derived samples are shown. Gray shaded areas represent ± 1 standard deviation.

The average spectra from both EVs and CM extracted from the identified cell sources showed the characteristic Raman bands of proteins (Amide I 1,650 cm^{-1}), lipids (2,700–3,200 cm^{-1}), and nucleic acids (720–820 cm^{-1}). The EV average spectra are in agreement with previously reported bulk characterization of vesicles by RS (Gualerzi et al., 2017, 2019). Interestingly, the lipid content described by the CH, CH_2, and CH_3 bonds (in the spectral range 2,600–3,200 cm^{-1}) was different between EV and CM samples, suggesting that the main differences between the two types of cell-free preparations might involve the lipid components.

To further investigate the reproducibility of the acquisition setting and the differences in the secretome of the two cell sources, Raman data from both EVs and CM preparations were considered for multivariate PCA-LDA analysis. The scatterplot shown in **Figure 3A** graphically represents the results of the multivariate analysis of EV- and CM-derived spectra from ASC and DF samples, with each dot representing one single spectrum. In accordance with our previous data (Gualerzi et al., 2017), the significant differences observed in the spectral profiles of EVs from ASCs and DFs, determine an error rate in the classification of EV samples of 21.92% for ASC-derived EVs and of 2.38% for DF-derived EVs. The spectral difference between the two EV samples is visually represented in the scatter plot of **Figure 3A**: the dots corresponding to the Raman spectra of ASC-derived EVs (pink) have a minimal overlap with those from DF-derived EVs (light blue). Interestingly, also CM preparations from ASCs and DFs could be distinguished by means of the PCA-LDA classification model. Although spectral similarities between CM samples determine a partial overlap in the scatter plot reported in **Figure 3A**, the proposed classification model suggests the possibility to distinguish between the secretome of ASCs and that of DFs by their Raman profile. This result is in agreement with previously reported data from differential proteomic analysis performed on CM samples from ASCs and DFs, demonstrating that CM from these cell types share common proteomic patterns (Niada et al., 2018). Collectively, the mean values of canonical variable 1 obtained for ASC- and DF-derived samples were demonstrated to be significantly different ($p < 0.001$, Kruskal-Wallis test, **Figure 3B**) for both EVs and CM. To verify that the difference between CM and EV preparations was related to the cell source and not due to donor-associated differences, Kruskal-Wallis test was performed demonstrating that the canonical variable 1 and 2 scores were not significantly different between donors at the 0.05 level. On the contrary, looking at the canonical variable 2 values, only those from DF-derived EV samples were shown to be significantly different from DF-derived CM and ASC-derived EVs and CM (**Figure 3C**).

Looking at the classification error rate after leave-one-out cross-validation, the calculated mean percentage of misclassification was 25.43%, with the lower value of error rate for DF-derived EVs (14.29%).

In order to deepen the reasons for the observed spectral differences, **Figure 4A** shows the subtraction spectra obtained by subtracting the EV average spectrum to the CM average spectrum for ASC (red line) and DF (blue line) preparations. We can speculate that the reported spectra represent mainly the contribution of soluble secretome factors to the CM samples, once the contribution of EVs was removed. Although PCA-LDA analysis highlighted partial overlap in the spectra from CM preparations, the subtraction of the EV spectral contribution made the differences between the non-EV secretome of ASCs and DFs apparent. It is worth noting that, in the present study, the non-EV secretome might include those particles that cannot

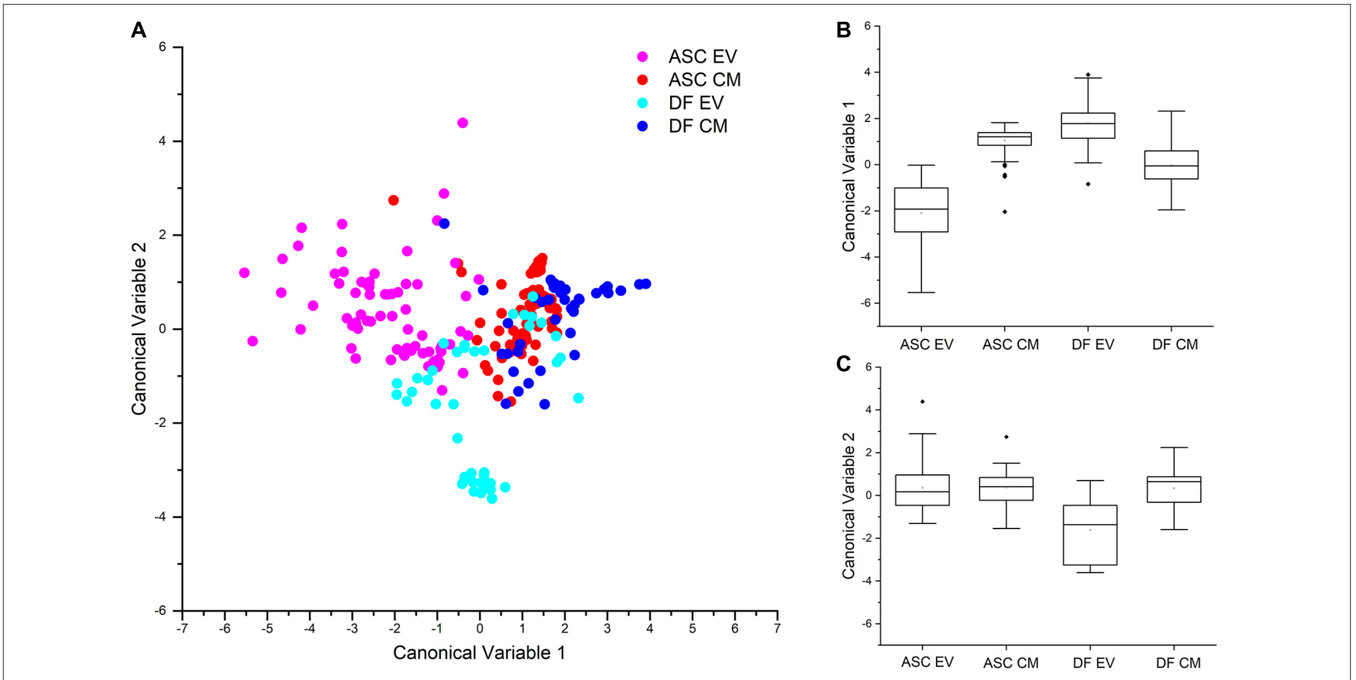

FIGURE 3 | (A) Scatterplot reporting the results of the PCA-LDA multivariate statistical analysis of ASC- and DF-derived secretome products, EVs and CM. Each dot represents one spectrum that has been assigned with canonical variable 1 and canonical variable 2 scores. As reported in the legend, different colors are assigned to spectra based on the source: ASC-derived EVs, pink; ASC-derived CM, red; DF-derived EVs, light blue; DF-derived CM, blue. Partial overlap of blue and red dots shows similarities in the spectra from ASC- and DF-derived CM. B, C: Box plots representing the canonical variable 1 **(B)** and canonical variable 2 **(C)** scores obtained after PCA-LDA analysis and the respective results of the non-parametric Kruskal-Wallis test for the analysis of variance. The statistical data demonstrate that CM and EV preparations can be distinguished by the PCA-LDA classification model.

be separated by the ultracentrifugation method due to poor yield and technical limitation (Thery et al., 2018). For this reason, we cannot exclude the contribution of a subpopulation of EVs, possibly both small and large EVs, to the reported spectral differences.

The main peaks of the subtraction spectrum were identified, revealing that the main differences can be attributed to the saccharide content of the samples (Movasaghi et al., 2007). In particular, 761–764 (Tryptophan ring or Pyrimidine ring); 832–836 (O-P-O stretching, Tyrosine/DNA); 941.6 (skeletal modes, polysaccharides); 1,049 (Glycogen); 1,440 (CH/CH_2 deformation); 2,836–2,839 and 2,890.3 cm^{-1} (contributions from CH2 asymmetric stretch of proteins and lipids) were identified as prominent peaks in the subtraction spectra of both cell types, thus describing the major differences in the biochemical composition of CM compared to EVs for both cell sources. On the contrary, the 971 cm^{-1}, attributed to the C-C stretching of proteins, was peculiar of ASC-derived data, whereas 2,930 and 2,949 cm^{-1} characterized the DF subtraction spectrum, underlying that lipids play a major role in the biochemical difference of cell-free preparations from this cell type.

Finally, we obtained the subtraction spectra for CM and EV preparations by subtracting the spectrum of the DF-derived samples to the ASC-derived one. **Figures 4B,C** show the results using the same scale on the *y*-axis, i.e., the same intensity scale. Spectral differences are more prominent between EV spectra than CM spectra from ASCs and DFs, suggesting that CM chemical composition and content are more similar than the EV cargo between the two cell sources. The subtraction spectra describe the differences highlighted by PCA-LDA from another point of view.

DISCUSSION

In the present work, we demonstrated that CM preparations, compared to EV ones, retained a 3–4 times higher number of particles per million donor cells. This result can be attributed to a suboptimal yield of the ultracentrifugation procedure, as already described in the literature (Tang et al., 2017; Takov et al., 2019). Nevertheless, the isolation procedure through ultracentrifugation did not affect EVs quality as far as size distribution and antigen profile are concerned.

The RS characterization of CM and EV preparations has demonstrated its usefulness in assessing the quality and repeatability of the cell-free product, but it has also brought to light biochemical similarities and differences between the two preparations. The present data confirm previously reported observations about the ability of RS to uncover the biochemical differences between EVs released by different cell sources (Gualerzi et al., 2017), as well as the possibility to use the spectroscopic method to highlight differences in the purity of EV samples obtained by different protocols (Gualerzi et al., 2019). Concerning this latter point, it was previously suggested that variations in the method of EV isolation influence the quality

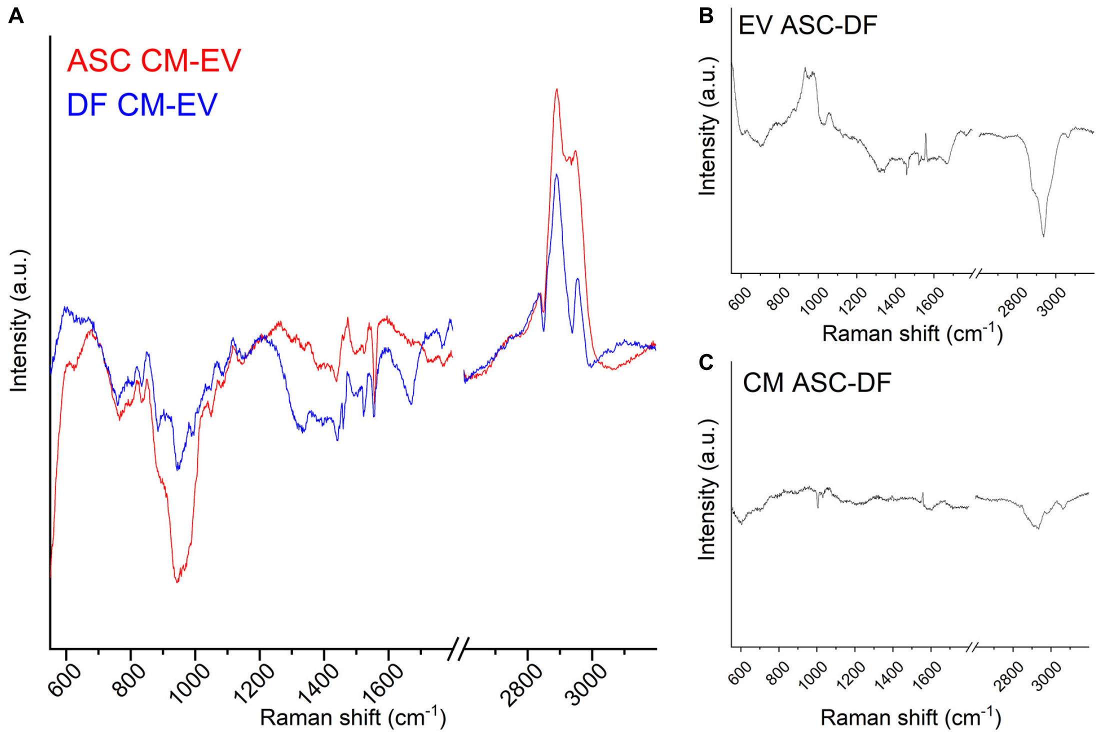

FIGURE 4 | (A) Subtraction spectra obtained for ASC (red line) and DF (blue line) preparations by subtracting the EV average spectrum to the CM average spectrum. **(B,C)** Subtraction spectra obtained for CM **(B)** and EV **(C)** preparations by subtracting the ASC average spectrum to the DF average spectrum. All graphs display the same scale for the *y*-axis (Intensity of the Raman signal).

and quantity of co-isolated soluble factors (quantified also by the purity scores) and induce the selection of subpopulations of EVs. The data herein reported confirm the possibility of using Raman analysis to characterize EV products with variable purity index, but also different cell-free preparations, like CM samples. The advantage of the proposed methodology is related to the identification of a spectroscopic fingerprint that does not imply the detection and labeling of a single or a limited panel of specific antigens but provides an overall description of the content of the preparation that is under investigation. In the search for the optimal protocol for EV or CM preparation, the Raman analysis can verify the repeatability of the downstream product. Once the adequate translational procedure is found, the Raman data can verify the content of multiple batches, repeatedly, without the need for *ad hoc* preparations to be "sacrificed" for the quality check. Despite the fact that most researchers dealing with cell-free products for regenerative medicine might find the methodology apparently complicated and possibly expensive, it is worth noting that, once optimized, the acquisition protocol does not require sample preparation and it could be performed using portable, cost-effective instruments, commercially available and widely used for diagnostic purposes. Differently from other interesting approaches for EV detection that take advantage of Surface Enhanced Raman Scattering (SERS) (Lee et al., 2017; Chalapathi et al., 2020), the proposed protocol relies on the bulk characterization of the specimen, with less intense signals but more versatile. The SERS approach is able to highly enhance the Raman effect provided by various biological molecules present in a specific fluid, but the enhancement is not selective because it relies on the non-specific formation of a hot spot between the nanostructured metallic material and the molecule. In our case, the CM characterized present various heterogeneous biological molecules, and consecutively, the application of the SERS regimen could provide the enhancement of the Raman signal of unwanted molecules, e.g., proteins, masking the effective CM Raman signature.

As for the similarities in the spectral signature of CM and EV samples within the same cell source, we can speculate that some of them might be related to the particles present within the CM preparation. Nonetheless, it should be noted that other soluble factors could be shared between CM and EV samples, i.e., molecules co-isolated with vesicles or bound to the external surface of EVs. Another interesting aspect is the partial overlap of ASC- and DF-derived CM samples obtained by PCA-LDA analysis, revealing that the impact of the cell source is more evident for EV preparations. We hypothesize that this result may in part depend on the different route of secretion between soluble factors and EV cargo, the latter being more selectively controlled by the cells, especially for miRNA sorting (Abels and Breakefield, 2016). Moreover, EV lipid composition shares common features with the cell of origin. Therefore, even though CM samples represent a complex cocktail accounting for a lot more than EVs, the presence of common freely secreted molecules between ASCs and DFs may flatten the statistical comparison and mask the impact of the observed differences on EV composition. Of note, through a differential proteomic approach, we recently gave evidence of a slightly lower similarity between the CM samples from the two cell populations in comparison to EV ones (93.4% vs. 97.2% of shared proteins between CM and EVs, respectively) (Niada et al., 2020). This discrepancy is most probably due to the contribution of non-protein molecules to the Raman profile of the samples. Here we suggest that the factors that majorly contribute in distinguishing ASC- and DF-EVs are lipids rather than proteins, confirming previously reported data (Gualerzi et al., 2017). It also has to be noted that the lipid components involved in the biochemical differences between the considered samples comprise but are not limited to the EV lipid bilayer. Both EVs and CM might include bioactive lipids, like endocannabinoids, that can be freely secreted by the cell and mediate communication among different cell types. As a consequence, deep lipidomic analysis should be performed to investigate the origin of the observed spectral differences between the two preparations.

Moreover, the subtraction spectra between CM and EV revealed that, for both cell types, remarkable differences seem to be related to saccharide content. Considering that theoretically CM samples contain naïve vesicles, since the process to obtain them consists simply of a filtration step, we can hypothesize that ultracentrifugation may enrich an EV subpopulation with specific carbohydrate contents, e.g., peculiar glycosylation profiles. Indeed, in recent years EV glycomics has attracted scientific interest for its implications both as a diagnostic tool (Williams et al., 2018) and in the study of EV uptake (Williams et al., 2019). From this perspective, a first report on the impact of the isolation method on the EV glycosylation profile has been recently published (Freitas et al., 2019).

CONCLUSION

In conclusion, with the present work we took a step forward in the characterization and molecular profiling of two secretome formulas derived from distinct cell sources by providing evidence of both a quantitative difference in the yield of vesicular elements per million cells between CM and EV preparations and a qualitative difference in the Raman spectra depending on sample type (CM or EVs) and cell of origin (ASCs or DFs). Our data demonstrate that RS can be a valuable tool in the quality and reproducibility assessment of cell-free products to be used in the pipeline of stem cell-derived products for regenerative medicine, as it does not focus on a specific component but rather looks at the true complexity of their composition in which nucleic acids, lipids, carbohydrates, and proteins play specific and key roles.

DATA AVAILABILITY STATEMENT

The raw data supporting the conclusions of this article will be made available by the authors, without undue reservation.

AUTHOR CONTRIBUTIONS

CC, CG, SN, AG, and AB: conceptualization. CC, CG, SN, and AG: methodology. CC, CG, SN, MB, AG, and AB: resources. CC, CG, and AG: data curation and writing and preparation of the original draft. SN, MB, and AB: editing and review of writing. AG and AB: supervision. CC, CG, AG, and AB: project administration. CG, MB, AG, and AB funding acquisition. All authors have read and agreed to the published version of the manuscript.

FUNDING

This research was funded by the Italian Ministry of Health, grant number RC L1039 (IRCCS Istituto Ortopedico Galeazzi) and RC2020-2022 (IRCCS Fondazione Don Carlo Gnocchi ONLUS). Funds for open access publication fees were received from IRCCS Istituto Ortopedico Galeazzi.

REFERENCES

Abels, E. R., and Breakefield, X. O. (2016). Introduction to extracellular vesicles: biogenesis, RNA cargo selection, content, release, and uptake. *Cell. Mol. Neurobiol.* 36, 301–312. doi: 10.1007/s10571-016-0366-z

Bogatcheva, N. V., and Coleman, M. E. (2019). Conditioned medium of mesenchymal stromal cells: a new class of therapeutics. *Biochemistry (Mosc.)* 84, 1375–1389. doi: 10.1134/s0006297919110129

Chalapathi, D., Padmanabhan, S., Manjithaya, R., and Narayana, C. (2020). Surface-enhanced raman spectroscopy as a tool for distinguishing extracellular vesicles under autophagic conditions: a marker for disease diagnostics. *J. Phys. Chem. B* 124, 10952–10960. doi: 10.1021/acs.jpcb.0c06910

Chu, D. T., Nguyen Thi Phuong, T., Tien, N. L. B., Tran, D. K., Minh, L. B., Thanh, V. V., et al. (2019). Adipose tissue stem cells for therapy: an update on the progress of isolation, culture, storage, and clinical application. *J. Clin. Med.* 8:917. doi: 10.3390/jcm8070917

D'Arrigo, D., Roffi, A., Cucchiarini, M., Moretti, M., Candrian, C., and Filardo, G. (2019). Secretome and extracellular vesicles as new biological therapies for knee osteoarthritis: a systematic review. *J. Clin. Med.* 8:1867. doi: 10.3390/jcm8111867

de Girolamo, L., Lopa, S., Arrigoni, E., Sartori, M. F., Baruffaldi Preis, F. W., and Brini, A. T. (2009). Human adipose-derived stem cells isolated from young and elderly women: their differentiation potential and scaffold interaction during in vitro osteoblastic differentiation. *Cytotherapy* 11, 793–803. doi: 10.3109/14653240903079393

Freitas, D., Balmaña, M., Poças, J., Campos, D., Osório, H., Konstantinidi, A., et al. (2019). Different isolation approaches lead to diverse glycosylated extracellular vesicle populations. *J. Extracell. Vesicles* 8:1621131. doi: 10.1080/20013078.2019.1621131

Gualerzi, A., Kooijmans, S. A. A., Niada, S., Picciolini, S., Brini, A. T., Camussi, G., et al. (2019). Raman spectroscopy as a quick tool to assess purity of extracellular vesicle preparations and predict their functionality. *J. Extracell. Vesicles* 8:1568780. doi: 10.1080/20013078.2019.1568780

Gualerzi, A., Niada, S., Giannasi, C., Picciolini, S., Morasso, C., Vanna, R., et al. (2017). Raman spectroscopy uncovers biochemical tissue-related features of extracellular vesicles from mesenchymal stromal cells. *Sci. Rep.* 7:9820.

Ichim, T. E., O'Heeron, P., and Kesari, S. (2018). Fibroblasts as a practical alternative to mesenchymal stem cells. *J. Transl. Med.* 16:212.

Lee, C., Carney, R., Lam, K., and Chan, J. W. (2017). SERS analysis of selectively captured exosomes using an integrin-specific peptide ligand. *J. Raman Spectrosc.* 48, 1771–1776. doi: 10.1002/jrs.5234

Movasaghi, Z., Rehman, S., and Rehman, I. U. (2007). Raman spectroscopy of biological tissues. *Appl. Spectrosc. Rev.* 42, 493–541. doi: 10.1080/05704920701551530

Niada, S., Giannasi, C., Gualerzi, A., Banfi, G., and Brini, A. T. (2018). Differential proteomic analysis predicts appropriate applications for the secretome of adipose-derived mesenchymal stem/stromal cells and dermal fibroblasts. *Stem Cells Int.* 2018:7309031.

Niada, S., Giannasi, C., Magagnotti, C., Andolfo, A., and Brini, A. T. (2020). Proteomic analysis of extracellular vesicles and conditioned medium from human adipose-derived stem/stromal cells and dermal fibroblasts. *J. Proteom.* 232:104069. doi: 10.1016/j.jprot.2020.104069

Nilforoushzadeh, M. A., Ahmadi Ashtiani, H. R., Jaffary, F., Jahangiri, F., Nikkhah, N., Mahmoudbeyk, M., et al. (2017). Dermal fibroblast cells: biology and function in skin regeneration. *J. Skin Stem Cell* 4:e69080.

Rogers, C. J., Harman, R. J., Bunnell, B. A., Schreiber, M. A., Xiang, C., Wang, F. S., et al. (2020). Rationale for the clinical use of adipose-derived mesenchymal stem cells for COVID-19 patients. *J. Transl. Med.* 18:203.

Sriramulu, S., Banerjee, A., Di Liddo, R., Jothimani, G., Gopinath, M., Murugesan, R., et al. (2018). Concise review on clinical applications of conditioned medium derived from human Umbilical Cord-Mesenchymal Stem Cells (UC-MSCs). *Int. J. Hematol. Oncol. Stem Cell Res.* 12, 230–234.

Takov, K., Yellon, D. M., and Davidson, S. M. (2019). Comparison of small extracellular vesicles isolated from plasma by ultracentrifugation or size-exclusion chromatography: yield, purity and functional potential. *J. Extracell. Vesicles* 8:1560809. doi: 10.1080/20013078.2018.1560809

Tang, Y. T., Huang, Y. Y., Zheng, L., Qin, S. H., Xu, X. P., An, T. X., et al. (2017). Comparison of isolation methods of exosomes and exosomal RNA from cell culture medium and serum. *Int. J. Mol. Med.* 40, 834–844. doi: 10.3892/ijmm.2017.3080

Thery, C., Witwer, K. W., Aikawa, E., Alcaraz, M. J., Anderson, J. D., Andriantsitohaina, R., et al. (2018). Minimal information for studies of extracellular vesicles 2018 (MISEV2018): a position statement of the International Society for Extracellular Vesicles and update of the MISEV2014 guidelines. *J. Extracell. Vesicles* 7:1535750.

Willett, N. J., Boninger, M. L., Miller, L. J., Alvarez, L., Aoyama, T., Bedoni, M., et al. (2020). Taking the next steps in regenerative rehabilitation: establishment of a new interdisciplinary field. *Arch. Phys. Med. Rehabil.* 101, 917–923. doi: 10.1016/j.apmr.2020.01.007

Williams, C., Pazos, R., Royo, F., González, E., Roura-Ferrer, M., Martinez, A., et al. (2019). Assessing the role of surface glycans of extracellular vesicles on cellular uptake. *Sci. Rep.* 9:11920.

Williams, C., Royo, F., Aizpurua-Olaizola, O., Pazos, R., Boons, G. J., Reichardt, N. C., et al. (2018). Glycosylation of extracellular vesicles: current knowledge, tools and clinical perspectives. *J. Extracell. Vesicles* 7:1442985. doi: 10.1080/20013078.2018.1442985

Conflict of Interest: The authors declare that the research was conducted in the absence of any commercial or financial relationships that could be construed as a potential conflict of interest.

Copyright © 2021 Carlomagno, Giannasi, Niada, Bedoni, Gualerzi and Brini. This is an open-access article distributed under the terms of the Creative Commons Attribution License (CC BY). The use, distribution or reproduction in other forums is permitted, provided the original author(s) and the copyright owner(s) are credited and that the original publication in this journal is cited, in accordance with accepted academic practice. No use, distribution or reproduction is permitted which does not comply with these terms.

frontiers in Bioengineering and Biotechnology

REVIEW
published: 13 May 2021
doi: 10.3389/fbioe.2021.652970

Mesenchymal Stromal Cells and Their Secretome: New Therapeutic Perspectives for Skeletal Muscle Regeneration

Martina Sandonà[1†], *Lorena Di Pietro*[2†], *Federica Esposito*[1], *Alessia Ventura*[1], *Antonietta Rosa Silini*[3], *Ornella Parolini*[2,4] *and Valentina Saccone*[1,2*]

[1] *Istituto di Ricovero e Cura a Carattere Scientifico (IRCCS), Fondazione Santa Lucia, Rome, Italy,* [2] *Dipartimento di Scienze della Vita e Sanità Pubblica, Università Cattolica del Sacro Cuore, Rome, Italy,* [3] *Centro di Ricerca "E. Menni", Fondazione Poliambulanza – Istituto Ospedaliero, Brescia, Italy,* [4] *Fondazione Policlinico Universitario "Agostino Gemelli" IRCCS, Rome, Italy*

OPEN ACCESS

Edited by:
Johannes Grillari,
Ludwig Boltzmann Institute for Experimental and Clinical Traumatology, Austria

Reviewed by:
Janina Burk,
University of Giessen, Germany
Bruna Corradetti,
Houston Methodist Research Institute, United States

***Correspondence:**
Valentina Saccone
valentina.saccone@unicatt.it;
v.saccone@hsantalucia.it

[†] *These authors have contributed equally to this work*

Specialty section:
This article was submitted to Preclinical Cell and Gene Therapy, a section of the journal Frontiers in Bioengineering and Biotechnology

Received: *13 January 2021*
Accepted: *01 April 2021*
Published: *13 May 2021*

Citation:
Sandonà M, Di Pietro L, Esposito F, Ventura A, Silini AR, Parolini O and Saccone V (2021) Mesenchymal Stromal Cells and Their Secretome: New Therapeutic Perspectives for Skeletal Muscle Regeneration. Front. Bioeng. Biotechnol. 9:652970. doi: 10.3389/fbioe.2021.652970

Mesenchymal stromal cells (MSCs) are multipotent cells found in different tissues: bone marrow, peripheral blood, adipose tissues, skeletal muscle, perinatal tissues, and dental pulp. MSCs are able to self-renew and to differentiate into multiple lineages, and they have been extensively used for cell therapy mostly owing to their anti-fibrotic and immunoregulatory properties that have been suggested to be at the basis for their regenerative capability. MSCs exert their effects by releasing a variety of biologically active molecules such as growth factors, chemokines, and cytokines, either as soluble proteins or enclosed in extracellular vesicles (EVs). Analyses of MSC-derived secretome and in particular studies on EVs are attracting great attention from a medical point of view due to their ability to mimic all the therapeutic effects produced by the MSCs (i.e., endogenous tissue repair and regulation of the immune system). MSC-EVs could be advantageous compared with the parental cells because of their specific cargo containing mRNAs, miRNAs, and proteins that can be biologically transferred to recipient cells. MSC-EV storage, transfer, and production are easier; and their administration is also safer than MSC therapy. The skeletal muscle is a very adaptive tissue, but its regenerative potential is altered during acute and chronic conditions. Recent works demonstrate that both MSCs and their secretome are able to help myofiber regeneration enhancing myogenesis and, interestingly, can be manipulated as a novel strategy for therapeutic interventions in muscular diseases like muscular dystrophies or atrophy. In particular, MSC-EVs represent promising candidates for cell free-based muscle regeneration. In this review, we aim to give a complete picture of the therapeutic properties and advantages of MSCs and their products (MSC-derived EVs and secreted factors) relevant for skeletal muscle regeneration in main muscular diseases.

Keywords: mesenchymal stromal cells, secretome, extracellular vesicles, muscle, muscle regeneration, atrophy, muscular dystrophy

INTRODUCTION

Mesenchymal "stromal" cells (MSCs) are adult, multipotent non-hematopoietic stem cells (Dominici et al., 2006). Over the last years, MSCs have emerged as a promising tool for cell therapy due to numerous features: their ability to self-renew and differentiate into several cell lineages, their ability to migrate to target tissues, and their immunomodulatory and anti-fibrotic properties, which can be attributed to their ability to secrete a plethora of biologically active molecules.

MSCs and/or mesenchymal-like cells can be isolated from numerous adult and perinatal tissues. MSCs were originally extracted from the bone marrow (Friedenstein et al., 1974) but have now been isolated from different sources: skeletal muscle (Kisiel et al., 2012), adipose tissue (Zuk et al., 2002), synovial membranes (De Bari et al., 2001), dental pulp (Rajendran et al., 2013), periodontal ligaments (Otabe et al., 2012), cervical tissue (Montesinos et al., 2013), peripheral blood (Longhini et al., 2019), suture mesenchyme of the skull (Lattanzi et al., 2013; Di Pietro et al., 2020), menstrual blood (Ren et al., 2016), perinatal tissues (Silini et al., 2015), and fetal blood (Campagnoli et al., 2001).

The International Society for Cellular Therapy (ISCT) established the minimal criteria necessary to identify MSCs: plastic adherence; positive for CD105, CD73, and CD90 surface markers; and negative (<2% expression) for CD11b, CD14, CD34, CD45, CD79a or CD19, and HLA class II (Dominici et al., 2006). Moreover, as multipotent cells, they must have the ability to differentiate into osteoblasts, adipocytes, and chondroblasts in *in vitro* differentiation conditions (Dominici et al., 2006). According to a few studies, MSCs can also express embryonic stem cell markers, such as Oct-4, Rex-1, and Sox-2 (Izadpanah et al., 2006; Riekstina et al., 2009). In 2008, similar criteria were established for MSCs from fetal membranes, with the addition that MSCs from fetal membranes must be of fetal origin (Parolini et al., 2008).

MSCs have gained much attention due to their *in vitro* and *in vivo* immunoregulatory capabilities that make them useful as guardians against excessive inflammatory responses (Prockop and Youn Oh, 2012; Magatti et al., 2017). Their protective and regenerative properties, as well as their immunoregulation skills, make them a valuable therapeutic strategy both for regenerative medicine and for the treatment of disorders characterized by alterations of the immune system.

MSCs have been shown to exert most of their effects through the release of molecules with paracrine and anti-inflammatory effects (Galderisi and Giordano, 2014). For this reason, more recently, different studies have focused on the secretome of MSCs, the set of biologically active molecules and extracellular vesicles (EVs) that these cells release. The secretome is nowadays considered a possible substitute for MSCs in cell therapy due to its comparable ability to enhance/favor tissue regeneration and modulate the immune response (Eleuteri and Fierabracci, 2019).

A hallmark in the study of the MSC secretome [or conditioned medium (CM)] was reached by Timmers and collaborators who fractionated the CM-MSC and discovered that the 50- to 200-nm component was the one with the most activity (Timmers et al., 2007). Subsequent characterization studies identified this fraction as EVs, which are lipid endogenous nanoparticles that mediate the transfer of their content across cellular boundaries (Guescini et al., 2010; Andaloussi et al., 2013; Romancino et al., 2013; Forterre et al., 2014).

EV is the generic term accepted by the International Society for Extracellular Vesicles (ISEV) to describe vesicles, characterized by the absence of a nucleus and the inability to replicate, that are released by cells into the extracellular space (Théry et al., 2018).

EVs are found in several biological fluids such as blood, urine, saliva, amniotic fluid, and milk (Iraci et al., 2016), and they can interact with the recipient cell by direct binding or ligand–receptor binding (Kahroba et al., 2019). EVs released by cells can be classified into different subtypes based on their physical features such as size or density. Small EVs (sEVs) have a typical size lower than 200 nm, while medium/large vesicles are characterized by a size greater than 200 nm. The classification of EVs is also based on their biochemical composition: the presence of transmembrane or glycosylphosphatidylinositol (GPI)-anchored proteins (e.g., CD63, CD81, and MHC class I), cytosolic proteins or periplasmic proteins (e.g., TSG101, Flotillin-1, Alix, and HSP-70), and proteins associated with non-EV structures (e.g., albumin and ApoA1/2).

EVs are characterized by a specific cargo composed of mRNAs, microRNAs (miRs), proteins, or DNA. This genetic material is protected by the oxidative extracellular environment and can be shuttled to distant cells in order to modulate the repair of damaged tissue (Cantaluppi et al., 2012; Borges et al., 2013).

In this review, we summarize the current research in the use of MSCs and of their secreted factors as alternative therapeutic strategies to improve skeletal muscle regeneration in the context of several muscle diseases. The MSC immune-modulatory and anti-fibrotic properties represent an attractive strategy to counteract the progression of chronic and in some cases lethal muscle diseases by reducing inflammation and fibrosis and stimulating the regenerative potential of muscle stem cells.

THERAPEUTIC POTENTIAL OF MESENCHYMAL STROMAL CELLS IN SKELETAL MUSCLE REGENERATION

The skeletal muscle is an adaptive tissue able to regenerate following damage due to trauma or genetic conditions. A complex stem cell niche resides in the muscle in which several cell types cooperate to regulate the balance between quiescence/activation/differentiation of the resident muscle stem cells, namely, satellite cells (MuSCs). In recent years, the role of other cell types has emerged, including inflammatory cells (Kharraz et al., 2013; Tidball et al., 2014) and mesenchymal cells residing in the muscle interstitium named fibro-adipogenic progenitors (FAPs), which maintain the homeostasis of the muscle niche and cooperate to support muscle regeneration (Mitchell et al., 2010; Uezumi et al., 2010, 2011; Malecova and Puri, 2012). For this reason, the muscle niche is a complex setting with different protagonists: FAPs play a pivotal role in coordinating tissue regeneration by supporting MuSC activity and by cooperating with inflammatory cells that mediate the activation of the regenerative response (Mozzetta et al., 2013; Madaro et al., 2018). During acute muscle injury, the myogenic program is properly activated, and inflammatory and muscle resident cells play a central role in modulating repair and regeneration; but, on the other hand, this does not occur during chronic injuries, in which myogenic regeneration is deregulated. Muscle degeneration, observed in chronic muscular injury diseases such as Duchenne muscular dystrophy (DMD), is in fact characterized by a gradual decline of regenerative potential.

DMD is the most severe muscular genetic disease in which the loss of dystrophin in the muscle leads to myofiber fragility and successive cycles of muscle necrosis and regeneration. Over time, the capacity of dystrophic muscle to regenerate becomes impaired, and muscle quality declines on account of increased fibrosis and adipose tissue deposition due to an abnormal persistence of FAPs. Indeed, the detrimental environment due to disease causes a decreased ability of MuSCs to replace degenerating muscles and an increase in the fibro-adipogenic activity of FAPs, the latter of which has proven to be a source of pro-atrophic and pro-fibrotic signals. In this dramatic context, the crosstalk between the different cell populations fails, and the regeneration ability of the entire tissue is hampered leading to muscle atrophy (Mozzetta et al., 2013; Madaro et al., 2018).

Several efforts have been devoted to the identification of effective treatments able to support the regeneration of skeletal muscle in both acute and chronic conditions. MSCs from different tissues are being studied for their ability to regenerate or repair skeletal muscle. In particular, MSCs are able to induce the proliferation and differentiation of resident MuSCs and are also able to act on the other cellular components of the muscle cell niche by reducing inflammation and infiltration.

In the following sections, we will describe evidence of the therapeutic effects of MSCs in different preclinical models of skeletal muscle injury. We will first focus on studies on acute muscle injury models in which skeletal muscle tissue is physiologically induced to activate a myogenic program and, then, on chronic pathologic damage associated with different diseases.

Acute Muscle Injuries

Skeletal muscle is a tissue with a great regenerative capacity; but if profoundly scratched due to car accidents or sport injuries, it recovers only 50% in strength and 80% of its ability to shorten (Noonan and Garrett, 1999). Up to 20% of muscle mass loss can be compensated by the high adaptability and regenerative potential of skeletal muscle (Liu et al., 2018).

MSCs can be used to regenerate or repair skeletal muscle that has been damaged by acute injuries.

MSCs from the bone marrow (BM-MSCs) were the first and are the most studied. Intramuscular transplantation of BM-MSCs in rats with severe muscle injury has been shown to contribute to skeletal muscle healing by downregulating inflammatory cytokines levels [interleukin (IL)-1b, IL-6, TNF-α, and IFN-α] and by inducing anti-inflammatory cytokines (IL-10) (Helal et al., 2016). In addition, when compared with untreated controls, BM-MSC-treated muscles were characterized by the presence of regenerating myofibers and angiogenesis restoration (Helal et al., 2016). Moreover, BM-MSC transplantation has been shown to counteract the accumulation of fibrotic tissue in injured muscles by inhibiting the downstream signaling of the pro-fibrotic cytokine transforming growth factor beta 1 (TGF-β1) (Helal et al., 2016). Additionally, allogeneic BM-MSCs have also been shown to support the formation of new muscle fibers (Andrade et al., 2015) when directly injected in the muscles of rats with acute damage. The results showed an acceleration of muscle function recovery (Andrade et al., 2015).

Interestingly, in addition to BM-MSCs, adipose tissue-derived MSCs (AT-MSCs) and synovial membrane-derived MSCs (SM-MSCs) have also been shown to be active contributors to skeletal muscle regeneration (De La Garza-Rodea et al., 2012). More in detail, De la Garza-Rodea and collaborators demonstrated that all three types of MSCs were able to contribute to skeletal muscle regeneration in the cardiotoxin-injured mouse (CTX mouse), a model of acute damage in the skeletal muscle tissue (De La Garza-Rodea et al., 2012). However, they demonstrated enhanced effects of AT-MSCs on myofiber formation/regeneration when compared with BM-MSCs, and this was attributed to higher engraftment in the tibialis anterior muscles (De La Garza-Rodea et al., 2012).

The regenerative effects of both allogenic BM-MSCs and AT-MSCs were also described in the treatment of skeletal muscle laceration injury in Wistar rats (Moussa et al., 2020). In particular, both types of MSCs were shown to be effective and lasted up to 8 weeks post treatment, even if intramuscular injection of AT-MSCs displayed a stronger effect leading to an increase of myotube formation in parallel to a decrease of collagen deposition (Moussa et al., 2020). Similar results were obtained after immortalized BM-MSCs embedded within Pluronic F-127 hydrogel were locally injected in a muscle contusion murine model (Chiu et al., 2020). As a matter of fact, mice treated with BM-MSCs embedded in the hydrogel displayed numerous regenerating myofibers, as well as improved muscle strength, when compared with the control group (Chiu et al., 2020).

The long-term effects of the local injection of autologous BM-MSCs, combined with plastic surgery, to treat muscle necrosis were also recently investigated in a pig model of severe radiation burn (Linard et al., 2018). Very interestingly, BM-MSC treatment supported muscle regeneration even 1 year after surgery, leading to the restoration of myofiber diameter and density, stimulation of fast-twitch to slow-twitch fiber conversion, accelerated restoration of vascular structures, and regulation of M1/M2 macrophage balance in the muscle (Linard et al., 2018).

Intriguingly, transplantation of Wharton's jelly-derived MSCs (WJ-MSCs) in a mouse model of skeletal muscle injury was shown to attenuate neutrophil-mediated acute inflammation post injury and to reduce fibrous tissue accumulation by modulating TGF-β1 levels in the muscle (Su et al., 2019). The effects of WJ-MSCs were also evaluated by Kwon and colleagues who reported anti-apoptotic properties of WJ-MSCs exerted in a mouse skeletal myoblast cell line (C2C12) (Kwon et al., 2016). They demonstrated that when co-cultured in serum-deprived with C2C12, WJ-MSCs secrete high levels of the chemokine

CXCL1 (Chemokine C Motif Ligand 1) that was responsible for the anti-apoptotic effect of human WJ-MSCs (Kwon et al., 2016).

Taken together, these studies sustain the therapeutic efficacy of MSCs derived from different sources and demonstrate that they promote muscle regeneration in different animal models of acute muscle injury. Comparative studies have demonstrated the great effectiveness of MSCs in different directions: inducing new muscle fibers; decreasing inflammation by acting on cytokines, neutrophils, and macrophages; decreasing fibrosis by the modulation of TGF-β1 levels in muscles; increasing vascularization; and improving also muscle functionality. Very interestingly, a long-term beneficial effect upon MSC transplantation has also been observed, further supporting future translation into the clinical practice.

Chronic Muscle Injuries

MSCs have been also applied as a therapeutic strategy to promote muscle regeneration in the presence of conditions due to genetic alterations (i.e., muscular dystrophies).

Seminal works have discovered that BM-MSCs have the intriguing potential to induce skeletal muscle regeneration in the mdx mouse, a model for DMD, in which mutations in exon 23 of the dystrophin gene lead to the protein deletion, thus mimicking the human pathology characterized by progressive muscle degeneration. As a matter of fact, when injected intraperitoneally into the mdx mouse, BM-MSCs, isolated from the femoral and tibial bone marrow of dystrophin/utrophin double-knockout mice, were able to improve disease symptoms by increasing locomotor activity and prolonging mouse survival (Maeda et al., 2017). Noteworthy, BM-MSC transplantation also increased the number of MuSCs and significantly decreased fibrosis in the diaphragm (one of the most affected organs in DMD). Furthermore, when MuSCs were co-cultured with BM-MSCs, an improvement of myotube differentiation was observed (Maeda et al., 2017).

The therapeutic potential of BM-MSCs in dystrophin/utrophin double-knockout mice was also previously reported (Li et al., 2011). BM-MSC administration via the caudal vein ameliorated the symptoms, strengthened the muscle functionality, and, noteworthy, induced the expression of dystrophin and utrophin genes in the treated mice (Li et al., 2011).

A recent work reported the beneficial effects of intravenous injection of WJ-MSCs in the mdx mouse model (Choi et al., 2020). Indeed, treatment determined a decrease of fibrosis and of the percentage of necrotic fibers (Choi et al., 2020). The authors also indicated the paracrine secretion of the matrix metalloproteinase-1 (MMP-1) as the key factor that exerted the anti-fibrotic effect of WJ-MSCs in the muscle (Choi et al., 2020).

The ability of AT-MSCs to promote skeletal muscle regeneration in dystrophin-deficient mice was also demonstrated (Pinheiro et al., 2012). Local injection of AT-MSCs improved muscle strength and resistance to fatigue, and this was mediated by modulation of inflammation and regulation of different genes involved in the regenerative process [i.e., myogenin, vascular endothelial growth factor (VEGF), TGF-β1, IL-6, IL-10, and IL-4] (Pinheiro et al., 2012).

Very interestingly, the effect of the $CD146^{+}$ cell (i.e., pericytes) subpopulation of the stromal fraction of human adipose tissue was investigated and compared with that of AT-MSCs from the same sample. Weekly intraperitoneal transplantations of $CD146^{+}$ cells in the DMD mouse model were able to sustain muscle regeneration for up to 8 weeks after transplantation, and this effect was stronger when compared with that of AT-MSCs (Gomes et al., 2018).

The potential of human dental pulp stem cells (DP-MSCs) and of human amniotic fluid stem cells (AF-MSCs) was also assessed in an immune-compromised mdx/SCID model (Pisciotta et al., 2015). MSCs were pre-committed *in vitro* toward the myogenic lineage by means of a DNA demethylation treatment, in both the presence and absence of CM from differentiated C2C12 cell cultures, that induced the expression of specific myogenic commitment markers (i.e., myogenin, myosin heavy chain, and desmin). Pre-differentiated DP-MSCs and AF-MSCs were then injected intramuscularly in mice, and both cell types were able to restore dystrophin expression and slow down muscle degeneration by exerting pro-angiogenic and anti-fibrotic effects (Pisciotta et al., 2015).

MSCs have also been tested in sarcoglycanopathies, another chronic muscular disorder (Shabbir et al., 2009). These diseases result from the absence of sarcoglycan proteins whose role is to connect the cytoskeleton of muscle fibers to the sarcolemma in order to maintain structural integrity of the myofibers (Gao et al., 2015). Indeed, Shabbir and colleagues demonstrated that intramuscular transplantation of human or pig BM-MSCs in delta-sarcoglycan-deficient dystrophic hamsters was able to significantly decrease CD45 and NFkB expression. In addition, MSC treatment was able to decrease malondialdehyde (MDA) expression, the final product of lipid peroxidation induced by inflammation that characterizes dystrophic muscles, similar to that of wild-type mice (Shabbir et al., 2009).

Based on these findings, the authors concluded that the immunomodulatory properties of MSCs can be exploited as a possible therapy for chronic inflammatory conditions such as muscular dystrophies (Shabbir et al., 2009).

Altogether, several studies have shown how MSCs derived from different sources, injected both locally and systemically, can also exert beneficial effects in severe forms of muscular dystrophies by acting at different levels to hamper muscle degeneration.

Atrophic Muscle

Muscular atrophy can be a physiological process due to aging or long-term immobilization, or it can be a consequence of pathogenic conditions such as spinal muscular atrophy (SMA) or other chronic diseases like muscular dystrophies, amyotrophic lateral sclerosis (ALS), cancer, acquired immunodeficiency syndrome (AIDS), and diabetes (Bonaldo and Sandri, 2013). Muscular atrophy is characterized by the loss of muscle mass due to myofiber death, change in fiber types and myosin isoforms, reduction of cell cytoplasm, loss of cellular organelles, and, in particular, protein degradation that exceeds the synthesis of new proteins.

Kim and colleagues demonstrated how human MSCs isolated from different sources (bone marrow, adipose tissue, and umbilical cord) can induce muscle regeneration after transplantation into the soleus of rats with hindlimb suspension-induced muscle atrophy (Kim et al., 2015). In particular, the authors observed activation of the phosphoinositide-3-kinase (PI3K)/Akt pathway and consequently a reduction of muscle-specific RING finger protein-1 (MuRF-1) and atrophy F-box (MAFbx/Atrogin-1) expression in rats treated with MSCs (Kim et al., 2015).

ALS is a serious progressive neurodegenerative pathology characterized by the loss of motor neurons with consequent atrophy and loss of muscle movements (Hardiman et al., 2017). Numerous studies conducted in mice with the Gly93Ala mutation in the SOD1 gene (SOD1-G93A mice), which leads to the development of ALS symptoms (progressive loss of muscle strength, onset of the disease at about 5 months, and a life span of about 6 months) (Julien and Kriz, 2006), have demonstrated that BM-MSCs induce important therapeutic effects (Zhao et al., 2007; Vercelli et al., 2008; Zhou et al., 2013). Different works highlighted how BM-MSC transplantation in ALS mice improves disease phenotype, delays disease progression, and induces partial recovery of the motor function (Zhao et al., 2007; Vercelli et al., 2008; Gugliandolo et al., 2019).

In particular, it has been shown that intravenous injection of human BM-MSCs injected into SOD1-G93A mice was able to delay the development of pathology-related symptoms and to promote survival when compared with untreated and vehicle-injected mice (Zhao et al., 2007). Moreover, the functions of neuromotors were also analyzed, and again, significant differences were found. In particular, when compared with untreated mice, those that received human BM-MSCs lost motor function almost a month after treatment and had a higher number of motor neurons (Zhao et al., 2007). Furthermore, human BM-MSCs prevented the loss of peripheral motor nerves, and reinnervation took longer for treated mice.

Zhang and collaborators also demonstrated that multiple intrathecal injections of human BM-MSCs induced therapeutic effects in SOD1-G93A mice by enhancing motor performance, decreasing motor neuron loss, and increasing survival through the inhibition of the inflammatory response as shown by downregulation of TNF-α and iNOS protein levels (Zhang et al., 2009; Zhou et al., 2013).

Another study also demonstrated that when transplanted into the lumbar spinal cord of SOD1-G93A mice, BM-MSCs were able to migrate in the lumbar spinal cord, prevent microglial activation, and delay disease onset associated with a decrease in the number of motor neurons, thus globally leading to a better muscle performance (Vercelli et al., 2008).

The striking effectiveness of AT-MSCs for ALS has also been demonstrated. Systemic injection of AT-MSCs into the SOD-1 mutant mouse was able to modulate the secretome of local glial cells and increase glial-derived neurotrophic factor (GDNF) levels, which consequently led to neuroprotection and increased the number, survival, and functionality of motor neurons (Marconi et al., 2013).

Taken together, administration of MSCs, and especially of BM-MSCs, in ALS models is effective in decelerating disease symptoms as well as in sustaining muscle innervation, acting on both muscle and motor neuron sides.

THE THERAPEUTIC POTENTIAL OF THE MESENCHYMAL STROMAL CELL SECRETOME

In recent years, the regenerative potential of MSCs has not been attributed so much to the ability of these cells to engraft into target tissue and differentiate but to their ability to secrete factors capable of supporting tissue regeneration through activation of resident cells.

CM-MSCs have been shown to be a valid alternative to its cellular counterpart (MSCs) by numerous *in vitro* and *in vivo* studies, which describe similar beneficial effects between the two (Gnecchi et al., 2006; Aslam et al., 2009; Rossi et al., 2012; Goolaerts et al., 2014).

Different *in vitro* studies have shown that CM-MSC affects different immune cell populations of the innate (macrophages, dendritic cells, neutrophils, and natural killer cells) and adaptive (T and B cell) immunity. For example, CM-MSCs obtained from different tissues, such as bone marrow, adipose tissue, and muscle tissue, inhibit T-cell proliferation (Di Nicola et al., 2002; Keyser et al., 2007; Hegyi et al., 2012; Lang et al., 2018), support the expansion of T regulatory cells (Nasef et al., 2007; Yang et al., 2009; Sattler et al., 2011; Tasso et al., 2012), and inhibit B-cell proliferation (Augello et al., 2005; Corcione et al., 2006) and B-cell differentiation (Asari et al., 2009). Furthermore, CM-MSCs have been shown to induce a phenotype and functional switch of monocytes toward macrophages with anti-inflammatory, M2-like features (Onishi et al., 2015; Pischiutta et al., 2016; Magatti et al., 2017; Giampà et al., 2019), to inhibit natural killer cell proliferation and cytotoxicity (Rasmusson et al., 2003; Sotiropoulou et al., 2006), and to inhibit dendritic cell differentiation (Nauta et al., 2006; Djouad et al., 2007; Ramasamy et al., 2007; Li et al., 2008). Moreover, the administration of CM-MSC has been shown to induce therapeutic effects in a wide variety of disease models, such as sepsis (Németh et al., 2009), and to support the repair of several tissues such as the liver (Zagoura et al., 2012), lungs (Ray et al., 2003; Cargnoni et al., 2012; Turner et al., 2013), skin (Lee et al., 2011), and heart (Mirabella et al., 2011) and moreover, it possesses neuroprotective and neurotrophic abilities (Mead et al., 2014; Caseiro et al., 2016; Giampà et al., 2019).

The advantages of using CM-MSCs lie in its composition of soluble factors and EVs. In particular, EVs are very attractive for a cell-free therapeutic approach in regenerative medicine since they bypass some undesirable side effects of MSCs, such as their ability to enhance tumor growth by chemokine or cytokine secretion (Liu et al., 2011; Tsai et al., 2011; Yan et al., 2012), and their inability to proliferate overcomes the tumorigenesis potential of MSCs (Rani et al., 2015; Mardpour et al., 2019).

The use of MSC-EVs as a therapeutic approach is advantageous also for other reasons: (i) the ability to migrate specifically into the target organ while MSCs often become entrapped in the microvasculature leading to a high risk of thrombosis (Gowen et al., 2020; Zhao et al., 2020); (ii) the systemic injection of EVs has an improved safety profile and lower immunogenicity with any histopathological changes or increases of liver transaminases or cytokine levels (Koniusz et al., 2016; Zhu et al., 2017; Leavitt et al., 2019; Saleh et al., 2019; Shiue et al., 2019); (iii) EVs are a putative delivery system of genes, drugs, enzymes, and RNAs, and they can be engineered to target specific cells or pathways (Yeo et al., 2013; Pascucci et al., 2014; Tian et al., 2018; Asgarpour et al., 2020; Conceição et al., 2021). All these characteristics make MSC-EVs promising tools for cell-free therapeutics.

Therapeutic Effects of the Mesenchymal Stromal Cells Secretome in Muscle Regeneration

As for other pathologies, it has been proven that when locally or systemically injected, MSCs activate muscle resident cells due to the release of paracrine factors, such as VEGFa, improving muscle regeneration and/or modulating muscle inflammation and muscle fibrosis (Pinheiro et al., 2012; Secco et al., 2013; Valadares et al., 2014).

In the context of skeletal muscle diseases, Assoni and colleagues demonstrated *in vitro* that CM from adipose tissue, skeletal muscle, and uterine tube MSCs has the ability to modulate apoptosis of dystrophic myoblasts, also enhancing cell migration and proliferation (Assoni et al., 2017). Through proteomic profiling of the CM, they also demonstrated the great variability of proteins from the different sources analyzed but also highlighted common enriched pathways related to extracellular matrix organization, axon guidance, antigen processing, metabolic processes, and positive regulation of nitric oxide (Assoni et al., 2017).

Another study demonstrated that the transplantation of CM-WJ-MSCs showed better results on inflammation and collagen deposition in muscle tissue than transplantation of the source cells (Pereira et al., 2014). These effects were due to the presence of cytokines and growth factors involved in the suppression of local immune system, such as hepatocyte growth factor (HGF) and IL-10, in the improvement of angiogenesis, such as fibroblast growth factor (FGF) and VEGFA, and in the inhibition of scar formation (Chen et al., 2008; Li et al., 2009; Jackson et al., 2012).

In a different study, Kim and collaborators showed that injection of human CM-UC-MSCs in a mouse model of muscle atrophy induced recovery of the muscle mass through the activation of PI3K/Akt pathway (Kim et al., 2016). In addition, using an antibody-based protein array, the authors characterized factors released by human umbilical cord-derived MSCs (UC-MSCs) (Kim et al., 2016). Interestingly, several regulators of muscle regeneration were identified: ectodysplasin-A2, thrombospondin-1, IL-6, monocyte chemoattractant protein-1 (MCP-1), dickkopf-related protein 1 (DKK1), HGF, VEGF, FGF7, tissue inhibitor of metalloproteinase 1 (TIMP-1), SMAD family member 4 (SMAD4), macrophage inflammatory protein 2 (MIP-2), activin A, insulin-like growth factor-binding protein (IGFBP)-related protein 1, and MMP-1 (Kim et al., 2016).

These seminal works clearly demonstrate that the efficacy of MSCs in supporting skeletal muscle regeneration is attributed to secreted factors that exert a bioactive effect in damaged muscles.

Therapeutic Effects of Extracellular Vesicles Derived From Mesenchymal Stromal Cells in Muscle Regeneration

MSC-EV-derived therapeutic approaches have been exploited in several pathologies, such as liver diseases (Lou et al., 2015; Qu et al., 2017; Chen et al., 2018; Shao et al., 2020; Zhang et al., 2020), brain diseases including brain tumors (Xin et al., 2012, 2013; Xu et al., 2019; Allahverdi et al., 2020), cardiac dysfunctions, and myocardial infarction (Feng et al., 2014; Yu et al., 2015).

The therapeutic potential of MSC-EVs in supporting skeletal muscle regeneration in the context of muscle diseases has also been evaluated. Nakamura et al. (2015) described the *in vitro* beneficial effect of EVs isolated from BM-MSCs on myogenesis and angiogenesis of C2C12 myoblasts and HUVECs, respectively. The authors confirmed these data in the CTX mouse model, in which they performed an intramuscular injection of MSC-EVs and observed an increase of muscle cross-sectional area, a decrease of fibrotic area, and an improvement of capillary density (Nakamura et al., 2015). The interest toward MSC-EVs as an efficacious treatment for degenerative neuromuscular diseases has also escalated due to the fact that EVs are lipid vesicles of endocytic origin that can cross the blood–brain barrier (BBB) in a non-invasive manner (Zhuang et al., 2011; Zhou et al., 2014). Several studies have reported that the beneficial effects are associated with EV cargo. In particular, a comparison of miR content in MSC-EVs and in CM-MSCs has revealed several miRs in common and others exclusive for MSC-EVs (Nakamura et al., 2015). For example, miR-21, an anti-apoptotic miR, was present in both the MSC-EVs and MSC-CM, but as already reported by others, miRs encapsulated in EVs appeared to have enhanced functions when compared with miRs released in the total CMs (Shimbo et al., 2014; Nakamura et al., 2015). The analysis of miRs cargo showed the presence of myogenic miRs, such as miR-1, miR-133, and miR-206, but also of miR-494, which has been shown to induce a protective effect against ischemia-induced cardiac injury (Wang et al., 2010; Nakamura et al., 2015). Lo Sicco and colleagues investigated the angiogenic effect of EVs isolated from AT-MSCs in a mouse model of muscle damage (Lo Sicco et al., 2017). They implanted matrigel plugs containing MSC-EVs in mice and observed that 3 weeks after the implantation, there was an increase of vessels along the periphery of the plugs (Lo Sicco et al., 2017). The described effect of MSC-EVs was associated with the high expression, in their cargo, of the angiogenic factors platelet and endothelial cell adhesion molecule (PECAM) and VEGFA (Lo Sicco et al., 2017). Moreover, EVs isolated from MSCs cultured in hypoxic conditions were able to upregulate the expression of several miRs implicated in muscle repair, in particular miR-223, miR-146b, miR-126, and miR-199a (Lo Sicco et al., 2017). By *in vitro* and *in vivo* experiments, MSC-EVs, especially when isolated from MSCs cultured in hypoxic conditions, were able to modulate inflammation by regulating macrophage polarization and accelerating muscle regeneration (Lo Sicco et al., 2017). Concordantly, others described the beneficial effects of the secretome (the whole CM and EV fraction) of human AF-MSCs on muscle homeostasis, highlighting their anti-inflammatory activity, their ability to enhance proliferation, and their capacity to protect against cellular senescence in the CTX mouse model (Mellows et al., 2017). In particular, the beneficial effect observed was mediated, at least in part, through the repression of NF-κB pathway, which appears stronger in MSC-EVs compared with the whole CM. Interestingly, the pro-regenerative effect of MSC-EVs in CTX mice was also associated with their miR content, which was predicted to promote angiogenesis, proliferation, migration, differentiation, autophagy, apoptosis, and inflammation (Mellows et al., 2017). A comparison of the effects of the whole CM and EVs from AF-MSCs in the CTX mouse model revealed very few differences in muscle regeneration. CM-AF-MSCs increased regenerating fiber size, the number of capillaries/fibers, and the level of committed muscle stem cells, while AF-EVs increased the regenerating fiber size and the number of capillaries/fiber (Mellows et al., 2017).

On the other hand, the recent comparison of the whole secretome with the EV fraction with AT-MSCs showed differences in protein and miR expression leading to a different impact from secretome and/or EVs on biological processes. Several factors (both proteins and miRs) are described as potentially involved in different processes (Mitchell et al., 2019). For example, the whole secretome but not the EV fraction influenced senescence, while EVs but not the whole secretome impacted inflammation (Mitchell et al., 2019). Notably, Mitchell and colleagues highlighted the greater effect of EVs in muscle repair in acute damage conditions in CTX mice. Indeed, by studying the miR contents in MSC-EVs, they observed the presence of anti-inflammatory (i.e., miR-let7 family), pro-regenerative (i.e., miR-145), and angiogenic miRs (i.e., miR-23a), all able to improve muscle regeneration in CTX mice (Mitchell et al., 2019).

Local injection of exosomes isolated from the CM of BM-MSCs was very recently shown to accelerate the recovery of contractile function of muscles in a rat model of muscle injury (Iyer et al., 2020). Treatment stimulated the formation of new fibers and modulated the expression of genes involved in inflammation, fibrosis, and myogenesis mechanisms (Iyer et al., 2020). Furthermore, another study demonstrated that intramuscular injection of exosomes from BM-MSCs after muscle contusion in mice modified the polarization status of macrophages, alleviated the inflammatory reaction, reduced fibrosis size, promoted muscle regeneration, and improved fast-twitch and tetanus strength (Luo et al., 2020).

The therapeutic effects of placenta-derived MSCs (PL-MSCs) and their secreted EV exosomes were assessed *in vitro* in myoblasts isolated from DMD patients and mdx mice and *in vivo* by intramuscular transplantation of PL-MSCs in mdx mice (Bier et al., 2018). In particular, both PL-MSCs and their EVs promoted fusion and differentiation of human muscle cells from DMD patients, as well as decreased the expression of TGF-β and thus the fibrogenic differentiation of DMD myoblasts. MiR-29 was identified as a mediator of this effect since it has been associated with various pathological pathways in DMD, and it is downregulated in myoblasts from DMD patients compared with muscle cells from healthy donors (Bier et al., 2018). Intriguingly, both PL-MSCs and their EVs induced the dystrophin homolog utrophin in C2C12 cells and in human myoblasts derived from healthy donors and DMD patients. Intramuscular transplantation of PL-MSCs and EVs in mdx mice showed comparable effects; in fact, both treatments inhibited fibrosis and inflammation (Bier et al., 2018). Also, local injections of EVs isolated from UC-MSCs or systemic administration of murine BM-MSC-EVs in mdx mice counteracted DMD pathology. Both treatments induced the recovery of muscle function, the decline of creatinine kinase (CK) blood levels, and the decrease of muscle fibrosis and inflammation due to the re-localization of the dystrophin-associated protein complex (DAPC) (Leng et al., 2020).

Our recent studies have also demonstrated how miR content of EVs derived from muscular interstitial MSCs, FAPs, could play a pivotal role in muscle regeneration (Sandonà et al., 2020). We demonstrated that EVs mediate the communication between FAPs and MuSCs in dystrophic mice; and additionally, we reported the first evidence of pharmacological treatment ability to fine-tune EV cargo, enhancing their regenerating effects on muscle fibers (Sandonà et al., 2020). The pharmacological treatment of mdx with an epigenetic drug, histone deacetylase (HDAC) inhibitor [HDACi; i.e., Trichostatin A (TSA)], induced a significant upregulation of 14 miRs inside the EVs released by FAPs of dystrophic mice (miR-206, miR-542, miR-449a, miR-342, miR-320, miR-192, miR-423, miR-376a, miR-145a, miR-224, miR-30a, miR-494, miR-29a, and miR-7b), which are mainly involved in muscle regeneration and muscle homeostasis (Sandonà et al., 2020). Among them, miR-206 was found to be the most upregulated following HDACi treatment and was found to be crucial to confer the ability to drive muscle regeneration, and to reduce fibrotic tissue deposition and muscle inflammation, to EVs injected in dystrophic muscles. This was confirmed by antagomiR inhibition of miR-206 expression in EVs, which led to the loss of the ability of EVs to impact muscle regeneration and muscle fibrosis but did not affect muscle inflammation (Sandonà et al., 2020). In addition, the inhibition of the expression of miR-145a, another HDACi-induced miR in EVs, reduced inflammation in the muscles of mdx mice. Therefore, we concluded that the specific assembly of miRs inside the EVs is fundamental to reveal their therapeutic effect in DMD (Sandonà et al., 2020).

Interestingly, the therapeutic efficacy of MSCs secreted vesicles has also been recently demonstrated in muscle atrophy. In particular, EVs from human UC-MSC (hUC-MSC-EVs) injected in rats with sciatic nerve defects were capable of restoring hind leg muscle mass thanks to extensive muscle innervation (Ma et al., 2019). The hUC-MSC-EVs promoted the nerve regeneration by the modulation of the inflammation, as observed by the downregulation of IL−6 and IL−1β and the up−regulation of IL−10, improving functional recovery.

There is also reported evidence that the increment of muscle mass in atrophic muscles could be restored by the injection of MSC-EVs in injured muscles of rat with massive rotator cuff tear (MRCT) (Wang et al., 2019). In this model, EVs inhibited macrophage migration and the release of pro-inflammatory cytokines, preventing secondary muscle damage; moreover, vesicles were able to reduce the apoptosis of tenocytes and myocytes and to increase myogenesis of endogenous stem cell residing in the muscle (Wang et al., 2019).

Therapeutic approaches with MSC-EVs have also been tested on other chronic pathologies such as ALS. There are new and promising therapeutic approaches for ALS using MSC-EVs, in particular those isolated from AT-MSCs. AT-MSCs possess neuroprotective properties mediated by their EVs. EVs derived from AT-MSCs and in particular exosomes could be used for therapeutic approaches for ALS because they are capable of acting on different hallmarks of the disease. Indeed, an *in vitro* study using the NSC-34 motorneuron cell line overexpressing hSOD1 has shown that AT-MSC-EVs prevented H_2O_2-induced damage and increased cell viability (Bonafede et al., 2016).

The subsequent proteomic analyses of AT-MSC-derived exosomes revealed that it contains proteins that affect pathways crucial for ALS pathology, such as cell adhesion, apoptosis, response to oxidative stress, and PI3K/Akt signaling pathway (Bonafede et al., 2019). The neuroprotective effect of AT-MSC-derived exosomes in ALS could be associated with the presence of the ribonuclease RNAse4, a protein mutated in ALS patient, which is known to display angiogenic, neurogenic, and neuroprotective activities (Li et al., 2013; Bonafede et al., 2019; Padhi and Gomes, 2019). With the use of an *in vitro* model of ALS, the transfer of SOD1 and SOD3 through exosomes destroyed free superoxide radicals generating a protective effect replacing the enzymatic function of mutated SOD1, thus improving response to oxidative stress. In addition, Igf1, which activates the PI3K/Akt signaling pathway and binds Igf1R promoting proliferation and inhibiting apoptosis, was also found inside AT-MSC-derived exosomes (Bonafede et al., 2019). Other *in vitro* studies on neural stem cells (NSCs) isolated from the SOD1-G93A ALS mouse model have demonstrated that treatment with AT-MSC-EVs could reduce the increase of SOD1 aggregation in the cytoplasm of cells (Lee et al., 2016). Moreover, EV treatment had also effects on mitochondrial defects: NSCs treated with AT-MSC-EVs showed an increase in mitochondrial protein expression, such as p-CREB/CREB and PGC1α involved in the activation of mitochondrial biogenesis and have been reported to be abnormally expressed in ALS (Kong and Xu, 1998; Lee et al., 2016).

The recent available literature clearly suggests that the intravesicular portion of CM-MSCs has therapeutic implications for musculoskeletal diseases and, at the same time, assesses the feasibility of using EVs in treatment of diseases that have no cure to date.

The deep investigation of the identity of EV cargo in terms of proteins, mRNA, and miRNAs can be harnessed therapeutically in the more immediate future by engineering vesicles for specifically delivering therapeutic components to the target tissue.

CLINICAL TRIALS IN HUMANS

Thanks to their regenerative potential, MSCs have been tested in different clinical trials for cardiovascular, neurological, and immunological diseases, among others (Chen et al., 2004; Bang et al., 2005; Lazarus et al., 2005; Ringden et al., 2006; Ripa et al., 2007; Markert et al., 2009; Lee et al., 2012; Rajput et al., 2015; Pezzi et al., 2017; Kim et al., 2018; Winkler et al., 2018). Despite several advantages of using MSCs in clinical trials, most of them have failed to reach primary endpoints. The therapeutic ineffectiveness resides mostly on the age of the MSC donor, on the different MSC isolation and culture methods, on the various MSC administration routes, and on the MSC recipient (host) (Yukawa et al., 2012; Siegel et al., 2013; Stubbendorff et al., 2013; Pezzi et al., 2017).

For example, cell isolation methods can yield non-homogenous cell populations that can consequently affect clinical outcome. In addition, long-term culture has been shown to decrease differentiation ability (Drela et al., 2019), increase malignant transformation of MSCs from BM (Røsland et al., 2009; Drela et al., 2019), and reduce engraftment *in vivo* (Bonab et al., 2006; Tolar et al., 2007; Yang et al., 2018).

Although several studies have shown the efficacy of both MSCs and their secretome in preclinical models of muscle diseases, there are very few clinical trials.

With the use of the key terms "muscle" and "mesenchymal cells" and selecting only studies concerning the use of MSCs in muscular diseases, eight clinical trials are registered on ClinicalTrial.gov[1]. Amongst these, six are in DMD patients, one in patients with facioscapulohumeral dystrophy (FSHD), and one in Werdnig–Hoffman patients. Four trials involved the use of umbilical cord MSCs, two used adipose-derived MSCs, and the remaining two used BM-MSCs. There are no results available for these eight selected studies on ClinicalTrial.gov[1].

Twenty-two approved and registered clinical trials were found on www.clinicaltrials.gov using the search terms "ALS" and "mesenchymal cells"; and they also evaluated the efficacy of MSCs, isolated from different sources, in ALS patients. The results were recently reviewed in detail by Gugliandolo and colleagues (Gugliandolo et al., 2019).

Very interestingly, a phase 2 clinical trial (ClinicalTrials.gov Identifier: NCT03406780) investigated the safety and efficacy of a cell therapy called CAP-1002 in DMD patients. CAP-1002 is a therapeutic product composed of allogenic cardiac progenitor cells, namely, cardiosphere-derived cells, and it has been previously demonstrated that intracoronary infusion of CAP-1002 is feasible, safe, and potentially effective in DMD patients (Taylor et al., 2019). These cardiospheres have been proposed to act through the secretion of different growth factors and exosomes exerting anti-inflammatory, anti-fibrotic, and regenerative actions in the target organ (Taylor et al., 2019).

In the last couple of years, different publications have reported clinical trials results. For example, the suitability, safety, and efficacy of intra-arterial and intramuscular administration of allogeneic WJ-MSCs in ambulatory and non-ambulatory DMD

[1] https://www.clinicaltrials.gov/

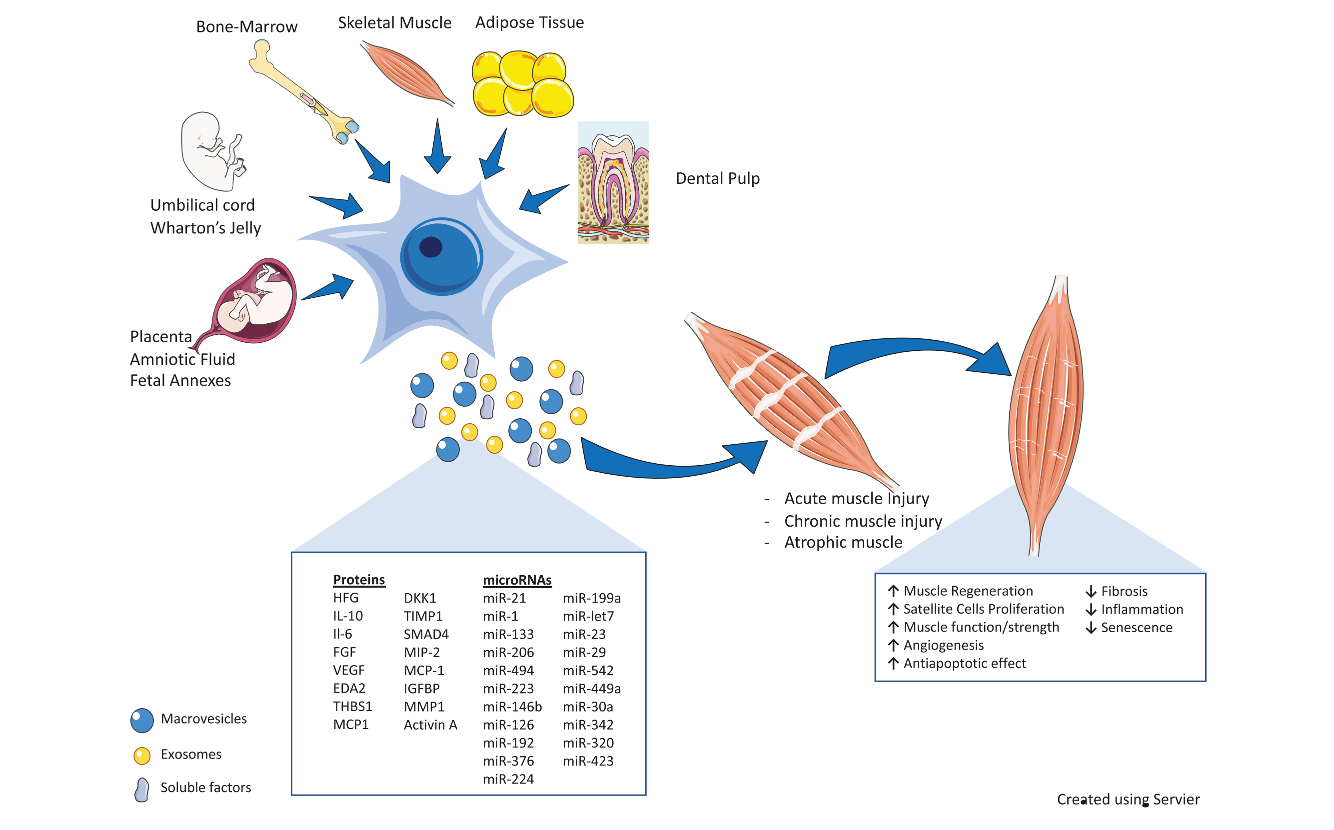

FIGURE 1 | Therapeutic properties of mesenchymal stromal cells (MSCs) and their secretome [soluble factors and extracellular vesicles (EVs)] in various muscle injury models. MSCs derived from different tissues participate in skeletal muscle tissue regeneration, directly or through their secretome (soluble factors and EVs). The cartoon reports the bioactive fraction of the MSC secretome (cytokines, miRs, and growth factors) and the main regenerative processes induced by these factors, as discussed in the main text (↑, upregulation/induction; ↓, downregulation/inhibition). The schematic art pieces used in this figure were provided by Servier Medical art (https://smart.servier.com). Servier Medical Art by Servier is licensed under a Creative Commons Attribution 3.0 Unported License.

patients were found be well tolerated, ameliorated symptoms, and slowed the progression of the disease in the first year following the administration (Dai et al., 2018). Furthermore, the feasibility of treatment with BM-MSCs in patients with DMD (Sharma et al., 2014; Klimczak et al., 2020) and with ALS (Nabavi et al., 2019) has been also evaluated. In particular, intravenous and intrathecal injections of autologous BM-MSCs in ALS patients were found to be safe and feasible (Nabavi et al., 2019). Klimczak and colleagues tested the effects of the intramuscular co-transplantation of BM-MSCs and myogenic progenitor cells in three DMD patients, based on the rationale that both cell types can merge with damaged myofibers to regenerate skeletal muscle and from the knowledge that BM-MSCs are involved in myogenesis due to their ability to differentiate into myoblasts and to inhibit chronic inflammation that characterizes DMD (Klimczak and Kozlowska, 2016; Klimczak et al., 2018). They demonstrated that BM-MSCs had immunomodulatory properties that supported the regenerative potential of the myogenic precursors *in vivo* (Klimczak et al., 2020).

Finally, intravenous administration of UC-MSCs in patients affected by Becker muscular dystrophy was found to be safe and determined an increase of muscle strength, a result that is interestingly more evident in patients with a shorter course of disease (Li et al., 2015).

CONCLUSION

The incredible and multifaceted properties of MSCs have attracted great scientific interest for the possible development of numerous therapeutic applications, making them the most commonly used cells, especially in the regenerative medicine field. They can be obtained from many different adult tissues and, for the most part, are easy to isolate and culture. When tissues are damaged, administrated MSCs have the ability to migrate to the site of injury and to release molecules (growth factors, cytokines, and EVs) that establish a favorable microenvironment and promote tissue homeostasis that supports or directly favors regeneration by the induction of pleiotropic effects: anti-inflammatory, immune-modulating, anti-fibrotic, angiogenic, and anti-apoptotic (Chapel et al., 2003; Caplan, 2009; Singer and Caplan, 2011; Le Blanc and Mougiakakos, 2012; Bronckaers et al., 2014).

In this review, we have emphasized the current knowledge about MSCs and how MSCs derived from different origins are widely used in the treatment of various diseases with a particular focus on muscular diseases. In the last decade, we have learned that MSCs act through paracrine factors, and in particular through the EVs they release. For all these reasons, we have provided insights into the possible therapeutic employment of the

MSCs with a special attention to their secretome and EVs as novel off-the-shelf approaches for muscle regeneration.

Although different studies described the ability of MSCs to target specific damaged tissues, long-term engraftment is not often observed (Toma et al., 2002), and several alternative mechanisms have changed the "cell replacement theory" behind the beneficial effect of MSCs of promoting tissue repair.

Numerous recent preclinical and clinical studies here discussed demonstrated that the therapeutic effect of MSCs secretome in skeletal muscle regeneration could be partly due to secreted EVs, which can mirror the therapeutic effect of their parent cells. We have discussed in detail how EVs released by MSCs are able to mediate intercellular communication that is translated into pleiotropic actions generating therapeutic potential through the transfer of active molecules, also in different muscle injury models (**Figure 1**).

The use of MSC-CM and in particular of MSC-derived EVs as a cell-free therapy is quickly developing as a promising option that could bypass the safety concerns associated with the use of live cells, ethical concerns associated with the origin of cells, and also immune-compatibility issues.

The MSC secretome is considered a potential bioactive pharmaceutical component, in which its vesicular portion, containing genetic information transmitted between cells of different types, is promising as a drug delivery system mainly due to homing capabilities, thereby opening an opportune window to specific and targeted compound (drugs, proteins, etc.) release into damaged lesions (Bari et al., 2018). A secretome-based approach should also minimize biological variability, allow precise dosing, and thus lead to the development of safe and effective therapeutic strategies with possibly predictable outcomes.

EVs isolated from MSCs constitute the best alternative to cell-free therapy due to low immunogenicity, high biocompatibility, and low cytotoxicity to tissues. They can also be used for nano-regenerative medicine since they can be engineered to target specific cells or tissues and can work as drug carriers.

We and others demonstrated the beneficial effects and efficacious employment of EVs in reducing muscle injury effects and enhancing tissue repair (Ma et al., 2019; Wang et al., 2019; Sandonà et al., 2020; **Figure 1**). The alteration in the content of these vesicles leads to a miscommunication between cells in the diseased muscles (i.e., dystrophic muscles) and alters their behavior. This study showed the ability of MSC-EVs to transfer the benefits of drugs without causing the unwanted systemic side effects of these treatments, bringing new hope to regenerative medicine for DMD (Sandonà et al., 2020).

Although there is a large body of evidence that has demonstrated the regenerative capacity of MSCs and their secretome in disease models of acute injury, chronic damage, and atrophy of the skeletal muscle, to date, little clinical evidence is reported in patients and is anyhow limited to the use of MSCs.

Unfortunately, clinical applications of EVs remain challenging due to lack of standardized protocols to produce vesicles for therapeutic use. There are open debates in the EV community (ISEV) about the diversity and preparation of MSCs and consequently about the methods of EV isolation and purification. These points, together with the lack of standardized quality assurance assays, and limited accuracy of *in vitro* and *in vivo* functional assays can affect the reproducibility of research results. In addition to these obstacles, low yield (Shao et al., 2018) and heterogeneity (Pegtel and Gould, 2019) need to be urgently addressed (Ayers et al., 2019).

A full understanding of the potential and efficacy of MSCs, and especially of their products, to support muscle regeneration will be a breakthrough for regenerative medicine that will identify new molecules for the repair and regeneration of skeletal muscle tissue.

AUTHOR CONTRIBUTIONS

MS, LDP, FE, AV, and VS: writing—original draft preparation. ARS, MS, LDP, OP, and VS: writing—review and editing. OP and VS: supervision. All authors final approval of the manuscript.

FUNDING

This work has been supported by the following funding: Association Francaise contre les Myopathies (AFM no. 21657) and Italian Ministry of Health (GR-2016-02362451) to VS; Italian Ministry of Research and University, PRIN 2017 (MIUR, grant no. 2017RSAFK7) to OP; 5×1000 year 2018; and Fondazione Poliambulanza.

ACKNOWLEDGMENTS

We thank Università Cattolica del Sacro Cuore, Rome, and Fondazione Santa Lucia, Rome. We would like to acknowledge the Regenerative Medicine Research Center (CROME) of Università Cattolica del Sacro Cuore. This work contributes to the COST Action CA17116 International Network for Translating Research on Perinatal Derivatives into Therapeutic Approaches (SPRINT) and supported by COST (European Cooperation in Science and Technology).

REFERENCES

Allahverdi, A., Arefian, E., Soleimani, M., Ai, J., Nahanmoghaddam, N., Yousefi-Ahmadipour, A., et al. (2020). MicroRNA-4731-5p delivered by AD-mesenchymal stem cells induces cell cycle arrest and apoptosis in glioblastoma. *J. Cell. Physiol.* 235, 8167–8175. doi: 10.1002/jcp.29472

Andaloussi, E. L. S., Mäger, I., Breakefield, X. O., and Wood, M. J. A. (2013). Extracellular vesicles: biology and emerging therapeutic opportunities. *Nat. Rev. Drug Discov.* 12, 347–357. doi: 10.1038/nrd3978

Andrade, B. M., Baldanza, M. R., Ribeiro, K. C., Porto, A., Peçanha, R., Fortes, F. S. A., et al. (2015). Bone marrow mesenchymal cells improve muscle function in a skeletal muscle re-injury model. *PLoS One* 10:e127561. doi: 10.1371/journal.pone.0127561

Asari, S., Itakura, S., Ferreri, K., Liu, C.-P., Kuroda, Y., Kandeel, F., et al. (2009). Mesenchymal stem cells suppress B-cell terminal differentiation. *Exp. Hematol.* 37, 604–615. doi: 10.1016/j.exphem.2009.01.005

Asgarpour, K., Shojaei, Z., Amiri, F., Ai, J., Mahjoubin-Tehran, M., Ghasemi, F., et al. (2020). Exosomal microRNAs derived from mesenchymal stem cells: cell-to-cell messages. *Cell Commun. Signal.* 18:149. doi: 10.1186/s12964-020-00650-6

Aslam, M., Baveja, R., Liang, O. D., Fernandez-Gonzalez, A., Lee, C., Mitsialis, S. A., et al. (2009). Bone marrow stromal cells attenuate lung injury in a murine model of neonatal chronic lung disease. *Am. J. Respir. Crit. Care Med.* 180, 1122–1130. doi: 10.1164/rccm.200902-0242OC

Assoni, A., Coatti, G., Valadares, M. C., Beccari, M., Gomes, J., Pelatti, M., et al. (2017). Different donors mesenchymal stromal cells secretomes reveal heterogeneous profile of relevance for therapeutic use. *Stem Cells Dev.* 26, 206–214. doi: 10.1089/scd.2016.0218

Augello, A., Tasso, R., Negrini, S. M., Amateis, A., Indiveri, F., Cancedda, R., et al. (2005). Bone marrow mesenchymal progenitor cells inhibit lymphocyte proliferation by activation of the programmed death 1 pathway. *Eur. J. Immunol.* 35, 1482–1490. doi: 10.1002/eji.200425405

Ayers, L., Pink, R., Carter, D. R. F., and Nieuwland, R. (2019). Clinical requirements for extracellular vesicle assays. *J. Extracell. Ves.* 8:1593755. doi: 10.1080/20013078.2019.1593755

Bang, O. Y., Lee, J. S., Lee, P. H., and Lee, G. (2005). Autologous mesenchymal stem cell transplantation in stroke patients. *Ann. Neurol.* 57, 874–882. doi: 10.1002/ana.20501

Bari, E., Perteghella, S., Di Silvestre, D., Sorlini, M., Catenacci, L., Sorrenti, M., et al. (2018). Pilot Production of mesenchymal Stem/stromal freeze-dried secretome for cell-free regenerative nanomedicine: a validated GMP-compliant process. *Cells* 7:190. doi: 10.3390/cells7110190

Bier, A., Berenstein, P., Kronfeld, N., Morgoulis, D., Ziv-Av, A., Goldstein, H., et al. (2018). Placenta-derived mesenchymal stromal cells and their exosomes exert therapeutic effects in Duchenne muscular dystrophy. *Biomaterials* 174, 67–78. doi: 10.1016/j.biomaterials.2018.04.055

Bonab, M. M., Alimoghaddam, K., Talebian, F., Ghaffari, S. H., Ghavamzadeh, A., and Nikbin, B. (2006). Aging of mesenchymal stem cell in vitro. *BMC Cell Biol.* 7:14. doi: 10.1186/1471-2121-7-14

Bonafede, R., Brandi, J., Manfredi, M., Scambi, I., Schiaffino, L., Merigo, F., et al. (2019). The anti-apoptotic effect of ASC-exosomes in an in vitro ALS model and their proteomic analysis. *Cells* 8:1087. doi: 10.3390/cells8091087

Bonafede, R., Scambi, I., Peroni, D., Potrich, V., Boschi, F., Benati, D., et al. (2016). Exosome derived from murine adipose-derived stromal cells: neuroprotective effect on in vitro model of amyotrophic lateral sclerosis. *Exp. Cell Res.* 340, 150–158. doi: 10.1016/j.yexcr.2015.12.009

Bonaldo, P., and Sandri, M. (2013). Cellular and molecular mechanisms of muscle atrophy. *Dis. Model. Mech.* 6, 25–39. doi: 10.1242/dmm.010389

Borges, F. T., Reis, L. A., Schor, N., Borges, F. T., Reis, L. A., and Schor, N. (2013). Extracellular vesicles: structure, function, and potential clinical uses in renal diseases. *Braz. J. Med. Biol. Res.* 46, 824–830. doi: 10.1590/1414-431X20132964

Bronckaers, A., Hilkens, P., Martens, W., Gervois, P., Ratajczak, J., Struys, T., et al. (2014). Mesenchymal stem/stromal cells as a pharmacological and therapeutic approach to accelerate angiogenesis. *Pharmacol. Ther.* 143, 181–196. doi: 10.1016/j.pharmthera.2014.02.013

Campagnoli, C., Roberts, I. A., Kumar, S., Bennett, P. R., Bellantuono, I., and Fisk, N. M. (2001). Identification of mesenchymal stem/progenitor cells in human first-trimester fetal blood, liver, and bone marrow. *Blood* 98, 2396–2402. doi: 10.1182/blood.v98.8.2396

Cantaluppi, V., Gatti, S., Medica, D., Figliolini, F., Bruno, S., Deregibus, M. C., et al. (2012). Microvesicles derived from endothelial progenitor cells protect the kidney from ischemia-reperfusion injury by microRNA-dependent reprogramming of resident renal cells. *Kidney Int.* 82, 412–427. doi: 10.1038/ki.2012.105

Caplan, A. I. (2009). Why are MSCs therapeutic? New data: new insight. *J. Pathol.* 217, 318–324. doi: 10.1002/path.2469

Cargnoni, A., Ressel, L., Rossi, D., Poli, A., Arienti, D., Lombardi, G., et al. (2012). Conditioned medium from amniotic mesenchymal tissue cells reduces progression of bleomycin-induced lung fibrosis. *Cytotherapy* 14, 153–161. doi: 10.3109/14653249.2011.613930

Caseiro, A. R., Pereira, T., Ivanova, G., Luís, A. L., and Maurício, A. C. (2016). Neuromuscular regeneration: perspective on the application of Mesenchymal stem cells and their secretion products. *Stem Cells Int.* 2016, e9756973. doi: 10.1155/2016/9756973

Chapel, A., Bertho, J. M., Bensidhoum, M., Fouillard, L., Young, R. G., Frick, J., et al. (2003). Mesenchymal stem cells home to injured tissues when co-infused with hematopoietic cells to treat a radiation-induced multi-organ failure syndrome. *J. Gene Med.* 5, 1028–1038. doi: 10.1002/jgm.452

Chen, C., Yang, Q., Wang, D., Luo, F., Liu, X., Xue, J., et al. (2018). MicroRNA-191, regulated by HIF-2α, is involved in EMT and acquisition of a stem cell-like phenotype in arsenite-transformed human liver epithelial cells. *Toxicol. Vitro Int. J. Publ. Assoc. BIBRA* 48, 128–136. doi: 10.1016/j.tiv.2017.12.016

Chen, L., Tredget, E. E., Wu, P. Y. G., and Wu, Y. (2008). Paracrine factors of mesenchymal stem cells recruit macrophages and endothelial lineage cells and enhance wound healing. *PLoS One* 3:e1886. doi: 10.1371/journal.pone.0001886

Chen, S., Fang, W., Ye, F., Liu, Y.-H., Qian, J., Shan, S., et al. (2004). Effect on left ventricular function of intracoronary transplantation of autologous bone marrow mesenchymal stem cell in patients with acute myocardial infarction. *Am. J. Cardiol.* 94, 92–95. doi: 10.1016/j.amjcard.2004.03.034

Chiu, C.-H., Chang, T.-H., Chang, S.-S., Chang, G.-J., Chen, A. C.-Y., Cheng, C.-Y., et al. (2020). Application of bone marrow-derived mesenchymal stem cells for muscle healing after contusion injury in mice. *Am. J. Sports Med.* 48, 1226–1235. doi: 10.1177/0363546520905853

Choi, A., Park, S. E., Jeong, J. B., Choi, S., Oh, S., Ryu, G. H., et al. (2020). Anti-fibrotic effect of human Wharton's Jelly-derived mesenchymal stem cells on skeletal muscle cells, mediated by secretion of MMP-1. *Int. J. Mol. Sci.* 21:6269. doi: 10.3390/ijms21176269

Conceição, M., Forcina, L., Wiklander, O. P. B., Gupta, D., Nordin, J. Z., Vrellaku, B., et al. (2021). Engineered extracellular vesicle decoy receptor-mediated modulation of the IL6 trans-signalling pathway in muscle. *Biomaterials* 266:120435. doi: 10.1016/j.biomaterials.2020.120435

Corcione, A., Benvenuto, F., Ferretti, E., Giunti, D., Cappiello, V., Cazzanti, F., et al. (2006). Human mesenchymal stem cells modulate B-cell functions. *Blood* 107, 367–372. doi: 10.1182/blood-2005-07-2657

Dai, A., Baspinar, O., Yeşilyurt, A., Sun, E., Aydemir, ÇÝ, Öztel, O. N., et al. (2018). Efficacy of stem cell therapy in ambulatory and nonambulatory children with Duchenne muscular dystrophy - Phase I-II. *Degener. Neurol. Neuromuscul. Dis.* 8, 63–77. doi: 10.2147/DNND.S170087

De Bari, C., Dell'Accio, F., Tylzanowski, P., and Luyten, F. P. (2001). Multipotent mesenchymal stem cells from adult human synovial membrane. *Arthrit. Rheum.* 44, 1928–1942. doi: 10.1002/1529-0131(200108)44:8<1928: AID-ART331>3.0.CO;2-P

De La Garza-Rodea, A. S., Van Der Velde-Van Dijke, I., Boersma, H., Gonçalves, M. A. F. V., Van Bekkum, D. W., De Vries, A. A. F., et al. (2012). Myogenic properties of human Mesenchymal stem cells derived from three different sources. *Cell Transplant.* 21, 153–173. doi: 10.3727/096368911X580554

Di Nicola, M., Carlo-Stella, C., Magni, M., Milanesi, M., Longoni, P. D., Matteucci, P., et al. (2002). Human bone marrow stromal cells suppress T-lymphocyte proliferation induced by cellular or nonspecific mitogenic stimuli. *Blood* 99, 3838–3843. doi: 10.1182/blood.v99.10.3838

Di Pietro, L., Barba, M., Prampolini, C., Ceccariglia, S., Frassanito, P., Vita, A., et al. (2020). GLI1 and AXIN2 are distinctive markers of human Calvarial Mesenchymal stromal cells in nonsyndromic craniosynostosis. *Int. J. Mol. Sci.* 21:4356. doi: 10.3390/ijms21124356

Djouad, F., Charbonnier, L.-M., Bouffi, C., Louis-Plence, P., Bony, C., Apparailly, F., et al. (2007). Mesenchymal stem cells inhibit the differentiation of dendritic cells through an interleukin-6-dependent mechanism. *Stem Cells* 25, 2025–2032. doi: 10.1634/stemcells.2006-0548

Dominici, M., Le Blanc, K., Mueller, I., Slaper-Cortenbach, I., Marini, F., Krause, D., et al. (2006). Minimal criteria for defining multipotent mesenchymal stromal cells. The international society for cellular therapy position statement. *Cytotherapy* 8, 315–317. doi: 10.1080/14653240600855905

Drela, K., Stanaszek, L., Nowakowski, A., Kuczynska, Z., and Lukomska, B. (2019). Experimental strategies of mesenchymal stem cell propagation: adverse events and potential risk of functional changes. *Stem Cells Int.* 2019, 7012692. doi: 10.1155/2019/7012692

Eleuteri, S., and Fierabracci, A. (2019). Insights into the secretome of mesenchymal stem cells and its potential applications. *Int. J. Mol. Sci.* 20:4597. doi: 10.3390/ijms20184597

Feng, Y., Huang, W., Wani, M., Yu, X., and Ashraf, M. (2014). Ischemic preconditioning potentiates the protective effect of stem cells through secretion of Exosomes by targeting Mecp2 via miR-22. *PLoS One* 9:e88685. doi: 10.1371/journal.pone.0088685

Forterre, A., Jalabert, A., Berger, E., Baudet, M., Chikh, K., Errazuriz, E., et al. (2014). Proteomic analysis of C2C12 Myoblast and Myotube Exosome-like vesicles: a new paradigm for Myoblast-Myotube cross talk? *PLoS One* 9:e84153. doi: 10.1371/journal.pone.0084153

Friedenstein, A. J., Chailakhyan, R. K., Latsinik, N. V., Panasyuk, A. F., and Keiliss-Borok, I. V. (1974). Stromal cells responsible for transferring the microenvironment of the hemopoietic tissues. Cloning in vitro and retransplantation in vivo. *Transplantation* 17, 331–340. doi: 10.1097/00007890-197404000-00001

Galderisi, U., and Giordano, A. (2014). The gap between the physiological and therapeutic roles of mesenchymal stem cells. *Med. Res. Rev.* 34, 1100–1126. doi: 10.1002/med.21322

Gao, Q. Q., Wyatt, E., Goldstein, J. A., LoPresti, P., Castillo, L. M., Gazda, A., et al. (2015). Reengineering a transmembrane protein to treat muscular dystrophy using exon skipping. *J. Clin. Invest.* 125, 4186–4195. doi: 10.1172/JCI82768

Giampà, C., Alvino, A., Magatti, M., Silini, A. R., Cardinale, A., Paldino, E., et al. (2019). Conditioned medium from amniotic cells protects striatal degeneration and ameliorates motor deficits in the R6/2 mouse model of Huntington's disease. *J. Cell. Mol. Med.* 23, 1581–1592. doi: 10.1111/jcmm.14113

Gnecchi, M., He, H., Noiseux, N., Liang, O. D., Zhang, L., Morello, F., et al. (2006). Evidence supporting paracrine hypothesis for Akt-modified mesenchymal stem cell-mediated cardiac protection and functional improvement. *FASEB J.* 20, 661–669. doi: 10.1096/fj.05-5211com

Gomes, J. P., Coatti, G. C., Valadares, M. C., Assoni, A. F., Pelatti, M. V., Secco, M., et al. (2018). Human Adipose-Derived CD146+ stem cells increase life span of a muscular dystrophy mouse model more efficiently than Mesenchymal stromal cells. *DNA Cell Biol.* 37, 798–804. doi: 10.1089/dna.2018.4158

Goolaerts, A., Pellan-Randrianarison, N., Larghero, J., Vanneaux, V., Uzunhan, Y., Gille, T., et al. (2014). Conditioned media from mesenchymal stromal cells restore sodium transport and preserve epithelial permeability in an in vitro model of acute alveolar injury. *Am. J. Physiol. Lung Cell. Mol. Physiol.* 306, L975–L985. doi: 10.1152/ajplung.00242.2013

Gowen, A., Shahjin, F., Chand, S., Odegaard, K. E., and Yelamanchili, S. V. (2020). Mesenchymal stem cell-derived extracellular vesicles: challenges in clinical applications. *Front. Cell Dev. Biol.* 8:149. doi: 10.3389/fcell.2020.00149

Guescini, M., Guidolin, D., Vallorani, L., Casadei, L., Gioacchini, A. M., Tibollo, P., et al. (2010). C2C12 myoblasts release micro-vesicles containing mtDNA and proteins involved in signal transduction. *Exp. Cell Res.* 316, 1977–1984. doi: 10.1016/j.yexcr.2010.04.006

Gugliandolo, A., Bramanti, P., and Mazzon, E. (2019). Mesenchymal stem cells: a potential therapeutic approach for amyotrophic lateral sclerosis? *Stem Cells Int.* 2019:e3675627. doi: 10.1155/2019/3675627

Hardiman, O., Al-Chalabi, A., Chio, A., Corr, E. M., Logroscino, G., Robberecht, W., et al. (2017). Amyotrophic lateral sclerosis. *Nat. Rev. Dis. Primer.* 3, 1–19. doi: 10.1038/nrdp.2017.71

Hegyi, B., Kudlik, G., Monostori, É, and Uher, F. (2012). Activated T-cells and pro-inflammatory cytokines differentially regulate prostaglandin E2 secretion by mesenchymal stem cells. *Biochem. Biophys. Res. Commun.* 419, 215–220. doi: 10.1016/j.bbrc.2012.01.150

Helal, M. A. M., Shaheen, N. E. M., and Abu Zahra, F. A. (2016). Immunomodulatory capacity of the local mesenchymal stem cells transplantation after severe skeletal muscle injury in female rats. *Immunopharmacol. Immunotoxicol.* 38, 414–422. doi: 10.1080/08923973.2016.1222617

Iraci, N., Leonardi, T., Gessler, F., Vega, B., and Pluchino, S. (2016). Focus on extracellular vesicles: physiological role and signalling properties of Extracellular membrane vesicles. *Int. J. Mol. Sci.* 17:171. doi: 10.3390/ijms17020171

Iyer, S. R., Scheiber, A. L., Yarowsky, P., Henn, R. F., Otsuru, S., and Lovering, R. M. (2020). Exosomes isolated from platelet-rich plasma and mesenchymal stem cells promote recovery of function after muscle injury. *Am. J. Sports Med.* 48, 2277–2286. doi: 10.1177/0363546520926462

Izadpanah, R., Trygg, C., Patel, B., Kriedt, C., Dufour, J., Gimble, J. M., et al. (2006). Biologic properties of mesenchymal stem cells derived from bone marrow and adipose tissue. *J. Cell. Biochem.* 99, 1285–1297. doi: 10.1002/jcb.20904

Jackson, W. M., Nesti, L. J., and Tuan, R. S. (2012). Mesenchymal stem cell therapy for attenuation of scar formation during wound healing. *Stem Cell Res. Ther.* 3:20. doi: 10.1186/scrt111

Julien, J.-P., and Kriz, J. (2006). Transgenic mouse models of amyotrophic lateral sclerosis. *Biochim. Biophys. Acta BBA Mol. Basis Dis.* 1762, 1013–1024. doi: 10.1016/j.bbadis.2006.03.006

Kahroba, H., Hejazi, M. S., and Samadi, N. (2019). Exosomes: from carcinogenesis and metastasis to diagnosis and treatment of gastric cancer. *Cell. Mol. Life Sci.* 76, 1747–1758. doi: 10.1007/s00018-019-03035-2

Keyser, K. A., Beagles, K. E., and Kiem, H.-P. (2007). Comparison of Mesenchymal stem cells from different tissues to suppress T-Cell activation. *Cell Transplant.* 16, 555–562. doi: 10.3727/000000007783464939

Kharraz, Y., Guerra, J., Mann, C. J., Serrano, A. L., and Muñoz-Cánoves, P. (2013). Macrophage plasticity and the role of inflammation in skeletal muscle repair. *Med. Inflamm.* 2013:491497. doi: 10.1155/2013/491497

Kim, M. J., Kim, Y., Kim, Z.-H., and Heo, S.-H. (2015). Mesenchymal stem cells suppress muscle atrophy induced by Hindlimb suspension. *Stem Cell Res. Ther.* 5, 1–9.

Kim, M. J., Kim, Z.-H., Kim, S.-M., and Choi, Y.-S. (2016). Conditioned medium derived from umbilical cord mesenchymal stem cells regenerates atrophied muscles. *Tissue Cell* 48, 533–543. doi: 10.1016/j.tice.2016.06.010

Kim, S. H., Cho, J. H., Lee, Y. H., Lee, J. H., Kim, S. S., Kim, M. Y., et al. (2018). Improvement in left ventricular function with intracoronary Mesenchymal stem cell therapy in a patient with anterior wall st-segment elevation myocardial infarction. *Cardiovasc. Drugs Ther.* 32, 329–338. doi: 10.1007/s10557-018-6804-z

Kisiel, A. H., McDuffee, L. A., Masaoud, E., Bailey, T. R., Esparza Gonzalez, B. P., and Nino-Fong, R. (2012). Isolation, characterization, and in vitro proliferation of canine mesenchymal stem cells derived from bone marrow, adipose tissue, muscle, and periosteum. *Am. J. Vet. Res.* 73, 1305–1317. doi: 10.2460/ajvr.73.8.1305

Klimczak, A., and Kozlowska, U. (2016). Mesenchymal stromal cells and tissue-specific progenitor cells: their role in tissue homeostasis. *Stem Cells Int.* 2016, 4285215. doi: 10.1155/2016/4285215

Klimczak, A., Kozlowska, U., and Kurpisz, M. (2018). Muscle Stem/progenitor cells and Mesenchymal stem cells of bone marrow origin for skeletal muscle regeneration in muscular dystrophies. *Arch. Immunol. Ther. Exp.* 66, 341–354. doi: 10.1007/s00005-018-0509-7

Klimczak, A., Zimna, A., Malcher, A., Kozlowska, U., Futoma, K., Czarnota, J., et al. (2020). Co-Transplantation of bone marrow-MSCs and Myogenic Stem/progenitor cells from adult donors improves muscle function of patients with Duchenne muscular dystrophy. *Cells* 9:1119. doi: 10.3390/cells9051119

Kong, J., and Xu, Z. (1998). Massive mitochondrial degeneration in motor neurons triggers the onset of amyotrophic lateral sclerosis in mice expressing a mutant SOD1. *J. Neurosci. Off. J. Soc. Neurosci.* 18, 3241–3250. doi: 10.1523/jneurosci.18-09-03241.1998

Koniusz, S., Andrzejewska, A., Muraca, M., Srivastava, A. K., Janowski, M., and Lukomska, B. (2016). Extracellular vesicles in physiology, pathology, and therapy of the immune and central nervous system, with focus on extracellular vesicles derived from mesenchymal stem cells as therapeutic tools. *Front. Cell. Neurosci.* 10:109. doi: 10.3389/fncel.2016.00109

Kwon, S., Ki, S. M., Park, S. E., Kim, M.-J., Hyung, B., Lee, N. K., et al. (2016). Anti-apoptotic effects of human Wharton's jelly-derived mesenchymal stem cells on skeletal muscle cells mediated via secretion of XCL1. *Mol. Ther. J. Am. Soc. Gene Ther.* 24, 1550–1560. doi: 10.1038/mt.2016.125

Lang, F. M., Hossain, A., Gumin, J., Momin, E. N., Shimizu, Y., Ledbetter, D., et al. (2018). Mesenchymal stem cells as natural biofactories for exosomes carrying miR-124a in the treatment of gliomas. *Neuro Oncol.* 20, 380–390. doi: 10.1093/neuonc/nox152

Lattanzi, W., Barba, M., Novegno, F., Massimi, L., Tesori, V., Tamburrini, G., et al. (2013). Lim mineralization protein is involved in the premature calvarial ossification in sporadic Craniosynostoses. *Bone* 52, 474–484. doi: 10.1016/j.bone.2012.09.004

Lazarus, H. M., Koc, O. N., Devine, S. M., Curtin, P., Maziarz, R. T., Holland, H. K., et al. (2005). Cotransplantation of HLA-identical sibling culture-expanded mesenchymal stem cells and hematopoietic stem cells in hematologic malignancy patients. *Biol. Blood Marrow Transplant.* 11, 389–398. doi: 10.1016/j.bbmt.2005.02.001

Le Blanc, K., and Mougiakakos, D. (2012). Multipotent mesenchymal stromal cells and the innate immune system. *Nat. Rev. Immunol.* 12, 383–396. doi: 10.1038/nri3209

Leavitt, R. J., Limoli, C. L., and Baulch, J. E. (2019). miRNA-based therapeutic potential of stem cell-derived extracellular vesicles: a safe cell-free treatment to ameliorate radiation-induced brain injury. *Int. J. Radiat. Biol.* 95, 427–435. doi: 10.1080/09553002.2018.1522012

Lee, M., Ban, J.-J., Kim, K. Y., Jeon, G. S., Im, W., Sung, J.-J., et al. (2016). Adipose-derived stem cell exosomes alleviate pathology of amyotrophic lateral sclerosis in vitro. *Biochem. Biophys. Res. Commun.* 479, 434–439. doi: 10.1016/j.bbrc.2016.09.069

Lee, P. H., Lee, J. E., Kim, H.-S., Song, S. K., Lee, H. S., Nam, H. S., et al. (2012). A randomized trial of mesenchymal stem cells in multiple system atrophy. *Ann. Neurol.* 72, 32–40. doi: 10.1002/ana.23612

Lee, R. H., Oh, J. Y., Choi, H., and Bazhanov, N. (2011). Therapeutic factors secreted by mesenchymal stromal cells and tissue repair. *J. Cell. Biochem.* 112, 3073–3078. doi: 10.1002/jcb.23250

Leng, L., Dong, X., Gao, X., Ran, N., Geng, M., Zuo, B., et al. (2020). Exosome-mediated improvement in membrane integrity and muscle function in dystrophic mice. *Mol. Ther.* 29, 1459–1470. doi: 10.1016/j.ymthe.2020.12.018

Li, L., Zhang, S., Zhang, Y., Yu, B., Xu, Y., and Guan, Z. (2009). Paracrine action mediate the antifibrotic effect of transplanted mesenchymal stem cells in a rat model of global heart failure. *Mol. Biol. Rep.* 36, 725–731. doi: 10.1007/s11033-008-9235-2

Li, P., Cui, K., Zhang, B., Wang, Z., Shen, Y., Wang, X., et al. (2015). Transplantation of human umbilical cord-derived mesenchymal stems cells for the treatment of Becker muscular dystrophy in affected pedigree members. *Int. J. Mol. Med.* 35, 1051–1057. doi: 10.3892/ijmm.2015.2084

Li, S., Sheng, J., Hu, J. K., Yu, W., Kishikawa, H., Hu, M. G., et al. (2013). Ribonuclease 4 protects neuron degeneration by promoting angiogenesis, neurogenesis, and neuronal survival under stress. *Angiogenesis* 16, 387–404. doi: 10.1007/s10456-012-9322-9

Li, Y.-P., Paczesny, S., Lauret, E., Poirault, S., Bordigoni, P., Mekhloufi, F., et al. (2008). Human Mesenchymal stem cells license adult CD34+ Hemopoietic progenitor cells to differentiate into regulatory dendritic cells through activation of the Notch pathway. *J. Immunol.* 180, 1598–1608. doi: 10.4049/jimmunol.180.3.1598

Li, Z., Liu, H.-Y., Lei, Q.-F., Zhang, C., and Li, S.-N. (2011). Improved motor function in dko mice by intravenous transplantation of bone marrow-derived mesenchymal stromal cells. *Cytotherapy* 13, 69–77. doi: 10.3109/14653249.2010.510502

Linard, C., Brachet, M., L'homme, B., Strup-Perrot, C., Busson, E., Bonneau, M., et al. (2018). Long-term effectiveness of local BM-MSCs for skeletal muscle regeneration: a proof of concept obtained on a pig model of severe radiation burn. *Stem Cell Res. Ther.* 9:299. doi: 10.1186/s13287-018-1051-6

Liu, J., Saul, D., Böker, K. O., Ernst, J., Lehman, W., and Schilling, A. F. (2018). Current methods for skeletal muscle tissue repair and regeneration. *Bio Med. Res. Int.* 2018:e1984879. doi: 10.1155/2018/1984879

Liu, S., Ginestier, C., Ou, S. J., Clouthier, S. G., Patel, S. H., Monville, F., et al. (2011). Breast cancer stem cells are regulated by mesenchymal stem cells through cytokine networks. *Cancer Res.* 71, 614–624. doi: 10.1158/0008-5472.CAN-10-0538

Lo Sicco, C., Reverberi, D., Balbi, C., Ulivi, V., Principi, E., Pascucci, L., et al. (2017). Mesenchymal Stem cell-derived extracellular vesicles as mediators of anti-inflammatory effects: endorsement of macrophage polarization: msc-derived ev promote macrophage polarization. *Stem Cells Transl. Med.* 6, 1018–1028. doi: 10.1002/sctm.16-0363

Longhini, A. L. F., Salazar, T. E., Vieira, C., Trinh, T., Duan, Y., Pay, L. M., et al. (2019). Peripheral blood-derived mesenchymal stem cells demonstrate immunomodulatory potential for therapeutic use in horses. *PLoS One* 14:e0212642. doi: 10.1371/journal.pone.0212642

Lou, G., Song, X., Yang, F., Wu, S., Wang, J., Chen, Z., et al. (2015). Exosomes derived from miR-122-modified adipose tissue-derived MSCs increase chemosensitivity of hepatocellular carcinoma. *J. Hematol. Oncol.J Hematol Oncol* 8:122. doi: 10.1186/s13045-015-0220-7

Luo, Z., Lin, J., Sun, Y., Wang, C., and Chen, J. (2020). Bone marrow stromal cell-derived exosomes promote muscle healing following contusion through macrophage polarization. *Stem Cells Dev.* 30, 167. doi: 10.1089/scd.2020.0167

Ma, Y., Dong, L., Zhou, D., Li, L., Zhang, W., Zhen, Y., et al. (2019). Extracellular vesicles from human umbilical cord mesenchymal stem cells improve nerve regeneration after sciatic nerve transection in rats. *J. Cell. Mol. Med.* 23, 2822–2835. doi: 10.1111/jcmm.14190

Madaro, L., Passafaro, M., Sala, D., Etxaniz, U., Lugarini, F., Proietti, D., et al. (2018). Denervation-activated STAT3-IL-6 signalling in fibro-adipogenic progenitors promotes myofibres atrophy and fibrosis. *Nat. Cell Biol.* 20, 917–927. doi: 10.1038/s41556-018-0151-y

Maeda, Y., Yonemochi, Y., Nakajyo, Y., Hidaka, H., Ikeda, T., and Ando, Y. (2017). CXCL12 and osteopontin from bone marrow-derived mesenchymal stromal cells improve muscle regeneration. *Sci. Rep.* 7:3305. doi: 10.1038/s41598-017-02928-1

Magatti, M., Vertua, E., Munari, S. D., Caro, M., Caruso, M., Silini, A., et al. (2017). Human amnion favours tissue repair by inducing the M1-to-M2 switch and enhancing M2 macrophage features. *J. Tissue Eng. Regen. Med.* 11, 2895–2911. doi: 10.1002/term.2193

Malecova, B., and Puri, P. L. (2012). "Mix of Mics"- phenotypic and biological heterogeneity of "Multipotent" muscle interstitial cells (MICs). *J. Stem Cell Res. Ther.* (Suppl. 11):4.

Marconi, S., Bonaconsa, M., Scambi, I., Squintani, G. M., Rui, W., Turano, E., et al. (2013). Systemic treatment with adipose-derived mesenchymal stem cells ameliorates clinical and pathological features in the amyotrophic lateral sclerosis murine model. *Neuroscience* 248, 333–343. doi: 10.1016/j.neuroscience.2013.05.034

Mardpour, S., Ghanian, M. H., Sadeghi-abandansari, H., Mardpour, S., Nazari, A., Shekari, F., et al. (2019). Hydrogel-mediated sustained systemic delivery of mesenchymal stem cell-derived extracellular vesicles improves hepatic regeneration in chronic liver failure. *ACS Appl. Mater. Interf.* 11, 37421–37433. doi: 10.1021/acsami.9b10126

Markert, C. D., Atala, A., Cann, J. K., Christ, G., Furth, M., Ambrosio, F., et al. (2009). Mesenchymal stem cells: emerging therapy for duchenne muscular dystrophy. *PM R* 1, 547–559. doi: 10.1016/j.pmrj.2009.02.013

Mead, B., Logan, A., Berry, M., Leadbeater, W., and Scheven, B. A. (2014). Paracrine-mediated neuroprotection and neuritogenesis of axotomised retinal ganglion cells by human dental pulp stem cells: comparison with human bone marrow and adipose-derived mesenchymal stem cells. *PLoS One* 9:e109305. doi: 10.1371/journal.pone.0109305

Mellows, B., Mitchell, R., Antonioli, M., Kretz, O., Chambers, D., Zeuner, M.-T., et al. (2017). Protein and molecular characterization of a clinically compliant amniotic fluid stem cell-derived extracellular vesicle fraction capable of accelerating muscle regeneration through enhancement of angiogenesis. *Stem Cells Dev.* 26, 1316–1333. doi: 10.1089/scd.2017.0089

Mirabella, T., Cilli, M., Carlone, S., Cancedda, R., and Gentili, C. (2011). Amniotic liquid derived stem cells as reservoir of secreted angiogenic factors capable of stimulating neo-arteriogenesis in an ischemic model. *Biomaterials* 32, 3689–3699. doi: 10.1016/j.biomaterials.2011.01.071

Mitchell, K. J., Pannérec, A., Cadot, B., Parlakian, A., Besson, V., Gomes, E. R., et al. (2010). Identification and characterization of a non-satellite cell muscle resident progenitor during postnatal development. *Nat. Cell Biol.* 12, 257–266. doi: 10.1038/ncb2025

Mitchell, R., Mellows, B., Sheard, J., Antonioli, M., Kretz, O., Chambers, D., et al. (2019). Secretome of adipose-derived mesenchymal stem cells promotes skeletal muscle regeneration through synergistic action of extracellular vesicle cargo and soluble proteins. *Stem Cell Res. Ther.* 10:116. 10.1186/s13287-019-1213-1

Montesinos, J. J., Mora-García, M., de, L., Mayani, H., Flores-Figueroa, E., García-Rocha, R., et al. (2013). In vitro evidence of the presence of mesenchymal stromal cells in cervical cancer and their role in protecting cancer cells from cytotoxic T cell activity. *Stem Cells Dev.* 22, 2508–2519. doi: 10.1089/scd.2013.0084

Moussa, M. H., Hamam, G. G., Abd Elaziz, A. E., Rahoma, M. A., Abd El Samad, A. A., El-Waseef, D. A. A., et al. (2020). Comparative study on bone marrow-versus adipose-derived stem cells on regeneration and re-innervation of skeletal muscle injury in wistar rats. *Tissue Eng. Regen. Med.* 17, 887–900. doi: 10.1007/s13770-020-00288-y

Mozzetta, C., Consalvi, S., Saccone, V., Tierney, M., Diamantini, A., Mitchell, K. J., et al. (2013). Fibroadipogenic progenitors mediate the ability of HDAC inhibitors to promote regeneration in dystrophic muscles of young, but not old Mdx mice. *EMBO Mol. Med.* 5, 626–639. doi: 10.1002/emmm.201202096

Nabavi, S. M., Arab, L., Jarooghi, N., Bolurieh, T., Abbasi, F., Mardpour, S., et al. (2019). Safety, feasibility of intravenous and Intrathecal injection of Autologous bone marrow derived mesenchymal stromal cells in patients with amyotrophic lateral sclerosis: an open label Phase I clinical trial. *Cell J.* 20, 592–598. doi: 10.22074/cellj.2019.5370

Nakamura, Y., Miyaki, S., Ishitobi, H., Matsuyama, S., Nakasa, T., Kamei, N., et al. (2015). Mesenchymal-stem-cell-derived exosomes accelerate skeletal muscle regeneration. *FEBS Lett.* 589, 1257–1265. doi: 10.1016/j.febslet.2015.03.031

Nasef, A., Mathieu, N., Chapel, A., Frick, J., François, S., Mazurier, C., et al. (2007). Immunosuppressive effects of mesenchymal stem cells: involvement of HLA-G. *Transplantation* 84, 231–237. doi: 10.1097/01.tp.0000267918.07906.08

Nauta, A. J., Kruisselbrink, A. B., Lurvink, E., Willemze, R., and Fibbe, W. E. (2006). Mesenchymal stem cells inhibit generation and function of both CD34+-derived and monocyte-derived dendritic cells. *J. Immunol. Baltim. Md* 1950, 2080–2087. doi: 10.4049/jimmunol.177.4.2080

Németh, K., Leelahavanichkul, A., Yuen, P. S. T., Mayer, B., Parmelee, A., Doi, K., et al. (2009). Bone marrow stromal cells attenuate sepsis via prostaglandin E 2 - dependent reprogramming of host macrophages to increase their interleukin-10 production. *Nat. Med.* 15, 42–49. doi: 10.1038/nm.1905

Noonan, T. J., and Garrett, W. E. (1999). Muscle strain injury: diagnosis and treatment. *J. Am. Acad. Orthop. Surg.* 7, 262–269. doi: 10.5435/00124635-199907000-00006

Onishi, R., Ohnishi, S., Higashi, R., Watari, M., Yamahara, K., Okubo, N., et al. (2015). Human amnion-derived mesenchymal stem cell transplantation ameliorates dextran sulfate sodium-induced severe colitis in rats. *Cell Transplant.* 24, 2601–2614. doi: 10.3727/096368915X687570

Otabe, K., Muneta, T., Kawashima, N., Suda, H., Tsuji, K., and Sekiya, I. (2012). Comparison of Gingiva, dental pulp, and periodontal ligament cells from the standpoint of Mesenchymal stem cell properties. *Cell Med.* 4, 13–21. doi: 10.3727/215517912X653319

Padhi, A. K., and Gomes, J. (2019). A molecular dynamics based investigation reveals the role of rare Ribonuclease 4 variants in amyotrophic lateral sclerosis susceptibility. *Mutat. Res.* 813, 1–12. doi: 10.1016/j.mrfmmm.2018.11.002

Parolini, O., Alviano, F., Bagnara, G. P., Bilic, G., Bühring, H.-J., Evangelista, M., et al. (2008). Concise review: isolation and characterization of cells from human term placenta: outcome of the first international workshop on placenta derived stem cells. *Stem Cells* 26, 300–311. doi: 10.1634/stemcells.2007-0594

Pascucci, L., Coccè, V., Bonomi, A., Ami, D., Ceccarelli, P., Ciusani, E., et al. (2014). Paclitaxel is incorporated by mesenchymal stromal cells and released in exosomes that inhibit in vitro tumor growth: a new approach for drug delivery. *J. Control. Release Off. J. Control. Release Soc.* 192, 262–270. doi: 10.1016/j.jconrel.2014.07.042

Pegtel, D. M., and Gould, S. J. (2019). Exosomes. *Annu. Rev. Biochem.* 88, 487–514. doi: 10.1146/annurev-biochem-013118-111902

Pereira, T., Armada-da Silva, P. A. S., Amorim, I., Rêma, A., Caseiro, A. R., Gärtner, A., et al. (2014). Effects of human Mesenchymal stem cells isolated from Wharton's Jelly of the umbilical cord and conditioned media on skeletal muscle regeneration using a myectomy model. *Stem Cells Int.* 2014, 1–16. doi: 10.1155/2014/376918

Pezzi, A., Amorin, B., Laureano, Á., Valim, V., Dahmer, A., Zambonato, B., et al. (2017). Effects of hypoxia in long-term in vitro expansion of human bone marrow derived Mesenchymal stem cells. *J. Cell. Biochem.* 118, 3072–3079. doi: 10.1002/jcb.25953

Pinheiro, C. H. D. J., de Queiroz, J. C. F., Guimarães-Ferreira, L., Vitzel, K. F., Nachbar, R. T., de Sousa, L. G. O., et al. (2012). Local injections of adipose-derived mesenchymal stem cells modulate inflammation and increase angiogenesis ameliorating the dystrophic phenotype in dystrophin-deficient skeletal muscle. *Stem Cell Rev. Rep.* 8, 363–374. doi: 10.1007/s12015-011-9304-0

Pischiutta, F., Brunelli, L., Romele, P., Silini, A., Sammali, E., Paracchini, L., et al. (2016). Protection of brain injury by amniotic mesenchymal stromal cell-secreted metabolites. *Crit. Care Med.* 44:e01118-31. doi: 10.1097/CCM.0000000000001864

Pisciotta, A., Riccio, M., Carnevale, G., Lu, A., De Biasi, S., Gibellini, L., et al. (2015). Stem cells isolated from human dental pulp and amniotic fluid improve skeletal muscle histopathology in mdx/SCID mice. *Stem Cell Res. Ther.* 6:156. doi: 10.1186/s13287-015-0141-y

Prockop, D. J., and Youn Oh, J. (2012). Mesenchymal Stem/Stromal Cells (MSCs): role as guardians of inflammation. *Mol. Ther.* 20, 14–20. doi: 10.1038/mt.2011.211

Qu, Y., Zhang, Q., Cai, X., Li, F., Ma, Z., Xu, M., et al. (2017). Exosomes derived from miR-181-5p-modified adipose-derived mesenchymal stem cells prevent liver fibrosis via autophagy activation. *J. Cell. Mol. Med.* 21, 2491–2502. doi: 10.1111/jcmm.13170

Rajendran, R., Gopal, S., Masood, H., Vivek, P., and Deb, K. (2013). Regenerative potential of dental pulp mesenchymal stem cells harvested from high caries patient's teeth. *J. Stem Cells* 8, 25–41.

Rajput, B. S., Chakrabarti, S. K., Dongare, V. S., Ramirez, C. M., and Deb, K. D. (2015). Human Umbilical cord Mesenchymal stem cells in the treatment of duchenne muscular dystrophy: safety and feasibility study in India. *J. Stem Cells* 10, 141–156.

Ramasamy, R., Fazekasova, H., Lam, E. W.-F., Soeiro, I., Lombardi, G., and Dazzi, F. (2007). Mesenchymal stem cells inhibit dendritic cell differentiation and function by preventing entry into the cell cycle. *Transplantation* 83, 71–76. doi: 10.1097/01.tp.0000244572.24780.54

Rani, S., Ryan, A. E., Griffin, M. D., and Ritter, T. (2015). Mesenchymal stem cell-derived extracellular vesicles: toward cell-free therapeutic applications. *Mol. Ther.* 23, 812–823. doi: 10.1038/mt.2015.44

Rasmusson, I., Ringdén, O., Sundberg, B., and Le Blanc, K. (2003). Mesenchymal stem cells inhibit the formation of cytotoxic T lymphocytes, but not activated cytotoxic T lymphocytes or natural killer cells. *Transplantation* 76, 1208–1213. doi: 10.1097/01.TP.0000082540.43730.80

Ray, P., Devaux, Y., Stolz, D. B., Yarlagadda, M., Watkins, S. C., Lu, Y., et al. (2003). Inducible expression of keratinocyte growth factor (KGF) in mice inhibits lung epithelial cell death induced by hyperoxia. *Proc. Natl. Acad. Sci. U.S.A.* 100, 6098–6103. doi: 10.1073/pnas.1031851100

Riekstina, U., Cakstina, I., Parfejevs, V., Hoogduijn, M., Jankovskis, G., Muiznieks, I., et al. (2009). Embryonic stem cell marker expression pattern in human mesenchymal stem cells derived from bone marrow, adipose tissue, heart and dermis. *Stem Cell Rev. Rep.* 5, 378–386. doi: 10.1007/s12015-009-9094-9

Ren, H., Sang, Y., Zhang, F., Liu, Z., Qi, N., and Chen, Y. (2016). Comparative analysis of human Mesenchymal stem cells from umbilical cord, dental pulp, and menstrual blood as sources for cell therapy. *Stem Cells Int.* 2016, 3516574. doi: 10.1155/2016/3516574

Ringden, O., Uzunel, M., Rasmusson, I., Remberger, M., Sundberg, B., Lnnies, H., et al. (2006). Mesenchymal stem cells for treatment of therapy-resistant graft-versus-host disease. *Transplantation* 81, 1390–1397. doi: 10.1097/01.tp.0000214462.63943.14

Ripa, R. S., Haack-Sorensen, M., Wang, Y., Jorgensen, E., Mortensen, S., Bindslev, L., et al. (2007). Bone Marrow derived Mesenchymal cell mobilization by granulocyte-colony stimulating factor after acute myocardial infarction: results from the stem cells in myocardial infarction (STEMMI) trial. *Circulation* 116, I–24–I–30. doi: 10.1161/CIRCULATIONAHA.106.678649

Romancino, D. P., Paterniti, G., Campos, Y., De Luca, A., Di Felice, V., d'Azzo, A., et al. (2013). Identification and characterization of the nano-sized vesicles released by muscle cells. *FEBS Lett.* 587, 1379–1384. doi: 10.1016/j.febslet.2013.03.012

Røsland, G., Svendsen, A., Torsvik, A., Sobala, E., Mc Cormack, E., Immervoll, H., et al. (2009). Long-term cultures of bone marrow-derived human mesenchymal stem cells frequently undergo spontaneous malignant transformation. *Cancer Res.* 69, 5331–5339. doi: 10.1158/0008-5472.CAN-08-4630

Rossi, D., Pianta, S., Magatti, M., Sedlmayr, P., and Parolini, O. (2012). Characterization of the conditioned medium from amniotic membrane cells: prostaglandins as key effectors of its immunomodulatory activity. *PLoS One* 7:e46956. doi: 10.1371/journal.pone.0046956

Saleh, A. F., Lázaro-Ibáñez, E., Forsgard, M. A.-M., Shatnyeva, O., Osteikoetxea, X., Karlsson, F., et al. (2019). Extracellular vesicles induce minimal hepatotoxicity and immunogenicity. *Nanoscale* 11, 6990–7001. doi: 10.1039/c8nr08720b

Sandonà, M., Consalvi, S., Tucciarone, L., De Bardi, M., Scimeca, M., Angelini, D. F., et al. (2020). HDAC inhibitors tune miRNAs in extracellular vesicles of dystrophic muscle-resident mesenchymal cells. *EMBO Rep.* 21:e50863. doi: 10.15252/embr.202050863

Sattler, C., Steinsdoerfer, M., Offers, M., Fischer, E., Schierl, R., Heseler, K., et al. (2011). Inhibition of T-cell proliferation by Murine Multipotent Mesenchymal stromal cells is mediated by CD39 expression and adenosine generation. *Cell Transplant.* 20, 1221–1230. doi: 10.3727/096368910X546553

Secco, M., Bueno, C., Vieira, N. M., Almeida, C., Pelatti, M., Zucconi, E., et al. (2013). Systemic delivery of human Mesenchymal stromal cells combined with IGF-1 enhances muscle functional recovery in LAMA2dy/2jDystrophic mice. *Stem Cell Rev. Rep.* 9, 93–109. doi: 10.1007/s12015-012-9380-9

Shabbir, A., Zisa, D., Leiker, M., Johnston, C., Lin, H., and Lee, T. (2009). Muscular dystrophy therapy by nonautologous mesenchymal stem cells: muscle regeneration without immunosuppression and inflammation. *Transplantation* 87, 1275–1282. doi: 10.1097/TP.0b013e3181a1719b

Shao, H., Im, H., Castro, C. M., Breakefield, X., Weissleder, R., and Lee, H. (2018). New technologies for analysis of extracellular vesicles. *Chem. Rev.* 118, 1917–1950. doi: 10.1021/acs.chemrev.7b00534

Shao, M., Xu, Q., Wu, Z., Chen, Y., Shu, Y., Cao, X., et al. (2020). Exosomes derived from human umbilical cord mesenchymal stem cells ameliorate IL-6-induced acute liver injury through miR-455-3p. *Stem Cell Res. Ther.* 11:37. doi: 10.1186/s13287-020-1550-0

Sharma, A., Sane, H., Paranjape, A., Bhagawanani, K., Gokulchandran, N., and Badhe, P. (2014). Autologous bone marrow mononuclear cell transplantation in Duchenne muscular dystrophy - a case report. *Am. J. Case Rep.* 15, 128–134. doi: 10.12659/AJCR.890078

Shimbo, K., Miyaki, S., Ishitobi, H., Kato, Y., Kubo, T., Shimose, S., et al. (2014). Exosome-formed synthetic microRNA-143 is transferred to osteosarcoma cells and inhibits their migration. *Biochem. Biophys. Res. Commun.* 445, 381–387. doi: 10.1016/j.bbrc.2014.02.007

Shiue, S.-J., Rau, R.-H., Shiue, H.-S., Hung, Y.-W., Li, Z.-X., Yang, K. D., et al. (2019). Mesenchymal stem cell exosomes as a cell-free therapy for nerve injury-induced pain in rats. *Pain* 160, 210–223. doi: 10.1097/j.pain.0000000000001395

Siegel, G., Kluba, T., Hermanutz-Klein, U., Bieback, K., Northoff, H., and Schäfer, R. (2013). Phenotype, donor age and gender affect function of human bone marrow-derived mesenchymal stromal cells. *BMC Med.* 11:146. doi: 10.1186/1741-7015-11-146

Silini, A. R., Cargnoni, A., Magatti, M., Pianta, S., and Parolini, O. (2015). The long path of human placenta, and its derivatives, in regenerative medicine. *Front. Bioeng. Biotechnol.* 3:162. doi: 10.3389/fbioe.2015.00162

Singer, N. G., and Caplan, A. I. (2011). Mesenchymal stem cells: mechanisms of inflammation. *Annu. Rev. Pathol.* 6, 457–478. doi: 10.1146/annurev-pathol-011110-130230

Sotiropoulou, P. A., Perez, S. A., Gritzapis, A. D., Baxevanis, C. N., and Papamichail, M. (2006). Interactions between human Mesenchymal stem cells and natural killer cells. *Stem Cells* 24, 74–85. doi: 10.1634/stemcells.2004-0359

Stubbendorff, M., Deuse, T., Hua, X., Phan, T. T., Bieback, K., Atkinson, K., et al. (2013). Immunological properties of extraembryonic human mesenchymal stromal cells derived from gestational tissue. *Stem Cells Dev.* 22, 2619–2629. doi: 10.1089/scd.2013.0043

Su, W.-H., Wang, C.-J., Fu, H.-C., Sheng, C.-M., Tsai, C.-C., Cheng, J.-H., et al. (2019). Human umbilical cord Mesenchymal stem cells extricate Bupivacaine-impaired skeletal muscle function via mitigating Neutrophil-mediated acute inflammation and protecting against fibrosis. *Int. J. Mol. Sci.* 20:4321. doi: 10.3390/ijms20174312

Tasso, R., Ilengo, C., Quarto, R., Cancedda, R., Caspi, R. R., and Pennesi, G. (2012). Mesenchymal stem cells induce functionally active t-regulatory lymphocytes in a Paracrine fashion and ameliorate experimental autoimmune Uveitis. *Invest. Ophthalmol. Vis. Sci.* 53, 786–793. doi: 10.1167/iovs.11-8211

Taylor, M., Jefferies, J., Byrne, B., Lima, J., Ambale-Venkatesh, B., Ostovaneh, M. R., et al. (2019). Cardiac and skeletal muscle effects in the randomized HOPE-Duchenne trial. *Neurology* 92:e00866-78. doi: 10.1212/WNL.0000000000006950

Théry, C., Witwer, K. W., Aikawa, E., Alcaraz, M. J., Anderson, J. D., Andriantsitohaina, R., et al. (2018). Minimal information for studies of extracellular vesicles 2018 (MISEV2018): a position statement of the International Society for Extracellular Vesicles and update of the MISEV2014 guidelines. *J. Extracell. Vesicles* 7:1535750. doi: 10.1080/20013078.2018.1535750

Tian, T., Zhang, H.-X., He, C.-P., Fan, S., Zhu, Y.-L., Qi, C., et al. (2018). Surface functionalized exosomes as targeted drug delivery vehicles for cerebral ischemia therapy. *Biomaterials* 150, 137–149. doi: 10.1016/j.biomaterials.2017.10.012

Tidball, J. G., Dorshkind, K., and Wehling-Henricks, M. (2014). Shared signaling systems in myeloid cell-mediated muscle regeneration. *Development* 141, 1184–1196. doi: 10.1242/dev.098285

Timmers, L., Lim, S. K., Arslan, F., Armstrong, J. S., Hoefer, I. E., Doevendans, P. A., et al. (2007). Reduction of myocardial infarct size by human mesenchymal stem cell conditioned medium. *Stem Cell Res.* 1, 129–137. doi: 10.1016/j.scr.2008.02.002

Tolar, J., Nauta, A. J., Osborn, M. J., Panoskaltsis Mortari, A., McElmurry, R. T., Bell, S., et al. (2007). Sarcoma derived from cultured mesenchymal stem cells. *Stem Cells Dayt. Ohio* 25, 371–379. doi: 10.1634/stemcells.2005-0620

Toma, C., Pittenger, M. F., Cahill, K. S., Byrne, B. J., and Kessler, P. D. (2002). Human Mesenchymal stem cells differentiate to a cardiomyocyte phenotype in the adult Murine heart. *Circulation* 105, 93–98. doi: 10.1161/hc0102.101442

Tsai, K.-S., Yang, S.-H., Lei, Y.-P., Tsai, C.-C., Chen, H.-W., Hsu, C.-Y., et al. (2011). Mesenchymal stem cells promote formation of colorectal tumors in mice. *Gastroenterology* 141, 1046–1056. doi: 10.1053/j.gastro.2011.05.045

Turner, J.-E., Morrison, P. J., Wilhelm, C., Wilson, M., Ahlfors, H., Renauld, J.-C., et al. (2013). IL-9-mediated survival of type 2 innate lymphoid cells promotes damage control in helminth-induced lung inflammation. *J. Exp. Med.* 210, 2951–2965. doi: 10.1084/jem.20130071

Uezumi, A., Fukada, S., Yamamoto, N., Takeda, S., and Tsuchida, K. (2010). Mesenchymal progenitors distinct from satellite cells contribute to ectopic fat cell formation in skeletal muscle. *Nat. Cell Biol.* 12, 143–152. doi: 10.1038/ncb2014

Uezumi, A., Ito, T., Morikawa, D., Shimizu, N., Yoneda, T., Segawa, M., et al. (2011). Fibrosis and adipogenesis originate from a common mesenchymal progenitor in skeletal muscle. *J. Cell Sci.* 124, 3654–3664. doi: 10.1242/jcs.086629

Valadares, M. C., Gomes, J. P., Castello, G., Assoni, A., Pellati, M., Bueno, C., et al. (2014). Human Adipose tissue derived pericytes increase life span in utrntm1KedDmdmdx/J mice. *Stem Cell Rev. Rep.* 10, 830–840. doi: 10.1007/s12015-014-9537-9

Vercelli, A., Mereuta, O. M., Garbossa, D., Muraca, G., Mareschi, K., Rustichelli, D., et al. (2008). Human mesenchymal stem cell transplantation extends survival, improves motor performance and decreases neuroinflammation in mouse model of amyotrophic lateral sclerosis. *Neurobiol. Dis.* 31, 395–405. doi: 10.1016/j.nbd.2008.05.016

Wang, C., Song, W., Chen, B., Liu, X., and He, Y. (2019). Exosomes isolated from adipose-derived stem cells: a new cell-free approach to prevent the muscle degeneration associated with torn rotator cuffs. *Am. J. Sports Med.* 47, 3247–3255. doi: 10.1177/0363546519876323

Wang, X., Zhang, X., Ren, X.-P., Chen, J., Liu, H., Yang, J., et al. (2010). MicroRNA-494 targeting both Proapoptotic and Antiapoptotic proteins protects against ischemia/reperfusion-induced cardiac injury. *Circulation* 122, 1308–1318. doi: 10.1161/CIRCULATIONAHA.110.964684

Winkler, T., Perka, C., Roth, P., von Agres, A. N., Plage, H., Preininger, B., et al. (2018). Immunomodulatory placental-expanded, mesenchymal stromal cells improve muscle function following hip arthroplasty. *J. Cachexia Sarcopenia Muscle* 9, 880–897. doi: 10.1002/jcsm.12316

Xin, H., Li, Y., Buller, B., Katakowski, M., Zhang, Y., Wang, X., et al. (2012). Exosome-Mediated Transfer of miR-133b from Multipotent Mesenchymal Stromal cells to neural cells contributes to neurite outgrowth. *Stem Cells* 30, 1556–1564. doi: 10.1002/stem.1129

Xin, H., Li, Y., Liu, Z., Wang, X., Shang, X., Cui, Y., et al. (2013). MiR-133b promotes neural plasticity and functional recovery after treatment of stroke with multipotent mesenchymal stromal cells in rats via transfer of exosome-enriched extracellular particles. *Stem Cells* 31, 2737–2746. doi: 10.1002/stem.1409

Xu, H., Zhao, G., Zhang, Y., Jiang, H., Wang, W., Zhao, D., et al. (2019). Mesenchymal stem cell-derived exosomal microRNA-133b suppresses glioma progression via Wnt/β-catenin signaling pathway by targeting EZH2. *Stem Cell Res. Ther.* 10:381. doi: 10.1186/s13287-019-1446-z

Yan, X., Fu, C., Chen, L., Qin, J., Zeng, Q., Yuan, H., et al. (2012). Mesenchymal stem cells from primary breast cancer tissue promote cancer proliferation and enhance mammosphere formation partially via EGF/EGFR/Akt pathway. *Breast Cancer Res. Treat.* 132, 153–164. doi: 10.1007/s10549-011-1577-0

Yang, S.-H., Park, M.-J., Yoon, I.-H., Kim, S.-Y., Hong, S.-H., Shin, J.-Y., et al. (2009). Soluble mediators from mesenchymal stem cells suppress T cell proliferation by inducing IL-10. *Exp. Mol. Med.* 41, 315–324. doi: 10.3858/emm.2009.41.5.035

Yang, Y.-H. K., Ogando, C. R., Wang See, C., Chang, T.-Y., and Barabino, G. A. (2018). Changes in phenotype and differentiation potential of human mesenchymal stem cells aging in vitro. *Stem Cell Res. Ther.* 9, 131. doi: 10.1186/s13287-018-0876-3

Yeo, R., Lai, R. C., Tan, K. H., and Lim, S. K. (2013). Exosome: a novel and safer therapeutic refinement of Mesenchymal Stem Cell. *Exosomes Microvesicles* 1:1. doi: 10.5772/57460

Yu, B., Kim, H. W., Gong, M., Wang, J., Millard, R. W., Wang, Y., et al. (2015). Exosomes secreted from GATA-4 overexpressing mesenchymal stem cells serve as a reservoir of anti-apoptotic microRNAs for cardioprotection. *Int. J. Cardiol.* 182, 349–360. doi: 10.1016/j.ijcard.2014.12.043

Yukawa, H., Watanabe, M., Kaji, N., Okamoto, Y., Tokeshi, M., Miyamoto, Y., et al. (2012). Monitoring transplanted adipose tissue-derived stem cells combined with heparin in the liver by fluorescence imaging using quantum dots. *Biomaterials* 33, 2177–2186. doi: 10.1016/j.biomaterials.2011.12.009

Zagoura, D. S., Roubelakis, M. G., Bitsika, V., Trohatou, O., Pappa, K. I., Kapelouzou, A., et al. (2012). Therapeutic potential of a distinct population of human amniotic fluid mesenchymal stem cells and their secreted molecules in mice with acute hepatic failure. *Gut* 61, 894–906. doi: 10.1136/gutjnl-2011-300908

Zhang, C., Zhou, C., Teng, J.-J., Zhao, R.-L., Song, Y.-Q., and Zhang, C. (2009). Multiple administrations of human marrow stromal cells through cerebrospinal fluid prolong survival in a transgenic mouse model of amyotrophic lateral sclerosis. *Cytotherapy* 11, 299–306. doi: 10.1080/14653240902806986

Zhang, L., Song, Y., Chen, L., Li, D., Feng, H., Lu, Z., et al. (2020). MiR-20a-containing exosomes from umbilical cord mesenchymal stem cells alleviates liver ischemia/reperfusion injury. *J. Cell. Physiol.* 235, 3698–3710. doi: 10.1002/jcp.29264

Zhao, C.-P., Zhang, C., Zhou, S.-N., Xie, Y.-M., Wang, Y.-H., Huang, H., et al. (2007). Human mesenchymal stromal cells ameliorate the phenotype of SOD1-G93A ALS mice. *Cytotherapy* 9, 414–426. doi: 10.1080/14653240701376413

Zhao, Y., Wei, W., and Liu, M.-L. (2020). Extracellular vesicles and lupus nephritis - new insights into pathophysiology and clinical implications. *J. Autoimmun.* 115:102540. doi: 10.1016/j.jaut.2020.102540

Zhou, F., Guan, Y., Chen, Y., Zhang, C., Yu, L., Gao, H., et al. (2013). miRNA-9 expression is upregulated in the spinal cord of G93A-SOD1 transgenic mice. *Int. J. Clin. Exp. Pathol.* 6, 1826–1838.

Zhou, W., Fong, M. Y., Min, Y., Somlo, G., Liu, L., Palomares, M. R., et al. (2014). Cancer-secreted miR-105 destroys vascular endothelial barriers to promote metastasis. *Cancer Cell* 25, 501–515. doi: 10.1016/j.ccr.2014.03.007

Zhu, X., Badawi, M., Pomeroy, S., Sutaria, D. S., Xie, Z., Baek, A., et al. (2017). Comprehensive toxicity and immunogenicity studies reveal minimal effects in mice following sustained dosing of extracellular vesicles derived from HEK293T cells. *J. Extracell. Vesicles* 6:1324730. doi: 10.1080/20013078.2017.1324730

Zhuang, X., Xiang, X., Grizzle, W., Sun, D., Zhang, S., Axtell, R. C., et al. (2011). Treatment of brain inflammatory diseases by delivering exosome encapsulated anti-inflammatory drugs from the nasal region to the brain. *Mol. Ther.* 19, 1769–1779. doi: 10.1038/mt.2011.164

Zuk, P. A., Zhu, M., Ashjian, P., De Ugarte, D. A., Huang, J. I., Mizuno, H., et al. (2002). Human adipose tissue is a source of multipotent stem cells. *Mol. Biol. Cell* 13, 4279–4295. doi: 10.1091/mbc.e02-02-0105

Conflict of Interest: The authors declare that the research was conducted in the absence of any commercial or financial relationships that could be construed as a potential conflict of interest.

Copyright © 2021 Sandonà, Di Pietro, Esposito, Ventura, Silini, Parolini and Saccone. This is an open-access article distributed under the terms of the Creative Commons Attribution License (CC BY). The use, distribution or reproduction in other forums is permitted, provided the original author(s) and the copyright owner(s) are credited and that the original publication in this journal is cited, in accordance with accepted academic practice. No use, distribution or reproduction is permitted which does not comply with these terms.

frontiers in Bioengineering and Biotechnology

ORIGINAL RESEARCH
published: 07 June 2021
doi: 10.3389/fbioe.2021.669537

New Multiscale Characterization Methodology for Effective Determination of Isolation–Structure–Function Relationship of Extracellular Vesicles

Thanh Huyen Phan[1], Shiva Kamini Divakarla[1], Jia Hao Yeo[2], Qingyu Lei[1], Priyanka Tharkar[1], Taisa Nogueira Pansani[3], Kathryn G. Leslie[2], Maggie Tong[2], Victoria A. Coleman[4], Åsa Jämting[4], Mar-Dean Du Plessis[4], Elizabeth J. New[2,5], Bill Kalionis[6], Philip Demokritou[7], Hyun-Kyung Woo[8,9], Yoon-Kyoung Cho[8,9] and Wojciech Chrzanowski[1]*

[1] Sydney School of Pharmacy, Faculty of Medicine and Health, Sydney Nano Institute, The University of Sydney, Camperdown, NSW, Australia, [2] School of Chemistry, The University of Sydney, Camperdown, NSW, Australia, [3] Department of Dental Materials and Prosthodontics, Araraquara School of Dentistry, UNESP-Universidade Estadual Paulista, Araraquara, Brazil, [4] Nanometrology Section, National Measurement Institute Australia, Lindfield, NSW, Australia, [5] School of Chemistry, Faculty of Science, Sydney Nano Institute, The University of Sydney, Camperdown, NSW, Australia, [6] Maternal-Fetal Medicine Pregnancy Research Centre, The Royal Women's Hospital, and Department of Obstetrics and Gynaecology, The University of Melbourne, Parkville, VIC, Australia, [7] Department of Environmental Health, Center for Nanotechnology and Nanotoxicology, Harvard T.H. Chan School of Public Health, Boston, MA, United States, [8] Center for Soft and Living Matter, Institute for Basic Science (IBS), Ulsan, South Korea, [9] Department of Biomedical Engineering, Ulsan National Institute of Science and Technology (UNIST), Ulsan, South Korea

OPEN ACCESS

Edited by:
Antonietta Rosa Silini, Fondazione Poliambulanza Istituto Ospedaliero, Italy

Reviewed by:
Carolina Balbi, University of Zurich, Switzerland
Ryan Michael Porter, University of Arkansas for Medical Sciences, United States

***Correspondence:**
Wojciech Chrzanowski
wojciech.chrzanowski@sydney.edu.au

Specialty section:
This article was submitted to Preclinical Cell and Gene Therapy, a section of the journal Frontiers in Bioengineering and Biotechnology

Received: *19 February 2021*
Accepted: *12 April 2021*
Published: *07 June 2021*

Citation:
Phan TH, Divakarla SK, Yeo JH, Lei Q, Tharkar P, Pansani TN, Leslie KG, Tong M, Coleman VA, Jämting Å, Du Plessis M-D, New EJ, Kalionis B, Demokritou P, Woo H-K, Cho Y-K and Chrzanowski W (2021) New Multiscale Characterization Methodology for Effective Determination of Isolation–Structure–Function Relationship of Extracellular Vesicles. Front. Bioeng. Biotechnol. 9:669537. doi: 10.3389/fbioe.2021.669537

Extracellular vesicles (EVs) have been lauded as next-generation medicines, but very few EV-based therapeutics have progressed to clinical use. Limited clinical translation is largely due to technical barriers that hamper our ability to mass produce EVs, i.e., to isolate, purify, and characterize them effectively. Technical limitations in comprehensive characterization of EVs lead to unpredicted biological effects of EVs. Here, using a range of optical and non-optical techniques, we showed that the differences in molecular composition of EVs isolated using two isolation methods correlated with the differences in their biological function. Our results demonstrated that the isolation method determines the composition of isolated EVs at single and sub-population levels. Besides the composition, we measured for the first time the dry mass and predicted sedimentation of EVs. These parameters were likely to contribute to the biological and functional effects of EVs on single cell and cell cultures. We anticipate that our new multiscale characterization approach, which goes beyond traditional experimental methodology, will support fundamental understanding of EVs as well as elucidate the functional effects of EVs in *in vitro* and *in vivo* studies. Our findings and methodology will be pivotal for developing optimal isolation methods and establishing EVs as mainstream therapeutics and diagnostics. This innovative approach is applicable to a wide range of sectors including biopharma and biotechnology as well as to regulatory agencies.

Keywords: extracellular vesicles, mesenchymal stromal/stem cell, isolation methods, ultracentrifugation, tangential flow filtration, nanodosimetry, single vesicle analysis, exosomes

INTRODUCTION

Current medicine has only taken us so far in reducing disease and the tissue damage that it causes. Extracellular vesicles (EVs) have been hailed as the next generation of medicines. EVs are membrane-surrounded nanoscale structures secreted ubiquitously by cells. They contain multiple substances that influence the function of surrounding cells (Lötvall et al., 2014; Iraci et al., 2016). Since EV composition reflects the composition of the parent cell, EVs are ideal candidates for use in disease diagnosis (Candelario and Steindler, 2014). EVs are already considered as diagnostic biomarkers for cancer, cardiovascular, neurodegeneration, and kidney diseases (Taylor and Gercel-Taylor, 2008; Candelario and Steindler, 2014; Danielson and Das, 2014). It is also well established that EVs transfer numerous molecules including proteins, lipids, and nucleic acids between cells, and these molecules can act synergistically and influence the behavior of surrounding cells (Yanez-Mo et al., 2015). Since EVs can deliver multiple molecules to reprogram the injured cells and mediate the de-differentiation of cells, EVs can be used for tissue repair/regeneration (Guo et al., 2011). EVs derived from stem cells are recognized as "second generation" stem cell therapies (Candelario and Steindler, 2014; György et al., 2015)—made by cells for cells. Compared with stem cells, EVs have key advantages including low immunogenicity, no ability to self-replicate (no risk of cancer), high resistance to hostile environments, and improved bioactivity and stability upon storage (Piffoux et al., 2017). However, despite all these potential advantages, very few EV applications have progressed to clinical use (Yekula et al., 2020).

The limited clinical translation of EVs is largely due to technical barriers that hamper the mass production of EVs, i.e., the ability to isolate, purify, and characterize them effectively at single vesicle (nano), sub-population, and population levels (Ramirez et al., 2018). Since EV sizes range from 50 to 150 nm and they are secreted into rich multicomponent media or body fluids, isolation and characterization are not trivial and remain as key challenges in the field (Ramirez et al., 2018). The molecular corona, which cloaks EVs and is likely to cover some of the surface markers, adds to the complexity of these challenges (Simonsen and Munter, 2020). Since the corona changes the physicochemical characteristics of EVs and their affinity to the substrates used in some isolation methods, it is difficult to isolate and characterize EVs effectively. Moreover, EV isolates often contain lipoproteins, protein aggregates, and non-vesicle macromolecules (Sunkara et al., 2016). We also know that cell-free DNA can adsorb to lipid nanoparticles (Gardner et al., 2020), which is likely to occur for circulating EVs too, but surprisingly, this phenomenon is largely overlooked in the field. These "contaminants" influence the biological function of EVs and are not trivial to detect due to the sensitivity of experimental methods. This also means that it is difficult to decouple them from the isolated EV populations (Mateescu et al., 2017). However, these contaminants could potentially work synergistically with EVs to achieve specific therapeutic function in the body (Thery et al., 2018). Therefore, for practical utilization of isolation protocols, it is necessary first to perform comprehensive physicochemical and molecular characterization of EV isolates at sub/population and single vesicle levels and to measure functional responses to EVs in adequate cell/animal-based models.

The most commonly used approach to isolate EVs is ultracentrifugation, which involves multistep differential centrifugations to pellet vesicles (Ismail et al., 2013; Gardiner et al., 2016). However, ultracentrifugation is labor intensive, requires large sample volumes, and produces a relatively low yield of enriched EVs (Kang et al., 2017). Numerous alternative isolation methods have been developed including density gradients (DG) and size exclusion chromatography (SEC). Although DG and SEC usually result in high-purity EV, these protocols are time consuming, characterized by poor yields and suitable for small input volumes only (less than 5 ml) (Witwer et al., 2013; Coumans et al., 2017). Immunoaffinity-based approaches can also be used for EV isolation (Li et al., 2019). In these approaches, EVs are "collected" by beads functionalized with EV-specific antibodies; thus, the isolation process is solely related to affinity of EVs to selected antibodies. The collection of EVs is based on the assumption that specific markers are present on the surface of EVs. This means that these approaches are highly selective and likely to isolate only some fractions of EV populations. More importantly, these methods fail to account for the aforementioned corona making these approaches even more selective (Simonsen and Munter, 2020). Furthermore, at this stage, only small quantities of biological samples can be processed in immunoaffinity-based isolation (Momen-Heravi et al., 2013). In contrast, tangential flow filtration (TFF) is capable of processing scalable volumes of biological fluids and producing high EV yield (Busatto et al., 2018). TFF is technically simple to operate and requires low-cost instrumentation. These features make TFF well suited to isolate EVs at large scale. However, to enable broader applications of TFF, its advantages in comparison with ultracentrifugation (and other methods) must be determined.

Previous studies investigated the differences in physical properties between EVs isolated using TFF and ultracentrifugation (Busatto et al., 2018; Heath et al., 2018). However, the results are limited to selected physical characteristics of EVs (e.g., yield, size distribution, morphology, and surface markers) and do not show their correlation with biological effects. To the best of our knowledge, there is no available studies investigating how the physicochemical properties of EVs contribute to the EV functionality. Here, using a combination of high-resolution optical and non-optical techniques, as well as functional assays, we interrogated the differences between EVs isolated using ultracentrifugation and TFF at single vesicle, sub-population, and population levels. The significance of this work is in a new methodology, which

Abbreviations: AFM, atomic force microscopy; AFM-IR, atomic force microscope infrared-spectroscopy; CMSC29, chorionic mesenchymal stromal/stem cell line; CEVs, extracellular vesicles derived from chorionic mesenchymal stromal/stem cell; DMSC23, decidual mesenchymal stromal/stem cell line; DEVs, extracellular vesicles derived from decidual mesenchymal stromal/stem cell; EVs, extracellular vesicles; HBSS(-), Hank's balanced salt solution; LPS, lipopolysaccharide; MSC, mesenchymal stromal/stem cell; PTA, particle tracking analysis; nFCM, nano-flow cytometry; RMM, resonant mass measurement; TRPS, tunable resistive pulse sensing; TFF, tangential flow filtration.

enables characterizing EVs and demonstrating how the isolation methods influence the physicochemical/molecular composition of EVs and functional cell responses to EVs. For the first time, we measured the dry mass of large EVs or EV agglomerates (>100 nm), predicted the sedimentation of EVs, and developed a new fluorescent probe to assess the functionality of EVs. The key strength of this study lies in the comprehensive characterization of EVs at single vesicle, EV sub-population, and EV population levels, as well as in the analysis of cellular responses (i.e., EV uptake) at single-cell level. To achieve desired statistical and scientific validation of our approach, we used two cell types, which produce different quantities of EVs and that these EVs characterize with different molecular cargo; specifically, we used chorionic and decidual mesenchymal stem cells (CMSC29 and DMSC23, respectively) (Qin et al., 2016; Kim et al., 2019a).

Our study provides evidence that EVs' physicochemical characteristics (at single vesicle, subpopulation, and population level) as well as their biological function, depends on the isolation method. The differences in physicochemical properties of EVs were shown to correlate well with the functional effects of EVs. We concluded that isolation method determines the composition of EV isolates. These findings are of critical significance in the field because they suggest that isolation method is pivotal in establishing downstream applications of EV as diagnostic biomarkers, therapeutics, and in fundamental biology. Notably, this work highlights the importance of nanoscale and single-particle characterization methods in EV research and the need for the integrated use of physicochemical and functional assays.

MATERIALS AND METHODS

Cell Culture and Maintenance

Both chorionic and decidual MSCs cell lines (CMSC29 and DMSC23) were obtained from the Royal Women's Hospital in Melbourne, Australia. Telomerase reverse transcriptase (hTERT) was transduced into primary MSCs from the fetal chorion and maternal decidual components of human placenta to create the CMSC29 and DMSC23 cell lines, respectively (Qin et al., 2016). Since CMSC29 and DMSC23 were derived from different parts of the placenta, they are exposed to different levels of oxidative stress (Kusuma et al., 2016); thus, they required different types of medium. CMSC29 cells were cultured in 85% AmnioMAX^{TM} C-100 basal medium and 15% AminoMAX^{TM} C-100 supplement (Invitrogen^{TM}, ThermoFisher Scientific). DMSC23 cells were cultured in MesenCult^{TM} MSC basal medium (Human), 10% Mesenchymal stem cell stimulatory supplement (STEMCELL Technologies, Canada), GlutaMAX^{TM} (Life Technologies, Australia), and antibiotics (Pen/Strep) (100 U of penicillin and 0.1 mg/ml of streptomycin, Sigma-Aldrich, Australia). BEAS-2B cells were cultured in medium containing Dulbecco's modified Eagle's medium (DMEM medium-high glucose, Sigma-Aldrich, Australia) supplemented with 10% fetal bovine serum (FBS, Bovogen, Australia), and antibiotics (Pen/Strep). Cells were sub-cultured every 2–3 days and maintained in the incubator at 37°C supplemented with 5% CO_2. Hanks' balanced salt solution (HBSS, Sigma-Aldrich, Australia) was used for washing CMSC29 and DMSC23 cells. TrypLE^{TM} Express (Gibco, Denmark) was used to dissociate the adherent cells. EV isolation and collection were from CMSC29 and DMSC23 cells at passages P23–28.

Isolation of Extracellular Vesicles by Ultracentrifugation

CMSC29 and DMSC23 cells were cultured to 80% confluency. Cells were washed twice with HBSS before incubating cells with EV isolation media (MesenCult^{TM} MSC basal medium) containing 0.5% (w/v) bovine serum albumin (BSA, Sigma-Aldrich, Australia) for 48 h. After 48 h, EV-containing media was collected and centrifuged at 500 × *g* for 5 min and 2,000 × *g* for 10 min to remove cells and debris. The supernatant was then transferred to thick-wall polycarbonate ultracentrifuge tubes (Seton Scientific Inc, United States) and centrifuged at 100,000 × *g* for 60 min at 4°C using rotor Ti-70 in an Optima LE-80K Ultra Centrifuge (Beckman Coulter, Australia). The harvested EV pellet was resuspended in 1 ml of RNase-free phosphate-buffered saline (RNase-free PBS, Lonza, Australia) and washed using ultracentrifugation at 100,000 × *g* for 60 min at 4°C. The pellet was resuspended in 1 ml of RNase-free PBS and transferred to RNase-free microcentrifuge tubes. The EV pellets were stored at 4°C to avoid losing biological function during the freezing process.

Isolation of Extracellular Vesicles by Tangential Flow Filtration

After removing cells and debris by centrifugation at 500 × *g* (5 min) and 2,000 × *g* (10 min) as described above, the EV containing supernatant was filtered (0.45 μm) and transferred to TFF-Easy 20-nm pores (HansaBioMed/Lonza, Tallinn, Estonia) for EV concentration. The EV concentration process was described in the manufacturer's protocol (HansaBioMed/Lonza), and EVs were finally diafiltrated in RNase-free PBS.

Size and Concentration Measurement Using Nano-Flow Cytometry

The size and concentration of EVs were measured using NanoFCM (Xiamen Fuliu Biological Technology Co., Ltd, Xiamen, China). A mixture of silica nanospheres (68, 91, 113, and 155 nm) was used as the size standard for the construction of a calibration curve and standard 200-nm polystyrene spheres were used for laser alignment. All events were collected for 120 s, and size (SSC) triggering was used to detect EVs. The total events collected ranged from 3,000 to 6,000 events. The representative histogram was conducted from triplicate measurements of each EV sample.

Size and Concentration Measurement Using Particle Tracking Analysis

EV samples were diluted with RNase-free water to achieve a concentration between 1×10^8 and 1×10^9 EVs/ml and measured using a NanoSight NS300 (Malvern Panalytical Ltd, Malvern, United Kingdom). A syringe pump with a speed of

40 μl/min was used, and cell temperature was set at 25°C. Embedded laser wavelength was 488 nm, and the particles were imaged with an auto-focus camera for 60 s. Data were obtained at camera-level 11. The analysis settings were set to "auto," and the detection threshold was set to 5 in the NanoSight Software NTA (version 3.2) to assess mean and modal particle diameters, D50 values (which represents the 50th percentile of the averaged cumulative number-weighted particle size distribution) and particle number concentration. For each EV sample, three repeat measurements were conducted.

Size Measurement Using Dynamic Light Scattering

EV samples were diluted in RNase-free water to achieve a particle concentration ranging from 1×10^9 to 1×10^{10} EVs/ml and were measured in a Zetasizer Ultra (Malvern Panalytical Ltd, Malvern, United Kingdom). The manufacturer's default software setting for EVs (liposomes) was selected, and three cycles were performed for each measurement at 4°C. Data were analyzed using general purpose mode in ZS XPLORER software (version 1.2.0.91), and the size distribution of EV populations was presented as a percentage of intensity. Three consecutive runs were performed for each sample.

Size and Concentration Measurement Using Tunable Resistive Pulse Sensing

TRPS was performed using a qNano (IZON, New Zealand) to measure the particle size and the concentration of EVs. EVs were suspended in electrolytes and passed through an engineered pore (NP100), which provided direct measurement of size and concentration. Buffers and reagents were freshly prepared and filtered (0.22 μm) before the measurement. The detailed protocol for qNano measurements was described in the study by Vogel et al. (2011). Three independent measurements were done for each individual EV sample.

Morphology Analysis of Extracellular Vesicles Using Atomic Force Microscopy

EV samples were placed onto zinc selenide prism, dried overnight, and subsequently imaged using atomic force microscopy (AnasysInstruments, United States). Images were obtained in contact mode at a scan rate of 0.5 Hz using EX-T125 probe with nominal resonance frequency 200–400 kHz and spring constant 13–77 Nm^{-1} (AnasysInstruments, United States).

Dry Mass Measurement of Extracellular Vesicles Using Resonant Mass Measurement

The buoyant mass of the particles was measured with the Archimedes Particle Metrology System (Malvern Panalytical, Malvern, United Kingdom). The microchannel sensor used consisted of a microfluidic channel with a cross section of $2 \times 2\ \mu m^2$. In order to determine the dry mass and size of the EVs from the measured buoyant mass, EVs of known size were used to determine EV density. Monodisperse control EVs with 200 nm diameter were measured, and a spherical model was applied, from which a density of 1.4 g/cm^3 was determined (**Supplementary Figure 1**). The sensitivity factor of the microchannel resonator was determined using monomodal gold calibration particles (NIST RM 8016, 60 nm, United States). From this sensitivity factor, the mass resolution of the sensor is $\sim 10^{-15}$ g, which for EVs corresponds to a limit of detection (LOD) of 100 nm.

Quantification of Extracellular Vesicle Surface Markers Using nFCM

The monoclonal antibodies, anti-CD9 Alexa Fluor 488-conjugated (R & D systems, Canada), anti-CD63 Alexa Fluor 488-conjugated (Invitrogen, ThermoFisher Scientific), or anti-CD81 Alexa Fluor 488-conjugated (R & D systems, Canada) were used to assess protein surface markers of EVs. Approximately 1×10^{10} EVs/ml was stained using 8 μg/ml of each antibody and incubated 30 min at 37°C in dark condition. The EV samples were then washed with 2 ml of RNase-free PBS three times using ultracentrifugation 100,000 × *g*, 4°C, 70 min each. The supernatants were carefully aspirated from the bottom of the tubes in every wash. Subsequently, the pellets were dissolved in RNase-free PBS, and the fluorescence intensity was measured using a nFCM. The control sample was the basal medium with 0.05% (w/v) BSA without EVs. All fluorescence events were detected in FITC triggering of nFCM, and the threshold level was set by default in NF Profession 1.0 acquisition software.

Quantification of Nucleic Acid Using nFCM

EVs isolated using TFF and ultracentrifugation were stained using 10 μM SYTO RNASelect green fluorescent cell stain (Invitrogen™, ThermoFisher Scientific) at 37°C for 30 min. The EV samples were loaded on the exosome spin column MW 3000 (Invitrogen™, ThermoFisher Scientific) to remove unbound dyes and measured using nFCM. The control sample was basal medium without EVs. All fluorescence events were collected for 120 s and fluorescence (FITC) triggering of an nFCM was used to detect fluorescence EVs. Data were analyzed using FlowJo software (version 10.6). The threshold level was set above the background level by the NF Profession 1.0 acquisition software by default.

Quantification of Lipid Content Using nFCM

PKH67 and Diluent C (ThermoFisher Scientific) was selected to be the general membrane labeling for EVs. PKH67 was diluted in 100 μl of Diluent C to a final concentration of 15 μM (dye solution). Approximately 1×10^{10} EVs/ml were diluted with 80 μl of Diluent C, added to a dye solution, and incubated for 3 min with gentle pipetting. Excess dye was bound with 10% (w/v) BSA in RNase-free water. The EV samples were then diluted to 2 ml with RNase-free PBS and washed three times using ultracentrifugation 100,000 × *g*, 4°C, 70 min each. The pellet was gently resuspended in 100 μl of RNase-free PBS, and nFCM was used to measure the fluorescence intensity of EVs. The control sample was the basal medium only and the basal medium with 0.05% (w/v) BSA without EVs. All fluorescence events were triggered in the FITC channel and collected for 120 s. The threshold was set by default in NF Profession 1.0 acquisition software.

Molecular Composition Analysis of Extracellular Vesicles Using Atomic Force Nanoscale Infrared Spectroscopy (AFM-IR)

The protocol for EV characterization using AFM-IR (nanoIR, Anasys Instruments, United States) was described in our previous study (Khanal et al., 2016). Briefly, each EV sample was placed on a zinc selenide prism and dried overnight. The laser signal was optimized before acquiring the nanoIR spectra ranging from 1,000 to 1,800 cm^{-1} at 4-cm^{-1} intervals with a scan rate of 0.5 Hz. A gold-coated tip and a silicon nitride cantilever with a nominal spring constant of 0.5 Nm^{-1} were used for all measurements. The acquired scan sizes were 10 × 5 μm for each sample, and Analysis Studio™ software was used for data analyses. The "Savitzky–Golay" function was used to achieve smoothing of the spectra with the polynomial function of 3, and eight numbers of points.

Measurement of Predicted Sedimentation of Extracellular Vesicles—Distorted Grid Model

The predicted transport modeling of TFF and ultracentrifugation isolated EVs, which was originally applied for the engineered nanomaterials (ENMs), was modified and adapted for EVs (Cohen et al., 2014). Briefly, the protocol comprised three interconnected parts: ENM dispersion preparation and characterization in suspension, effective density calculation, and delivered dose computation (Cohen et al., 2014). The dispersion preparation and characterization were not applied to EVs. The delivered dose metric was used to calculate the fraction of administered EVs in a 96-well plate over 24 h. Data were acquired using Matlab.

The effective density of EVs ($\rho_{effective\ density}$) was determined using the equation:

$$\rho_{effective\ density} = \rho_{media} + \left[\left(\frac{M_{EV} - M_{EVsol}}{V_{pellet}SF}\right)\left(1 - \frac{\rho_{media}}{\rho_{EV}}\right)\right] \quad (1)$$

whereby:

ρ_{media} is the density of the medium (g/cm^3).

M_{EV} is the total mass of EVs (g) in the dispensed volume of suspension.

M_{EVsol} is the mass of dissolved EVs in the dispensed volume of suspension.

V_{pellet} is the measured pellet size in centimeters squared inside the PCV tube.

SF is the stacking factor, which is the portion of the pellet that is composed of agglomerates (theoretical maximum of 0.74 for ordered stacking).

ρ_{EV} is the density of EVs (g/cm^3).

Visualization of Extracellular Vesicle Uptake Using Holotomography and Fluorescence Microscopy

CMSC29 EVs isolated using TFF and ultracentrifugation were labeled with PKH67 followed the lipid staining protocol as described in section 'Quantification of Lipid Content Using nFCM'. The staining of EVs was done 1 h prior to incubation. Approximately 2 × 10^4 BEAS-2B cells were dosed with 1 × 10^9 PKH67-stained EVs/ml and incubated with the dye for 3 h. Uptake of EVs by cells was performed on a holotomography microscope Tomocube HT-2H (Tomocube Inc., Daejeon, South Korea). A water immersion objective (60×, N.A = 1.2) was used to acquire the images. Z-stacked images were acquired across each field-of-view, with a minimum of four field-of-views imaged for each type of EVs. The images were acquired in TomoStudio™ 2.0 software, and they were further analyzed using ImageJ FIJI.

Analysis of Cell Migration to Extracellular Vesicle Treatment After Lipopolysaccharides Injury

Cell migration in the presence of isolated EVs was measured by comparing the area of closure of a two-dimensional scratch wound. BEAS-2B cells were seeded at 1 × 10^4 cells per well on Image Lock 96-well plates and allowed to adhere overnight. "Injury" was induced using 10 μg/ml of lipopolysaccharides (LPS) for 24 h (Xu and Zhou, 2020). A wound on the midline of culture well was then created using a 96-pin wound making tool (IncuCyte WoundMaker™). After washing the cells with RNase-free PBS once, EVs isolated using TFF and ultracentrifugation were added at an ascending concentration ranging from 10 to 1,000 EVs per cell. Wound images were taken every 2 h with a 10× magnification objective lens using the IncuCyte live cell imaging system and IncuCyte ZOOM software program (Essen BioScience, United States). Wound confluence (%), which was represented as the wound closure (%), was assessed for all images using IncuCyte ZOOM software. Data were analyzed using GraphPad, and measurements of eight samples ($n = 8$) were performed for each condition.

Analysis of Cellular Responses to Extracellular Vesicle Treatment After Lipopolysaccharide Injury

Cellular responses post-injury in the presence of TFF and ultracentrifugation isolated EVs were assessed by measuring intracellular nitric oxide (NO) levels. Approximately 5 × 10^3 BEAS-2B cells were seeded on a glass bottom dish precoated in L-poline (MatTek) and allowed to adhere overnight. Cells were then exposed to 10 μg/ml of LPS for 24 h. Cells were next incubated with 50 μM NpNO1 probe for 24 h at 37°C, at 5% CO_2. Excess NpNO1 probe was washed and imaged in FluoroBrite^{TM} DMEM media (Gibco, ThermoFisher Scientific) supplemented with 10% FBS and antibiotics (Pen/Strep). Samples were imaged using Olympus FV3000 microscope equipped with a 405-nm laser, a water 60× objective lens, and an incubator stage maintained at 37°C and 5% CO_2. A minimum of three field-of-views were imaged for each condition per experiment with Z-stacked images per field-of-view. Maximum projected micrographs of the Z-stacks were presented in this study. Regions of interest were drawn around each cell, and mean fluorescence intensities were quantified using ImageJ FIJI. Statistical analyses were performed on the mean fluorescence intensity values and plotted using GraphPad.

Statistical Analyses

Data were analyzed and presented as mean ± standard deviation (SD). For cell migration and cellular stress assays, a minimum of three independent preparations of each sample were made for each of the experiments (n = 3). Ordinary one-way ANOVA followed by Dunn's multiple comparison's test for pair-wise comparisons were used to determine the differences between multiple groups. A P-value <0.05 is considered to be statistically significant.

RESULTS

To measure EV size and concentration, we used particle tracking analysis (PTA), dynamic light scattering (DLS) (size only), nano-flow cytometry (nFCM), tunable resistive pulse sensing (TRPS), and asymmetric flow-field fractionation (AF4) (size only). Nanoscale infrared spectroscopy (AFM-IR) and nFCM were used to determine EV composition at the single EV and EV sub-population levels. For the first time, we used resonant mass measurement (RMM) for the characterization of dry mass and buoyant mass of large EVs (>100 nm) and distorted grid (DG) for the sedimentation prediction of EVs. Sedimentation of nanoparticles reveals the actual concentration of nanoparticles on the cell surface, which correlates with cellular uptake (Momen-Heravi et al., 2013). Therefore, sedimentation is the key factor in the interpretation of downstream biological effects of EVs on the cellular response. The actual functional effects of EV isolates on cells were determined using newly developed nitric oxide fluorescent probe to measure intracellular stress in an *in vitro* model of acute lung injury.

Comparison of Extracellular Vesicle Size Distribution and Concentration

Chorionic and decidual MSC cell lines (CMSC29 and DMSC23) were used as cell sources to isolate EVs. EVs isolated from CMSC29 and EVs isolated from DMSC23 cells were referred to as CEVs and DEVs, respectively.

The size distribution of CEVs and DEVs was assessed using four independent techniques: PTA, DLS, nFCM, and TRPS.

Particle Tracking Analysis

PTA analyses showed that both CEVs and DEVs isolated using TFF and ultracentrifugation had a similar particle size distribution ranging from 100 to 300 nm (**Figures 1A,B**). However, there was a small peak at around 50 nm in the size distribution spectrum of DEVs isolated using TFF, which was not present in EVs isolated using ultracentrifugation (**Figure 1B**).

Dynamic Light Scattering

Size analyses using DLS showed that the intensity-based size distribution of CEVs and DEVs, isolated using TFF and ultracentrifugation, were different (**Figures 1C,D**). CEVs isolated using TFF had one high-intensity peak at around 200 nm with one low-intensity peak at approximately 8 nm. In contrast, CEVs isolated using ultracentrifugation had one dominant peak at around 300 nm (**Figure 1C**). The intensity-based size distribution for DEVs isolated using TFF had two peaks at 8 and 200 nm, while DEVs isolated using ultracentrifugation had one broad peak at around 1,000 nm with one small shoulder at around 200 nm (**Figure 1D**).

The presence of small particles (around 8 nm) in CEVs isolated using TFF was verified using preliminary asymmetric flow-field fractionation (AF4) measurement (**Supplementary Figure 2**). Since the elution peak of CEVs isolated using TFF at 18 min coincides with pure BSA, the small-size particles in CEVs isolated using TFF were identified as BSA contaminants.

Overall, the size of both CEVs and DEVs isolated using ultracentrifugation as assessed by DLS were larger than the EVs isolated using TFF. This is likely to be related to the presence of a few larger entities (potentially agglomerates during the ultracentrifugation process). Since DLS is extremely sensitive to the presence of large entities, even with a low amount of these would account for the shape of the intensity-weighted data (Bishop et al., 1991).

Nano-Flow Cytometry

nFCM measurements showed a broad size distribution ranging from 50 to 200 nm for both CEVs and DEVs isolated using TFF and ultracentrifugation (**Figures 1E,F**). While the size of most of EVs isolated using TFF (for both CEVs and DEVs) was around 60 nm, the size of EVs isolated using ultracentrifugation was evenly distributed from 50 to 200 nm.

Tunable Resistive Pulse Sensing

TRPS measurements showed that CEVs isolated using TFF and ultracentrifugation had a similar size distribution spectrum (**Figure 1G**). The size of DEVs isolated using TFF showed a broad distribution ranging from 70 to 200 nm, while the size distribution obtained for DEVs isolated using ultracentrifugation could not be used for comparison due to a much lower sample concentration (**Figure 1H**).

The mode sizes of both CEVs and DEVs were consistent for each individual method (with differences between methods) regardless of the isolation method. PTA, nFCM, and TRPS showed that the mode sizes of CEVs and DEVs were around 150, 90, and 110 nm, respectively (**Figure 1I**). However, DLS showed differences in mode sizes of CEVs and DEVs depending on the isolation method. Ultracentrifugation yielded larger CEVs with mode size around 270 nm, while CEVs isolated with TFF was approximately 197 nm. Similarly, the mode size of DEVs isolated using ultracentrifugation was approximately

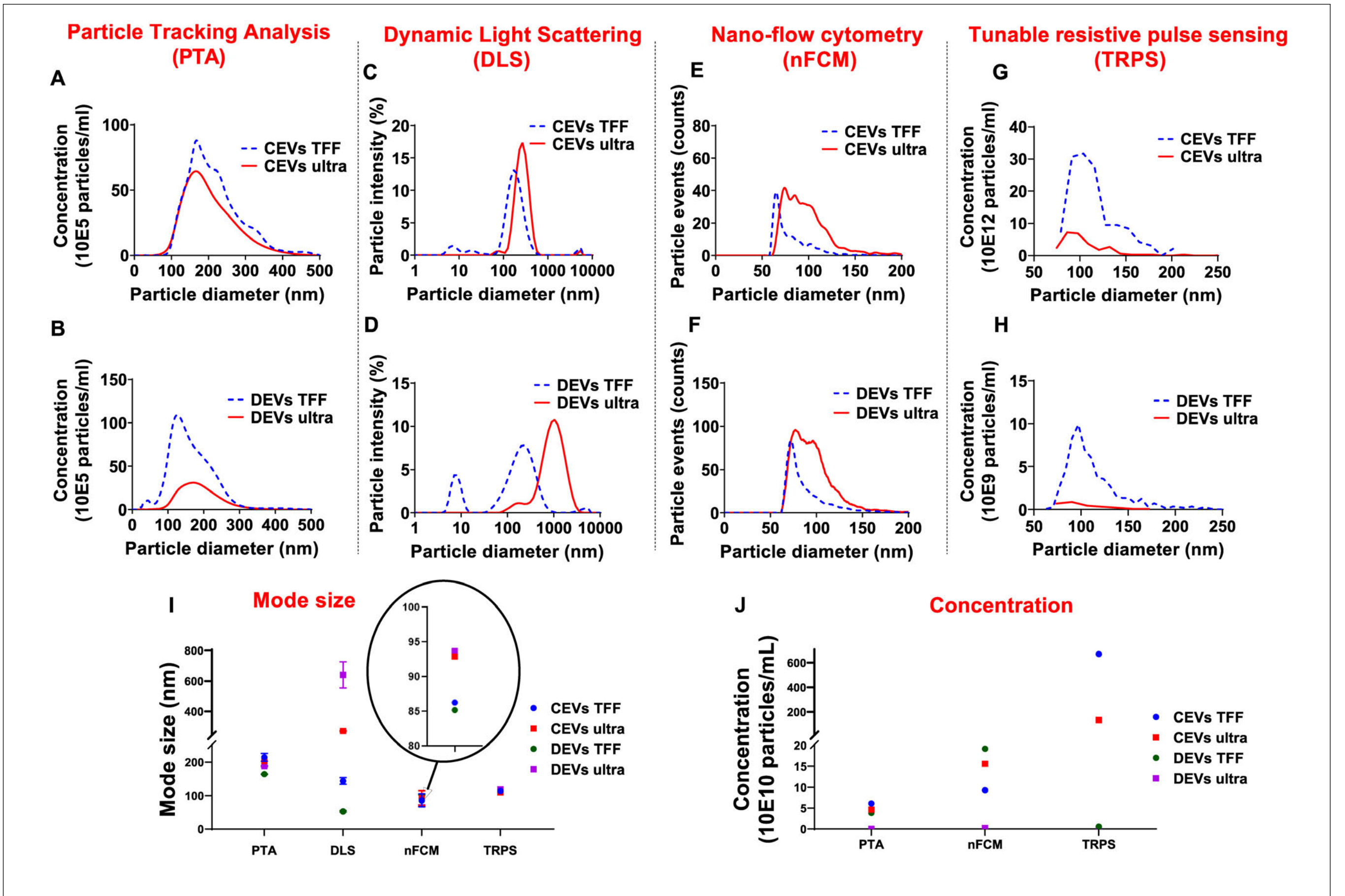

FIGURE 1 | Comparison of the size distribution for different isolated extracellular vesicles (EVs). Representative histograms revealing size distribution of extracellular vesicles derived from chorionic mesenchymal stromal/stem cell (CEVs) and extracellular vesicles derived from decidual mesenchymal stromal/stem cell (DEVs) isolated using tangential flow filtration (TFF) and ultracentrifugation by four different methods. The size distributions of these EVs were assessed by **(A,B)** particle tracking analysis (PTA), **(C,D)** dynamic light scattering (DLS), **(E,F)** nano-flow cytometry (nFCM), and **(G,H)** tunable resistive pulse sensing (TRPS), respectively. The mode size **(I)** and concentration **(J)** of all EV samples were presented. The graphs represent the averaged values based on three repeated measurements of each EV sample.

1,120 nm, and TFF isolated DEVs was approximately 240 nm. It is important to notice that the scattering intensity depends on the 6th power of the size of the macromolecules, therefore, large agglomerates—even a very small amount will overwhelm the intensity from small size particles in DLS (Barnett, 1942). Thus, the observation of small size particles in EVs isolated using TFF in DLS indicated the substantial amount of small size particles and the absence of agglomerates in TFF isolated EVs. To further explore the possibility of the presence of small size particles in the samples, AF4 was used (**Supplementary Figure 2**) to fractionate and measure the hydrodynamic diameter of the entities as they eluted.

The concentration of EVs was determined using three techniques: PTA, nFCM, and TRPS (**Figure 1J**). The concentration of CEVs isolated using TFF and ultracentrifugation determined by PTA and nFCM was approximately 10^{11} EVs/ml. In contrast, TRPS measured approximately 10^{12} CEVs/ml isolated using TFF, one order of magnitude larger than PTA and nFCM. The concentration of DEVs isolated using TFF measured using PTA and TRPS was $\sim 10^9$ EVs/ml, while the measurement made using nFCM was 10^{11} EVs/ml, two orders of magnitude higher. The concentration of DEVs isolated using ultracentrifugation was consistent for all measurement methods, 10^9 EVs/ml.

In summary, both PTA and nFCM measurements showed a consistent average size for both DEVs and CEVs regardless of isolation method; however, the concentration of EVs was around two orders of magnitude lower for DEVs isolated using ultracentrifugation. Overall, results suggested that PTA was less sensitive than nFCM for the detection of EVs smaller than 100 nm.

Mass Analysis

Besides the size distribution, the buoyant mass and dry mass of different isolated EVs were quantified. Previously, buoyant mass and dry mass were used to determine the exact amount of nanoparticles interacting with cells and tissues in toxicity studies (Cohen et al., 2013). Here, we used resonant mass measurement (RMM) for the first time to characterize EVs for buoyant mass and dry mass. The advantage of this approach is that both

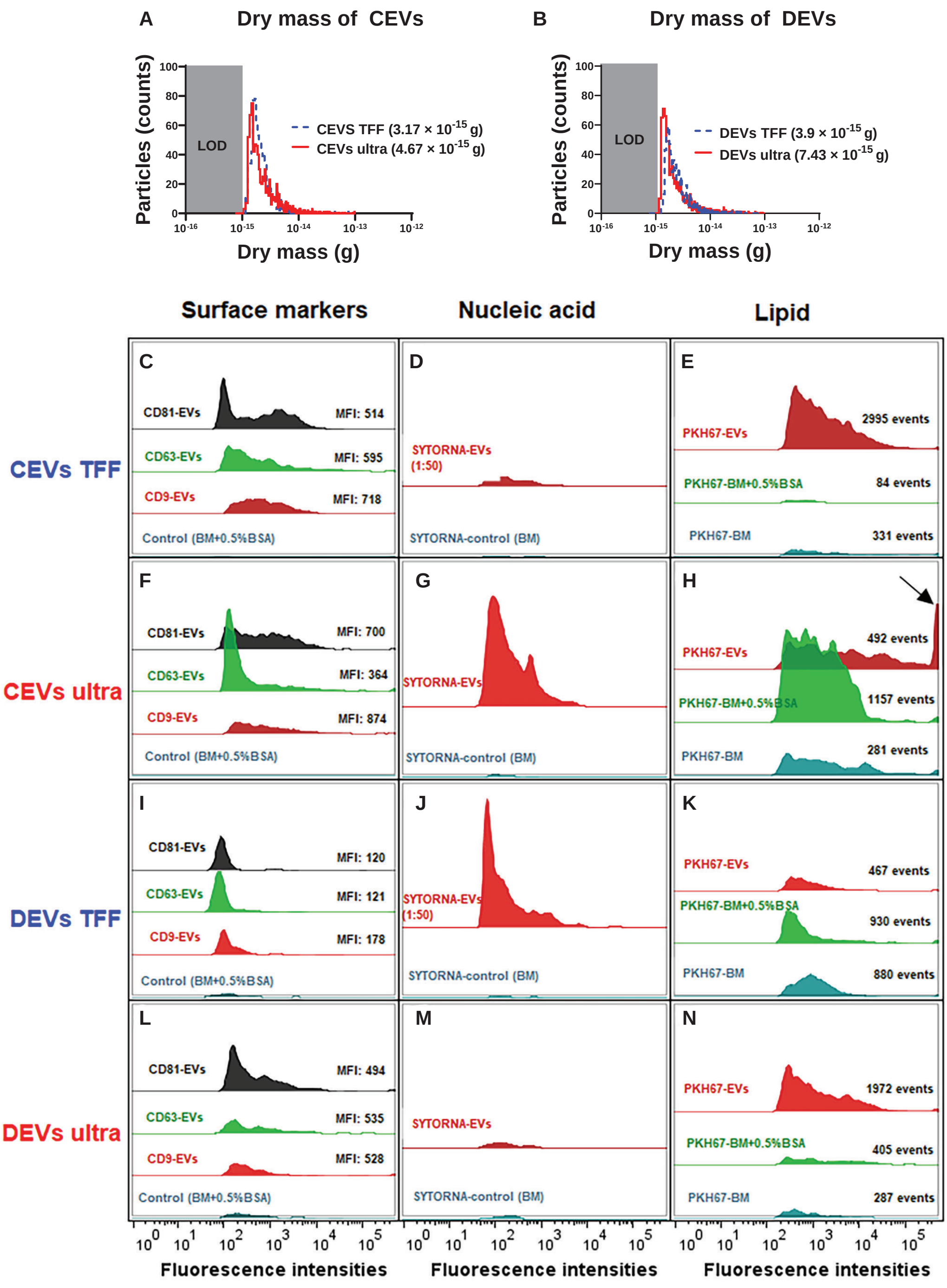

FIGURE 2 | The dry mass of different isolated EVs, and EV molecular composition was analyzed using nano-flow cytometry (nFCM). The dry mass of TFF and ultracentrifugation-isolated **(A)** CEVs and **(B)** DEVs. LOD, limit of detection. Representative histograms showing the presence of three surface markers CD9, CD63, and CD81 **(C,F,I,L)**, nucleic acid **(D,G,J,M)**, and lipid content **(E,H,K,N)** in CEVs and DEVs isolated using TFF and ultracentrifugation. The arrow indicates the saturated fluorescence peak. MFI, mean fluorescence intensity.

mass parameters can be measured for individual vesicles, which in turn reveals the total mass, including molecular cargo, of each vesicle (Rupert et al., 2017). Precise knowledge of the amount of EV cargo is pivotal to define the biological function of EVs.

The dry mass of EVs isolated using ultracentrifugation and TFF was measured and presented in **Figures 2A,B**. The size distribution of each EV type was calculated from the measured buoyant mass, with a particle density of 1.4 g/cm^3 (**Supplementary Figure 3**). It is important to notice that the limit of detection (LOD) of RMM for dry mass is 10^{-15} g, and for size distribution, it is 100 nm. Therefore, only sub-population of EVs with the high mass was detected and measured. When plotted as a function of dry mass, both detectable CEVs and DEVs isolated using ultracentrifugation showed higher dry mass than EVs isolated using TFF (**Figure 2**). The dry mass of measurable CEVs isolated using ultracentrifugation (4.67×10^{-15} g) was higher than CEVs isolated using TFF (3.17×10^{-15} g) (**Figure 2A**). Similarly, measurable DEVs isolated using ultracentrifugation (7.43×10^{-15} g) showed higher dry mass than DEVs isolated using TFF (3.9×10^{-15} g) (**Figure 2B**). Interestingly, a sub-population of DEVs isolated using TFF, which has a positive buoyancy was detected, and its size was estimated using a density of 0.01 g/cm^3 (**Supplementary Figure 3**). This positively buoyant sub-population of DEVs isolated using TFF could be bubbles or empty vesicles. The higher mass for detectable EVs (above 100 nm) (CEVs and DEVs) isolated using ultracentrifugation suggested the presence of more agglomerates in ultracentrifugation-isolated EVs.

Cumulatively, size and mass measurements suggested that these EVs contained some amounts of agglomerates. The agglomeration of EVs during ultracentrifugation was reported in previous studies (Linares et al., 2015; Nordin et al., 2015; Taylor and Shah, 2015).

Extracellular Vesicle Molecular Composition Assessed Using Nano-Flow Cytometry and Nanoscale Infrared Spectroscopy

Extracellular Vesicle Surface Markers

The differences in the dry mass of EVs isolated using ultracentrifugation, and TFF suggested that there were differences in molecular composition of EVs. Therefore, we assessed the presence of three common EV surface markers (i.e., CD9, CD63, and CD81) on different isolated EVs by using nFCM. CD9, CD63, and CD81-positive were EVs defined as the events that were above the threshold level and detected by fluorescence triggering (**Supplementary Figure 4**). A control using basal medium with 0.5% (w/v) BSA (**Supplementary Figure 4**) showed negligible fluorescence in fluorescence triggering, which demonstrated that the free dye was successfully removed by our washing procedure. The histogram analyses showed that both CEVs and DEVs regardless of isolation method were positive for CD9, CD63, and CD81 (**Figures 2C,F,I,L**). The overall mean fluorescence intensity (MFI) of CD9, CD63, and CD81 was higher for CEVs isolated using the same method. Profile analysis of individual surface markers showed that their expression was not uniform across different sub-populations of EVs. CD9 was detected as strongly positive in CEVs isolated using TFF (MFI: 718), followed by CD63 (MFI: 595) and CD81 (MFI: 514) (**Figure 2C**), whereas the expression of CD9 (MFI: 874) and CD81 (MFI: 700) was higher than CD63 (MFI: 364) in CEVs isolated using ultracentrifugation (**Figure 2F**).

The expression of the markers was more uniform for DEVs than CEVs when using the same isolation method. All three markers of DEVs isolated using TFF were uniformly detected at a low MFI level (under 200) (**Figure 2I**). Specifically, the MFI value for CD9 (178) was higher than CD63 and CD81 (121 and 120, respectively). Since DEVs isolated using TFF had a substantial amount of small size particles (~8 and 200 nm) assessed using DLS, the expressions of the markers were lowest. Meanwhile, DEVs isolated using ultracentrifugation showed a higher expression of the markers than TFF. The MFI values for CD9, CD63, and CD81 were 494, 535, and 528, respectively, in DEVs isolated using ultracentrifugation (**Figure 2L**).

The profile of the surface markers for EVs isolated from each of the cell type was different depending on the isolation method. This result suggested that each of the isolation method provided different EV populations. However, regardless of the isolation method, EVs isolated from DMSC23 consistently showed more uniform expression of all three markers, which implied that exosome-specific markers were more homogenously expressed on DEVs.

Nucleic Acid Profiling

We next quantify the total nucleic acid content inside EVs by staining EVs with SYTO RNASelect green fluorescent cell stain. The percentage of nucleic acid was calculated by dividing the concentration of SYTO RNASelect green-positive events by the total concentration of EVs (**Table 1**). EVs isolated using TFF were diluted 50 times before staining to achieve the same threshold level as EVs isolated using ultracentrifugation. Since TFF isolated EVs were diluted, a smaller fluorescence intensity peak was shown in CEVs isolated using TFF in comparison with CEVs isolated using ultracentrifugation (**Figures 2D,G**). However, the analyses after the calculation showed that CEVs isolated using TFF contained 22 times more of the nucleic acid (2.46%) than CEVs isolated using ultracentrifugation (0.11%) (**Table 1**). Similarly, the nucleic acid content of DEVs isolated using TFF (3.31%) was seven times higher than DEVs isolated using ultracentrifugation (0.46%) (**Table 1** and **Figures 2J,M**). Overall, we concluded that the total amount of nucleic acid in DEVs was higher than CEVs when using the same isolation method. The low percentage of SYTO RNASelect green-positive events could be due to the low amount of RNA inside EVs. Moreover, since the nucleic acids are considered to be small molecules and may have low fluorescence intensities, the fluorescence events from the nucleic acid may fall below the detection limit of nFCM.

TABLE 1 | The percentage of nucleic acid content in extracellular vesicles derived from chorionic mesenchymal stromal/stem cell (CEVs) and extracellular vesicles derived from decidual mesenchymal stromal/stem cell (DEVs) isolated using tangential flow filtration (TFF) and ultracentrifugation assessed using nano-flow cytometry (nFCM).

EV type	Percentage of nucleic acid (%)
CEVs TFF	2.46
CEVs ultra	0.11
DEVs TFF	3.31
DEVs ultra	0.46

Lipid Membrane Profiling

We next assessed the lipid content in each EV type by staining EVs with green fluorescence lipophilic dye, PKH67. PKH67, which labels the cell membrane by inserting its aliphatic chains into the lipid membrane, has been used extensively to label the lipid membrane of EVs (Ohno et al., 2013). The lipid compositions of DEVs and CEVs were measured and compared with two controls: basal medium only (BM) and basal medium with 0.5% (w/v) BSA (BM + 0.5% BSA) (**Figure 2**). We used two controls as PKH67 may label other components in the medium (non-specific binding) (Lai et al., 2015; Takov et al., 2017). Hence, two control groups were essential to eliminate false positives due to fluorescence from non-EV components.

The total fluorescence events of CEVs isolated using TFF (2,995 events) was nine- and 35-fold higher than BM (84 events) and BM + 0.5% BSA (331 events) (**Figure 2E**), which showed substantial PKH67-positive EVs. On the other hand, CEVs isolated using ultracentrifugation (492 events) had 221 more fluorescence events than BM (281 events), but they had 665 less events than BM + 0.5% BSA (1,157 events) (**Figure 2H**). The fluorescence-positive events in controls indicated that there were some "contaminants" in the controls, which bound to PKH67 and caused the fluorescence. The saturated fluorescence intensity peak in CEVs isolated using ultracentrifugation, which was not detected in controls, suggested the presence of larger size vesicles or agglomerates (**Figure 2H**; arrow).

The total fluorescence events of DEVs isolated using TFF (467 events) were approximately twofold lower than BM (880 events) and BM + 0.5% BSA (930 events) (**Figure 2K**). DEVs isolated using ultracentrifugation (1,972 events) had 1,685 and 1,567 more events than BM (287 events) and BM + 0.5% BSA (405 events), respectively (**Figure 2N**). This result indicated that DEVs isolated using ultracentrifugation contained a high concentration of PKH67-positive EVs. Since DEVs isolated using ultracentrifugation had the lowest concentration of EVs among all EV groups, this result could be a false-positive result. One possible explanation could be that during ultracentrifugation, lipid–protein aggregates and other media components are isolated beside EVs. These undesired components can potentially bind PKH67, which causes a misleading result.

As observed in **Figures 2H,N**, the number of events shown in the controls (BM and BM + 0.5% BSA) emphasized the non-selective binding of PKH67 to other components. These results are consistent with the findings that the PKH67 lipophilic dyes is not specific to EVs (Lai et al., 2015). Therefore, this study was inconclusive regarding to the amount of lipid of EV isolates.

Molecular Composition of Individual Extracellular Vesicles Using Nanoscale Infrared Spectroscopy

While nFCM proved to be a very effective method to determine size and composition of EVs at bulk population level, this method, similar to other size measurements methods, cannot effectively distinguish between a single large EV and an agglomerate of several small EVs (Linares et al., 2015). Therefore, to characterize EVs at single vesicle level, we used nanoscale infrared spectroscopy (AFM-IR) (**Figure 3**; Kim et al., 2018, 2019b). Topographical AFM images showed that both CEVs and DEVs were spherical and their size ranged between 20 and 300 nm regardless of isolation method (**Figure 3A**). Molecular analysis at the single vesicle level employed state-of-the-art nanoscale infrared spectroscopy (AFM-IR), which showed that individual EVs contained proteins, nucleic acids, and lipids (**Supplementary Figure 5** and **Figures 3B,C**). However, the compositions of both types of EVs were different depending on the isolation method.

The spectra of CEVs isolated using TFF had dominant peaks for all three main components of EVs: protein (1,670, 1,544, and 1,260 cm^{-1}), nucleic acid (1,450, 1,404, and 1,320 cm^{-1}), and lipid (1,105 and 1,020 cm^{-1}), which confirmed the presence of all three components in individual EVs (Lee et al., 2017). The intensity ratio of protein amide I (1,670 cm^{-1}) and amide II (1,544 cm^{-1}) was 2:1, which indicated ordinary protein conformation in CEVs isolated using TFF. Peaks at 1,450 and 1,404 cm^{-1} in the spectra of CEVs isolated using TFF were attributed to phosphatidylcholine head group and thymine of RNAs (Kim et al., 2019b). In contrast, the spectra of CEVs isolated using ultracentrifugation had a broad band with low intensity in amide I peak at 1,660 cm^{-1}. They also showed a dominant peak at 1,068 cm^{-1} (lipid) and five minor peaks at 1,768, 1,560, 1,480, 1,296, and 1,248 cm^{-1}. Since the intensity of amide II peak (1,560 cm^{-1}) was low in the spectra of CEVs isolated using ultracentrifugation, it suggested that protein conformation for these EVs was altered. Moreover, the absence of peaks in the 1,450–1,350 cm^{-1} region in the spectra of CEVs isolated using ultracentrifugation suggested smaller amounts of nucleic acid (i.e., RNAs), which was consistent with the nFCM result (**Table 1**). The dominant peak at $\sim$1,068 cm^{-1} in the spectra of CEVs isolated using ultracentrifugation was associated with the ester C–O–C symmetric stretching vibration (Mohan et al., 2020). This peak was shifted to $\sim$1,105 cm^{-1} in the spectra of CEVs isolated using TFF. The peak at 1,768 cm^{-1} in the spectra of CEVs isolated using ultracentrifugation could be related to ester groups, primarily from lipid and fatty acids (Kim et al., 2018).

The spectra of DEVs isolated using TFF characterized showed dominant peaks at 1,624, 1,544, 1,256 cm^{-1}, and a shoulder at 1,672 cm^{-1} (protein), 1,450, 1,392 cm^{-1} (nucleic acid), and 1,080 and 1,040 cm^{-1} (lipid). The intensity ratio of amide I (1,624 cm^{-1}) and amide II (1,544 cm^{-1}) peaks was $\sim$2:1, which suggested unaltered protein conformation in the spectra of DEVs isolated using TFF. Peaks at 1,450 and 1,392 cm^{-1} in the spectra of DEVs isolated using TFF confirmed the presence of RNAs (Kim et al., 2019b). In contrast, the spectra of DEVs isolated using ultracentrifugation had dominating peaks at 1,592 cm^{-1} (protein amide II), 1,280 cm^{-1} (nucleic acid, protein), and broad bands at 1,680, 1,440, and 1,164 cm^{-1}. The low intensity of the amide I (1,680 cm^{-1}) peak in the spectra of DEVs isolated using ultracentrifugation suggested some alterations in protein structures of these EVs. The broad band with low intensity at 1,440 cm^{-1} in the spectra of DEVs isolated using ultracentrifugation suggested a reduced amount of RNAs, which was consistent with the nFCM result (**Table 1**). In addition,

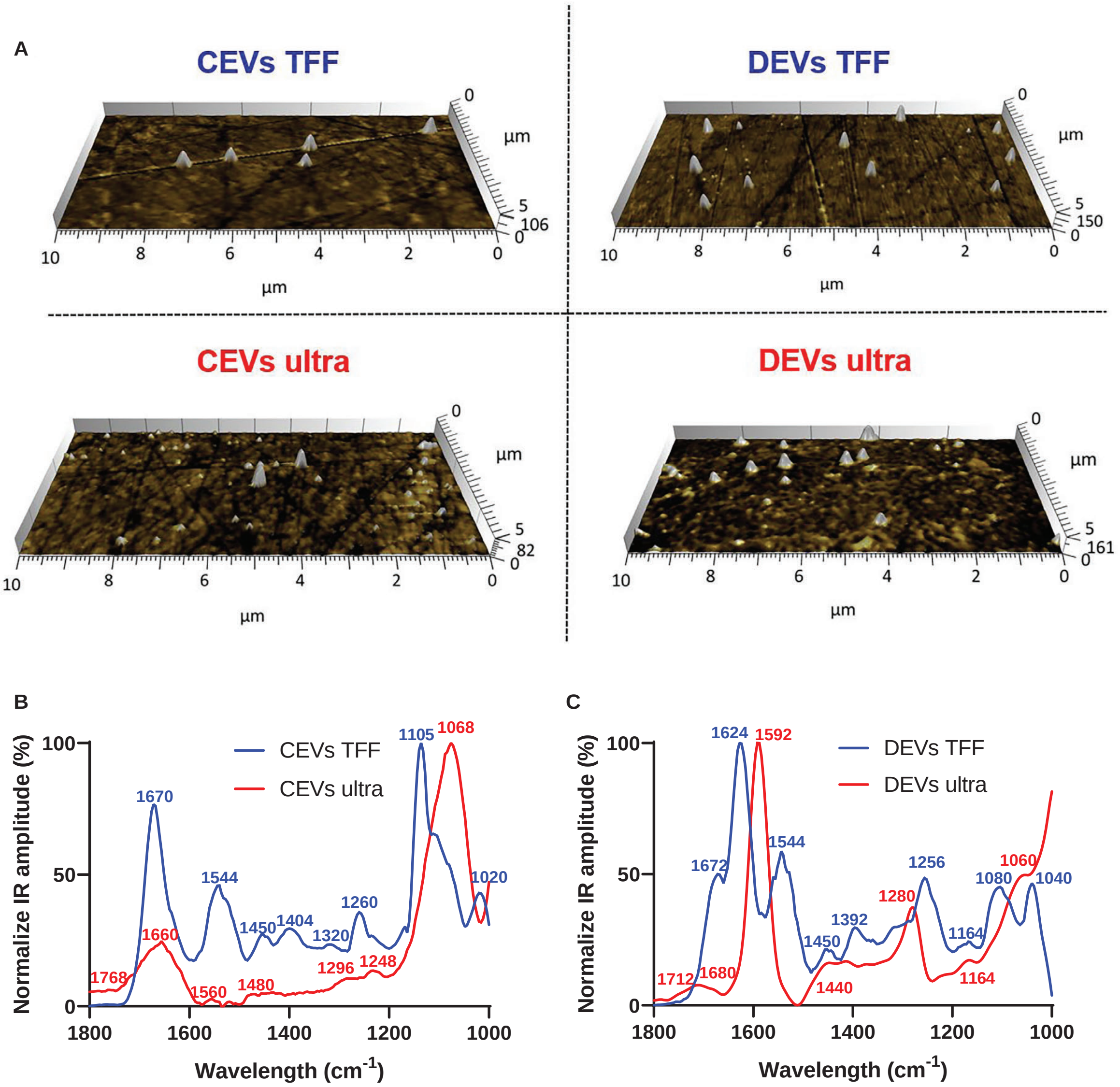

FIGURE 3 | Average infrared absorption spectra of extracellular vesicle (EV) molecular composition corresponding topographical atomic force microscopy (AFM) images for EVs. **(A)** AFM images (10 × 5 µm) of individual EVs (indicated as white protrusions) deposited on prism. Normalization of the average AFM-IR spectra of **(B)** CEVs isolated using TFF and ultracentrifugation; **(C)** DEVs isolated using TFF and ultracentrifugation. At least 15 individual EVs were randomly selected and analyzed using Analysis Studio^{TM} software.

the bands in the 1,080–1,040 cm^{-1} region were associated with vibration from phosphate stretch of RNA/DNA or lipid (Balan et al., 2019). While the spectra of DEVs isolated using TFF had two peaks at 1,080 and 1,040 cm^{-1}, the spectra of DEVs isolated using ultracentrifugation only had one peak at 1,060 cm^{-1} suggesting changes in RNA/DNA structures and lipid. The peak at 1,712 cm^{-1} in the spectra of DEVs isolated using ultracentrifugation could be related to ester groups, primarily from lipid and fatty acids.

Overall, the structures of all three key molecular/structural components of EVs, proteins, lipids, and nucleic acid were maintained in the spectra of both CEVs and DEVs isolated using TFF. In contrast, for the spectra of EVs isolated using ultracentrifugation, the intensity, position, and the width of the peaks changed, indicating changes to the molecular structure of these components. These changes were observed for both CEVs and DEVs.

Since both nucleic acid and lipid peaks are centered around the same frequency, it was necessary to validate the results using an alternative technique, e.g., nFCM. We showed that the amount of nucleic acid in the spectra of EVs isolated using ultracentrifugation was smaller than TFF regardless of the origin of EVs, which was consistent with the nFCM result. Therefore, combining both nFCM and nanoscale infrared spectroscopy are necessary to gain precise understanding of the molecular/structural composition of individual EVs.

Predicted Sedimentation of Isolated Extracellular Vesicles Using Distorted Grid Model

The differences in physicochemical properties of EV types suggested that their colloidal stability, interactions with the cell membrane, internalization, and downstream biological effects could also be different (Willms et al., 2018). While largely ignored, the colloidal stability is a critical parameter that shows ability of EVs to move toward, and reach cells ("sediment"), hence, likely to affect the biological effectiveness of EVs. The transport modeling for EVs was completed for the first time based on their size, size distribution, effective density to calculate the particles sedimentation, and diffusion in cell culture media.

The predicted sedimentation of different EV isolates was assessed using the DG model. All the values used for the modeling are shown in **Supplementary Table 2**. The results indicated the differences in sedimentation between EVs depending on the isolation method (**Figure 4**). CEVs isolated using TFF showed that the deposited fraction was predicted to reach 0.00354 within 1 h, then slowly reach the mean fraction deposited (0.003587) after ∼10 h (**Figure 4B**). Meanwhile, CEVs isolated using ultracentrifugation was predicted to reach the mean fraction deposited (0.2169) after ∼7.5 h (**Figure 4D**). For DEVs, the mean fraction deposit was predicted to be reached after ∼8 h for EVs isolated using TFF (0.003588)(**Figure 4C**) and ∼10 h for EVs isolated using ultracentrifugation (0.3198)(**Figure 4E**). Overall, the mean of fraction deposit of EVs isolated using ultracentrifugation was 65 and 100 times higher than EVs isolated using TFF for CEVs and DEVs, respectively. A previous study reported that less agglomeration resulted in a smaller deposited fraction (DeLoid et al., 2015), which confirmed that EVs isolated using TFF do not contain agglomerates. In contrast, EVs isolated using ultracentrifugation may contain the agglomerates, and these agglomerates could be attributed to the higher sedimentation. This result was consistent with our size distribution (DLS), mass (RMM), and the visualization of EV (holotomography) internalization by a single cell (see below).

Extracellular Vesicles Internalization by Living BEAS-2B Cells Using Holotomography

To attest the relevance of the predicted sedimentation study in assessing EV uptake, we used EVs isolated using TFF and ultracentrifugation and visualized their presence in and on single cells using correlative holotomography and fluorescence microscopy (**Figure 5**). This method, unlike confocal microscopy, does not require any fluorescent labeling for cells, which imparted no stress on cells. Additionally, holotomography microscopy enables us to visualize the differences in refractive index; thus, we can observe subcellular organelles of the cells without labeling with nanometer resolution (Kim et al., 2020).

DEVs isolated using TFF had a substantial amount of small size particles (**Figure 1**), which caused the difficulties in visualizing EVs. Therefore, to demonstrate the differences between TFF and ultracentrifugation-isolated EVs, the EVs localization study using a holotomography microscope was conducted only for CEVs. BEAS-2B cells were dosed with PKH67-labeled CEVs and imaged 3 h later. We observed fluorescence inside the cells and not on the plasma membrane, which suggested that EVs were internalized by the cells. In order to confirm whether EVs are inside cell cytoplasm, we used digital staining for cells and processed them into dynamic 3D images based on the rotation of one axis (**Supplementary Video 1**). The analysis of the dynamic images evidenced that EVs were internalized by BEAS-2B cells after 3 h. The results showed that the punctate CEVs isolated using TFF were qualitatively and homogenously distributed in the cytoplasm (**Figure 5A**) and are of uniform sizes. The size of CEVs isolated using ultracentrifugation were heterogenous, ranging from 100 to 500 nm (**Figure 5B**). These observations confirmed agglomeration had occurred during ultracentrifugation. The control experiment using BM + 0.5% BSA showed no fluorescently labeled particles (data not shown).

Cell Migration Assay With Different Concentrations of Isolated Extracellular Vesicles

The actual biological effects of different EV isolates were investigated using the scratch wound assay, which was modified to measure the wound closure of cells toward the "wound." Lung epithelial cells (BEAS-2B) were selected, and 10 μg/ml of lipopolysaccharides (LPS) was used before wound scratch as an *in vitro* model of acute lung injury. LPS is a key pathogenic factor that induces various inflammatory mediators, which resulted in lung inflammatory and epithelial damage (Nova et al., 2019). Concentrations of CEVs and DEVs isolated using TFF and ultracentrifugation, ranging from 10 to 1,000 EVs per cell, were used in order to test their ability to promote cell migration and increase wound closure after injury. Both CEV- and DEV-treated cells enhanced wound closure percentage when compared with LPS-treated only cells (**Figure 6**). Increasing the concentration of CEVs isolated using both TFF and ultracentrifugation (from 10 to 1,000 EVs per cell) increased the wound closure percentage of BEAS-2B cells (**Figures 6A,C**). Especially, at the concentration of 10 EVs per cell for CEVs isolated using TFF, the wound closure percentage was significantly increased compared with LPS-treated only cells (**Figure 6A**).

Treatment with DEVs isolated using TFF resulted in increased wound closure percentage of BEAS-2B cells (**Figure 6B**). The wound closure percentage of BEAS-2B was significantly increased at the concentration of 100 and 1,000 EVs per cell for DEVs isolated using TFF. In contrast, with a high concentration of DEVs isolated using ultracentrifugation (100 and 1,000 EVs per cell), the wound closure percentage remains as low as the LPS-treated cells (**Figure 6D**). This was supported by the highest sedimented amount for DEVs isolated using ultracentrifugation using the DG model, which resulted in the highest dose for cells.

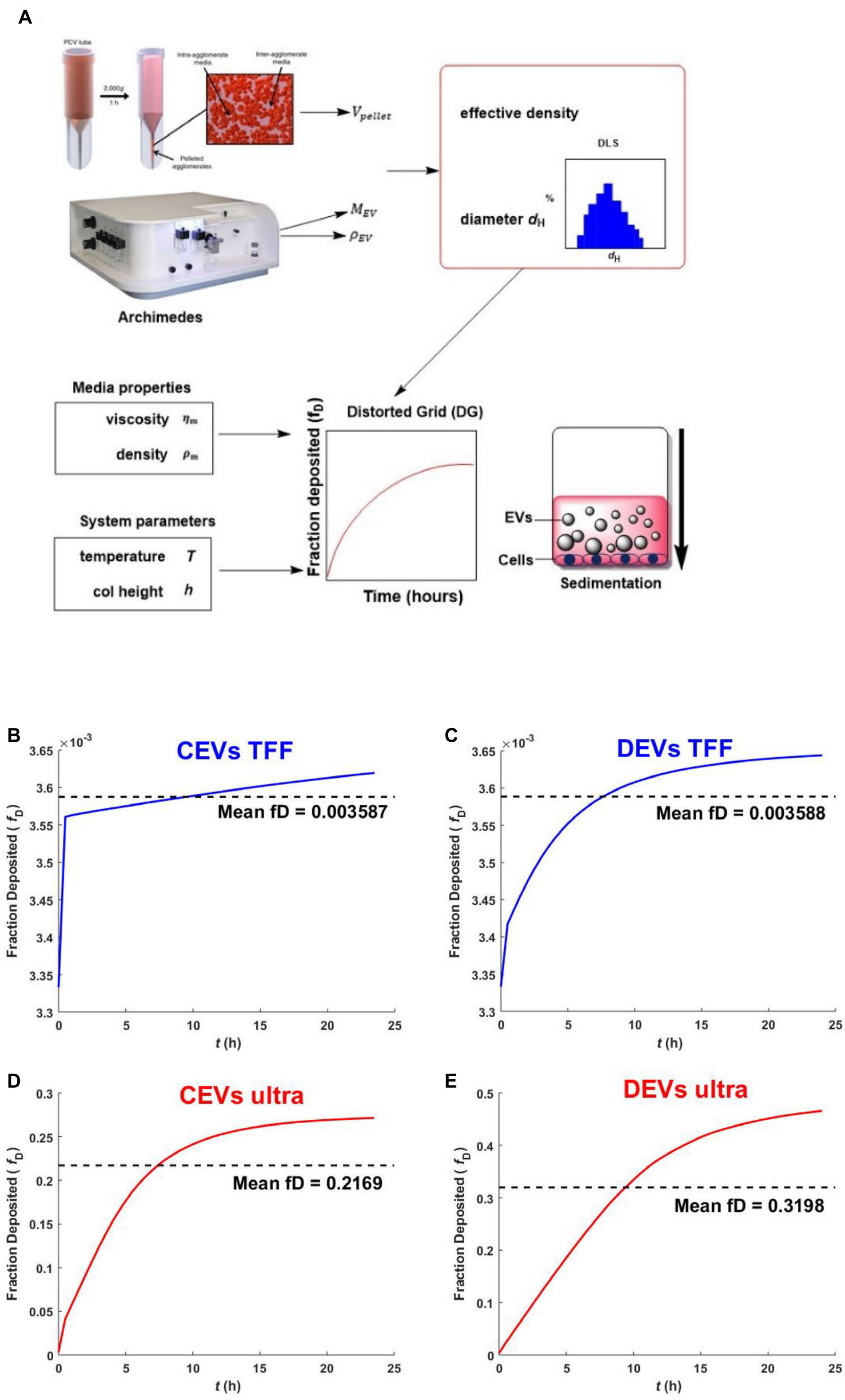

FIGURE 4 | Schematic overview of nanodosimetry approach and the predicted fraction deposited of EVs. The schematic overview of DG modeling adapted from DeLoid et al. (2017) **(A)**. The predicted fraction deposited of CEVs isolated using **(B)** TFF and **(D)** ultracentrifugation; DEVs isolated using **(C)** TFF and **(E)** ultracentrifugation into each well in a 96-well plate was generated by Matlab. Mean fD is the mean fraction deposited.

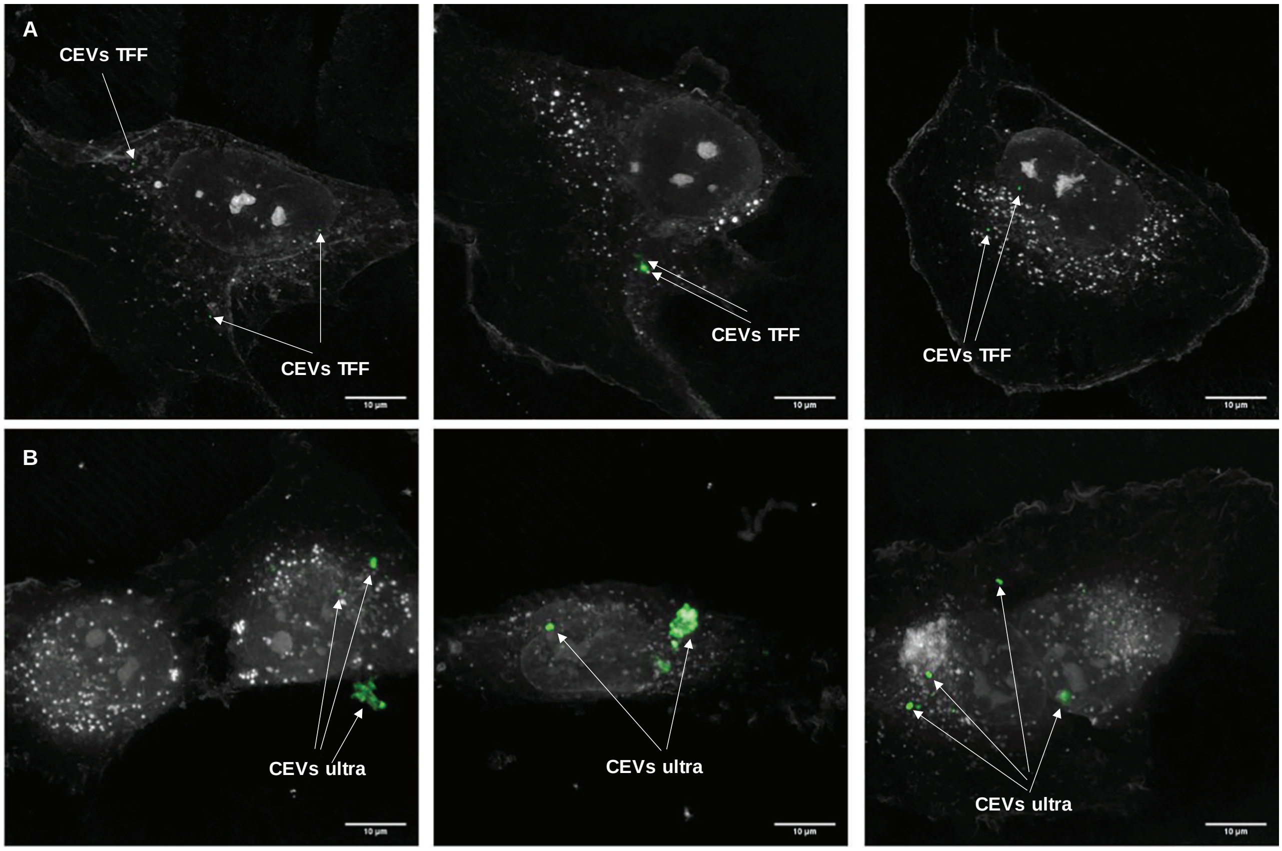

FIGURE 5 | The localization of EVs with BEAS-2B cells. Three representative images of BEAS-2B cells and stained CEVs (green color) isolated using **(A)** TFF and **(B)** ultracentrifugation. Scale bar represents 10 μm. Bright white dots inside BEAS-2B cells indicate the lipid droplets.

We postulate that the high DEV dose could be causing adverse effects on the cells.

Cellular Stress After Injury in Response to Different Concentration of Isolated Extracellular Vesicles

Nitric oxide (NO) measurement allows the measurement of cellular stress levels in response to injury (Nasyrova et al., 2015). NO participates in diverse physiological and pathological processes, such as inflammation (van der Vliet et al., 2000). In response to inflammatory stimuli, NO production is markedly elevated (Coleman, 2001). Given the importance in studying and understanding NO for health and disease, a number of fluorescent sensors have been reported to date (Iverson et al., 2018). However, a common feature of small molecule sensors is poor water solubility, arising from the highly aromatic structures. This has two main drawbacks in cellular studies: first, a need to prepare a stock solution of the dye in an organic solvent such as dimethyl sulfoxide (DMSO), which itself can perturb the system, and second, a tendency for the dye to aggregate and self-quench. We therefore sought to prepare a water-soluble fluorescent sensor for NO by utilizing the previously-reported selective conversion of aromatic ortho-diamines to triazoles in the presence of nitric oxide and oxygen (Iverson et al., 2018), conjugating this reactive group to a 4-amino-1,8-naphthalimide fluorophore, which we have previously shown to have great potential for sensing applications (Leslie et al., 2018; Yang et al., 2018). Water solubility was achieved by incorporating a triethylene glycol (TEG) group to give the final probe, NpNO1 (**Figure 7A**). NpNO1 was prepared in four synthetic steps from commercially available bromoacetic naphthalic anhydride, in 42% overall yield as detailed in the **Supplementary Information** (Scheme 1). NpNO1 was found to have excellent aqueous solubility up to 1 mM (**Supplementary Figure 6**) and a strong fluorescence turn-on at 455 nm with NO addition (**Figure 7B**).

The ability of NpNO1 to detect changes in intracellular NO levels by confocal microscopy was confirmed in A549 (human alveolar basal epithelial) cells treated with 50 μM of NpNO1 overnight, in the presence or absence of 5 mM MAHMA NONOate (**Figure 7C** and **Supplementary Figure 6**). MAHMA NONOate spontaneously releases NO and, hereafter, will be referred to as the NO donor. We observed minimal/basal fluorescence from untreated cells (no stain), cells treated with only MAHMA NONOate, or cells treated with NpNO1 alone. In A549 cells treated with both the NpNO1 and the NO donor, we observed fluorescent puncta in every cell, and a significant increase in mean fluorescence intensity.

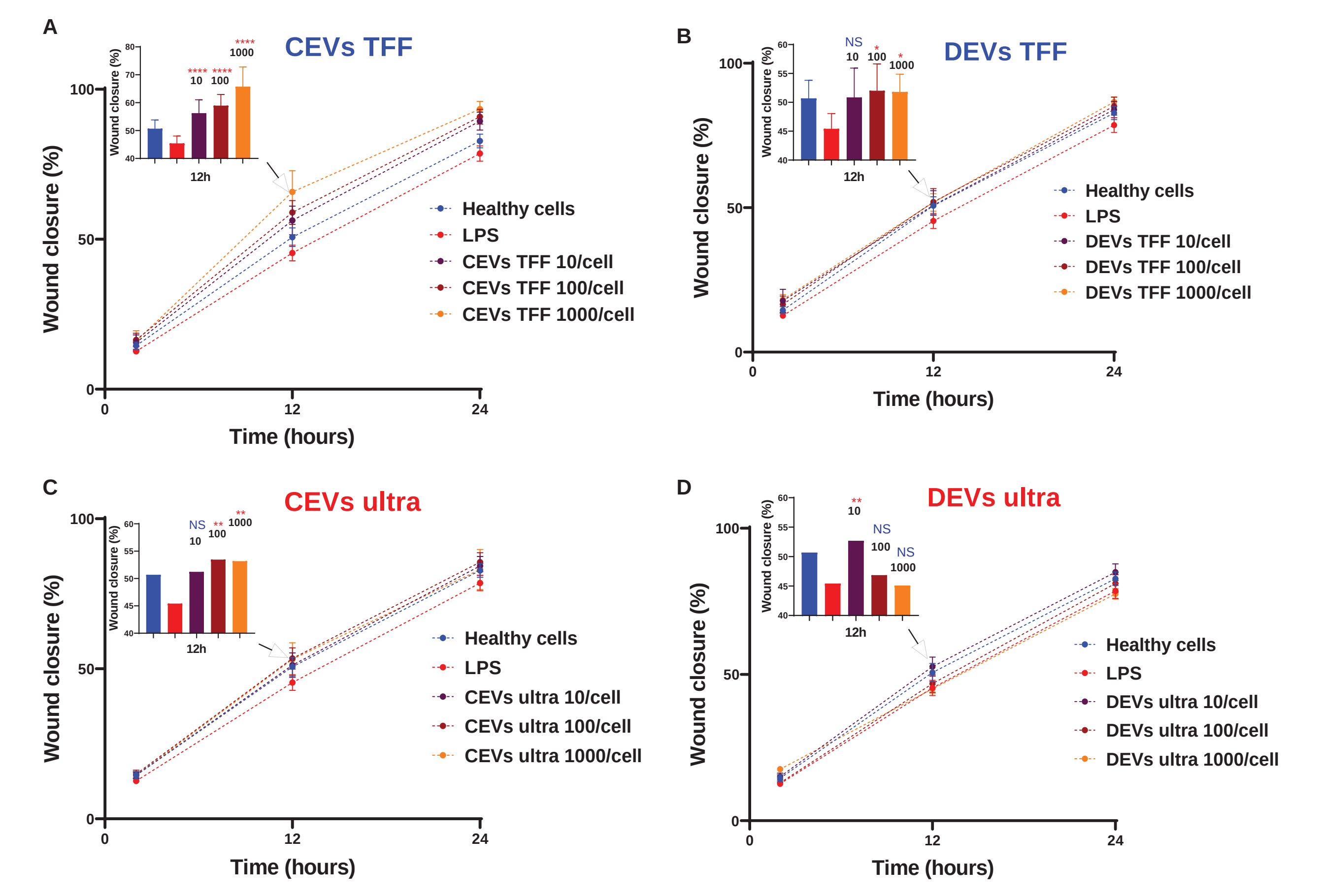

FIGURE 6 | Assessment of wound closure in injured BEAS-2B in response to EV treatment. BEAS-2B cells were "injured" with 10 μg/ml of LPS and treated with CEVs isolated using **(A)** TFF and **(C)** ultracentrifugation; DEVs isolated using **(B)** TFF and **(D)** ultracentrifugation. Error bars represent standard deviation (SD), $n = 8$. Statistics significance was determined by ordinary one-way ANOVA test, followed by Dunn's multiple comparisons test for pair-wise comparisons. Statistical significance shown was between LPS treatment and other groups at time point 12 h. $^*P < 0.1$; $^{**}P < 0.01$; $^{****}P < 0.0001$; NS, not significant.

We then assessed intracellular NO levels after adding various EVs, by quantifying the NpNO1 fluorescence intensity in cells imaged using confocal microscopy (**Supplementary Figure 7**).

Similar to the scratch wound assay, we modeled cellular injury by treating human BEAS-2B epithelial cells with 10 μg/ml of LPS. The intracellular NO, as indicated by the fluorescence intensity of NpNO1, increases after LPS injury (**Figure 7**), which is consistent with the literature (Chokshi et al., 2008). Next, we assessed the fluorescence intensity of NpNO1, which corresponds to the levels of intracellular NO present, in LPS-treated cells dosed with various isolated EVs. Upon adding the concentration of 10–1,000 EVs/cells for CEVs isolated using TFF, the NO levels diminished compared with LPS-treated cells (**Figure 7E**), whereas, dosing the LPS-treated cells with 10 EVs/cell for CEVs isolated using ultracentrifugation, the intracellular NO levels remain high, as in the LPS-treated cells (**Figure 7E**). The intracellular NO levels decreased when 100 and 1,000 EVs/cells for CEVs isolated using ultracentrifugation were added compared with LPS-treated cells.

The NpNO1 fluorescence intensity remained as high as LPS-treated cells using the concentration of 10 DEVs/cell isolated using TFF (**Figure 7F**). The intracellular NO levels, as indicated by NpNO1 fluorescence intensity, decreased when the cells were treated with 100 and 1,000 DEVs isolated using TFF. For DEVs isolated using ultracentrifugation, the intracellular NO levels remain as high as the LPS-treated cells at all concentrations (**Figure 7F**).

DISCUSSION

While there is palpable excitement about the future of EV-based medicine, a current major limitation is the lack of understanding about how to effectively and uniformly isolate them from complex biological milieu (Li et al., 2019). Furthermore, it has not been clear whether different isolation methods extract different sub-populations of EVs, which would impact on their downstream applications. This gap in knowledge is associated with conceptual and technical limitations in EV characterization. We have addressed this challenge by using multiple techniques including optical, non-optical, and high-resolution single vesicle characterization methods, and

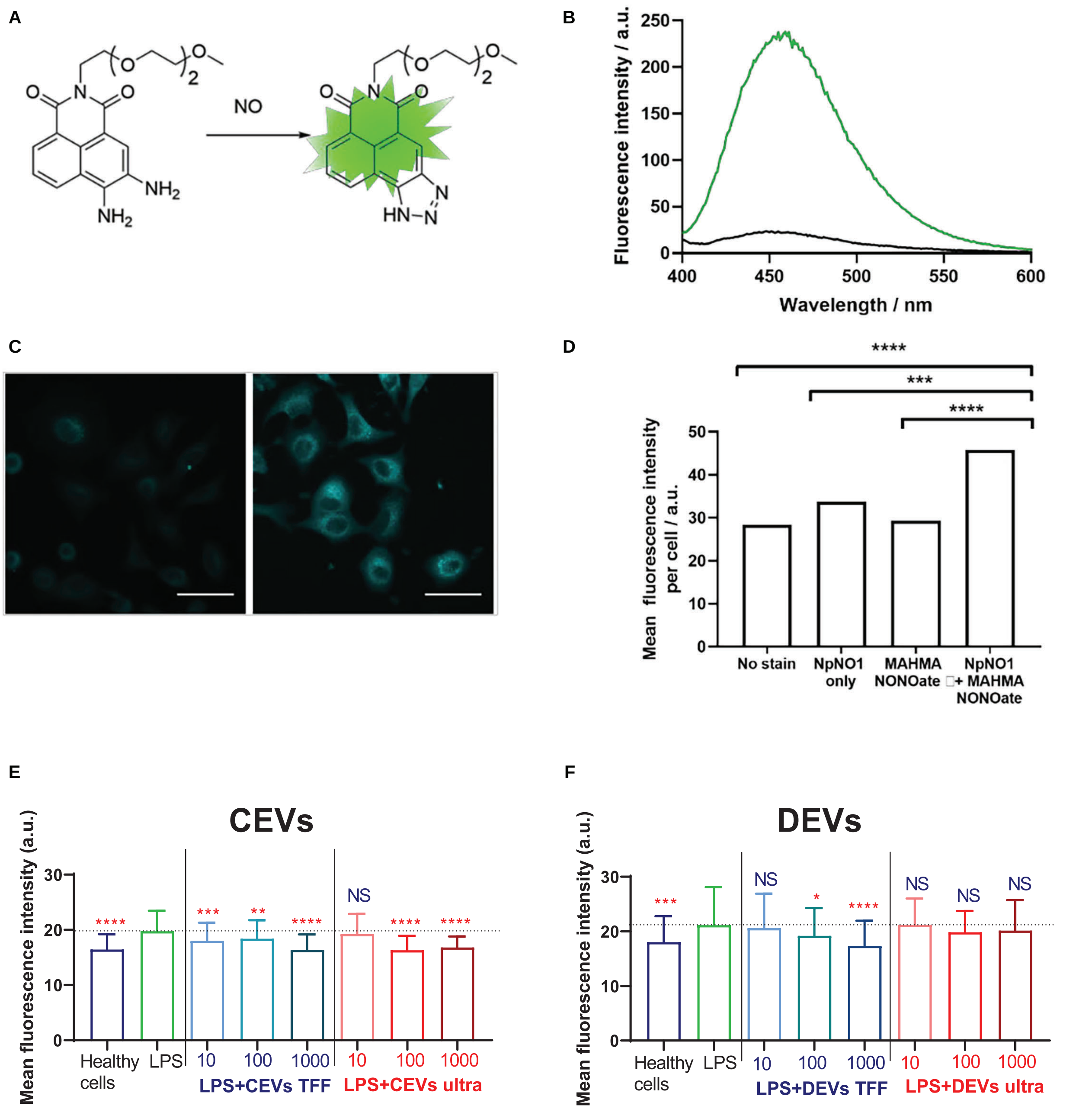

FIGURE 7 | A novel, water soluble fluorescent sensor for intracellular nitric oxide (NO) and assessing NO levels in BEAS-2B cells. **(A)** Water-soluble NO sensor NpNO1 and the product of its reaction with nitric oxide to give a fluorescent triazole derivative. **(B)** Fluorescence emission response of NpNO1 (10 μM) in the presence of diethylamine NONOate (1 mM). **(C)** Representative micrographs of A549 cells treated with NpNO1 (50 μM) in the absence (left) and presence (right) of MAHMA NONOate (5 mM). Scale bar represents 50 μm. **(D)** Mean fluorescence intensity of A549 cells treated as indicated measured across at least three different field of views in each of the three independent experiments performed ($n = 3$). MAHMA NONOate, (Z)-1-{N-methyl-N-[6-(N-methylammoniohexyl)amino]}diazen-1-ium-1,2-diolate, an NO donor. BEAS-2B cells were "injured" with 10 μg/ml of LPS and dosed with **(E)** CEVs isolated using TFF and ultracentrifugation and **(F)** DEVs isolated using TFF and ultracentrifugation. Statistical significance was determined by ordinary one-way ANOVA, followed by Dunn's multiple comparisons test for pair-wise comparisons, $n = 3$. Statistical significance shown was between LPS treatment and other groups. *$P < 0.1$; **$P < 0.01$; ***$P < 0.001$; ****$P < 0.0001$; NS, not significant. Error bars denote standard deviation (SD). The dash line represents the mean level of the LPS group.

we provide extensive experimental evidence that *isolation method determines the composition and biological function of EV isolates.*

Two common isolation methods were used in this study: ultracentrifugation and TFF. Using four different techniques, we demonstrated that the size distributions of EVs isolated using ultracentrifugation and TFF were different. Since EVs are heterogenous and each characterization technique has its own limits of detection (Gandham et al., 2020), it is essential to measure the size distribution using multiple techniques. Here we used four techniques to measure the size distribution and concentration of EVs including PTA, DLS, nFCM, and TRPS. PTA is based on light scattering and Brownian motion, which cannot differentiate between large protein aggregates and single large particles (Gercel-Taylor et al., 2012). For DLS, the size distribution depends on the intensity of light scattering; therefore, the intensity of the scattered light from small particles is normally surpassed by large particles (Tosi et al., 2020). Hence, DLS is not suitable to provide the accurate size distribution for heterogenous populations. In addition, many EVs have protein corona on their surfaces, which may impact on the accuracy of the results as EVs with and without corona (or unspecific corona) have different hydrodynamic diameters (Varga et al., 2020). Similar to PTA and DLS, nFCM is based on the light scattering from the samples. However, nFCM detects the light scattering from individual nanoparticles passing through the lasers, which prevents the bulk analysis of samples like PTA and DLS. In addition, with the incorporation of multiparameter fluorescence detection, nFCM allows the size detection of individual EVs down to 40 nm (Tian et al., 2018; Gandham et al., 2020). However, the large particles or agglomerates (>200 nm) could not be detected using nFCM since the size distribution of EVs was calibrated based on the size standard of a mixture of silica nanospheres, which was below 200 nm. Finally, we used TRPS with a nanopore NP100, which was calibrated to measure nanoparticles in the range between 50 and 300 nm. Since TRPS detects vesicles within the range of the selected nanopore (Maas et al., 2015), TRPS was less sensitive for detection of EV particles below 50 nm. Size and concentration measurement results showed that each characterization technique has its own limitations due to principles of the measurement, the way samples are prepared, as well as calibration standards (for nFCM and TRPS). Consequently, it led to discrepancies between the results obtained with each of the techniques. These findings highlighted the need to use multiple and complementary techniques to capture the whole population of EVs. Our study also emphasized the need for the careful interpretation of the measurement results, which should account for theoretical and physical principles of each technique, sample preparation, and sample state, which all can impact on the results.

In addition, for the first time, we have demonstrated that large EVs (>100 nm) isolated using ultracentrifugation have a higher dry mass than large EVs isolated using TFF. Here we have introduced the parameter of EV dry mass as a metric to reveal the total mass of molecular cargo inside each vesicle, a measurement not previously made in the EV field. The differences in dry mass between EV isolates suggested different molecular compositions. Indeed, we showed that there were variations between the expression levels of surface markers (CD9, CD63, and CD81) between different EV isolates at sub-population level by using nano-flow cytometry. It has been reported that the presence of each surface marker in EV populations was different depending on the isolation methods of EVs (Tian et al., 2020), which clearly indicated that different subpopulations of EVs have been extracted using different isolation methods. Furthermore, our study showed that the amount of nucleic acid content in EVs isolated using TFF was higher than in EVs isolated using ultracentrifugation for both EV types. The higher nucleic acid content for EVs isolated using TFF was further confirmed at individual vesicle characterization using atomic force nanoscale infrared spectroscopy. By combining multiscale characterization techniques, our study allows robust and precise quantification of molecular composition of EVs. This methodology goes a step beyond conventional characterization methods such as immunoassays or mass spectroscopy, which not only lack single vesicle and subpopulation resolution and flexibility in practical applications but also are very expensive (Trenchevska et al., 2016). This study paves the way to the future diagnostic and therapeutic applications of EVs that depend on identification/quantification of specific cargo.

We have also showed for the first time that the variations in the physicochemical properties of different EV types correlate to their different interactions with cell membranes. By using a distorted grid model to predict how quickly different types of EVs can reach the cell membrane, we demonstrated that the predicted sedimented amount of EVs isolated using ultracentrifugation were 60–100 times higher than EVs isolated using TFF. The calculated higher sedimentation of EVs isolated using ultracentrifugation is likely to be due to the presence of agglomerates, which was consistent with the size distribution and mass results. The agglomerates in EVs isolated using ultracentrifugation were confirmed further using correlative holotomography and fluorescence microscopy. The results of the sedimentation study predict the amount of EVs, which is likely to reach and interact with cells. Depending on the amount of internalized EVs, there may be beneficial or deleterious effects in recipient cells. For example, we showed that DEVs isolated using ultracentrifugation had the highest predicted sedimentation and induced both decreased cell migration and high intracellular NO levels, which indicated an increase in cellular stress post-injury. However, these undesired effects could be associated with EV agglomerates that sedimented rapidly to the cell surface, or with "contaminations" that are typically co-isolated with EV samples during ultracentrifugation. Differences in biological responses to different EV isolates were confirmed using newly developed nitric oxide (NO) probe, which allowed for quantitative and qualitative assessment of intracellular stress (Nasyrova et al., 2015). NO probe enabled us to determine the ability of each EV isolates to promote cell recovery from injury.

In conclusion, we have shown that the physicochemical properties, molecular composition, presence of surface markers, and subsequent biological effects of EVs isolated using ultracentrifugation are markedly different from those isolated by TFF. This study confirms that the isolation method determines which composition of EV sub-populations is isolated. Demonstrated here is the correlation between physicochemical properties and biological effects of EVs, which confirmed that the downstream applications of EVs are determined by the effectiveness of the isolation methods to isolate and fractionate different subpopulations of EVs.

The methodology that we present here for the high-resolution and multiscale measurement of physicochemical and functional properties of EVs is likely to accelerate progress in the development and refinement of isolation methods. Our findings, which uncovered that different EV subpopulations are isolated by different methods, shed new light in our understanding of EV secretion by cells. Furthermore, knowing what the differences in EV composition are depending on the isolation method will support the development of accurate EV-based diagnostic tools for early disease detection. We will also be able to define populations of EVs which have therapeutic potential for specific medical conditions. Taken together, the presented study advanced current understanding of the effect of isolation methods on EV composition and functionality. Our results are likely to contribute to future EV research and provide a backbone for rapid translation of EVs to practical applications.

DATA AVAILABILITY STATEMENT

The raw data supporting the conclusions of this article will be made available by the authors, without undue reservation.

AUTHOR CONTRIBUTIONS

THP, SD, JY, and WC contributed to conception and design of the study. QL, PT, TNP, KL, and MT performed some experiments. VC, ÅJ, M-DD, H-KW, and Y-KC performed the statistical analysis. EN, BK, and PD provided the experimental sources. THP wrote the first draft of the manuscript. All authors contributed to manuscript revision, read, and approved the submitted version.

ACKNOWLEDGMENTS

The authors acknowledge the facilities and the scientific and technical assistance of the Bosch Molecular Biological Facility and Australian Microscopy and Microanalysis Research Facility at the Australian Centre for Microscopy and Microanalysis, The University of Sydney, Tomocube Company, South Korea. The authors would like to acknowledge the Australian Research Council (DP180101353 and DP180101897) for funding, the Westpac Scholars Trust for a Research Fellowship (EN), the University of Sydney for a SOAR Fellowship (EN and WC), the Australian government for Research Training Program Scholarships (KL), and the Medical Advances Without Animals Trust MAWA (THP and WC).

SUPPLEMENTARY MATERIAL

The Supplementary Material for this article can be found online at: https://www.frontiersin.org/articles/10.3389/fbioe.2021.669537/full#supplementary-material

REFERENCES

Balan, V., Mihai, C. T., Cojocaru, F. D., Uritu, C. M., Dodi, G., Botezat, D., et al. (2019). Vibrational spectroscopy fingerprinting in medicine: from molecular to clinical practice. *Materials (Basel)* 12:2884. doi: 10.3390/ma12182884

Barnett, C. E. (1942). Some applications of wave-length turbidimetry in the infrared. *J. Phys. Chem.* 46, 69–75. doi: 10.1021/j150415a009

Bishop, J. B., Martin, J. C., and Rosenblum, W. M. (1991). A light-scattering method for qualitatively monitoring aggregation rates in macromolecular systems. *J. Cryst. Growth* 110, 164–170. doi: 10.1016/0022-0248(91)90880-e

Busatto, S., Vilanilam, G., Ticer, T., Lin, W. L., Dickson, D. W., Shapiro, S., et al. (2018). Tangential flow filtration for highly efficient concentration of extracellular vesicles from large volumes of fluid. *Cells* 7:273. doi: 10.3390/cells7120273

Candelario, K. M., and Steindler, D. A. (2014). The role of extracellular vesicles in the progression of neurodegenerative disease and cancer. *Trends Mol. Med.* 20, 368–374. doi: 10.1016/j.molmed.2014.04.003

Chokshi, N. K., Guner, Y. S., Hunter, C. J., Upperman, J. S., Grishin, A., and Ford, H. R. (2008). The role of nitric oxide in intestinal epithelial injury and restitution in neonatal necrotizing enterocolitis. *Semin. Perinatol.* 32, 92–99. doi: 10.1053/j.semperi.2008.01.002

Cohen, J., Deloid, G., Pyrgiotakis, G., and Demokritou, P. (2013). Interactions of engineered nanomaterials in physiological media and implications for in vitro dosimetry. *Nanotoxicology* 7, 417–431. doi: 10.3109/17435390.2012.666576

Cohen, J. M., Teeguarden, J. G., and Demokritou, P. (2014). An integrated approach for the in vitro dosimetry of engineered nanomaterials. *Part Fibre Toxicol.* 11:20.

Coleman, J. W. (2001). Nitric oxide in immunity and inflammation. *Int. Immunopharmacol.* 1, 1397–1406. doi: 10.1016/s1567-5769(01)00086-8

Coumans, F. A. W., Brisson, A. R., Buzas, E. I., Dignat-George, F., Drees, E. E. E., El-Andaloussi, S., et al. (2017). Methodological guidelines to study extracellular vesicles. *Circ. Res.* 120, 1632–1648.

Danielson, K. M., and Das, S. (2014). Extracellular vesicles in heart disease: excitement for the future ? *Exosomes Microvesicles* 2:10.5772/58390. doi: 10.5772/58390

DeLoid, G. M., Cohen, J. M., Pyrgiotakis, G., and Demokritou, P. (2017). Preparation, characterization, and in vitro dosimetry of dispersed, engineered nanomaterials. *Nat. Protoc.* 12, 355–371. doi: 10.1038/nprot.2016.172

DeLoid, G. M., Cohen, J. M., Pyrgiotakis, G., Pirela, S. V., Pal, A., Liu, J., et al. (2015). Advanced computational modeling for in vitro nanomaterial dosimetry. *Part Fibre Toxicol.* 12:32.

Gandham, S., Su, X., Wood, J., Nocera, A. L., Alli, S. C., Milane, L., et al. (2020). Technologies and standardization in research on extracellular vesicles. *Trends Biotechnol.* 38, 1066–1098.

Gardiner, C., Di Vizio, D., Sahoo, S., Théry, C., Witwer, K. W., Wauben, M., et al. (2016). Techniques used for the isolation and characterization of extracellular vesicles: results of a worldwide survey. *J. Extracell. Vesicles* 5, 32945–32945. doi: 10.3402/jev.v5.32945

Gardner, L., Warrington, J., Rogan, J., Rothwell, D. G., Brady, G., Dive, C., et al. (2020). The biomolecule corona of lipid nanoparticles contains circulating cell-free DNA. *Nanoscale Horiz.* 5, 1476–1486. doi: 10.1039/d0nh00333f

Gercel-Taylor, C., Atay, S., Tullis, R. H., Kesimer, M., and Taylor, D. D. (2012). Nanoparticle analysis of circulating cell-derived vesicles in ovarian cancer patients. *Anal. Biochem.* 428, 44–53. doi: 10.1016/j.ab.2012.06.004

Guo, L., Zhao, R. C., and Wu, Y. (2011). The role of microRNAs in self-renewal and differentiation of mesenchymal stem cells. *Exp. Hematol.* 39, 608–616. doi: 10.1016/j.exphem.2011.01.011

György, B., Hung, M. E., Breakefield, X. O., and Leonard, J. N. (2015). Therapeutic applications of extracellular vesicles: clinical promise and open questions. *Annu. Rev. Pharmacol. Toxicol.* 55, 439–464. doi: 10.1146/annurev-pharmtox-010814-124630

Heath, N., Grant, L., De Oliveira, T. M., Rowlinson, R., Osteikoetxea, X., Dekker, N., et al. (2018). Rapid isolation and enrichment of extracellular vesicle preparations using anion exchange chromatography. *Sci. Rep.* 8:5730.

Iraci, N., Leonardi, T., Gessler, F., Vega, B., and Pluchino, S. (2016). Focus on extracellular vesicles: physiological role and signalling properties of extracellular membrane vesicles. *Int. J. Mol. Sci.* 17, 171–171. doi: 10.3390/ijms17020171

Ismail, N., Wang, Y., Dakhlallah, D., Moldovan, L., Agarwal, K., and Batte, K. (2013). Macrophage microvesicles induce macrophage differentiation and miR-223 transfer. *Blood* 121, 984–995. doi: 10.1182/blood-2011-08-374793

Iverson, N. M., Hofferber, E. M., and Stapleton, J. A. (2018). Nitric oxide sensors for biological applications. *Chemosensors* 6:8. doi: 10.3390/chemosensors6010008

Kang, H., Kim, J., and Park, J. (2017). Methods to isolate extracellular vesicles for diagnosis. *Micro Nano Syst. Lett.* 5:15.

Khanal, D., Kondyurin, A., Hau, H., Knowles, J. C., Levinson, O., Ramzan, I., et al. (2016). Biospectroscopy of nanodiamond-induced alterations in conformation of intra- and extracellular proteins: a nanoscale IR study. *Anal. Chem.* 88, 7530–7538. doi: 10.1021/acs.analchem.6b00665

Kim, S., Hun, K. S., Byun, S. H., Kim, H.-J., Park, I.-K., and Hirschberg, H. (2020). Intercellular bioimaging and biodistribution of gold nanoparticle-loaded macrophages for targeted drug delivery. *Electronics* 9:1105. doi: 10.3390/electronics9071105

Kim, S. Y., Joglekar, M. V., Hardikar, A. A., Phan, T. H., Khanal, D., Tharkar, P., et al. (2019a). Placenta stem/stromal cell–derived extracellular vesicles for potential use in lung repair. *Proteomics* 19:1800166. doi: 10.1002/pmic.201800166

Kim, S. Y., Khanal, D., Kalionis, B., and Chrzanowski, W. (2019b). High-fidelity probing of the structure and heterogeneity of extracellular vesicles by resonance-enhanced atomic force microscopy infrared spectroscopy. *Nat. Protoc.* 14, 576–593. doi: 10.1038/s41596-018-0109-3

Kim, S. Y., Khanal, D., Tharkar, P., Kalionis, B., and Chrzanowski, W. (2018). None of us is the same as all of us: resolving the heterogeneity of extracellular vesicles using single-vesicle, nanoscale characterization with resonance enhanced atomic force microscope infrared spectroscopy (AFM-IR). *Nanoscale Horiz.* 3, 430–438. doi: 10.1039/c8nh00048d

Kusuma, G. D., Abumaree, M. H., Pertile, M. D., Perkins, A. V., Brennecke, S. P., and Kalionis, B. (2016). Mesenchymal stem/stromal cells derived from a reproductive tissue niche under oxidative stress have high aldehyde dehydrogenase activity. *Stem Cell Rev. Rep.* 12, 285–297. doi: 10.1007/s12015-016-9649-5

Lai, C. P., Kim, E. Y., Badr, C. E., Weissleder, R., Mempel, T. R., Tannous, B. A., et al. (2015). Visualization and tracking of tumour extracellular vesicle delivery and RNA translation using multiplexed reporters. *Nat. Commun.* 6:7029. doi: 10.1038/ncomms8029

Lee, J., Wen, B., Carter, E. A., Combes, V., Grau, G. E. R., and Lay, P. A. (2017). Infrared spectroscopic characterization of monocytic microvesicles (microparticles) released upon lipopolysaccharide stimulation. *FASEB J.* 31, 2817–2827. doi: 10.1096/fj.201601272r

Leslie, K. G., Jacquemin, D., New, E. J., and Jolliffe, K. A. (2018). Expanding the breadth of 4-Amino-1,8-naphthalimide photophysical properties through substitution of the naphthalimide core. *Chem. A Eur. J.* 24, 5569–5573. doi: 10.1002/chem.201705546

Li, X., Corbett, A. L., Taatizadeh, E., Tasnim, N., Little, J. P., Garnis, C., et al. (2019). Challenges and opportunities in exosome research-Perspectives from biology, engineering, and cancer therapy. *APL Bioeng* 3:011503. doi: 10.1063/1.5087122

Linares, R., Tan, S., Gounou, C., Arraud, N., and Brisson, A. R. (2015). High-speed centrifugation induces aggregation of extracellular vesicles. *J. Extracell. Vesicles* 4:29509. doi: 10.3402/jev.v4.29509

Lötvall, J., Hill, A. F., Hochberg, F., Buzás, E. I., Di Vizio, D., Gardiner, C., et al. (2014). Minimal experimental requirements for definition of extracellular vesicles and their functions: a position statement from the International Society for Extracellular Vesicles. *J. Extracell. Vesicles* 3, 26913–26913. doi: 10.3402/jev.v3.26913

Maas, S. L. N., de Vrij, J., van der Vlist, E. J., Geragousian, B., van Bloois, L., Mastrobattista, E., et al. (2015). Possibilities and limitations of current technologies for quantification of biological extracellular vesicles and synthetic mimics. *J. Control. Release* 200, 87–96. doi: 10.1016/j.jconrel.2014.12.041

Mateescu, B., Kowal, E. J., van Balkom, B. W., Bartel, S., Bhattacharyya, S. N., Buzás, E. I., et al. (2017). Obstacles and opportunities in the functional analysis of extracellular vesicle RNA - an ISEV position paper. *J. Extracell. Vesicles* 6:1286095. doi: 10.1080/20013078.2017.1286095

Mohan, V., Naske, C. D., Britten, C. N., Karimi, L., and Walters, K. B. (2020). Hydroxide-catalyzed cleavage of selective ester bonds in phosphatidylcholine: an FTIR study. *Vibrat. Spectrosc.* 109:103055. doi: 10.1016/j.vibspec.2020.103055

Momen-Heravi, F., Balaj, L., Alian, S., Mantel, P. Y., Halleck, A. E., Trachtenberg, A. J., et al. (2013). Current methods for the isolation of extracellular vesicles. *Biol. Chem.* 394, 1253–1262.

Nasyrova, R. F., Ivashchenko, D. V., Ivanov, M. V., and Neznanov, N. G. (2015). Role of nitric oxide and related molecules in schizophrenia pathogenesis: biochemical, genetic and clinical aspects. *Front. Physiol.* 6:139. doi: 10.3389/fphys.2015.00139

Nordin, J. Z., Lee, Y., Vader, P., Mäger, I., Johansson, H. J., Heusermann, W., et al. (2015). Ultrafiltration with size-exclusion liquid chromatography for high yield isolation of extracellular vesicles preserving intact biophysical and functional properties. *Nanomedicine* 11, 879–883. doi: 10.1016/j.nano.2015.01.003

Nova, Z., Skovierova, H., and Calkovska, A. (2019). Alveolar-capillary membrane-related pulmonary cells as a target in endotoxin-induced acute lung injury. *Int. J. Mol. Sci.* 20, 831. doi: 10.3390/ijms20040831

Ohno, S., Takanashi, M., Sudo, K., Ueda, S., Ishikawa, A., Matsuyama, N., et al. (2013). Systemically injected exosomes targeted to EGFR deliver antitumor microRNA to breast cancer cells. *Mol. Ther.* 21, 185–191. doi: 10.1038/mt.2012.180

Piffoux, M., Gazeau, F., Wilhelm, C., and Silva, A. K. A. (2017). "Imaging and therapeutic potential of extracellular vesicles," in *Design and Applications of Nanoparticles in Biomedical Imaging*, eds J. W. M. Bulte and M. M. J. Modo (Cham: Springer International Publishing), 43–68. doi: 10.1007/978-3-319-42169-8_3

Qin, S. Q., Kusuma, G. D., Al-Sowayan, B., Pace, R. A., Isenmann, S., Pertile, M. D., et al. (2016). Establishment and characterization of fetal and maternal mesenchymal stem/stromal cell lines from the human term placenta. *Placenta* 39, 134–146. doi: 10.1016/j.placenta.2016.01.018

Ramirez, M. I., Amorim, M. G., Gadelha, C., Milic, I., Welsh, J. A., Freitas, V. M., et al. (2018). Technical challenges of working with extracellular vesicles. *Nanoscale* 10, 881–906.

Rupert, D. L. M., Claudio, V., Lässer, C., and Bally, M. (2017). Methods for the physical characterization and quantification of extracellular vesicles in biological samples. *Biochim. Biophys. Acta* 1861, 3164–3179. doi: 10.1016/j.bbagen.2016.07.028

Simonsen, J. B., and Munter, R. (2020). Pay attention to biological nanoparticles when studying the protein corona on nanomedicines. *Angew. Chem. Int. Edn.* 59, 12584–12588. doi: 10.1002/anie.202004611

Sunkara, V., Woo, H. K., and Cho, Y. K. (2016). Emerging techniques in the isolation and characterization of extracellular vesicles and their roles in cancer diagnostics and prognostics. *Analyst* 141, 371–381. doi: 10.1039/c5an01775k

Takov, K., Yellon, D. M., and Davidson, S. M. (2017). Confounding factors in vesicle uptake studies using fluorescent lipophilic membrane dyes. *J. Extracell. Vesicles* 6:1388731. doi: 10.1080/20013078.2017.1388731

Taylor, D. D., and Gercel-Taylor, C. (2008). MicroRNA signatures of tumor-derived exosomes as diagnostic biomarkers of ovarian cancer. *Gynecol. Oncol.* 110, 13–21. doi: 10.1016/j.ygyno.2008.04.033

Taylor, D. D., and Shah, S. (2015). Methods of isolating extracellular vesicles impact down-stream analyses of their cargoes. *Methods* 87, 3–10. doi: 10.1016/j.ymeth.2015.02.019

Thery, C., Witwer, K. W., Aikawa, E., Alcaraz, M. J., Anderson, J. D., Andriantsitohaina, R., et al. (2018). Minimal information for studies of extracellular vesicles 2018 (MISEV2018): a position statement of the International Society for Extracellular Vesicles and update of the MISEV2014 guidelines. *J. Extracell. Vesicles* 7:1535750.

Tian, Y., Gong, M., Hu, Y., Liu, H., Zhang, W., Zhang, M., et al. (2020). Quality and efficiency assessment of six extracellular vesicle isolation methods by nano-flow cytometry. *J. Extracell. Vesicles* 9:1697028. doi: 10.1080/20013078.2019.1697028

Tian, Y., Ma, L., Gong, M., Su, G., Zhu, S., Zhang, W., et al. (2018). Protein profiling and sizing of extracellular vesicles from colorectal cancer patients via flow cytometry. *ACS Nano* 12, 671–680. doi: 10.1021/acsnano.7b07782

Tosi, M. M., Ramos, A. P., Esposto, B. S., and Jafari, S. M. (2020). "Chapter Six – dynamic light scattering (DLS) of nanoencapsulated food ingredients," in *Characterization of Nanoencapsulated Food Ingredients*, ed. S. M. Jafari (Cambridge, MA: Academic Press), 191–211. doi: 10.1016/b978-0-12-815667-4.00006-7

Trenchevska, O., Nelson, R. W., and Nedelkov, D. (2016). Mass spectrometric immunoassays in characterization of clinically significant proteoforms. *Proteomes* 4:13. doi: 10.3390/proteomes4010013

van der Vliet, A., Eiserich, J. P., and Cross, C. E. (2000). Nitric oxide: a pro-inflammatory mediator in lung disease? *Respir. Res.* 1, 67–72.

Varga, Z., Fehér, B., Kitka, D., Wacha, A., Bóta, A., Berényi, S., et al. (2020). Size measurement of extracellular vesicles and synthetic liposomes: the impact of the hydration shell and the protein corona. *Colloids Surf. B Biointerfaces* 192, 111053. doi: 10.1016/j.colsurfb.2020.111053

Vogel, R., Willmott, G., Kozak, D., Roberts, G. S., Anderson, W., Groenewegen, L., et al. (2011). Quantitative sizing of nano/microparticles with a tunable elastomeric pore sensor. *Anal. Chem.* 83, 3499–3506. doi: 10.1021/ac200195n

Willms, E., Cabañas, C., Mäger, I., Wood, M. J. A., and Vader, P. (2018). Extracellular vesicle heterogeneity: subpopulations, isolation techniques, and diverse functions in cancer progression. *Front. Immunol.* 9:738. doi: 10.3389/fimmu.2018.00738

Witwer, K. W., Buzás, E. I., Bemis, L. T., Bora, A., Lässer, C., Lötvall, J., et al. (2013). Standardization of sample collection, isolation and analysis methods in extracellular vesicle research. *J. Extracell. Vesicles* 2:10.3402/jev.v2i0.20360. doi: 10.3402/jev.v2i0.20360

Xu, F., and Zhou, F. C. (2020). Inhibition of microRNA-92a ameliorates lipopolysaccharide-induced endothelial barrier dysfunction by targeting ITGA5 through the PI3K/Akt signaling pathway in human pulmonary microvascular endothelial cells. *Int. Immunopharmacol.* 78:106060. doi: 10.1016/j.intimp.2019.106060

Yanez-Mo, M., Siljander, P. R. M., Andreu, Z., Zavec, A. B., Borràs, F. E., Buzas, E. I., et al. (2015). Biological properties of extracellular vesicles and their physiological functions. *J. Extracell. Vesicles* 4:27066.

Yang, K., Leslie, K. G., Kim, S. Y., Kalionis, B., Chrzanowski, W., Jolliffe, K. A., et al. (2018). Tailoring the properties of a hypoxia-responsive 1,8-naphthalimide for imaging applications. *Org. Biomol. Chem.* 16, 619–624. doi: 10.1039/c7ob03164e

Yekula, A., Muralidharan, K., Kang, K. M., Wang, L., Balaj, L., and Carter, B. S. (2020). From laboratory to clinic: translation of extracellular vesicle based cancer biomarkers. *Methods* 177, 58–66. doi: 10.1016/j.ymeth.2020.02.003

Conflict of Interest: The authors declare that the research was conducted in the absence of any commercial or financial relationships that could be construed as a potential conflict of interest.

Copyright © 2021 Phan, Divakarla, Yeo, Lei, Tharkar, Pansani, Leslie, Tong, Coleman, Jämting, Du Plessis, New, Kalionis, Demokritou, Woo, Cho and Chrzanowski. This is an open-access article distributed under the terms of the Creative Commons Attribution License (CC BY). The use, distribution or reproduction in other forums is permitted, provided the original author(s) and the copyright owner(s) are credited and that the original publication in this journal is cited, in accordance with accepted academic practice. No use, distribution or reproduction is permitted which does not comply with these terms.

frontiers in Bioengineering and Biotechnology

ORIGINAL RESEARCH
published: 09 June 2021
doi: 10.3389/fbioe.2021.686510

Check for updates

Fabrication and Characterization of a Biomaterial Based on Extracellular-Vesicle Functionalized Graphene Oxide

*Julia Driscoll, Anuradha Moirangthem, Irene K. Yan and Tushar Patel**

Department of Transplantation, Mayo Clinic, Jacksonville, FL, United States

OPEN ACCESS

Edited by:
*Antonietta Rosa Silini,
Fondazione Poliambulanza Istituto Ospedaliero, Italy*

Reviewed by:
*Katalin Lumniczky,
Frédéric Joliot-Curie National Research Institute for Radiobiology and Radiohygiene, Hungary
Valentina Palmieri,
Istituto dei Sistemi Complessi, ISC, CNR, Italy*

***Correspondence:**
*Tushar Patel
patel.tushar@mayo.edu*

Specialty section:
This article was submitted to Preclinical Cell and Gene Therapy, a section of the journal Frontiers in Bioengineering and Biotechnology

Received: *27 March 2021*
Accepted: *17 May 2021*
Published: *09 June 2021*

Citation:
Driscoll J, Moirangthem A, Yan IK and Patel T (2021) Fabrication and Characterization of a Biomaterial Based on Extracellular-Vesicle Functionalized Graphene Oxide. Front. Bioeng. Biotechnol. 9:686510. doi: 10.3389/fbioe.2021.686510

Mesenchymal stem cell (MSC) derived extracellular vesicles (EV) are emerging as acellular therapeutics for solid organ injury and as carriers for drug delivery. Graphene-based materials are novel two-dimensional crystal structure-based materials with unique characteristics of stiffness, strength and elasticity that are being explored for various structural and biological applications. We fabricated a biomaterial that would capture desirable properties of both graphene and stem cell derived EV. Metabolically engineered EV that express azide groups were cross-linked with alkyne-functionalized graphene oxide (GO) via a copper catalyzed alkyne-azide cycloaddition (CuAAC) reaction. The crosslinking between EV and GO was accomplished without the need for ligand expression on the metal. Scanning electron and fluorescence microscopy demonstrated excellent cross-linking between EV and GO. Biological effects were assessed by phagocytosis studies and cell viability studies. The uptake of GO or sonicated GO (sGO) resulted in a durable pro-inflammatory immune response. Cell studies further showed that crosslinked GO-EV scaffolds exhibited cell-type dependent cytotoxicity on liver cancer cells whereas there was minimal impact on healthy hepatocyte proliferation. *In vitro*, neither GO-EV nor sGO-EV induced DNA strand breaks. *In vivo* studies in zebrafish revealed gross developmental malformations but treatment-induced mortality was only seen with the highest doses of GO-EV and sGO-EV. With these advantages, this engineered biomaterial combining the versatility of graphene with the therapeutic effects of MSC-EV has potential for applications in tissue engineering and regenerative medicine.

Keywords: extracellular vesicles, graphene, therapeutics, biomaterials, toxicology

INTRODUCTION

Extracellular vesicles (EV) are membrane-bound nanovesicles that can be released from different cell types and are ubiquitous in biological fluids. EV can play an essential role in intercellular communication through the unilateral transfer of their cargo to recipient cells (Yáñez-Mó et al., 2015). Delivery of their cargo to recipient cells is facilitated by membrane proteins

Abbreviations: az-EV, azide tagged extracellular vesicles; BM, bone marrow; CM, conditioned media; CuAAC, copper catalyzed alkyne-azide cycloaddition; EV, extracellular vesicles; GO, alkyne functionalized graphene oxide; hpf, hours post-fertilization; miRNA, micro RNAs; MSC, mesenchymal stem cells; rGO, reduced GO; sGO, sonicated GO; siRNA, small interfering RNA; TFF, tangential flow filtration; TNF, tumor necrosis factor.

that promote cellular uptake by recipient cells. These properties facilitate the use of EVs as delivery agents for therapeutics. Moreover, EV derived from mesenchymal stem cells (MSC-EV) have potential as an acellular therapeutic, due to their intrinsic beneficial therapeutic properties such as promoting tissue repair (Reis et al., 2012; Yang et al., 2015; Haga et al., 2017). The cargo of EV can be modified to enhance their capability and utility as acellular therapeutics. Modification of the EV cargo can be accomplished by either loading the EV with therapeutic molecule(s) of interest or through protein engineering manipulations of the parent cells (Tian et al., 2014; Li et al., 2018; Matsuda et al., 2019).

Graphene is a carbon-based material that has garnered much recent attention in the scientific community. This unique material is comprised of carbon atoms arranged in a two-dimensional honeycomb lattice. The delocalization of one of the electrons in each carbon atom endows graphene with a high tensile strength and exceptional thermal and electrical conductivity that make it attractive for use in a variety of biomedical applications (Geim, 2009). Furthermore, the development of graphene-based drug and nucleic acid delivery vehicles is supported by the high surface area of graphene that allows for the loading of pharmaceutical agents or biological macromolecules. The surface chemistry of graphene can be modified to generate derivatives with different physicochemical properties. Oxidation of graphene generates graphene oxide (GO), a hydrophilic biomaterial, whereas reduction of GO results in the formation of reduced GO. The surface of graphene and its derivatives can be altered by covalent as well as non-covalent modifications. The most common surface modifications include the addition of functional group(s) to enable cycloaddition reactions, the conjugation of polymers to increase the biocompatibility of the biomaterial and the attachment of antibodies to enable the targeted delivery of the biomaterial (Mei et al., 2015; Xu et al., 2016; Zheng et al., 2016). The versatility of graphene enables its use for a variety of different biomedical applications. Indeed, graphene and its derivatives have already been effectively used for biosensing, drug and nucleic acid delivery, photothermal and photodynamic therapy for cancer treatment, and tissue engineering (Robinson et al., 2011; Hu et al., 2012; Lee et al., 2016; Shin et al., 2016; Vinothini et al., 2019).

The overall goals of our study were to develop a composite graphene-based biological material that would allow us to further exploit the use of EV for drug delivery or tissue repair. We postulated that the functional applications of EV-based therapeutic applications could be extended by combining them with the versatile properties offered by the application of graphene-based materials. Using a protein engineering and biorthogonal click conjugation strategy, we generated a biological graphene nanoparticle by conjugating EV to graphene oxide. This new biomaterial (GO-EV) can be readily generated, retains biological effects of EV, and could support the development of new applications in tissue engineering, repair and regenerative medicine.

MATERIALS AND METHODS

Cells and Cell Culture

Human bone marrow derived-mesenchymal stem cells (hBM-MSC) were purchased from Lonza (Walkersville, MD) and maintained in MSC basal media supplemented with L-glutamine, gentamicin sulfate, amphotericin and mesenchymal cell growth supplement (Lonza; Walkersville, MD). After the third passage, the cells were cultured in vesicle-depleted media. Vesicle depletion from media was performed by tangential flow filtration (TFF) using a sterile 500 kDa molecular weight cut off MidiKros filter lined with a modified polyethersulfone membrane (Repligen; Waltham, MA). The permeate, containing the vesicle-depleted MSC media, was collected and passed through a 0.22 μm filter before storing at 4°C. Human hepatocytes (HH; Sciencell, United Kingdom) and PLC cells (ATCC; Manassas, VA) were cultured in untreated plates. KMBC (provided by Dr. Gregory Gores, Mayo Clinic), HepG2 and Hep3B (ATCC; Manassas, VA) cells were cultured in collagen-coated plates. The aforementioned cells were maintained in Dulbecco's modified eagle media (DMEM) high glucose media supplemented with 1% penicillin-streptomycin and 10% fetal bovine serum (FBS). HL-60 promyeloblasts (ATCC; Manassas, VA) were cultured with Iscove's modified Dulbecco's medium supplemented with 20% FBS in T75 flasks. RAW264.7 murine macrophages (ATCC; Manassas, VA) were cultured with DMEM high glucose media supplemented with 10% FBS.

Isolation of EV

MSC-conditioned media (MSC-CM) was collected from azide-tagged or untagged MSC in culture and centrifuged to remove debris and apoptotic bodies. The MSC-CM was first centrifuged at 300 × g for 5 min at 4°C; the supernatant was transferred to new tube and centrifuged at 2,000 × g for an additional 30 min. The supernatant was transferred to a 250 mL reservoir for isolation by TFF with a 500 kDa molecular weight cut-off filter. The flow rate was maintained at 53 mL/min with a sheer rate that did not exceed 3,000 for the duration of the isolation process. The MSC-CM was concentrated 5 times to reduce the volume to 5 mL, diafiltrated 5 times with PBS and further concentrated to attain a final volume of approximately 2–5 mL. The filter was washed once with PBS prior to loading with subsequent batches of MSC-CM. Fifty microliters of untreated EV or azide-tagged EV (az-EV) were diluted in PBS (1:100) for quantitation of particle size and concentration using the nanosight (Malvern Panalytical, United Kingdom). A BCA assay (Thermo Fisher Scientific, Waltham, MA) was used to quantitate proteins, with concentrations of EV extrapolated from a standard curve that was constructed using a 4-parameter fit. Aliquots of the isolated EV were stored at 4°C for later use.

Generation of GO-EV

MSC were treated with 50 μM of N-azidoacetylmannosamine-tetraacetylated ($Ac_4ManNAz$; Kerafast, Boston, MA) for 72 h. Az-EV were isolated from $Ac_4ManNAz$-treated MSC. Alkyne functionalized graphene oxide (GO) was obtained from Nanocs (cat no. GO1-AK-1, New York, NY), and characteristics are reported in **Supplementary Table 1**. GO or sonicated GO (sGO) was covalently bound to az-EV by copper-catalyzed click chemistry. sGO was generated as described by Campbell et al. (2019) Briefly, GO was subjected to ultra-low power sonication for 20 min (Branson Sonifer 150; Danbury, CT), followed by centrifugation for 5 min at 2,000 × g to remove large aggregates, and repeat sonication of the supernatant for 30 min. GO-EV or sGO-EV were generated by incubating equivalent amounts of EV and GO or sGO at room temperature (RT) in the dark for 30 min using the reaction buffer kit (Click Chemistry Tools, Scottsdale, AZ). The reaction products were centrifuged at 14,000 × g for 10 min. The supernatants containing the reaction buffers and unbound substrates were removed by centrifugation and the GO-EV and sGO-EV pellets were resuspended in PBS and stored at 4°C for later use.

Fluorescence Imaging

Untreated EV and az-EV were diluted with PBS to a concentration of 2×10^{10} particles/mL and stained with 10 μM/L DiI (Life Technologies; Carlsbad, CA) for 60 min with periodic mixing, followed by ultracentrifugation at 100,000 × g for 70 min at 4°C. The supernatants were removed, and the pellets were resuspended in a working volume of PBS. Click chemistry reactions were performed using 5.7 μg GO and 2.9 μg DiI stained unmodified or az-EV. DiI stained unmodified EV-GO or az-EV-GO were transferred to microscope slides and visualized using fluorescence microscopy (Life technologies; Carlsbad, CA).

Spectral Analysis

GO or sGO were diluted in PBS to desired concentrations (200–800 μg/mL). The samples were transferred to quartz microcuvettes and absorbance spectrophotometry was performed using a Beckman Spectrophotometer (Beckman Coulter; DU800; Brea, CA). PBS was used as a blank.

Scanning Electron Microscopy (SEM)

GO-EV or sGO-EV were generated using 200 μg/mL azide tagged EV and 200 μg/mL GO or sGO by click chemistry. The reaction products underwent centrifugation at 14,000 × g for 10 min, the supernatants were discarded and the pellets were resuspended in a 4% glutaraldehyde/0.1 M PBS fixative. Small volumes of 200 μg/mL GO and sGO were aliquoted and centrifuged at 14,000 × g for 10 min. The supernatants were removed and the pellets were resuspended in water. The washing step was repeated once more to remove any residual salts from the samples. After the final wash step, the GO and sGO samples were air-dried on poly-L lysine coated coverslips after which they were mounted on an aluminum stub and sputter coated (E5100 SEM Sputter Coater, Bio-Rad, Hercules, CA) for 1 min with gold-palladium.

After the final wash, the GO-EV and sGO-EV samples were centrifuged at 14,000 × g for 10 min and fixed for 1 h at 4°C in Trump's fixative (4% formaldehyde, 1% glutaraldehyde in 1.0 M phosphate buffer with a pH of 7.2). Once fixed, the samples were transferred to poly-L lysine coated coverslips. First, they were washed with PBS, followed by water and subsequently dehydrated twice through a graded series of ethanol concentrations (10, 30, 50, 70, 90, 95, and 100%). The samples were then subjected to critical point drying (CPD) with liquid CO_2 (EMS 3100 CPD; Electron Microscopy Sciences; Hatfield, PA). The samples were then sputter coated using the method described above. SEM was performed by the Mayo EM core facility using a S-4700 cold field emission SEM set to a 5 kV accelerating voltage (Hitachi; Tokyo, Japan).

Cytotoxicity Assays

Cells were seeded in a 96 well plate and allowed to attach overnight. The following day, the media was aspirated and the cells were washed once with PBS. The PBS was removed and 100 μL of vesicle-depleted DMEM high glucose media was added to each well. The cells were then treated with the following: PBS (control), 0.4 μg of GO, sonicated GO (sGO), GO-EV or az-EV. To account for the background absorbance due to graphene, additional wells without cells were treated with similar amounts of GO or GO-EV. Cell viability was assessed using an MTS assay (Promega; Madison, WI) at 24–96 h post-treatment. Briefly, 20 μL of MTS reagent was added to each of the wells and the plates were maintained in complete darkness for 2 h at 37°C. The absorbance was measured at 490 nm to assess cell viability. Each treatment condition consisted of 4 technical replicates. The percent viability was calculated for each treatment condition and normalized to the control group.

DNA Damage Assay

An Oxiselect Comet assay (Fisher; Hampton, NH) was performed to assess the genotoxicity in HL-60 cells. Cells (100,000/well) were seeded in a 24 well plate, then incubated for 24 h with PBS (diluent control), 40 μg/mL GO-EV or sGO-EV or for 1 h with 20 μm etoposide (positive control). Cells were centrifuged at 600 × *g* for 2 min, and the pellets resuspended in ice cold PBS. Alkaline electrophoresis was performed and cells were visualized using fluorescence microscopy (EVOS FL; Invitrogen, Carlsbad, CA). Each treatment was performed in triplicate. Tail length quantitation and analysis was performed using the OpenComet software (CometBio, Chicago, IL). At least 15 images from each replicate were captured. The tail length quantitation was performed using the OpenComet software (CometBio, Chicago, IL).

Assessment of Developmental Toxicity

Zebrafish (*Danio rerio*) were obtained from the Zebrafish International Resource Center (Eugene, OR) and housed in the Mayo Clinic Jacksonville zebrafish facility. The zebrafish were fed live brine shrimp (*Artemia nauplii*) twice daily and also received dry flakes (pellets) once a day. A single male and female zebrafish were placed on opposite sides of a spawning aquarium, equipped with a separator and a mesh bottom to capture the embryos. The following morning, the separator was removed and the embryos were collected after 30–60 min and subsequently rinsed with embryo water (EW) (5 nM NaCl, 0.17 nM KCl, 0.33 nM $CaCl^2$, 0.33 $MgSO^4$, 0.00001% methylene blue). The fertilized embryos were transferred to single wells of a 96 well plate and maintained in 100 μL of EW. At 24 h post-fertilization (hpf), the EW was replaced with EW containing phenylthiourea 10% v/v PBS, 10 μg GO, 1 μg or 10 μg sGO, 1 or 10 μg GO-EV, 1 μg or 10 μg sGO-EV, 1 μg or 10 μg az-EV or nothing else. The treatments were refreshed every 24 h. Dechorionation was monitored every 3 h from 45 to 85 hpf. The heart rates of the zebrafish were recorded at 48, 72, 144, and 168 hpf. Furthermore, the zebrafish were examined for malformations and their survival was noted.

Visualization of EV-GO Uptake

One milliliter of az-EV was stained with an equal volume of 4x PKH67 dye (Sigma, St. Louis, MO) for 30 min with periodic mixing, after which the labeling reaction was terminated by the addition of 1 mL of 1% BSA. The az-EV underwent ultracentrifugation at 100,000 × g for 70 min at 4°C, after which the supernatant was removed and the pellet was resuspended in PBS. Click chemistry reactions were performed with PKH67 labeled EV and GO or sGO. RAW264.7 cells (10,000/well) were seeded onto a FluoroDish (Fisher; Hampton, NH) and allowed to attach overnight. The media was aspirated and the cells were washed once with PBS. One and a half milliliters of phenol red-free media with 50 μL of PKH67 stained GO-EV or sGO-EV was added on top of the cells. Bright field and fluorescence channel images were captured every 5 min using the Nanolive 3D cell explorer (Nanolive, Switzerland). Imaging was terminated once the cell(s) had successfully internalized the biomaterials.

Cytokine Assays

RAW264.7 cells (20,000/well) were seeded on a 96 well plate and allowed to attach overnight. The following day the cells were treated with PBS or 0.4 μg GO-EV for 3 h. The media was collected and centrifuged at 1,500 rpm for 10 min. The supernatant was collected and utilized to perform a mouse 31-plex cytokine and chemokine panel (Eve technologies, Alberta, Canada). For TNF-α assays, cells were treated with PBS, 0.4 μg GO, sGO, GO-EV, sGO-EV or az-EV for 24 h. Samples were diluted in PBS. TNF-α assays were performed by a high sensitivity TNF-α ELISA (Thermo Fisher Scientific, Waltham, MA) according to the manufacturer's protocol, using a FLUOstar Omega plate reader (BMG Labtech, Germany) to measure absorbance. A four-parameter fit standard curve was generated using RStudio. For cytokine assays, four technical replicates were included for each treatment condition.

Statistical Analysis

Data are reported as the average ± the standard deviation from studies performed using an appropriate number of replicates, or as otherwise indicated. For the cytokine and chemokine assays, the fold change in average concentration between treated and control cells was calculated. Comparisons across groups was performed by Student's *t*-test.

RESULTS

Generation of Bioengineered EV

Cell culture media was harvested from the media of early passage (passage 4–5) MSC-EV were isolated using TFF. A cell glycoprotein engineering approach involving $Ac_4ManNAz$ treatment was used to metabolically modify MSC. These cells integrate azide-bearing biomolecules such as amino acids and saccharides into the multivesicular bodies and can thereby introduce active azides as reaction sites on EV released by these cells. The metabolic engineering of these EVs can be performed without exposure of the cell to toxic agents, whilst maintaining their biochemical integrity and viability. $Ac_4ManNAz$ treated cells released EVs with azide tags. These engineered az-EV have a slightly greater mean diameter compared with unmodified EV, although the overall size distribution profile was very similar (**Figure 1**). A larger number of EVs and protein content (**Table 1**) were obtained from engineered cells compared with untreated controls.

Fabrication of GO-EV

Using bio-orthogonal click conjugation, az-EV were cross-linked to alkyne-functionalized GO. The reaction was catalyzed using copper through CuAAC cycloaddition. To determine if the EV were capable of binding to GO, fluorescently stained EV were reacted with GO. Fluorescence microscopy revealed DiI stained az-EV bound to GO, indicating successful conjugation. Furthermore, EV that lacked the azide tag were unable to bind to GO. Studies using alkyne-functionalized GO revealed size variations and large GO particles. To achieve size homogenization, GO was further sonicated prior to conjugation with EV for some studies. The sonicated GO (sGO) particles exhibited reduced diameters and a more homogenous size distribution profile in comparison to plain GO particles (**Figure 1**).

Characterization of GO-EV Based Biomaterials

Visualization of EV-GO biomaterial was performed by scanning EM (SEM). SEM revealed a highly heterogeneous size composition of GO flakes (**Figure 2**). The larger sized GO flakes had lateral dimensions ranging from 20 to 40 microns, while the smallest sized flakes were less than 2 microns. The sGO flakes were much more homogeneous in size, with the majority of the flakes measuring less than 10 microns. Therefore, we selected sGO for further detailed assessments. On SEM, surface modifications were present on GO-EV and sGO-EV when compared with GO or sGO, which is consistent with successful conjugation of EV following the CuAAC reaction. The optical properties of GO- and sGO-based biomaterials were determined by absorbance spectrophotometry. A peak was detected at 257 nm at each of four different dilutions of GO, and absorbance intensity increased with increasing concentrations of GO (**Figure 3**).

Effects of GO on Cell Viability

To evaluate the effects of GO on cell viability over time, HepG2 cells were treated with PBS or 0.4 μg GO for 24, 48, 72, or 96 h. A significant reduction in viable cell numbers was noted during incubation with GO compared with PBS at 24 hrs but

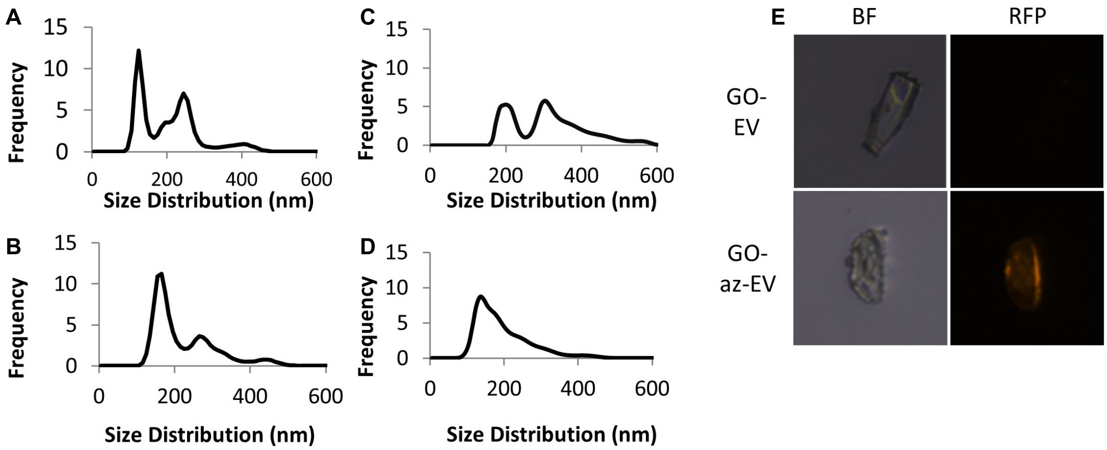

FIGURE 1 | Characterization of nanoparticles. The size distribution of **(A)** unmodified MSC-EV, **(B)** azide tagged MSC-EV (az-EV), **(C)** graphene oxide (GO) and **(D)** sonicated GO (sGO). **(E)** Bright field and fluorescence microscopy images of Dil stained plain (EV) and azide tagged (az-EV) MSC-derived EV covalently bound to graphene oxide (GO) were captured with a 40x magnification.

not at subsequent time points. Notably, there was an increase in the number of viable cells with longer durations up to 96 h post-treatment. These observations suggest that HepG2 cells are able to overcome the cytotoxic effects of GO with more prolonged exposure.

Cellular Effects of GO-EV and sGO-EV

To evaluate the effects of GO-EV in different cell types, cell viability was assessed in normal human hepatocytes (HH) and in HepG2, Hep3B, or PLC malignant hepatocyte cell lines after exposure to PBS, 4 μg/mL GO, GO-EV, or az-EV for 96 h. Although GO-EV did not reduce cell viability in HH cells, a reduction was observed in HepG2, Hep3B and PLC cells compared with PBS treated controls ($p < 0.05$, $p < 0.001$, $p < 0.001$, respectively) (**Figure 4**). Differences across cell lines were also noted, with Hep3B cells being the most sensitive to cytotoxic effects of GO-EV. These results suggest that cytotoxicity of GO-EV is cell type specific, with selective effects in malignant hepatocytes.

Synthetic approaches for GO can result in flakes of varying sizes. To evaluate whether these observed effects could reflect flake size, GO was first sonicated to prepare sonicated GO (sGO). Cell viability was assessed in HH, HepG2, and Hep3B cells treated with PBS, sGO, sGO-EV, and az-EV. Compared with controls, neither sGO nor sGO-EV altered cell viability in HH or HepG2 cells. However, sGO-EV, but not sGO treatment reduced viability in Hep3B cells after 96 h compared with PBS controls. These results suggest that exposure to GO-EV or sGO-EV can cause acute cytotoxicity in some HCC cell lines.

TABLE 1 | Size and protein characterization of unmodified and azide tagged MSC-EV.

	[Particles] (p/mL)	Average particle diameter (nm)	Protein concentration (μg/mL)
EV	8.03×10^{8}	221.8	1189.7
az-EV	9.58×10^{10}	224.3	1590.0

GO-EV and sGO-EV Do Not Induce DNA Damage

Since GO-EV and sGO-EV reduced the viability of several liver cancer cell lines, we performed an alkaline-based comet assay to determine if the GO-based biomaterials could induce DNA strand breaks (**Figure 5**). Suspension cells are more sensitive to GO-induced toxicity, and thus we selected HL-60 cells to evaluate the genotoxic potential of GO-EV and sGO-EV treatment. There was no DNA damage observed in HL-60 cells treated with 4 μg/mL GO-EV (**Figure 5**). Similarly, treatment with 4 μg/mL sGO-EV did not induce any considerable genotoxicity. On the contrary, treatment with 20 μM etoposide, which served as the positive control, induced noticeable DNA damage.

Biological Effects of GO-EV on Macrophages

Macrophage phagocytosis was assessed by time lapse photography of biomaterial uptake by RAW264.7 murine macrophages incubated with 50 μL of PKH67 stained GO-EV or sGO-EV. First, we observed that RAW264.7 could take up GO-EV by phagocytosis (**Figure 6**). Next, we assessed whether GO-EV would affect cell viability or proliferation. Compared with PBS treated controls, treatment with 4 μg/mL GO-EV slightly enhanced RAW264.7 cell proliferation at 96 h (data not shown). Similar changes were observed in cells treated with 4 μg/mL GO or az-EV. To elucidate the effects of GO-EV treatment on RAW264.7 activity, chemokine and cytokine production was assessed following incubation with PBS or 4 μg/mL GO-EV for 3 h (**Supplementary Table 2**). In comparison to the PBS treated controls, there was a greater than two-fold increase in the secretion of tumor necrosis factor-α (TNF-α; $p < 0.01$) and granulocyte-colony stimulating factor (G-CSF;

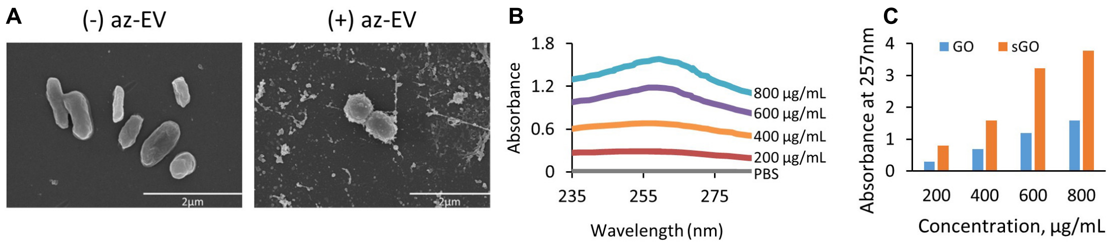

FIGURE 2 | Visualization and absorbance scanning of GO biomaterials. **(A)** Scanning electron microscopy images of GO and GO-EV were captured at 25 and 20 k magnification, respectively. **(B)** Absorbance scanning of GO dilutions over 200–300 nm revealed peak absorbance at 257 nm. **(C)** Absorbance of GO and sGO dilutions at 257 nm.

$p < 0.05$) in response to treatment with GO-EV. This suggests that exposure of RAW264.7 cells to GO-EV could induce the cells to differentiate into classically activated macrophages.

To confirm these findings and to evaluate the durability of TNF-α response, we performed a high sensitivity TNF-α assay in RAW264.7 cells incubated with PBS, 10 ng/mL lipopolysaccharide (LPS), 4 µg/mL GO, sGO, GO-EV, sGO-EV or az-EV for 24 h. In comparison to the PBS treated control cells, an increase in TNF-α secretion was observed in the RAW264.7 cells treated with GO, with levels similar to those observed with LPS ($p < 0.001$; **Figure 6D**). However, treatment with either GO-EV or az-EV alone did not increase TNF-α secretion. Similar to the effects observed in GO treated cells, sGO treatment also increased TNF-α secretion by RAW264.7 cells ($p < 0.001$). Similar increases in TNF-α secretion were also noted with sGO-EV (**Figure 6E**). These results indicated that the smaller-sized biomaterial elicit a more potent and longer-lasting immune response.

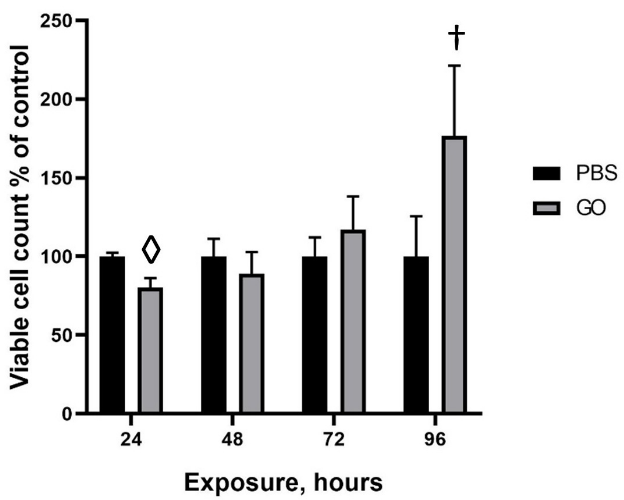

FIGURE 3 | Viability of HepG2 cells in response to GO exposure. To assess the cytotoxic effects of transient exposure of cells to GO-based biomaterials, HepG2 cells were treated with 0.4 µg GO, GO-EV, or EV and the viability was measured at 24, 48, 72, and 96 h post-treatment. The data depicted represents the mean ± SD; †$p < 0.05$, ◇$p < 0.0005$, relative to the control cells.

Developmental Toxicity of GO-EV Treatment

To determine if GO and sGO-based biomaterials have *in vivo* effects, we evaluated their toxicity using zebrafish. Dechorionation and hatching in zebrafish takes place between 48 and 72 hpf. First, we monitored the hatching rate of the zebrafish starting at 45 hpf. In comparison to vehicle treated control zebrafish, there was a modest delay in the hatching rates of the zebrafish treated with 100 µg/mLGO and GO-EV, conversely, the rates in zebrafish treated with 10 µg/mL EV were accelerated (**Figure 7**). A similar acceleration in hatching was observed in the zebrafish treated with 10 µg/mL sGO, whereas the zebrafish treated with 10 µg/mL sGO-EV, 100 µg/mL sGO and 100 µg/mL sGO-EV all exhibited delayed hatching rates (**Supplementary Figure 1**). Next, we evaluated for the development of any malformations. In zebrafish exposed to GO-EV, yolk sac edema and pericardial edema were observed. Pericardial edema was also observed in the zebrafish treated with either low or high concentrations of sGO-EV. On the contrary, there were no malformations observed in the zebrafish treated with PBS, GO, or sGO at either 10 or 100 µg/mL. The heart rate varied considerably at different time points, but we did not observe any trends toward decreased heart rate in any treatment groups (data not shown). We further assessed survival of zebrafish at 168 hpf. A slight increase in mortality was observed in zebrafish treated with GO-EV, and with higher concentrations of sGO or sGO-EV but there was no lethality observed in zebrafish treated with PBS, GO or lower concentrations of sGO.

DISCUSSION

In the present study we have developed a graphene oxide-based biomaterial synthesized by copper-catalyzed cycloaddition of azide tagged bone marrow derived-MSC-EV to alkyne functionalized graphene oxide. This novel biomaterial offers the ability to combine the structural physicochemical benefits of graphene with the biological effects of MSC-EV. MSC-EV retain the intrinsic therapeutic properties of their parent cells and have shown to be effective in promoting tissue repair and regeneration, mitigating oxidative stress and modulating immune cell activities.

The utility of MSC-EV as acellular therapeutics is being increasingly recognized. Their use is enhanced by several

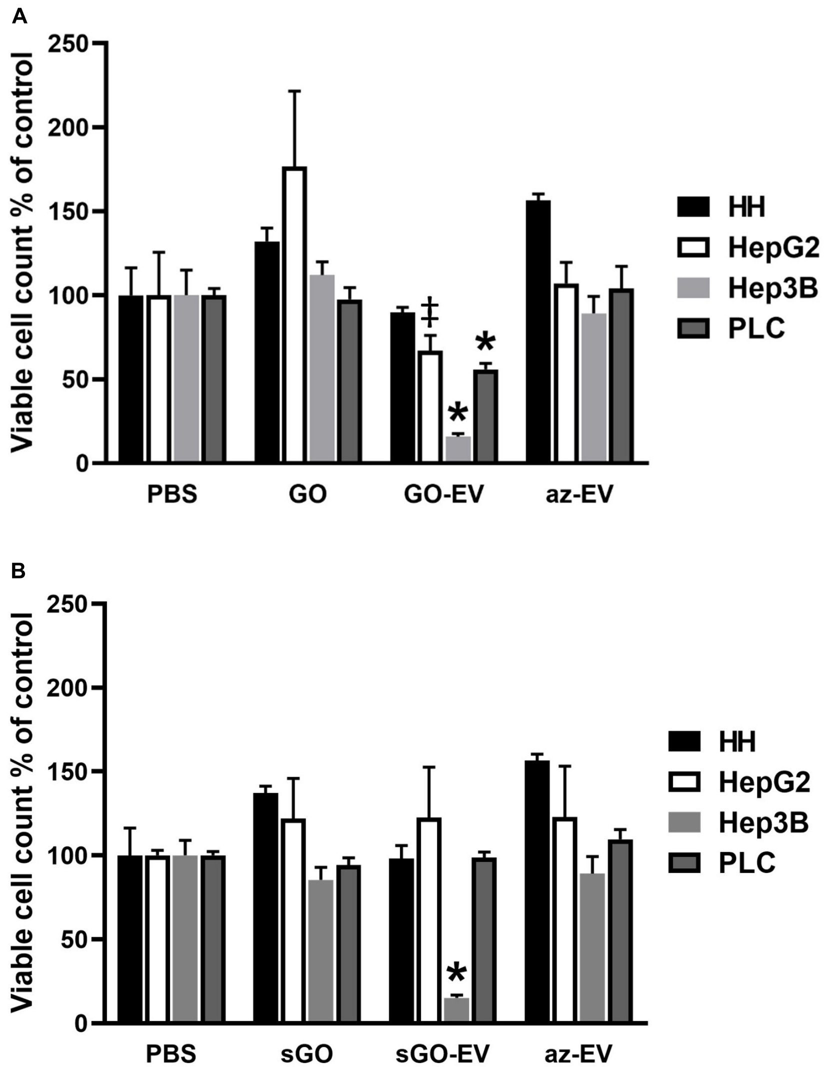

FIGURE 4 | Cytotoxicity of GO-EV and sGO-EV. Healthy human hepatocytes (HH) as well as three malignant hepatocyte cell lines (HepG2, Hep3B and PLC) were incubated with PBS, 4 μg/ml GO, GO-EV, sGO, sGO-EV and az-EV. At 96 h post-treatment the viability of the cells treated with **(A)** GO- and **(B)** sGO-based biomaterials was evaluated by an MTS assay. The data represents the average ± SD. $^{‡}p < 0.05$, $^{*}p < 0.001$ relative to PBS vehicle control.

properties. Their cargo can be altered by exogenous loading to selectively enrich them with modulatory agents such as antisense oligonucleotides (George et al., 2018), miRNAs (Pomatto et al., 2019) or siRNAs (Matsuda et al., 2019). In addition, selective manipulation of their content is feasible through genetic engineering of donor cells to express RNA or proteins of interest. Moreover, their surface can be engineered to express specific markers that facilitate tissue- or cell-targeted delivery of the EV. Furthermore, their cellular production can be modulated by microenvironmental perturbations (Yan et al., 2017; Zhang et al., 2020). Of particular therapeutic relevance, MSC-EV also retain an ability to home to sites of inflammation and injury, similar to their parental cells (Lai et al., 2013). For all of these reasons, MSC-EV are attractive acellular therapeutics as well as therapeutic delivery vehicles with the capacity for targeted delivery of bioactive therapeutic molecules.

The unique physicochemical properties and adaptability of graphene makes it attractive for development as a theranostic nanomaterial. Several biomedical applications such as drug and nucleic acid delivery, biosensing, photothermal, photodynamic therapy and tissue engineering have been proposed for graphene and its derivatives such as GO and rGO (Robinson et al., 2011; Hu et al., 2012; Lee et al., 2016; Shin et al., 2016; Vinothini et al., 2019). The oxygen-containing functional groups in GO and rGO contribute to their overall colloidal stability in aqueous solutions. These derivatives are often conjugated to polymers or other biomolecules in order to mitigate membrane-damaging effects or the effects of oxidative stress. Similarly, the conjugation of MSC-EV to GO may permit additional properties that can be exploited toward broader potential biomedical applications. The MSC-EV cargo contains a variety of bioactive molecules that can work alone, or in concert, to elicit a therapeutic effect

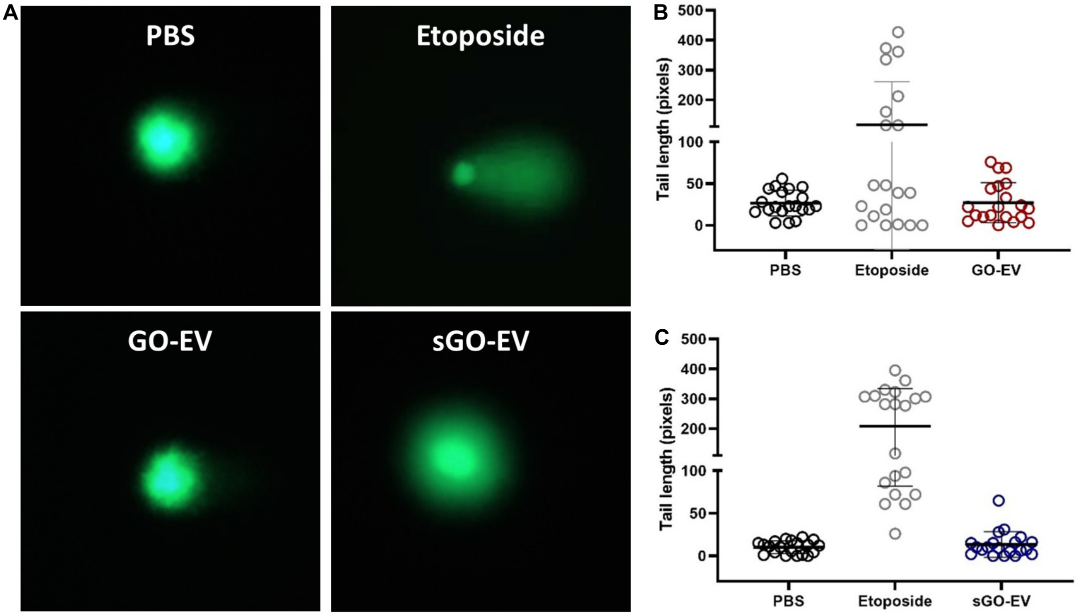

FIGURE 5 | GO-EV does not induce DNA damage. HL-60 cells were treated with PBS (control), 4 μg/ml GO-EV or sGO-EV for 24 h, or 20 μm etoposide (positive control) for 1 h. An alkaline-based comet assay was performed at the treatment end point to assess for the presence of DNA breaks. Images of the DNA tails were captured by fluorescence microscopy **(A)** and the average tail length **(B,C)** was calculated for each treatment condition using the OpenComet software. The lines mark the average DNA tail length for each population.

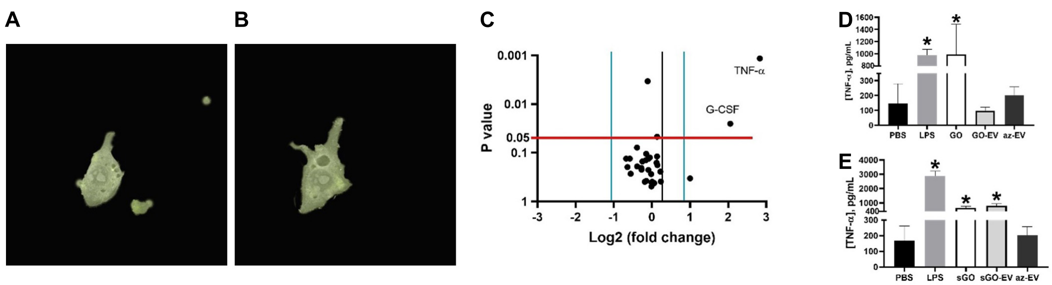

FIGURE 6 | Effects of GO-EV on macrophages. **(A)** Time-lapse imaging of RAW264.7 murine macrophages incubated with PKH67 labeled GO-EV was performed. Images were captured **(A)** before uptake, and every 5 min following the addition of GO-EV to the cells. Imaging was ceased once the biomaterial was **(B)** successfully internalized by the RAW264.7 cells. Extracellular background masks were applied to the image. **(C)** RAW264.7 cells were incubated with PBS or 4 μg/ml GO-EV. After 3 h, conditioned media was collected, and assays were performed to determine protein concentrations for a panel of 31 chemokines or cytokines. Proteins with a log-two-fold or more change in concentration in response to GO-EV treatment were identified. A TNF-α ELISA was performed to quantify the TNF-α secretion by RAW264.7 cells treated with **(D)** GO- and **(E)** sGO-based biomaterials. RAW264.7 cells were treated with PBS, 10 ng LPS, 0.4 μg GO, sGO, GO-EV, sGO-EV, or az-EV for 24 h. Data represents average ± SD, $^{*}p < 0.001$.

(Liang et al., 2016; Yan et al., 2017). The modifiability of the EV cargo and the EV surface profile can contribute to achieve the desired biological effects in a targeted fashion (Ye et al., 2018). Furthermore, considering that EV and GO are internalized by different mechanisms, conjugation of EV to GO could enhance GO uptake by recipient cells (Huang et al., 2012; McKelvey et al., 2015). Thus, the biological effects of MSC-EV such as reducing tissue injury can be coupled with physical, biochemical or structural functionalities offered by graphene.

An advantage of conjugation of EV to GO allows exploitation of the properties of graphene, such as surface modifications for additional functional properties. For example, cytotoxic effects of GO-EV could be augmented by loading chemotherapeutic that are released in a pH-responsive manner in tumor settings (Ardeshirzadeh et al., 2015; Wang et al., 2019). Other potential applications may involve fashioning the GO-EV as a structural biomolecule for implantation as an extracellular scaffold within tissues such as bone or teeth, or within endoprostheses and stents placed in the body (Diomede et al., 2018; Li et al., 2018). In this context, the ability to selectively load MSC-EV exogenously after isolation, or endogenously through genetic or protein manipulation of the parental cells offer the potential ability to use GO-EV as a therapeutic delivery platform. For such applications, further studies to determine the kinetics of EV release from

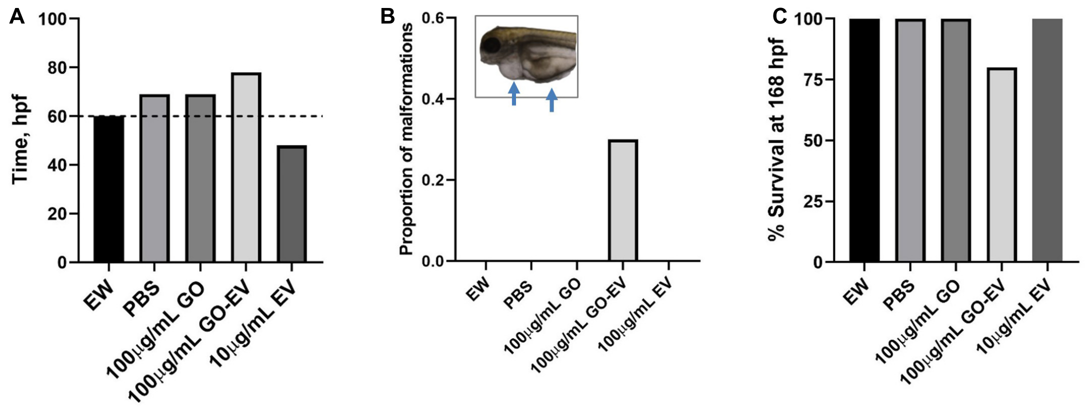

FIGURE 7 | Developmental toxicity of GO-EV in zebrafish. At 24 h post-fertilization (hpf) zebrafish (n = 10) were incubated in embryo water (EW) alone or EW containing 100 μg/mL GO, 100 μg/mL GO-EV or 10 μg/mL EV every 24 h for a total of 168 h. **(A)** The time at which 70% of the zebrafish hatched following treatment with GO-based biomaterials was recorded from 45 to 85 hpf. **(B)** The zebrafish treated with GO-based biomaterials were monitored for the development of any malformations and the proportion of malformations present in each treatment group was calculated. Pericardial and/or yolk sac edema was observed in some zebrafish treated with GO-EV. **(C)** The survival of the zebrafish treated with GO-based biomaterials was recorded at 168 hpf.

GO-EV would be valuable to determine whether controlled release of MSC-EV can be accomplished for therapeutic benefit.

The paucity of developmental or genotoxic effects of the GO-EV biomaterial paves the way for development of further applications in tissue engineering and regenerative medicine. Within the context of bone tissue engineering, GO elicits pro-osteoneogenic effects *in vitro* and *in vivo* (Hermenean et al., 2017). BM MSC-EV cargo has been shown to be enriched in several pro-osteogenic miRNAs (Ardeshirzadeh et al., 2015). Thus, GO-EV could augment the osteoinductive effects observed with GO. We observed variable effects on cytotoxicity of GO-EV and sGO-EV in liver cancer cell lines, though minimal cytotoxicity was observed in healthy hepatocytes. Notably, no genotoxicity was observed. Moreover, we did not detect any significant developmental toxicity in zebrafish. sGO-EV and GO-EV are readily recognized and phagocytosed by macrophages. Following their internalization by RAW264.7 cells, an alteration in the secretome profile with enhanced secretion of the pro-inflammatory cytokine, TNF-α was observed. The immunological impact of these biomaterials warrants further evaluation. Biocompatibility *in vivo* could be improved via the conjugation of GO with polymers that are capable of being cleaved upon internalization of the biomaterial to prevent the adverse accumulation of GO in cells (Li et al., 2014). Additional surface modifications may further reduce undesirable immune effects observed in our *in vitro* study.

This study developed a process for fabrication of a graphene-based biomaterial incorporating MSC-EV and examined their cytotoxicity and immunologic effects *in vitro* and developmental toxicity effects *in vivo*. GO-EV induced an inflammatory response and cell-specific cytotoxicity. While some developmental malformations were observed, these had a minimal impact on overall survival in zebrafish. There are opportunities to further improve the biocompatibility of GO-EV. For example, variable effects of cytotoxicity have been observed with GO in different study settings. Cytotoxicity can be influenced by the flake size and the degree of oxygenation of GO, with the smaller and more oxygenated forms of GO eliciting more potent cytotoxic effects (Pelin et al., 2017; Gurunathan et al., 2019). Differences in GO induced cytotoxicity have been observed between different malignant and non-malignant cells (Fiorillo et al., 2015). Attention to optimized approaches and selection of base materials is warranted in future studies because cytotoxic effects could be impacted by the physical differences in the lateral dimensions and overall shapes of graphene noted between top-down and bottom-up synthetic approaches (Lee et al., 2019). Such efforts are warranted to take full advantage of the use of GO-EV as a functional biomaterial that combines the versatility of graphene with the intrinsic therapeutic effects of cell derived EV for the development of biomedical applications.

DATA AVAILABILITY STATEMENT

The original contributions presented in the study are included in the article/**Supplementary Material**, further inquiries can be directed to the corresponding author/s.

ETHICS STATEMENT

The animal study was reviewed and approved by the Mayo Clinic Institutional Animal Care and Use Committee.

AUTHOR CONTRIBUTIONS

TP contributed to the conception of the study and acquired the funding and resources. TP, JD, AM, and IY designed the methodology. JD, AM, and IY performed the experiments. JD and AM formally analyzed and curated the data. TP and JD wrote the original draft and revised and edited the manuscript. All authors contributed to the article and approved the submitted version.

ACKNOWLEDGMENTS

We acknowledge funding support by the National Institutes of Health (RO1CA217833) and the Mayo Foundation and helpful discussions by members of the TP laboratory.

SUPPLEMENTARY MATERIAL

The Supplementary Material for this article can be found online at: https://www.frontiersin.org/articles/10.3389/fbioe.2021.686510/full#supplementary-material

REFERENCES

Ardeshirzadeh, B., Anaraki, N. A., Irani, M., Rad, L. R., and Shamshiri, S. (2015). Controlled release of doxorubicin from electrospun PEO/chitosan/graphene oxide nanocomposite nanofibrous scaffolds. *Mater. Sci. Eng. C Mater. Biol. Appl.* 48, 384–390. doi: 10.1016/j.msec.2014.12.039

Campbell, E., Hasan, M. T., Pho, C., Callaghan, K., Akkaraju, G.R., and Naumov, A. V. (2019). Graphene oxide as a multifunctional platform for intracellular delivery, imaging, and cancer sensing. *Sci. Rep.* 9:416. doi: 10.1038/s41598-018-36617-4

Diomede, F., Gugliandolo, A., Cardelli, P., Merciaro, I., Ettorre, V., Traini, T., et al. (2018). Three-dimensional printed PLA scaffold and human gingival stem cell-derived extracellular vesicles: a new tool for bone defect repair. *Stem Cell Res. Ther.* 9:104. doi: 10.1186/s13287-018-0850-0

Fiorillo, M., Verre, A. F., Iliut, M., Peiris-Pagés, M., Ozsvari, B., Gandara, R., et al. (2015). Graphene oxide selectively targets cancer stem cells, across multiple tumor types: implications for non-toxic cancer treatment, via "differentiation-based nano-therapy". *Oncotarget* 6, 3553–3562. doi: 10.18632/oncotarget.3348

Geim, A. K. (2009). Graphene: status and prospects. *Science* 324, 1530–1534. doi: 10.1126/science.1158877

George, J., Yan, I. K., and Patel, T. (2018). Nanovesicle-mediated delivery of anticancer agents effectively induced cell death and regressed intrahepatic tumors in athymic mice. *Lab. Invest.* 98, 895–910. doi: 10.1038/s41374-018-0053-4

Gurunathan, S., Kang, M. H., Jeyaraj, M., and Kim, J. H. (2019). Differential Cytotoxicity of Different Sizes of Graphene Oxide Nanoparticles in Leydig (TM3) and Sertoli (TM4) Cells. *Nanomaterials (Basel)* 9:139. doi: 10.3390/nano9020139

Haga, H., Yan, I. K., Borrelli, D. A., Matsuda, A., Parasramka, M., Shukla, N., et al. (2017). Extracellular vesicles from bone marrow-derived mesenchymal stem cells protect against murine hepatic ischemia/reperfusion injury. *Liver Transpl.* 23, 791–803. doi: 10.1002/lt.24770

Hermenean, A., Codreanu, A., Herman, H., Balta, C., Rosu, M., Mihali, C. V., et al. (2017). Chitosan-graphene oxide 3D scaffolds as promising tools for bone regeneration in critical-size mouse calvarial defects. *Sci. Rep.* 7:16641. doi: 10.1038/s41598-017-16599-5

Hu, Z., Huang, Y., Shun, S., Guan, W., Yan, Y., Tang, P., et al. (2012). Visible light drive photodynamic anticancer activity of graphene oxide/TiO2 hybrid. *Carbon* 50, 994–1004.

Huang, J., Zong, C., Shen, H., Liu, M., Chen, B., Ren, B., et al. (2012). Mechanism of cellular uptake of graphene oxide studied by surface-enhanced Raman spectroscopy. *Small* 8, 2577–2584. doi: 10.1002/smll.201102743

Lai, R. C., Yeo, R. W., Tan, K. H., and Lim, S. K. (2013). Exosomes for drug delivery - a novel application for the mesenchymal stem cell. *Biotechnol. Adv.* 31, 543–551. doi: 10.1016/j.biotechadv.2012.08.008

Lee, J., Kim, J., Kim, S., and Min, D. H. (2016). Biosensors based on graphene oxide and its biomedical application. *Adv. Drug Deliv. Rev.* 105(Pt B), 275–287. doi: 10.1016/j.addr.2016.06.001

Lee, X. J., Hiew, B. Y. Z., Lai, K. C., Lee, L. Y., Gan, S., Thangalazhy-Gopakumar, S., et al. (2019). Review on graphene and its derivatives: Synthesis methods and potential industrial implementation. *J. Taiwan Inst. Chem. Eng.* 98, 163–180.

Li, W., Liu, Y., Zhang, P., Tang, Y., Zhou, M., Jiang, W., et al. (2018). Tissue-engineered bone immobilized with human adipose stem cells-derived exosomes promotes bone regeneration. *ACS Appl. Mater. Interfaces* 10, 5240–5254. doi: 10.1021/acsami.7b17620

Li, Y., Feng, L., Shi, X., Wang, X., Yang, Y., Yang, K., et al. (2014). Surface coating-dependent cytotoxicity and degradation of graphene derivatives: towards the design of non-toxic, degradable nano-graphene. *Small* 10, 1544–1554. doi: 10.1002/smll.201303234

Liang, X., Zhang, L., Wang, S., Han, Q., and Zhao, R. C. (2016). Exosomes secreted by mesenchymal stem cells promote endothelial cell angiogenesis by transferring miR-125a. *J. Cell Sci.* 129, 2182–2189. doi: 10.1242/jcs.170373

Matsuda, A., Ishiguro, K., Yan, I. K., and Patel, T. (2019). Extracellular vesicle-based therapeutic targeting of β-Catenin to modulate anticancer immune responses in hepatocellular cancer. *Hepatol. Commun.* 3, 525–541. doi: 10.1002/hep4.1311

McKelvey, K. J., Powell, K. L., Ashton, A. W., Morris, J. M., and McCracken, S. A. (2015). Exosomes: mechanisms of uptake. *J. Circ. Biomark.* 4:7. doi: 10.5772/61186

Mei, K. C., Rubio, N., Costa, P. M., Kafa, H., Abbate, V., Festy, F., et al. (2015). Synthesis of double-clickable functionalised graphene oxide for biological applications. *Chem. Commun. (Camb)* 51, 14981–14984. doi: 10.1039/c5cc05412e

Pelin, M., Fusco, L., León, V., Martín, C., Criado, A., Sosa, S., et al. (2017). Differential cytotoxic effects of graphene and graphene oxide on skin keratinocytes. *Sci. Rep.* 7:40572. doi: 10.1038/srep40572

Pomatto, M. A. C., Bussolati, B., D'Antico, S., Ghiotto, S., Tetta, C., Brizzi, M. F., et al. (2019). Improved loading of plasma-derived extracellular vesicles to encapsulate antitumor miRNAs. *Mol. Ther. Methods Clin. Dev.* 13, 133–144. doi: 10.1016/j.omtm.2019.01.001

Reis, L. A., Borges, F. T., Simões, M. J., Borges, A. A., Sinigaglia-Coimbra, R., and Schor, N. (2012). Bone marrow-derived mesenchymal stem cells repaired but did not prevent gentamicin-induced acute kidney injury through paracrine effects in rats. *PLoS One* 7:e44092. doi: 10.1371/journal.pone.0044092

Robinson, J. T., Tabakman, S. M., Liang, Y., Wang, H., Casalongue, H. S., Vinh, D., et al. (2011). Ultrasmall reduced graphene oxide with high near-infrared absorbance for photothermal therapy. *J. Am. Chem. Soc.* 133, 6825–6831. doi: 10.1021/ja2010175

Shin, S. R., Li, Y. C., Jang, H. L., Khoshakhlagh, P., Akbari, M., Nasajpour, A., et al. (2016). Graphene-based materials for tissue engineering. *Adv. Drug Deliv. Rev.* 105(Pt B), 255–274. doi: 10.1016/j.addr.2016.03.007

Tian, Y., Li, S., Song, J., Ji, T., Zhu, M., Anderson, G. J., et al. (2014). A doxorubicin delivery platform using engineered natural membrane vesicle exosomes for targeted tumor therapy. *Biomaterials* 35, 2383–2390. doi: 10.1016/j.biomaterials.2013.11.083

Vinothini, K., Rajendran, N. K., Munusamy, M. A., Alarfaj, A. A., and Rajan, M. (2019). Development of biotin molecule targeted cancer cell drug delivery of doxorubicin loaded κ-carrageenan grafted graphene oxide nanocarrier. *Mater. Sci. Eng. C Mater. Biol. Appl.* 100, 676–687. doi: 10.1016/j.msec.2019.03.011

Wang, S. B., Ma, Y. Y., Chen, X. Y., Zhao, Y. Y., and Mou, X. Z. (2019). Ceramide-graphene oxide nanoparticles enhance cytotoxicity and decrease HCC xenograft development: a novel approach for targeted cancer therapy. *Front. Pharmacol.* 10:69. doi: 10.3389/fphar.2019.00069

Xu, M., Zhu, J., Wang, F., Xiong, Y., Wu, Y., Wang, Q., et al. (2016). Improved in vitro and in vivo biocompatibility of graphene oxide through surface modification: poly(Acrylic Acid)-functionalization is superior to PEGylation. *ACS Nano* 10, 3267–3281. doi: 10.1021/acsnano.6b00539

Yan, Y., Jiang, W., Tan, Y., Zou, S., Zhang, H., Mao, F., et al. (2017). hucMSC exosome-derived GPX1 is required for the recovery of hepatic oxidant injury. *Mol. Ther.* 25, 465–479. doi: 10.1016/j.ymthe.2016.11.019

Yáñez-Mó, M., Siljander, P. R., Andreu, Z., Zavec, A. B., Borràs, F. E., Buzas, E. I., et al. (2015). Biological properties of extracellular vesicles and their physiological functions. *J. Extracell. Vesicles* 4:27066. doi: 10.3402/jev.v4.27066

Yang, J., Liu, X. X., Fan, H., Tang, Q., Shou, Z. X., Zuo, D. M., et al. (2015). Extracellular vesicles derived from bone marrow mesenchymal stem cells protect against experimental colitis via attenuating colon inflammation, oxidative stress and apoptosis. *PLoS One* 10:e0140551. doi: 10.1371/journal.pone.0140551

Ye, Z., Zhang, T., He, W., Jin, H., Liu, C., Yang, Z., et al. (2018). Methotrexate-loaded extracellular vesicles functionalized with therapeutic and targeted peptides for the treatment of glioblastoma multiforme. *ACS Appl. Mater. Interfaces* 10, 12341–12350. doi: 10.1021/acsami.7b18135

Zhang, S., Jiang, L., Hu, H., Wang, H., Wang, X., Jiang, J., et al. (2020). Pretreatment of exosomes derived from hUCMSCs with TNF-α ameliorates acute liver failure by inhibiting the activation of NLRP3 in macrophage. *Life Sci.* 246:117401. doi: 10.1016/j.lfs.2020.117401

Zheng, X. T., Ma, X. Q., and Li, C. M. (2016). Highly efficient nuclear delivery of anti-cancer drugs using a bio-functionalized reduced graphene oxide. *J. Colloid Interface Sci.* 467, 35–42. doi: 10.1016/j.jcis.2015.12.052

Conflict of Interest: The authors declare that the research was conducted in the absence of any commercial or financial relationships that could be construed as a potential conflict of interest.

Copyright © 2021 Driscoll, Moirangthem, Yan and Patel. This is an open-access article distributed under the terms of the Creative Commons Attribution License (CC BY). The use, distribution or reproduction in other forums is permitted, provided the original author(s) and the copyright owner(s) are credited and that the original publication in this journal is cited, in accordance with accepted academic practice. No use, distribution or reproduction is permitted which does not comply with these terms.

frontiers in Bioengineering and Biotechnology

ORIGINAL RESEARCH
published: 25 August 2021
doi: 10.3389/fbioe.2021.703241

Extracellular Vesicles Derived From Human Umbilical Cord Mesenchymal Stem Cells Protect Against DOX-Induced Heart Failure Through the miR-100-5p/NOX4 Pathway

Zhenglong Zhong†, Yuqing Tian†, Xiaoming Luo, Jianjie Zou, Lin Wu and Julong Tian**

Department of Cardiology, Affiliated Hospital of Panzhihua University, Panzhihua, China

OPEN ACCESS

Edited by:
Enrico Ragni, Galeazzi Orthopedic Institute (IRCCS), Italy

Reviewed by:
Monica Reis, University of Edinburgh, United Kingdom
Andrea Mohr, University of Essex, United Kingdom

***Correspondence:**
Lin Wu
linwu71ch@yahoo.com
Julong Tian
551333202@qq.com

†These authors have contributed equally to this work

Received: 30 April 2021
Accepted: 12 July 2021
Published: 25 August 2021

Citation:
Zhong Z, Tian Y, Luo X, Zou J, Wu L and Tian J (2021) Extracellular Vesicles Derived From Human Umbilical Cord Mesenchymal Stem Cells Protect Against DOX-Induced Heart Failure Through the miR-100-5p/NOX4 Pathway. Front. Bioeng. Biotechnol. 9:703241. doi: 10.3389/fbioe.2021.703241

The end result of a variety of cardiovascular diseases is heart failure. Heart failure patients' morbidity and mortality rates are increasing year after year. Extracellular vesicles (EVs) derived from human umbilical cord mesenchymal stem cells (HucMSC-EVs) have recently been discovered to be an alternative treatment for heart failure, according to recent research. In this study, we aimed to explore the underlying mechanisms in which HucMSC-EVs inhibited doxorubicin (DOX)-induced heart failure in AC16 cells. An miR-100-5p inhibitor and an miR-100-5p mimic were used to transfect HucMSCs using Lipofectamine 2000. HucMSC-EVs were isolated and purified using the ultracentrifugation method. AC16 cells were treated with DOX combined with HucMSC-EVs or an EV miR-100-5-p inhibitor or EV miR-100-5-p mimic. ROS levels were measured by a flow cytometer. The levels of LDH, SOD, and MDA were measured by biochemical methods. Apoptotic cells were assessed by a flow cytometer. Cleaved-caspase-3 and NOX4 protein expression were determined by Western blot. The experiment results showed that HucMSC-EVs inhibited DOX-induced increased levels of ROS, LDH, and MDA, and decreased levels of SOD which were reversed by an EV miR-100-5-p inhibitor, while EV miR-100-5-p mimic had a similar effect to HucMSC-EVs. At the same time, HucMSC-EV-inhibited DOX induced the increases of apoptotic cells as well as NOX4 and cleaved-caspase-3 protein expression, which were reversed by an EV miR-100-5-p inhibitor. Furthermore, the NOX4 expression was negatively regulated by miR-100-5p. Overexpression of NOX4 abolished the effects in which HucMSC-EVs inhibited DOX-induced ROS, oxidative stress, and apoptosis increases. In conclusion, these results indicate that HucMSC-EVs inhibit DOX-induced heart failure through the miR-100-5p/NOX4 pathway.

Keywords: oxidative stress, miR-100-5p, NOX4, heart failure, human umbilical cord mesenchymal stem cells, extracellular vesicles

INTRODUCTION

Heart failure is the final result of various cardiovascular diseases, among which the most common causes include coronary heart disease, hypertension, cardiomyopathy, and valvular heart disease. Its morbidity and mortality are gradually increasing year by year, posing a serious threat to human health. Mesenchymal stem cells (MSCs) are a type of pluripotent stem cells with multiple differentiation potentials that implant in the mesoderm (Jaquet et al., 2005). MSCs can be derived from the bone marrow, placenta, adipose tissue, umbilical cord blood, *etc*. Human umbilical cord mesenchymal stem cells (HucMSCs) are easier to obtain and have proliferation and immunosuppressive effects. In addition, there are no ethical issues for HucMSCs in clinical applications (Li et al., 2018; Guan et al., 2019; Xie et al., 2020). HucMSCs are used to increase the number of cardiomyocytes with contractile function, thereby improving heart failure caused by various reasons (Bartolucci et al., 2017; Mao et al., 2017; Kobayashi et al., 2018; Matsushita, 2020).

Paracrine function is the main way for mesenchymal stem cells to exert therapeutic effects. As one of the main components of paracrine, EVs include mRNA, miRNA, circRNA, protein, and other functional molecules, which not only participate in the regulation of cell proliferation and survival but also play an important role in signal transmission and cell communication (Keerthikumar et al., 2016; Tkach and Théry, 2016). EVs are formed by eukaryotic cells through endocytosis of some signal molecules to form multivesicular endosomes, and then fused with the cell membrane and released into nanovesicles in the extracellular environment. EVs contain different kinds of lipids, proteins, RNAs, and other biologically active molecules, which play a variety of biological functions. EVs have been proven to be an important medium for MSCs to exert therapeutic effects. They can enter the cytoplasm through endocytosis or direct fusion with the cell membrane, or through receptor–ligand interactions, to transmit biological information to target cells, thereby exerting biological functions and regulating abnormal microenvironment (Davidson and Yellon, 2018; Balbi and Vassalli, 2020). Recent studies have shown that MSC-derived EVs (MSC-EVs) are expected to become a new alternative to stem cell therapy for heart failure (Fang et al., 2016).

DOX is an antitumor drug widely used clinically. It has a good effect on many tumors. However, DOX has very serious cardiotoxicity and finally leads to heart failure. DOX-induced cardiotoxicity can be used as an *in vitro* model to summarize the mechanism of heart failure. The application of the *in vitro* cardiotoxicity test system can greatly help understand the development of heart failure (Sachinidis, 2020). In this study, the effects of HucMSC-EVs on DOX-induced heart failure were studied. The aim of this study was to explore the molecular mechanism of HucMSC-EVs inhibiting DOX-induced heart failure.

MATERIALS AND METHODS

Cell Culture

Human AC16 cells were obtained from ATCC (Manassas, VA, United States) and cultured in a DMEM medium (Hyclone, SH30243.01, Logan, UT, United States) supplemented with 10% fetal bovine serum (Gibco, 16000e044, Carlsbad, CA, United States) and 1% penicillin–streptomycin (Solarbio, P1400, Beijing, China) and incubated at 37°C with 5% CO_2. AC16 cells were treated with 2 μmol/L DOX (Sigma-Aldrich, 25316-40-9, Shanghai, China) and HucMSC-EVs in different concentrations for 24 h.

Human Umbilical Cord Mesenchymal Stem Cell Characterization

HucMSCs were provided by Stem Cell Bank, Chinese Academy of Sciences and cultured in serum-free MSC NutriStem® XF Medium (Biological Industries, Beit HaEmek, Israel). When the cells grew to 80–90% confluence, they were digested with 0.25% trypsin containing 0.01% EDTA. The cells were resuspended in PBS and adjusted to 1×10^6 cells/ml. The mouse antihuman CD34, CD45, CD44, and CD105 were added and incubated at 4°C in dark for 15–30 min. Surface antigens of MSCs were characterized by using a Beckman CytoFLEX flow cytometer (Beckman Coulter Life Sciences, Tokyo, Japan) and the Human MSC Analysis Kit (BD Biosciences, San Jose, CA, United States).

Isolation and Characterization of Extracellular Vesicles

HucMSCs were cultured in EV-free production medium for 24–48 h before conditioned medium was collected. EVs were isolated and purified by ultracentrifugation according to the protocol (Théry et al., 2006). The morphology of isolated HucMSC-EVs was observed by transmission electron microscopy (FEI Tecnai G2 Spirit Twin, Philips, NL). The TSG101 and CD81 protein markers of EVs were detected by Western blot.

Extracellular Vesicle Uptake Assay

PKH67 EV green fluorescent dye (UR52303, Umibio, China) was used to trace EVs being endocytosed by AC16 cells. In brief, EVs were stained with PKH67 dying working solution, in which the PKH liker was mixed with diluent C at a ratio of 1:9 in dark at room temperature. Then they were mixed well and incubated for 10 min in dark. The labeled EVs were incubated on AC16 cells for 24 h at 37°C, and cells were washed with 1 × PBS. Cells were mounted in a mounting medium containing DAPI (4′,6-diamidino-2-phenylindole dihydrochloride) (DAPI-Fluoromount-GTM, Yeasen Biotechnology, Shanghai, China). A laser-scanning confocal microscope was applied to take all of the images (Youn et al., 2019).

Cell Transfection

The coding region of NOX4 (NM_001143837.2) was cloned into pCDNA3.1 (+) plasmids (Clontech, Mountain View, CA, United States) at Hind III and EcoR1 sites. It was designated to oeNOX4. oeNOX4 was transfected to AC16 cells using Lipofectamine 2000 Kit (Invitrogen, Carlsbad, CA, United States). The negative control included cells with blank vector pCDNA3.1 (+) transfection. The primers used for amplification of the coding sequence of NOX4 were as follows:

NOX4-F:5′-CCCAAGCTTATGAATGTCCTGCTTTTCTGGAAAAC-3’ (Hind III)

NOX4-R: 5′-CGGAATTCTCAGCTGAAAGACTCTTTATTGTATTC-3’ (EcoR I)

miRNA Transfection

miR-100-5p mimic (5′-AACCCGUAGAUCCGAACUUGUG-3′), miR-100-5p inhibitor (5′-CACAAGUUCGGAUCUACGGGUU-3′), and negative control (NC, 5′-CAGUACUUUUGUGUAGUACAA-3′) were synthesized by Beyotime (Beijing, China) and transfected to cells with Lipofectamine 2000 Kit individually.

Luciferase Reporter Assay

The NOX4 reporter gene plasmid is constructed by gene synthesis. The NOX4 (NM_001143837.2) sequence was found in NCBI. According to the NOX4 3′-UTR sequence, wild-type and mutant NOX4 3′-UTR sequences with Sac I and Xho I sticky ends were synthesized. The mutation site was based on the binding site of hsa-miR-100-5p and NOX4 3′-UTR sequence. The NOX4 3′-UTR binding site sequence containing mutation was inserted into the vector pGL3-promoter through Sac I and Xho I restriction sites to construct pGL3-Promoter-mutNOX4 3′-UTR. Wild-type NOX4 3′-UTR was inserted into the vector pGL3-Promoter through Sac I and Xho I restriction sites to construct pGL3-Promoter-wtNOX4-3′-UTR. PGL3-Promoter vector had firefly fluorescent gene (luc2) and pRL-TK with Renilla fluorescent gene (hRluc). A map of the predicted binding site of hsa-miR-100-5p to NOX4 and mutant was as following.

hsa-miR-100-5p	5′ GCCUAGAUGCCCAA 3′
–	|||||||
wtNOX4-3′-UTR	5′ TATTGATACGGGTACT 3′
mutNOX4-3′-UTR	5′ TATTGAGCATTAGCCT 3

293T cells were then co-transfected with miR-100-5p inhibitor, miR-100-5p mimic and pGL3-NOX4-WT or miR-100-5p inhibitor, miR-100-5p mimic, and pGL3-NOX4-MUT plasmids. After transfection, the cells were treated with a Dual-Luciferase Reporter Gene Detection System Test Kit. The firefly luciferase activity and Renilla luciferase activity were detected by a microplate reader. Luciferase activity ratio in this study was the ratio of the firefly luciferase activity to Renilla luciferase activity.

ROS Detection

A dichlorodihydrofluorescein diacetate (DCFH-DA) fluorescent probe (Sigma-Aldrich, D6883, Shanghai, China) combined with the flow cytometric analysis was used to detect the changes of reactive oxygen species (ROS) levels. The reactive oxygen species in the cell can oxidize nonfluorescent DCFH to produce fluorescent DCF. By detecting the fluorescence of DCF, the level of reactive oxygen species in the cell can be known. According to the production of red fluorescence in living cells, the amount and change of the cell ROS content can be judged. Briefly, AC16 cells were resuspended in 1x PBS, and the density was adjusted to 5×10^5 cells/ml. AC16 cells were then incubated with 10 μM DCFH-DA for 20 min in dark at 37°C and subsequently subjected to the flow cytometric analysis (Shi et al., 2016).

Cell Apoptosis

AC16 cells were seeded in 6-well plates with 1×10^5 per well and cultured for 12–24 h before use. AC16 cells were harvested 24 h after being treated with DOX combined with HucMSC-EVs or EV miR-100-5-p inhibitor or oeNOX4. Cells were prepared with the Annexin V-FITC Apoptosis Detection Kit (Beyotime, C1062s, Beijing, China) according to the manufacturer's recommendations. Briefly, AC16 cells were centrifuged at 1,000 g for 5 min and resuspended to a concentration of 1×10^6 cells/ml. 1×10^6 resuspended cells were centrifuged at 1,000 g for 5 min. The supernatant was discarded, and 195 μL of Annexin V-FITC binding solution was added to gently resuspend the cells. And 10 μL of Annexin V-FITC was added and mixed gently. Then 5 μL of propidium iodide staining solution was added to the mix gently. The cell suspension was gently vortexed and incubated in dark at room temperature for 15 min, and then placed in an ice bath. At the same time, a tube without Annexin V-FITC and PI was used as a negative control. Flow cytometry was performed within 1 h. The following method was used: The Annexin V-negative/PI-negative part represented viable cells. The Annexin V-positive/PI-negative part represented early apoptotic cells, and the Annexin V-positive/PI-positive part represented late apoptotic and dead cells.

Biochemical Detection

The levels of lactate dehydrogenase (LDH), superoxide dismutase (SOD), and malondialdehyde (MDA) in cells were measured, respectively, using the LDH (A020-2), SOD (A001-3), and MDA (A003-1) kits (Jiancheng Biotechnology Research Institute, Nanjing, Jiangsu, China) according to the manufacturer's recommendations. Assays were performed in triplicate, and the mean values of each sample were calculated manually.

QRT-PCR

Total RNA was extracted using Trizol reagent (Invitrogen, Carlsbad, CA, United States) according to the manufacturer's protocol, and reverse-transcribed with a RevertAid First Strand cDNA Synthesis Kit (Thermo Fisher Scientific Inc., Waltham, MA, United States). qRT-PCR was done using an SYBR green PCR Master Mix (Thermo Fisher Scientific Inc., Waltham, MA, United States) on the ABI 7300 system. The relative abundance of genes was quantified by using the comparative 2-ΔΔCt with β-actin or U6 as an internal control. The sequences of primers used in the study were as follows. Human NOX4, Primer F:

5′-TTTAGATACCCACCCTCCCG-3′, Primer R:

5′-GGCACAGTACAGGCACAAAGG-3′. Human cytochrome b-245 beta chain (CYBB), Primer F: 5′-CTAAGATAGCGGTTGATGGGC-3′, Primer R:

5′-CTTGAGAATGGATGCGAAGG-3′. Human β-actin, Primer F:

5′-CGTGGACATCCGCAAAGAC-3′, Primer R: 5′-TGC TGGGAGCCAGAGCAG-3’.

hsa-miR-100-5p, RT Primer:

5′-GTCGTATCCAGTGCAGGGTCCGAGGTATTCGCA CTGGATACGACCACAA

G-3′, Primer F: 5′-GCGAACCCGTAGATCCGAA-3′, Primer R:

5′-AGTGCAGGGTCCGAGGTATT-3′. Human U6, Primer F:

5′-CTCGCTTCGGCAGCACA, Primer R: 5′-AACGCTTCA CGAATTTGCGT-3′.

Western Blot

AC16 cells were lysed by the addition of RIPA lysis buffer supplemented with a protease and phosphatase inhibitor cocktail (p8340 and p8250, Sigma, St Louis, MO, United States). 25 μg of total protein was separated by SDS-PAGE and transferred onto a nitrocellulose membrane. Membranes were further blocked with 5% skim milk and immersed into antibody solutions against TSG101 (1:2000, ab120511, Abcam, Cambridge, MA, United States), CD81 (1:2000, ab109201, Abcam, Cambridge, MA, United States), NOX2 (1:5000, ab129068, Abcam, Cambridge, MA, United States), cleaved-caspase-3 (1:500, ab13847, Abcam, Cambridge, MA, United States), β-actin (1: 2000, ab8226, Abcam, Cambridge, MA, United States), and NOX4 (1: 2000, 14347-1-AP, Proteintech, Rosemont, IL, United States). Then the membranes were immersed into the secondary antibody solution linked to horseradish peroxidase (A0208 and A0216, Beyotime, Shanghai, China). Signals were captured by a chemiluminescence system.

Statistical Analysis

All data were expressed as mean ± standard deviation (SD). One-way analysis of variance (ANOVA) was applied to assess the statistically significant differences between more than two groups. Statistical analysis was performed by Prism 8.0.2 software (GraphPad, San Diego, United States). p value < 0.05 was considered significant.

RESULTS

Identification of Human Umbilical Cord Mesenchymal Stem Cell-Extracellular Vesicles

HucMSCs were cultured and collected. HucMSCs were identified by a flow cytometer to detect their surface markers. Flow cytometry exhibited that HucMSC surface markers, such as CD44 and CD105, were highly expressed, while hematopoietic stem marker CD34 and leukocyte surface antigen CD45 exhibited low expression (**Figure 1A**). Next, HucMSC-EVs were extracted and identified. Transmission electron microscope showed that HucMSC-EVs were small round or elliptical membranous bi-lipid membrane vesicles. Their diameters ranged in size from 30 to 100 nm. There were low electron densities in the vesicles (**Figure 1B**). The specific markers, namely, TSG101 and CD81, of HucMSC-EVs were detected by Western blot. While there were no expression for the specific markers TSG101 and CD81 of HucMSC-EVs in the HucMSC medium (**Figure 1C**). HucMSC-EVs were labeled by PKH67 and incubated with AC16 cells for 24 h. Under a laser scanning microscope, the green EVs were located in the cytoplasm (**Figure 1D**). These results suggest that HucMSC-EVs were successfully isolated.

Human Umbilical Cord Mesenchymal Stem Cell-Extracellular Vesicles Inhibit Doxorubicin-Induced Oxidative Stress and Apoptosis

AC16 cells were treated with 2 μmol/L DOX and HucMSC at concentrations of 0 μg/ml, 50 μg/ml, 100 μg/ml, and 200 μg/ml for 24 h. Flow cytometry showed that 2 μmol/L DOX obviously induced ROS levels to increase, while HucMSC-EV treatment decreased ROS levels that were increased by DOX. HucMSC-EVs significantly reduced ROS levels at the concentrations of 50 μg/ml, 100 μg/ml, and 200 μg/ml. The effect of HucMSC-EV treatment was concentration dependent (**Figure 2A**). Meanwhile, 2 μmol/L DOX increased LDH release and MDA levels, and decreased SOD levels. However, HucMSC-EV treatment inhibited the increases of LDH release and MDA levels, and the decreases of SOD levels which were induced by DOX. The functions of HucMSC-EVs on LDH release, SOD levels, and MDA levels were in a concentration-dependent manner (**Figures 2C–E**). Furthermore, 2 μmol/L DOX induced AC16 cell apoptosis. Flow cytometry displayed that HucMSC-EVs reduced apoptotic cells that were increased by DOX with the concentrations of 50, 100, and 200 μg/ml. The action of HucMSC-EVs on AC16 cell apoptosis was in a concentration-dependent manner (**Figure 2B**). Western blot exhibited that HucMSC-EVs markably repressed the cleaved-caspase-3 expression with the different concentrations of 50, 100, and 200 μg/ml, which were highly expressed by DOX (**Figure 2F**). These findings suggest that HucMSC-EVs obviously inhibit cardiomyocyte oxidative stress and apoptosis that are induced by DOX in AC16 cells.

Human Umbilical Cord Mesenchymal Stem Cell-Extracellular Vesicles Inhibit NOX4 Expression Induced by Doxorubicin

AC16 cells were treated with 2 μmol/L DOX and HucMSC-EVs with the concentrations of 0, 50, 100, and 200 μg/ml for 24 h. qRT-PCR indicated that DOX extremely increased the NOX2 and NOX4 mRNA expression. HucMSC-EVs could repress the mRNA expression of NOX2 and NOX4 at concentrations of 50, 100, and 200 μg/ml, which were increased by DOX. Compared to the 2 μmol/L_DOX+50 μg/ml_HucMSC-EV group, HucMSC-EV treatment at 100 μg/ml apparently suppressed NOX2 and NOX4 mRNA expression, which was induced by DOX (**Figure 3A**). Western blot displayed that HucMSC-EVs suppressed protein expression of NOX2 and NOX4 with the concentrations of 50, 100, and 200 μg/ml, which was increased by DOX (**Figure 3B**). AC16 cells were treated with 2 μmol/L DOX and 100 μg/ml HucMSC-EVs for 0, 6, 12, 24, and 48 h. qRT-PCR showed that 2 μmol/L DOX remarkably induced NOX4 mRNA expression increase. HucMSC-EVs attenuated NOX4 mRNA expression with a concentration of 100 μg/ml at

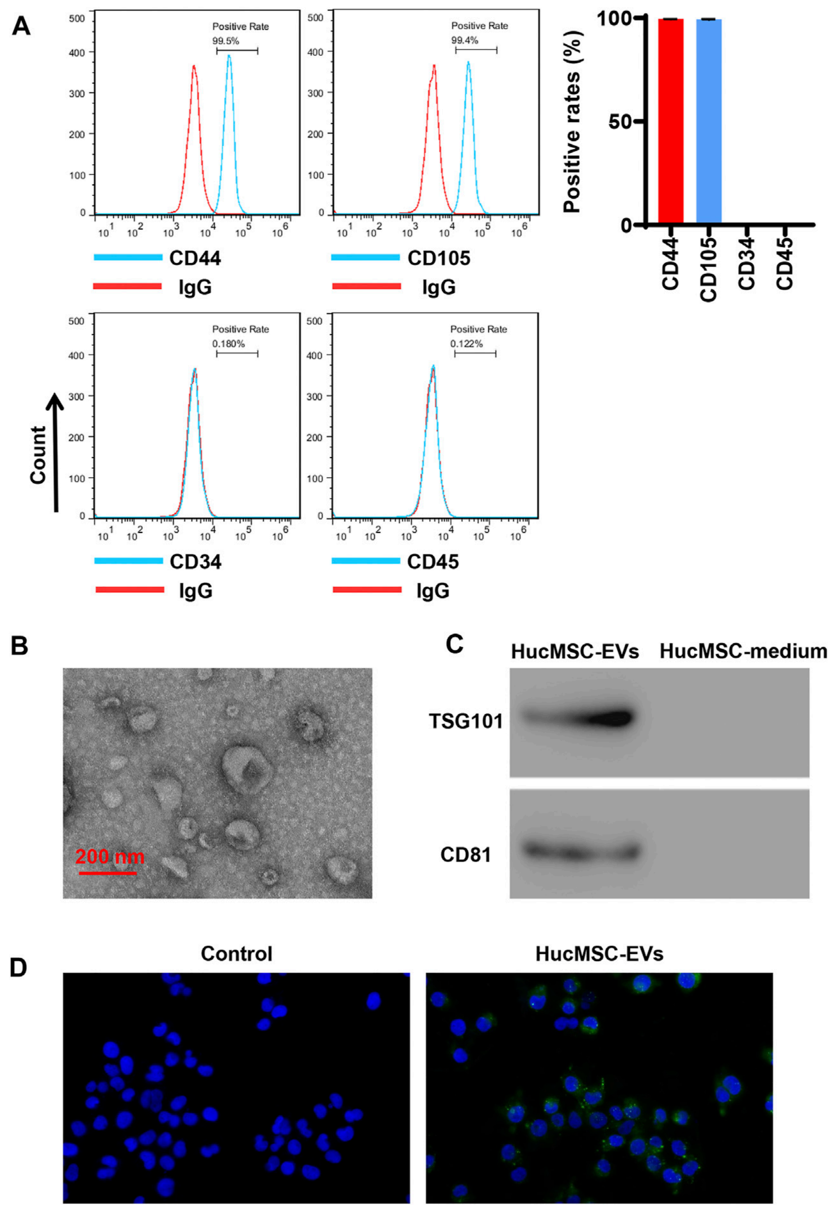

FIGURE 1 | Isolation and identification of HucMSC-EVs. **(A)** The surface markers CD44 and CD105 of HucMSCs were identified by flow cytometry. **(B)** The morphology of purified HucMSC-EVs was observed by transmission electron microscopy: scale bar: 200 nm. **(C)** The markers CD81 and TSG101 of HucMSC-EVs were detected by Western blot. **(D)** HucMSC-EV endocytosis traced by PKH67 was observed by a laser scanning microscope in AC16 cells.

6, 12, 24, and 48 h, which were increased by DOX. Compared to 12 h, HucMSC-EV treatment markedly suppressed NOX4 mRNA expression with 100 μg/ml at 24 h, which was increased by DOX (**Figure 3C**). Similarly, Western blot displayed that the NOX4 protein expression was ameliorated at a concentration of 100 μg/ml for 6, 12, 24, and 48 h, which was increased by DOX (**Figure 3D**). Collectively, the data suggest that HucMSC-EVs markedly inhibit NOX4 expression in a time- and concentration-dependent manner, which is induced by DOX.

Inhibition of EV miR-100-5-p Reverses Those Effects That Human Umbilical Cord Mesenchymal Stem Cell-Extracellular Vesicles Inhibit Doxorubicin-Induced Oxidative Stress and Apoptosis

HucMSCs were transfected with miR-100-5p inhibitor (Inhibitor) or miR-100-5p mimic (Mimic). Q-PCR displayed that miR-100-5p expression was abolished by miR-100-5p inhibitor, while the miR-100-5p expression was aggravated by

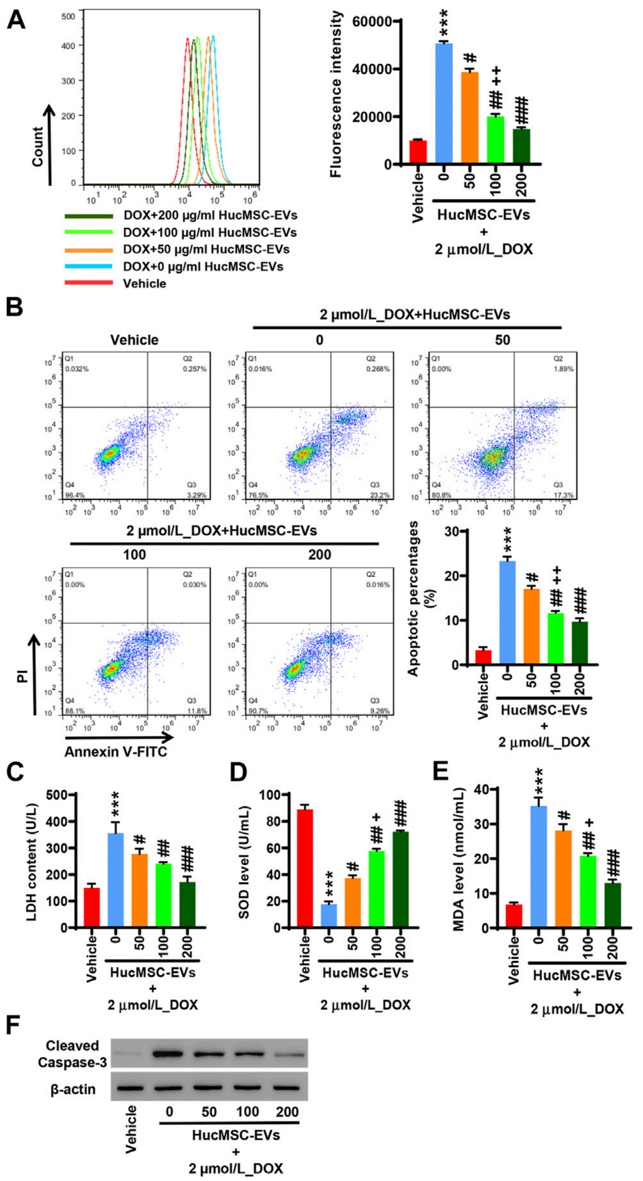

FIGURE 2 | HucMSC-EVs inhibit DOX-induced oxidative stress and apoptosis. AC16 cells were treated with 2 μmol/L DOX and HucMSC-EVs at different concentrations (0, 50, 100, and 200 μg/ml) for 24 h. **(A)** ROS levels were measured by flow cytometry. **(B)** The percentages of apoptotic cells were assessed by flow cytometry. Quadrant 1 represented dead cells. Quadrant 2 represented late apoptotic cells. Quadrant 3 represented early apoptotic cells. Quadrant 4 represented normal cells. **(C–E)** The levels of LDH **(C)**, SOD **(D)**, and MDA **(E)** were measured with biochemistry methods. **(F)** Western blot analysis of cleaved-caspase-3. $^{***}p$ < 0.001 vs. vehicle, $^{\#}p$ < 0.05, $^{\#\#}p$ < 0.01, $^{\#\#\#}p$ < 0.001 vs. 2 μmol/L_DOX + 0 μg/ml_HucMSC-EVs, ^{+}p < 0.05, ^{++}p < 0.01 vs. 2 μmol/L_DOX + 50 μg/ml_HucMSC-EVs.

miR-100-5p mimic (**Figure 3A**). After HucMSCs were transfected with miR-100-5p inhibitor or miR-100-5p mimic, HucMSC-EVs were extracted, and Q-PCR was performed. Q-PCR showed that miR-100-5p inhibitor abolished miR-100-5p expression in EVs compared to the negative control, whereas miR-100-5p mimic exceedingly exacerbated miR-100-5p expression in EVs (**Figure 3B**). AC16 cells were treated with 2 μmol/L DOX and 100 μg/ml miR-100-5p negative control in HucMSC-EVs (NC-EVs) or miR-100-5p inhibitor in HucMSC-EVs (Inhibitor-EVs) or miR-100-5p mimic in HucMSC-EVs (Mimic-EVs) for 24 h. Flow cytometry demonstrated that DOX remarkably increased ROS levels, which were decreased with supplement of NC-EVs or Mimic-EVs. Compared to NC-EVs, Inhibitor-EVs reversed those effects in which NC-EVs decreased ROS production which were increased by DOX, whereas Mimic-EVs had similar inhibitory effects to NC-EVs for ROS production (**Figure 4C**). Biochemical assay exhibited that 2 μmol/L DOX aggravated LDH release and MDA level increases as well as SOD level decreases, which were inhibited with supplement of NC-EVs or Mimic-EVs. In comparison to the NC-EV group, Inhibitor-EVs reversed those effects in which NC-EVs inhibited DOX induced the increases of LDH and MDA levels as well as the decreases of SOD levels, while Mimic-EVs had the similar effects to NC-EVs (**Figures 4E–G**). Furthermore, apoptosis was examined with flow cytometry and Western blot. NC-EVs and Mimic-EVs markedly reduced the percentages of apoptotic cells, which were induced to increase y DOX. Compared to the NC-EV group, Mimic-EVs had a similar effect to NC-EVs for reducing the percentages of apoptotic cells, while inhibitor-EVs reversed those effects in which NC-EVs inhibited DOX-induced apoptotic cell increases (**Figure 4D**). NOX4 and cleaved-caspase-3 protein expression were apparently attenuated by NC-EVs or Mimic-EVs, which was induced to increase by DOX. Compared to the NC-EV group, Inhibitor-EVs reversed those effects which NC-EVs decreased, NOX4 and cleaved-caspase-3 protein expression, which was increased by DOX, while Mimic-EVs had a similar effect to NC-EVs (**Figure 4H**). Taken together, these findings suggest that downregulation of EV miR-100-5-p reverses those effects in which HucMSC-EVs inhibit DOX-induced oxidative stress and apoptosis.

Overexpression of NOX4 Cancels Those Effects in Which Human Umbilical Cord Mesenchymal Stem Cells Inhibit Doxorubicin-Induced Oxidative Stress and Apoptosis

To study whether miR-100-5p targets the NOX4 protein, 293T cells were co-transfected with pGL3-NOX4-WT, miR-100-5p inhibitor (Inhibitor), and miR-100-5p mimic (Mimic) or pGL3-NOX4-MUT, miR-100-5p inhibitor (Inhibitor), and miR-100-5p mimic (Mimic). The miR-100-5p inhibitor markedly increased the luciferase activity of pGL3-NOX4-WT, while the miR-100-5p mimic obviously reduced the luciferase activity of pGL3-NOX4-WT. There was no change in the luciferase activity of pGL3-NOX4-MUT (**Figure 5A**). qRT-PCR exhibited that the miR-100-5p inhibitor increased the NOX4 mRNA expression, while the miR-100-5p mimic decreased the NOX4 mRNA expression (**Figure 5B**). Western blot illustrated that the NOX4 protein expression was increased by the miR-100-5p inhibitor, whereas the NOX4 protein expression was reduced by the miR-100-5p mimic

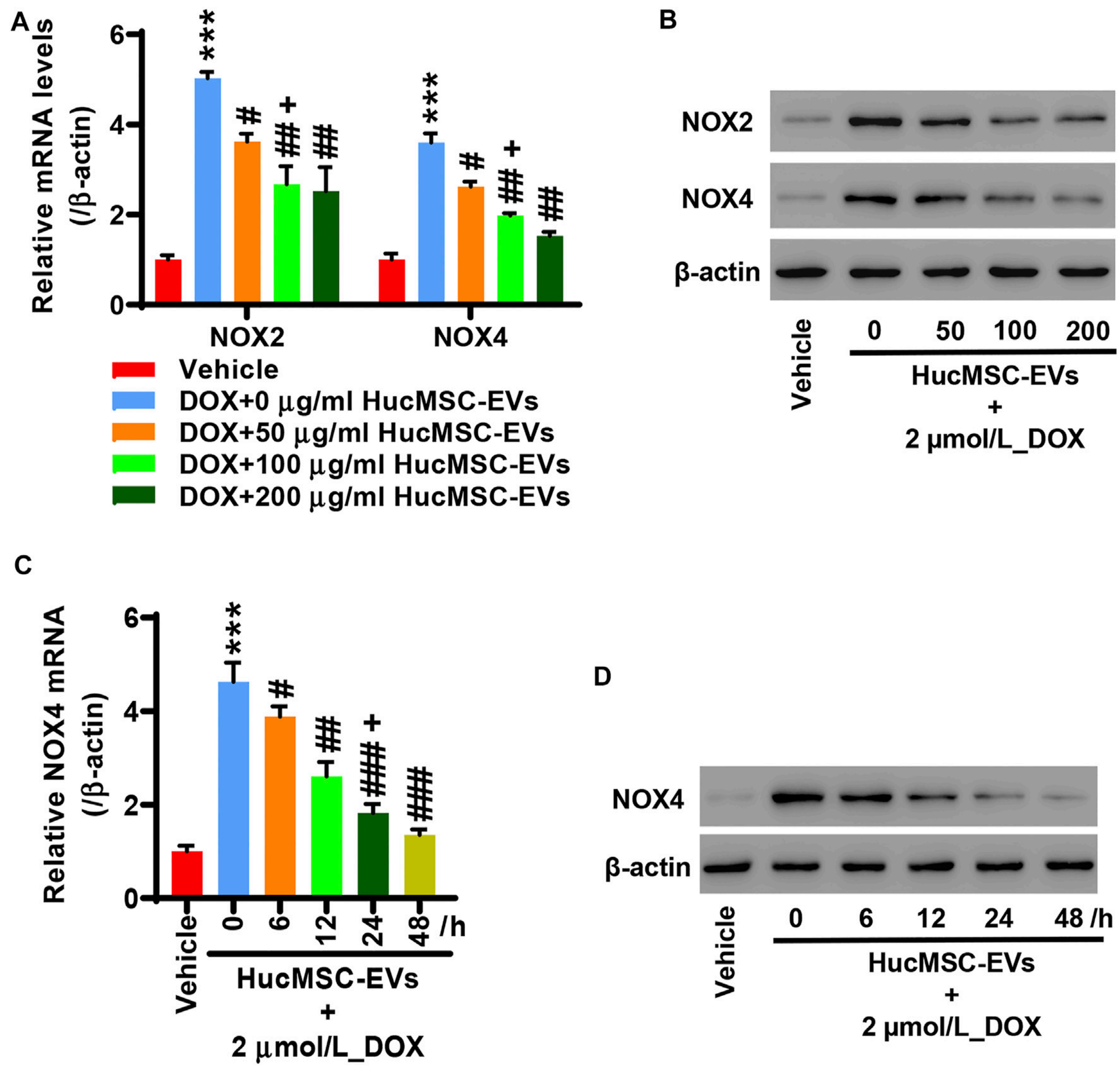

FIGURE 3 | HucMSC-EVs inhibits NOX4 expression. AC16 cells were treated with 2 μmol/L DOX and HucMSC-EVs at different concentrations (0, 50, 100, and 200 μg/ml) for 24 h. **(A)** qRT-PCR and **(B)** Western blot were performed to detect NOX2 and NOX4 expression, respectively. $^{***}p < 0.001$ vs. vehicle, $^{\#}p < 0.05$, $^{\#\#}p < 0.01$ vs. 2 μmol/L_DOX + 0 μg/ml_HucMSC-EVs, $^{+}p < 0.05$ vs. 2 μmol/L_DOX + 50 μg/ml_HucMSC-EVs. **(C–D)** AC16 cells were treated with 2 μmol/L DOX and HucMSC-EVs at a concentration of 100 μg/ml for different times (0, 6, 12, 24, and 48 h). **(C)** qRT-PCR and **(D)** Western blot were used for the detection of NOX4 expression. $^{***}p < 0.001$ vs. Vehicle, $^{\#}p < 0.05$, $^{\#\#}p < 0.01$, $^{\#\#\#}p < 0.001$ vs. 0 h, $^{+}p < 0.05$ vs. 12 h.

(**Figure 5C**). These results demonstrate that NOX4 is the targeting protein of miR-100-5p. NOX4 expression is negatively regulated by miR-100-5p. Next, NOX4 overexpression plasmid (oe-NOX4) was constructed and transfected to AC16 cells. oe-NOX4 markedly increased NOX4 mRNA expression (**Figure 5D**) and NOX4 protein expression (**Figure 5E**). Furthermore, AC16 cells were transfected with oe-NOX4 for 24 h, and then treated with 2 μmol/L DOX combined with 100 μg/ml HucMSC-EVs for another 24 h. Flow cytometry revealed that HucMSC-EVs reduced ROS levels which were induced to increase by DOX, and this was reversed by the overexpression of NOX4 (**Figure 5F**). At the same time, HucMSC-EVs inhibited increased LDH and MDA levels as well as decreased SOD levels which were induced by DOX; these effects were reversed by the overexpression of NOX4 (**Figures 5H–J**). Moreover, DOX induced the percentages of apoptotic cell increase. HucMSC-EVs ameliorated the percentages of apoptotic cells which were increased by DOX, and this was reversed by NOX4 overexpression (**Figure 5G**). Western blot showed that HucMSC-EVs ameliorated the expression of NOX4 and cleaved-caspase-3 which was increased by DOX, and this was reversed by NOX4 overexpression (**Figure 5K**). Collectively, these results indicate that overexpression of NOX4 abolishes those effects in which HucMSC-EVs inhibit DOX-induced oxidative stress and apoptosis.

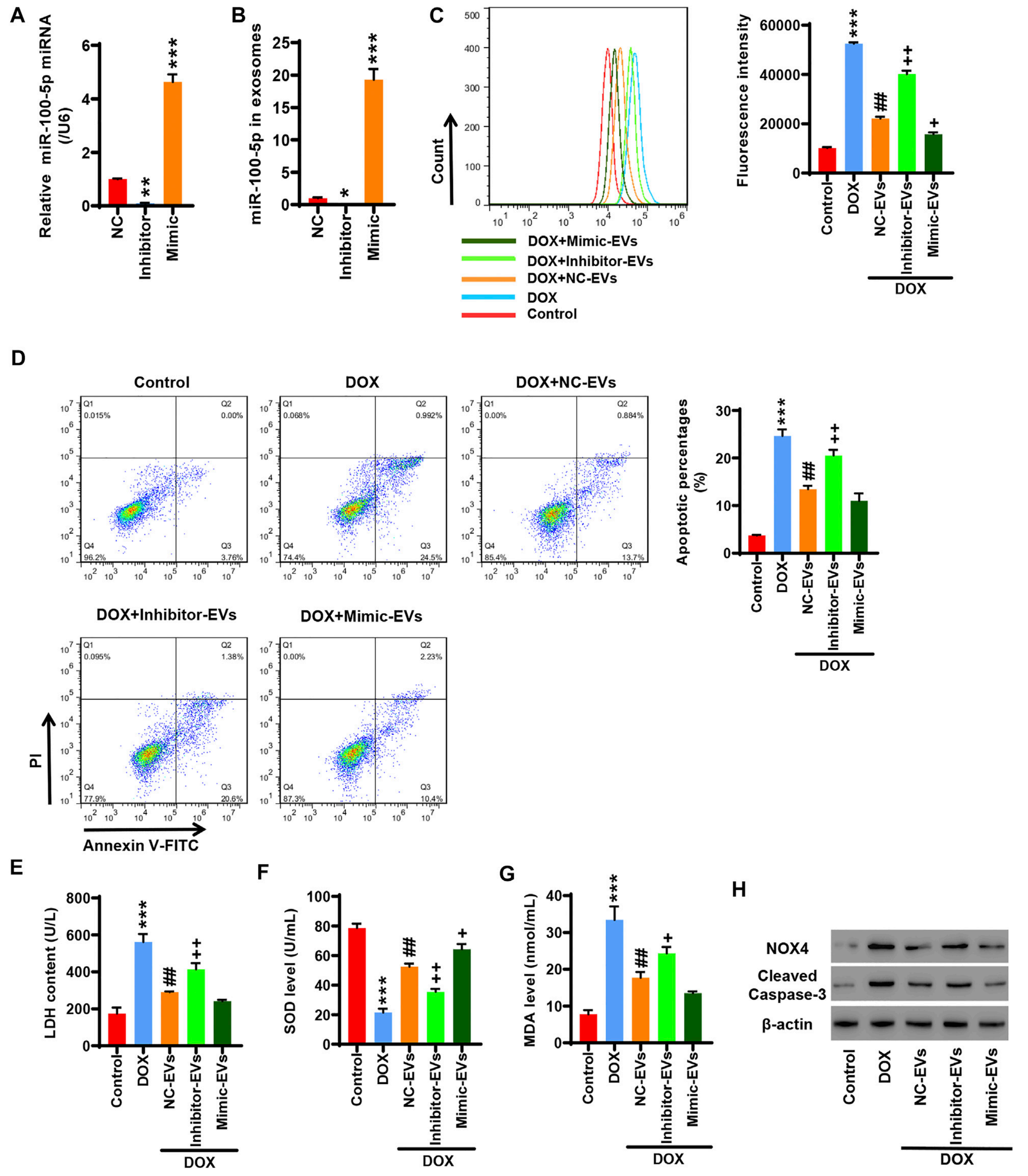

FIGURE 4 | Inhibition of EV miR-100-5-p reverses the effects in which HucMSC-EVs inhibit DOX-induced oxidative stress and apoptosis. **(A)** HucMSCs were transfected with miR-100-5p inhibitor (Inhibitor) or miR-100-5p mimic (Mimic). MiR-100-5p expression was determined by Q-PCR. **(B)** HucMSCs were transfected with miR-100-5p inhibitor or miR-100-5p mimic. After HucMSC-EVs were extracted, EV miR-100-5-p was determined by Q-PCR. $^{*}p < 0.05$, $^{**}p < 0.01$, $^{***}p < 0.001$ vs. NC. **(C–H)** AC16 cells were treated with 2 μmol/L DOX and EV miR-100-5p inhibitor (Inhibitor-EVs) or EV miR-100-5-p mimic (Mimic-EVs) at a concentration of 100 μg/ml. **(C)** ROS levels were measured by flow cytometry. **(D)** Apoptosis was determined by flow cytometry. Quadrant 1 represented dead cells. Quadrant 2 represented late apoptotic cells. Quadrant 3 represented early apoptotic cells, and Quadrant 4 represented normal cells. **(E–G)** LDH, SOD, and MDA levels were measured with biochemical assay. **(H)** NOX4 and cleaved-caspase-3 expression were examined by Western blot. $^{***}p < 0.001$ vs. control, $^{\#\#}p < 0.01$ vs. 2 μmol/DOX, $^{+}p < 0.05$, $^{++}p < 0.01$ vs. 2 μmol/L DOX + NC-EVs.

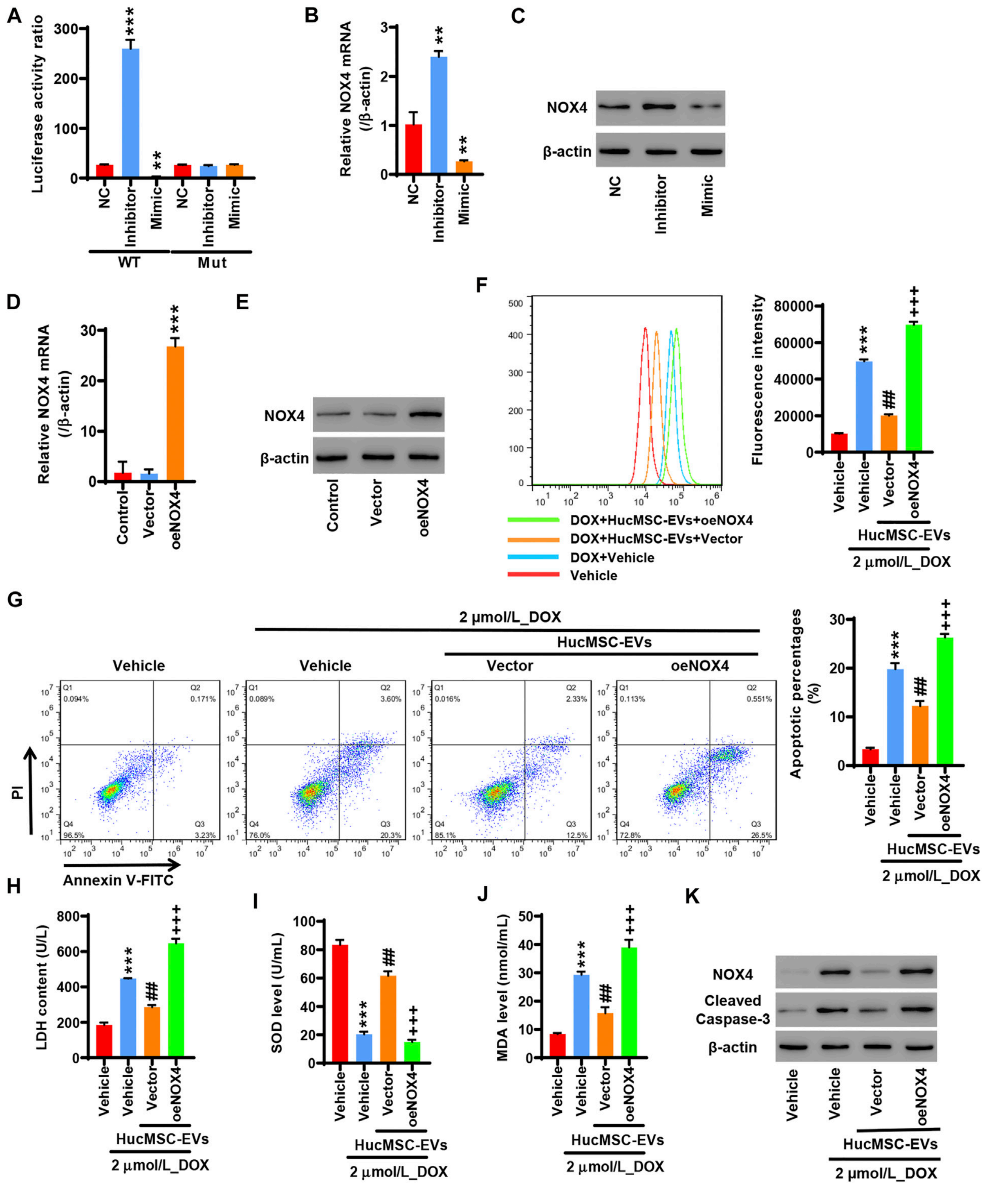

FIGURE 5 | Overexpression of NOX4 abolishes those effects in which HucMSC-EVs inhibit DOX-induced oxidative stress and apoptosis. 293T cells were co-transfected with either pGL3-NOX4-WT, miR-100-5p inhibitor (Inhibitor) and miR-100-5p Mimic, and pGL3-NOX4-MUT, mimic (Mimic) or pGL3-NOX4-MUT, miR-100-5p inhibitor (Inhibitor) and miR-100-5p mimic (Mimic). **(A)** Luciferase activity was quantified using a luminometer. $^{**}p < 0.01$, $^{***}p < 0.001$ vs. WT + NC. **(B)** NOX4 mRNA was examined by qRT-PCR. **(C)** NOX4 protein expression was detected by Western blot. $^{**}p < 0.01$ vs. NC. **(D)** AC16 cells were transfected with oeNOX4. NOX4 mRNA was examined by qRT-PCR. **(E)** AC16 cells were transfected with oeNOX4. NOX4 protein was detected by Western blot. $^{***}p < 0.001$ vs. vector. **(F–K)** AC16 cells were transfected with oeNOX4 for 24 h and then treated with 2 μmol/L DOX and 100 μg/ml HucMSC-EVs for 24 h. **(F)** ROS levels were measured by flow cytometry. **(G)** Apoptosis was measured by flow cytometry. Quadrant 1 represented dead cells. Quadrant 2 represented late apoptotic cells. Quadrant 3 represented early apoptotic cells, and Quadrant 4 represented normal cells. LDH **(H)**, SOD **(I)**, and MDA **(J)** were measured by biochemical assay. **(K)** NOX4 and cleaved-caspase-3 expression were determined by Western blot. $^{***}p < 0.001$ vs. vehicle, $^{\#\#}p < 0.01$ vs. 2 μmol/L_DOX + vehicle, $^{+++}p < 0.001$ vs. 2 μmol/L_DOX + HucMSC-EVs + vector.

DISCUSSION

With the aging of the population, the incidence of cardiovascular diseases such as hypertension and coronary heart disease has increased significantly. The consequence of the development of most cardiovascular diseases is heart failure, which has increasingly become a major disease that seriously threatens human health. Heart failure is manifested as insufficient cardiac output and the inability to maintain the oxygen supply required by the body's metabolism. It is an important reason for the loss of labor and death in patients with cardiovascular diseases. In recent years, MSCs are of great significance for the treatment of heart failure (Vrtovec et al., 2013; Narita and Suzuki, 2015; Guijarro et al., 2016; Bartunek et al., 2017). However, MSCs have a short curative effect time, whereas MSC-derived EVs have a long curative effect time. MSC-derived EVs have a protective effect on heart failure (Chen et al., 2020b; Tan et al., 2020; Zheng et al., 2020). Chen et al. reported that EVs derived from MSCs improved cardiac hypertrophy, heart function, fibrosis, and myocardial apoptosis after transverse aortic constriction (TAC). It may be a benefit for treatment of heart failure (Chen et al., 2020a). Gao et al. found that after myocardial infarction (MI), serum EVs were obtained from ischemic heart and kidney. Cardiorenal EV-derived miRNA-1956 promoted adipose-derived MSC-mediating angiogenesis, which is important for ischemic tissue repair (Gao et al., 2020). Nakamura et al. demonstrated that injection of adiponectin and hMSC significantly increased hMSC-derived EV release. Adiponectin accelerated hMSC-derived therapy in heart failure mice (Nakamura et al., 2020). In this study, DOX induced oxidative stress, ROS, and apoptosis increases in AC16 cells, which were inhibited by HucMSC-EVs, and these were further reversed by the inhibition of EV miR-100-5-p. Meanwhile, HucMSC-EVs inhibited NOX4 expression which was induced by DOX. Overexpression of NOX4 abolished the effects of HucMSC-EVs. NOX4 was negatively regulated by miR-100-5p. These data suggest that HucMSC-EVs have protective effects against DOX-induced heart failure in AC16 cells.

Oxidative stress refers to the pathological process in which the balance of the oxidation system and antioxidant system causes an increase in ROS in the body and causes cell oxidative damage. ROS is mainly produced by the mitochondria (Dietl and Maack, 2017). ROS is also produced by the NADPH oxidase (Shang et al., 2019). Oxidative stress in the myocardium causes the increase of ROS and causes damage of the cell membrane to release LDH. MDA is the final product of lipid oxidation. SOD is the most important member of the antioxidant system. In heart failure, SOD is decreased, and LDH, MDA, and ROS are increased (Agostini et al., 2015; Casieri et al., 2017; Zhou and Tian, 2018; Koju et al., 2019; Ni et al., 2019). Cardiomyocyte oxidative stress plays an important role in heart failure (Kim et al., 2020). In heart failure, oxidative stress is markedly increased (Wang et al., 2019; Lubrano and Balzan, 2020). Inhibition of oxidative stress in cardiomyocytes can improve the symptoms of heart failure (Kumar et al., 2019; Pop et al., 2020). Heart failure is associated with oxidative stress and apoptosis. Recent studies find that apoptosis and mitochondrial oxidative stress are markedly increased in heart failure rats. Whereas myocardial capillary and arteriolar density as well as SIRT1, FOXO3a, and MnSOD expression are decreased. Echinacoside improves the heart function by the SIRT1/FOXO3a/MnSOD signaling pathway in heart failure rats (Ni et al., 2021). In DOX-induced heart failure mice, SOD2, GPx-1, FOX3a, and SIRT3 expression are decreased, apoptotic cells and cleaved-caspase-3 expression are increased, as well as inflammatory cytokines such as IL-1β, IL-6, and TNF-α are increased. LongShengZhi capsule (LSZ) is a traditional Chinese medicine. After treatment of heart failure mice with LSZ, the indicators of heart failure are significantly improved. LSZ decreases oxidative stress, apoptosis, and inflammatory cytokine levels, which are increased by DOX. LSZ increases FoxO3a, SIRT3, and SOD2 expression, which are decreased by DOX (Xu et al., 2020). In our studies, HucMSC-EVs inhibited ROS production in a concentration-dependent manner, which was induced by DOX. LDH and MDA levels were decreased by HucMSC-EVs, which were increased by DOX. SOD levels were increased by HucMSC-EVs, which were decreased by DOX. HucMSC-EV treatment was concentration dependent. Additionally, HucMSC-EV treatment decreased apoptotic cells and cleaved-caspase-3 expression in a concentration-dependent fashion, which were increased by DOX. These results suggest that HucMSC-EVs inhibit DOX-induced heart failure in a concentration-dependent manner in AC16 cells.

Nicotinamide adenine dinucleotide phosphate (NADPH) oxidase is a peroxidase. There are NOX1, NOX2, NOX3, NOX4, NOX5, DUOX1, and DUOX2 in NADPH oxidase (NOX) family (Brandes et al., 2010). NOX2 and its homologue NOX4 function as the core catalytic subunit of NADPH oxidase, which are the key to the function of the enzyme. NADPH oxidase produces ROS as a signal molecule to participate in the signal transduction process that regulates cell proliferation, senescence, and apoptosis (Ray et al., 2011; Schröder et al., 2012; Guo and Chen, 2015). When NOX family proteins are abnormally expressed, ROS levels increase, which cause oxidative stress and participate in the formation of heart failure (Kumar et al., 2019). The main function of NOX family is to generate ROS (Panday et al., 2015). Previous studies found that NOX4 knockout mice exhibited severe cardiac hypertrophy and contractile dysfunction after pressure overload, whereas NOX4 transgenic mice showed enhanced angiogenesis and increased expression of VEGF and Hif1α as well as less cardiac hypertrophy after pressure overload. It was suggested that NOX4 had a protection against cardiac stress by pressure overload (Zhang et al., 2010). Cardiac-specific overexpression of NOX4 activates the nuclear transcription factor Nrf2 (Brewer et al., 2011). Nrf2 is a key transcription factor in the cellular antioxidative stress system. Nrf2 enters the nucleus and binds to ARE (antioxidant response elements) to generate GSTs and SOD, and play a role of antioxidant damage. Nrf2 shows a protection against load-induced cardiac hypertrophy (Li et al., 2009; Schröder et al., 2012). However, recent studies demonstrate that in heart failure rats, TLR4 and NOX4 expression is significantly increased, autophagy and ferroptosis are enhanced, as well as the heart function is abnormal. Downregulation of either TLR4 or NOX4 inhibits autophagy and ferroptosis, and obviously improves cardiac function and left ventricular remodeling (Chen et al., 2019). DOX-induced cardiac and renal toxicities have been reported (Uygur et al., 2014; Tulubas et al., 2015). DOX induces apoptosis and oxidative stress in heart and kidney tissues. NOX4 is also induced to increase by DOX in the renal tissues. Pretreatment with omega-3 fatty acids improves the cardiac function, illustrates antioxidant and antiapoptotic effects, and increases renal NOX4 expression (Saleh et al., 2020). In our experiments, HucMSC-EVs ameliorated the expression of NOX2 mRNA and NOX4 mRNA, which was enhanced by DOX. Similarly, HucMSC-EVs attenuated the expression of NOX2 and NOX4 proteins, which was increased by DOX. HucMSC-EV treatment was concentration dependent. Furthermore, HucMSC-EV treatment attenuated the expression of NOX4 mRNA and protein in a time–concentration–dependent fashion, which was induced to increase by DOX. Moreover, overexpression of NOX4 abolished that HucMSC-EVs inhibited DOX-induced ROS production, increased LDH and MDA, and decreased SOD. Overexpression of NOX4 abolished that HucMSC-EVs inhibited DOX-induced increased apoptotic cells, as well as cleaved-caspase-3 and NOX4 protein expression. These data indicate that HucMSC-EVs inhibit DOX-induced heart failure through targeting NOX4 in AC16 cells.

Research in recent years has shown that miRNAs are important epigenetic regulatory factors. miRNAs also play the important roles in EVs, which are benefit to treat cardiovascular diseases. EVs play a vital role in intercellular communication and their functions depend mainly on their internal contents (Vlassov et al., 2012). EVs act as miRNA carriers that carry miRNAs to nearby or distant cells. EVs act on target cells by directly releasing miRNAs to target cells through target cell endocytosis or membrane fusion, which is considered to be an important tool for intercellular signal transduction (Montecalvo et al., 2012; Zeringer et al., 2015). EVs can deliver specific miRNAs to target cells that are as an important component of the paracrine effect of stem cells. microRNAs encapsulated in EVs are the key genetic material that promotes the repair of myocardial damage. Inhibition of miR-342-5p reduces exercise-afforded cardiac protection in myocardial ischemia/reperfusion rats. MiR-342-5p agomir increases the miR-342-5p levels and decreases myocardial infarct size in rat hearts. Exercise-derived circulating EVs mediate the protective effects against myocardial ischemia/reperfusion injury through EV miR-342-5p (Hou et al., 2019). MiR-100-5p is believed to have anti-atherosclerotic effects because it inhibits the proliferation of endothelial cells and migration of blood vessels and smooth muscle cells (Shoeibi, 2020). In a mouse model of atherosclerosis, the expression of miR-100-5p can improve endothelial function, weaken atherosclerosis, and reduce plaque area (Linna-Kuosmanen et al., 2020). Further studies indicate that downregulation of miR-100-5p activates the VEGFA/MYC pathway, which leads to increased endothelial cell metabolism, proliferation, and angiogenesis, thereby promoting angiogenesis (Pankratz et al., 2018). Downregulation of miR-100 leads to the formation of angiogenic tubes, the increase in endothelial germination, and proliferation in HUVECs (Grundmann et al., 2011). NOX4 is the target of miR-100-5p. Inhibition of miR-100-5p targeting NOX4 leads to H_2O_2 release (Kriegel et al., 2015). The expression of miR-100-5p is decreased by hypoxia. EVs derived a human neural stem cell line that inhibits hypoxia-induced proliferation and migration through EV miR-100-5-p in pulmonary artery smooth muscle cells (Wang et al., 2020). Hromadnikova et al. found that downregulation of miR-100-5p was associated with gestational hypertension and preeclampsia (Hromadnikova et al., 2016). Onrat et al. compared 50 patients with dilated cardiomyopathy and 10 healthy persons. They found that miR-100-5p was overexpressed in the dilated cardiomyopathy (Onrat et al., 2018). In this study, HucMSC-EVs inhibited DOX-induced ROS, LDH, and MDA increases, and SOD decrease, which were reversed by the EV miR-100-5-p inhibitor. There were differences in reducing ROS levels and increasing SOD levels between EV miR-100-5p mimic treatment and HucMSC-EV treatment. But there were no differences in reducing LDH and MDA levels between EV miR-100-5-p mimic treatment and HucMSC-EV treatment. It means that the effects of EV miR-100-5p treatment and HucMSC-EV treatment are similar in reducing ROS and oxidative stress. Furthermore, HucMSC-EVs inhibited DOX-induced apoptotic cell increase, and cleaved-caspase-3 and NOX4 protein expression increase, which were reversed by the EV miR-100-5-p inhibitor, whereas the effects of EV miR-100-5p treatment and HucMSC-EV treatment were similar in reducing apoptosis. Moreover, miR-100-5p inhibited NOX4 mRNA and protein expression, whereas the inhibition of miR-100-5p increased NOX4 mRNA and protein expression. Taken together, these data indicate that EV miR-100-5-p treatment inhibits DOX-induced heart failure *via* targeting the NOX4 protein in AC16 cells, which is similar to the effects of HucMSC-EV treatment.

CONCLUSION

In summary, HucMSC-EV treatment inhibited DOX-induced oxidative stress, ROS, and apoptosis increases. HucMSC-EV treatment also inhibited DOX-induced NOX4 expression. Overexpression of NOX4 abolished those effects in which HucMSC-EVs inhibited DOX-induced oxidative stress, apoptosis, and ROS production. NOX4 protein expression was negatively regulated by EV miR-100-5-p. Inhibition of EV miR-100-5-p reversed those effects in which HucMSC-EVs inhibited DOX-induced oxidative stress, apoptosis, and ROS production, whereas EV miR-100-5-p played a role similar to HucMSC-EVs in reducing oxidative stress, apoptosis, and ROS production. It is suggested that HucMSC-EVs inhibit DOX-induced heart failure through the miR-100-5p/NOX4 pathway.

DATA AVAILABILITY STATEMENT

The datasets presented in this study can be found in online repositories. The names of the repository/repositories and accession number(s) can be found in the article/Supplementary Material.

AUTHOR CONTRIBUTIONS

ZZ and YT performed most of the experiments. XL performed part of the experiments. JZ analyzed data. LW designed the experiments and wrote the manuscript. JT designed the experiments and revised the manuscript. All authors read and approved the final manuscript.

FUNDING

This study was supported by Affiliated Hospital of Panzhihua University and supported by the grant from the Zhejiang Medical and Health Research Project, China (Grant Nos: 2018KY915 and 2019KY793).

REFERENCES

Agostini, S., Chiavacci, E., Matteucci, M., Torelli, M., Pitto, L., and Lionetti, V. (2015). Barley Beta-Glucan Promotes MnSOD Expression and Enhances Angiogenesis under Oxidative Microenvironment. *J. Cel. Mol. Med.* 19 (1), 227–238. doi:10.1111/jcmm.12442

Balbi, C., and Vassalli, G. (2020). Exosomes - beyond Stem Cells for Cardiac Protection and Repair. *Stem Cells* 38 (11), 1387–1399. doi:10.1002/stem.3261

Bartolucci, J., Verdugo, F. J., González, P. L., Larrea, R. E., Abarzua, E., Goset, C., et al. (2017). Safety and Efficacy of the Intravenous Infusion of Umbilical Cord Mesenchymal Stem Cells in Patients with Heart Failure. *Circ. Res.* 121 (10), 1192–1204. doi:10.1161/circresaha.117.310712

Bartunek, J., Terzic, A., Davison, B. A., Filippatos, G. S., Radovanovic, S., Beleslin, B., et al. (2017). Cardiopoietic Cell Therapy for Advanced Ischaemic Heart Failure: Results at 39 Weeks of the Prospective, Randomized, Double Blind, Sham-Controlled CHART-1 Clinical Trial. *Eur. Heart J.* 38 (9), 648–660. doi:10.1093/eurheartj/ehw543

Brandes, R. P., Weissmann, N., and Schröder, K. (2010). NADPH Oxidases in Cardiovascular Disease. *Free Radic. Biol. Med.* 49 (5), 687–706. doi:10.1016/j.freeradbiomed.2010.04.030

Brewer, A. C., Murray, T. V. A., Arno, M., Zhang, M., Anilkumar, N. P., Mann, G. E., et al. (2011). Nox4 Regulates Nrf2 and Glutathione Redox in Cardiomyocytes *In Vivo*. *Free Radic. Biol. Med.* 51 (1), 205–215. doi:10.1016/j.freeradbiomed.2011.04.022

Casieri, V., Matteucci, M., Cavallini, C., Torti, M., Torelli, M., and Lionetti, V. (2017). Long-term Intake of Pasta Containing Barley (1-3)Beta-D-Glucan Increases Neovascularization-Mediated Cardioprotection through Endothelial Upregulation of Vascular Endothelial Growth Factor and Parkin. *Sci. Rep.* 7 (1), 13424. doi:10.1038/s41598-017-13949-1

Chen, F., Li, X., Zhao, J., Geng, J., Xie, J., and Xu, B. (2020a). Bone Marrow Mesenchymal Stem Cell-Derived Exosomes Attenuate Cardiac Hypertrophy and Fibrosis in Pressure Overload Induced Remodeling. In Vitro *Cell.Dev.Biol.-Animal* 56 (7), 567–576. doi:10.1007/s11626-020-00481-2

Chen, F., Liang, P., Ye, F., Hou, C.-C., and Pi, L. (2020b). Mesenchymal Stem Cell Therapy for Patients with Ischemic Heart Failure -past, Present, and Future. *Cscr* 15. doi:10.2174/1574888x15666200309144906

Chen, X., Xu, S., Zhao, C., and Liu, B. (2019). Role of TLR4/NADPH Oxidase 4 Pathway in Promoting Cell Death through Autophagy and Ferroptosis during Heart Failure. *Biochem. Biophysical Res. Commun.* 516 (1), 37–43. doi:10.1016/j.bbrc.2019.06.015

Davidson, S. M., and Yellon, D. M. (2018). Exosomes and Cardioprotection - A Critical Analysis. *Mol. Aspects Med.* 60, 104–114. doi:10.1016/j.mam.2017.11.004

Dietl, A., and Maack, C. (2017). Targeting Mitochondrial Calcium Handling and Reactive Oxygen Species in Heart Failure. *Curr. Heart Fail. Rep.* 14 (4), 338–349. doi:10.1007/s11897-017-0347-7

Fang, Z., Yin, X., Wang, J., Tian, N., Ao, Q., Gu, Y., et al. (2016). Functional Characterization of Human Umbilical Cord-Derived Mesenchymal Stem Cells for Treatment of Systolic Heart Failure. *Exp. Ther. Med.* 12 (5), 3328–3332. doi:10.3892/etm.2016.3748

Gao, L., Mei, S., Zhang, S., Qin, Q., Li, H., Liao, Y., et al. (2020). Cardio-renal Exosomes in Myocardial Infarction Serum Regulate Proangiogenic Paracrine Signaling in Adipose Mesenchymal Stem Cells. *Theranostics* 10 (3), 1060–1073. doi:10.7150/thno.37678

Grundmann, S., Hans, F. P., Kinniry, S., Heinke, J., Helbing, T., Bluhm, F., et al. (2011). MicroRNA-100 Regulates Neovascularization by Suppression of Mammalian Target of Rapamycin in Endothelial and Vascular Smooth Muscle Cells. *Circulation* 123 (9), 999–1009. doi:10.1161/circulationaha.110.000323

Guan, Y. T., Xie, Y., Li, D. S., Zhu, Y. Y., Zhang, X. L., Feng, Y. L., et al. (2019). Comparison of Biological Characteristics of Mesenchymal Stem Cells Derived from the Human Umbilical Cord and Decidua Parietalis. *Mol. Med. Rep.* 20 (1), 633–639. doi:10.3892/mmr.2019.10286

Guijarro, D., Lebrin, M., Lairez, O., Bourin, P., Piriou, N., Pozzo, J., et al. (2016). Intramyocardial Transplantation of Mesenchymal Stromal Cells for Chronic Myocardial Ischemia and Impaired Left Ventricular Function: Results of the MESAMI 1 Pilot Trial. *Int. J. Cardiol.* 209, 258–265. doi:10.1016/j.ijcard.2016.02.016

Guo, S., and Chen, X. (2015). The Human Nox4: Gene, Structure, Physiological Function and Pathological Significance. *J. Drug Target.* 23 (10), 888–896. doi:10.3109/1061186x.2015.1036276

Hou, Z., Qin, X., Hu, Y., Zhang, X., Li, G., Wu, J., et al. (2019). Longterm Exercise-Derived Exosomal miR-342-5p. *Circ. Res.* 124 (9), 1386–1400. doi:10.1161/circresaha.118.314635

Hromadnikova, I., Kotlabova, K., Hympanova, L., and Krofta, L. (2016). Gestational Hypertension, Preeclampsia and Intrauterine Growth Restriction Induce Dysregulation of Cardiovascular and Cerebrovascular Disease Associated microRNAs in Maternal Whole Peripheral Blood. *Thromb. Res.* 137, 126–140. doi:10.1016/j.thromres.2015.11.032

Jaquet, K., Krause, K. T., Denschel, J., Faessler, P., Nauerz, M., Geidel, S., et al. (2005). Reduction of Myocardial Scar Size after Implantation of Mesenchymal Stem Cells in Rats: what Is the Mechanism? *Stem Cell Develop.* 14 (3), 299–309. doi:10.1089/scd.2005.14.299

Keerthikumar, S., Chisanga, D., Ariyaratne, D., Al Saffar, H., Anand, S., Zhao, K., et al. (2016). ExoCarta: A Web-Based Compendium of Exosomal Cargo. *J. Mol. Biol.* 428 (4), 688–692. doi:10.1016/j.jmb.2015.09.019

Kim, S., Song, J., Ernst, P., Latimer, M. N., Ha, C.-M., Goh, K. Y., et al. (20202019). MitoQ Regulates Redox-Related Noncoding RNAs to Preserve Mitochondrial Network Integrity in Pressure-Overload Heart Failure. *Am. J. Physiology-Heart Circulatory Physiol.* 318 (3), H682–h695. doi:10.1152/ajpheart.0061710.1152/ajpheart.00617.2019

Kobayashi, K., and Suzuki, K. (2018). Mesenchymal Stem/Stromal Cell-Based Therapy for Heart Failure — what Is the Best Source? —. *Circ. J.* 82 (9), 2222–2232. doi:10.1253/circj.CJ-18-0786

Koju, N., Taleb, A., Zhou, J., Lv, G., Yang, J., Cao, X., et al. (2019). Pharmacological Strategies to Lower Crosstalk between Nicotinamide Adenine Dinucleotide Phosphate (NADPH) Oxidase and Mitochondria. *Biomed. Pharmacother.* 111, 1478–1498. doi:10.1016/j.biopha.2018.11.128

Kriegel, A. J., Baker, M. A., Liu, Y., Liu, P., Cowley, A. W., Jr., and Liang, M. (2015). Endogenous MicroRNAs in Human Microvascular Endothelial Cells Regulate mRNAs Encoded by Hypertension-Related Genes. *Hypertension* 66 (4), 793–799. doi:10.1161/hypertensionaha.115.05645

Kumar, A., Supowit, S., Potts, J. D., and DiPette, D. J. (2019). Alpha-calcitonin Gene-related Peptide Prevents Pressure-overload Induced Heart Failure: Role of Apoptosis and Oxidative Stress. *Physiol. Rep.* 7 (21), e14269. doi:10.14814/phy2.14269

Li, J., Ichikawa, T., Villacorta, L., Janicki, J. S., Brower, G. L., Yamamoto, M., et al. (2009). Nrf2 Protects against Maladaptive Cardiac Responses to Hemodynamic Stress. *Atvb* 29 (11), 1843–1850. doi:10.1161/atvbaha.109.189480

Li, J., Xu, S. Q., Zhao, Y. M., Yu, S., Ge, L. H., and Xu, B. H. (2018). Comparison of the Biological Characteristics of Human Mesenchymal Stem Cells Derived from Exfoliated Deciduous Teeth, Bone Marrow, Gingival Tissue, and Umbilical Cord. *Mol. Med. Rep.* 18 (6), 4969–4977. doi:10.3892/mmr.2018.9501

Linna-Kuosmanen, S., Tomas Bosch, V., Moreau, P. R., Bouvy-Liivrand, M., Niskanen, H., Kansanen, E., et al. (2020). NRF2 Is a Key Regulator of Endothelial microRNA Expression under Proatherogenic Stimuli. *Cardiovasc. Res.* 117, 1339–1357. doi:10.1093/cvr/cvaa219

Lubrano, V., and Balzan, S. (2020). Role of Oxidative Stress-Related Biomarkers in Heart Failure: Galectin 3, α1-antitrypsin and LOX-1: New Therapeutic Perspective? *Mol. Cell Biochem* 464 (1-2), 143–152. doi:10.1007/s11010-019-03656-y

Mao, C., Hou, X., Wang, B., Chi, J., Jiang, Y., Zhang, C., et al. (2017). Intramuscular Injection of Human Umbilical Cord-Derived Mesenchymal Stem Cells Improves Cardiac Function in Dilated Cardiomyopathy Rats. *Stem Cell Res Ther* 8 (1), 18. doi:10.1186/s13287-017-0472-y

Matsushita, K. (2020). Heart Failure and Adipose Mesenchymal Stem Cells. *Trends Mol. Med.* 26 (4), 369–379. doi:10.1016/j.molmed.2020.01.003

Montecalvo, A., Larregina, A. T., Shufesky, W. J., Beer Stolz, D., Sullivan, M. L. G., Karlsson, J. M., et al. (2012). Mechanism of Transfer of Functional microRNAs between Mouse Dendritic Cells via Exosomes. *Blood* 119 (3), 756–766. doi:10.1182/blood-2011-02-338004

Nakamura, Y., Kita, S., Tanaka, Y., Fukuda, S., Obata, Y., Okita, T., et al. (2020). Adiponectin Stimulates Exosome Release to Enhance Mesenchymal Stem-Cell-Driven Therapy of Heart Failure in Mice. *Mol. Ther.* 28 (10), 2203–2219. doi:10.1016/j.ymthe.2020.06.026

Narita, T., and Suzuki, K. (2015). Bone Marrow-Derived Mesenchymal Stem Cells for the Treatment of Heart Failure. *Heart Fail. Rev.* 20 (1), 53–68. doi:10.1007/s10741-014-9435-x

Ni, J., Liu, X., Yin, Y., Zhang, P., Xu, Y.-W., and Liu, Z. (2019). Exosomes Derived from TIMP2-Modified Human Umbilical Cord Mesenchymal Stem Cells Enhance the Repair Effect in Rat Model with Myocardial Infarction Possibly by the Akt/Sfrp2 Pathway. *Oxidative Med. Cell Longevity* 2019, 1–19. doi:10.1155/2019/1958941

Ni, Y., Deng, J., Liu, X., Li, Q., Zhang, J., Bai, H., et al. (2021). Echinacoside Reverses Myocardial Remodeling and Improves Heart Function via Regulating SIRT1/FOXO3a/MnSOD axis in HF Rats Induced by Isoproterenol. *J. Cel. Mol. Med.* 25 (1), 203–216. doi:10.1111/jcmm.15904

Onrat, S. T., Onrat, E., Ercan Onay, E., Yalım, Z., and Avşar, A. (2018). The Genetic Determination of the Differentiation between Ischemic Dilated Cardiomyopathy and Idiopathic Dilated Cardiomyopathy. *Genet. Test. Mol. Biomarkers* 22 (11), 644–651. doi:10.1089/gtmb.2018.0188

Ozaki Tan, S. J., Floriano, J. F., Nicastro, L., Emanueli, C., and Catapano, F. (2020). Novel Applications of Mesenchymal Stem Cell-Derived Exosomes for Myocardial Infarction Therapeutics. *Biomolecules* 10 (5), 707. doi:10.3390/biom10050707

Panday, A., Sahoo, M. K., Osorio, D., and Batra, S. (2015). NADPH Oxidases: an Overview from Structure to Innate Immunity-Associated Pathologies. *Cell Mol Immunol* 12 (1), 5–23. doi:10.1038/cmi.2014.89

Pankratz, F., Hohnloser, C., Bemtgen, X., Jaenich, C., Kreuzaler, S., Hoefer, I., et al. (2018). MicroRNA-100 Suppresses Chronic Vascular Inflammation by Stimulation of Endothelial Autophagy. *Circ. Res.* 122 (3), 417–432. doi:10.1161/circresaha.117.311428

Pop, C., Berce, C., Ghibu, S., Scurtu, I., Soriţău, O., Login, C., et al. (2020). Effects of Lycium Barbarum L. Polysaccharides on Inflammation and Oxidative Stress Markers in a Pressure Overload-Induced Heart Failure Rat Model. *Molecules* 25 (3), 466. doi:10.3390/molecules25030466

Ray, R., Murdoch, C. E., Wang, M., Santos, C. X., Zhang, M., Alom-Ruiz, S., et al. (2011). Endothelial Nox4 NADPH Oxidase Enhances Vasodilatation and Reduces Blood Pressure *In Vivo*. *Atvb* 31 (6), 1368–1376. doi:10.1161/atvbaha.110.219238

Sachinidis, A. (2020). Cardiotoxicity and Heart Failure: Lessons from Human-Induced Pluripotent Stem Cell-Derived Cardiomyocytes and Anticancer Drugs. *Cells* 9 (4), 1001. doi:10.3390/cells9041001

Saleh, D., Abdelbaset, M., Hassan, A., Sharaf, O., Mahmoud, S., and Hegazy, R. (2020). Omega-3 Fatty Acids Ameliorate Doxorubicin-Induced Cardiorenal Toxicity: In-Vivo Regulation of Oxidative Stress, Apoptosis and Renal Nox4, and In-Vitro Preservation of the Cytotoxic Efficacy. *PLoS One* 15 (11), e0242175. doi:10.1371/journal.pone.0242175

Schröder, K., Zhang, M., Benkhoff, S., Mieth, A., Pliquett, R., Kosowski, J., et al. (2012). Nox4 Is a Protective Reactive Oxygen Species Generating Vascular NADPH Oxidase. *Circ. Res.* 110 (9), 1217–1225. doi:10.1161/circresaha.112.267054

Shang, L., Weng, X., Wang, D., Yue, W., Mernaugh, R., Amarnath, V., et al. (2019). Isolevuglandin Scavenger Attenuates Pressure Overload-Induced Cardiac Oxidative Stress, Cardiac Hypertrophy, Heart Failure and Lung Remodeling. *Free Radic. Biol. Med.* 141, 291–298. doi:10.1016/j.freeradbiomed.2019.06.029

Shi, J.-x., Wang, Q.-j., Li, H., and Huang, Q. (2016). Silencing of USP22 Suppresses High Glucose-Induced Apoptosis, ROS Production and Inflammation in Podocytes. *Mol. Biosyst.* 12 (5), 1445–1456. doi:10.1039/c5mb00722d

Shoeibi, S. (2020). Diagnostic and Theranostic microRNAs in the Pathogenesis of Atherosclerosis. *Acta Physiol.* 228 (1), e13353. doi:10.1111/apha.13353

Théry, C., Amigorena, S., Raposo, G., and Clayton, A. (2006). Isolation and Characterization of Exosomes from Cell Culture Supernatants and Biological Fluids. *Curr. Protoc. Cell Biol.* 30 (Unit 3.22). doi:10.1002/0471143030.cb0322s30

Tkach, M., and Théry, C. (2016). Communication by Extracellular Vesicles: Where We Are and where We Need to Go. *Cell* 164 (6), 1226–1232. doi:10.1016/j.cell.2016.01.043

Tulubas, F., Gurel, A., Oran, M., Topcu, B., Caglar, V., and Uygur, E. (2015). The Protective Effects of ω-3 Fatty Acids on Doxorubicin-Induced Hepatotoxicity and Nephrotoxicity in Rats. *Toxicol. Ind. Health* 31 (7), 638–644. doi:10.1177/0748233713483203

Uygur, R., Aktas, C., Tulubas, F., Alpsoy, S., Topcu, B., and Ozen, O. (2014). Cardioprotective Effects of Fish omega-3 Fatty Acids on Doxorubicin-Induced Cardiotoxicity in Rats. *Hum. Exp. Toxicol.* 33 (4), 435–445. doi:10.1177/0960327113493304

Vlassov, A. V., Magdaleno, S., Setterquist, R., and Conrad, R. (2012). Exosomes: Current Knowledge of Their Composition, Biological Functions, and Diagnostic and Therapeutic Potentials. *Biochim. Biophys. Acta (Bba) - Gen. Subjects* 1820 (7), 940–948. doi:10.1016/j.bbagen.2012.03.017

Vrtovec, B., Poglajen, G., and Haddad, F. (2013). Stem Cell Therapy in Patients with Heart Failure. *Methodist DeBakey Cardiovasc. J.* 9 (1), 6–10. doi:10.14797/mdcj-9-1-6

Wang, J., Hu, L., Huang, H., Yu, Y., Wang, J., Yu, Y., et al. (2020). CAR (CARSKNKDC) Peptide Modified ReNcell-Derived Extracellular Vesicles as a Novel Therapeutic Agent for Targeted Pulmonary Hypertension Therapy. *Hypertension* 76 (4), 1147–1160. doi:10.1161/hypertensionaha.120.15554

Wang, K., Zhu, Z. F., Chi, R. F., Li, Q., Yang, Z. J., Jie, X., et al. (2019). The NADPH Oxidase Inhibitor Apocynin Improves Cardiac Sympathetic Nerve Terminal Innervation and Function in Heart Failure. *Exp. Physiol.* 104 (11), 1638–1649. doi:10.1113/ep087552

Xie, Q., Liu, R., Jiang, J., Peng, J., Yang, C., Zhang, W., et al. (2020). What Is the Impact of Human Umbilical Cord Mesenchymal Stem Cell Transplantation on Clinical Treatment? *Stem Cell Res. Ther* 11 (1), 519. doi:10.1186/s13287-020-02011-z

Xu, S., Wang, Y., Yu, M., Wang, D., Liang, Y., Chen, Y., et al. (2020). LongShengZhi Capsule Inhibits Doxorubicin-Induced Heart Failure by Anti-oxidative Stress. *Biomed. Pharmacother.* 123, 109803. doi:10.1016/j.biopha.2019.109803

Youn, S.-W., Li, Y., Kim, Y.-M., Sudhahar, V., Abdelsaid, K., Kim, H., et al. (2019). Modification of Cardiac Progenitor Cell-Derived Exosomes by miR-322 Provides Protection against Myocardial Infarction through Nox2-dependent Angiogenesis. *Antioxidants* 8 (1), 18. doi:10.3390/antiox8010018

Zeringer, E., Barta, T., Li, M., and Vlassov, A. V. (2015). Strategies for Isolation of Exosomes. *Cold Spring Harb Protoc.* 2015 (4), pdb.top074476–323. doi:10.1101/pdb.top074476

Zhang, M., Brewer, A. C., Schröder, K., Santos, C. X. C., Grieve, D. J., Wang, M., et al. (2010). NADPH Oxidase-4 Mediates protection against Chronic Load-Induced Stress in Mouse Hearts by Enhancing Angiogenesis. *Proc. Natl. Acad. Sci.* 107 (42), 18121–18126. doi:10.1073/pnas.1009700107

Zheng, D., Huo, M., Li, B., Wang, W., Piao, H., Wang, Y., et al. (2020). The Role of Exosomes and Exosomal MicroRNA in Cardiovascular Disease. *Front. Cell Dev. Biol.* 8, 616161. doi:10.3389/fcell.2020.616161

Zhou, B., and Tian, R. (2018). Mitochondrial Dysfunction in Pathophysiology of Heart Failure. *J. Clin. Invest.* 128 (9), 3716–3726. doi:10.1172/jci120849

Conflict of Interest: The authors declare that the research was conducted in the absence of any commercial or financial relationships that could be construed as a potential conflict of interest.

Publisher's Note: All claims expressed in this article are solely those of the authors and do not necessarily represent those of their affiliated organizations, or those of the publisher, the editors and the reviewers. Any product that may be evaluated in this article, or claim that may be made by its manufacturer, is not guaranteed or endorsed by the publisher.

Copyright © 2021 Zhong, Tian, Luo, Zou, Wu and Tian. This is an open-access article distributed under the terms of the Creative Commons Attribution License (CC BY). The use, distribution or reproduction in other forums is permitted, provided the original author(s) and the copyright owner(s) are credited and that the original publication in this journal is cited, in accordance with accepted academic practice. No use, distribution or reproduction is permitted which does not comply with these terms.

frontiers in Bioengineering and Biotechnology

ORIGINAL RESEARCH
published: 17 September 2021
doi: 10.3389/fbioe.2021.694908

The Therapeutic Efficacy of Adipose Tissue-Derived Mesenchymal Stem Cell Conditioned Medium on Experimental Colitis Was Improved by the Serum From Colitis Rats

*Li-li Qi, Zhe-yu Fan, Hai-guang Mao and Jin-bo Wang**

School of Biological and Chemical Engineering, Ningbo Tech University, Ningbo, China

Adipose derived mesenchymal stem cells (AD-MSCs) have shown therapeutic potential in treatments of inflammatory bowel disease (IBD). Due to the harsh host environment and poor survival of the cells, controversy concerning the homing, proliferation and differentiation of MSCs in lesion tissue still remains. It has been reported that conditioned media from MSCs could improve the colitis, whereas the therapeutic efficiency could be significantly elevated by the stimulation of pro-cytokines. In this study, we pre-treated the adipose derived MSCs with the serum from colitis rats and then the activated conditioned media (CM-AcMSC) were collected. To compare the therapeutic effects of CM-MSC and CM-AcMSC on IBD, we constructed dextran sodium sulphate (DSS)-induced colitis rat models. The colitis was induced in rats by administrating 5% DSS in drinking water for 10 days, and the disease symptoms were recorded daily. The colon histopathological changes were observed by different staining methods (H&E and PAS). The expression levels of MUC2 and tight junctions (TJs) were determined by RT-qPCR. The levels of inflammatory cytokines were analyzed by ELISA and western blot analysis. Our findings suggested that CM-AcMSC was more effective in ameliorating the clinical features and histological damage scores. Treatment with CM-AcMSC significantly increased the expression of MUC2 and TJs and suppressed the production of pro-inflammatory cytokines in colonic tissues of colitis rats. The inhibitory effects of CM-AcMSC on inflammatory responses of colitis rats were mediated by NF-κB signaling pathway. These results suggested that pre-activation of MSCs with serum from colitis rats could promote the production of paracrine factors and improve the therapeutic effects of conditioned medium on colitis rats.

Keywords: adipose tissue-derived mesenchymal stem cell, serum from colitis model rat, conditioned medium, inflammatory bowel disease, therapeutic efficacy

OPEN ACCESS

Edited by:
Antonietta Rosa Silini, Fondazione Poliambulanza Istituto Ospedaliero, Italy

Reviewed by:
Federica Francesca Masieri, University of Suffolk, United Kingdom
Jehan J. El-Jawhari, Nottingham Trent University, United Kingdom
Maria Gazouli, National and Kapodistrian University of Athens, Greece

***Correspondence:**
Jin-bo Wang
wjb@nbt.edu.cn

Specialty section:
This article was submitted to Preclinical Cell and Gene Therapy, a section of the journal Frontiers in Bioengineering and Biotechnology

Received: *14 April 2021*
Accepted: *06 September 2021*
Published: *17 September 2021*

Citation:
Qi L-l, Fan Z-y, Mao H-g and Wang J-b (2021) The Therapeutic Efficacy of Adipose Tissue-Derived Mesenchymal Stem Cell Conditioned Medium on Experimental Colitis Was Improved by the Serum From Colitis Rats. Front. Bioeng. Biotechnol. 9:694908. doi: 10.3389/fbioe.2021.694908

INTRODUCTION

Inflammatory bowel disease (IBD), including ulcerative colitis (UC) and Crohn's disease (CD), is characterized by chronic and relapsing inflammation in the intestinal mucosa (Maloy and Powrie, 2011; Molodecky et al., 2012). Although the pathogenesis of IBD remains unclear, it is generally agreed that the disorders of immune system, genetic influences and environmental factors are involved in the initiation and development of the disease (Cho, 2008; Neurath, 2014). Gut microbiota is an important environmental factor in the progression of IBD (Marchesi et al., 2016). The IBD patients present with various severe symptoms, including abdominal pain, bloody stool, and persistent diarrhea (Strober et al., 2007). Current treatment options for IBD include anti-inflammatory and immune-modulating drugs, corticosteroids, biological agents and surgery (Pithadia and Jain, 2011). However, the effects of most therapies are scant. Anti-TNF treatment is an efficient therapy and has been increasingly employed in clinical practice. However, about 40% of IBD patients do not respond to this therapy (Hendy et al., 2016; Cohen and Sachar, 2017). Therefore, it is essential to find the alternative therapies for IBD.

Mesenchymal stromal cells (MSCs) are multipotent adult stem cells (Jiang et al., 2002), which are highly proliferative and fibroblast-like in appearance. MSCs claimed to derive only by bone marrow (BM-MSCs) and adipose tissue (AD-MSCs). (Katz et al., 2005). MSCs belong to pluripotent stem cells and have the potential for multidirectional differentiation. In 1999, it was first reported that Pittenger successfully induced bone marrow MSC into adipocytes, osteoblasts and chondrocytes *in vitro* (Pittenger et al., 1999), which was known as the classic tri-lineage differentiation capacity of MSCs.In addition to the ability of cell differentiation, MSCs suppress the inflammation via secretion of anti-inflammatory factors. MSCs can also exert angiogenic and anti-apoptotic effects through the secretion of paracrine factors (Stavely et al., 2015; Nammian et al., 2021). Therefore, MSCs have emerged as an attractive candidate therapy for many diseases, including IBD (Arranz et al., 2018; Silva et al., 2018; Kang et al., 2020). The previous investigations have indicated that the therapeutic efficacy of MSCs does not depend on cell-to-cell interactions, but on the effects mediated by the soluble active factors secreted by the cells (Eleuteri and Fierabracci, 2019; Gorgun et al., 2021). The components of MSCs, such as conditioned medium and extracellular vesicles, have been verified to ameliorate the experimental colitis in mice (Legaki et al., 2016). Interestingly, pre-activation of MSCs with pro-inflammatory factors could significantly elevate their therapeutic capacity (Fuenzalida et al., 2016; Shin et al., 2020; Lim et al., 2021). Dextran sodium sulfate (DSS)-induced colitis is one of the most common experimental models. In 1985, Ohkusa induced enteritis in hamsters by oral DSS feeding and reported that these lesions showed erosion, ulceration, inflammatory cell infiltration, crypt abscesses and epithelioglandular hyperplasia as in human UC (Bamba et al., 2012). Due to its simple preparation, high success rate, and similar to human UC lesions, it is an ideal model for studying the pathogenesis of UC and evaluating the efficacy of drugs, but the mechanism of colitis induction is unclear. However, the exogenous inflammatory stimuli might result in tissue damages or provoke seriously hypersensitive responses in host. The levels of inflammatory factors are considerably higher in the colitis patients at the active stage of the disease in comparison to control (Gholamrezayi et al., 2020).

In the present study, we separated the serum from the colitis model rats and preactivated the adipose MSCs with the serum. The activated MSC-derived conditioned medium (CM-AcMSC) was collected and then injected into the colitis rats via tail vein. Our results demonstrated that CM-MSC pre-activated with the serum from colitis rats had better therapeutic efficacy on IBD than untreated CM-MSC.

MATERIALS AND METHODS

Animal Maintenance

Male SD rats (weighing 300–320 g) were purchased from the Laboratory Animal Center of Zhejiang Province (Hangzhou, China). The rats had *ad libitum* access to food and water under a 12-h dark-light cycle. All procedures were performed under approval of the ethical committee in Zhejiang University and decided following the rule of the NIH Guide for the Care and Use of Laboratory Animals (NIH Publication No. 85-23, 1985, revised 1996).

Isolation and Culture of Rat Adipose Tissue-Derived MSCs

Subcutaneous fat was carefully dissected from the inguinal region of rats under inhalatory isoflurane anaesthesia. After rinsing with Hank's balanced salt solution (Gibco, Shanghai, China) and mincing, the fat tissue was digested in 0.1% collagenase type I (Gibco, Shanghai, China) in PBS at 37°C for 60 min. After being centrifugated for 15 min at 1,000×g, the cell pellets were resuspended in complete culture medium: DMEM/F12 (Gibco, Shanghai, China) supplemented with 100 U/ml penicillin, 100 mg/ml streptomycin, 2 mM L-glutamine, and 10% fetal bovine serum (Gibco, Shanghai, China). The cells were maintained in a humid atmosphere of 5% CO_2 and 95% air at 37°C.

Characterization of Rat Adipose MSCs

CD73-PE (Biolegend, Cat.127,205), CD90-APC (Biolegend, Cat.328,113), CD105-PE (Biolegend, Cat.120,407), CD34-APC (Biolegend, Cat.343,607) and CD45-PE (Biolegend, Cat.103,105) were measured by flow cytometry to confirm the minimum markers to define the MSCs as per standard criteria.

The classic tri-lineage differentiation experiment was also carried out. MSCs were phenotypically characterized by the capacity to differentiate into adipocytes, osteocytes and chondrocytes. Adipogenic differentiation is induced by supplementation of 50 μg/ml indomethacin (Sigma), 5.0 μg/ml insulin, and10^{-3} mM dexamethasone (Sigma) in the complete culture media. To detect the differentiation, the MSCs were fixed in 10% neutral formalin and stained with Oil red O (Sigma-Aldrich, Shanghai, China). To induce the MSCs to differentiate into osteocytes, the cells were cultured for 3 weeks in complete H-DMEM with 10^{-5} mM dexamethasone (Sigma), 10 mM β-glycerolphosphate (Sigma), and 50 mM ascorbic acid 2-phosphate (Sigma). To confirm the osteogenesis, the cells were fixed in 10% neutral formalin and then stained with 2% Alizarin Red S (Sigma-Aldrich, Shanghai, China). For chondrogenic differentiation, the cells were cultured for 3 weeks in complete H-DMEM with 1% Insulin-Transferrin-Selenium (ITS) (Gibco, Cat.41400045), 10 ng/ml TGF-β3 (Peprotech, Cat.100-36E), 50 nM ascorbate-2-phosphate (Gibco, Cat.11360070) and 1% antibiotic, and finally analyzed by staining with toluidine blue staining.

Induction of Experimental Colitis

Colitis was induced in SD rats by oral administration of dextran sulfate sodium (DSS) (Solarbio Life Sciences, Beijing, China) as described previously (Zhu et al., 2019). Briefly, the colitis was induced in rats by administrating 5% DSS in drinking water for 10 days.

MSC Pre-activation and Collection of MSC Conditioned Media

After euthanizing the colitis rats, blood was collected from the carotid artery and collected in the procoagulant tube. After being left at room temperature for about 30 min, the blood was centrifuged at 3,000 rpm for 10 min. The supernatant was the serum, which was then filtered by the membranes of 0.45 and 0.22 μm twice respectively, and finally obtained the serum of colitis rats.

Adipose MSCs were plated in 75 cm^2 flasks at a concentration of 1×10^6 cells/mL in the complete culture medium, and incubated at 37°C and 5% CO_2. When the cells reached to 80% confluency, the culture medium and nonadherent cells were removed. To obtain the activated MSC conditioned medium, the MSCs were pretreated with complete medium containing 10% of serum from colitis rat for 24 h. MSC conditioned media treated (CM-AcMSC) or untreated (CM-MSC) with colitis serum were collected and centrifuged at 2000 rpm for 10 min to remove impurities and then filtered twice by membranes of 0.45 and 0.22 μm respectively. Then the obtained conditioned media was intravenously injected into the colitis rats.

Study Design

Animals of 3 weeks of age were randomly divided into four groups: rats received no treatment for 10 days and then injected daily with 1.5 ml of PBS for another 10 days (control group), CTR; DSS+0.9% normal saline, rats received DSS in distilled water (5%) for 10 days and then injected daily with 1.5 ml of normal saline via tail vein for another 10 days; DSS + CM-MSC, mice received DSS in distilled water (5%) for 10 days and then injected daily with 1.5 ml of CM-MSC via tail vein for another 10 days; DSS + CM-AcMSC, rats received DSS in distilled water (5%) for 10 days and then injected daily with 1.5 ml of CM-AcMSC via tail vein for another 10 days. Each group included 15 rats.

Analysis of the Disease Activity Index

The body weight changes of the animal were recorded daily. The DAI was determined daily by body weight loss, stool consistency, and detection of rectal bleeding according to the method as previously described (**Table 1**) (Heidari et al., 2018). DAI = combined score of weight loss, stool consistency and bleeding.

Histological Damage Score Evaluation

After euthanasia, the animals were sacrificed and the colon was cut longitudinally. Each group contained 15 rats. The colon tissues were stained by Hematoxylin-eosin and Alcian Blue-Periodic Acid Schiff, respectively, and analyzed using a light microscope. The scoring criteria parameters were as followed: epithelial lesion (0, none damage; 1, some loss of goblet cells; 2, extensive loss of goblet cells; 3, some loss of crypts; 4, extensive loss of crypts); infiltration (0, none infiltration; 1, infiltration around crypt bases; 2, infiltration spreading to muscularis mucosa; 3, extensive infiltration in the muscularis mucosa with abundant oedema; 4, infiltration spreading to submucosa) (Wang et al., 2016). The total grades were calculated by adding the scores of each sample.

Hematoxylin-Eosin Staining

The colonic tissues of the rats were fixed in 10% neutral buffered formalin and then transferred to a series of graded ethanol baths (70, 80, 95, 100%). Fixed tissues were embedded in paraffin and cut into 4 μm thick slices. After deparaffinization and hydration, the colonic tissues were stained in hematoxylin for 3–5 min. And then the tissues were stained with 1% Eosin for 15 min. The slides were washed with tap water and cleared with xylene. The histological changes were observed with optical microscopy (Nikon, Tokyo, Japan). Sections were evaluated based on the cell infiltration of inflammatory cells and epithelial damage as previously described (Dai et al., 2015).

Alcian Blue-Periodic Acid Schiff Staining

Alcian blue-periodic acid schiff (AB/PAS) staining was conducted to observe the variation of goblet cells. 5 mm of colonic tissue was immediately fixed in Carnoy's fluid at 4°C for 2 h. Fixed colon tissues were embedded in paraffin and cut into 5 μm sections and subjected to AB/PAS staining. The variation of goblet cells and integrity of mucus were analyzed using a microscope (Nikon E100, Tokyo, Japan).

Quantitative Reverse Transcription PCR

Colonic RNA isolation was performed using the total RNA Kit (OMEGA Bio-Tek) according to the instructions. About 20 mg tissue mixed with Lysis Buffer was homogenized to extract total RNA. The purity and concentration of the extracted total RNA were tested by the NanoDropND2000 spectrophotometer (Thermo Fisher Scientific, United States). The cDNA was synthesized by the reverse transcription kit (Takara, China) at 42°C for 60 min with the oligo dT-adaptor primer according to the instruction. Real time PCR was performed with one-step qRT-PCR Kit (TOYOBO) in CFX Connect System (Bio-Rad, California, United States) with 20-μl volume, including 2 μl of cDNA, 0.8 μl of forward primer, 0.8 μl of reverse primer, 10 μl of

TABLE 1 | The standard of DAI score.

Score	Body weight change	Stool consistency	Bleeding
0	With no change/decrease	Formed	Negative
1	1–5% decrease	Soft	Positive occult blood
2	6–10% decrease	Loose	Visible bleeding
3	11–20% decrease	Watery	Severe bleeding
4	More than 20% decrease	—	—

TABLE 2 | Primers used for RT-qPCR.

	Forward primer (5–3′)	Reverse primer (5–3′)
claudin-1	AGCTGCCTGTTCCATGTACT	CTCCCATTTGTCTGCTGCTC
occludin	ACGGACCCTGACCACTATGA	TCAGCAGCAGCCATGTACTC
Z O -1	ACCCGAAACTGATGCTGTGGATAG	AAATGGCCGGGCAGAACTTGTGTA
MUC2	GCTGACGAGTGGTTGGTGAATG	GATGAGGTGGCAGACAGGAGAC
TNF-α	CCCTCACACTCAGATCATCTTCT	CTACGACGTGGGCTACAG
IL-1β	GCAACTGTTCCTGAACTCAAC	ATCTTTTGGGGTCCGTCAACT
IL-6	CTCTGGCGGAGCTATTGAGA	AAGTCTCCTGCGTGGAGAAA
IL-10	AGGGCCCTTTGCTATGGTGT	TGGCCACAGTTTTCAGGGAT
GAPDH	GAAGGTGAAGGTCGGAGTCAAC	CATCGCCCCACTTGATTTTGGA

2 × SYBR Premix Ex Taq II, 0.4 μl of ROX Reference Dye (50x) and 6 μl of nuclease-free water. Primer sequences were listed in **Table 2**. Real time PCR conditions were as follows: 5 min denaturation at 98 °C, followed by 33 cycles at 95°C at 30 s, 60°C for 30 s, and then 72 °C for 1 min. Data were analyzed using the CFX Manager software (Bio-Rad, California, United States). The data were normalized against GAPDH and expressed as fold change over mock ($2^{-\Delta\Delta Ct}$). Each sample was treated in triplicate to ensure statistical analysis significance.

Western Blot Analysis

The fresh colon tissue of about 100 mg was washed for three times with PBS, and then lysed in 300 μL RIPA buffer according to the manufacturer's instructions (Beyotime, Shanghai, China). The protein concentrations were measured using BCA kits (Beyotime, Shanghai, China). The colonic tissue proteins (10 μg/lane) were loaded onto 12.5% separation gels for SDS-PAGE and then transfer to 0.45-μm nitrocellulose membranes (Merck). The membranes were blocked with 5% skim milk in TBS-T for 1.5 h, then shaken with primary antibody at 4°C overnight. After being washed with TBS-T for three times, the membranes were shaken with secondary antibodies conjugated with horseradish peroxidase for 1.5 h at room temperature. Chemiluminescent signals were detected with imaging analyzer (ChemiDocXRS system). Densitometry analysis was visualized using ImageJ Software. The primary antibodies include anti-P-NF-κB p65 (CST, Cat. 3003), anti-NF-κB p65 (CST, Cat.8242), anti-IκBα (CST, Cat. 9,242),anti-P-IκBα (CST, Cat.2859), the secondary antibody includes goat anti-rabbit antibody (Abcam, ab6721)

Cytokine Measurements

To detect the levels of inflammatory cytokines such as interferon-γ (IFN-γ), interleukin-1β (IL-1β), IL-6, and TNF-α, the colon tissue was homogenized in cold PBS (containing 1 mM phenylmethylsulfonyl fluoride). After that, the mixture was centrifuged (11,000×g, 15 min at 4 °C) and the supernatants were collected. The levels of IFN-γ, IL-1β, IL-6 and TNF-α were determined with ELISA kits (Multisciences Biotech, Hangzhou, China) according to the manufacturer's instructions. The colonic tissue cytokine levels were expressed as picograms per Gram of tissue protein.

Statistical Analysis

The results are presented as mean values ±S.E. The data were analyzed using the SPSS statistics software. Analyses of variance with Student's *t* tests were used for intergroup comparisons. Comparisons between three or more groups were performed with a one-way ANOVA, followed by a post hoc Bonferroni's test for significance. p value <0.05 was considered significant.

RESULTS

Rat Adipose-Derived Mesenchymal Stem Cells Showed the Characteristics of MSCs

As shown in **Figure 1A**, the flow cytometry results showed that surface markers of MSCs, CD73 (99.79%), CD90 (99.92%) and CD105 (99.82%) were all positive (>95%), while CD34 (0.30%) and CD45 (0.16%) were all negative. These results meet the minimum markers to confirm the MSCs as the International Society for Cellular Therapy (ISCT) defined.

As shown in **Figure 1B**, the cells exhibited spindle-shaped morphology at passage 3. The differentiation potentials of Ad-MSCs to osteocytes, adipocytes, and chondrocytes were assessed with Oil Red-O staining and Alizarin Red staining and Alcian Blue staining, respectively. As shown in **Figure 1C**, 3 weeks after osteogenic induction, the cell morphology disappeared and mineralized nodules could be observed in the MSC media

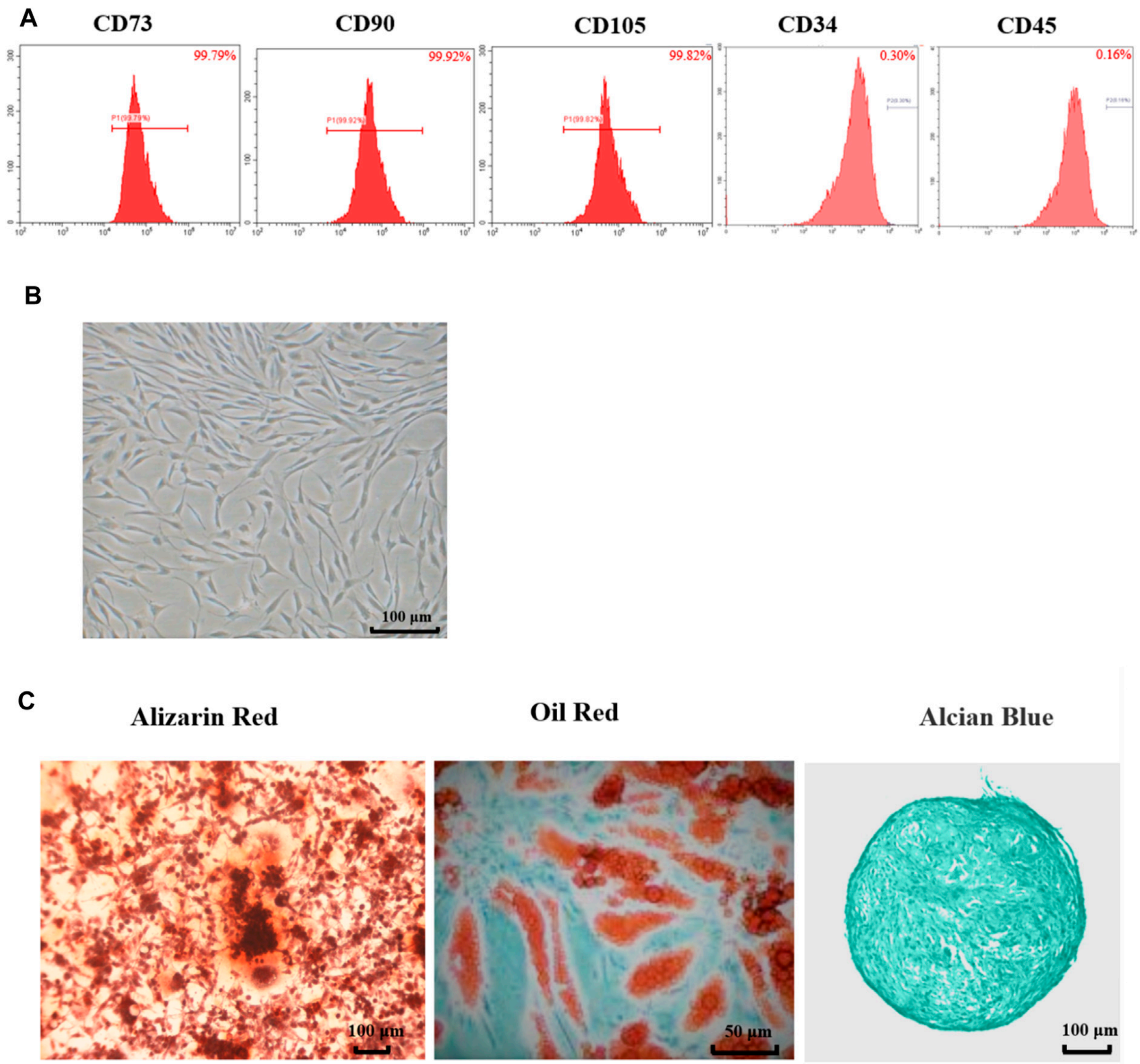

FIGURE 1 | Characteristics of adipose-derived mesenchymal stem cell from rats. **(A)** Flow cytometry of Ad-MSCs by CD73, CD90, CD105, CD34 and CD45. **(B)** The morphology of Ad-MSCs. **(C)** Tri-lineage differentiation capacity of MSCs: stained with Oil Red-O after induction into adipocytes, stained with Alizarin Red after induction into osteocytes and stained with Alcian Blue after induction into chondrocytes.

stained with Alizarin Red. Three weeks after adipogenic induction, lipid vacuoles were visible in Ad-MSCs. Three weeks after chondrogenic induction, blue tint could be seen under the microscope. These results confirmed that the cells we obtained were Ad-MSCs, meeting the capacity for trilineage mesenchymal differentiation of MSCs as ISCT defined, which could be used in subsequent experiments.

CM-AcMSC Were More Effective Than CM-MSC to Ameliorate the DSS-Induced Colitis in Rats

Acute colon inflammatory responses were induced in rats by administration of 5% DSS for 5 days. The symptoms of weight loss, diarrhea, bloody stools and reduced activities appeared in the DSS induced colitis rats. As shown in **Figure 2**, treatment with CM-MSC or CM-AcMSC significantly inhibited the body weight loss and decreased the DAI of colitis model rats (**Figure 2**). From day 4, the treatment groups began to show body weight loss, and from day 6 the DSS + CM-AcMSC treatment group showed significantly lower body weight loss ($p < 0.05$), compared to DSS + CM-MSC group and DSS group, the decreases were about 32.8 and 9.9%, respectively. Finally, DSS + CM-AcMSC group showed the lowest body weight loss ($p < 0.01$) from day 8 to day 10 among the three treatment groups (**Figure 2A**). In the terms of DAI, from day 4, the DAI of treatment groups began to rise, and from day 6 the group of treatment with CM-AcMSC showed significantly lower ($p < 0.05$) DAI than the groups of

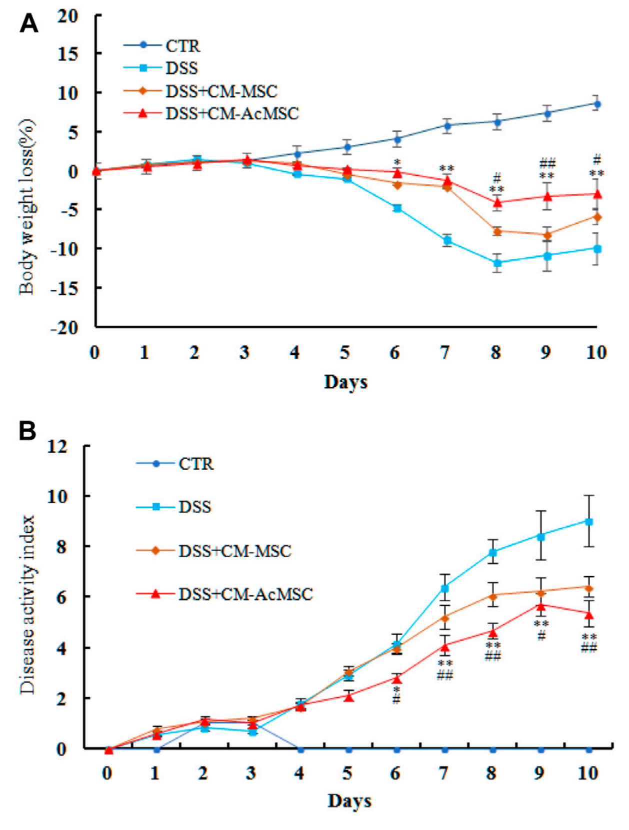

FIGURE 2 | CM-AcMSC effectively alleviated the body weight loss and DAIof DSS induced colitis model rats, $n = 15$. **(A)** Body weight was measured daily (DSS *vs* DSS + CM-Ac-MSC, $^{*}p < 0.05$, $^{**}p < 0.01$; DSS + CM-MSC *vs* DSS + CM-Ac-MSC, $^{\#}p < 0.05$, $^{\#\#}p < 0.01$). (B) DAI was measured during the disease process (DSS *vs* DSS + CM-Ac-MSC, $^{*}p < 0.05$, $^{**}p < 0.01$; DSS + CM-MSC *vs* DSS + CM-Ac-MSC, $^{\#}p < 0.05$, $^{\#\#}p < 0.01$).

treatment with DSS and CM-MSC, and finally showed the significantly lowest ($p < 0.01$) among the three treatment groups. The results indicated that CM-AcMSC could more effectively impede the disease progress than CM-MSC.

On the twenty-first day, macroscopic evaluation of the abdominal cavity was conducted. In the DSS induced colitis model rats, the signs of colon hyperaemia and colonic wall thickening were obviously observed, whereas the symptoms were significantly ameliorated by the injection of CM-MSC or CM-AcMSC (**Figure 3A**). The colonic paraffin sections were stained with H&E. CTR group showed expected colonic mucosal histology with normal crypts and intact structure. However, the colonic mucosal epithelium and crypts were all destructed in the colitis model rats treated with DSS. Mucosal edema, inflammatory cell infiltration and muscle thickening were also observed in the colonic sections of DSS induced colitis rats. Compared to the DSS group, the CM-MSC group possessed more intact colonic epithelium and crypts with reduced inflammatory cell infiltration. Treatment with CM-AcMSC almost diminished the DSS induced morphologic changes, significantly reduced the muscle thickening, and prevented inflammatory cell infiltration compared to the CM-MSC group (**Figure 3A**). Mucus is the primary barrier to protect the intestine from the invasion of pathogens and harmful macromolecules. PAS staining was performed to assess the integrity of colonic mucus layer and the abundance of goblet cells. The colonic mucus was extensively damaged and goblet cell abundance was evidently decreased in DSS induced colitis group compared with the control group. Treatment with CM-MSC improved the mucus integrity and goblet abundance. In the CM-AcMSC group, the degree of the mucus integrity is similar to the control group (**Figure 3A**). As shown in **Figure 3C**, both CM-MSC and CM-AcMSC significantly reduced the histological damage scores, whereas CM-AcMSC were more effective than CM-MSC. These results suggested that CM-AcMSC could efficiently improve DSS induced colitis. DSS treatment could significantly result in the shortening of colon length in colitis rats, while treatment with CM-MSC or CM-AcMSc could markedly restored the colon length to a threshold close to control (**Figure 3B**).

CM-AcMSC Upregulated the Expression of MUC2 and Tight Junctions

DSS induced colitis could result in the injury of intestinal mucosal barrier. Intestinal mucosal barrier mainly consists of tight junctions (TJs), gap junctions and adherens junctions. Among these, TJs are the major components of mucosal barrier. In this study, the expression levels of TJs (Claudin-1, Occludin and ZO-1) and MUC2 were determined by RT-qPCR. As described in **Figure 4**, both CM-MSC and CM-Ac-MSC prominently up-regulated the mRNA levels of Claudin-1, Occludin, ZO-1 and MUC2 compared with the DSS group. The CM-MSC and CM-Ac-MSC group showed about 41.2 and 58.8% higher ($p < 0.01$) Claudin-1 mRNA expression level than DSS group, while no difference was showed between the CM-MSC and CM-Ac-MSC groups ($p > 0.05$). For Occludin mRNA expression level, the CM-MSC and CM-Ac-MSC group showed about 59.5 and 97.6% higher ($p < 0.01$) than DSS group, and CM-Ac-MSC group showed significantly higher than CM-MSC group ($p < 0.01$). For ZO-1 mRNA expression level, CM-Ac-MSC group showed 36.5% higher ($p < 0.05$) than DSS group, while no difference was showed between the CM-MSC and DSS group ($p > 0.05$). For MUC2 mRNA expression level, the CM-MSC and CM-Ac-MSC group showed 29.3% ($p < 0.05$) and 61.0% ($p < 0.01$) higher than DSS group, and CM-Ac-MSC group also showed 24.5% higher than CM-MSC group ($p < 0.01$). Overall, as compared with CM-MSC group, CM-AcMSC group significantly up-regulated the mRNA levels of Occludin, ZO-1 and MUC2, but no obvious difference was shown in the mRNA level of Claudin-1.

CM-AcMSC Attenuated the Pro-inflammatory Cytokines of Colonic Tissues

TNF-α, IL-1β and IL-6 are the cytokines which play pro-inflammatory roles in the process of ulcerative colitis. RT-qPCR results indicated that mRNA levels of these cytokines were markedly increased in the DSS group compared with the control, whereas treatment with CM-MSC or CM-AcMSC

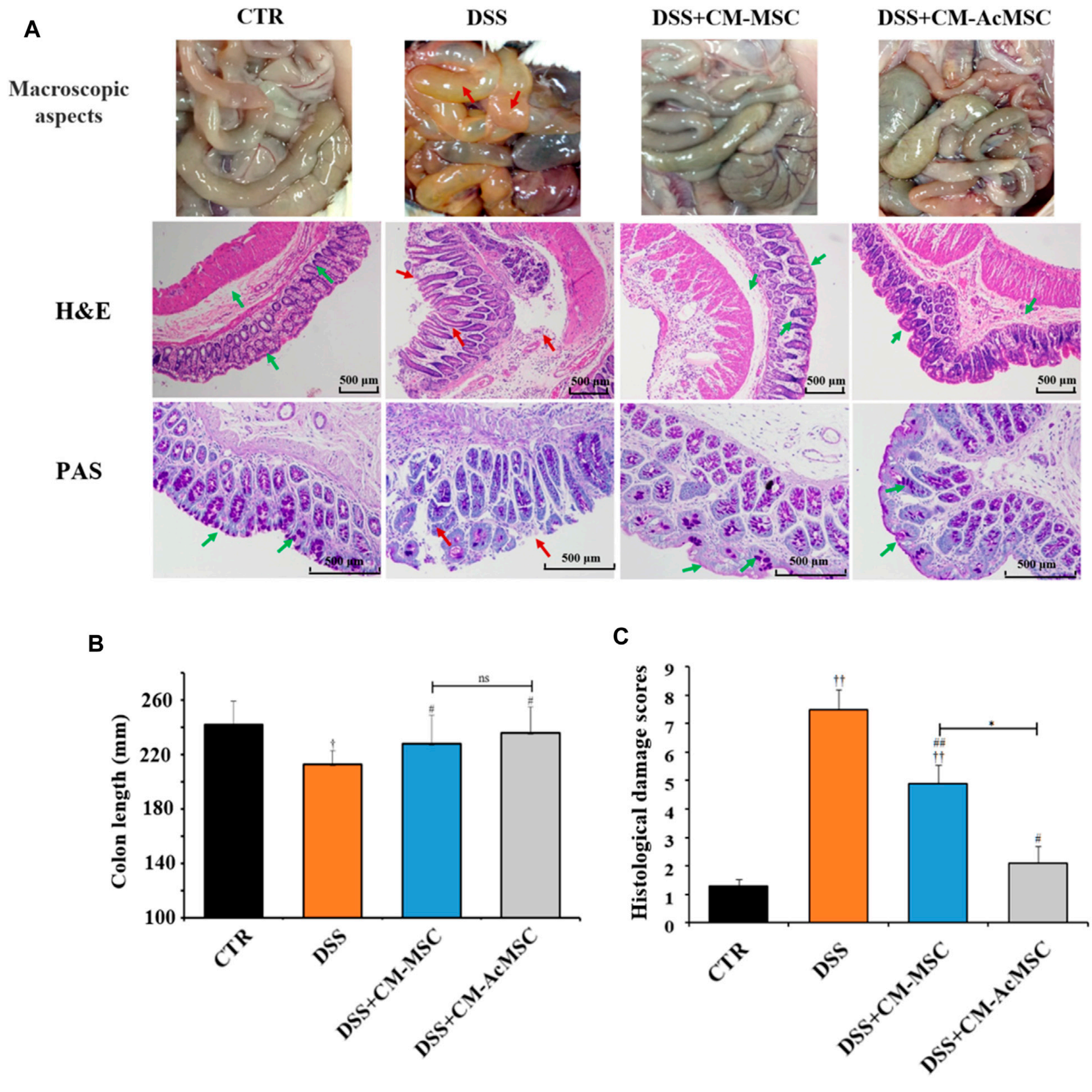

FIGURE 3 | CM-AcMSC significantly improved colonic histopathological feature in model rats, $n = 15$. **(A)** Macroscopic aspects of the colon in rats, paraffin sections of colon tissues were stained with hematoxylin and eosin (H&E), and paraffin sections of colon tissues were stained with Periodic Acid-Schiff (PAS), respectively. **(B)** The length of colons was measured per group. $^{\dagger}p < 0.05$, $^{\dagger\dagger}p < 0.01$ *vs* CTR; $^{\#}p < 0.05$, $^{\#\#}p < 0.01$ *vs* DSS; $^{*}p < 0.05$, $^{**}p < 0.01$. **(C)** Histological damage scores were evaluated according to scoring criteria parameters.

suppressed the expression of TNF-α, IL-1β and IL-6 (**Figure 5A**). The CM-AcMSC group had significantly lower levels of these cytokines in comparison with CM-MSC group (**Figure 5A**). ELISA results showed that the production of TNF-α, IL-1β and IL-6 in the colon tissues was significantly elevated in the DSS-induced rats but was markedly reduced in the rats treated with CM-MSC or CM-AcMSC (**Figure 5B**). CM-AcMSC exhibited lower levels of pro-cytokines than that of CM-MSC group (**Figure 5B**). As an important anti-inflammatory cytokine, the expression level of IL-10 was determined with RT-qPCR and ELISA. Compared to the DSS and CM-MSC group, CM-AcMSC group had higher expression level of IL-10 (**Figure 5B**).

CM-AcMSC Inhibited the Activation of NF-κB Signaling Pathway in the Colon Tissues

To investigate whether the effects of CM-AcMSC or CM-MSC on colitis were mediated by NF-κB signaling pathway, western

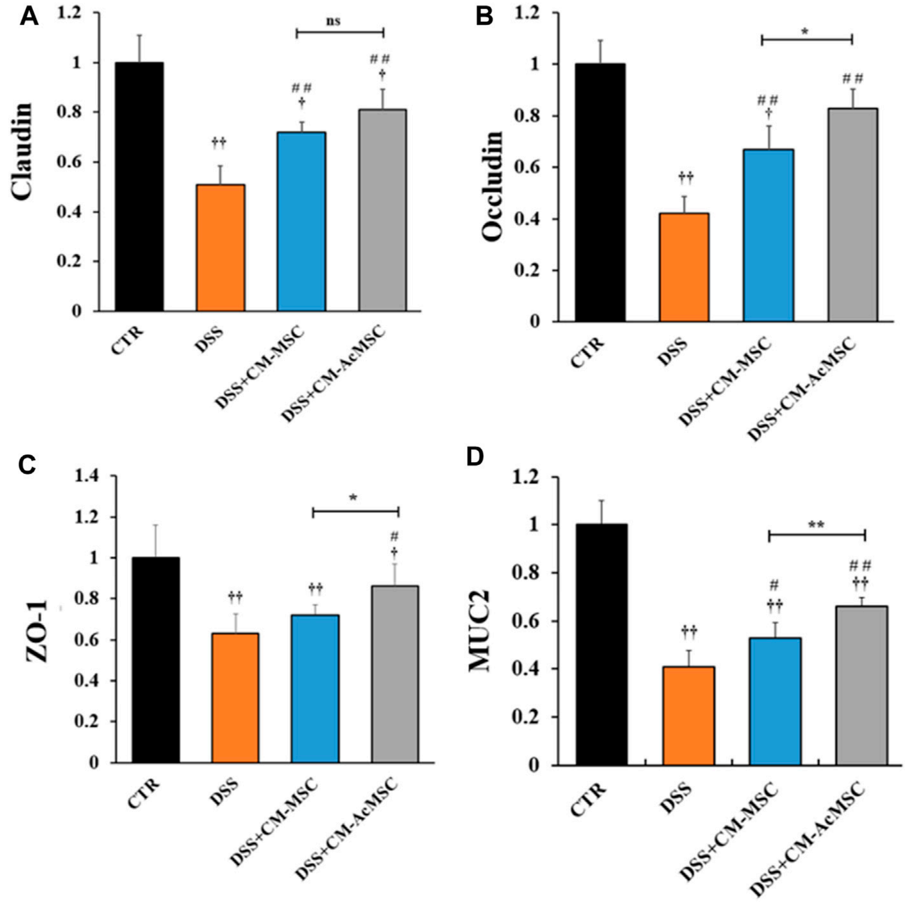

FIGURE 4 | CM-AcMSC enhanced the mRNA expression levels of tight junctions (Claudin, Occludin and ZO-1) and MUC2 in colon tissues, $n = 6$. The mRNA expression levels determined by real time PCR, normalized by β-actin. **(A)** Claudin-1. **(B)** Occludin. **(C)**ZO-1. **(D)**MUC2. $^{\dagger}p < 0.05$, $^{\dagger\dagger}p < 0.01$ *vs* CTR; $^{\#}p < 0.05$, $^{\#\#}p < 0.01$ *vs* DSS; $^{*}p < 0.05$, $^{**}p < 0.01$.

blot analysis was performed to examine the expression levels of the key proteins in this pathway. As described in **Figure 6**, treatment with CM-AcMSC or CM-MSC significantly suppressed the phosphorylation of p65 subunit which was highly activated in DSS group. The level of p-NF-κB (p65) in CM-AcMSC group was obviously lower than that of CM-MSC group. In unstimulated cells, NF-κB is associated with IκB including IκBα, IκBβ and IκBγ. After activated by IKK, IκB dissociated from NF-κB complex (p50/p65). Then the p50/p65 complexes are activated and then promote the expression of down-streaming proteins. As shown in **Figure 6**, IκBα was highly phosphorylated in the colonic tissues from colitis model rats induced by DSS, while treatment with CM-MSC or CM-AcMSC markedly inhibited the activation of IκBα by IKK. The levels of *p*-IκBα in CM-AcMSC group was significantly lower than those of CM-MSC. There was no difference in the levels of *p*-IκBα between CM-AcMSC group and control group (**Figures 6A**,**B**). These results demonstrated that treatment with CM-MSC or CM-AcMSC could effectively suppress the activation of NF-κB signaling pathway whereas CM-AcMSC was more effective.

DISCUSSION

In the clinical practice, it is difficult to effectively treat ulcerative colitis. Most therapies exhibited many side effects or failed to maintain the remission (Lee et al., 2016). Cell therapy is a promising treatment for IBD (Pak et al., 2018). MSCs are multipotent cells which have been tested in clinical studies for the treatment of IBD. In recent years, MSCs have garnered substantial interest because they have low immunogenicity and are easy to be extracted from adult adipose and bone marrow tissues (Grim et al., 2021). One of the important features of MSCs is the capacity of tri-lineage differentiation, and our result in **Figure 1C** showed that the cells we obtained had the potentials to differentiate into osteocytes, adipocytes and chondrocytes. Moreover, the flow cytometry results in **Figure 1A** showed CD73 (99.79%), CD90 (99.92%) and CD105 (99.82%) were all positive (>95%), while CD34 (0.30%) and CD45 (0.16%) were all negative. These are the key surface markers of MSCs, which play important roles in the identification of stem cells suggested by the International Society for Cellular Therapy (ISCT) (Pittenger et al., 1999). These results indicated that the cells we obtained meet the

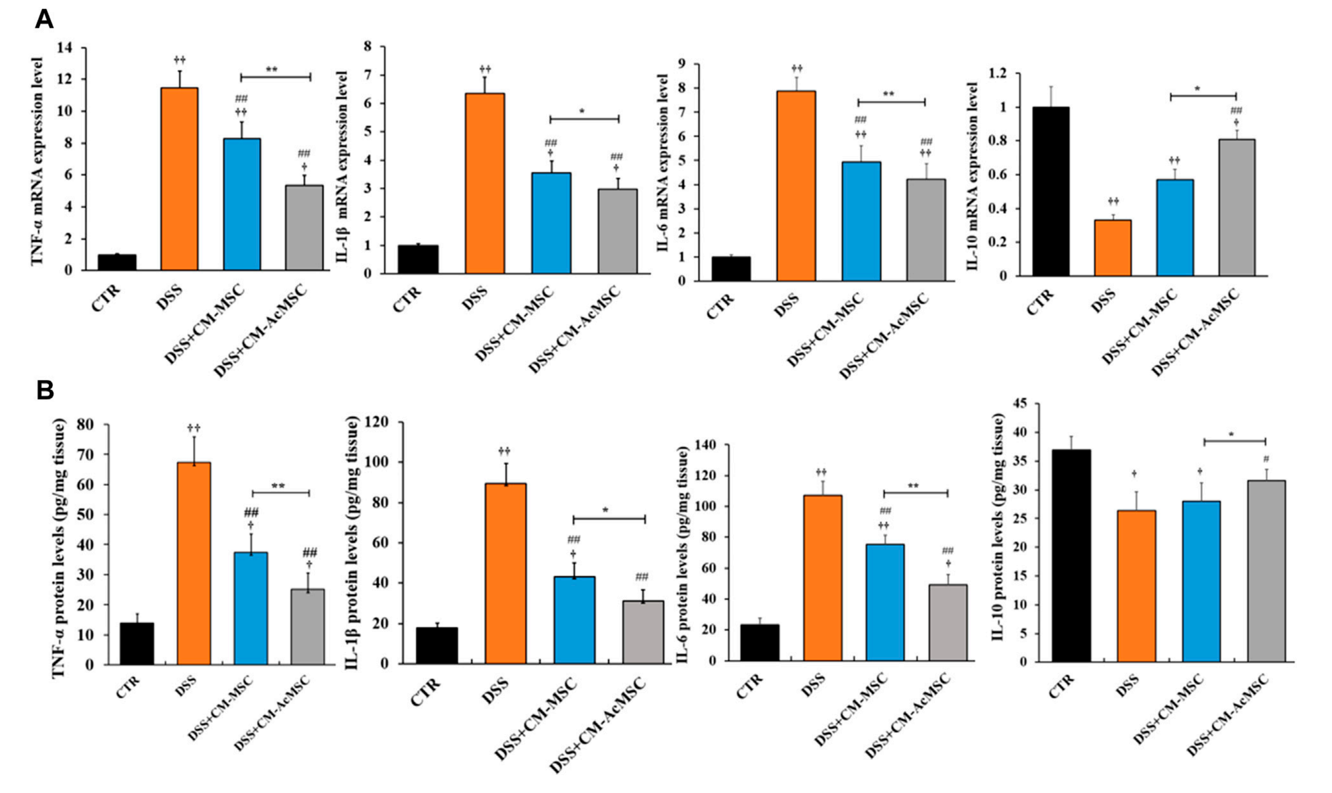

FIGURE 5 | CM-AcMSC inhibited the expression and production of cytokines in colon tissues, $n = 6$. **(A)** The mRNA levels of cytokines such as TNF-α, IL-1β, IL-6, and IL-10 were determined by quantitative reverse-transcription PCR, normalized by β-actin. **(B)** The protein levels of TNF-α,IL-1β, IL-6, and IL-10 were detected by ELISA. Data are presented as means ± SEM. $^{\dagger}p < 0.05$, $^{\dagger\dagger}p < 0.01$ *vs* CTR; $^{\#}p < 0.05$, $^{\#\#}p < 0.01$ *vs* DSS; $^{*}p < 0.05$, $^{**}p < 0.01$.

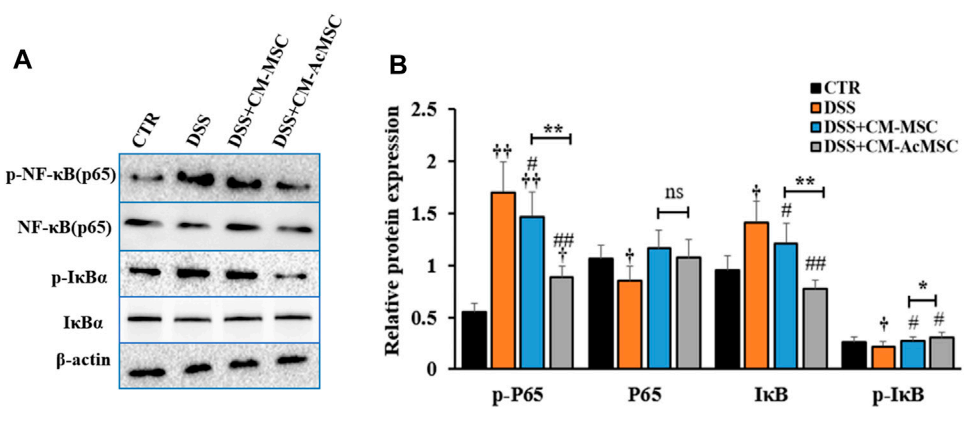

FIGURE 6 | CM-AcMSC inhibited the activation of NF-κB signaling pathway in DSS induced colitis rats. **(A)** Changes of p-P65, P65, IκB, *p*-IκB, and β-actin were measured by western blot analysis. **(B)** Densitometric analysis was performed to evaluate the relative ratios of each protein. Data are presented as means ± SEM. $^{\dagger}p < 0.05$, $^{\dagger\dagger}p < 0.01$ *vs* CTR; $^{\#}p < 0.05$, $^{\#\#}p < 0.01$ *vs* DSS; $^{*}p < 0.05$, $^{**}p < 0.01$. The same enhancement was applied to all sections of the WB to emphasize the bands.

minimum markers to confirm the MSCs. Previous investigations have found that MSCs or the exosome secreted from MSCs could significantly alleviate ulcerative colitis (Yang et al., 2020; Grim et al., 2021). Consistent with these results, our study showed the conditioned media from MSC significantly attenuated inflammatory responses and improve the colitis. Preconditioning of MSCs with cytokines, growth factors or other active molecules could enhance the therapeutic effects of MSCs (Noronha et al., 2019). However, these preconditioning factors might result in some unexpected side effects to the patients. Serum from the colitis individuals contains high levels of cytokines, which has low immunogenicity and could be used as a priming factor to enhance the immunomodulatory capabilities of MSCs. It is reported that autologous-derived MSCs were able to inhibit autologous peripheral blood mononuclear cell (PBMC) proliferation and inhibit TNFα production *in vitro*. Furthermore, autologous MSCs infusion appeared to be safe as intravenous MSC infusions were clinically well tolerated (Duijvestein et al., 2010). In the present study, we preconditioned the adipose MSCs with the serum from colitis rat with high levels of inflammatory cytokines. Then we studied the effects of CM-Ac-MSC on the experimental colitis induced by DSS. Although CM-AcMSC and CM-MSC candidate therapy resulted in alleviation of colitis, treatment with CM-AcMSC was more effective in inhibiting body weight loss, reducing DAI and protecting mucus integrity.

Administration of adipose-or bone marrow-derived MSCs could attenuate inflammatory responses, repair the damaged colon tissue and modulate intestinal immune homeostasis in experimental colitis models (Li et al., 2015; Barnhoorn et al., 2018; Lopez-Santalla et al., 2020). The results of this study are consistent with previous studies, which suggest that the CM-AcMSC could significantly heal the process of inflammation of colitis rats and improve the effectiveness of treatment. Currently, MSCs have been used to study the effects on the Crohn's disease. Intravenous infusions of MSCs were weekly given to 15 Crohn's disease patients for 4 weeks. The results showed that 80% of patients had clinical response, 53% of patient had clinical remission and 47% of patients had endoscopic improvement (Forbes et al., 2014). Adipose-derived MSC injection for 8 weeks led to complete healing of fistula in 82% patients (27/33) (Lee et al., 2013). In another study, bone marrow-derived MSC was intravenously injected to Crohn's disease patients at the dose of $1–2×10^6$ cells/kg body weight. The results demonstrated only three of 10 patients showed clinical response, but three patients required surgery due to disease worsening (Duijvestein et al., 2010). However, MSCs must survive in the harsh host environment and reach the lesion sites. Accordingly, the transplantation efficacy of MSCs is low and the effects are inconsistent in different clinical trials. The therapeutic capabilities of MSCs are not limited to the regenerative capabilities. MSCs could secret various trophic factors and extracellular vesicles (EVs), which were defined as secretom (Lai et al., 2011; Harrell et al., 2020). An increasing number of investigators consider that the secretom plays key therapeutic roles in the treatment of disease instead of the tissue-homing property of MSCs (Yang et al., 2020). The secretom contains many active factors such as functional proteins (cytokines, chemokines, trophic factors, and growth factors), microRNAs, noncoding RNA, fatty acid and fatty acid binding protein (FABP) (Monsel et al., 2016; Ko et al., 2020). The above researches suggested us that secretom of MSCs might play an important role in cellular immunity or tissue damage repair processes. Previous studies have indicated that mesenchymal stem cells-conditioned medium could ameliorate colitis in the DSS induced models (Gonçalves et al., 2018; Heidari et al., 2018). Preconditioning could enhance the immunomodulatory functions of MSCs and increase the secretion of paracrine factors (Ankrum et al., 2014; Saparov et al., 2016; Hu and Li, 2018; Yang et al., 2018; Lee and Kang, 2020). IFN-γ, TNF-α and other agents have been used to precondition MSCs to improve their therapeutic efficacy on ulcerative colitis (Fuenzalida et al., 2016; Shin et al., 2020; Lim et al., 2021). This might explain why CM-Ac-MSC has better therapeutic effect than CM-MSC. It is an ideal approach to boost the expression and secretion of immunomodulatory factors of MSCs with molecules that mimic the physiological conditions (Ankrum et al., 2014). However, a major limitation of our study is that we did not identify the specific active components in the CM-Ac-MSC and CM-MSC, which might be one of our next research focuses. In this study, we preconditioned the adipose mesenchymal stem cells with the serum from colitis rats, and then investigated the therapeutic effects of CM-AcMSC on the colitis rats. The results showed that CM-AcMSC significantly decreased the expressions of pro-inflammatory cytokines such as TNF-α, IL-1β, and IL-6, upregulated the expression of MUC2 and TJs such as ZO-1, claudin-1and occludin, and protected the colonic mucus integrity. The effects of CM-AcMSC were better than those of CM-MSC.

NF-κB plays key roles in the inflammatory responses of mucosal inflammation in IBD (Nairz et al., 2011). The activated NF-κB translocated into the nucleus and triggered expression of pro-inflammatory cytokines including TNF-α, IL-1β, and IL-6 (Murano et al., 2000). In this study, we demonstrated that CM-AcMSC and CM-MSC significantly inhibited the phosphorylation of p65 and IκB in the colonic cells of colitis model rats induced by DSS. The levels of p-P65 and *p*-IκBα of CM-AcMSC group were similar to those of the control group. The comparison between CM-AcMSC and CM-MSC illustrated that CM-AcMSC was more effective than CM-MSC in suppressing the activation of NF-κB pathway.

CONCLUSION

Our study demonstrated that conditioned media from MSCs ameliorated DSS induced colitis in rats. Conditioned media from MSCs pre-activated with the serum from colitis rats exert superior therapeutic efficacy for IBD. Further studies should be carried out to explore the molecular mechanism. Clinic investigations based on human specimens are required to be performed to verify the therapeutic efficacy.

DATA AVAILABILITY STATEMENT

The original contributions presented in the study are included in the article/Supplementary Material, further inquiries can be directed to the corresponding author.

ETHICS STATEMENT

The animal study was reviewed and approved by The Ethical Committee in Zhejiang University.

AUTHOR CONTRIBUTIONS

L-LQ: Investigation, Methodology, Writing-original draft. Z-YF: Methodology, Investigation, Data curation. H-GM: Methodology, Resources. J-BW: Conceptualization, Writing-review and editing, Funding acquisition.

FUNDING

This work was funded by the National Natural Science Foundation of China (No. 31272461), the financial support from Ningbo Science and Technology Bureau Project (No.202003N4305, 2018B10095, 2017C110017).

REFERENCES

Ankrum, J. A., Ong, J. F., and Karp, J. M. (2014). Mesenchymal Stem Cells: Immune Evasive, Not Immune Privileged. *Nat. Biotechnol.* 32, 252–260. doi:10.1038/nbt.2816

Martín Arranz, E., Martín Arranz, M. D., Robredo, T., Mancheño-Corvo, P., Menta, R., Alves, F. J., et al. (2018). Endoscopic Submucosal Injection of Adipose-Derived Mesenchymal Stem Cells Ameliorates TNBS-Induced Colitis in Rats and Prevents Stenosis. *Stem Cel Res. Ther.* 9, 95. doi:10.1186/s13287-018-0837-x

Bamba, S., Andoh, A., Ban, H., Imaeda, H., Aomatsu, T., Kobori, A., et al. (2012). The Severity of Dextran Sodium Sulfate-Induced Colitis Can Differ between Dextran Sodium Sulfate Preparations of the Same Molecular Weight Range. *Dig. Dis. Sci.* 57, 327–334. doi:10.1007/s10620-011-1881-x

Barnhoorn, M., de Jonge-Muller, E., Molendijk, I., van Gulijk, M., Lebbink, O., Janson, S., et al. (2018). Endoscopic Administration of Mesenchymal Stromal Cells Reduces Inflammation in Experimental Colitis. *Inflamm. Bowel Dis.* 24, 1755–1767. doi:10.1093/ibd/izy130

Cho, J. H. (2008). The Genetics and Immunopathogenesis of Inflammatory Bowel Disease. *Nat. Rev. Immunol.* 8, 458–466. doi:10.1038/nri2340

Cohen, B. L., and Sachar, D. B. (2017). Update on Anti-Tumor Necrosis Factor Agents and Other New Drugs for Inflammatory Bowel Disease. *Bmj* 357, j2505. doi:10.1136/bmj.j2505

Dai, X., Chen, X., Chen, Q., Shi, L., Liang, H., Zhou, Z., et al. (2015). MicroRNA-193a-3p Reduces Intestinal Inflammation in Response to Microbiota via Down-Regulation of Colonic PepT1. *J. Biol. Chem.* 290, 16099–16115. doi:10.1074/jbc.M115.659318

Duijvestein, M., Vos, A. C. W., Roelofs, H., Wildenberg, M. E., Wendrich, B. B., Verspaget, H. W., et al. (2010). Autologous Bone Marrow-Derived Mesenchymal Stromal Cell Treatment for Refractory Luminal Crohn's Disease: Results of a Phase I Study. *Gut* 59, 1662–1669. doi:10.1136/gut.2010.215152

Eleuteri, S., and Fierabracci, A. (2019). Insights into the Secretome of Mesenchymal Stem Cells and its Potential Applications. *Ijms* 20, 4597. doi:10.3390/ijms20184597

Forbes, G. M., Sturm, M. J., Leong, R. W., Sparrow, M. P., Segarajasingam, D., Cummins, A. G., et al. (2014). A Phase 2 Study of Allogeneic Mesenchymal Stromal Cells for Luminal Crohn's Disease Refractory to Biologic Therapy. *Clin. Gastroenterol. Hepatol.* 12, 64–71. doi:10.1016/j.cgh.2013.06.021

Fuenzalida, P., Kurte, M., Fernández-O'ryan, C., Ibañez, C., Gauthier-Abeliuk, M., Vega-Letter, A. M., et al. (2016). Toll-like Receptor 3 Pre-conditioning Increases the Therapeutic Efficacy of Umbilical Cord Mesenchymal Stromal Cells in a Dextran Sulfate Sodium-Induced Colitis Model. *Cytotherapy* 18, 630–641. doi:10.1016/j.jcyt.2016.02.002

Gholamrezayi, A., Mohamadinarab, M., Rahbarinejad, P., Fallah, S., Barez, S. R., Setayesh, L., et al. (2020). Characterization of the Serum Levels of Meteorin-like in Patients with Inflammatory Bowel Disease and its Association with Inflammatory Cytokines. *Lipids Health Dis.* 19, 230. doi:10.1186/s12944-020-01404-6

Da Costa Gonçalves, F., Serafini, M. A., Mello, H. F., Pfaffenseller, B., Araújo, A. B., Visioli, F., et al. (2018). Bioactive Factors Secreted from Mesenchymal Stromal Cells Protect the Intestines from Experimental Colitis in a Three-Dimensional Culture. *Cytotherapy* 20, 1459–1471. doi:10.1016/j.jcyt.2018.06.007

Gorgun, C., Ceresa, D., Lesage, R., Villa, F., Reverberi, D., Balbi, C., et al. (2021). Dissecting the Effects of Preconditioning with Inflammatory Cytokines and Hypoxia on the Angiogenic Potential of Mesenchymal Stromal Cell (MSC)-derived Soluble Proteins and Extracellular Vesicles (EVs). *Biomaterials* 269, 120633. doi:10.1016/j.biomaterials.2020.120633

Grim, C., Noble, R., Uribe, G., Khanipov, K., Johnson, P., Koltun, W. A., et al. (2021). Impairment of Tissue-Resident Mesenchymal Stem Cells in Chronic Ulcerative Colitis and Crohn's Disease. *J. Crohns Colitis* 15, 1362–1375. doi:10.1093/ecco-jcc/jjab001

Harrell, C. R., Jovicic, N., Djonov, V., and Volarevic, V. (2020). Therapeutic Use of Mesenchymal Stem Cell-Derived Exosomes: From Basic Science to Clinics. *Pharmaceutics* 12, 474. doi:10.3390/pharmaceutics12050474

Heidari, M., Pouya, S., Baghaei, K., Aghdaei, H. A., Namaki, S., Zali, M. R., et al. (2018). The Immunomodulatory Effects of Adipose-derived Mesenchymal Stem Cells and Mesenchymal Stem Cells-conditioned Medium in Chronic Colitis. *J. Cel. Physiol.* 233, 8754–8766. doi:10.1002/jcp.26765

Hendy, P., Hart, A., and Irving, P. (2016). Anti-TNF Drug and Antidrug Antibody Level Monitoring in IBD: a Practical Guide. *Frontline Gastroenterol.* 7, 122–128. doi:10.1136/flgastro-2014-100527

Hu, C., and Li, L. (2018). Preconditioning Influences Mesenchymal Stem Cell Properties *In Vitro* and *In Vivo*. *J. Cel. Mol. Med.* 22, 1428–1442. doi:10.1111/jcmm.13492

Jiang, Y., Jahagirdar, B. N., Reinhardt, R. L., Schwartz, R. E., Keene, C. D., Ortiz-Gonzalez, X. R., et al. (2002). Pluripotency of Mesenchymal Stem Cells Derived from Adult Marrow. *Nature* 418, 41–49. doi:10.1038/nature00870

Kang, S. H., Kim, M. Y., Eom, Y. W., and Baik, S. K. (2020). Mesenchymal Stem Cells for the Treatment of Liver Disease: Present and Perspectives. *Gut Liver* 14, 306–315. doi:10.5009/gnl18412

Katz, A. J., Tholpady, A., Tholpady, S. S., Shang, H., and Ogle, R. C. (2005). Cell Surface and Transcriptional Characterization of Human Adipose-Derived Adherent Stromal (hADAS) Cells. *Stem Cells* 23, 412–423. doi:10.1634/stemcells.2004-0021

Ko, K.-W., Yoo, Y.-I., Kim, J. Y., Choi, B., Park, S.-B., Park, W., et al. (2020). Attenuation of Tumor Necrosis Factor-α Induced Inflammation by Umbilical Cord-Mesenchymal Stem Cell Derived Exosome-Mimetic Nanovesicles in Endothelial Cells. *Tissue Eng. Regen. Med.* 17, 155–163. doi:10.1007/s13770-019-00234-7

Lai, R. C., Chen, T. S., and Lim, S. K. (2011). Mesenchymal Stem Cell Exosome: a Novel Stem Cell-Based Therapy for Cardiovascular Disease. *Regener. Med.* 6, 481–492. doi:10.2217/rme.11.35

Lee, B.-C., and Kang, K.-S. (2020). Functional Enhancement Strategies for Immunomodulation of Mesenchymal Stem Cells and Their Therapeutic Application. *Stem Cel Res. Ther.* 11, 397. doi:10.1186/s13287-020-01920-3

Lee, W. Y., Park, K. J., Cho, Y. B., Yoon, S. N., Song, K. H., Kim, D. S., et al. (2013). Autologous Adipose Tissue-Derived Stem Cells Treatment Demonstrated Favorable and Sustainable Therapeutic Effect for Crohn's Fistula. *Stem Cells* 31, 2575–2581. doi:10.1002/stem.1357

Lee, J., Moraes-Vieira, P. M., Castoldi, A., Aryal, P., Yee, E. U., Vickers, C., et al. (2016). Branched Fatty Acid Esters of Hydroxy Fatty Acids (FAHFAs) Protect against Colitis by Regulating Gut Innate and Adaptive Immune Responses. *J. Biol. Chem.* 291, 22207–22217. doi:10.1074/jbc.M115.703835

Legaki, E., Roubelakis, M. G., Theodoropoulos, G. E., Lazaris, A., Kollia, A., Karamanolis, G., et al. (2016). Therapeutic Potential of Secreted Molecules Derived from Human Amniotic Fluid Mesenchymal Stem/Stroma Cells in a Mice Model of Colitis. *Stem Cel Rev Rep.* 12, 604–612. doi:10.1007/s12015-016-9677-1

Li, M., Zhang, Y.-X., Zhang, Z., Zhou, X.-Y., Zuo, X.-L., Cong, Y., et al. (2015). Endomicroscopy Will Track Injected Mesenchymal Stem Cells in Rat Colitis Models. *Inflamm. Bowel Dis.* 21, 2068–2077. doi:10.1097/MIB.0000000000000458

Lim, J.-Y., Kim, B.-S., Ryu, D.-B., Kim, T. W., Park, G., and Min, C.-K. (2021). The Therapeutic Efficacy of Mesenchymal Stromal Cells on Experimental Colitis was Improved by the IFN-γ and poly(I:C) Priming Through Promoting the Expression of Indoleamine 2,3-Dioxygenase. *Stem Cel Res. Ther.* 12, 37. doi:10.1186/s13287-020-02087-7

Lopez-Santalla, M., Hervas-Salcedo, R., Fernandez-Garcia, M., Bueren, J. A., and Garin, M. I. (2020). Cell Therapy with Mesenchymal Stem Cells Induces an Innate Immune Memory Response that Attenuates Experimental Colitis in the Long Term. *J. Crohns Colitis* 14, 1424–1435. doi:10.1093/ecco-jcc/jjaa079

Maloy, K. J., and Powrie, F. (2011). Intestinal Homeostasis and its Breakdown in Inflammatory Bowel Disease. *Nature* 474, 298–306. doi:10.1038/nature10208

Marchesi, J. R., Adams, D. H., Fava, F., Hermes, G. D. A., Hirschfield, G. M., Hold, G., et al. (2016). The Gut Microbiota and Host Health: A New Clinical Frontier. *Gut* 65, 330–339. doi:10.1136/gutjnl-2015-309990

Molodecky, N. A., Soon, I. S., Rabi, D. M., Ghali, W. A., Ferris, M., Chernoff, G., et al. (2012). Increasing Incidence and Prevalence of the Inflammatory Bowel Diseases with Time, Based on Systematic Review. *Gastroenterology* 142, 46–54. doi:10.1053/j.gastro.2011.10.001

Monsel, A., Zhu, Y.-g., Gudapati, V., Lim, H., and Lee, J. W. (2016). Mesenchymal Stem Cell Derived Secretome and Extracellular Vesicles for Acute Lung Injury and Other Inflammatory Lung Diseases. *Expert Opin. Biol. Ther.* 16, 859–871. doi:10.1517/14712598.2016.1170804

Murano, M., Maemura, K., Hirata, I., Toshina, K., Nishikawa, T., Hamamoto, N., et al. (2000). Therapeutic Effect of Intracolonically Administered Nuclear Factor κ B (P65) Antisense Oligonucleotide on Mouse Dextran Sulphate Sodium (DSS)-Induced Colitis. *Clin. Exp. Immunol.* 120, 51–58. doi:10.1046/j.1365-2249.2000.01183.x

Nairz, M., Schroll, A., Moschen, A. R., Sonnweber, T., Theurl, M., Theurl, I., et al. (2011). Erythropoietin Contrastingly Affects Bacterial Infection and Experimental Colitis by Inhibiting Nuclear Factor-κB-Inducible Immune Pathways. *Immunity* 34, 61–74. doi:10.1016/j.immuni.2011.01.002

Nammian, P., Asadi-Yousefabad, S.-L., Daneshi, S., Sheikhha, M. H., Tabei, S. M. B., and Razban, V. (2021). Comparative Analysis of Mouse Bone Marrow and Adipose Tissue Mesenchymal Stem Cells for Critical Limb Ischemia Cell Therapy. *Stem Cel Res. Ther.* 12, 58. doi:10.1186/s13287-020-02110-x

Neurath, M. F. (2014). Cytokines in Inflammatory Bowel Disease. *Nat. Rev. Immunol.* 14, 329–342. doi:10.1038/nri3661

Noronha, N. d. C., Mizukami, A., Caliári-Oliveira, C., Cominal, J. G., Rocha, J. L. M., Covas, D. T., et al. (2019). Priming Approaches to Improve the Efficacy of Mesenchymal Stromal Cell-Based Therapies. *Stem Cel Res. Ther.* 10, 131. doi:10.1186/s13287-019-1224-y

Pak, S., Hwang, S. W., Shim, I. K., Bae, S. M., Ryu, Y. M., Kim, H.-B., et al. (2018). Endoscopic Transplantation of Mesenchymal Stem Cell Sheets in Experimental Colitis in Rats. *Sci. Rep.* 8, 11314. doi:10.1038/s41598-018-29617-x

Pithadia, A. B., and Jain, S. (2011). Treatment of Inflammatory Bowel Disease (IBD). *Pharmacol. Rep.* 63, 629–642. doi:10.1016/S1734-1140(11)70575-8

Pittenger, M. F., Mackay, A. M., Beck, S. C., Jaiswal, R. K., Douglas, R., Mosca, J. D., et al. (1999). Multilineage Potential of Adult Human Mesenchymal Stem Cells. *Science* 284, 143–147. doi:10.1126/science.284.5411.143

Saparov, A., Ogay, V., Nurgozhin, T., Jumabay, M., and Chen, W. C. W. (2016). Preconditioning of Human Mesenchymal Stem Cells to Enhance Their Regulation of the Immune Response. *Stem Cell Int.* 2016, 3924858. doi:10.1155/2016/3924858

Shin, T.-H., Ahn, J.-S., Oh, S.-J., Shin, Y. Y., Yang, J. W., Kang, M.-J., et al. (2020). TNF-α Priming Elicits Robust Immunomodulatory Potential of Human Tonsil-Derived Mesenchymal Stem Cells to Alleviate Murine Colitis. *Biomedicines* 8, 561. doi:10.3390/biomedicines8120561

Silva, J. D., Lopes-Pacheco, M., Paz, A. H. R., Cruz, F. F., Melo, E. B., de Oliveira, M. V., et al. (2018). Mesenchymal Stem Cells from Bone Marrow, Adipose Tissue, and Lung Tissue Differentially Mitigate Lung and Distal Organ Damage in Experimental Acute Respiratory Distress Syndrome*. *Crit. Care Med.* 46, e132–e140. doi:10.1097/ccm.0000000000002833

Stavely, R., Robinson, A. M., Miller, S., Boyd, R., Sakkal, S., and Nurgali, K. (2015). Allogeneic guinea Pig Mesenchymal Stem Cells Ameliorate Neurological Changes in Experimental Colitis. *Stem Cel Res. Ther.* 6, 263. doi:10.1186/s13287-015-0254-3

Strober, W., Fuss, I., and Mannon, P. (2007). The Fundamental Basis of Inflammatory Bowel Disease. *J. Clin. Invest.* 117, 514–521. doi:10.1172/JCI30587

Wang, S., Xie, Y., Yang, X., Wang, X., Yan, K., Zhong, Z., et al. (2016). Therapeutic Potential of Recombinant Cystatin from Schistosoma Japonicum in TNBS-Induced Experimental Colitis of Mice. *Parasites Vectors* 9, 6. doi:10.1186/s13071-015-1288-1

Yang, F. Y., Chen, R., Zhang, X., Huang, B., Tsang, L. L., Li, X., et al. (2018). Preconditioning Enhances the Therapeutic Effects of Mesenchymal Stem Cells on Colitis through PGE2-Mediated T-Cell Modulation. *Cel Transpl.* 27, 1352–1367. doi:10.1177/0963689718780304

Yang, R., Huang, H., Cui, S., Zhou, Y., Zhang, T., and Zhou, Y. (2020). IFN-γ Promoted Exosomes from Mesenchymal Stem Cells to Attenuate Colitis via miR-125a and miR-125b. *Cell Death Dis.* 11, 603. doi:10.1038/s41419-020-02788-0

Zhu, L., Gu, P., and Shen, H. (2019). Protective Effects of Berberine Hydrochloride on DSS-Induced Ulcerative Colitis in Rats. *Int. Immunopharmacol.* 68, 242–251. doi:10.1016/j.intimp.2018.12.036

Conflict of Interest: The authors declare that the research was conducted in the absence of any commercial or financial relationships that could be construed as a potential conflict of interest.

Publisher's Note: All claims expressed in this article are solely those of the authors and do not necessarily represent those of their affiliated organizations, or those of the publisher, the editors, and the reviewers. Any product that may be evaluated in this article, or claim that may be made by its manufacturer, is not guaranteed or endorsed by the publisher.

Copyright © 2021 Qi, Fan, Mao and Wang. This is an open-access article distributed under the terms of the Creative Commons Attribution License (CC BY). The use, distribution or reproduction in other forums is permitted, provided the original author(s) and the copyright owner(s) are credited and that the original publication in this journal is cited, in accordance with accepted academic practice. No use, distribution or reproduction is permitted which does not comply with these terms.

frontiers in Bioengineering and Biotechnology

ORIGINAL RESEARCH
published: 15 December 2021
doi: 10.3389/fbioe.2021.772002

LncRNA Malat-1 From MSCs-Derived Extracellular Vesicles Suppresses Inflammation and Cartilage Degradation in Osteoarthritis

Chongzhi Pan[1,2,3], *Wenzhou Huang*[1,2,3], *Qi Chen*[1,2,3], *Jiu Xu*[4], *Guoyu Yao*[4], *Bin Li*[1,2,3,4], *Tianlong Wu*[1,2,3], *Changchang Yin*[5] *and Xigao Cheng*[1,2,3,4]*

[1]*Department of Orthopedics, The Second Affiliated Hospital of Nanchang University, Nanchang, China,* [2]*Institute of Orthopedics of Jiangxi Province, Nanchang, China,* [3]*Institute of Minimally Invasive Orthopedics, Nanchang University, Nanchang, China,* [4]*Second Clinical College, Nanchang University, Nanchang, China,* [5]*Jiujiang University, Key Laboratory of Medical Transformation of Jiujiang, Jiujiang, China*

OPEN ACCESS

Edited by:
Enrico Ragni,
Galeazzi Orthopedic Institute (IRCCS), Italy

Reviewed by:
Jehan J. El-Jawhari,
Nottingham Trent University, United Kingdom
Susana G. Santos,
Universidade do Porto, Portugal

***Correspondence:**
Xigao Cheng
228206846@qq.com

Specialty section:
This article was submitted to Preclinical Cell and Gene Therapy, a section of the journal Frontiers in Bioengineering and Biotechnology

Received: *07 September 2021*
Accepted: *30 November 2021*
Published: *15 December 2021*

Citation:
Pan C, Huang W, Chen Q, Xu J, Yao G, Li B, Wu T, Yin C and Cheng X (2021) LncRNA Malat-1 From MSCs-Derived Extracellular Vesicles Suppresses Inflammation and Cartilage Degradation in Osteoarthritis. Front. Bioeng. Biotechnol. 9:772002. doi: 10.3389/fbioe.2021.772002

Purpose: Extracellular Vesicles (EVs) derived from hMSCs, have the potential to alleviate cartilage damage and inflammation. We aimed to explore the effects of EVs derived from lncRNA malat-1-overexpressing human mesenchymal stem cells (hMSCs) on chondrocytes.

Material and Methods: hMSCs-derived Extracellular Vesicles (hMSCs-EVs) were identified by transmission electron microscopy and western blot. We used a Sprague-Dawley (SD) rat model of CollagenaseII-induced osteoarthritis (OA) as well as IL-1β-induced OA chondrocytes. Lentiviral vectors were used to overexpress lncRNA malat-1 in hMSCs. Chondrocyte proliferation, inflammation, extracellular matrix degradation, and cell migration were measured by Edu staining, ELISA, western blot analysis, and transwell assay. Chondrocyte apoptosis was evaluated by flow cytometry, Hoechst 33342/PI Staining, and western blot. Safranine O-fast green (S-O) staining and HE staining were used to assess morphologic alterations of the rat knee joint.

Results: hMSCs$^{malat-1}$-EVs decreased MMP-13, IL-6, and Caspase-3 expression in IL-1β-induced OA chondrocytes. Moreover, hMSCs$^{malat-1}$-EVs promoted chondrocyte proliferation and migration, suppressed apoptosis, and attenuated IL-1β-induced chondrocyte injury. Our animal experiments suggested that hMSCs$^{malat-1}$-EVs were sufficient to prevent cartilage degeneration.

Conclusion: Our findings show that lncRNA malat-1from hMSCs-delivered EVs can promote chondrocyte proliferation, alleviate chondrocyte inflammation and cartilage degeneration, and enhance chondrocyte repair. Overall, hMSCs$^{malat-1}$-EVs might be a new potential therapeutic option for patients with OA.

Keywords: mesenchymal stem cells, chondrocyte, osteoarthritis, inflammation, extracellular vesicles

INTRODUCTION

Osteoarthritis (OA) is one of the most common age-related degenerative joint diseases and public health problems worldwide, and can cause pain, disability, social and economic loss (Glyn-Jones et al., 2015). OA is characterized by the destruction of articular cartilage, synovial inflammation, osteophyte formation, and extracellular matrix (ECM) loss (Guilak et al., 2018). The molecular mechanisms underlying the occurrence and progression of OA remain unclear, and currently there are no interventions that can successfully restore the degenerated cartilage and slow down disease progression. Therefore, it is a clinical priority to seek new treatments for OA. Targeting cartilage cell regeneration, apoptosis and of extracellular matrix loss might represent new therapeutic avenues for the management and treatment of OA.

Mesenchymal stem cells (MSCs) are a type of pluripotent stem cells with self-renewal ability, have anti-inflammatory and immune roles, and have the ability of tissue repair. Bone marrow mesenchymal stem cells are used for fracture healing, cartilage repair, kidney injury, articular cartilage injury, myocardial injury and regenerative medicine due to their superior repair ability (Zhang et al., 2015; Chen et al., 2016; Li et al., 2018a; Wang et al., 2018; Yang et al., 2018; Fu et al., 2019). Existing animal experiments and clinical studies have confirmed that intra-articular injection of MSCs can effectively delay the degeneration of articular cartilage, relieve pain and improve joint function (Desando et al., 2013; Matas et al., 2019). At present, MSCs treatment still has certain limitations and side effects, such as thrombosis (Furlani et al., 2009) and abnormal ossification (Breitbach et al., 2007). Therefore, its therapeutic effect needs further research.

In recent years, EVs have gradually become the focus and entered people's field of vision. Evs carry proteins, mRNA, and non-coding RNA (including miRNA, lncRNA, circRNA) (Tao et al., 2017; Foers et al., 2018). Many current studies have shown that EVs have a huge potential for the MSCs to treating OA (Batrakova and Kim, 2015). The research results of Lei He et show bone marrow mesenchymal stem cell-derived EVs played an important role at protecting cartilage damage and relieving knee osteoarthritis pain in a rat model of osteoarthritis (He et al., 2020). It can be seen that EVs have great potential in the treatment of OA.

LncRNA is a new non-coding RNA widely expressed in the human genome, with a well-conserved sequence and high tissue specificity (Washietl et al., 2014). Metastasis-associated lung adenocarcinoma transcript 1 (malat-1) is a novel transcript of over 8000 nucleotides which has been shown to regulate inflammation (Puthanveetil et al., 2015), promotes chondrocyte proliferation (Yang et al., 2017). LncRNA malat-1 has been extensively studied in human systemic lupus erythematosus (SLE) (Li et al., 2020a), myasthenia gravis (MG) (Felson et al., 2000), cardiovascular disease (Zhu et al., 2019), osteoporosis (Yang et al., 2019), and cancer (Fu et al., 2020). Our previous studies have also found that lncRNA malat-1 in chondrocytes promotes chondrocyte proliferation, suppresses chondrocyte apoptosis, and reduces extracellular matrix degradation (Kong et al., 2019). But to the best of our knowledge no studies have confirmed whether malat-1 in the EVs can protect chondrocytes in OA. Therefore, the specific role of lncRNA malat-1 needs further study. We hypothesized that EVs expressing lncRNA malat-1 can delay chondrocyte degeneration, promote chondrocyte repair, and have a therapeutic potential in OA, and might be a reliable therapeutic approach for OA.

MATERIALS AND METHODS

Cell Culture and Co-Culture of Chondrocytes and EVs

Human MSCs (hMSCs) and human chondrocyte C28/I2 cells were acquired from ATCC (Manassas, United States) and BeNa Culture Collection (Beijing, China), respectively. Cells were cultured in DMED/F12 (Gibco, United States), containing 10% FBS (Gibco, United States) in a humidified incubator at 37°C and 5% CO_2. Cells were passaged every 2–3 days.

To establish an OA cell model, C28/I2 cells at 60–70% confluency were treated with or without 10 ng/ml human IL-1β recombinant protein (Sigma, United States) for 24 h. Following establishment of the vitro OA model, chondrocytes were treated with normal medium, hMSCs-EVs (10 μg/ml), and hMSCs$^{malat-1}$-EVs (EVs derived from lncRNA malat-1-overexpressing-hMSCs) for 24 h to investigate the effect of EVs, derived from lncRNA malat-1-overexpressing-hMSCs, on IL-1β-induced chondrocyte damage.

Isolation and Identification of EVs

HMSCs were grown at 80–90% confluency, at which time EVs -free medium (UR51101, Umibio, Shanghai, China) was added. Following 48 h of culture, supernatant was collected. Cell culture media was centrifuged to remove cell debris and then mixed with EVs isolate kit (UR52121, Umibio, Shanghai, China). According to the manufacturer's instructions, an initial spin was performed at 3000 ×g, at 4°C for 10 min to remove cells and cell debris. Then, the corresponding amount of reagents were added proportionally to the starting sample volume, mixed and incubated at 4°C for 2–4 h, followed by another centrifugation at 10,000 ×g for 60 min to obtain EVs pellets. Pellets were then resuspended with PBS, and purified with an EVs purification filter at 3,000 ×g for 10 min. EVs pellets were resuspended in 400 μl for 40 ml according to the manufacturer's instructions. EVs were stored at −80°C immediately after isolation until further analysis.

BCA protein assay kit (Beyotime, China) was used to assess EVs concentration. EVs morphological appearance was observed by transmission electron microscopy (TEM, H-7700, Hitachi, Japan), and EVs surface markers were analyzed by western blot (WB).

Uptake of PKH26-Labelled hMSCs-EVs

For up-take experiments, hMSCs-EVs were labeled with a red fluorescent color PKH26 kit (Sigma-Aldrich, United States), according to the manufacturer's instructions. Briefly, hMSCs-EVs were resuspended in 500 μl Diluent C, 2 μl PKH26 dye was then added to 500 μl Diluent C and incubated for 5 min at room temperature (RT). Then, 1 ml of 0.5% EVs-depleted FBS was added and incubated for 5 min to allow binding to excess dye. hMSCs-EVs were then collected by centrifugation at 100,000 ×g, at 4°C for 1 h. Next, hMSCs-EVs were resuspended in PBS and co-cultured with chondrocyte cells. Twenty-four hours later, cells samples were fixed in 4% paraformaldehyde, stained by 4′, 6-diamidine-2′2phenylindole dihydrochloride (DAPI) (Beyotime, Shanghai, China) for 10 min at RT, and observed under a fluorescence microscope (Novel, China) at a magnification of ×400.

Cell Transduction and Transfection

Lentiviral vectors targeting malat-1 were purchased from Focus Bioscience (Nanchang, China). Briefly, lentiviral vectors were transfected into competent cell 293T by using Lipofectamine 2000 (Thermo Fisher Scientific, United States). Culture medium was collected and co-cultured with hMSCs. HMSCs were infected lentivirus medium for 16 h, following which medium was replaced with fresh medium for another 48 h. Then, expression of lncRNA malat-1 was assessed by qRT-PCR. Infected hMSCs cells were co-cultured with puromycin (1 μg/ml) until all cells in the control group were dead. hMSCs overexpressing lncRNA malat-1 were filtrated and used for the next experiments.

Cell Viability Assay

CCK-8 was used to detect the effect of EVs on IL-1β-induced-chondrocyte injury. Chondrocyte cells (2×10^3) were cultured in a 96-well plate overnight, and co-cultured with different EVs concentrations (0, 1, 5, 10, 25, and 50 μg/ml) for 24 h. A control group was only co-cultured with normal culture media. According to the manufacturer's protocol, cells were incubated with 10 μl of CCK-8 solution (TransGen, Beijing, China) in each well for 4 h at 37°C. Finally, the optical density (OD) value at 450 nm of each well was measured by using a microplate reader (Perlong, Beijing, China).

Edu Proliferation Assay

The effects of EVs on chondrocytes were assessed with the Edu Cell Proliferation Assay Kit (Beyotime, China). Cells were seeded in 12-well plates and treated with IL-1β or EVs for 24 h. Following the manufacturer's manual, 10 μM of Edu solution was added to the plates in an incubator at 37°C for 2 h before fixation and permeabilization. Then, cells were incubated with Click Additive Solution at RT and kept away from light for 30 min. Next, chondrocytes cell nuclei were stained with Hoechst 33342 according to the manufacturer's instructions. The proportion of cells incorporating Edu was assessed under a fluorescence microscope.

Transwell Assay

Transwell cell culture chamber assay was used to assess cell migration. After treatment with IL-1β or different EVs for 24 h, chondrocytes were digested and resuspended in 2 ml serum-free medium. Then count the cells to ensure that the cell concentration is 7.5×10^4/ml. Next, 400 μl of cell suspension was added to the upper chamber (Corning, United States), and 700 μl DMEM containing 10% FBS was added to each bottom chamber of the 24-well plate. Following co-cultured for 24 h chondrocytes were washed twice with PBS, and fixed 4% paraformaldehyde for 20 min at RT. Then, chondrocytes were stained with 0.5% crystal violet dye for 30 min. Finally, the number of migrating cells was counted under a microscope.

Annexin V-FITC/Propidium Iodide Flow Cytometry Assay

Chondrocytes were cultured in 6-well plates and treated with IL-1β and EVs. After 24 h incubation, cells were resuspended with PBS, cells were counted, then resuspended in binding buffer, followed by incubation with Annexin V-FITC and PI (Beyotime, China) for 20 min at RT in a dark place. The rate of apoptosis was measured by flow cytometry (BD, San Jose, CA, United States).

Hoechst 33342/PI Assay

Hoechst 33342/PI staining kit was acquired from Solarbio (Beijing, China). According to the manufacturer's instructions, dye and cell staining buffers were added to each well incubated at 4°C for 30 min in a dark place after cell treatment with IL-1β, hMSCs-EVs, or $\text{hMSCs}^{\text{malat-1}}$-EVs. Finally, cells were observed with a fluorescence microscope.

IL-6 ELISA Assay

Following culture and treatment of chondrocyte cells with IL-1β or EVs for 24 h, the supernatants of each group were collected. The concentration of IL-6 was measured with a specific ELISA kit (Neobioscience, Shenzhen, China) following the manufacturer's instructions. In brief, 100 μl of the control, standard, or sample was added to each well and incubated for 90 min at 37°C. Then, wells were washed five times and incubated with 100 μl of human IL-6 conjugate antibody for 1 h at 37°C and washed again five times. 100 μl of the enzyme combination solution was added into each well and incubated for 30 min at 37°C away from light, followed by another step of washes. 100 μl of substrate solution was then added to each well and incubated for 15 min at 37°C away from the light. Finally, 100 μl of Stop Solution was added, and the OD values were measured at 450 nm by using a microplate reader.

Quantitative Real-Time Polymerase Chain Reaction

Total RNA was isolated from cells using Trizol reagent (Takara, Japan). Reverse transcription was carried out with the PrimeScrip RT reagent Kit with gDNA Eraser (Takara, Japan). TB Green Premix Ex Taq kit (Takara, Japan) was used to perform real-time PCR, and we used the CFX96 Real-Time PCR Detection System (Bio-Rad, United States) with the following primers: HMSC GAPDH: forward, 5′-GGTGGTCTCCTCTGACTTCAACA-3′ and reverse, 5′-TTGCTGTAGCCAAATTCGTTGT-3′; HMSC malat-1:forward, 5′- TCAGGATAATCAGACCACCACAG-3′ and reverse, 5′- GTAACTACCAGCCATTTCTCCAA-3′; Internal control was GAPDH.

Western Blot

Cells were washed three times with PBS and lysed in RIPA buffer with a protease inhibitor cocktail at the ice temperature for 20 min. After centrifugation at 10,000 ×g and 4°C for 10 min, the concentration of total protein levels was measured using the BCA kit. Protein extracts were separated by polyacrylamide gel electrophoresis (12–15%) and transferred to polyvinylidene difluoride (PVDF) membranes. Then, blots were incubated overnight at 4°C with antibodies specific for GAPDH (1: 5000,Abcam,United States), CD63 (1:1000, Proteintech, China), CD81 (1:1000,Abcam, United States), TSG101 (1: 1000,Abcam, United States), caspase-3 (1:5000,Abcam, United States), IL-6 (1:3000,Proteintech, China),MMP-13 (1:500, Proteintech, China). After washing with TBST 3 times, membranes were incubated with a goat anti-rabbit IgG–horseradish peroxidase antibody. Proteins were visualized using the ECL Chemiluminescent Kit (UE, Suzhou, China), and the chemical luminescence reaction was detected by the TECAN luminescent imaging system.

Animal Studies

All animal experiments were approved by the Institutional Animal Care and Use Committee of Nanchang University (China) and followed by the Guide for the Care and Use of Laboratory Animals by the National Institutes of Health (NIH). 10-week-old male Sprague-Dawley (SD rats) were obtained from the Experimental Animal Center of Nanchang University (Nanchang, China). Animals were kept in an environment with a dark/light cycle at 20–25°C, at ad libitum access to water and food. Animals were randomly divided into four groups randomly (n = 4 per group): Normal; OA + PBS; OA + hMSCs-EVs; OA + hMSCs$^{malat-1}$-EVs. To establish the OA model, collagenase II was injected into the knee joint cavity of SD rats under anesthesia. Three weeks after the injection, hMSCs-derived EVs were injected into the articular cavity of rats once a week at a concentration of 40 μg/100 μl. Six weeks later, histologic analysis was performed on the knee joint specimens.

Haematoxylin and Eosin and Safranine O-Fast Green Staining

Six weeks after treatment with EVs, all animals were sacrificed and articular cartilage samples were collected, fixed in paraformaldehyde for 24 h and subject to calcium removal for 21 days in 10% EDTA (pH 7.4). Then, knee-joint tissues were embedded in paraffin and sectioned into 5-μm-thick sections. Serial sections were obtained from the medial and lateral compartments at 200-μm intervals. Selected sections were deparaffinized in xylene, rehydrated through a graded series of ethanol washes, and stained by hematoxylin and eosin (H&E) and Safranin O/Fast Green staining (Solarbio, China). The degree of articulatio genus cartilage degeneration on the medial and lateral tibial plateau joint was evaluated according to the Osteoarthritis Research Society International (OARSI) score and the modified Mankin's score.

Statistical Analysis

All experiments were performed in triplicate. Mean ± standard deviation (SD) was used to present the data. Graphics and statistical analyses were conducted by GraphPad Prism 8 software (GraphPad Inc., La Jolla, CA, United States). Student's t-test for two groups and one-way ANOVA with Tukey post hoc test for three or more groups were used for group comparisons. A p value of less than 0.05 was considered statistically significant.

RESULTS

Identification of EVs and Isolated From Human BMSCs

After 48 h in culture, bone marrow mesenchymal stem cells (hMSCs) showed a uniform spindle morphology (**Figure 1A**). When the cell confluency reached 80%, EVs were extracted and identified by TEM, NTA, and WB. TEM results showed that EVs exhibited a classic approximate circular cup-shaped structure (**Figure 1B**). NTA showed a main peak of the particle size of approximately 144 nm (**Figure 1C**). Furthermore, WB showed that surface molecular markers CD63, CD81, TSG101 of the EVs were highly expressed compared to those of the negative group PBS (**Figure 1D**, **Supplementary Data Sheet S2**). These results show that EVs were successfully separated from the hMSCs.

Establishment of OA Model of Chondrocytes and EVs Uptake Experiment

According to previous literature, IL-1β (10 ng/ml) is appropriate for establishing an inflammatory injury model of chondrocytes to simulate the microenvironment of OA. ELISA experiments have shown that, after IL-1β treatment, the expression of the inflammatory cytokine IL-6 in chondrocytes was significantly higher than in the control group ($p < 0.05$) (**Figure 2A**). The expression of this inflammatory factors was also detected by western blot, with the results showing that IL-6 protein expression in the OA model group was increased by 3.89 times ($p < 0.05$) (**Figures 2B,C**, **Supplementary Data Sheet S1**). All data were statistically significant. These results indicate that the inflammatory injury model of chondrocytes has been successfully established.

To test the potential of EVs in the treatment of OA, we used PKH26 labeled EVs (red fluorescence), which were then co-cultured with chondrocytes. After 24 h of co-culture, EVs labeled with PKH26 were successfully observed in the cytoplasm of chondrocytes by fluorescence microscopy, suggesting that the EVs had been taken up by chondrocytes (**Figure 2D**).

LncRNA Malat-1 Overexpression in the EVs Reduces IL-1β Induced Inhibition of Chondrocyte Proliferation

To obtain lncRNA malat-1-rich EVs, lentiviral vectors were used to overexpress malat-1 in hMSCs. qRT-PCR data showed that

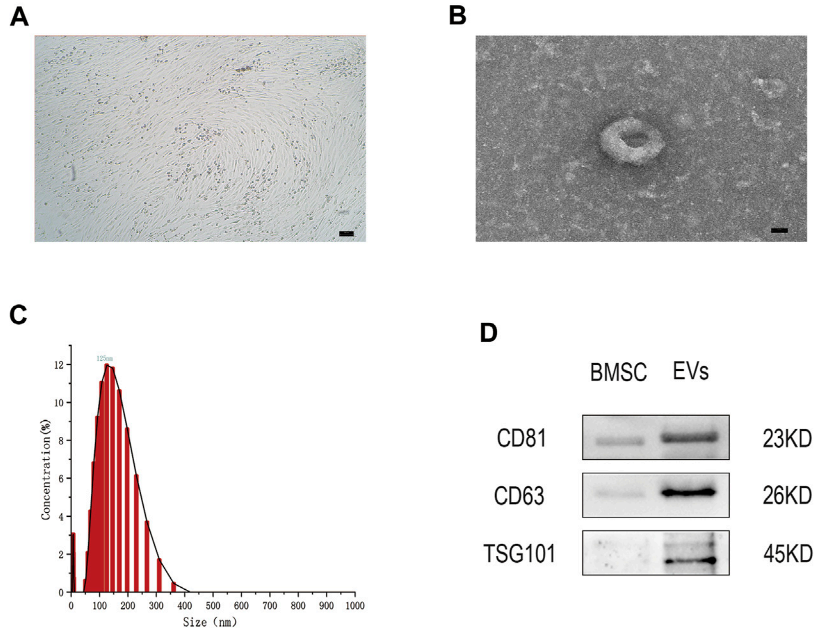

FIGURE 1 | (A) The hMSCs were observed by optical microscope. Scale bar = 100 μm. **(B)** The cup-shaped EVs under TEM. Scale bar = 25 nm **(C)** Size and concentration of EVs analyzed by NTA. **(D)** The indicated protein (CD9, CD63, and TSG101) in EVs were detected *via* western blotting. *n* = 3.

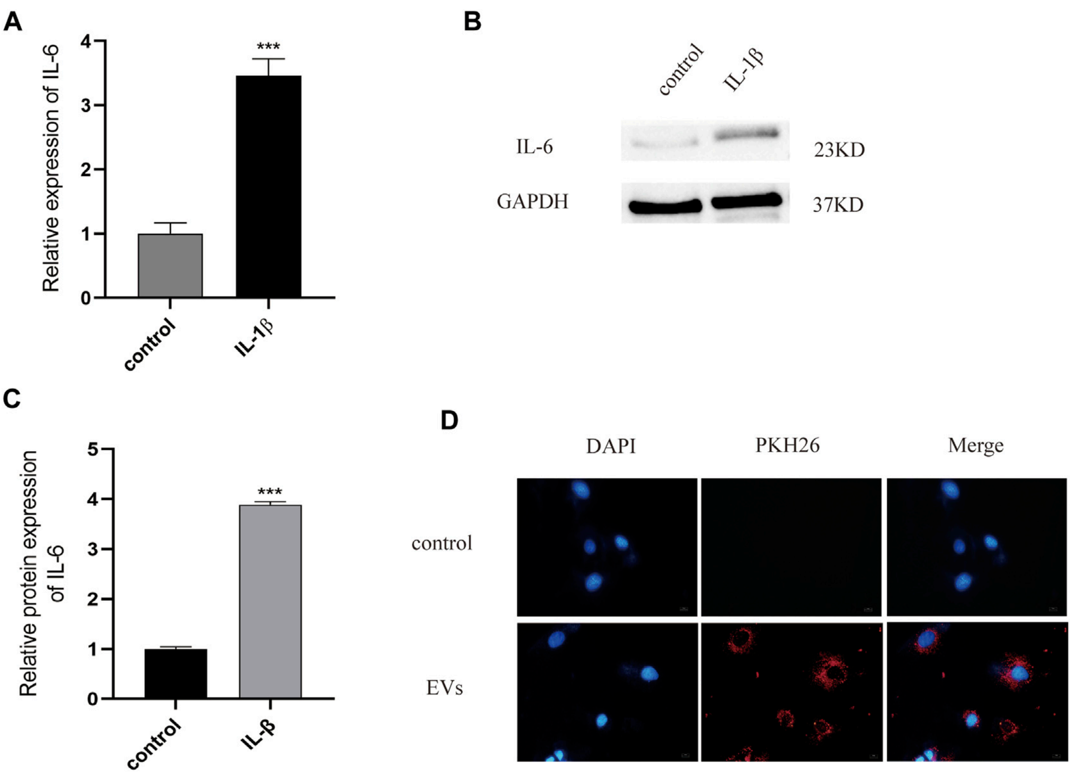

FIGURE 2 | (A) The expression of inflammatory factor IL-6 analyzed by Elisa. **(B)** and **(C)** The protein of IL-6 measured by western blot. **(D)** PKH26-labeled were uptaked by chondrocyte. Scale bar = 10 μm, *n* = 3, ***p < 0.001, t-test for all.

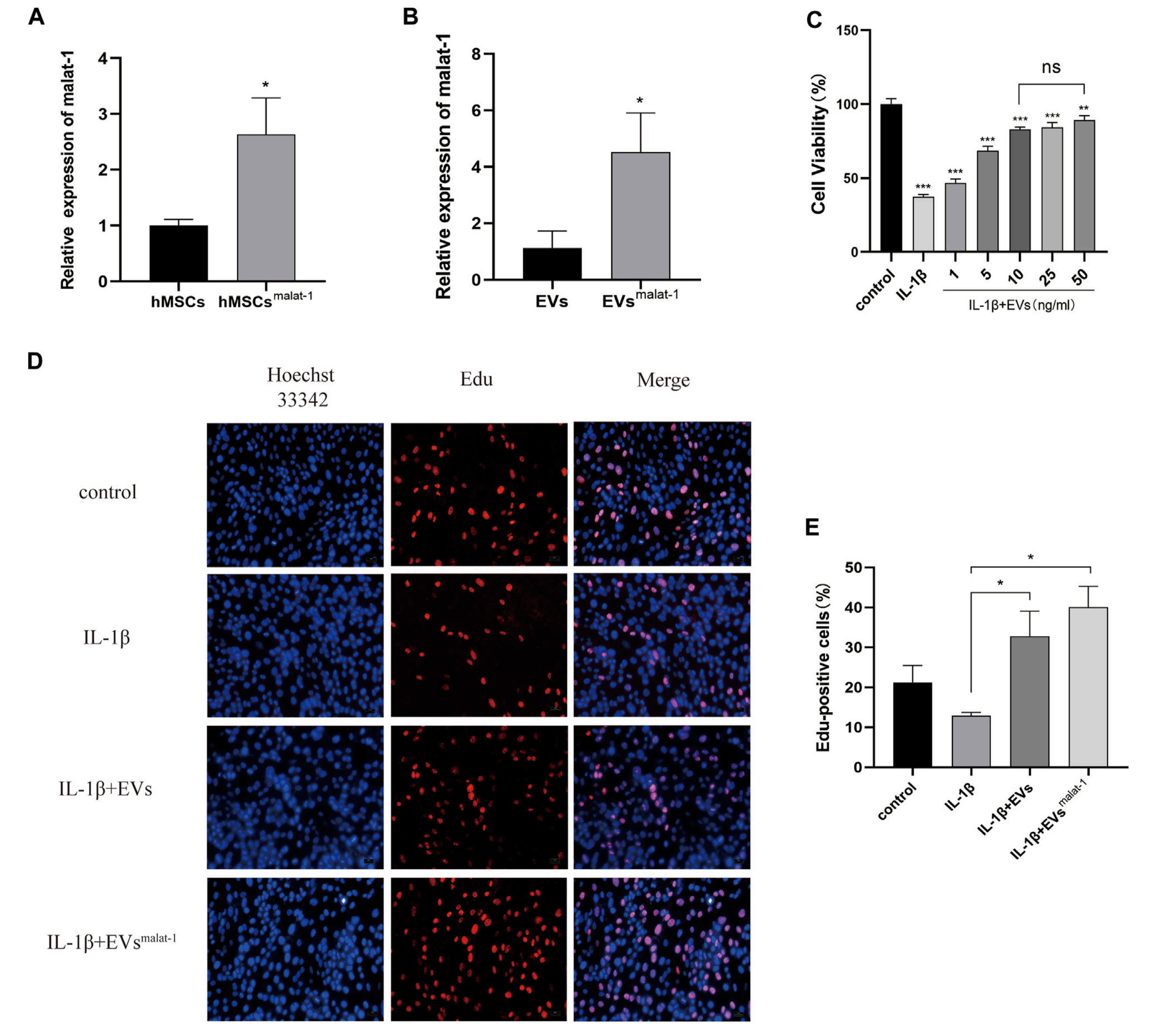

FIGURE 3 | (A) The expression of lncRNA malat-1 were analyze between hMSCs and hMSCs$^{over\text{-}malat-1}$ by qRT-PCR, $n = 3$, $^{*}p < 0.05$, t-test. **(B)** The expression of lncRNA malat-1 in two EVs analyzed by qRT-PCR, n = 3, $^{*}p < 0.05$, t-test. **(C)** Cell viability of chondrocytes treated with different concentrations of EVs by CCK-8 assay. $n = 3$, $^{*}p < 0.05$, one-way ANOVA **(D)** and **(E)** Edu assay was performed to detect proliferation of chondrocytes, $n = 3$, $^{*}p < 0.05$, one-way ANOVA.

malat-1 expression increased by approximately 2.6 times compared to the control group ($p < 0.05$) (**Figure 3A**). EVs were then extracted from the hMSCs cell serum, and lncRNA malat-1 expression in hMSCsmalat-1-EVs, detected by qRT-PCR, was about 4.03 times higher than in hMSCs-EVs ($p < 0.05$) (**Figure 3B**), indicating that lncRNA malat-1 was successfully expressed in EVs. To investigate the role of EVs in OA, we investigated the effects of different concentrations of EVs on chondrocyte vitality after IL-1β treatment. We found chondrocyte vitality was significantly decreased after IL-1β treatment ($p < 0.05$). There was no significant difference in the 10 μg/ml groups compared to 25 μg/ml and 50 μg/ml concentrations ($p > 0.05$) (**Figure 3C**). Therefore, the concentration of 10 μg/ml was selected for subsequent experiments.

Then, the effects of hMSCs-EVs and hMSCs$^{malat-1}$-EVs on chondrocyte proliferation were examined in the different groups. Edu staining confirmed that chondrocytes from the hMSCs$^{malat-1}$-EVs group showed better proliferation promotion compared to the hMSCs-EVs group ($p < 0.05$) (**Figures 3D,E**).

hMSCs$^{malat-1}$-EVs Inhibited Apoptosis and Inflammation of Chondrocytes Induced by IL-1β

We performed additional experiments to further explore the effect of LncRNA malat-1 in EVs on IL -1β induced

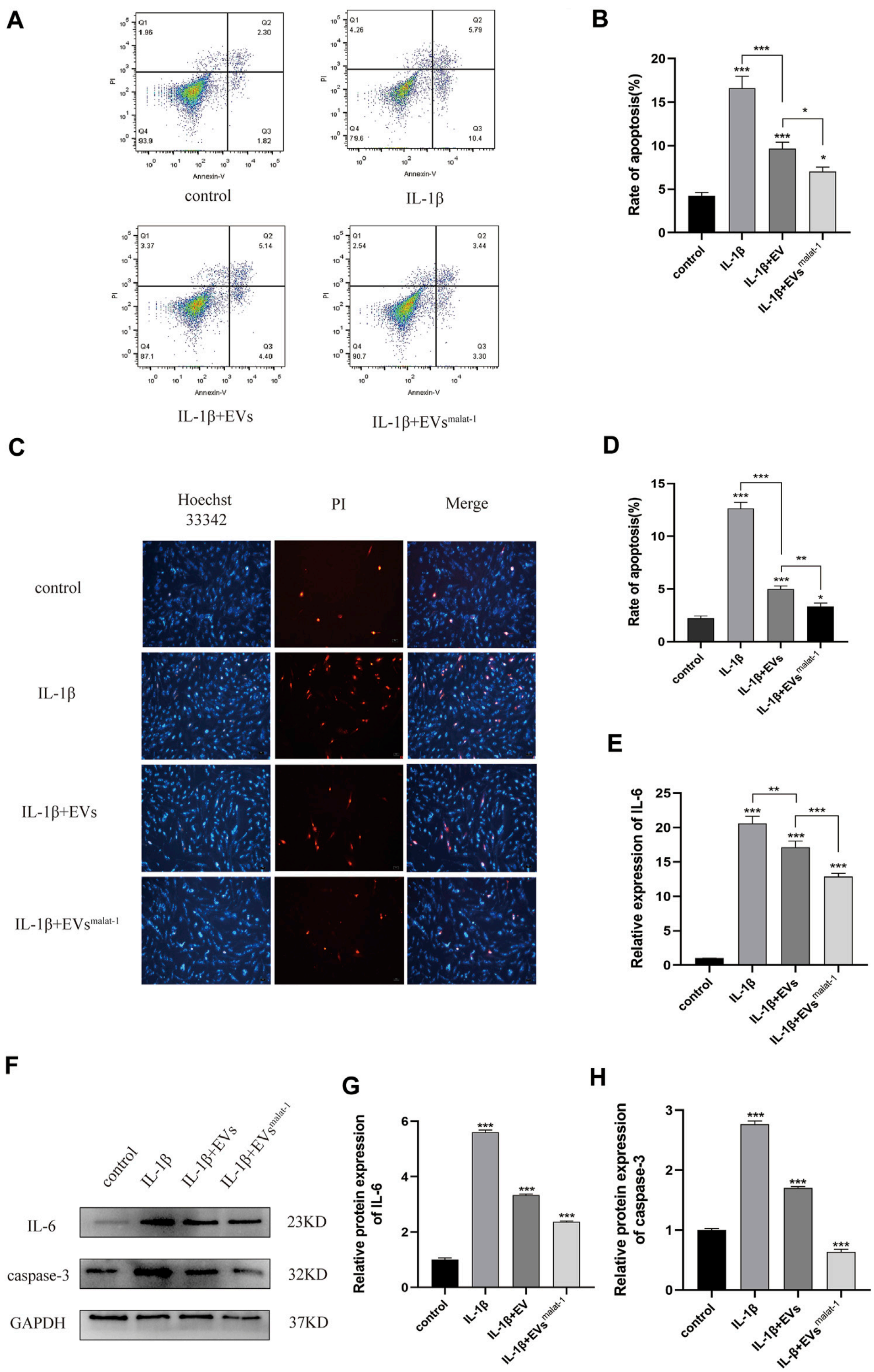

FIGURE 4 | (A) and **(B)** The apoptosis rate of chondrocytes treated with EVs analyzed by flow cytometry assay. **(C)** and **(D)** Hoechst 33342/PI assay was used to analyze the apoptosis rate of chondrocytes. **(E)** Inflammatory factor IL-6 expression was measured using Elisa in chondrocytes after treated with EVs. **(F–H)** The protein expression of IL-6 and Caspase-3 analyzed by western blot. $^{*}p < 0.05$, $^{**}p < 0.01$, $^{***}p < 0.001$, vs. control group. $n = 3$, one-way ANOVA for all.

chondrocyte apoptosis. We measured the apoptosis rate by flow cytometry. As the result show (**Figures 4A,B**), the apoptosis rate of the IL-1β group (16.62 ± 1.12%, $p < 0.05$) was significantly higher than that from the normal group (4.25 ± 0.32%, $p < 0.05$). After treatment with the hMSCs-EVs, the apoptosis rate of chondrocytes (9.67 ± 0.6%, $p < 0.05$) decreased by a third. At

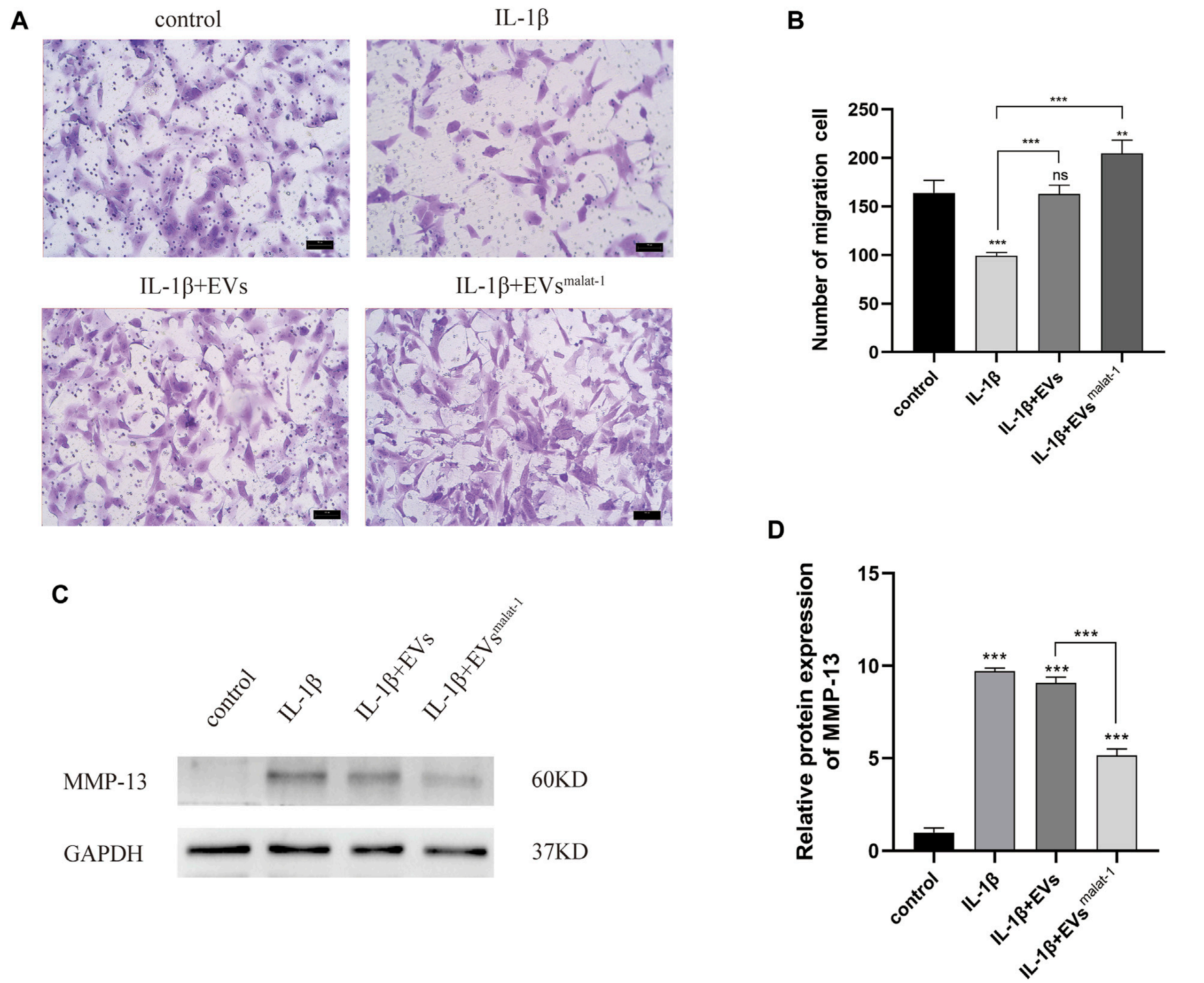

FIGURE 5 | (A) and **(B)** Migration of chondrocytes was detected by Transwell assays. $^{**}p < 0.01$, $^{***}p < 0.001$ vs. IL-1β group. **(C)** and **(D)** The protein expression of MMP-13 was detected by western blot, $^{*}p < 0.05$, $^{**}p < 0.01$, $^{***}p < 0.001$, vs. control group. $n = 3$, one-way ANOVA for all.

the same time, we found that the apoptosis rate of hMSCsmalat-1-EVs group (7.02 ± 0.42%, $p < 0.05$) decreased more substantially and was closer to the normal rate. Similarly, Hoechst 33342/PI staining results showed that after IL-1β treatment, the number of apoptotic cells increased significantly (**Figures 4C,D**). After adding hMSCs-EVs, the number of apoptotic cells decreased, but after adding hMSCs$^{malat-1}$-EVs, the number of apoptotic cells decreased even more substantially, suggesting a stronger anti-apoptotic effect of hMSCs$^{malat-1}$-EVs. Caspase-3 protein expression was detected by WB, and the results were consistent with those from flow cytometry and Hoechst 33342/PI staining.

In addition, the effect of LncRNA malat - 1 in EVs on IL - 1β induced chondrocyte inflammatory injury. Based on results from ELISA and WB (**Figures 4E,H**, **Supplementary Data Sheet S1**), chondrocyte in the normal group appeared to produce only a small amount of IL - 6 inflammatory-related factors and the OA inflammatory damage was significantly higher ($p < 0.05$). following EVs treatment, expression levels of IL-6 inflammation-related factors decreased ($p < 0.05$), but compared with the hMSCs-EVs group, the decrease in the hMSCs$^{malat-1}$-EVs group was more substantial ($p < 0.05$). These results suggest that chondrocyte apoptosis and inflammation induced by IL-1β can be inhibited by lncRNA malat-1 of the EVs, which appears protective for chondrocytes of OA.

hMSCs$^{malat-1}$-EVs Reversed IL-1β -Induced Decline of Chondrocyte Migration and Reeducation of MMP-13

We then performed transwell experiments to test the effects of hMSCs-EVs and hMSCs$^{malat-1}$-EVs on the ability of chondrocytes to migrate in OA. Our results showed that the number of migrating cells of IL-1β group decreased significantly compared to control groups ($p < 0.05$) (**Figures 5A,B**), while no significant differences were observed in the hMSCs-EVs group ($p > 0.05$). All groups, when treated with hMSCs$^{malat-1}$-EVs,

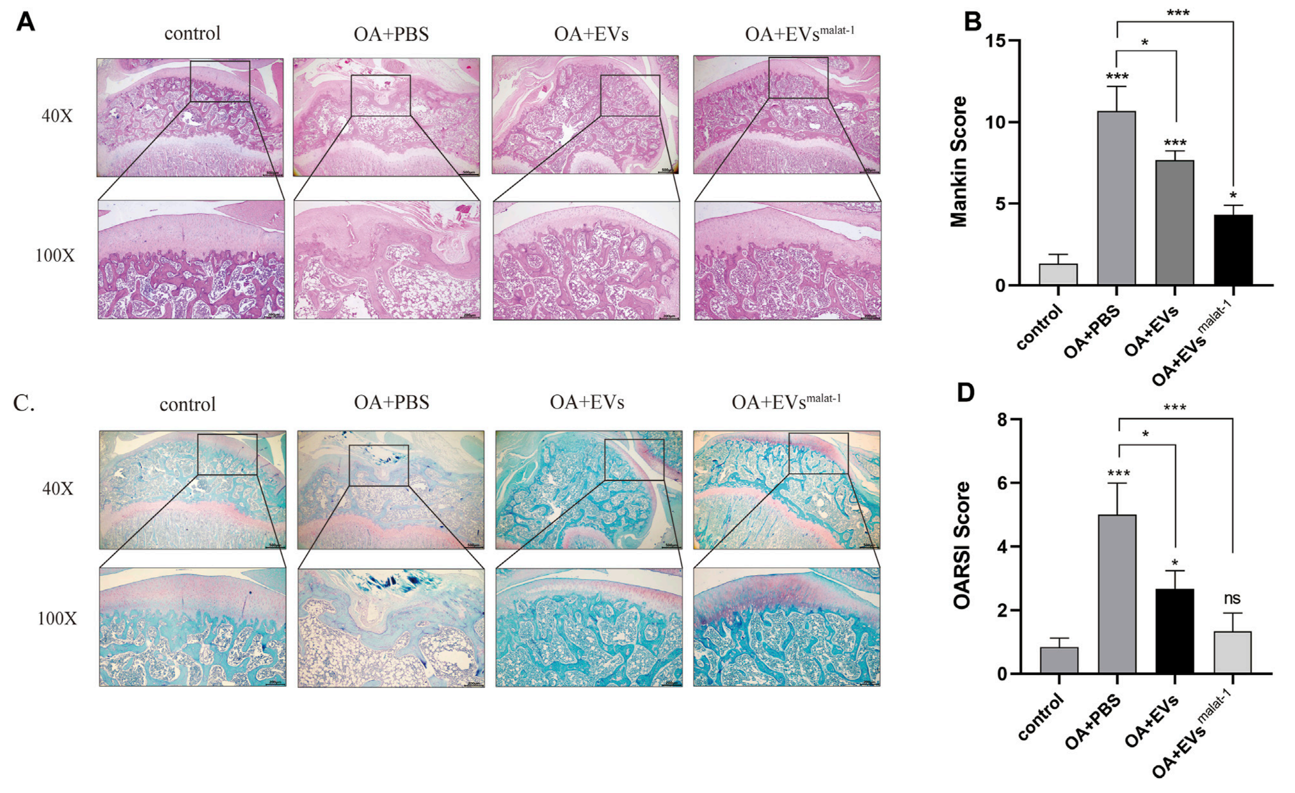

FIGURE 6 | (A) Haematoxylin and Eosin staining of SD rat knee joints after injecting EVs for 6 weeks. Scale bar: 200 μm (40X) and 500 μm (100X). **(B)** The modified Mankin's score of the SD rat knee joints. **(C)** Safranin O/Fast Green staining of SD rat knee joints after injecting EVs for 6 weeks. Scale bar: 200 μm (40X) and 500 μm (100X). **(D)** OARSI scores of the SD rat knee joints. $^{*}p < 0.05$, $^{**}p < 0.01$, $^{***}p < 0.001$, vs. control group. $n = 3$, one-way ANOVA for all.

exhibited a larger number of migrating cells compared to the IL-1β group and the hMSCs-EVs group ($p < 0.05$). The results from these experiments showed that IL-1β reduced chondrocyte migration ability, while the EVs reversed these effects *via* lncRNA malat-1.

To investigate the effect of EVs by malat-1 on the extracellular matrix (ECM) in OA, matrix metalloproteinase 13 (MMP-13) protein expression was tested. We found that both EVs downregulated the increased MMP-13 protein levels induced by IL-1β ($p < 0.05$) (**Figures 5C,D, Supplementary Data Sheet S1**). A more substantial decrease in MMP-13 protein levels was observed in the hMSCs$^{malat-1}$-EVs group compared to the hMSCs-EVs group ($p < 0.05$), suggesting that the EVs delayed IL-1β -induced chondrocyte degeneration through lncRNA malat-1.

hMSCs$^{malat-1}$-EVs Alleviated Cartilage Damage in a Rat OA Model

To confirm the protective effect of hMSCs$^{malat-1}$-EVs on chondrocytes *in vivo*, hMSCs-EVs and hMSCs$^{malat-1}$-EVs were injected into the articular cavity of OA rats. Six weeks later, OA articular surface changes were observed by HE staining and Safranine O-fast green (S-O) staining. The articular cartilage structure of OA rats was clear and exhibited a smooth surface. In the OA group, the surface was rough and had an irregular shape, the fibers were broken, and the cartilage was substantially damaged (**Figures 6A,B**). The score of OARSI and Mankin ($p < 0.05$) increased significantly (**Figures 6B,C**). After hMSCs-EVs treatment, articular cartilage injury of OA rats was alleviated and OARSI scores and Mankin score both decreases. Compared with hMSCs-EVs, the joint surface of the hMSCs$^{malat-1}$-EVs group was smoother, the cartilage damage was substantially alleviated, and the scores decreased ($p < 0.05$). These results indicate that hMSCs-EVs can alleviate cartilage damage caused by OA *via* LncRNA malat-1 in a rat model of OA.

DISCUSSION

The causes of OA are complex and multifactorial, and involve age, gender, degree of obesity, aging, genetic factors, joint damage, and other factors (Felson et al., 2000). In this study, we investigated a new potential treatment for OA. We successfully isolated EVs from hMSCs and used them to treat chondrocytes induced by IL-1β. After that, we harvested lncRNA malat-1-rich EVs through transfecting hMSCs to stably express lncRNA malat-1, which were used in subsequent experiments for evaluating their therapeutic effect on IL-1β induced-cartilage injury. Our results showed that overexpression of lncRNA malat-1 of EVs significantly reduced expression of IL-6, caspase-3, MMP-13 in OA, increased apoptosis, reversed IL-1β induced inhibition of proliferation, and increased the proliferation and migration rates of chondrocytes.

EVs are a type of vesicular structure of 40–160 nm in diameter that is actively secreted by almost all cells (Kalluri and LeBleu, 2020). EVs contain signaling factors such as mRNA, miRNA, and lncRNA, targeting adjacent cells by autocrine and paracrine mechanisms, or distal cells through the circulatory system (Colombo et al., 2014). Compared with stem cell transplantation, EVs became a hot topic given their potential for the treatment of OA due to their characteristics such as immunogenicity, and ease to save. Previous studies have suggested their huge therapeutic potential in hMSCs derived EVs in joint disease (Li et al., 2018b), and the importance of hMSCs paracrine in various diseases (Linero and Chaparro, 2014). In this study, the results of TEM, NTA, and WB indicate that we successfully extracted MSCs-derived EVs Furthermore, we confirmed that cartilage cells successfully uptake EVs by using the PKH26 probe, indicating that EVs can play a role in chondrocytes. EVs have attracted the attention of many scientists as a good carrier for treating the diseases, such as Qing Mao has researched that lncRNA KLF3-AS1 in human mesenchymal stem cell-derived EVs ameliorates pyroptosis of cardiomyocytes and myocardial infarction through miR-138-5p/Sirt1 axis (Mao et al., 2019). Huaxia Yang et also has found that lncRNA malat-1 is a novel inflammatory regulator in human systemic lupus erythematosus (SLE), and has great potential in treating inflammation (Li et al., 2020b). LncRNA malat-1 is a novel transcript of over 8000 nucleotides, and one of the most widely studied lncRNAs. It was first discovered in transcript screening related to non-small cell lung cancer (NSCLC) metastasis and patient survival (Hutchinson et al., 2007). A study of Tony Gutschner shows that lncRNA malat-1 is a critical regulator of the metastasis phenotype of lung cancer cells (Gutschner et al., 2013). In recent years, Jongchan Kim et found that malat-1 can inhibit the metastasis of breast cancer. In other diseases, lncRNA malat-1 is also widely studied, such as Huaxia Yang et has shown stem cell-derived EVs prevent aging-induced cardiac dysfunction through a novel EVs/lncRNA malat-1/NF-κB/TNF-α signaling pathway (Zhu et al., 2019). Furthermore, Xucheng Yang confirmed that lncRNA malat-1 shuttled by EVs derived from bone marrow mesenchymal stem cells-secreted EVs alleviates osteoporosis through mediating microRNA-34c/SATB2 axis (Yang et al., 2019). The exciting thing is that Hongxi Li et found that lncRNA malat-1 can regulate ECM catabolism, inflammation, apoptosis and proliferation in chondrocyte (Li et al., 2020a). Our study show lncRNA malat-1 from EVs reduced expression of IL-6, caspase-3, MMP-13 in OA, decrease apoptosis, promote proliferation and migration. It shows that lncRNA malat-1 from EVs has the ability to delay the degeneration of chondrocytes.

Inflammation plays an important role in the pathogenesis of OA, in which the chondrocytes, synovial membrane, and surrounding tissues produce large amounts of inflammatory factors such as IL-1β, IL-6, TNF-α, that accelerate the progression of osteoarthritis (Eymard et al., 2014; Li et al., 2020a). The up-regulation of inflammatory factors IL-1β, IL-6, TNF-α and other catabolic factors, such as MMP-13, can accelerate apoptosis and matrix degradation of chondrocytes. Inhibition of inflammation is therefore an important part of preventing OA development. In our study, we have detected through both ELISA and WB experiments that malat1 reduces the expression of the inflammatory factor IL-6 in the IL-1β induced OA cell model through EVs. Minqiu et al. found that SFC-miR-126-3p-Exos inhibited apoptosis and inflammation of articular cartilage and chondrocyte degradation in an SD rat model of OA (Zhou et al., 2021). In another study, Shipin Zhang et also researchers and finds that MSC EVs can effectively alleviate temporomandibular joint osteoarthritis by attenuating inflammation and restoring matrix homeostasis. Jiaping Wu et al. found reported lncRNA malat-1 inhibited inflammation of microglia through the miR-154-5p/AQP9 axis (Wu et al., 2020). In this study, we examined the effect of hMSCs$^{malat-1}$-EVs on OA inflammation and found that hMSCs$^{malat-1}$-EVs can reduce IL-6 levels in the OA model, in agreement with the results of Jiyong Zhang et al. (Zhang et al., 2020) Ruizhang et al. found that lncRNA malat-1 in EVs promoted proliferation and migration of non-small cell lung cancer cells (Zhang et al., 2017). In our study, chondrocyte proliferation decreased significantly, and increased apoptosis and decreased migration capacity were observed, after IL-1β treatment. After treatment with hMSCs-EVs and hMSCs$^{malat-1}$-EVs, the negative effect of IL-1β was ameliorated, and the function and vitality of chondrocytes were restored. Moreover, comparison of the two EVs revealed that hMSCs$^{malat-1}$-EVs had a better therapeutic effect, which was consistent with our original hypothesis. These results indicated that EVs promoted chondrocyte proliferation, inhibited apoptosis, and enhanced the migration ability of chondrocytes *via* lncRNA malat-1.

Inflammatory cytokines, such as IL-1β, IL-6, TNF-α, and others, promote the production of MMPs and aggravate the progression of OA (Goldring and Otero, 2011). MMPs are involved in the degradation of various proteins in the ECM. MMP-13 is an important member of the MMPs family, which plays an important role in degrading collagen type II in OA articular cartilage and bones, and is highly expressed in OA patients but barely expressed in healthy people (Burrage et al., 2006). MMP-13 is the main key enzyme of cartilage degeneration and can degrade the ECM. MMP-13 is considered as one of the major contributing factors in the onset of OA (Wan et al., 2020), hence inhibiting MMP-13 expression could represent a new strategy to prevent OA. Xue Chen and others found that EVs secreted by MSCs inhibited the expression of MMP-13 in the traumatic arthritis model by microRNA-136-5p targeting ELF3 (Chen et al., 2011). In the inflammatory injury model of OA generated in this work, we also found that chondrocytes highly expressed MMP-13 after IL-1β treatment, and the effect of hMSCs$^{malat-1}$-EVs on MMP-13 was further explored. We found that both hMSCs-EVs and hMSCs$^{malat-1}$-EVs downregulated IL-1β-induced MMP-13 increase, but hMSCs$^{malat-1}$-EVs appeared to have a stronger protective effect. This result is consistent with our hypothesis, suggesting that hMSCs$^{malat-1}$-EVs provide better protection to the ECM and might be a more promising treatment of OA than hMSCs-EVs. Similarly, our animal experiments showed that hMSCs$^{malat-1}$-EVs significantly delayed the degeneration of the articular cartilage in SD rats. In this study, we did not investigate the protein changes following hMSCs$^{malat-1}$-EVs uptake by chondrocytes, which is a topic that will be investigated in future studies.

CONCLUSION

All together, our results based on an IL-1β induced OA model, indicate that EVs derived from hMSCs with lncRNA malat-1 overexpression promote chondrocyte proliferation and migration, suppress inflammation, degradation of the ECM, and appear to have a good protective effect in OA, providing a new potential therapeutic option for the prevention and treatment of OA.

DATA AVAILABILITY STATEMENT

The raw data supporting the conclusions of this article will be made available by the authors, without undue reservation.

ETHICS STATEMENT

The animal study was reviewed and approved by Institutional Animal Care and Use Committee of Nanchang University.

AUTHOR CONTRIBUTIONS

XC, CP, CY, and WH: conception and design. TW: provision of study materials. QC, CP, and BL: collection and assembly of data. CP and WH: data analysis and interpretation. XC, CP, JX, and GY: manuscript writing. All authors final approval of manuscript.

FUNDING

This research was supported by the Double Thousand Plan Foundation of Jiangxi Province Human Resources And Social Security Department (Grant number: G/Y2577). Key Intervertebral Disc Laboratory of Jiangxi Province (Grant number: 2020ACBL206012).

SUPPLEMENTARY MATERIAL

The Supplementary Material for this article can be found online at: https://www.frontiersin.org/articles/10.3389/fbioe.2021.772002/full#supplementary-material

REFERENCES

Batrakova, E. V., and Kim, M. S. (2015). Using Exosomes, Naturally-Equipped Nanocarriers, for Drug Delivery. *J. Control. Release*, 396–405. doi:10.1016/j.jconrel.2015.07.030

Breitbach, M., Bostani, T., and Roell, W. (2007). Potential Risks of Bone Marrow Cell Transplantation into Infarcted Hearts. *Blood* 110, 1362–1369. doi:10.1182/blood-2006-12-063412

Burrage, P. S., and Mix, K. S. (2006). Mix and C E Brinckerhoff, Matrix Metalloproteinases: Role in Arthritis. *Front. Biosci. : a J. virtual Libr.* 11, 529–543. doi:10.2741/1817

Chen, X., Shi, Y., Xue, P., Zheng, J., Ma, X., Li, J., et al. (2020). Mesenchymal Stem Cell-Derived Exosomal microRNA-136-5p Inhibits Chondrocyte Degeneration in Traumatic Osteoarthritis by Targeting ELF3. *Arthritis Res. Ther.* 22, 256. doi:10.1186/s13075-020-02325-6

Chen, Y., Chen, Y., Zhang, S., Du, X., and Bai, B. (2016). Parathyroid Hormone-Induced Bone Marrow Mesenchymal Stem Cell Chondrogenic Differentiation and its Repair of Articular Cartilage Injury in Rabbits. *Med. Sci. Monit. Basic Res.* 22, 132–145. doi:10.12659/msmbr.900242

Colombo, M., Raposo, G., and Thery, C. (2014). Biogenesis, Secretion, and Intercellular Interactions of Exosomes and Other Extracellular Vesicles. *Annu. Rev. Cel Dev Biol* 30, 255–289. doi:10.1146/annurev-cellbio-101512-122326

Desando, G., Cavallo, C., Sartoni, F., Martini, L., Parrilli, A., Veronesi, F., et al. (2013). Intra-articular Delivery of Adipose Derived Stromal Cells Attenuates Osteoarthritis Progression in an Experimental Rabbit Model. *Arthritis Res. Ther.* 15, R22. doi:10.1186/ar4156

Eymard, F., Pigenet, A., Citadelle, D., Beneli, C., Chevalier, X., Houard, X., et al. (2014). Induction of an Inflammatory and Prodegradative Phenotype in Autologous Fibroblast-like Synoviocytes by the Infrapatellar Fat Pad from Patients with Knee Osteoarthritis. *Arthritis Rheumatol. (Hoboken, N.J).* 66, 2165–2174. doi:10.1002/art.38657

Felson, D. T., Lawrence, R. C., Dieppe, P. A., Jorden, J. M., Sharma, L., Zhang, Y., et al. (2000). Osteoarthritis: New Insights. Part 1: the Disease and its Risk Factors. *Ann. Intern. Med.* 133, 635–646. doi:10.7326/0003-4819-133-8-200010170-00016

Foers, A. D., Chatfield, S., and Dagley, L. F. (2018). Enrichment of Extracellular Vesicles from Human Synovial Fluid Using Size Exclusion Chromatography. *J. Extracell Vesicles* 7, 1490145. doi:10.1080/20013078.2018.1490145

Fu, S., Wang, Y., Li, H., Chen, L., and Liu, Q. (2020). Regulatory Networks of LncRNA MALAT-1 in Cancer. *Cancer Manag. Res.* 12, 10181–10198. doi:10.2147/cmar.s276022

Fu, X., Liu, G., Halim, A., Yung, J., Qing, L., and Guanbin, S. (2019). Mesenchymal Stem Cell Migration and Tissue Repair. *Cells* 8, 784. doi:10.3390/cells8080784

Furlani, D., Ugurlucan, M., and Ong, L. (2009). Is the Intravascular Administration of Mesenchymal Stem Cells Safe? Mesenchymal Stem Cells and Intravital Microscopy. *Microvasc. Res.* 77, 370–376. doi:10.1016/j.mvr.2009.02.001

Glyn-Jones, S., Palmer, A. J. R., and Agricola, R. (2015). Osteoarthritis. *Lancet*, 376–387. doi:10.1016/s0140-6736(14)60802-3

Goldring, M. B., and Otero, M. (2011). Inflammation in Osteoarthritis. *Curr. Opin. Rheumatol.* 23, 471–478. doi:10.1097/BOR.0b013e328349c2b1

Guilak, F., Nims, R. J., Dicks, A., Wu, C. L., and Meulenbelt, I. (2018). Osteoarthritis as a Disease of the Cartilage Pericellular Matrix. *Matrix Biol.* 71, 40–50. doi:10.1016/j.matbio.2018.05.008

Gutschner, T., Hammerle, M., Eissmann, M., Hsu, J., Kim, Y., Hung, G., et al. (2013). The Noncoding RNA MALAT1 Is a Critical Regulator of the Metastasis Phenotype of Lung Cancer Cells. *Cancer Res.* 73, 1180–1189. doi:10.1158/0008-5472.can-12-2850

Hutchinson, J. N., Ensminger, A. W., Clemson, C. M., Lynch, C. R., Lawrence, J. B., and Andrew, C. (2007). A Screen for Nuclear Transcripts Identifies Two Linked Noncoding RNAs Associated with SC35 Splicing Domains. *BMC Genomics* 8, 39. doi:10.1186/1471-2164-8-39

Kalluri, R., and LeBleu, V. S. (2020). The Biology, Function, and Biomedical Applications of Exosomes. *Science* 367, eaau6977. doi:10.1126/science.aau6977

Kong, X., Wang, J., Cao, Y., Zhang, H., Lu, X., Wang, Y., et al. (2019). The Long Noncoding RNA MALAT-1 Functions as a Competing Endogenous RNA to Regulate MSL2 Expression by Sponging miR-338-3p in Myasthenia Gravis. *J. Cell. Biochem.* 120, 5542–5550. doi:10.1002/jcb.27838

Li, H., Xie, S., and Li, H. (2020). LncRNA MALAT1 Mediates Proliferation of LPS Treated-Articular Chondrocytes by Targeting the miR-146a-PI3K/Akt/mTOR axis. *Life Sci.* 254, 116801. doi:10.1016/j.lfs.2019.116801

Li, H., Xie, S., Li, H., Zhang, R., and Zhang, H. (2020). LncRNA MALAT1 Mediates Proliferation of LPS Treated-Articular Chondrocytes by Targeting the miR-146a-PI3K/Akt/mTOR axis. *Life Sci.* 254, 116801. doi:10.1016/j.lfs.2019.116801

Li, L., Duan, X., and Fan, Z. (2018). Mesenchymal Stem Cells in Combination with Hyaluronic Acid for Articular Cartilage Defects. *Scientific Rep.* 8, 9900. doi:10.1038/s41598-018-27737-y

Li, Z., Wang, Y., Xiao, K., Weng, X., Xiang, S., and Li, Z. (2018). Emerging Role of Exosomes in the Joint Diseases. *Cell Physiol. Biochem. : Int. J. Exp. Cell. Physiol. Biochem. Pharmacol.* 47, 2008–2017. doi:10.1159/000491469

Linero, I., and Chaparro, O. (2014). Paracrine Effect of Mesenchymal Stem Cells Derived from Human Adipose Tissue in Bone Regeneration. *PloS one* 9, e107001. doi:10.1371/journal.pone.0107001

Mao, Q., Liang, X. L., Zhang, C. L., Pang, Y. H., and Lu, Y. X. (2019). LncRNA KLF3-AS1 in Human Mesenchymal Stem Cell-Derived Exosomes Ameliorates Pyroptosis of Cardiomyocytes and Myocardial Infarction through miR-138-5p/Sirt1 axis. *Stem Cel. Res. Ther.* 10, 393. doi:10.1186/s13287-019-1522-4

Matas, J., Orrego, M., Amenabar, D., Infante, C., Tapia-Limonchi, R., Cadiz, M. I., et al. (2019). Umbilical Cord-Derived Mesenchymal Stromal Cells (MSCs) for Knee Osteoarthritis: Repeated MSC Dosing Is Superior to a Single MSC Dose and to Hyaluronic Acid in a Controlled Randomized Phase I/II Trial. *Stem Cell Transl Med* 8, 215–224. doi:10.1002/sctm.18-0053

Puthanveetil, P., Chen, S., Feng, B., and Gautam, A. (2015). Long Non-coding RNA MALAT1 Regulates Hyperglycaemia Induced Inflammatory Process in the Endothelial Cells. *J. Cell. Mol. Med.*, 1418–1425. doi:10.1111/jcmm.12576

He, T., He, L., Xing, J., Fan, L., Liu, C., Wu, D., et al. (2020). Bone Marrow Mesenchymal Stem Cell-Derived Exosomes Protect Cartilage Damage and Relieve Knee Osteoarthritis Pain in a Rat Model of Osteoarthritis. *Stem Cel. Res. Ther.* 11, 276. doi:10.1186/s13287-020-01781-w

Tao, S. C., Yuan, T., and Zhang, Y. L. (2017). Exosomes Derived from miR-140-5p-Overexpressing Human Synovial Mesenchymal Stem Cells Enhance Cartilage Tissue Regeneration and Prevent Osteoarthritis of the Knee in a Rat Model. *Theranostics* 7, 180–195. doi:10.7150/thno.17133

Wan, Y., Li, W., Liao, Z., Chen, X., Yan, M., Tang, Z., et al. (2020). Selective MMP-13 Inhibitors: Promising Agents for the Therapy of Osteoarthritis. *Curr. Med. Chem.* 27, 3753–3769. doi:10.2174/0929867326666181217153118

Wang, X., Wang, C., Gou, W., Xu, X., Wang, Y., Wang, A., et al. (2018). The Optimal Time to Inject Bone Mesenchymal Stem Cells for Fracture Healing in a Murine Model. *Stem Cel. Res. Ther.*, 272. doi:10.1186/s13287-018-1034-7

Washietl, S., Kellis, M., and Garber, M. (2014). Evolutionary Dynamics and Tissue Specificity of Human Long Noncoding RNAs in Six Mammals. *Genome Res.* 24, 616–628. doi:10.1101/gr.165035.113

Wu, J., Wang, C., and Ding, H. (2020). LncRNA MALAT1 Promotes Neuropathic Pain Progression through the miR1545p/AQP9 axis in CCI Rat Models. *Mol. Med. Rep.* 21, 291–303. doi:10.3892/mmr.2019.10829

Yang, H., Liang, N., Wang, M., Fei, Y., Sun, J., Li, Z., et al. (2017). Long Noncoding RNA MALAT-1 Is a Novel Inflammatory Regulator in Human Systemic Lupus Erythematosus. *Oncotarget* 8, 77400–77406. doi:10.18632/oncotarget.20490

Yang, R. C., Zhu, X. L., Wang, J., Wan, F., Lin, Y., Zhu, B., et al. (2018). Bone Marrow Mesenchymal Stem Cells Attenuate the Progression of Focal Segmental Glomerulosclerosis in Rat Models. *BMC Nephrol.* 19, 335. doi:10.1186/s12882-018-1137-5

Yang, X., Yang, J., Lei, P., and Wen, T. (2019). LncRNA MALAT1 Shuttled by Bone Marrow-Derived Mesenchymal Stem Cells-Secreted Exosomes Alleviates Osteoporosis through Mediating microRNA-34c/SATB2 axis. *Aging* 11, 8777–8791. doi:10.18632/aging.102264

Zhang, J., Rong, Y., Luo, C., and Cui, W. (2020). Bone Marrow Mesenchymal Stem Cell-Derived Exosomes Prevent Osteoarthritis by Regulating Synovial Macrophage Polarization. *Aging* 12, 25138–25152. doi:10.18632/aging.104110

Zhang, M., Liu, D., Li, S., Zhang, Y., Chang, L., Sun, F., et al. (2015). Bone Marrow Mesenchymal Stem Cell Transplantation Retards the Natural Senescence of Rat Hearts. *Stem Cell Transl Med* 4, 494–502. doi:10.5966/sctm.2014-0206

Zhang, R., Xia, Y., Wang, Z., Zheng, J., Chen, Y., Li, X., et al. (2017). Serum Long Non Coding RNA MALAT-1 Protected by Exosomes Is Up-Regulated and Promotes Cell Proliferation and Migration in Non-small Cell Lung Cancer. *Biochem. Biophys. Res. Commun.* 19, 406–414. doi:10.1016/j.bbrc.2017.06.055

Zhou, Y., Ming, J., Li, Y., Li, B., Li, J., Liu, S., et al. (2021). Exosomes Derived from miR-126-3p-Overexpressing Synovial Fibroblasts Suppress Chondrocyte Inflammation and Cartilage Degradation in a Rat Model of Osteoarthritis. *Cel Death Discov.* 7, 37. doi:10.1038/s41420-021-00418-y

Zhu, B., Zhang, L., Liang, C., Liu, B., Pan, X., Wang, Y., et al. (2019). Stem Cell-Derived Exosomes Prevent Aging-Induced Cardiac Dysfunction through a Novel Exosome/lncRNA MALAT1/NF-kappaB/TNF-Alpha. *Oxid Med. Cel Longev* 2019, 9739258. doi:10.1155/2019/9739258

Conflict of Interest: The authors declare that the research was conducted in the absence of any commercial or financial relationships that could be construed as a potential conflict of interest.

Publisher's Note: All claims expressed in this article are solely those of the authors and do not necessarily represent those of their affiliated organizations, or those of the publisher, the editors and the reviewers. Any product that may be evaluated in this article, or claim that may be made by its manufacturer, is not guaranteed or endorsed by the publisher.

Copyright © 2021 Pan, Huang, Chen, Xu, Yao, Li, Wu, Yin and Cheng. This is an open-access article distributed under the terms of the Creative Commons Attribution License (CC BY). The use, distribution or reproduction in other forums is permitted, provided the original author(s) and the copyright owner(s) are credited and that the original publication in this journal is cited, in accordance with accepted academic practice. No use, distribution or reproduction is permitted which does not comply with these terms.

Advantages of publishing in Frontiers

OPEN ACCESS
Articles are free to read for greatest visibility and readership

FAST PUBLICATION
Around 90 days from submission to decision

HIGH QUALITY PEER-REVIEW
Rigorous, collaborative, and constructive peer-review

TRANSPARENT PEER-REVIEW
Editors and reviewers acknowledged by name on published articles

Frontiers
Avenue du Tribunal-Fédéral 34
1005 Lausanne | Switzerland

Visit us: www.frontiersin.org
Contact us: frontiersin.org/about/contact

REPRODUCIBILITY OF RESEARCH
Support open data and methods to enhance research reproducibility

DIGITAL PUBLISHING
Articles designed for optimal readership across devices

FOLLOW US
@frontiersin

IMPACT METRICS
Advanced article metrics track visibility across digital media

EXTENSIVE PROMOTION
Marketing and promotion of impactful research

LOOP RESEARCH NETWORK
Our network increases your article's readership